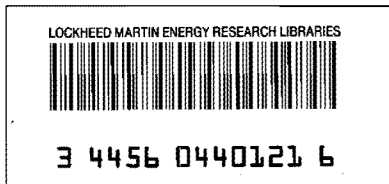


TID-7642

12



R D Chewerton

**Research Reactor
FUEL ELEMENT
Conference**

September 17-19, 1962

Gatlinburg, Tennessee

BOOK 1

Oak Ridge National Laboratory
Research Library

4500N, MS-6191

LIBRARY LOAN COPY

DO NOT TRANSFER TO ANOTHER PERSON.
If you wish someone else to see this report, send in
name with report and the library will arrange a loan.

ORNL 118(10-05)

UNITED STATES ATOMIC ENERGY COMMISSION
Division of Technical Information

LEGAL NOTICE

This report was prepared as an account of Government sponsored work. Neither the United States, nor the Commission, nor any person acting on behalf of the Commission:

A. Makes any warranty or representation, expressed or implied, with respect to the accuracy, completeness, or usefulness of the information contained in this report, or that the use of any information, apparatus, method, or process disclosed in this report may not infringe privately owned rights; or

B. Assumes any liabilities with respect to the use of, or for damages resulting from the use of any information, apparatus, method, or process disclosed in this report.

As used in the above, "person acting on behalf of the Commission" includes any employee or contractor of the Commission, or employee of such contractor, to the extent that such employee or contractor of the Commission, or employee of such contractor prepares, disseminates, or provides access to, any information pursuant to his employment or contract with the Commission, or his employment with such contractor.

This report has been reproduced directly from the best available copy.

Printed in USA. This report consists of 2 books, total price \$7.50. Available from the Office of Technical Services, Department of Commerce, Washington 25, D. C.

TID-7642

REACTOR TECHNOLOGY

Research Reactor
FUEL ELEMENT
Conference

September 17-19, 1962
Gatlinburg, Tennessee

BOOK 1

Sponsored by
AEC Divisions of
Research and Reactor Development
and
Oak Ridge National Laboratory

LOCKHEED MARTIN ENERGY RESEARCH LIBRARIES



3 4456 0440121 6

FOREWORD

The Research Reactor Fuel Element Conference was convened to bring together persons actively engaged in, or concerned with, the technology of research reactor fuel elements and to provide for interchange of information through presentation of formal papers and informal discussions. It was held in Gatlinburg, Tennessee, on September 17-19, 1962, under the sponsorship of the Division of Reactor Development of the U. S. Atomic Energy Commission. Oak Ridge National Laboratory served as host for the unclassified meeting which was attended by 150 participants, including 31 registered foreign guests.

The scope of the Conference embraced the broad topics of nuclear, thermal, and mechanical design; materials evaluation and selection; component fabrication and assembly; nondestructive testing and inspection; radiation damage; corrosion performance; and some economical aspects. A total of 36 technical papers was presented—2 from Belgium, 1 from Canada, 1 from Switzerland, 1 from France, and 31 from the United States. Many of the United States papers dealt with the new generation of research reactors now under design and construction. These are to provide unperturbed neutron flux densities in the range of 1 to 5×10^{15} neutrons/cm²/sec for (1) beam experiments designed to advance the study of elementary particles, (2) in-reactor performance tests on various materials and components in the coolant environment of water, liquid sodium, and gaseous media, and (3) production of research quantities of the transuranic elements. Included in this new group of reactors are the Advanced Test Reactor to be located at the National Reactor Testing Station in Idaho, the Argonne Advanced Research Reactor at Argonne, Illinois, the High Flux Isotope Reactor at Oak Ridge, and the High Flux Beam Reactor at Brookhaven National Laboratory, Upton, Long Island, New York.

These Proceedings contain the manuscripts of all papers presented. The paper entitled "General Design of the Argonne Advanced Research Reactor" by L. W. Fromm has been enlarged to include more information on the fuel element for the subject reactor. This change is the result of the fact that the original paper dealing with this information was eliminated from the program for reasons of patent clearance.

The presentation of these Proceedings represents the unstinting efforts of many, and, as general chairman, in behalf of the U. S. Atomic Energy Commission and the Oak Ridge National Laboratory, I would like to express my sincere appreciation to (1) the authors without whose contributions the Conference could not have been held; (2) the session chairmen, consisting of W. L. R. Rice, U. S. Atomic Energy Commission; A. L. Boch, Oak Ridge National Laboratory; G. M. Adamson, Jr., Oak Ridge National Laboratory; D. R. deBoisblanc, Phillips Petroleum Company; and J. M. Martin, U. S. Atomic Energy Commission; (3) the program committee composed of G. M. Adamson, Jr. and A. L. Boch; (4) the receptionists, Freda Finn, Marjorie White, and Evelyn Webb; (5) E. E. Sinclair of the U. S. Atomic Energy Commission who gave the opening remarks; and (6) J. A. Swartout, Deputy Director of the Oak Ridge National Laboratory, who presented a most interesting and satirical after-dinner talk on the subject of research reactors. In addition, a vote of thanks goes to D. D. Cowen, Director of Public Relations at the Oak Ridge National Laboratory, whose office was responsible for many of the Conference arrangements, and, finally, to the Division of Technical Information of the U. S. Atomic Energy Commission for the reproduction of these Proceedings.

J. E. Cunningham
General Chairman

TABLE OF CONTENTS

	Page
Foreword	i
Fuel Element and Core Design of the Brookhaven High Flux Beam Reactor	1
General Design of the Argonne Advanced Research Reactor	22
Physics Advantages of Stainless Steel Cores	38
Description and Objectives of the ATR	47
The Nuclear Design of the ATR	51
The Mechanical Design of the Advanced Test Reactor Fuel Element	61
The Thermal and Hydraulic Design of the Advanced Test Reactor	75
Nuclear Design of the HFIR	89
Mechanical and Hydraulic Design of the HFIR	99
Burnout Heat Flux Prediction for Flowing, Subcooled, Wetting Liquids	112
Thermal Design of the HFIR Fuel Element	138
Fuel Elements for the Belgian High Flux Test Reactor BR2	152
Part I: Design and hydraulic tests of some special fuel elements	
Fuel Elements for the Belgian High Flux Test Reactor BR2	182
Part II: Non-destructive testing of plates	
Bottle Type Fuel Element for Pool Type Reactors	197
Prototype Studies of Modified Fuel Element Geometries	244
Fabrication Development of the Involute-shaped High Flux Isotope Reactor Fuel Plates	268
Assembly and Welding Development for the High-Flux Isotope Reactor Fuel Element	290
Fabrication Development of the Advanced Test Reactor Fuel Element	315
Nondestructive Testing of High-Flux Isotope Reactor and Advanced Test Reactor Fuel Elements	337
Fuel Elements for the Belgian High Flux Test Reactor BR2	360
Fabrication and testing of a standard type fuel element made by spot- welding	

TABLE OF CONTENTS (Continued)

	Page
A New Concept for Aluminum Base Fuel Elements	369
Fabrication of Composite Plate Assemblies Containing Graded or Contour Fuel and/or Poison Loadings by Powder Metallurgy Techniques	376
Fabrication and Irradiation of Bonded Flat Type Rods for the NRU Reactor	398
Performance of Aluminum-Uranium Alloy Fuel Plates Under High Temperature and High Burnup Conditions	425
Some Results of Uranium Aluminum Irradiations at the MTR/ETR	444
Radiation Performance and Induced Transformations in Aluminum-Base Fuels	469
Effects of Fuel Burnup on Aluminum Plates Reinforced with Fueled-Glass Fibers	489
Mechanical Properties of X8001 Aluminum Cladding and X8001 Aluminum-Base Fuel Dispersion at Elevated Temperatures	549
Aluminum-Aluminum Oxide Alloy Wrought Products	565
Observations on the Thermal Stability of S.A.P.	588
Aluminum Alloy Corrosion	601
The Corrosion of Aluminum Alloys Under Simulated ATR and HFIR Conditions	612
Corrosion of Aluminum-Clad Fuel Elements	635
Exothermic Reactions in Al-U ₃ O ₈ Composites	649
The Relation of Uranium Homogeneity Requirements to the Yield of Uranium-Aluminum Alloy Fuel Plates	667
Use of Chip and Shot Methods for Producing Homogeneous Aluminum-Uranium Fuel	682
Applications of Scintillation Spectrometry to Research Reactor Fuel Assay	716

FUEL ELEMENT AND CORE DESIGN OF THE
BROOKHAVEN HIGH FLUX BEAM REACTOR

by

Joseph M. Hendrie
Brookhaven National Laboratory
Upton, New York

It is a pleasure to be able to present a report on the fuel element and core design of the Brookhaven High Flux Beam Reactor as the first paper of this conference on research reactor fuel elements. To place these remarks on fuel element and core design in the proper context, our objective in building the HFBR must first be understood. Second, some idea of the general arrangement of the system is necessary. We shall deal first with these introductory matters.

The objective of the HFBR Project is to build a machine to produce neutron beams for research. The neutron energies of interest are mainly those in the thermal range, with some interest in the resonance region up to perhaps 100 volts. These beams are to be as intense as the dual boundaries of technical knowledge and fiscal limitation will permit, and they should contain as small a fast neutron component as possible. The latter condition arises because most of the experiments in neutron beam physics are done against a background "noise" of

scattered and degraded fast neutrons, and the signal to noise ratio rather than the absolute counting rate is the limiting factor in determining what can be measured and in the accuracy of measurement.

The early theoretical work by Auerbach, Chernick, and co-workers⁽¹⁾ showed that if we could construct a small, under-moderated core, run it at high power density, and immerse the core in a very good reflector, the basic requirements for the machine could be met at modest total power levels. Undermoderating the core means that it will leak epithermal neutrons into the reflector at a great rate. The reflector then acts as a moderator and neutrons thermalized there stack up in a flux peak which is many times higher than the core thermal flux.

Because this system effects a spacial separation of the thermal range neutron source from the fast source, beam tubes can be placed to reduce the fast component at little cost to the low energy beam, and thus achieve the desired signal to noise ratio improvement. This system is essentially an inversion of the flux trap system, of which a great deal more will be heard at this conference.

Figure 1 shows both calculated and measured flux plots for the HFBR system. Note that the ordinate scale is in terms of flux per unit power. The high peaking of the thermal group neutron flux outside the reactor core is clearly shown in this illustration. At the design power of 40 Mw, the peak thermal flux is about 7×10^{14} n/cm²-sec.

We had hoped from the beginning to avoid the problems and expense of developing new and advanced fuel elements. We were, therefore, pleased to find that for core volumes of 50 to 80 liters the peak power density of 1.5 Mw/liter available in plate-type, water-cooled fuel elements of the MTR-ETR variety was sufficient for our needs. At a core volume split of about half moderator, half metal, and with D_2O rather than H_2O as moderator, the desired undermoderation of the core could be achieved with reasonable fuel alloys in the familiar .050 in. thick plates. Our fuel elements, then, are modifications of the MTR-ETR plate-type elements.

Note that the high epithermal leakage rate from the core could have been achieved with H_2O as moderator and coolant by reducing the water channel width in the fuel element, and increasing the uranium loading of the fuel plates by a larger factor. This approach is, in fact, what has been done in other designs. We have chosen, however, to retain the basic water channel width and plate thickness of the well-established MTR-ETR fuel element, to make a moderate increase in the uranium loading of the fuel alloy, and to achieve the desired epithermal leakage rate (or undermoderation of the core) by using D_2O as moderator and coolant. With D_2O chosen as the in-core fluid, and the need for a good quality reflector, the use of D_2O as the reflector is obvious.

So much for the objectives of the HFBR Project and the reasons for the core design taking the direction which it has.

Let us now look at the general arrangement of the reactor system.

An elevation of the biological shield and reactor vessel is shown in Figure 2. The reactor vessel rests in a pit formed by the concrete biological shield and the steel and lead thermal shield. Neutron beams are taken out horizontally, through beam ports with appropriate shutters and plugs. An assortment of vertical tubes and thimbles extend downward around and into the vessel for instrument ports and irradiation purposes. Fuel handling is done through the top cover of the vessel, moving one element at a time. The vessel itself is of aluminum, and has the shape of a large florence flask. The diameter of the spherical section which contains the core is 7 feet.

The water flow pattern within the reactor vessel is shown in Figure 3. Both inlet and outlet nozzles on the reactor vessel are well above the fuel region of the core. The water flow direction is downward through the core, and back up through the reflector. Process conditions in the vessel are indicated in Table 1, which is a general summary of HFBR design parameters.

A plan view of the reactor core is shown in Figure 4. The core is formed of 28 fuel elements, each of which is rectangular in cross section. The central two positions in the core are filled by fast flux irradiation thimbles. The structure around the perimeter of the core seen in Figure 4 is part of the control rod structure.

Nominal core volume is 86 liters, with a loading of 7.3 kilograms of U^{235} . The volume split into water and metal is 55% D_2O ,

45% metal. The atom ratios are D-U²³⁵-Al = 169-1-123. With this composition, the cold, clean core has an excess reactivity of 11% k. The volume reactivity co-efficient is about 0.25% k/liter, so that about half of the total core volume is necessary to provide reactivity for operation (xenon, temperature, and burn-up) and half is the cold, clean critical size.

The burn-up of U²³⁵ and the poisoning due to fission products other than xenon account for 5% k, or half the excess reactivity. Xenon takes 3.4% k, temperature 1.2% k, and the balance of 1.4% k is in experiments and control margin. The core life is 40 days. The cycle is broken every 20 days, however, and half of the core is loaded. The partially burned elements are shifted to the high power density regions and new fuel is placed in the low power density regions. This cycling is done to reduce the peak to average power ratio. Further core data is given in Table 1.

The control rod configuration is of some interest, and this is shown schematically in Figure 5. There are eight top and eight bottom rods, with the top rods covering the sides of the core for shutdown margin. During operation, the top and bottom rods are in symmetrical positions about the horizontal mid-plane of the core, and the power distribution is, therefore, balanced about this plane.

We turn now to the fuel elements. We say "fuel elements" in the plural, not only because there are 28 to a full core, but also because there are several types of elements. Figure 6 shows the first of these. It is the most compact and inexpensive of

the element types. The over-all dimensions of the element are 3 x 2.7 x 26 inches. The fuel is contained in 19 plates of .050 in. total thickness, with .020 in. fuel alloy thickness. The plate cladding material and picture frame material is 6061 aluminum. The meat alloy is 30 w% uranium, 93% enriched in U^{235} , 3 w% silicon, and the balance 1100 alloy aluminum. The silicon addition promotes the formation of UAl_3 rather than UAl_4 , and improves the grain structure of the meat alloy.

The fuel plates are cold rolled with a 15% reduction as a final operation to work harden the plates. The plates are then mechanically fastened to 6061 aluminum side plates. Fuel length is 21 inches, with a total plate length of 22 inches. The fuel loading is 260 grams of U^{235} per element. The water channels are .105 in. thick.

Elements of this type have been fabricated for ETR irradiation with fuel alloy loadings of 30, 35, and 40 w% uranium. The fuel plates were stable in the 30 w% alloy up to perhaps 30% burn-up of the fissionable material. At higher burn-ups a swelling of the fuel alloy caused constriction of the water channels in the test elements. In the worst spots, burn-up of about 55% of the U^{235} caused swelling and buckling of the plates so that a .030 in. thick feeler gauge could not be inserted in water channels which were initially .110 in. wide. There may have been some cross-coupling between the plate swelling from burn-up and difficulties in the fabrication method of joining

the fuel plates to the element side plates. This effect is not at present understood, and further testing is now in progress.

The higher weight per cent alloy elements showed similar swelling and buckling at somewhat lower fractional burn-up. Since the design core life of 40 days corresponds to only 20% burn-up, the HFBR design is on safe grounds, but the prospects of reducing fuel costs by extending the burn-up is not promising in these elements at the moment.

The short fuel element shown in Figure 6 is supported by a Zircaloy-2 core basket which also acts as a water flow shroud. The core basket is suspended from structures above the core in the vessel. Each element rests in an individual cell in the Zircaloy shroud.

An alternate version of this element is shown in Figure 7. Here the fuel section is the same as in the previous element, but the side plates are extended below the core to form a support column which rests on a grid plate in the base of the vessel. Here the Zircaloy flow shroud is still necessary. The merit of this element is that the Zircaloy flow shroud does not have to support the fuel elements against the downward forces due to water flow.

Figure 8 shows a different element configuration which avoids the necessity of the Zircaloy water flow shroud. Here the element is a sort of pressure tube, with the outside fuel plates thickened to .170 in. to withstand the full core pressure drop. The thick plates contain only half as much fuel alloy as

the inner plates since the cooling is to one side only. The internal plates are .050 in. thick, as in the previous versions. Nuclear properties of the core of pressure tube elements is the same as that with the standard plate elements.

Test elements of the thick plate type have been sent to ETR for irradiation and have at this point successfully completed about 14% burn-up of the U²³⁵.

It will be noted in Figure 8 that with this element, as with the one shown in Figure 7, the element side plates have been extended to form a support column which rests on a grid plate in the bottom of the reactor vessel. It should be remarked that we find it helpful in the design to remove heavy structures such as grid plates from the immediate region of the core. First of all, the thermal stresses in such structures are hard to accommodate with conservative design practice, and second, there is a severe reactivity penalty for absorbing structures close to the edge of the core.

Finally, there is a version of the pressure tube fuel element which has all fuel plates bent in MTR fashion to a 6 in. radius. Again, elements of this type has been fabricated and sent to the MTR for testing and are currently behaving well.

The next matter for our consideration is the power distribution in the core. As one might expect from the flux plot, Figure 1, there is a large thermal neutron return current from the reflector to the core. This results in the power peaks being at ^{the} core boundary, as shown in Figure 9. To understand

this lovely illustration, which is a result of very careful experimental work by Kenneth Downes, Anita Court, and Herbert Kouts, look first at the isometric drawing of the core. Note that a quadrant of the core is shown in plan on the power distribution graph, and that the height of a point on the power surface is proportional to the power developed along the length of the fuel plate below it. The whole plot is normalized to the core average power. Note the peaks on the outer corners and the slight rise around the experimental holes in the center of the core.

It is clear that the hot channel will lie along one of the outer fuel plates and that the hot spots will be at the corner of this plate. The next illustration, Figure 10, shows the vertical traverses along these regions. There is not much variation in power along the outside fuel plates in the vertical, or Z direction. A traverse along an inner fuel plate, however, would show the peaking at the core boundary typical of the under-moderated, highly reflected system. The over-all peak to average power ratio is 2.82, with most of the effect being in the radial distribution.

At 40 Mw total power, the average power density is 0.465 Mw/liter and the peak power density is 1.31 Mw/liter. This is somewhat below the going maximum at ETR, and leaves some margin for upgrading the HFBR total power level.

The thermal design calls for an average heat flux of 387,000 BTU/hr-ft², with a maximum heat flux of 1,090,000 BTU/hr-ft². The water flow velocity through the element water channels is

35 ft/sec, which gives an element pressure drop of about 25 psi. The inlet water temperature is 120°F, the bulk rise is 13.4°F, and the outlet, therefore, is at 133.4°F. The blanket gas pressure at the water surface, some 16 feet above the core, is 196 psig, which leads to a hot spot water pressure of 175 psig. The corresponding saturation temperature in D₂O is 377°F.

The transfer co-efficient for the water film is about 9,000 BTU/hr-ft²°F, varying somewhat with the film temperature. The hot spot analysis is done in the old cumulative way of multiplying together the assorted bulk rise and film temperature drop variable factors to get total bulk water and film drop hot channel factors. These have values of 1.36 for the bulk water and 1.87 for the film drop. The resulting hot spot temperature is 340°F, to which 20°F is added to cover inlet temperature and blanket gas pressure variations, with a final maximum hot spot temperature of 360°F. This compares to the saturation temperature of 377°F and again leaves some margin for increased power.

The burn-out analysis has been done using Bernath's correlation.⁽²⁾ With the hot spot running at 175 psig, water velocity of 35 ft/sec, equivalent channel diameter 0.0167 feet, heated diameter 0.106 feet, and bulk temperature of 360°F, the Bernath correlation indicates a burn-out heat flux of 4,760,000 BTU/hr-ft². The margin from operating conditions at the hot spot to burn-out conditions is, therefore, quite large, and we regard the HFBR core as being very conservatively rated from the thermal design standpoint.

REFERENCES

- (1) T. Auerbach, J. Chernick, J. Juliens, G. Lellouche, W. Zinn and Associates, Preliminary Design of a High Flux, Epithermal Research Reactor for the Brookhaven National Laboratory, Proc. Second Int. Conf. Geneva, 1958, P/424, Vol. 10, P. 60, (1958).

P. Michael and W. Rothenstein, Preliminary Theoretical Studies of the Brookhaven Beam Research Reactor, Trans. Am. Nuc. Soc., 2, 120, (June 1959).
- (2) L. Bernath, Extension of the Method of Burn-out Prediction, AECU 3901 (1958).

Table I. "HFBR Design Parameters"

<u>Power</u>	40 MW	<u>Core thermal design data</u>	
<u>Neutron flux</u>		Water channel thickness	0.105 in.
Core, total epithermal	$\sim 1.6 \times 10^{15} \text{ cm}^{-2} \text{ sec}^{-1}$	Fuel plate thickness	0.050 in.
Reflector thermal flux, max.	$7 \times 10^{14} \text{ cm}^{-2} \text{ sec}^{-1}$	Fuel plate length, active	21 in.
<u>Materials</u>		Water channel width	2.231 in.
Coolant, moderator, and reflector	D ₂ O	Core alloy width	2.00 in.
Fuel	U-235-Al alloy	Heat transfer surface per element	11.1 ft ²
Core structure, beam tubes	6061 aluminum	Total heat transfer surface, core	311 ft ²
Lower vessel	6061 aluminum	<u>Water flow data</u>	
Upper vessel	stainless steel	Water channel flow area per element	0.0326 ft ²
Primary pipes & process equipment	stainless steel	Total channel flow area, core	0.912 ft ²
<u>Fuel element and core</u>		Water velocity in channels	35 ft/sec
Type	ETR, flat-plate	Water flow per element	520 gpm
Uranium concentration in meat alloy	30 wt. %	Water flow, 28 elements	14,560 gpm
Meat thickness	.020 in. U-Al	Water flow in control rods, approx.	2,000 gpm
Cladding thickness	.015 in. 8001 Al	Water flow in bypass, approx.	1,000 gpm
Fuel region dimensions per element	2.6 x 3.0 x 21 in.	Total water flow, approx.	17,600 gpm
U-235 loading per element	260 gm	Total primary loop pressure drop	60 psi
Number of fuel elements	28	Pressure drop in fuel elements	25 psi
Core volume	86 liters	<u>Process system design</u>	
Total U-235 loading	7.28 Kgm	Maximum operating pressure	250 psig
Water-to-metal volume ratio	1.23	Maximum operating temperature	150°F
D/U-235 atom ratio	169	Vessel design temperature	200°F
Al/U-235 atom ratio	123	Beam tube design temperature	400°F
Cycle time for 20% burn-up	40 days	<u>Core power conditions</u>	
<u>Temperature and void coefficients</u>		Radial peak-to-average power ratio	2.15
Core metal coefficient	$-0.36 \times 10^{-3} \text{ \% k/}^\circ\text{C}$	Over-all peak-to-average power ratio	2.82
Core water coefficient	$-9.31 \times 10^{-3} \text{ \% k/}^\circ\text{C}$	Bulk hot channel factor	1.36
Reflector water coefficient	$-28.4 \times 10^{-3} \text{ \% k/}^\circ\text{C}$	Film hot channel factor	1.87
Total temperature coefficient	$-38.0 \times 10^{-3} \text{ \% k/}^\circ\text{C}$	Average power density	0.465 MW/L
Core void coefficient	$-0.33 \times 10^{-3} \text{ \% k/cm}^3$	Maximum power density	1.31 MW/L
<u>Excess reactivity requirements</u>		<u>Core thermal analysis results</u>	
	<u>Maximum</u> <u>Normal</u>	Reactor inlet temperature	120°F
Burn-up, plus Sm and stable f.p.'s	5.0 % 2.8 %	Reactor outlet temperature	133.4°F
Xenon, steady state	3.4 % 3.4 %	Δ T bulk	13.4°F
Temperature	1.2 % 1.2 %	Hot spot surface temperature	360°F
Control and experiments	1.1 % 1.1 %	Operating hot spot pressure	175 psig
Total	10.7 % 8.5 %	Saturation temperature at hot spot	377°F
<u>Control rods</u>		Blanket gas pressure	196 psig
Number of main rods	8	Average heat flux, BTU/hr-ft ²	.387 x 10 ⁶
Individual main rod, total worth	4.1 % k	Maximum heat flux, BTU/hr-ft ²	1.09 x 10 ⁶
8 main rods in gang, total worth	31 % k	Burn-out heat flux, BTU/hr-ft ²	4.76 x 10 ⁶
Number of auxiliary rods	8	<u>Neutron prompt lifetime</u>	672 μsec
Individual auxiliary rod, total worth	1.07 % k	<u>Delayed neutron fraction</u>	0.78 % k
8 auxiliary rods in gang, total worth	8 % k		
Total worth of all rods	39 % k		

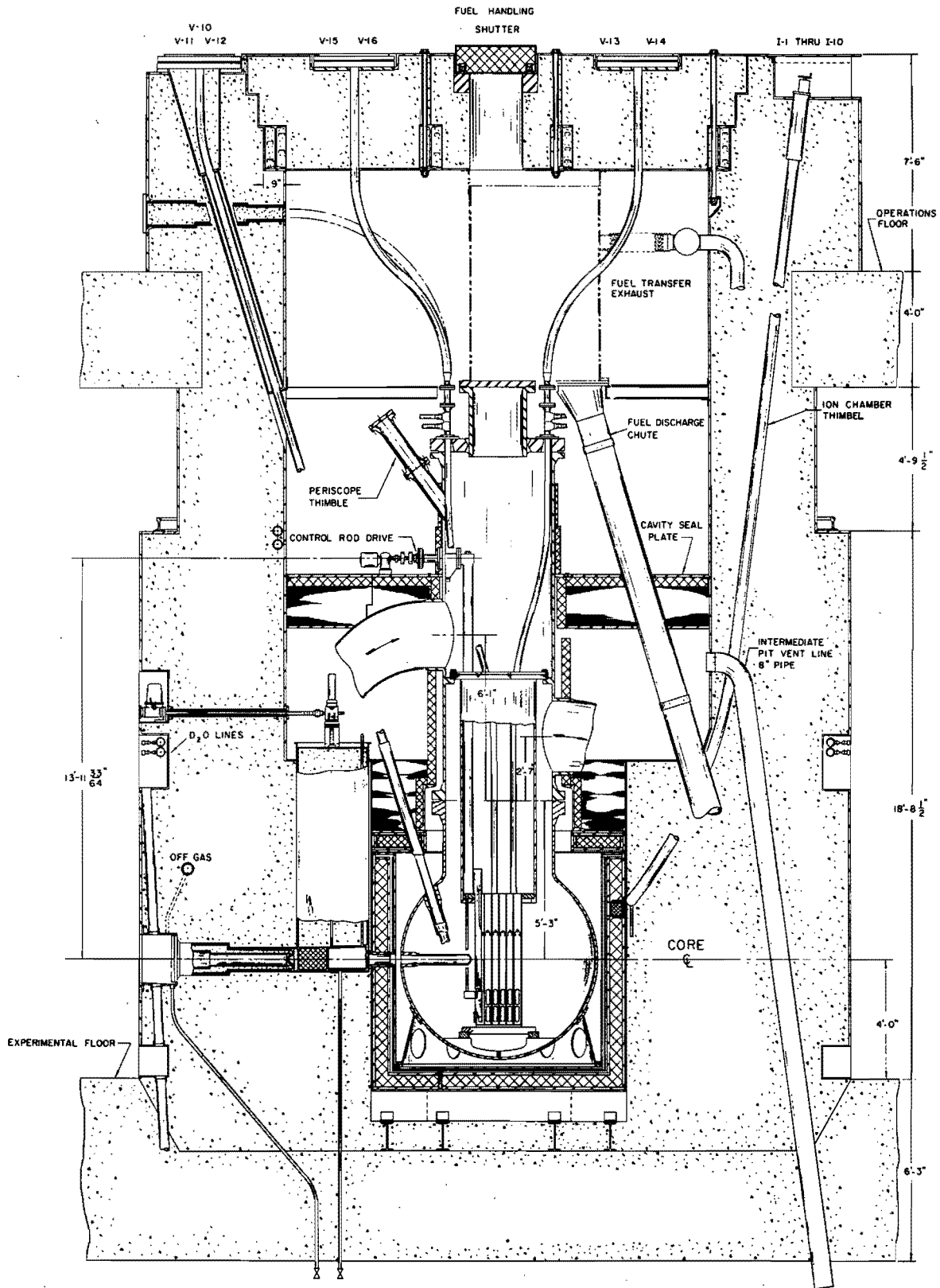


Figure 2 "Vertical section of HFBR shield and reactor vessel."

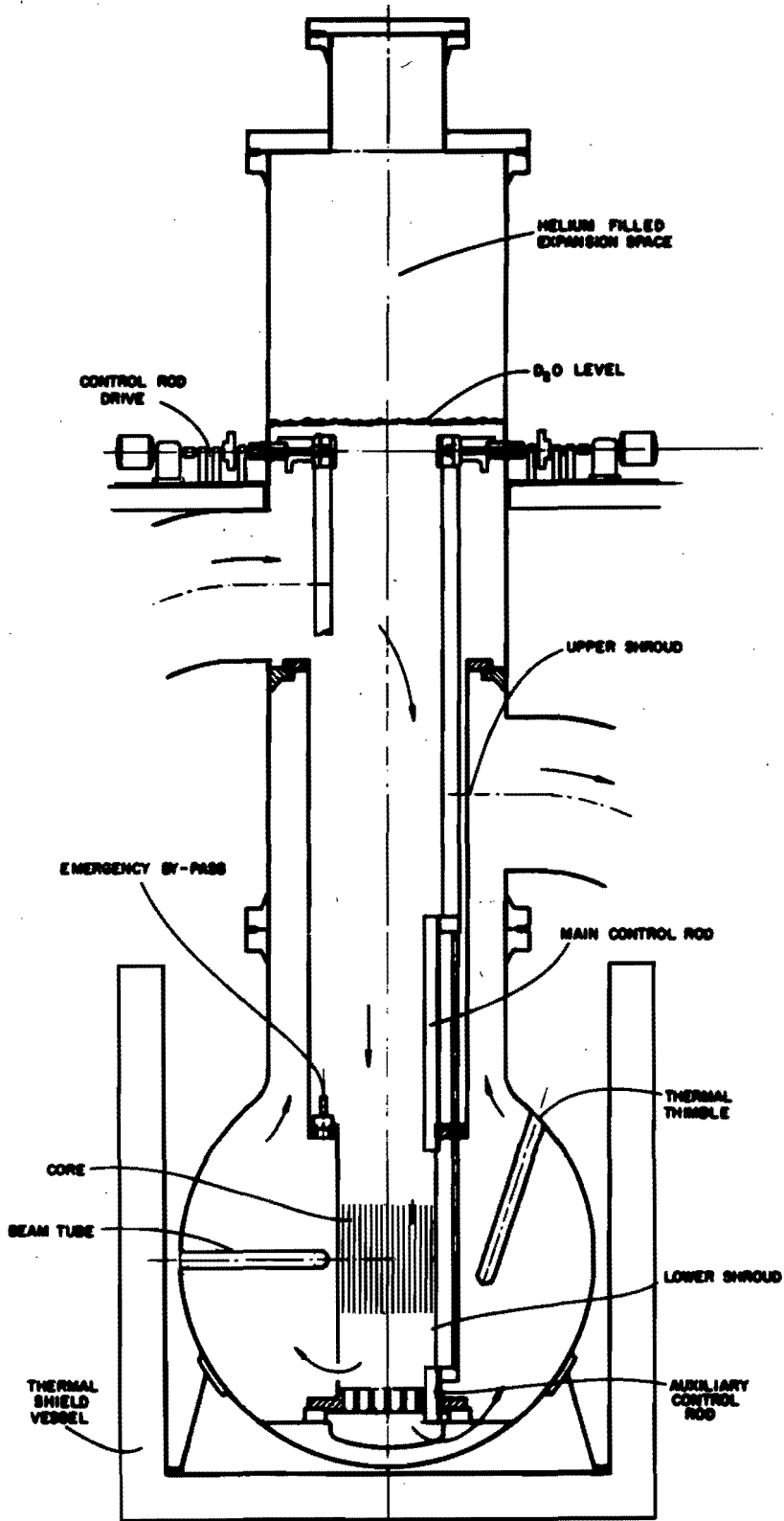


Figure 3 "Schematic elevation of HFBR vessel, showing water flow paths and internal shrouds."

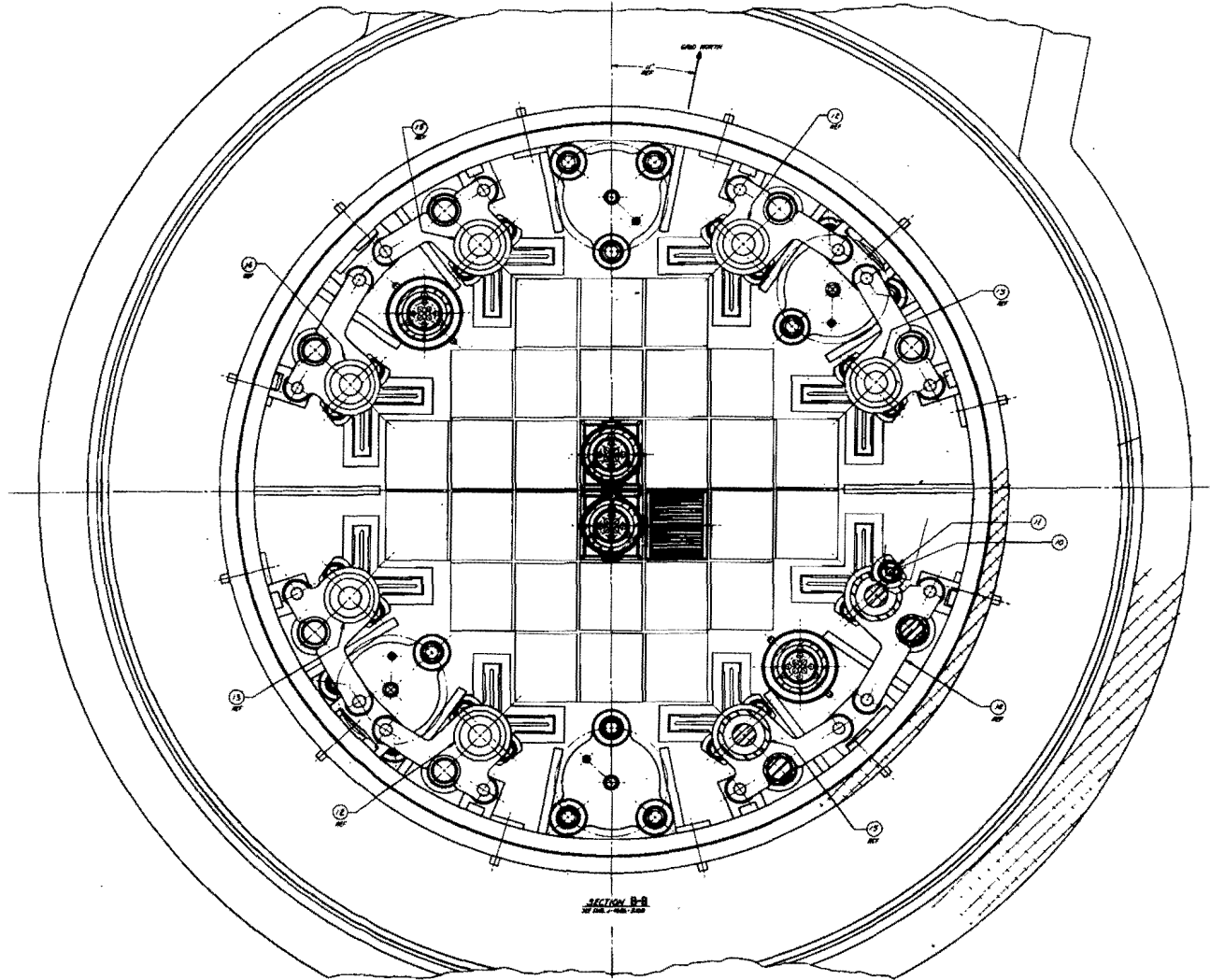


Figure 4 "Plan view of HFBR core."

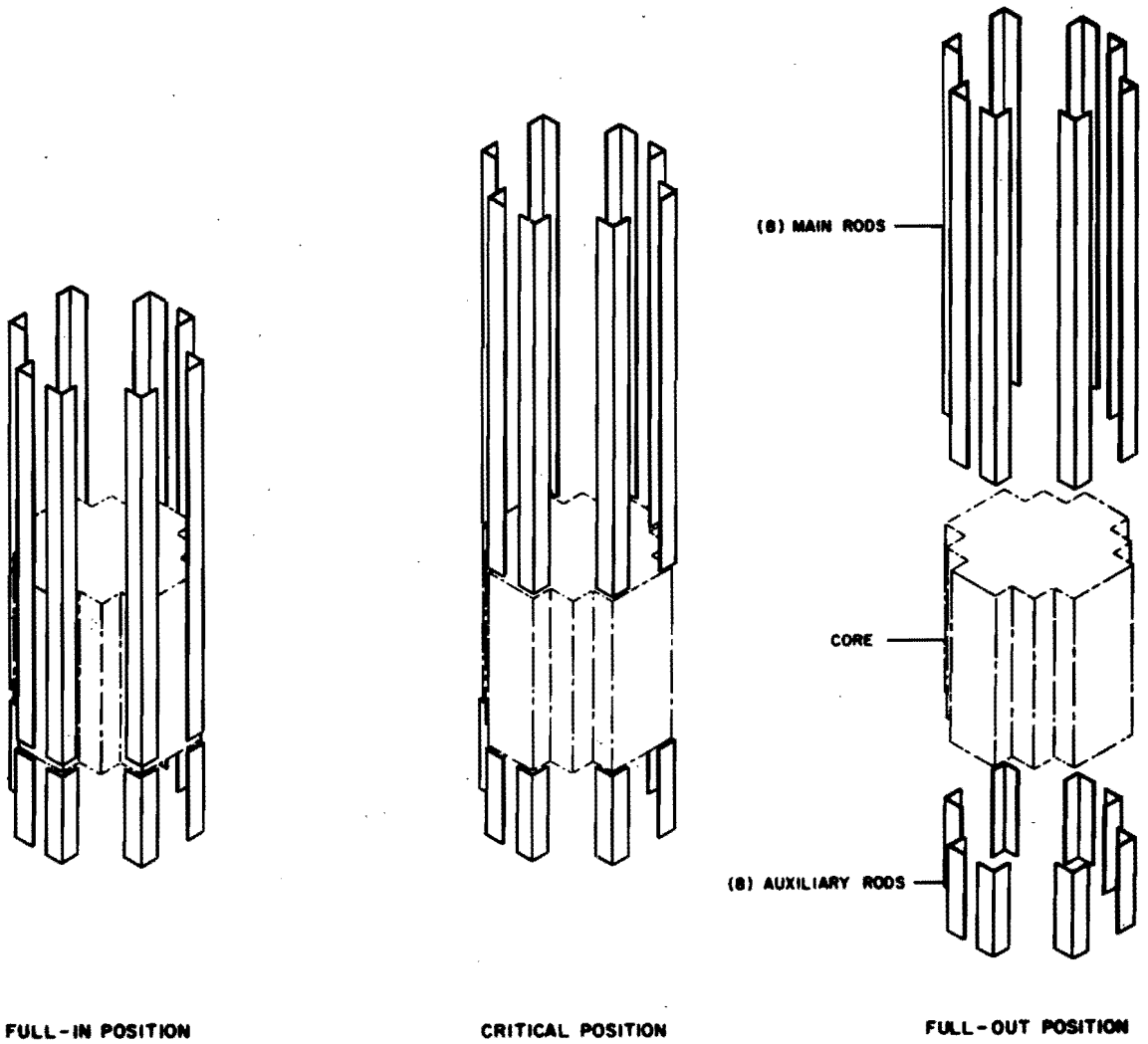


Figure 5 "Location and mode of operation of HFBR control rods."

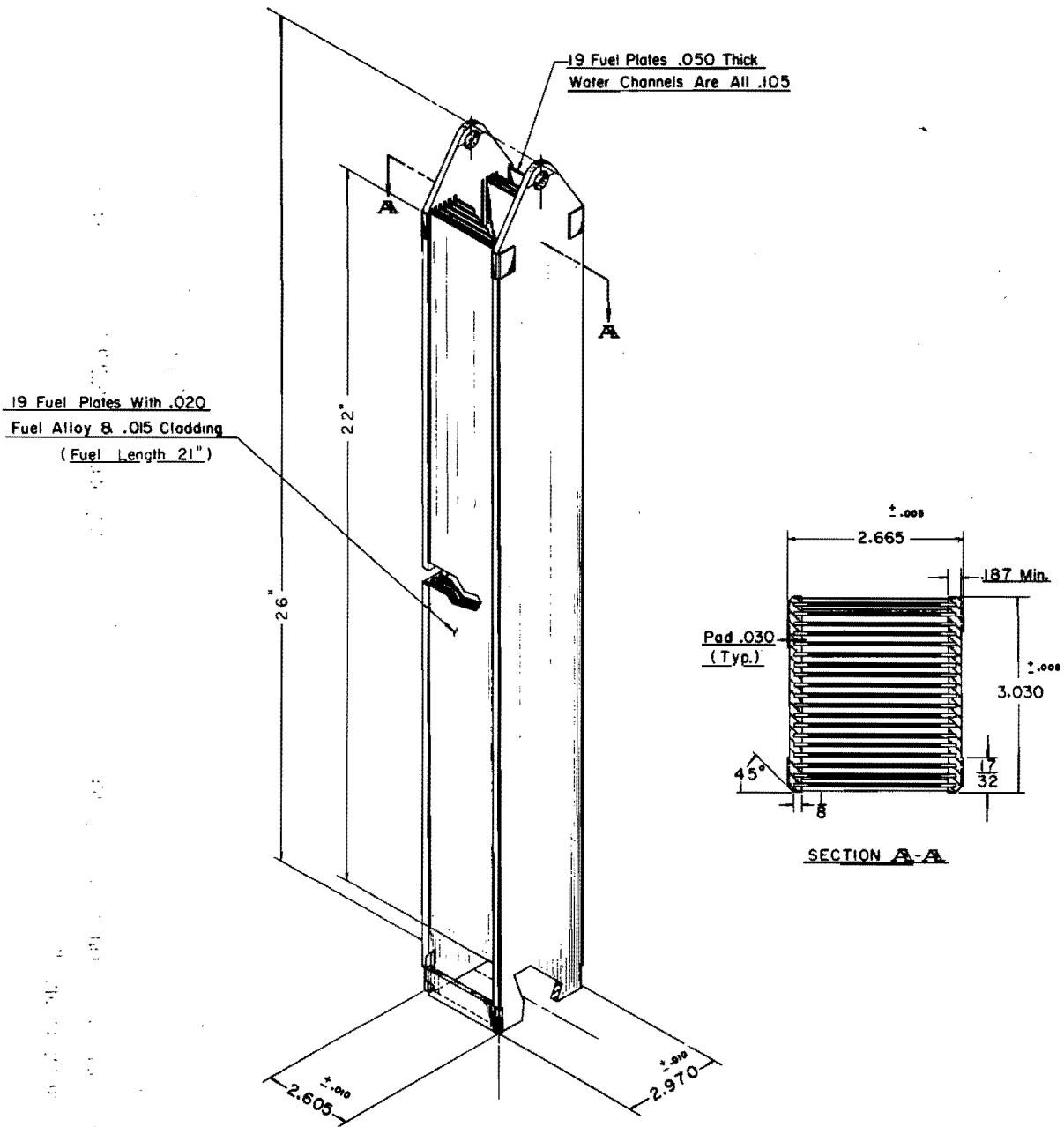


Figure 6 "HFBR fuel element, type J, short version."

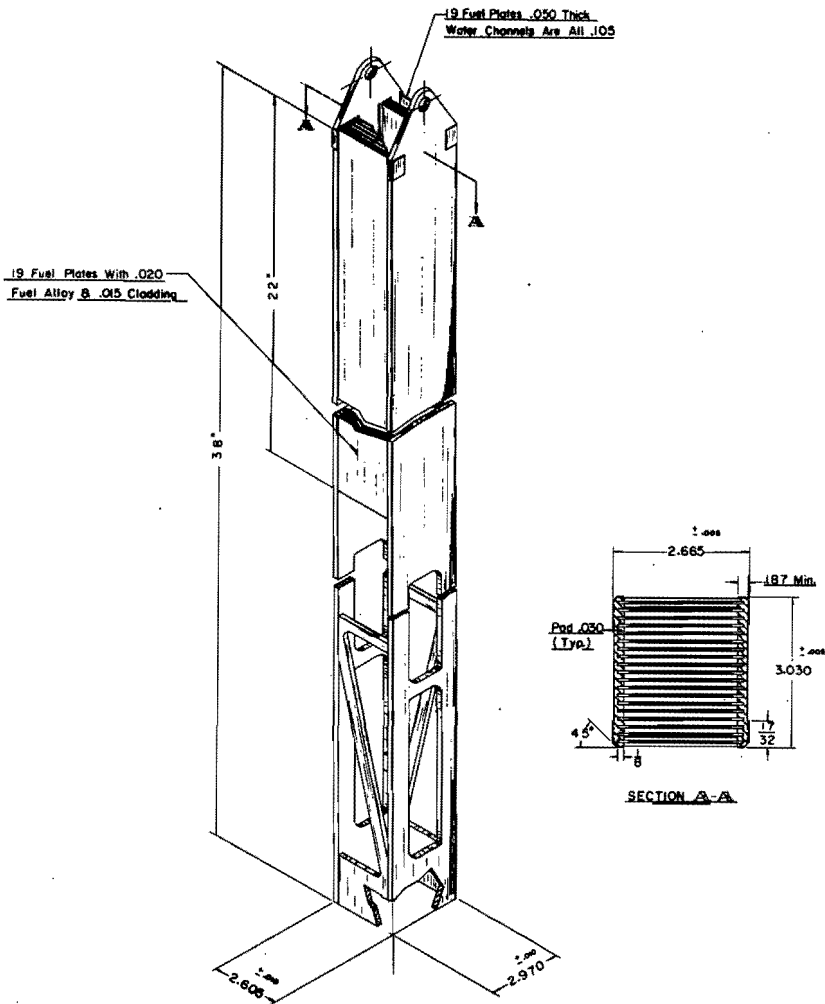


Figure 7 "HFBR fuel element, type J, long version."

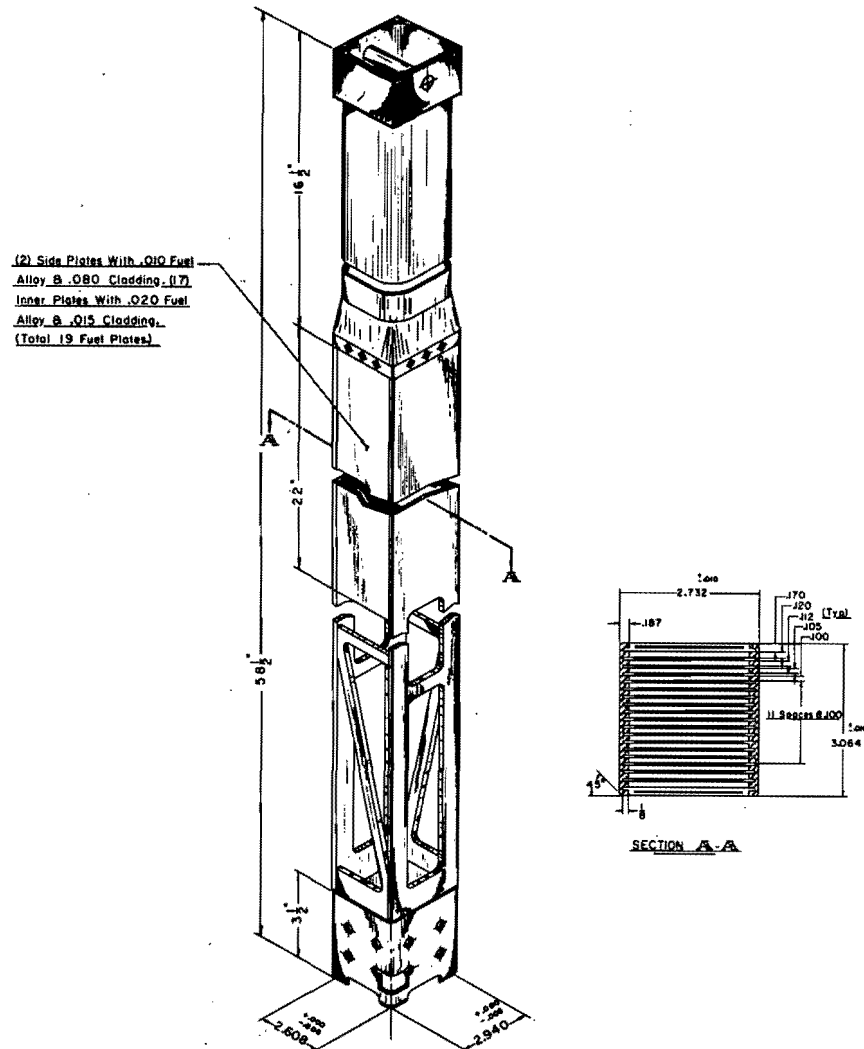


Figure 8 "HFBR fuel element, type D."

Z AVERAGE POWER DISTRIBUTION
 OVER ONE QUADRANT OF HFBR CORE 15
 HOLD-DOWN DISTRIBUTION
 5% IN COPPER
 5% IN CONTROL RODS

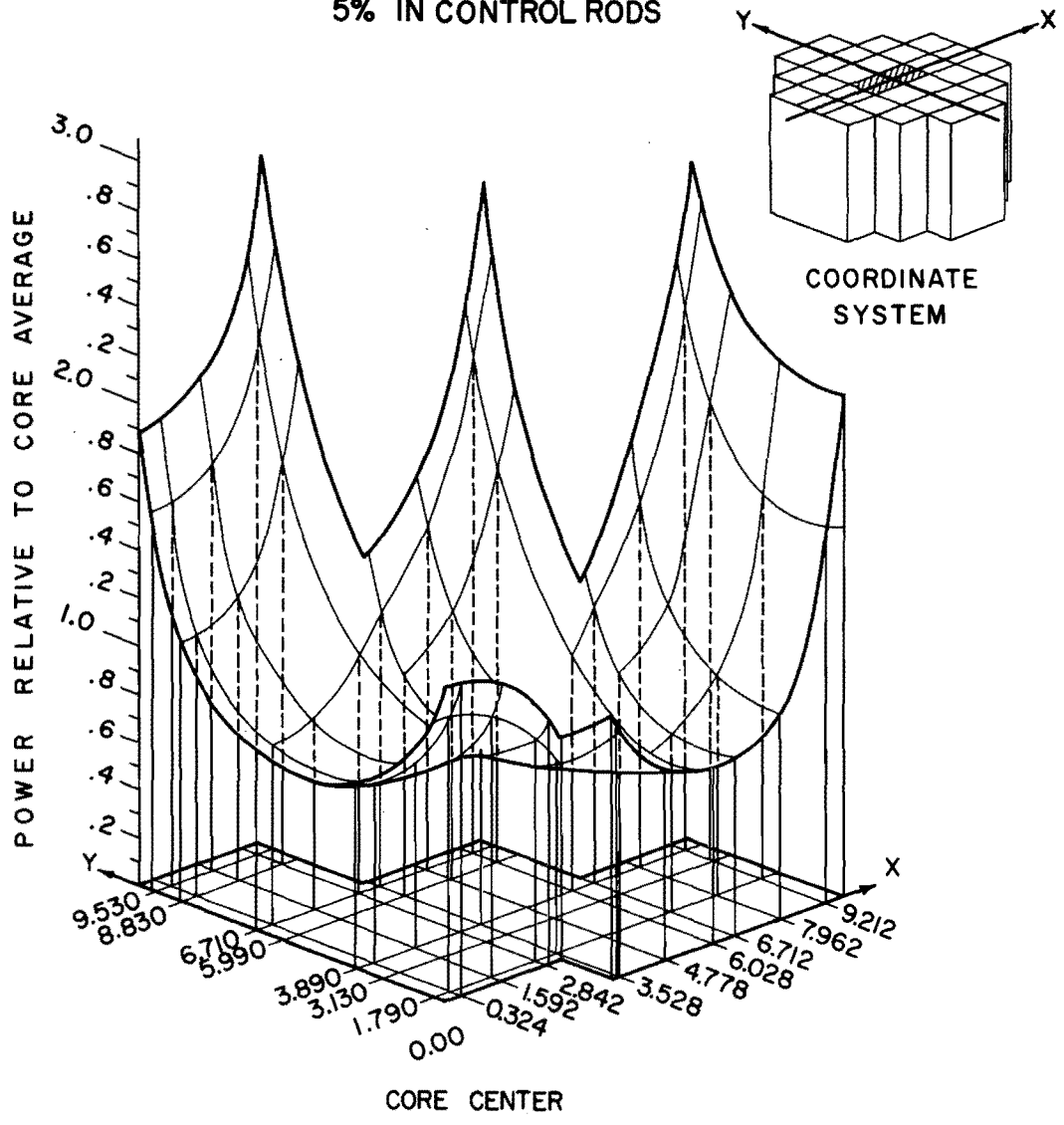


Figure 9 "Power distribution surface in HFBR core."

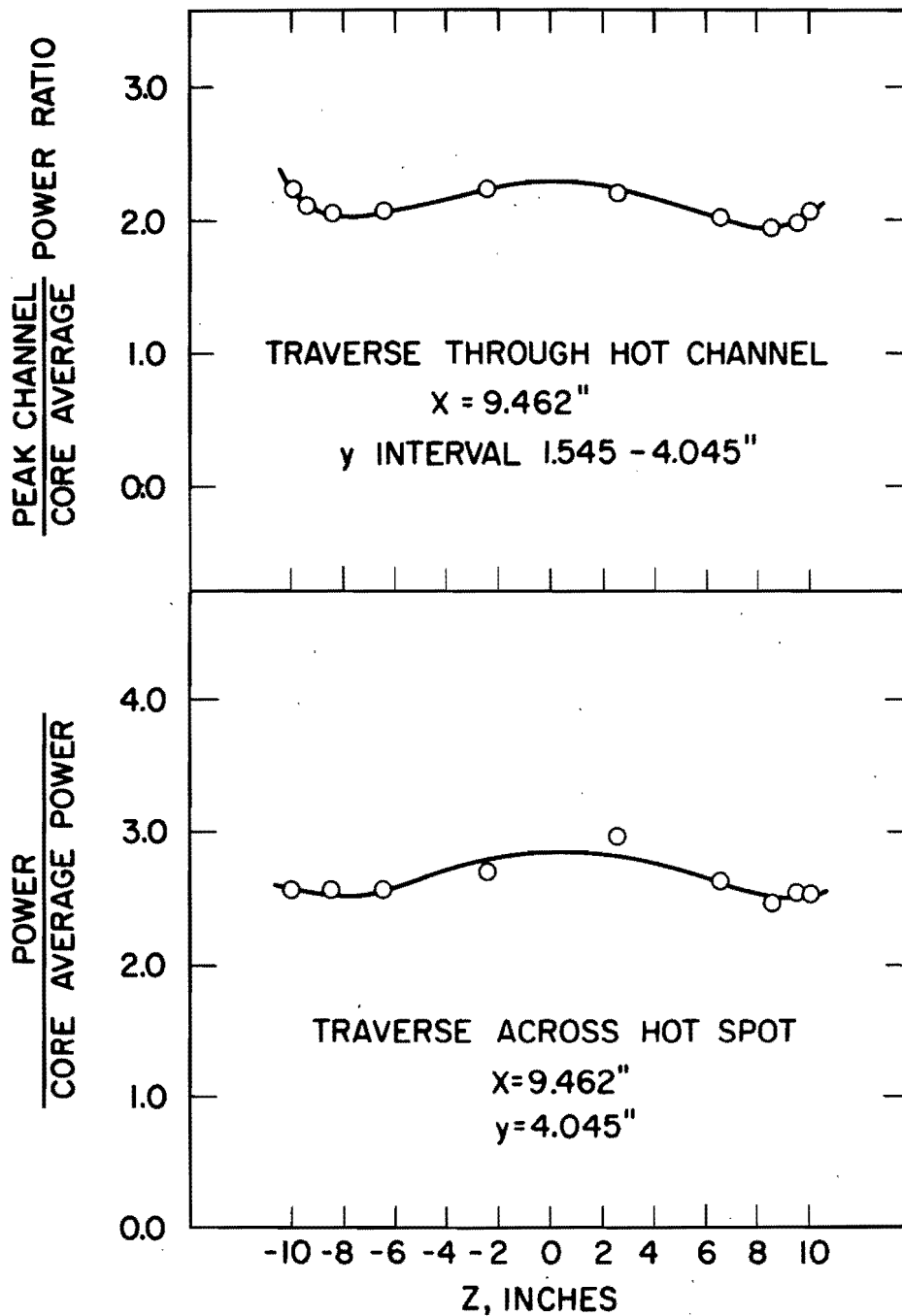


Figure 10 "Vertical power distribution along HFBR hot channel and hot spot."

GENERAL DESIGN OF THE
ARGONNE ADVANCED RESEARCH REACTOR*

L. W. Fromm

Argonne National Laboratory

Introduction and General Description

For the past several years, Argonne National Laboratory has recognized an increasing need for a source of higher neutron fluxes to permit the logical extension of basic research in nuclear physics, nuclear chemistry and solid state science, and has carried on a program to develop design concepts for general purpose higher flux research reactors to fill this need. The Argonne Advanced Research Reactor (AARR) is a product of this study program.

The reactor is light water cooled and moderated, and beryllium reflected. Heat removal provisions are included for an initial operating power level of 100 Mw. However, shielding is provided for higher core operating powers, the reactor design includes flexibility for adaptation to improved cores capable of higher power densities, and the plant arrangement permits easy installation of additional heat removal capacity. These features will permit later incorporation of the results of a continuing development program to produce neutron fluxes significantly higher than the $3-5 \times 10^{15}$ expected with the reference first core.

The AARR complex is designed as a complete unit to fill all practical needs of experimenters. In addition to the central thermal column, or flux trap, in the core, twelve horizontal beam tubes and two horizontal through

tubes are provided. Eight of the beam tubes are tangential to the core, while four are radial. Tube diameters (o.d.) range from 3 3/4 to 7 in. All beam and through tubes penetrate the reactor vessel and the beryllium reflector surrounding the core.

Other experimental facilities penetrating the reflector include six vertical irradiation tubes and two hydraulic rabbit facilities. A third but smaller hydraulic rabbit facility enters the central thermal column to permit short term sample exposures in the highest flux available in the reactor, without disturbing the long term samples installed there for quantity preparation of higher transuranic isotopes. In addition, eight vertical irradiation tubes are located within the reactor vessel in the water reflector-shield surrounding the beryllium reflector.

Since the normal offices and laboratories of experimenters are located in another area of the Argonne site, seventeen laboratories and nine offices are provided for the use of experimenters at the AARR, in the Laboratory and Office Building immediately adjacent to the Reactor Containment Building. The Laboratory and Office Building also contains offices and complete facilities for operations, radiation safety, special materials and service personnel associated with reactor operation. A wing of this building provides a high bay area for the mocking up and testing of experimental equipment prior to insertion into the reactor.

Because of the high power densities necessary in the reactor to produce high fluxes, the possibility of accidental core melt-down is somewhat more real in AARR than in reactors heretofore constructed. For this reason, a waste treatment facility is provided on the site to permit shielded storage of all water in the primary system, as well as water used for system flushing, and to remove fission products from the water by ion exchange prior to discharge or re-use.

Other auxiliary facilities include an exhaust air filtration system, cooling towers for dissipation of the reactor power and for air conditioning,

retention ponds for emergency storage of secondary cooling water, should it become contaminated, and an electrical substation.

Reactor

The reactor core consists of a 37 weight percent dispersion of UO_2 , fully enriched, in stainless steel, arranged in plates around the central flux trap. The plates are 0.040 in. thick, including 0.005 in. stainless steel cladding on each side, and coolant gaps between plates are also 0.040 in. thick. The initial fuel loading is 50.7 kg of U^{235} , contained in the stainless steel- UO_2 cermet fuel plates. Fuel plates with reduced fuel loading have been used in the core regions adjacent to the internal thermal column and beryllium reflector to reduce the power peaks which result from the inflow of thermalized neutrons in these regions.

The use of a stainless steel rather than aluminum core in AARR affords a number of advantages:

1. Much longer core life - 90 days as compared with 12 days for aluminum, achieved by virtue of the higher critical mass and attendant higher uranium burnup per unit of available excess reactivity achieved with the highly absorbing steel core.
2. Greater structural strength and stability in the presence of high flow velocity.
3. Elimination of corrosion as a consideration at the high fuel plate temperatures (over $400^\circ F$) required for high power density.
4. Elimination of xenon and samarium buildup after reactor shutdown as an impediment to operation during the first 75 days of core life, by virtue of the epithermal (median fission energy 8 ev) rather than thermal spectrum in the stainless steel core.

A summary of the core thermal and nuclear characteristics is given in Table I. The basic thermal design criterion has been the prevention of local boiling anywhere in the core during full power operation. This has been

assured by requiring that the maximum fuel plate surface temperature not exceed the local saturation temperature.

The core operates at higher heat fluxes than heretofore demanded of research reactors, but the levels appear within limits of acceptability. Critical ("burnout") heat flux for 100 Mw operation is more than twice the predicted maximum hot spot value. Considerable margin is included, particularly by choice of a 450 psia operating pressure, to permit the possibility of eventual 150 Mw operation.

The mechanical design of the core uses the package concept in which entire cores, including fuel, grid structure, control blades, and shrouds, are shop assembled and inserted or removed in AARR as a unit.

A longitudinal section through the reactor vessel is shown in Fig. 1.

A 12 in. thick radial beryllium reflector surrounds the core. Axial reflection at the top and bottom of the core is provided by the primary coolant water. The primary coolant water, which also serves as moderator, flows downward through the reflector and core in a single pass. The core and reflector are contained in an 8 ft. diameter spherical stainless steel pressure vessel having cylindrical extensions at its top and bottom for coolant entry and exit. Primary cooling water fills the region between the beryllium reflector and the pressure vessel, serving the dual role of a shield and reflector. Control rod drive mechanisms are located below the vessel.

Twelve horizontal beam tubes penetrate the pressure vessel and reflector and terminate in the peak flux region of the beryllium about 3 in. from the core boundary. The beam tubes are circular but are filled with slotted beryllium inserts in order to obtain a desired beam shape. The pressure vessel is provided with an integral nozzle at each beam tube penetration which is bolted to a flange on the beam tube. In addition, there are two horizontal through tubes which penetrate the reflector below the midplane of the core. All horizontal beam tubes are equipped with water-cooled rotary shutters which cut off the

Table I

AARR CORE THERMAL AND NUCLEAR CHARACTERISTICS

Power, Mw	100
Coolant	
Flow rate, lb/hr	7×10^6
Velocity, ft/sec	40
Inlet temp, °F	135
Outlet temp, °F	183
Inlet pressure, psia	450
Heat Flux, Btu/hr-ft ²	
Average	0.56×10^6
Nominal maximum*	1.79×10^6
Hot spot	2.35×10^6
Critical (or burnout)	5.49×10^6
Power Density, Mw/liter	
Core average	1.35
Nominal maximum	4.6
Hot spot	6.0
Fuel Loading, kg U ²³⁵	50.7
Core Volume, liters	74.2
Core Lifetime at Full Power, days	
	90
Core Lifetime at Full Power with Full Xenon Override Capability, days	
	75
k _{eff} Cold, Clean	1.173

* With power flattening by radial variation of fuel loading.

neutron beam when a tube is not being used. Details of the beam tube design are shown in Fig. 2.

A total of 18 vertical irradiation facilities are provided in the reactor. The largest of these is the internal thermal column located on the core vertical center line. The maximum flux in the reactor is obtained in this facility which is planned primarily for use in the production of transuranic isotopes. There are three hydraulic rabbit facilities for short-time irradiations; two of the rabbit tubes terminate in the beryllium reflector and one in the internal thermal column. Six vertical irradiation thimbles penetrate the top cover of the vessel and terminate in the beryllium reflector, while eight thimbles penetrate the spherical section of the reactor pressure vessel and terminate in the water region between the beryllium reflector and the vessel wall.

Other reactor vessel penetrations include instrument thimbles and an inlet for emergency boron injection.

Heat Removal and Auxiliary Systems

The reactor pressure vessel and primary cooling system (with the exception of the heat exchanger tubes) are fabricated of type-304 stainless steel and are designed for an operating pressure of 450 psia at an operating temperature of 200°F. This pressurization will assure a high degree of subcooling for prevention of coolant boiling within the core at 100 Mw operation. It also permits the possibility of future operation at higher power. In order to accommodate such a possibility, all piping and equipment are sized and arranged so that additional primary heat exchangers and additional cooling towers can be added at a later date to permit 150 Mw operation, and all shielding is initially designed on the basis of 150 Mw operation.

A simplified flow diagram for the primary and secondary cooling systems and some of the auxiliary systems required is shown in Fig. 3.

At 100 Mw operation, 18,000 gpm of cooling water enters the reactor vessel at a temperature of 135°F through a 24-in. diameter in the top cylin-

dricial extension, flows downward through the core and vessel, and leaves at a temperature of 174°F through two 16-in. nozzles at the bottom. At 150 Mw operation the coolant exit temperature would rise to 193°F. After leaving the reactor vessel, the water passes first through settling tanks whose prime function is the removal of active particulate matter which might be released to the water during an excursion accident, through four parallel water-to-water primary heat exchangers, and is returned to the reactor vessel by circulating pumps.

From the reactor vessel exit nozzles to the circulating pump inlet header, two flow loops are provided, each containing one settling tank followed by two parallel primary heat exchangers (with provision for a third to be added later). Three circulating pumps (one a stand-by unit) and one smaller shutdown cooling pump, all in parallel, are provided. The emergency shutdown pump is always connected to the emergency power supply, consisting of batteries and a diesel-generator set, and will supply cooling water to the reactor for after-shutdown heat removal in the event of an electric power failure. From the circulating pump outlet header, the water returns to the reactor vessel via a single 24-in. line.

Primary water is degassed and purified (the latter by ion exchange) in a by-pass system which also serves to pressurize the primary system to its operating pressure.

Secondary cooling water is circulated through the shell sides of the primary heat exchangers and rejects heat to the atmosphere by means of four cooling towers located on the site. Four secondary system circulating pumps operate in the same fashion as the primary system pumps, i.e., two for normal operation, one spare, and one for emergency shutdown cooling with power supplied by the batteries and diesel-generator unit.

The cooling towers also serve as the heat sink for auxiliaries such as the experiment cooling system, the primary purification system coolers, and the reactor pool and canal cooling system. In the latter system, chilling

equipment is also provided to maintain the pool and canal at comfortable working temperatures.

Make-up water for the cooling tower is obtained from the nearby Chicago Sanitary and Ship Canal via an existing water treatment plant at the Laboratory. Since this water contains high concentrations of chlorine and oxygen, the tubes in the primary heat exchangers and all auxiliary system heat exchangers using this water are made of Inconel to avoid the stress corrosion problem associated with the use of stainless steel in water having a high chloride content.

Reactor Building

A cutaway view of the reactor building is shown in Fig. 4.

The building is a concrete and steel shell, 122 ft. in diameter and 125 ft. in over-all height, with 87 ft. above grade and 38 ft. below grade. The building is designed to contain all the fission products which may be released in the event of a nuclear incident. It houses the reactor with its surrounding shielding and reactor shield pool above, areas for experiment equipment, the control room, the fuel storage and handling canal, a reactivity measurement facility, a hot cell, and the primary system process equipment. Service facilities include a 40-ton rotary crane which covers the main operating floor area, called the experiment level, as well as the reactor pool.

The building is divided into three principal functional levels: an equipment level on the lowest floor below grade, a canal level on an intermediate floor below grade, and an experiment level at grade. The primary system process equipment is located on the equipment level. The canal level is a working floor for the handling of spent fuel and radioactive experimental samples in the canal. In addition, the reactivity measurement facility, the hot cell, and the control rod drive room beneath the reactor are located at this level. The experiment level provides unimpeded working area around the reactor face for experimenters using the beam tubes, except for one sector (where there are no beam ports) reserved for equipment ingress and egress through a large vehicle and equipment

air lock. Various instrument and observation balconies are located above the experiment level, both around the reactor shield and along the outer periphery of the building. The control room is located on the peripheral observation balcony, at the same level as the top of the reactor pool. The crane runway is above the observation balcony.

In order to provide large working floor areas for specific beam tube experiments, the reactor is located off-center with respect to the building center line. This permits a range of neutron beam lengths within the reactor building, measured from shield face to building outer wall, varying from 33.5 ft. to 55 ft.

In refueling the reactor, the spent core is first cooled by forced convection until the afterheat has decayed to a point where sufficient cooling can be obtained by natural convection. The reactor vessel cover is then removed, and the core cartridge is lifted from the vessel into the pool above, moved laterally and lowered through a water filled chute to the equipment level, which is the level of the bottom of the fuel handling and storage canal. Here it is deposited on a hydraulically operated transfer cart. After the hoist grapple is withdrawn from the chute, the upper chute cover is closed, the lower door is opened, and the transfer cart is moved into the canal. The canal crane is then used to move the core cartridge from the transfer cart to the storage area, where the afterheat decays further by natural convection until such time as the core can be dismantled and shipped from the site for reprocessing.

A special area of the canal designated as the core disassembly area is isolated from the spent fuel storage area by a bulkhead and is provided with a separate cooling system. Spent cores known or suspected of having cladding failures are moved to this area after removal from the reactor, to prevent contamination of the entire canal by released fission products. Here the core may be disassembled to investigate the failure. A small hot cell is provided on the canal floor, and provision is made for direct transfer of fuel assemblies from the canal into the hot cell for close examination if

desired. The core disassembly area is also used for disassembly of undamaged spent cores and placement of the individual fuel subassemblies in casks for shipment, after completion of the afterheat decay period. Casks are brought into the reactor building through the vehicle air lock, and lowered directly into the canal by the main building crane through a hatch in the experiment floor just inside the air lock opening. This hatch is located so as not to interfere with any beam hole experiment equipment.

Experiment samples which have been irradiated in vertical thimbles in the reactor are also removed from the reactor through the fuel transfer chute to the canal. They may then be transferred into the hot cell for examination or placed in casks for removal from the building.

Primary system settling tanks, heat exchangers, circulating pumps and purifying and degassing equipment are located in shielded cells on the lowest, or equipment level, of the reactor building. Space is provided in these cells for the later installation of additional equipment for 150 Mw operation. The fuel storage and handling canal provides a sizeable portion of the shielding required. Certain other auxiliary equipment is also arranged in available space on this level.

Normal access to the reactor building is through two personnel air locks. These connect the experiment level and experiment balcony in the reactor building with the first and second floors of the adjacent laboratory and office building. The upper of these air locks is a special convenience to experimenters, since most of the experimenters' laboratories are located on the second floor of the laboratory and office building, and a major portion of the controls and instrumentation for beam hole experiments can be conveniently located on the experiment balcony, safe from damage during the handling of heavy equipment on the main experiment level.

Large, heavy equipment is moved in and out of the reactor building through a vehicle air lock, which connects to the equipment mock-up and storage area of the laboratory and office building. The arrangement of the latter

area is such that trucks may be backed into the building from the outside, across the mock-up area and straight into the reactor building through the vehicle air lock.

An equipment door (openable only during reactor shutdown) is provided on the canal level, and hatches in the canal level floor permit the transfer of heavy process equipment between the equipment level and the outside without disturbing experiment apparatus on the levels above. Three emergency air locks, at various levels of the reactor building, are provided for the safety of experimental and operating personnel.

Site Arrangement

The arrangement of the reactor building, laboratory and office building, and supporting facilities, is shown in Fig. 5. The site chosen is immediately adjacent to the Laboratory's CP-5 research reactor, for the convenience of experimental groups using both reactors in their programs of research.

Acknowledgement

A preliminary engineering feasibility and cost study on the Argonne Advanced Research Reactor has recently been completed by United Nuclear Corporation's Development Division (NDA), under an Argonne sub-contract. The design for the AARR facility presented in this paper was developed from Argonne concepts in a joint effort by Argonne and United Nuclear during the course of the study. The contribution of United Nuclear Corporation personnel, M. S. Silberstein, N. R. Adolph, S. A. Davis, and others, is hereby acknowledged with appreciation.

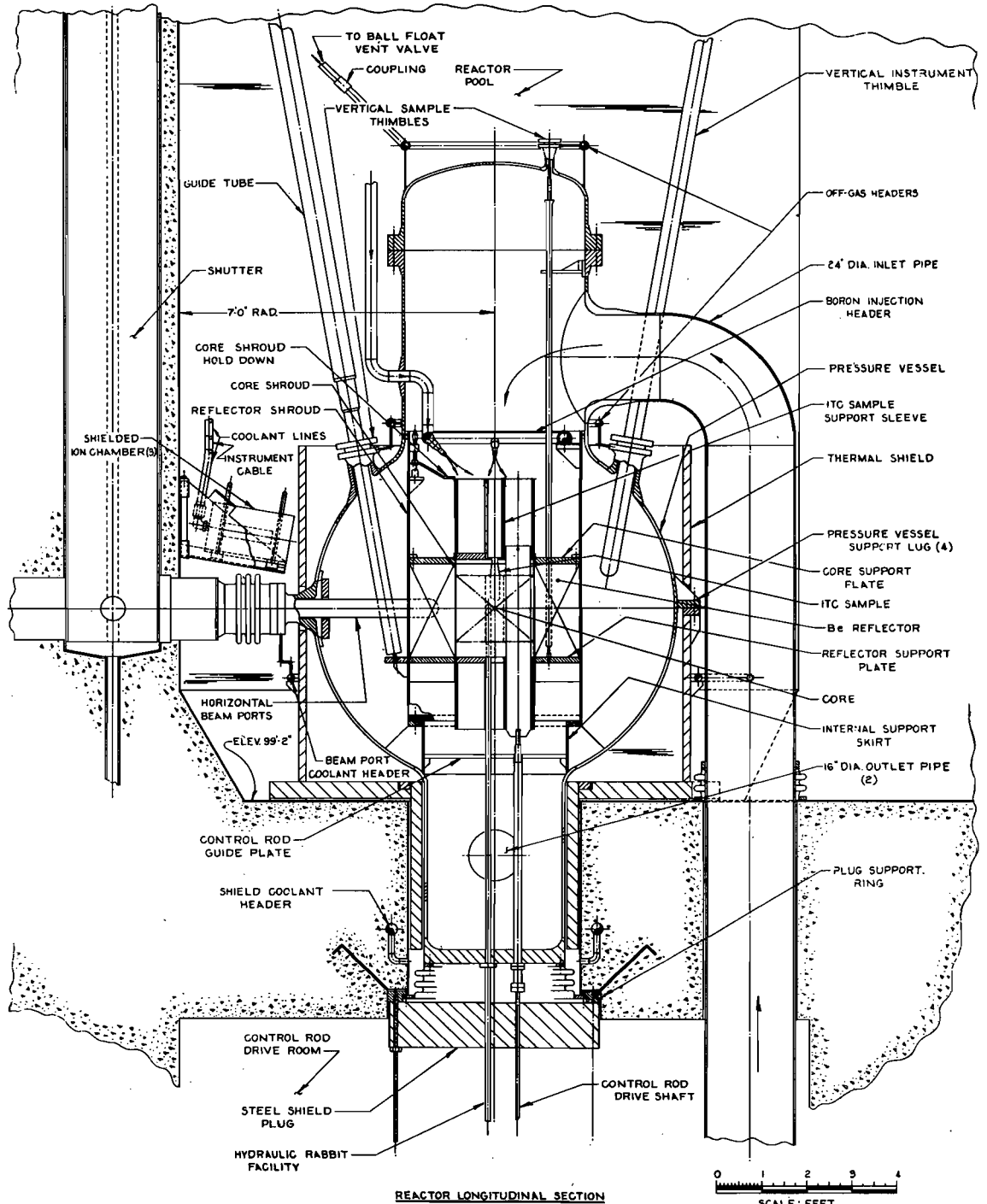
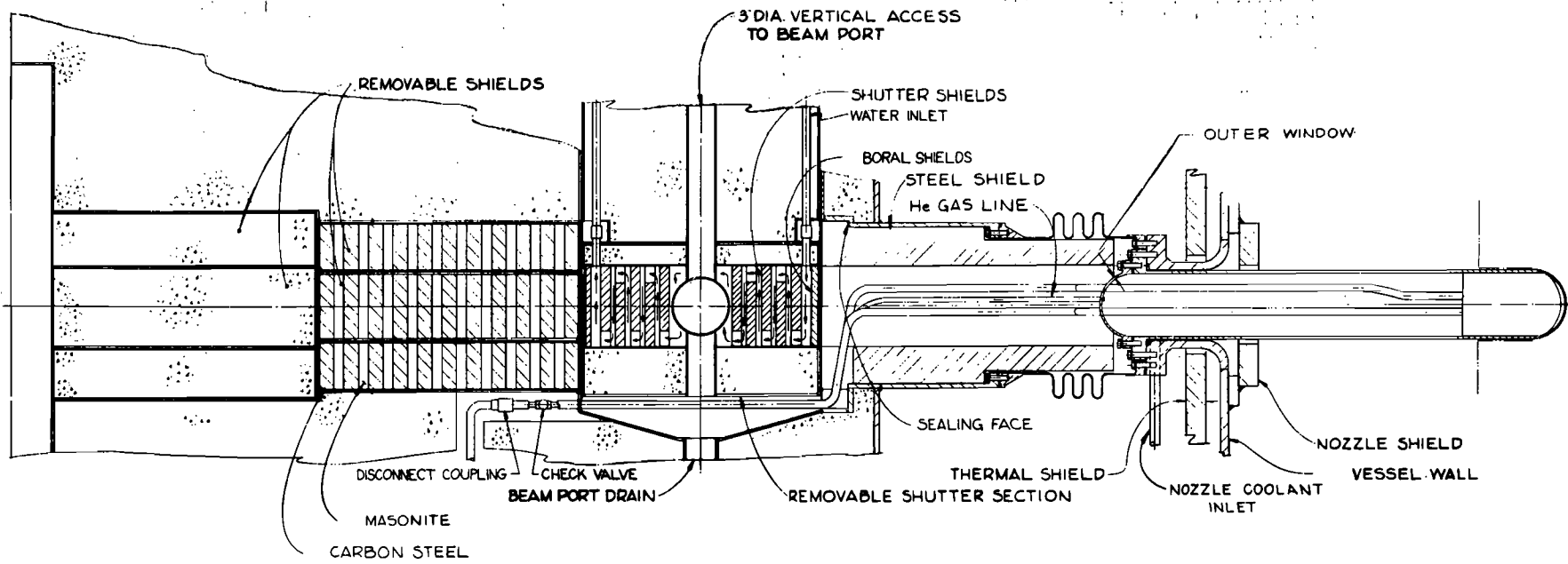
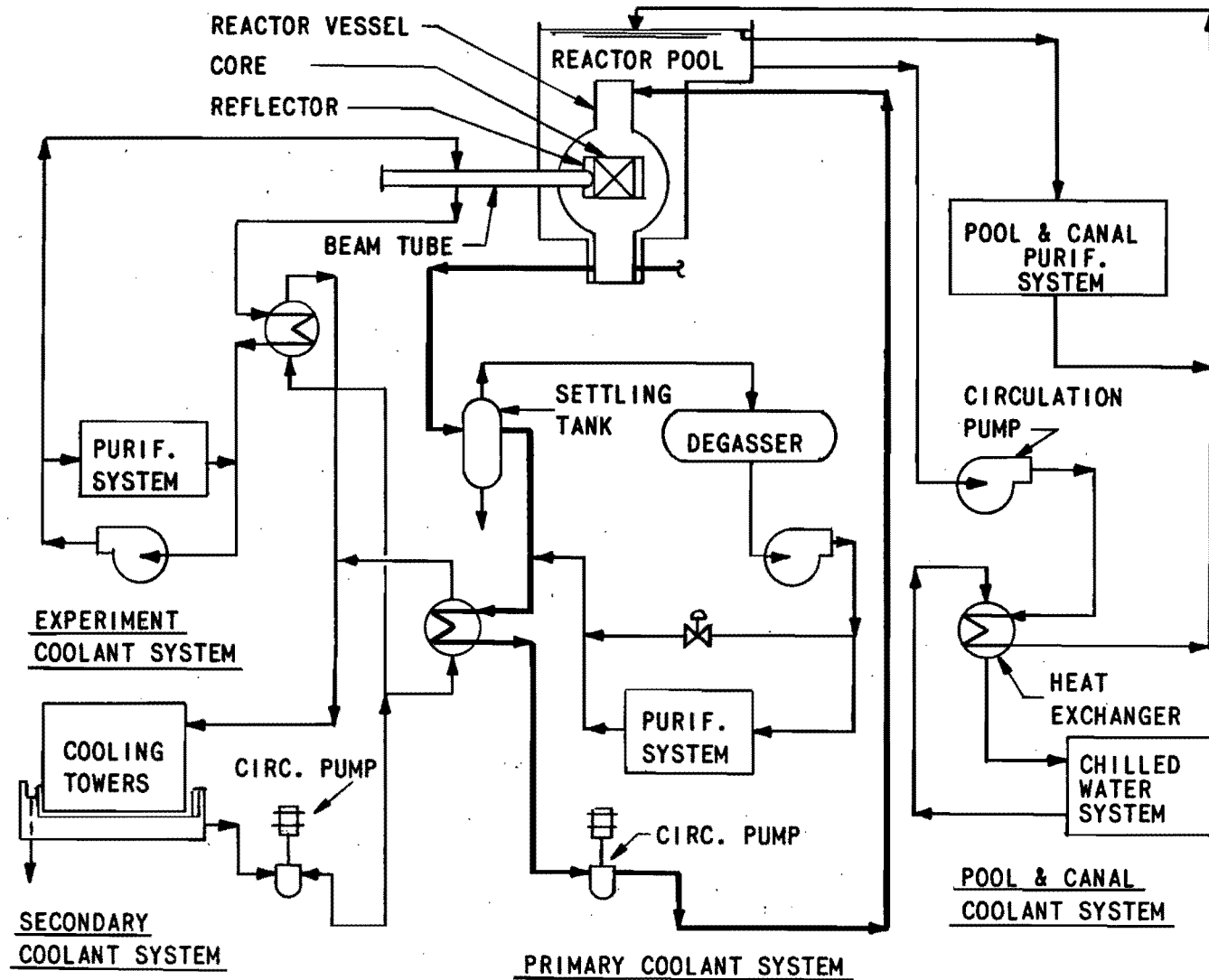


FIG. 1



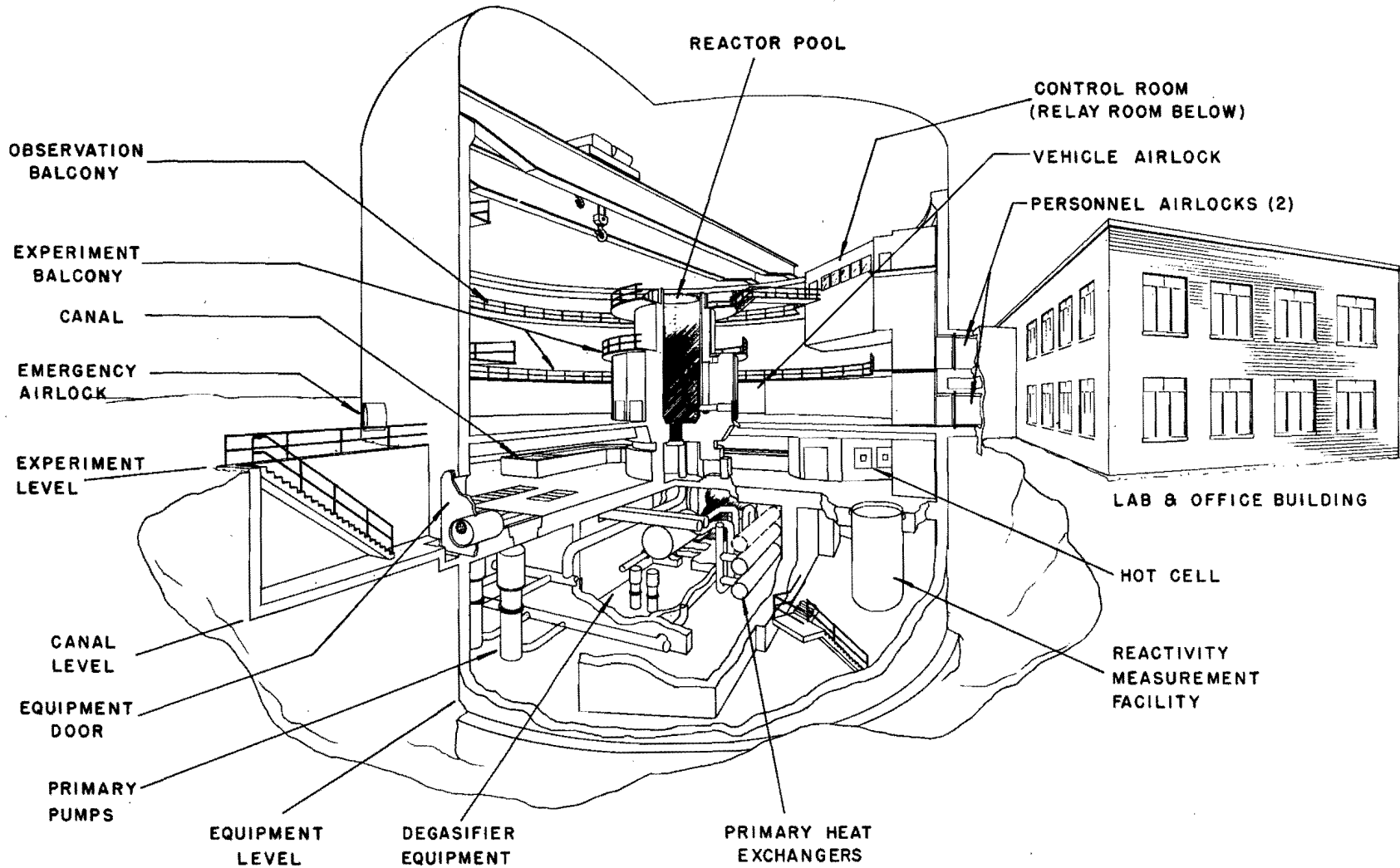
HORIZONTAL BEAM TUBE SECTION

FIG. 2



AARR SIMPLIFIED FLOW DIAGRAM

FIG. 3



AARR REACTOR BUILDING

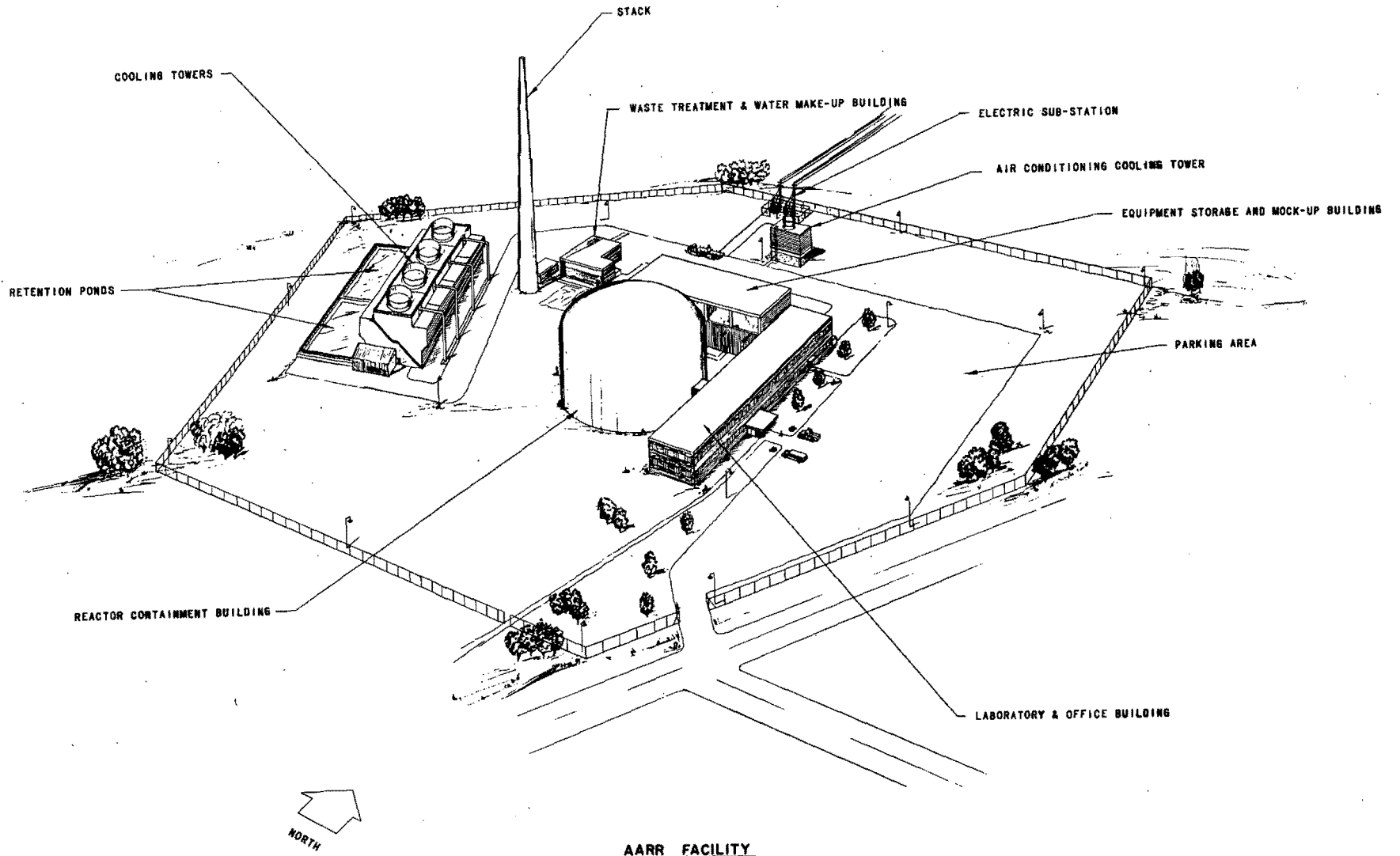


FIG. 5

PHYSICS ADVANTAGES
OF STAINLESS STEEL CORES

Charles N. Kelber

Argonne National Laboratory

The outstanding reason for the use of low cross section materials in research reactor fuels is the fact that in a homogeneous medium the thermal neutron flux is inversely proportional to the absorption cross section. The demand for higher fluxes (hence power densities) coupled with increasingly complex experimental arrays has led to the design of research reactors in which neutrons are thermalized in specific locations well removed from the core. Under these conditions the penalty in flux level and reactivity from the use of moderately high cross section materials may be small.

As the fuel investment increases, however, we expect the incremental reactivity of fuel added for burn up to decrease, so that the reactivity swing over a cycle of given length is decreased; alternatively longer cycle times are available without the use of unusual control methods. Of at least as great importance is the possibility of retaining complete Xenon override even at power densities of the order of a few megawatts per kilogram of fuel, or more. This implies that we will have an intermediate core,

and this is the case. Since the disadvantages of these cores are well known, we will not dwell on them.

The intermediate nature of the core spectrum can be illustrated by examining the energy distribution of fissions in a typical core. Figures 1 and 2 are based on calculations made for some designs suggested for the Argonne Advanced Research Reactor*: they do not necessarily represent any actual or proposed core.

Figure 1 is a plot of the cumulative fission distribution in the center of the core. These curves represent very nearly the infinite medium distribution. The lower curve represents the distribution (beginning of life) with a typical H:U ratio of 14. The median energy of fission is 15 ev. After a core cycle of moderate length the H:U ratio has changed only slightly, to 16, but the median energy has decreased to 10 ev.

By itself the change in median energy is not significant since, as Figure 1 shows, small changes in the distribution cause large changes in median energy. The change is indicative, however, of tendency of the η (neutrons per absorption in U) of the fuel to increase as burn up proceeds. Infinite medium calculations have shown that a reactivity increase of about 2% at very high burn ups can be obtained in this way. This increment helps to overcome the losses to fission products.

An effect of the spatial variation in neutron spectrum is illustrated by Figure 2. Here we graph the cumulative fission distribution at a core-reflector interface. The sensitivity of the median energy of fission to

* See: "General Design of the Argonne Advanced Research Reactor," L. W. Fromm, these proceedings.

small changes in spectrum is evident here as in Figure 1. More striking is the change in magnitude of this quantity showing the influence thermal neutrons entering from the reflectors. At a very high burn up the upper most curve (H:U = 94) is obtained. The η of Uranium-235 in such a distribution is very nearly 2.05; the harder distributions such as those of Figure 1 are characterized by η 's of 1.81. A crude relationship illustrating the reduced reactivity worth of incremental fuel is $\delta k = .2 \ln(M/M_0)$ where M_0 is the mass of U-235 at $k = 1.0$.

The hardness of the spectrum also implies a reduction in the worth of typical control rod materials. Thus we expect Hafnium or Europium in the core to be three to four times as effective as Cadmium. In typical thermal reactor cores massive Hafnium rods are typically 15 to 20% more effective than Cadmium; but in cores such as we are discussing the flux in the range 1 to 10 ev. (the region of Hafnium resonances) is 5 to 10 times that in the range 0 to .4 ev. At the core edge this is not the case; the discrepancy between Cadmium and Hafnium is much less there.

Concomittant with the reduction of effective cross section of thermal resonance absorbers such as Cadmium is a reduction in Xe-135 on Sm-149 worth. Figure 3 is a graph of the ratio $\overline{\sigma_a(Xe)} / \overline{\sigma_f(U-235)}$ (flux weighted average over energy) vs. radius in a typical stainless steel core. Except for small regions near the core edges the effective Xenon cross section is much less than encountered in typical thermal reactor cores.

In a high flux thermal core the Xenon residence time is governed almost completely by the lifetime to absorption; in these cores the lifetime to absorption is about the same as the decay time and the mean residence time is thus very long. In terms of recovery from partial or complete scrams this means the kinetic behavior of the system resembles that of a

thermal reactor in the $1-5 \times 10^{13}$ flux range. The necessary response time is long; typically an hour or more is allowed for recovery if only 1% δk is available.

Even more important, the total δk needed for override at any time is small $\sim 2.3\%$ so that recovery from scrams need be considered a problem only near the end of a fuel cycle. For the same reason Sm-149 is not a problem even in irradiated cores stored for a long time; the reactivity gain from decay of Xenon more than compensates for the buildup of Samarium.

By way of summary we give in Table 1 a typical neutron inventory. The U-235 captures includes the captures in equilibrium Xenon and Samarium. These two hold down about 3% in k . The term fission products refers to non-saturating fission products. The core studied here included some burnable poison, Samarium, and a small amount of poison is still present at this stage, which is about halfway through a core cycle. Captures directly associated with the fuel are thus .185 (per virgin neutron). Captures in hydrogen (in water) account for .053 while the remaining moderator or light elements capture only .031 neutrons. The stainless steel captures are (coincidentally) the same: .031; so that the parasitic capture in hydrogen is actually larger than that of stainless steel. In this core design power flattening shims were employed and they captured excessively: .09 neutrons per virgin neutron. Spatial fuel variation accomplishes the same end; excessive parasitic losses are at the same time decreased. We conclude that the stainless steel does not add an objectionable amount of parasitic capture.

The full utilization of such heavily loaded cores requires as large a fuel inventory as can be obtained and controlled. With 37 weight per cent UO_2 dispersed in stainless steel plates we have designed cores with

cycle lengths of 35 to 90 days at 100 Mw. The plates themselves, however, can probably take irradiations of 120-150 days. It is desirable that the reactivity life be comparable to the irradiation life in costly cores. Desirable improvements in these fuels center on increasing the fuel content. Alternative fuels include dispersions in Zircalloy or Zirconium-clad, metal fuels.

The use of heavily loaded cores implies some disadvantages. At the interfaces incoming thermal neutrons are absorbed readily and a power peak is created. This may be avoided by the use of shims which absorb mainly thermal neutrons or by spatial variation of the fuel loading. We have found the latter to be the more satisfactory method. Since the diffusion area for thermal neutrons in such cores is typically of the order 0.1 cm^2 , fuel variations must be sizeable over distances of 0.3 cm (.1") or less.

Another problem is that a heavily absorbing core in a diffusive medium creates a thermal neutron sink and hence a neutron concentration gradient in the reflector: this depletes the neutron flux in the reflector. A crude estimate of this depletion is $2 \exp^{-2 \sqrt{\tau/L^2}}$. In H_2O this is small, but in pure Beryllium the relative variation can be extremely large, approximately a factor of 2.5.

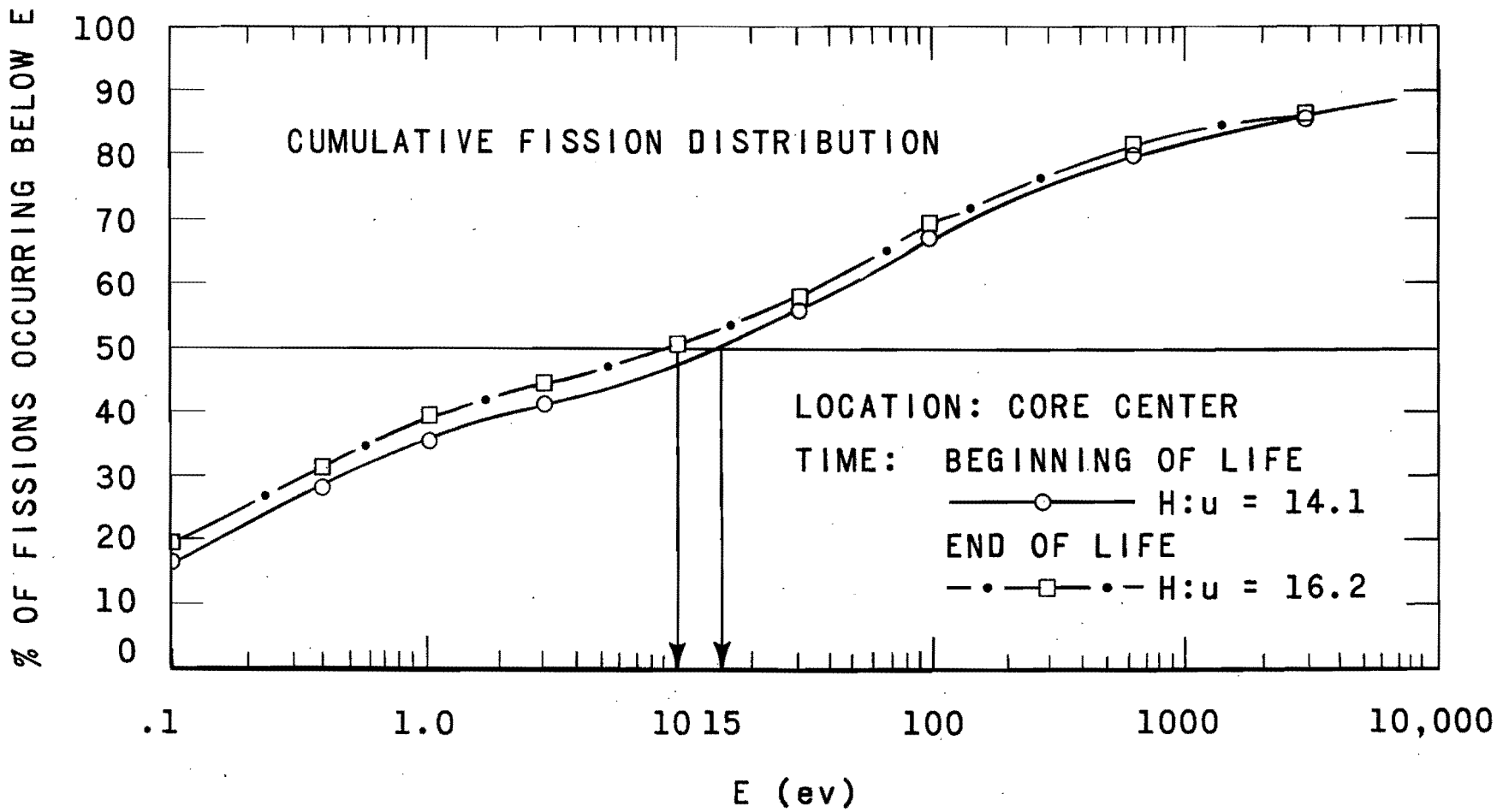


FIG. 1

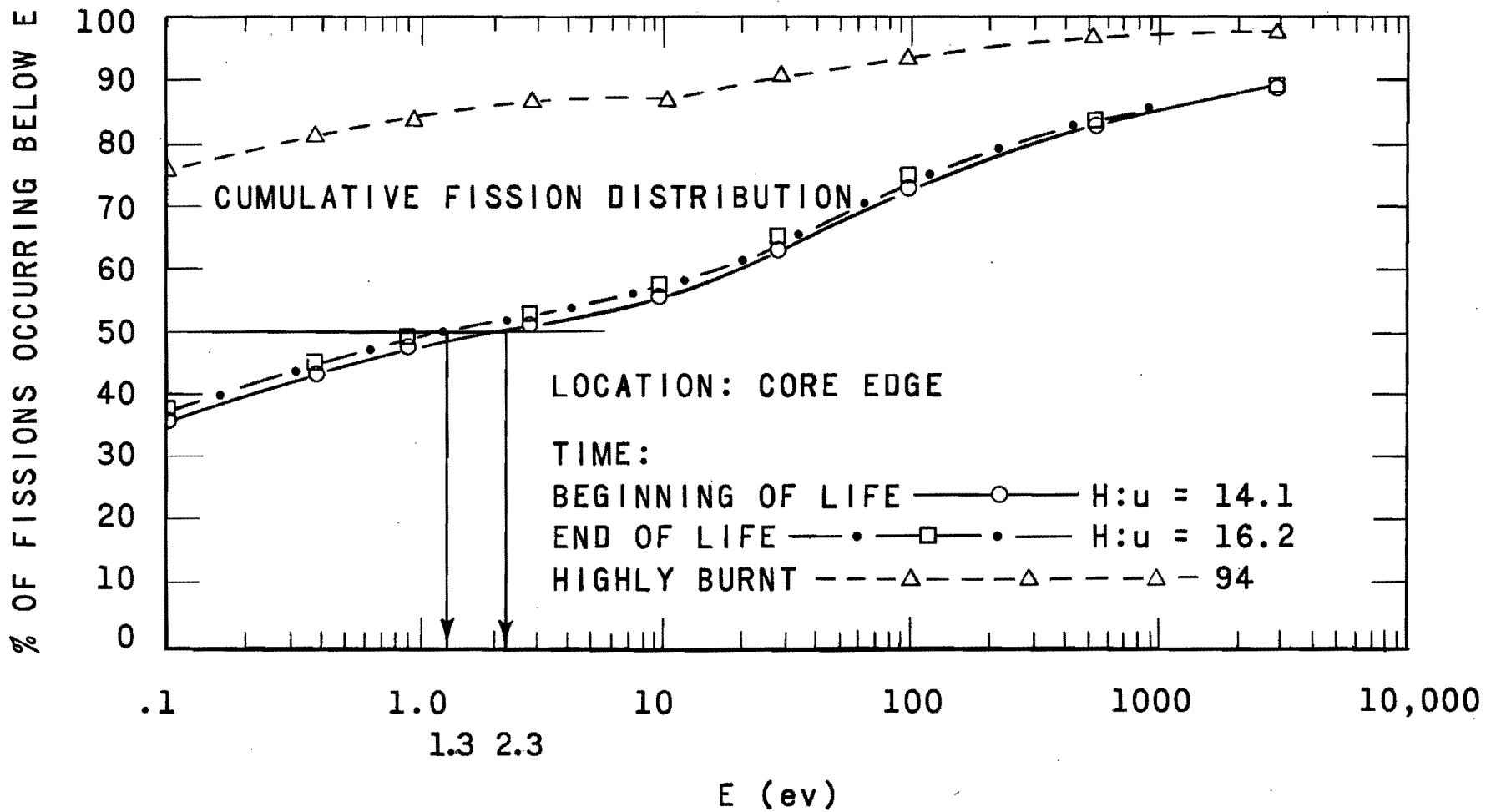


FIG. 2

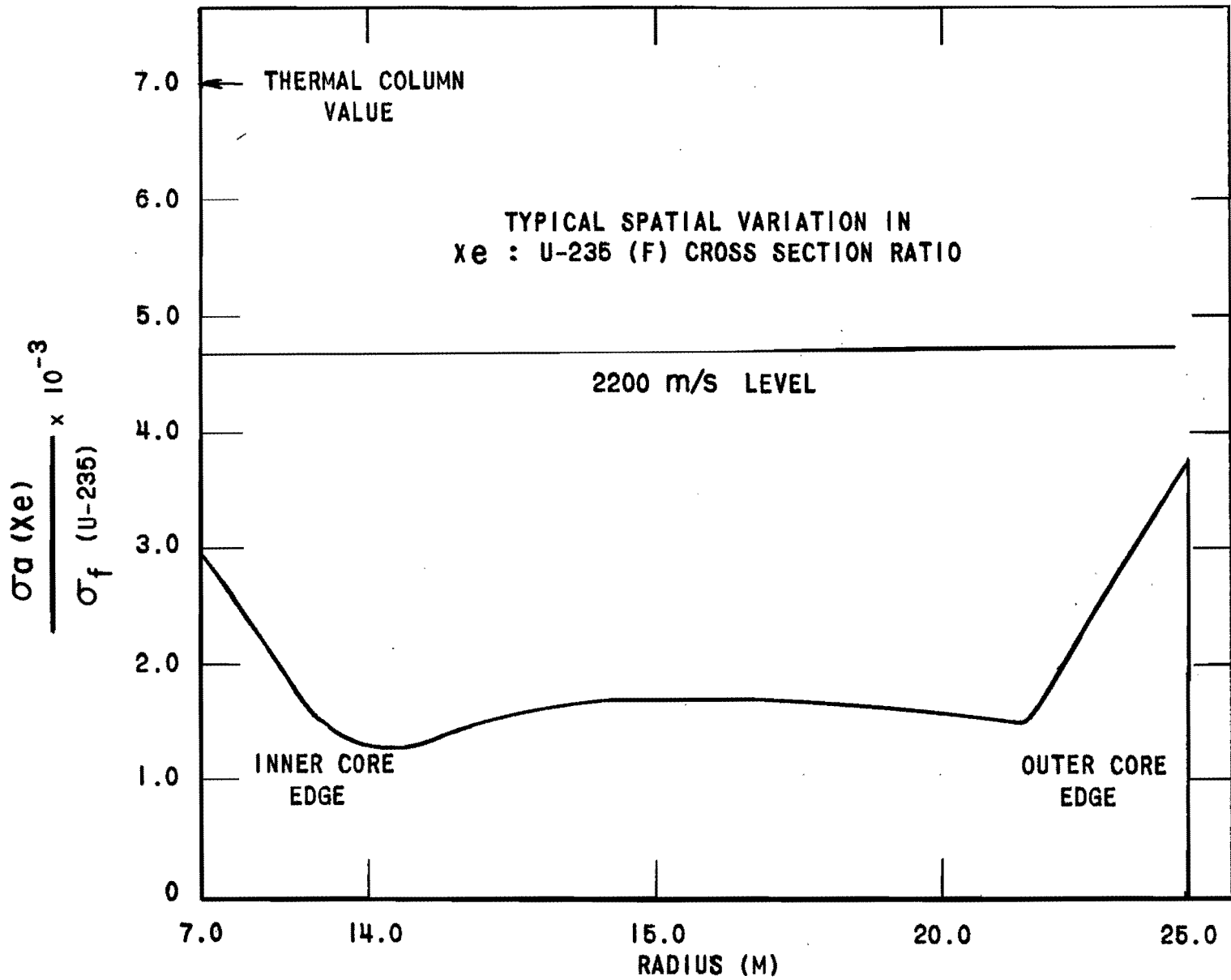


FIG. 3

TABLE 1

A TYPICAL NEUTRON INVENTORY
 BASED ON ONE VIRGIN NEUTRON PER REACTOR

CAPTURES: TOTAL = .39

U-235 (PLUS EQ. Xe, Sm-149)	.17	H: IN CORE	.003	O	.001	Fe	.02
FISSION PRODUCTS	.01	IN I.T.C.	.02	Be	.02	N:	.007
BURNABLE POISON (Sm)	.005	IN Be	.03	Al OR Zr	.01	Cr	.004

CAPTURES IN POWER FLATTENERS .09

FISSIONS IN U-235 .43

LEAKAGE .18

Description and Objectives of the ATR
A. W. Flynn and R. H. Gordon
Ebasco Services Inc.
New York, N. Y.

The Advanced Test Reactor (ATR) is being built to provide experimenters with facilities to irradiate engineering loop experiments in test holes 48 inches long, in neutron fluxes over 10^{15} adjustable as to intensity and spectrum, and constant within 10% over a 17 day operating cycle. This will be attained with a thermal power of 250 mw. The constancy of flux is maintained both axially and radially. In addition, the reactor is designed for a short refuelling time by provisions for refuelling both the core and the loops without removing the reactor head.

The objectives of the reactor have been achieved through the use of a multiple flux trap design. In a single flux trap reactor (Figure 1) the experimental space in the flux trap is completely surrounded by fuel. In the ATR four such flux traps have been combined to achieve an arrangement which permits 9 experiments to be installed in flux traps with each bounded over at least 180 degrees by fuel. (Figure 2). This 4 lobed configuration results in a serpentine fuel region which is built up from 40 identical elements.

Each element is a 45 degree slice out of a circular ring. The reactor fuel ring is assembled out of the identical elements by reversing the orientation of certain elements. An element is constructed of an array of 19 plates each formed as an arc of a circle.

The region outside of the fuel is filled with a beryllium reflector which contains 20 capsule holes and the reflector control elements. The spaces in the 9 flux traps contain the experiments and material to modify the spectrum through displacement of moderating water by metal, neutron filters, and converter assemblies. The reactor will contain an initial loading of experiments consisting of 6 pressurized water loops, one gas cooled loop, one liquid metal cooled fast loop and one liquid metal cooled thermal loop.

The control elements were selected to permit adjustment of the power pattern within the core without distorting the axial flux distribution. This is accomplished by using rotary control drums

in the reflector and reciprocating rod in the lobe neck regions as shown in Figure 2. To reduce the axial distortion which might result from moving the neck rods they are operated one at a time and positioned either all in or all out. Regulation is performed by one neck rod with a worth low enough to limit the degree of axial distortion. The control system is capable of maintaining a power shift which generates 60 mw in each of 2 diagonally opposite lobes, 40 mw in each of the other lobes while the center elements generate 50 mw. The reactor has a total of 45 control elements as follows:

- 16 Reflector control drums
- 20 Neck Shim Rods
- 4 Neck regulating rods (used one at a time)
- 5 Safety rods (installed in the pressurized water loop flux traps)

The details of the design will be presented in the next three papers. The nuclear design will be presented by Messrs T. M. Schuler and S. W. Spetz, the thermal and hydraulic design by Mr. W. M. Vannoy, and the mechanical design of the ATR fuel element by Messrs D. M. Collings and H. D. Ferris all of the Babcock and Wilcox Company.

SINGLE FLUX TRAP REACTOR

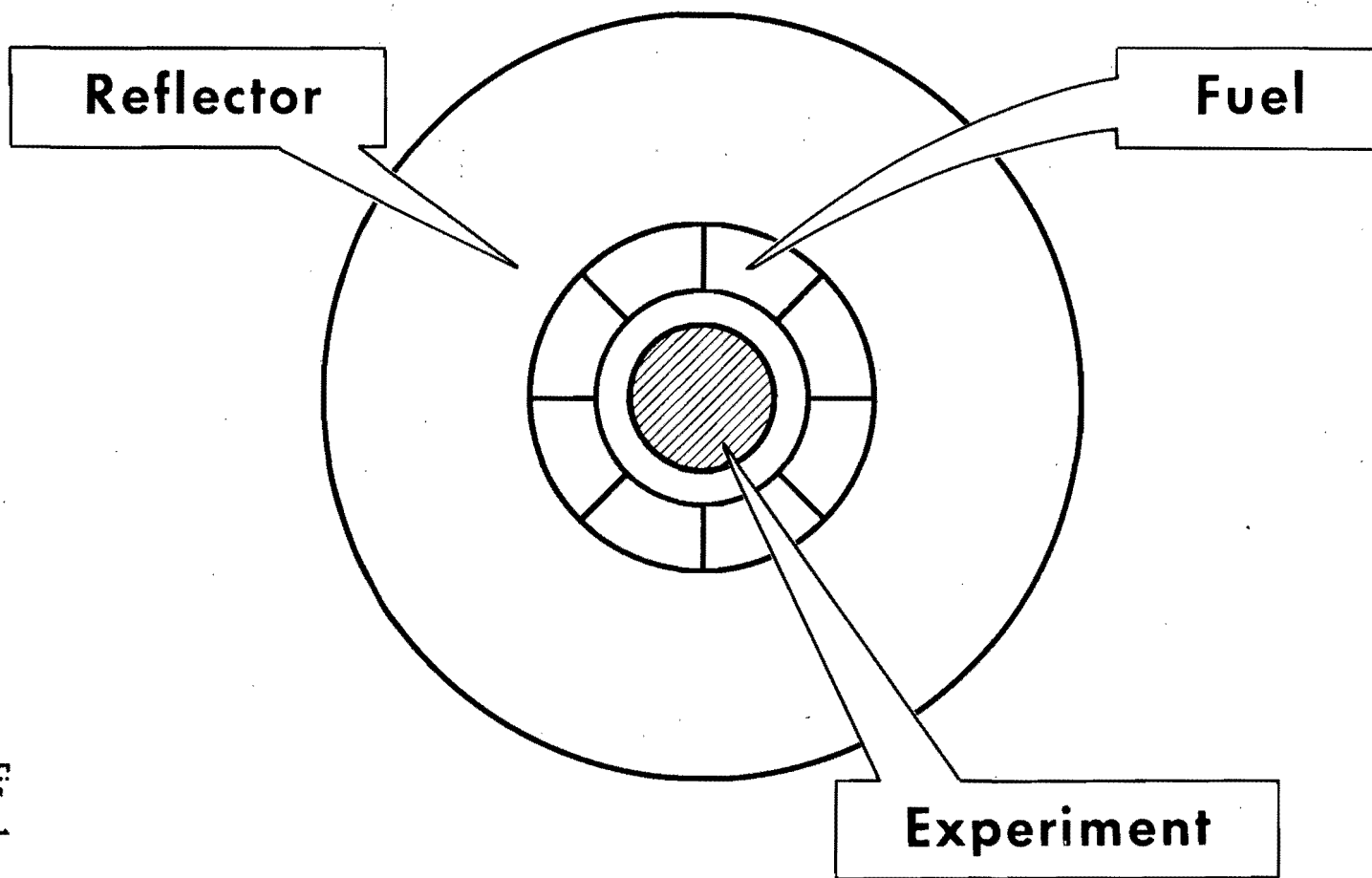
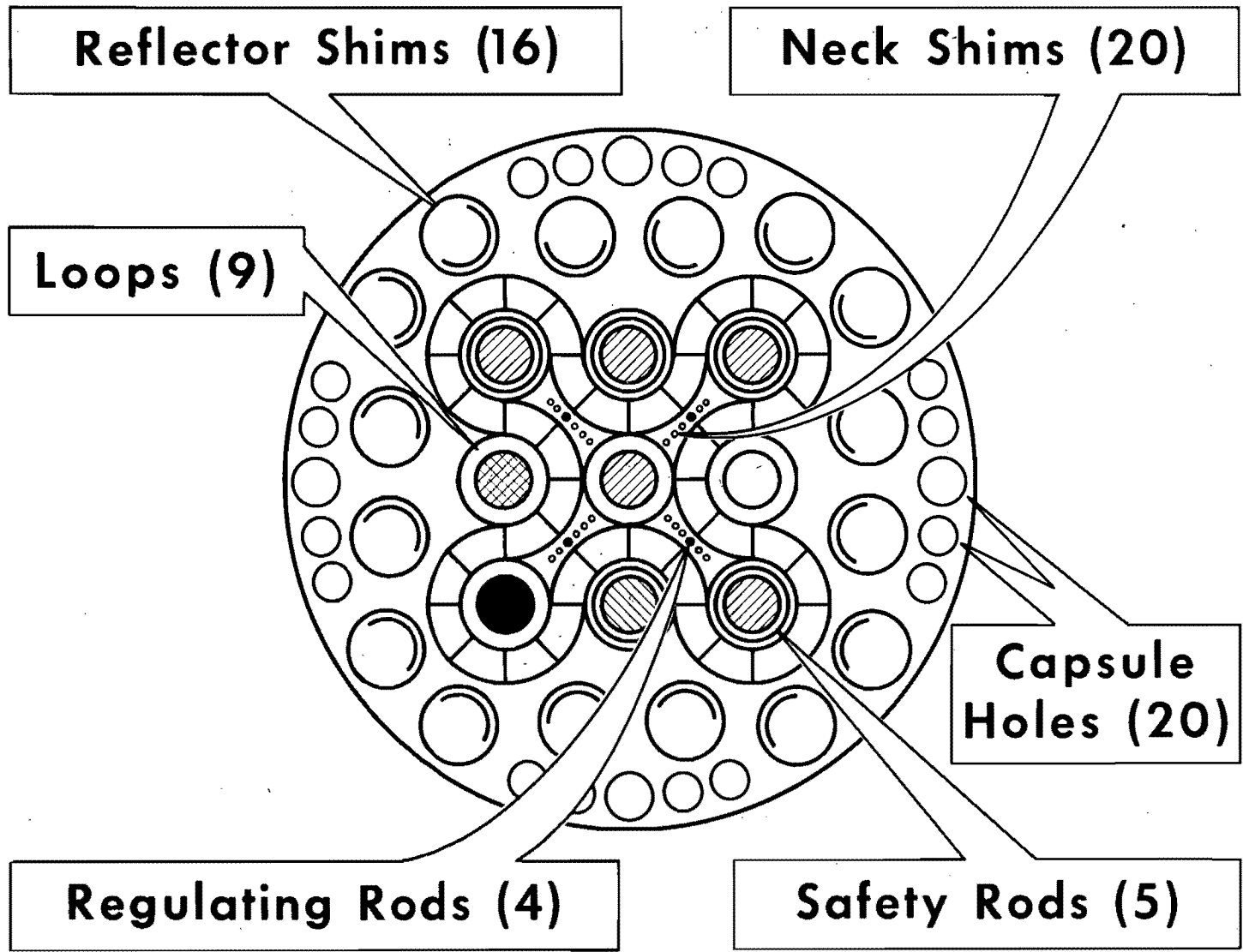


Fig. 1

ATR CORE ARRANGEMENT



50

Fig. 2

THE NUCLEAR DESIGN OF THE ATR

By

T. M. Schuler

S. W. Spetz

The Babcock and Wilcox Company

The Advanced Test Reactor is a 250 Mwt test reactor designed to provide additional experimental loop irradiation space for the AEC testing program. The core design incorporates many advanced ideas in test reactor technology and is expected to contribute a substantial body of information for further reactor development.

Design calculations to date have been done mainly to establish the basic nuclear characteristics of the reactor system. Final values of core parameters, such as core loading, burnable poison content in the fuel, control system worths, and experiment performance, will be confirmed or adjusted with the aid of the experimental program now under way.

The ATR has a unique core layout. A one quarter representation of the core is shown in Figure 1. Nine experimental loop flux traps are provided by a fuel geometry similar to that of a four leaf clover. Each leaf of the clover contains one flux trap, with an additional trap located between each pair of leaves. The ninth trap is formed by the intersection of the four leaves. Twenty inner capsule irradiation facilities are located in the outer regions of the beryllium reflector. Additional irradiation facilities are located just outside the core reflector tank.

The core fuel loading consists of fully enriched U_{308} dispersed in, and clad with, an aluminum alloy. Boron is included in the fuel matrix as a burnable poison for the control of lifetime reactivity. Each fuel element consists of nineteen curved plates which form a 45 degree sector of a circular annulus in cross section. Forty elements constitute the serpentine fuel annulus which surrounds five of these trap regions to form the basic four leaf clover pattern.

The ATR is designed to operate at a power level of 250 Mwt. Gross vertical and radial peak-to-average power ratios of 1.4/1 and 2.0/1 are basic design objectives. The homogenized fuel element produces approximately .95 Mwt/liter at rated power. A basic objective of the ATR is to provide perturbed neutron flux levels in the experiments of greater than 1×10^{15} (n/cm²-sec) thermal and 1.5×10^{15} (n/cm²-sec) epithermal. These maximum flux levels are to be maintained for the entire fuel cycle of 17 days with less than a 10%

variation in each experiment. Unperturbed thermal flux levels in the central test loop are expected to run as high as 2×10^{15} n/cm²-sec. Variation in desired neutron flux levels from lobe to lobe is accomplished by changing lobe power level. The neutron energy spectrum in each experiment may be varied by adjustment of the flux trap composition. The vertical flux distribution of each loop is held constant during the irradiation period, since essentially all controls cover the full 48 inch loop length (one regulating rod is partially inserted, but will have little or no effect on the axial flux profile in the experimental loops).

Core reactivity and experiment flux levels are controlled by combination of the two shim systems employed in the reactor. (These control systems are in addition to the burnable poison). The reflector shims are rotating cylinders located in the beryllium reflector region. Each cylinder has a hafnium plate insert which covers one-third (an arc of 120°) of its periphery and extends over the total 48 inch height of the core. The rest of the cylinder is beryllium. There are a total of sixteen reflector cylinders which operate in pairs. Each leaf of the fuel pattern is controlled by two pair of reflector shims. These cylinders rotate the absorber material toward or away from the core as needed for reactivity control. Under operating conditions the power level of each lobe and the resulting power distribution between lobes is controlled by a push-pull action of the reflector shims on either side of the core. These shims constitute a total control worth of approximately 8.6% in excess reactivity (ΔK_{excess}).

The neck shim system is made up of 24 small hafnium rods with aluminum followers which operate vertically in the neck region or stem portion of the leaf design. These neck shims operate either fully inserted or fully withdrawn, except for the regulating rod, and represent approximately 8.7% in excess reactivity (ΔK_{excess}) holddown. The calculated interaction between the two shim systems provides an additional 2.5% (ΔK_{excess}) control and give the total movable control system a worth of approximately 19.8% in excess reactivity.

A typical reactivity balance for the ATR at the beginning and end of life is shown in Table I. This data was taken from a TURBO lifetime calculation with an initial core loading of 26 kg U-235 and 128 grams of natural boron.

TABLE IReactivity Balance and Control

<u>Reactivity Available</u>	<u>0 Days</u>	<u>17 Days</u>
Max. Cold Clean K_{eff} (No Burnable)	1.241	-
Excess Reactivity Held by Poison (ΔK_{excess})		
Burnable Poison (B-10)	.111	.034
Xenon	-	.050
Samarium	-	.008
Fission Products	-	.027
Temperature Deficit (ΔK_{excess})	.010	.010
Max. Cold Clean K_{eff} (With Burnable)	1.130	1.059
Max. Hot Clean K_{eff} (With Burnable)	1.120	1.049
Movable Control Required to Maintain Reference		
Power Shift of 40-50-60 MW Over Core Life	.066	.066
Total Control Required	1.196	1.125
<u>Movable Control Available, ΔK_{excess}</u>		
Rotating Reflector Shims	.086	
Neck Shim (6 per neck)	.087	
Shim Interaction	.025	
Total Movable Control	.198	

Core reactivity regulation is provided by two neck rods located on opposite sides of the central flux trap. Each rod represents approximately $0.3 \Delta K_{\text{excess}}$ fully inserted. The rods operate either individually or as a pair to smooth out background reactivity changes. The regulating rod or rods are partially inserted during operation. Investigation indicates negligible power tilting as a result of partial insertion.

A composite curve indicating the reactivity contribution of each reactor parameter during one life cycle is shown in Figure 2. This composite separates the various parameters and indicates the influence of each during the life cycle. The curve designated " K_{excess} WITH NO CONTROL" represents the expected excess neutron multiplication factor with the neck rods fully withdrawn and the reflector shims rotated completely away from the fuel region at operating temperature. Data for the composite was taken from one and two dimensional lifetime and criticality calculations. Areas between adjacent curves are indicative of the total reactivity held by each parameter as noted.

The high flux levels in the ATR result in a nearly saturated xenon condition. Approximately 5.0% in excess reactivity is held by equilibrium xenon. Following a complete reactor shutdown, the xenon worth builds up at the rate of 0.1% reactivity per minute. At the start of core life, xenon override can be accomplished for about 120 minutes after shutdown by the existing control system. The startup period is reduced toward the end of core life.

Samarium accounts for approximately 0.8% reactivity during a life cycle. The reactivity loss due to the buildup of stable fission products reaches a maximum value of approximately 2.7%.

The next reactivity region represents the loss of fuel due to burnup in both the fuel and the experimental region. Some portion of this area must also be attributed to the variation of the importance of various fuel regions with core life.

A reactivity gain is indicated in the area representing the B^{10} holddown. Approximately 72% of the initial boron concentration is consumed during one 17 day period. This poison burnup is based on the initial fuel and natural boron loadings of 26 kg and 128 grams, respectively.

The temperature deficit is shown as the upper region and represents about 1.0% in excess reactivity between ambient and the operating temperatures. The total change in the effective neutron multiplication factor is $7.1\% \Delta K$ during the 17 day cycle.

One dimensional calculations of xenon stability have been made using analytical techniques, digital computer codes, and analog simulations. The results of this work indicate that the reactor is stable in all dimensions but may exhibit an underdamped response to some perturbations. The greatest emphasis has been on axial stability since the rotating reflector shims provide an automatic control over interlobe xenon reactions. Although the flux is very high, the core is short enough to keep the system within the bounds of stability. Changes in lobe power level do not have a strong effect upon stability because the xenon is nearly saturated at the average level of 50 MW per lobe. An increase in length would have a more pronounced influence on core stability.

Reactor power shifts from lobe to lobe or changes in total power level are made by systematic rotation of the various reflector shims and the insertion or withdrawal of the neck shims. A power distribution of 40-50-60 MW in the fuel regions was selected as a reasonable maximum imbalance in power for normal operation. This distribution produces 40 MW in each of two diagonally opposite lobes, 60 MW in each of the two remaining outer lobes, and 50 MW in the central fuel region. The central fuel region consists of the eight fuel elements closest to the central flux trap. Initial calculations indicate that this reference power distribution can be held for the full 17 day life cycle.

The versatility in operation of the ATR core has given rise to a need for some type of scheme which predicts the manipulation of the various control shims during each life cycle. The ATR critical (ATRC) is to be operated in conjunction with the ATR in much the same way as the ETR and ETRC are presently operated. That is, all experiment loadings and power shifts are first mocked up in the critical experiment to insure safe and successful results during the actual exposure period. A graphical control programming scheme has been developed to predict the manipulation of controls during each core cycle of the ATR. This scheme could be used as a first order approximation tool in operating both the ATR and the ATRC.

In addition to setting the initial burnable poison concentration and Uranium-235 loading for various cycle conditions, the proposed control scheme estimates five reactor criticality and power distribution effects. These effects are:

1. Reflector shim rotation
2. Neck shim withdrawal
3. Reflector and neck shim interaction
4. Experiment and trap composition
5. Fuel burnup and fission product accumulations.

Each effect is calculated separately and the resulting reactivity and power level changes are arrived at by summation of all individual effects.

Figure III illustrates one of these effects. This power distribution surface was generated from two dimensional calculations of the core layout with varying degrees of reflector shim rotation. The four reflector shims associated with each outer lobe were rotated as a unit. Calculations of various base points resulted in this surface which predicts the relative power level in each lobe (based on a total output power of 250 MW) and the total reactivity holddown involved in any particular shift. Similar curves and surfaces have been generated for the other effects mentioned. The scheme is set up to cover essentially all practical Uranium-235 loadings and burnable poison concentrations. The philosophy of core operation will determine whether a large or small ratio of fuel to poison will be used. The burnable poison concentration determines the amount of movable reactivity required for each core cycle. A large movable reactivity during the life cycle would lower resulting fuel costs and fuel element peak to average power factor. On the other hand a smaller movable reactivity would require less movement of control and less total shim control.

The application of the graphical control program to the ATR operation is widespread. The three basic advantages of this program are:

1. Helps determine the feasibility of various power distributions in terms of fuel loading, poison concentration, and length of cycle during which the desired power shift can be maintained with available movable control.
2. Predicts step by step shim movement for any practical power distribution throughout core cycle.
3. Introduces the possibility of automatic core operation using some computer facility in conjunction with the flow of data from core instrumentation.

The control program at present has two outstanding limitations. These are (1) in its present state of development the power distribution and shim positions are limited to one-eighth and one-quarter core symmetries, and (2) the scheme is based on the assumption that fresh fuel must be used for each cycle. Should the scheme be used extensively, further development would be necessary to eliminate these shortcomings.

Net void and temperature coefficients are negative for the fuel region and the reactor as a whole. Initial calculations on single and multi-lobe models give results comparable with earlier work on the ATR by Phillips Petroleum Co. The reference core has a negative temperature coefficient ($1/K \Delta K / \Delta T$ ($^{\circ}F$)) which ranges from approximately $-2 \times 10^{-4}/^{\circ}F$ to $-1.6 \times 10^{-4}/^{\circ}F$ as the reflector shims are rotated from the position closest to the fuel region (zero degrees rotation) to the fully withdrawn position (180° rotation). The temperature coefficient of the entire core is approximately $-1 \times 10^{-4}/^{\circ}F$. More detailed evaluation of the temperature and void coefficients are now under way. This study will result in coefficients for specific regions of the core for both void and temperature changes.

The nuclear design of the ATR is being substantiated by a large R&D program, which includes a full scale critical experiment now in operation. The versatility of this new test reactor has been demonstrated by the various experimental data accumulated to date. Final parameters for the reference core such as fuel loading, burnable poison content, control worths, and experiment performance will be set with the aid of these experimental results.

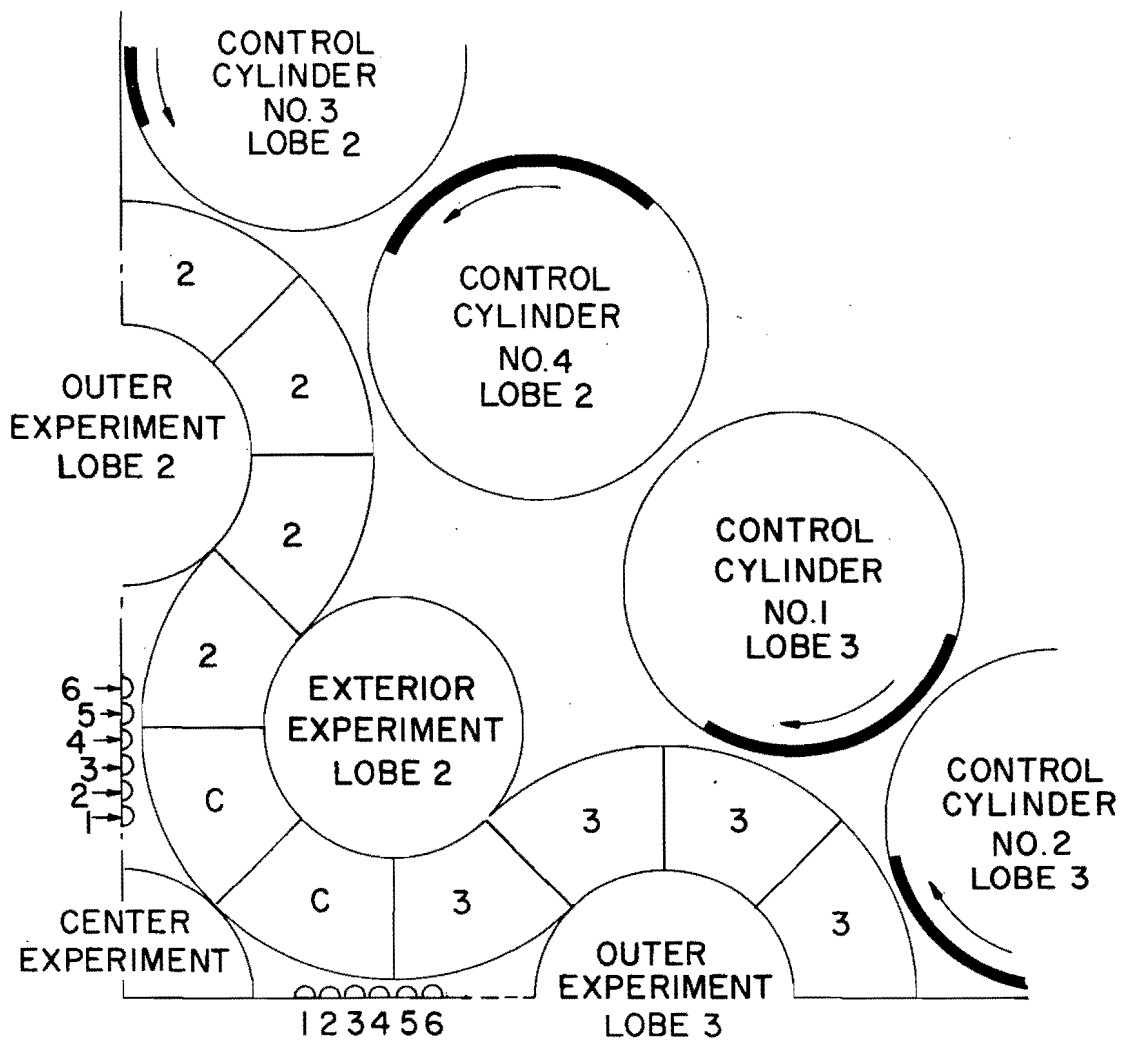


Figure 1. Layout and Nomenclature for One-Quarter Core Symmetry

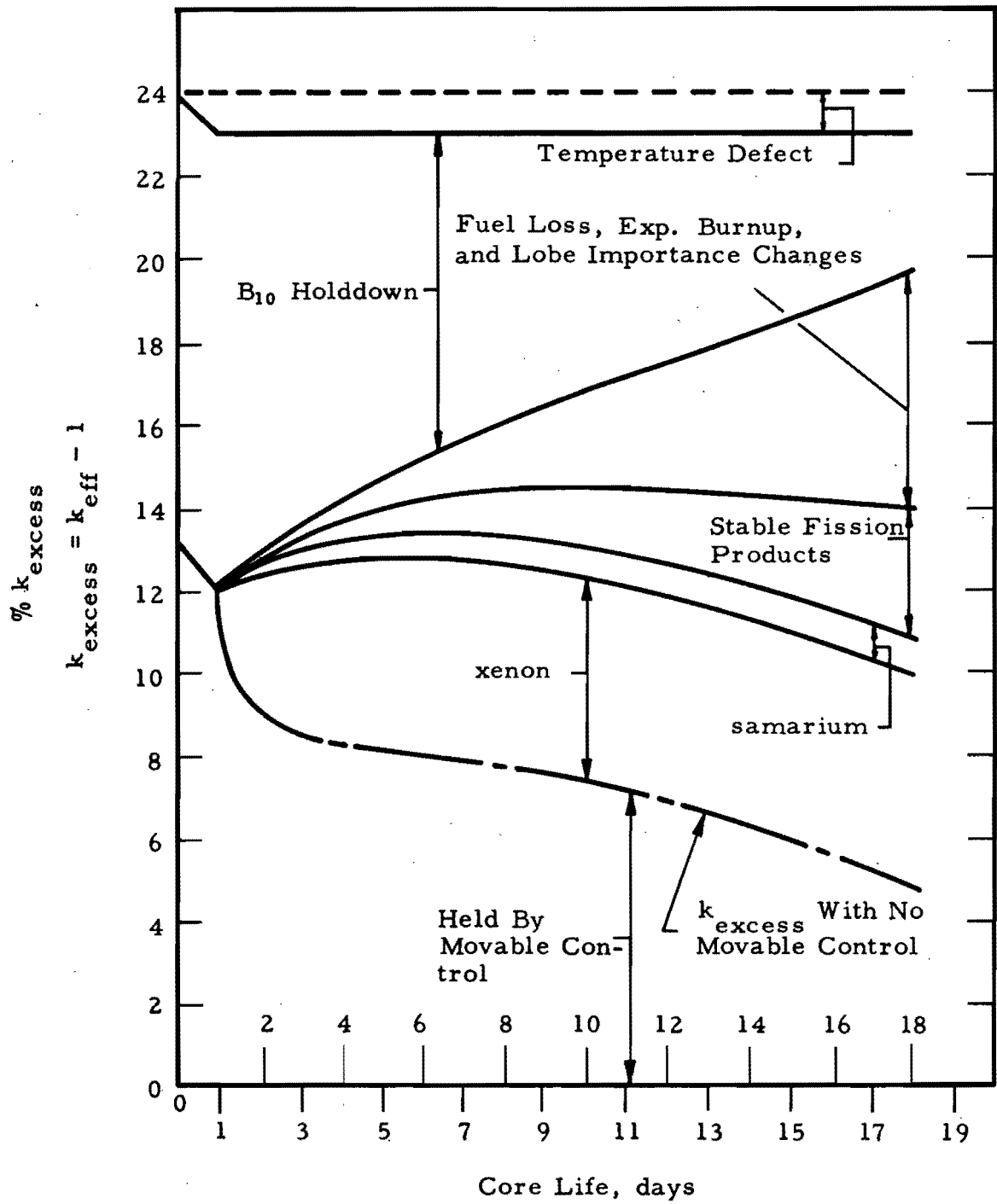


Figure 2. Reactivity Composite for Core Life

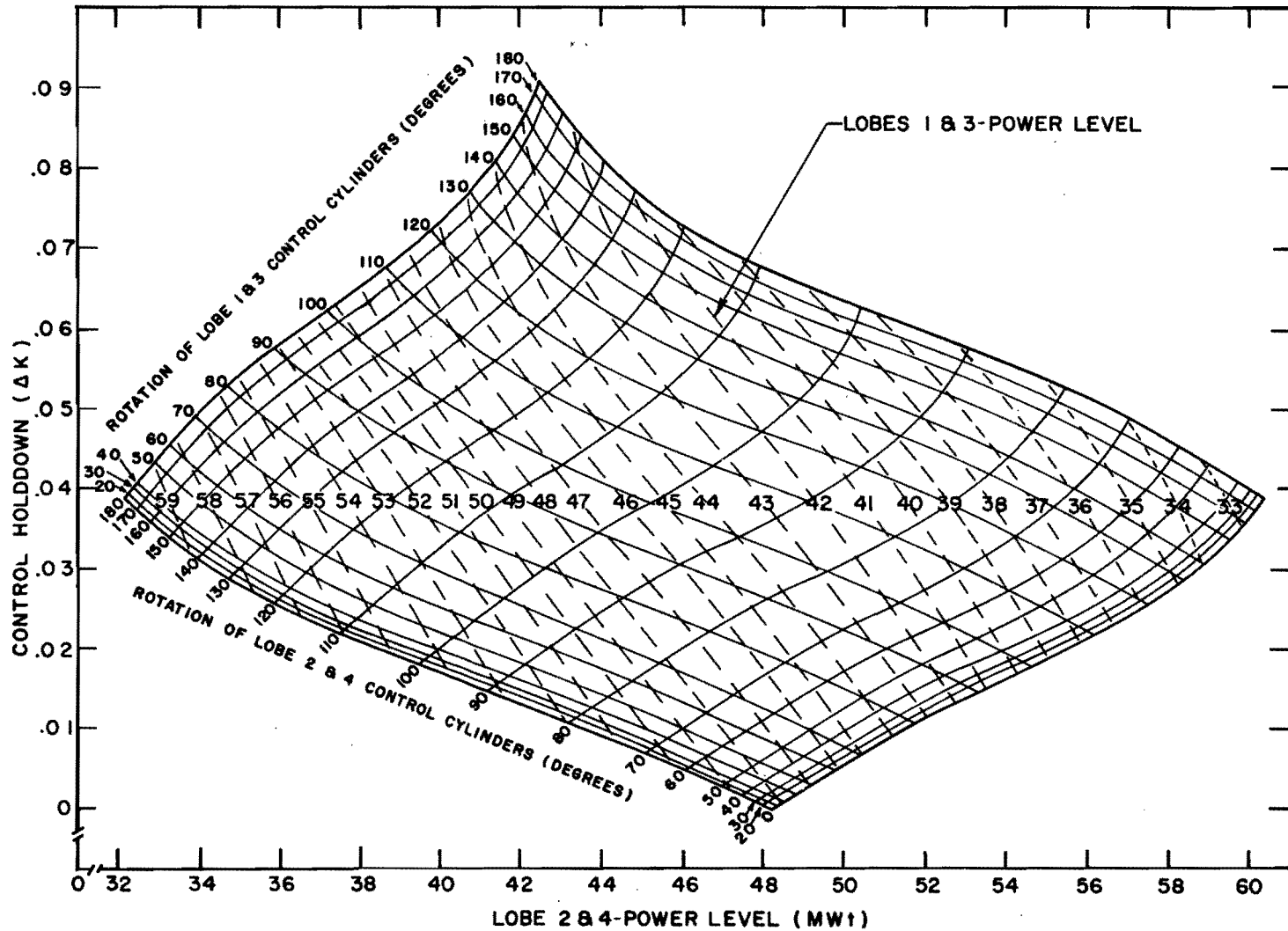


Figure 3. Control Cylinder Reactivity Holddown and Core Power Distribution as a Function of Cylinder Rotation (Degrees Inserted)

THE MECHANICAL DESIGN OF THE
ADVANCED TEST REACTOR FUEL ELEMENT

AUTHORS: D. M. COLLINGS, H. D. FERRIS

The Babcock and Wilcox Company

The intent is to present a brief description of the ATR fuel element, outline the major mechanical or structural problems encountered in the design, and to discuss the approaches employed to solve those problems.

As previously mentioned, the ATR fuel element forms a 45° segment of an annulus. It is made up of 19 fueled plates - curved with a common center, and two side plates - inclined at 45° to one another. All fuel plates have .020" thickness of fueled "meat" centrally located. The innermost plate (nearest the common center) is .080" thick and the outermost plate is .100" thick. All other fuel plates are .050" thick.

Initially, the clad material was X-8001*, but this has been replaced with 6061-0 material, because of the latter's superior strength. The 6061 T-6* side plates are nominally .188" thick. The fuel plates are joined to the side plates by a "roll-swaging" process.

The nominal water channel is .078". Because of the curvature, the channels, and fuel plates, vary in peripheral width from 2.2" to 4.0".

The fuel plates are slightly over 4-feet long and the nominal flow velocity is 44 ft/sec. The vertical pressure drop across the core is 92 psi.

* Aluminum Alloy

Fig. II shows a list of the major problems encountered so far in the design of the fuel element. By showing that there is a test set up to evaluate each problem, the chart illustrates the largely empirical nature of the mechanical design.

1. STEADY-STATE HYDRAULIC LOADS

Typical of the steady-state hydraulic loads are the radial pressure differences across fuel plates due to variations in overall channel size. Because of the tight tolerances possible within the fuel element, the channels formed by two fuel plates tend to become uniform with small deflections and stresses are therefore not expected to be troublesome.

Because of the general configuration of the reactor, the width of the annular space in which the fuel elements are located cannot be accurately controlled, and it is possible for the flow channel on the outside of the fuel element to become two or three times as large as the .078" nominal size.

For such a large flow channel between fuel plates and the reflector, the pressure differentials across the plates may not stabilize at acceptable deflections.

Both analytical and experimental approaches are being employed to evaluate the effects of this type of loading.

The analytical work consists of a stress and deflection analysis which estimates the stress and deflection of the fuel plates, taking credit for the membrane support from the side plates as well as the bending resistance of the fuel plates themselves.

The membrane loads applied to the outer fuel plates by the side plates are evaluated by determining the spring-rate of the side plates - as beams supported on an elastic foundation provided by the other fuel plates. The product of this spring-rate and the chordwise deflection of the fuel plate gives the membrane load. The innermost and outermost fuel plates are expected to have about the

same pressure load, but the outermost plate will have larger stresses and deflection because of its greater span. In addition, the plate adjacent to the outermost plate has high stresses because it supplies a large portion of the membrane support for the outermost fuel plate, and is only half as thick as the outermost plate.

Experimental support for this analysis has been obtained from several of the tests and will be discussed later, with the pertinent tests.

The experimental work to evaluate the mechanical effects of large channels consists of the Hot Flow Test, the Fuel Plate Pressure Deflection Test, and the Swaged Joint Strength Test.

The Hot Flow Test consists of a full size element mounted in a hot hydraulic loop which simulates the reactor, hydraulically, and is capable of flow velocities up to 1-1/2 times the reactor flow rates. Sufficient instrumentation is provided to determine pertinent flow velocities as well as pressure loading on the outside fuel plates.

The first specimen, which was tested at 420^oF, failed at about 120% of design velocity. The outside fuel plate failed by pulling out of the side plate over the middle half of its length until it was supported by the simulated reflector.

The pressure differences across the fuel plates during this test were lower than expected for the flow velocity, but the failure occurred at a pressure difference across the outside fuel plate which was quite close to the value predicted from the analysis, as indicated on Fig. III.

The initial test specimen was one of the first fuel bundles resulting from the fabrication development program and was accepted "as is". Later specimens will be up-dated design-wise (including the material change) and will include, if possible, simulated thermal "ripples" and/or other deformations which may exist

in the reactor. The final specimen will be tested for 30 days at about 400° F and 125% of design velocity.

In order to demonstrate the fuel plate stress levels and deflections, and confirm the analysis, several specimens made up of a single fuel plate swaged in two side plates have been tested at 420° F in a rig as shown in Fig. IV. The side plates are held by the fixture so that the chordwise stiffness of the unsupported span of the side plates approximates the stiffness in the fuel bundle, so as to provide the correct membrane force to the fuel plate. Internal and external pressures were applied to the specimen, and plate mid-span deflection and stress recorded.

The measured stress levels were in very good agreement with the values calculated by the analysis (discussed above) for this arrangement, as shown on Fig. V. In the plastic range, the stresses (primarily bending) do not increase as rapidly because the load is then mainly carried by the membrane support. The calculations are elastic and do not reflect this effect.

As indicated on Fig. VI, the agreement between calculated and test deflections is also good in the elastic range. Like the stress numbers, the deflection calculations are valid only in the elastic range, so that the disagreement in the plastic range is not surprising. The trend is as predicted, however.

Later specimens will consist of a complete fuel element with similar pressure loading.

2. UNSTABLE HYDRAULIC LOADS

The unstable hydraulic loads are characterized by smooth, local, channel restrictions, called "ripples", which produce a venturi effect without appreciably influencing the flow through that channel. In contrast to the stable small channel of constant width, the narrow part of a "rippled" channel sees a pressure decrease, which tends to further reduce the local channel

width. Where this resultant loading exceeds the strength of the fuel plate, the fuel element will probably collapse, at least locally.

Ripples can result from manufacturing or from thermal and mechanical loads during operation.

Thermal "ripples" may result from compressive longitudinal strains produced in the hotter fuel plates by the various thermal gradients. Examination of Fig. VIII indicates that the two outermost fuel plates are the worst from this standpoint.

Straightforward stress analysis indicates that a flat plate under these conditions would deform in the shape of a series of "ripples" in the longitudinal direction. In the plastic range, we are not able to handle the stiffening influence of the curvature of the fuel plates, analytically, and therefore, the Thermal Ripple Test has been set up to determine the length and amplitude of thermal "ripples". Similar "ripples" are to be built mechanically into the specimens for the Hot Flow Test.

The fuel plates were tested by bolting relatively low expansion stainless steel bars to the long edges and increasing the temperature of the assembly uniformly.

The material in the steel bars was selected so that the fuel plate thermal strain at uniform temperature in the test equals the strain expected in the reactor due to temperature differences.

This test work has been completed for X-8001 material and the results indicate that the curvature of the fuel plates virtually eliminates any tendency for thermal "ripples" to occur. Several flat plates were tested in the rig to demonstrate that it was performing as planned, and the flat plates "rippled" severely as predicted. It does appear that the effect of the thermal loading is to increase any imperfections in a fuel element. This will be investigated further.

3. FUEL PLATE RADIAL THERMAL DEFLECTION

Due to flux peaking, there is a radial thermal gradient in the fuel element with the central plates being the coolest and the outermost plate the hottest. This is shown on Fig. VIII. We are concerned that the hotter plate will deflect excessively in a transverse direction.

We plan a test to measure this deflection using a full cross section, partial length fuel element specimen. The test procedure is to heat the outer plate above the temperature of the rest of the specimen and record the plate deflection.

4. UNKNOWNNS

The observer may note that many problems which will occur simultaneously in the reactor, and may interact, are being treated separately in the test program. An irradiation test is contemplated in the ETR, but of course all pertinent loads cannot be correctly simulated at once, and it is desirable to have the ETR specimen as safe structurally as possible. Toward that end, we intend to build as many loads, imperfections, deformations, etc., as is practical into the last specimen for the hot flow test. This will give considerable confidence in the design going into the ETR test, and that test will cover irradiation effects as far as possible.

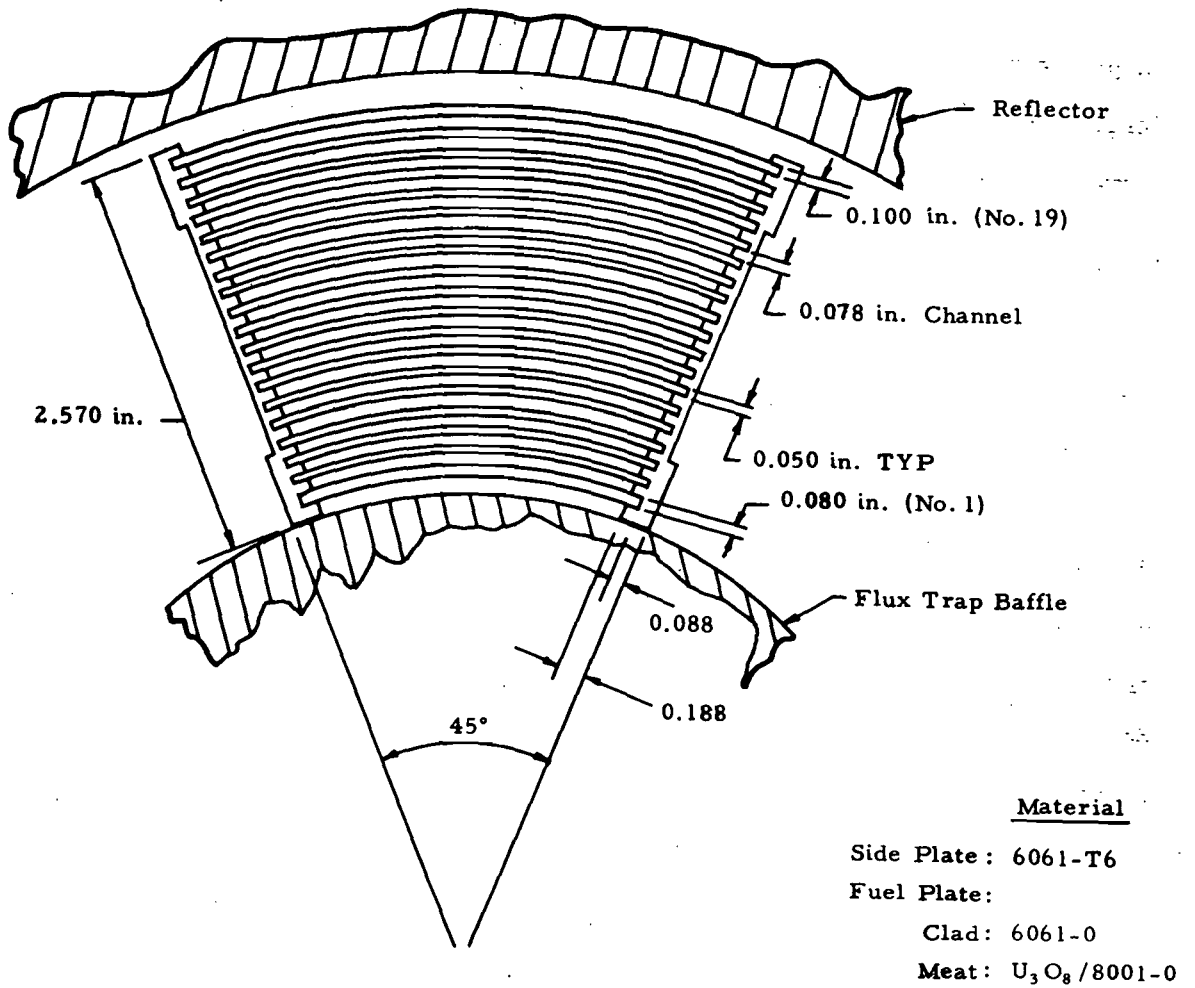


Fig. 1: ATR Fuel Element Cross-Section

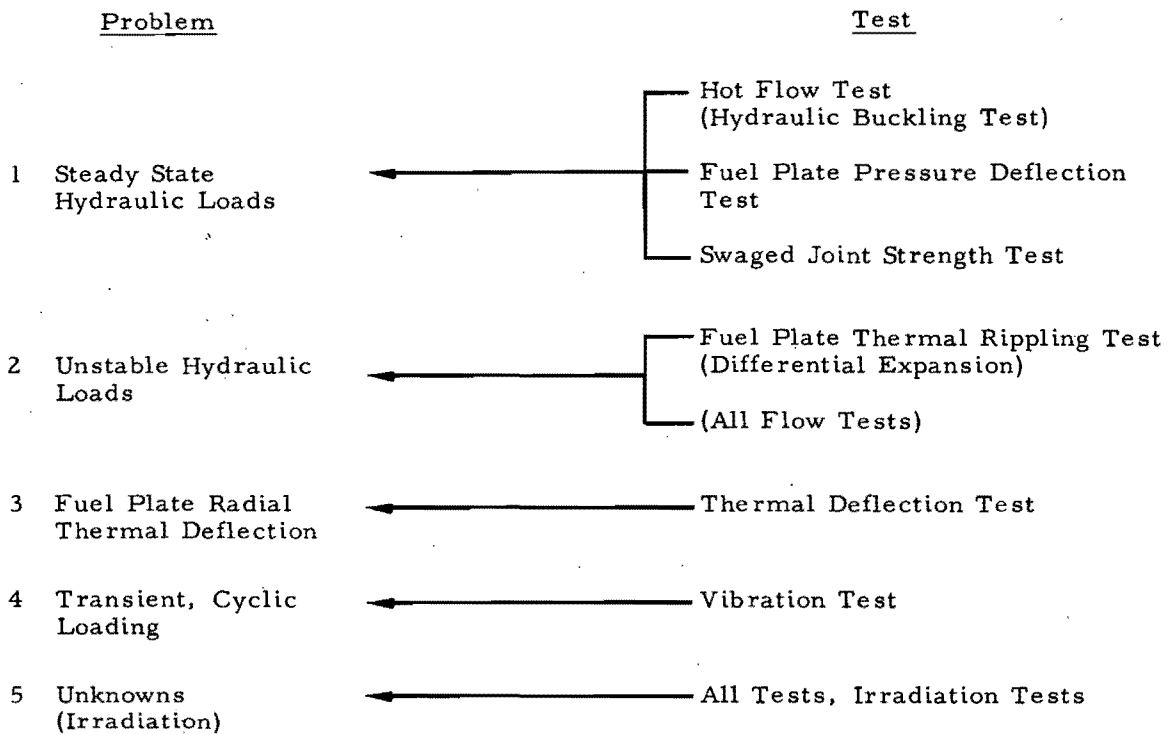


Fig. II: Major Mechanical Problems and Related Tests

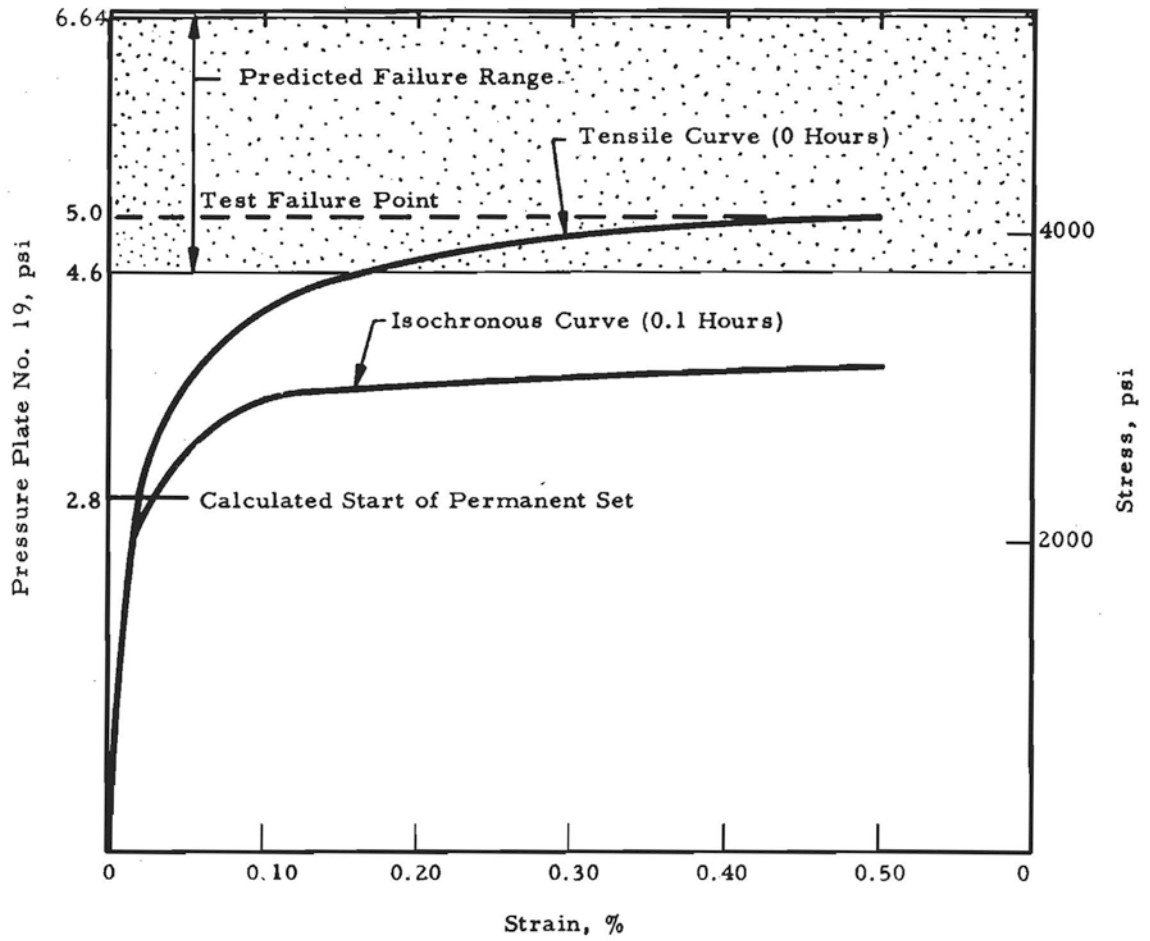


Fig. III: Hot Flow Test Performance, Actual Vs Calculated Results

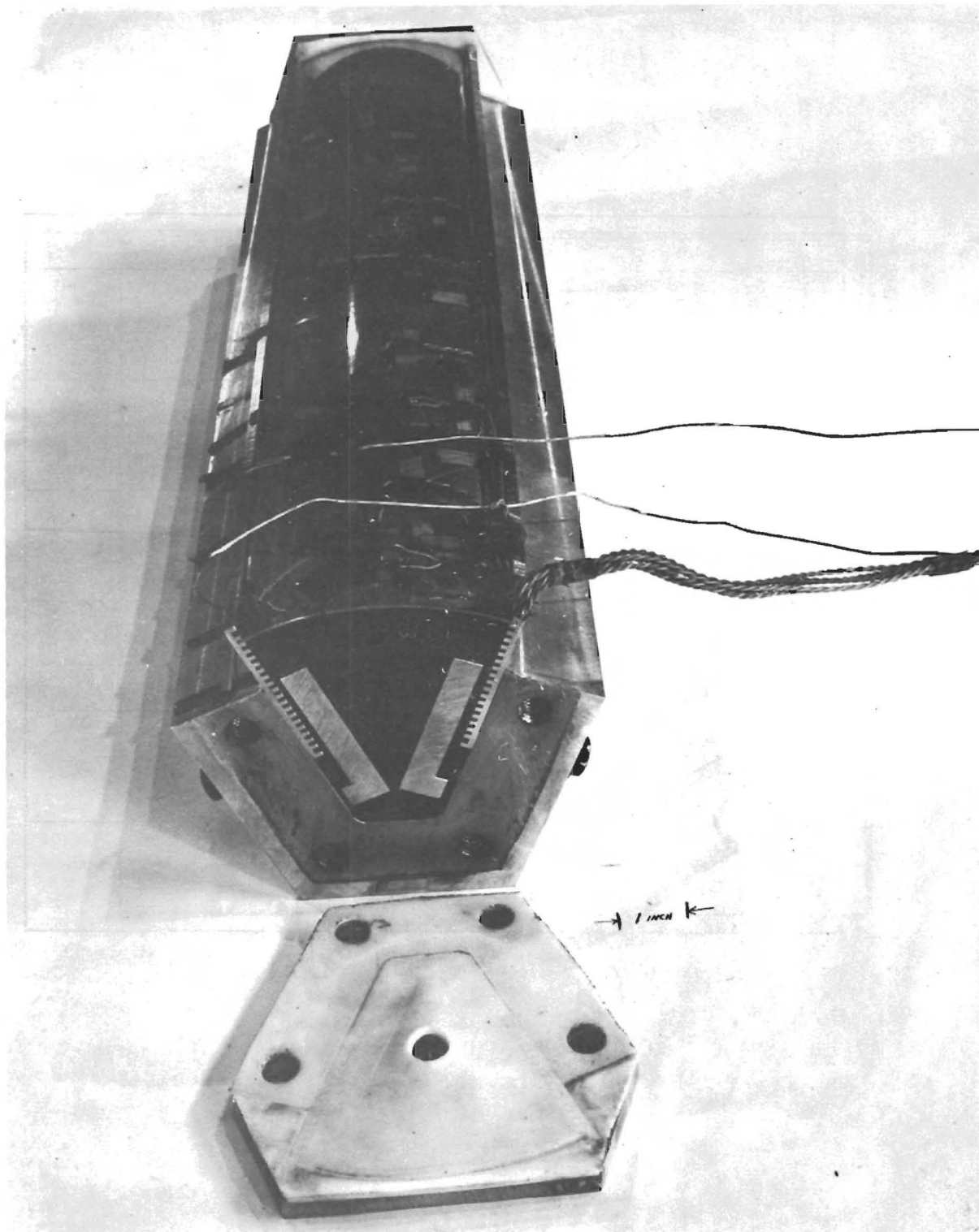


Fig. IV: Pressure Deflection Test

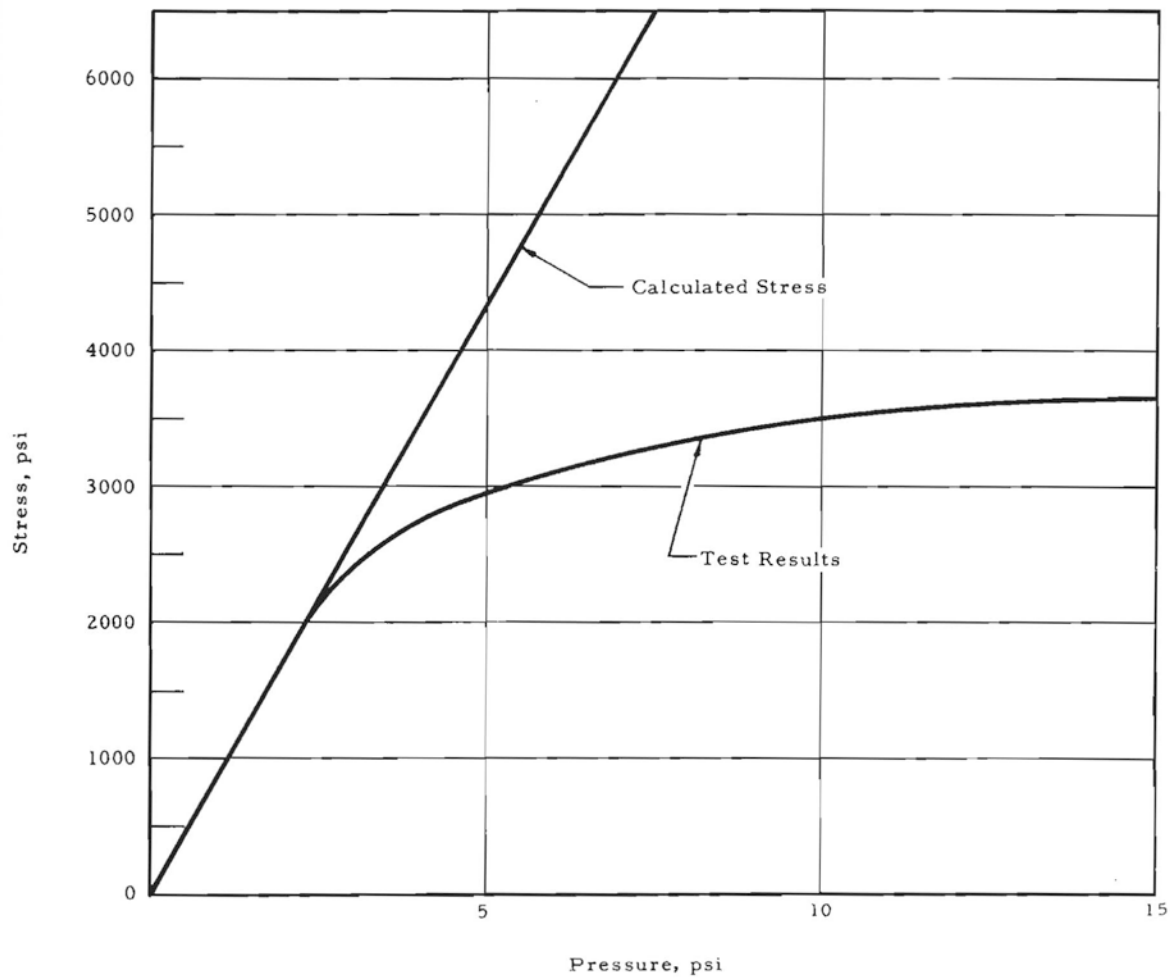


Fig. V: Fuel Plate Bending Stress Vs Pressure

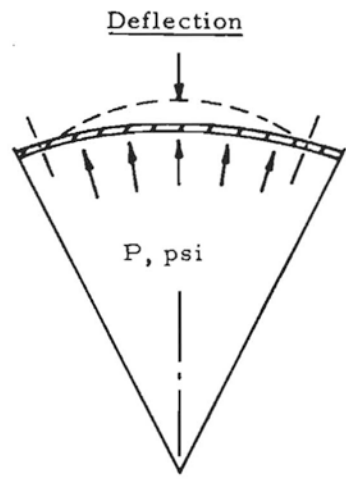
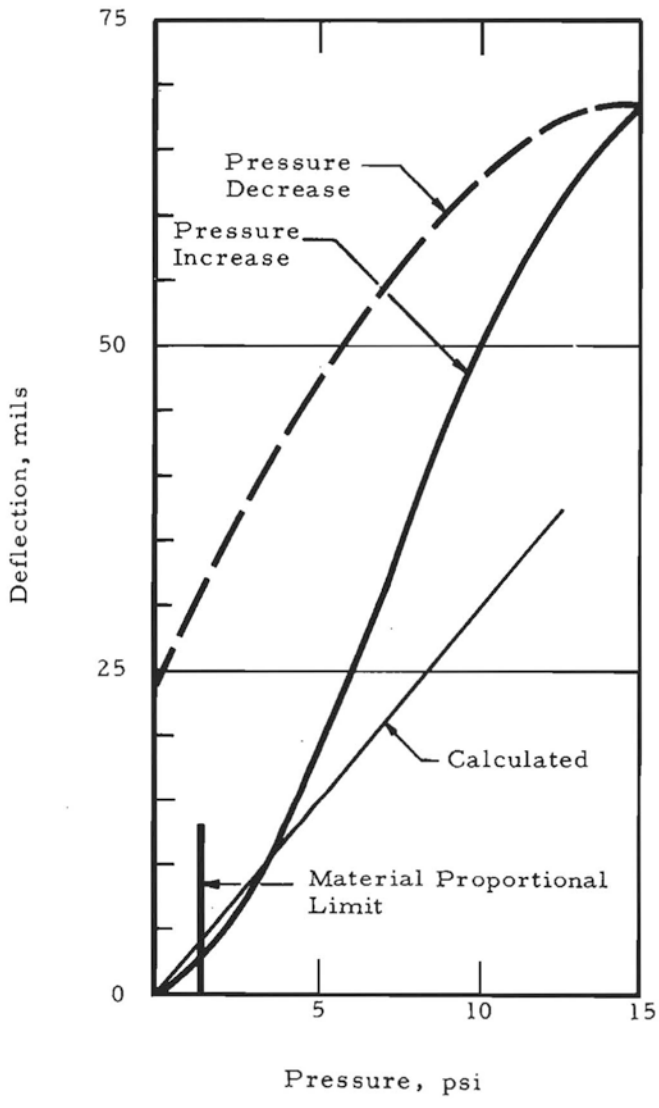


Fig. VI: Fuel Plate Deflection Vs Pressure

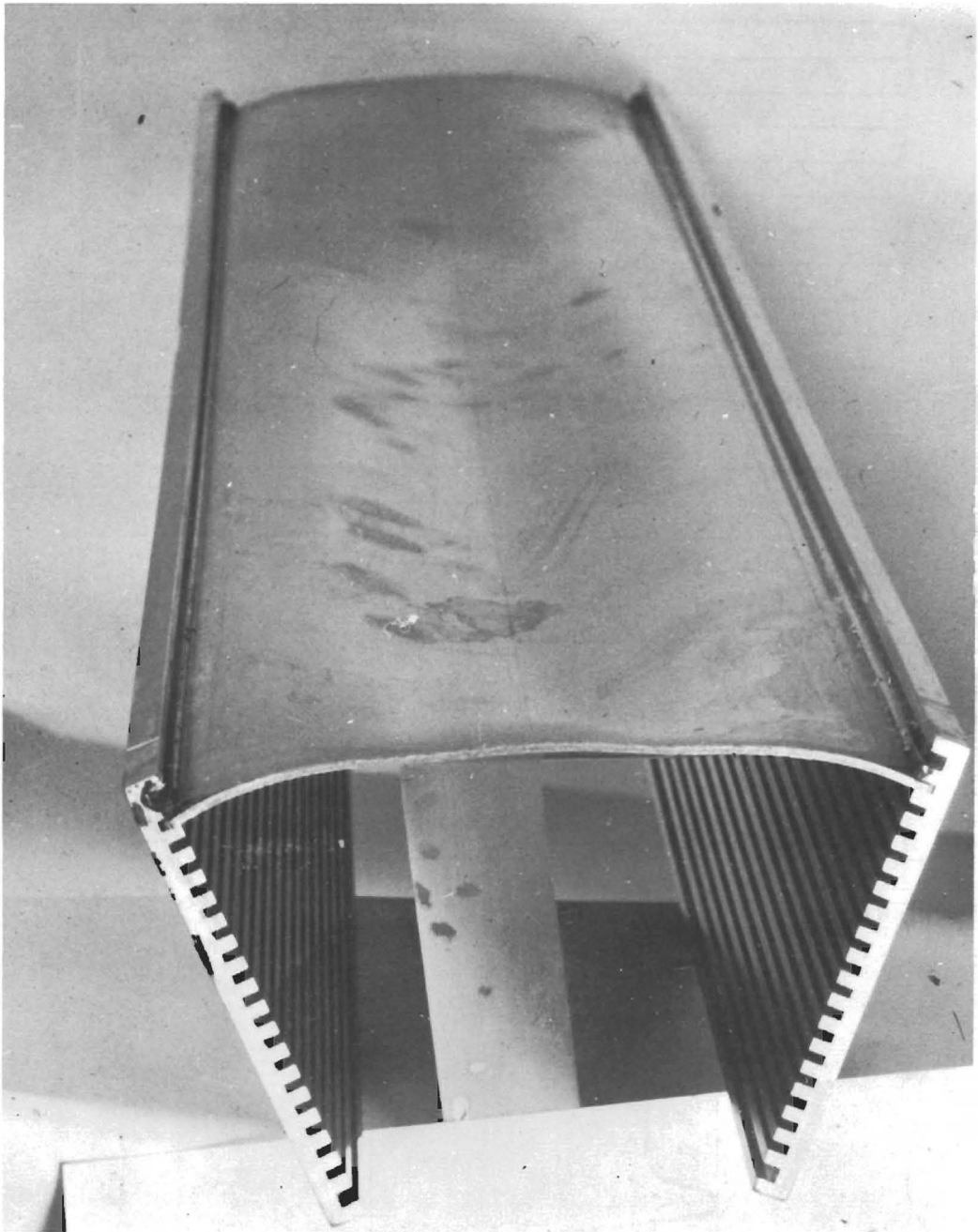


Fig. VII: Convex Pressure Failure

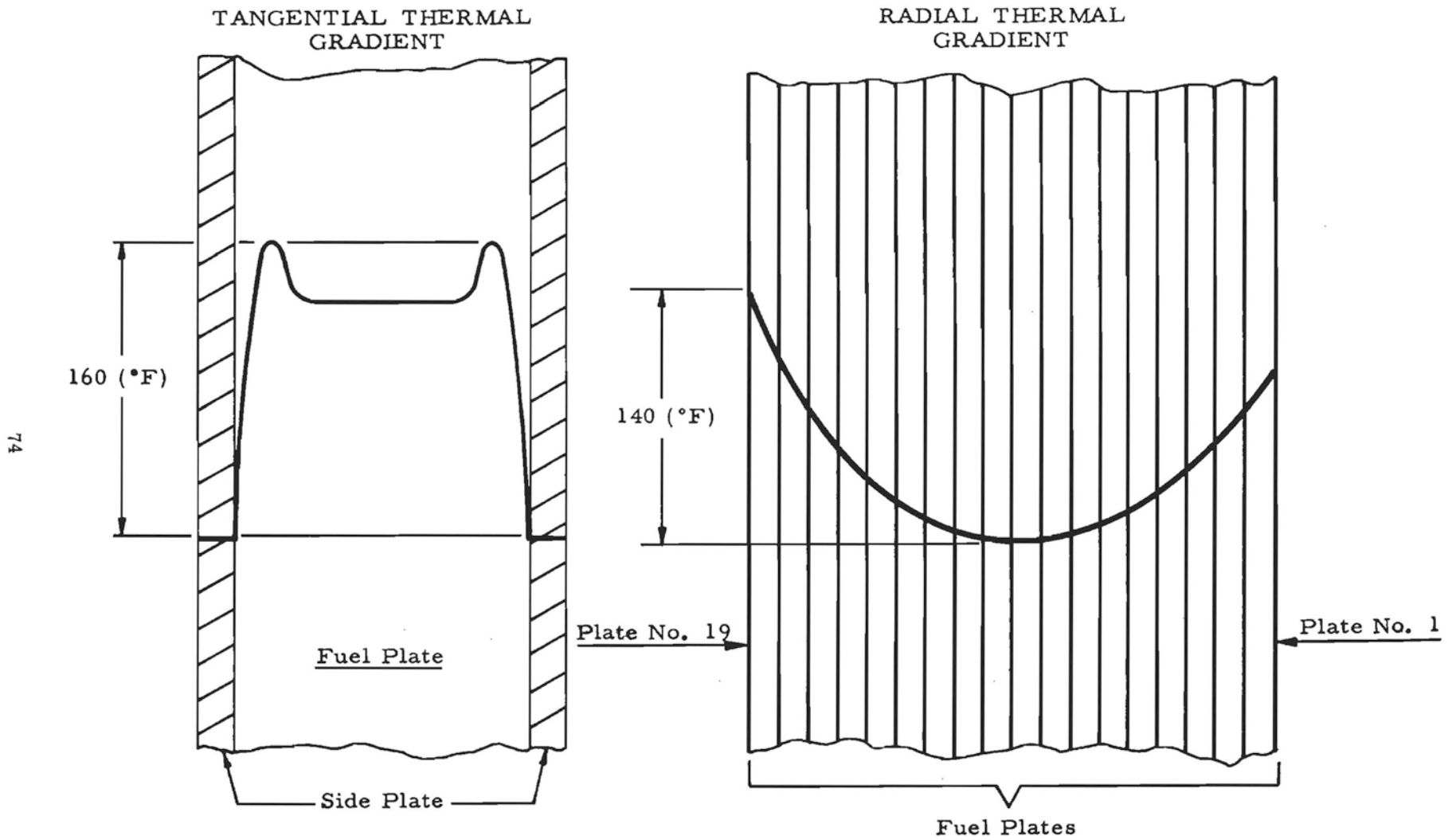


Fig. VIII: Thermal Gradients

THE THERMAL AND HYDRAULIC DESIGN OF THE ADVANCED TEST REACTOR

W. M. Vannoy

The Babcock and Wilcox Company

The Advanced Test Reactor (ATR) has a maximum power density of 2.6 MW/liter of core volume, or about twice the power density of the Engineering Test Reactor (ETR). Most thermal and hydraulic design problems are caused by the high power density and the coolant velocities required for adequate heat removal. The ATR design takes advantage of MTR and ETR experience to improve performance and reduce uncertainties in design calculations. Test programs are being conducted to investigate uncertain areas extending beyond current technology, but final results are not yet available. Discussed here are design features, calculations, and the scope and objectives of test programs affecting the thermal and hydraulic performance of the ATR fuel elements and reactor internals.

During normal operation at 250 MW-t, the pressurized light water coolant enters the core at 300 psig and 130 F, and leaves at 208 psig and 169 F. Figure 1 shows the coolant flow path. The coolant enters the reactor vessel through two 24-inch pipes, and approximately 95% flows upward through the thermal shields. The remaining 5% is diverted into the large space between the core reflector tank and the inlet flow baffle to provide a cool heat sink for natural circulation cooling of irradiated fuel elements stored in this region. Coolant from both paths flows into a large pool above the core, then reverses; and flows downward through the fuel elements, reactor internals, and irradiation facilities. A flow distribution tank beneath the core separates the flow into four quadrants; the coolant exits through four 18-inch outlet pipes.

The high core power density and the compact arrangement of the internals (Fig. 2) result in high gamma heating rates in the reactor components. Temperature gradients, average temperatures, pressure

differentials, and hydraulic forces are calculated for use in the stress analyses of reactor internals. These calculations are made for steady-state operation with equal lobe power and with the maximum shift of power between lobes (60-50-40), for normal transients, and for accident conditions. The coolant flow rates shown in Table 1 are sufficient to prevent local boiling and unacceptable thermal distortions.

Table 1. Reactor Flow Distribution

<u>Reactor region</u>	<u>Flow rate, gpm</u>
Fuel elements	25,800
Reflector blocks	1,890
Reflector control cylinders	6,040
Neck region	270
Flux traps	6,000
Inner capsule irradiation facilities	600
Between reflector and tank	1,145
Seal and syphon breaker leakage	1,110
Outer capsule irradiation facility	1,200
Total	<u>44,055</u>

Ample allowance is made for excess cooling capacity since the expected cooling requirement is 44,000 gpm and the three primary coolant pumps have a combined capacity of 54,000 gpm. There is also a standby pump rated at 18,000 gpm. The fuel element flow rate in each quadrant of the core is determined from pressure drop measurements calibrated against flow tests. The primary coolant flow rate is adjusted to the required value by a motor operated butterfly-type valve that is positioned before reactor startup. Decay heat removal is provided by two emergency coolant pumps, each with a capacity of 4500 gpm or a combined capacity of not less than 5400 gpm.

Table 2 shows some of the significant parameters related to the core thermal and hydraulic performance. The performance of the hot

channel, which is of principal design concern, assumes that the worst possible combination of manufacturing and operational tolerances exists where the power peaking is at a maximum.

Table 2. ATR Thermal and Hydraulic Parameters

Reactor power, MW-t	250
Maximum power density, kw/liter	2600
Operating pressure — core inlet, psig	300
Coolant flow rate, gpm	44,000
Coolant velocity in fuel elements, fps	44
Core pressure drop, psi	92
Coolant temperature — reactor inlet, F	130
Coolant temperature — reactor outlet, F	169
Core heat transfer area, ft ²	1390
Average heat flux, Btu/hr-ft ²	570,000
Maximum heat flux, Btu/hr-ft ²	1,920,000
Horizontal power peaking factor	2.0
Axial power peaking factor	1.4
Maximum surface temperature — hot spot, F	408
Burnout power, % design power	138

Hot channel calculations are based on a horizontal power peaking factor of 2.0 and a vertical power peaking factor of 1.4. Power distribution measurements from the B&W Critical Experiment Laboratory will be used in the final design analysis. Operating procedures provide for power distribution measurements for each core loading at the on-site critical facility. During operation, the power generated in each quadrant is measured, and the control system permits the power level in each lobe to be regulated independently. The vertical motion of the control poisons is limited to preserve a cosine vertical power distribution throughout a cycle.

ATR hot channel factors (Table 3) are estimated from MTR and ETR experience. Hot channel factors related to manufacturing tolerances will be modified on the basis of the results of the Fuel Element Development Program at Oak Ridge National Laboratory. At present, the heat transfer coefficient is calculated by the Colburn equation with a 1.25 safety factor. Heat transfer data from ETR, HFIR, and ATR test programs are being correlated against the Colburn, Hausen, and Sieder-Tate equations in an effort to minimize the uncertainty in the heat transfer coefficient for ATR conditions. The channel velocity distribution will be measured in the Flow Distribution Test at ORNL, and the hot channel factors will be modified accordingly.

Figure 3 shows the bulk coolant and fuel plate surface temperatures (at the beginning of life) obtained with the hot channel factors in Table 3 and a horizontal power peaking factor of 2.0. This power peaking factor exists locally near the edge of a single fuel plate; the power generation rate decreases with distance from the edge of the plate. The hot channel calculations, therefore, conservatively neglect any mixing of the coolant with respect to coolant temperature rise. Heat flow by conduction from the fuel plate to the side plate is also neglected.

The maximum permissible power of the ATR is calculated to be 138% of normal power at the onset of bulk boiling in the hot channel. The increased flow resistance due to steam formation in the hottest channel of the parallel-channel arrangement causes a flow reduction, and vapor binding may occur. This condition is illustrated in Figure 4, which shows the pressure drop versus flow characteristics of the hot channel for three different power levels. The plenum-to-plenum pressure drop, shown as the available head, is the same for each of the parallel fuel element channels. At 100% power, the hot channel has single-phase flow and a flow rate essentially the same as the other channels. At 118% power, local boiling begins in the hot channel, and the increased flow resistance causes a flow reduction. At 138% power, the pressure drop curve is tangent to the available head curve at point A, and a flow instability is probable. At power levels above 138%, the pressure drop curve intersects the available head curve at point C only, indicating a large flow reduction and probable vapor binding.

TABLE 3. ATR HOT CHANNEL FACTORS

	F_{Θ} (Film drop)	$F_{q''}$ (Heat flux)	$F_{\Delta T}$ (Coolant temp. rise)
<u>Manufacturing tolerances</u>			
Channel geometry	1.041	1.0	1.155
Surface roughness	1.015	1.0	1.018
Fuel content			
Local	1.10	1.10	1.0
Channel	1.0	1.0	1.04
Fuel heat transfer area	1.04	1.04	1.0
Fuel eccentricity	1.0	1.0	1.0
Sub-products	1.209	1.144	1.223
<u>Calculational factors</u>			
Film coefficient correlation	1.25	1.0	1.0
Plenum distribution	1.04	1.0	1.05
Channel velocity distribution	1.04	1.0	1.05
Sub-products	1.352	1.0	1.103
<u>Operational factors</u>			
Power measurement and regulation	1.05	1.05	1.05
Flow control	1.016	1.0	1.02
Inlet temperature regulation			+ 3 F
Sub-products	<u>1.067</u>	<u>1.05</u>	<u>1.071</u>
Total products	1.744	1.201	1.445

It is possible that a flow instability or burnout could occur before bulk boiling occurs in the hot channel. A flow instability may be initiated by the increased flow resistance caused by local boiling, or sub-cooled burnout may be caused by film blanketing when steam bubbles form so rapidly that they coalesce on the surface. Local boiling pressure drop and sub-cooled burnout data for ATR pressure, geometry, flow rate, and heat flux are not available. Therefore, the objectives of the heat transfer tests at the Argonne National Laboratory are to determine the method and magnitude of the power limitation.

The burnout and flow stability tests are designed to simulate as closely as possible ATR operating heat flux, pressure, coolant velocity, coolant temperature, channel thickness, and power distribution. The power generation rate in the test specimen has a cosine distribution, and the bypass flow rate is approximately ten times the specimen flow rate to maintain a constant pressure drop across the test section and simulate the parallel-channel effect. Tests are being made on full-length (48 inches) rectangular specimens with nominal channel thicknesses of 0.054, 0.072, and 0.094 inches.

Thermal design analyses include investigations of possible fuel element damage during accidents, such as a loss of flow and a loss of pressure. The loss of flow accident is illustrated in Figure 5. A scram is required to protect the reactor since a burnout condition will occur in 460 milliseconds if the power is not reduced. The voltage monitoring and flow sensing devices initiate a scram signal, and rods will start to insert in 340 milliseconds to prevent fuel element damage. Burnout tests are being run at reduced pressure and flow to obtain data applicable to the loss of flow and loss of pressure accidents.

The structural integrity of the fuel element depends on thermal and hydraulic conditions. Thermal gradients, hydraulic forces, and lateral pressure differentials cause fuel element stresses. Also, the strength and corrosion properties of the fuel elements are temperature dependent.

Lateral pressure differentials are caused by differences in the dimensions of two adjacent coolant channels. Tolerances on the fuel element and its annulus allow the flow channel between the fuel element and the beryllium reflector to vary between approximately 0.060

and 0.200 inches. The effect of a large external channel is shown in Figure 6. The external channel has a larger hydraulic diameter and less frictional resistance than the adjacent internal channel. For the same over-all pressure drop across both channels, the external channel, therefore, must have a higher coolant velocity and entrance loss that will result in a lateral pressure differential. The magnitude of the lateral pressure differential for different external channel dimensions is being measured in flow tests at ORNL. Deformation of the outside fuel plate tends to reduce the lateral pressure differential; but, if fuel plate deformation is excessive, minor modifications of the fuel element will be studied experimentally. Possible modifications fall into three basic categories: (1) increasing the flow resistance of the external channel, (2) reducing the entrance loss to the external channel, and (3) equalizing pressure by interconnecting external and internal channels.

A fuel plate ripple will also cause a lateral pressure differential. A local ripple, acting like a Venturi, causes a decrease in static pressure in the reduced channel and an increase in static pressure in the enlarged channel. Fuel plate deformation tends to increase the lateral pressure differential in this case. The effect of ripples is being determined in the hydraulic tests at ORNL.

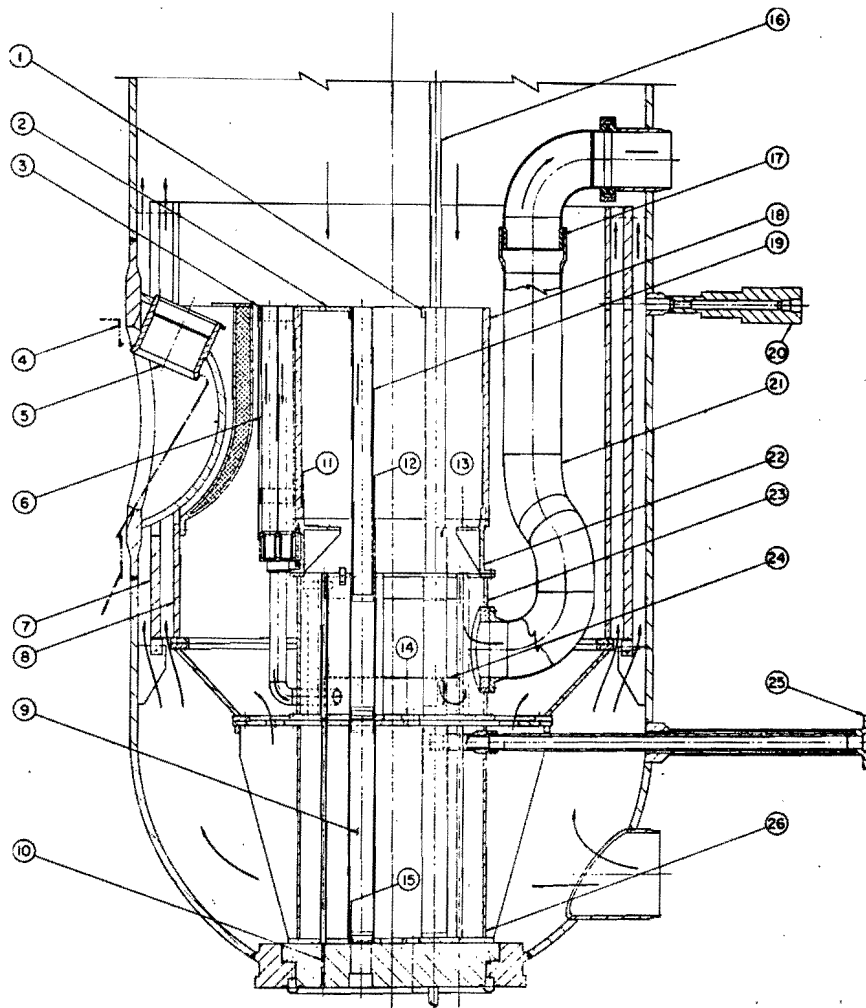
Since the existence of the temperatures calculated from hot channel analyses is statistically improbable, a more realistic appraisal of fuel plate temperatures is necessary to determine fuel plate stresses and corrosion rates. Corrosion tests show that the corrosion rate increases exponentially with the metal surface temperature. Corrosion tests with descending heat rates to simulate fuel burnup show that, with an initial metal surface temperature of 360 F, the end of life temperature exceeds 430 F due to film buildup. Whereas, an initial temperature of 340 F results in an end of life temperature of less than 400 F. However, corrosion film stripping does not occur in either case.

Fuel plate temperatures for the mechanical design are calculated from the detailed power distribution and a statistical treatment of hot channel factors. Figure 7 shows the maximum fuel plate surface area that may be expected to be above 340 F on the outside fuel plate of the hottest element. This fuel plate has the maximum temperature, lateral pressure differential, and span. Structural integrity depends on the

fuel plate area at a given temperature, the distribution of this area, and the distribution of stress with relation to the temperature distribution.

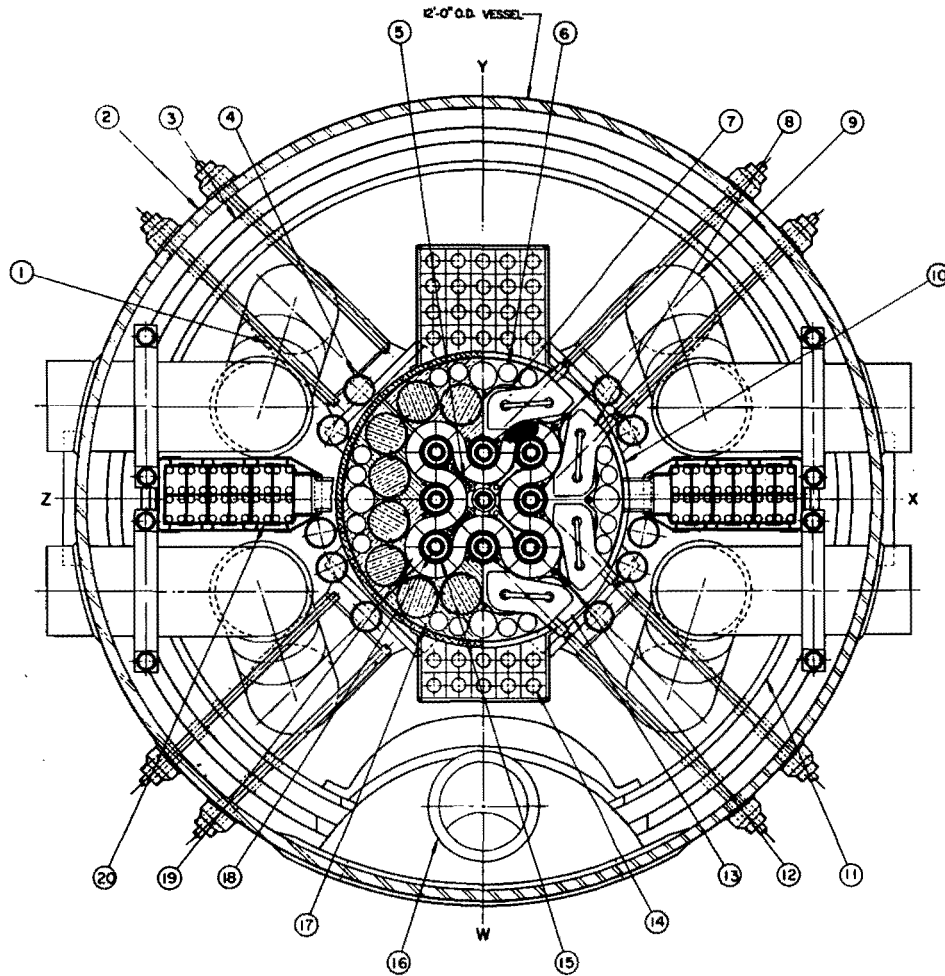
A similar analysis of the entire core shows that less than 40 square inches of heat transfer surface can be expected to be above 340 F, and an insignificant area is above 360 F at the beginning of life. Descending heat rate corrosion tests show that film stripping does not occur on either X-8001 or 6061-0 aluminum cladding with a starting temperature of 360 F. Therefore, any addition of activity to the primary system through film stripping cannot be detected.

In summary, the major problems in the thermal and hydraulic design are caused by the high power density and high coolant velocities. The operational features of the ATR design that allow an improved performance are excess flow capability and flow control, power and flow measurements for each quadrant of the core, independent control of lobe power, limited vertical motion of control poisons, and an on-site critical facility. The major uncertainties in the thermal and hydraulic design are being investigated in heat transfer and hydraulic tests. The final design of the ATR will be strongly guided by the results of these tests.



1. Attachment to Neck Shim Housing
2. Gear Box Support Plate
3. Outer Capsule Irradiation Facility (Aluminum)
4. Canal Liner
5. Drop Tube
6. Outer Reflector Blocks (Aluminum)
7. Thermal Shield
8. Inlet Flow Baffle
9. Safety Rod Cavity
10. N-16 Sample Tube Penetration
11. Beryllium Reflector Support Point
12. Fuel Element Support Point
13. Outer Shim Control Cylinder Bearing Support
14. Neck Shim Housing support Point
15. Safety Rod Assembly Support Point
16. Pressure and Insulation Tube Assembly
17. Thermal Expansion Joint
18. Core-Reflector Tank (Aluminum)
19. Flux Trap Baffle (Aluminum)
20. Outer Shim Drive Nozzle
21. Outlet Flow Pipe
22. Reflector Support Tank (Aluminum)
23. Flow Distribution Tank (Stainless Steel)
24. Flux Trap Coolant Plenum
25. Safety Rod Drive Nozzle
26. Core Support Tank (Stainless Steel)

Figure 1. Reactor Internals Elevation



1. Outer Shim Drive Shaft
2. Reactor Vessel
3. Thermal Shield
4. Instrument Thimble
5. Neck Shim Rod Housing
6. Inner Capsule Irradiation Facility
7. Outer Shim Control Cylinder
8. Outer Shim Gear Box
9. Outlet Flow Pipe
10. Core-Reflector Tank

11. Inlet Flow Baffle Assembly
12. N-16 Sample Tube
13. Outer Shim Gear Box Support Plate
14. Outer Capsule Irradiation Facility
15. Safety Rod
16. Drop Tube
17. Beryllium Reflector Block
18. Pressure Tube and Insulation Can Assembly
19. Fuel Element
20. Fuel Storage Rack

Figure 2. Reactor Internals Plan View

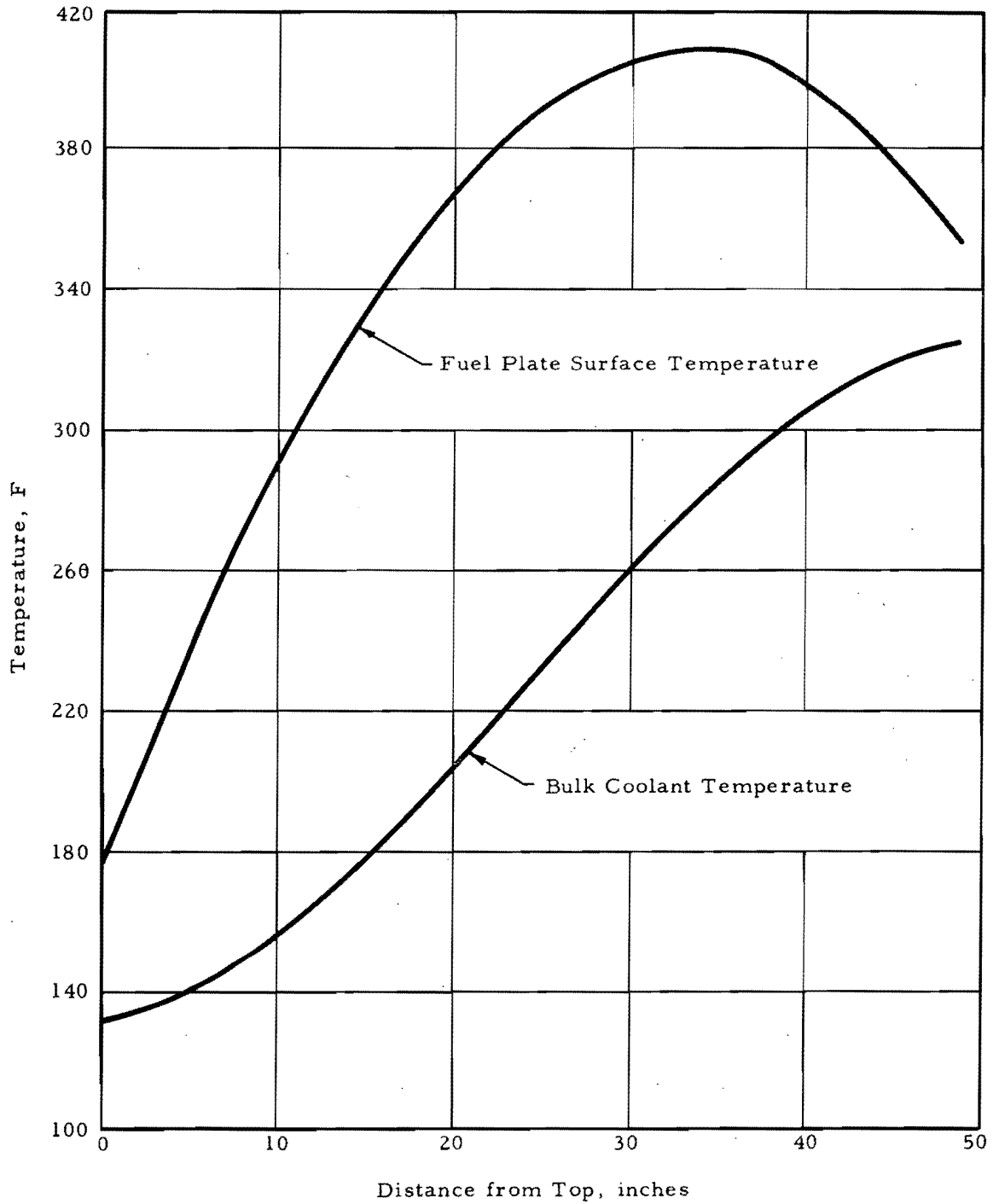


Figure 3. Temperature Vs Distance From Entrance to Hot Channel

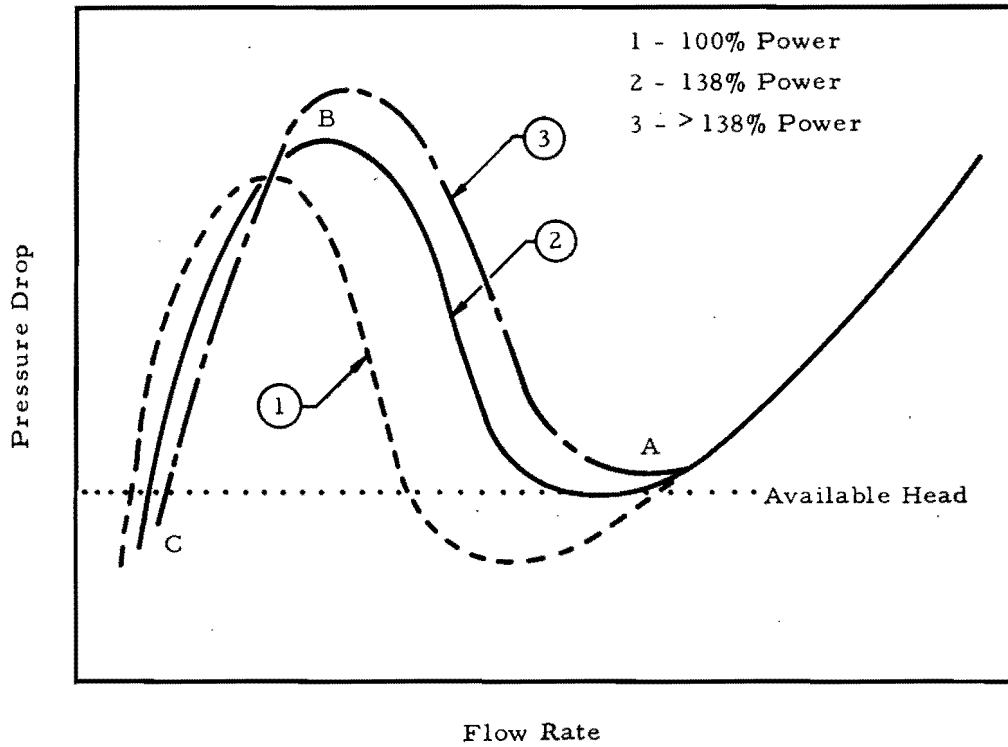


Figure 4. Effect of Boiling on Channel Pressure Drop

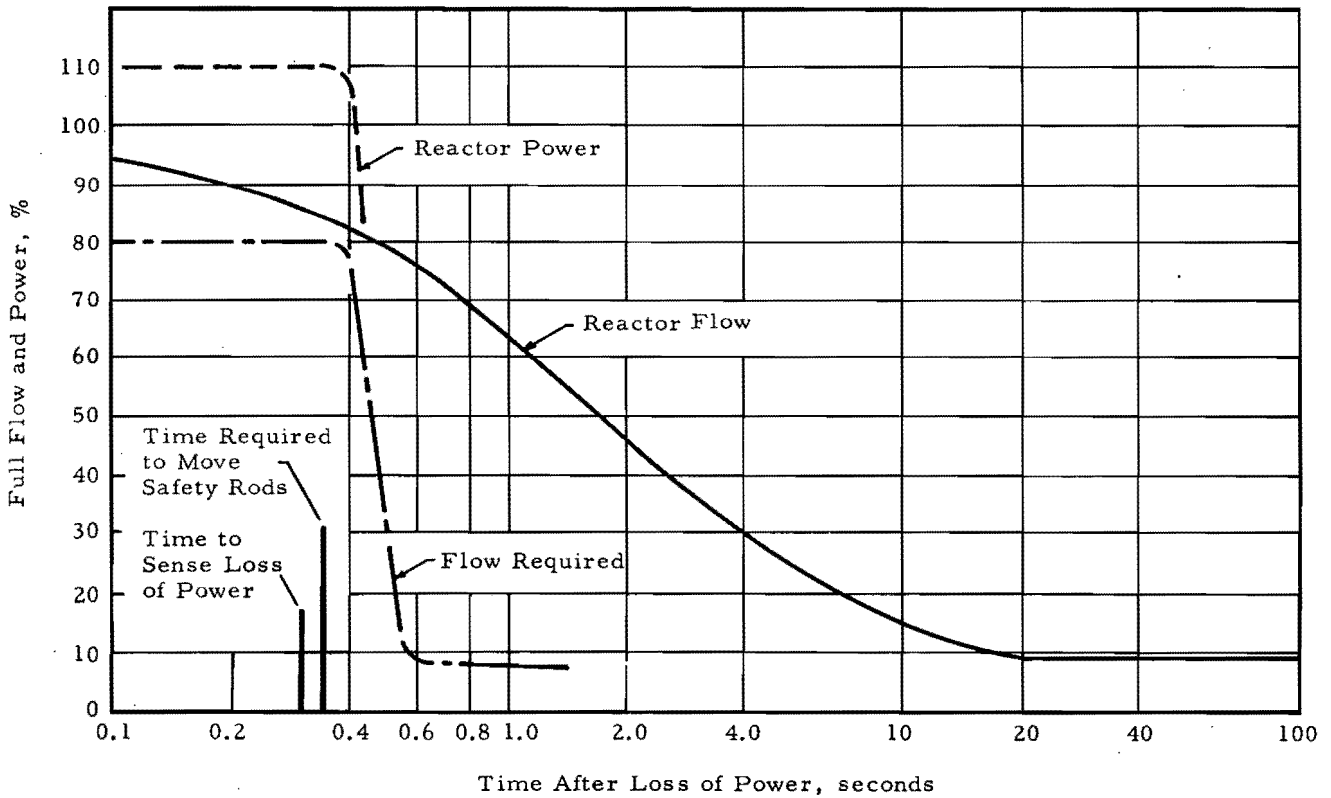


Figure 5. Loss of Power to Primary Coolant Pumps

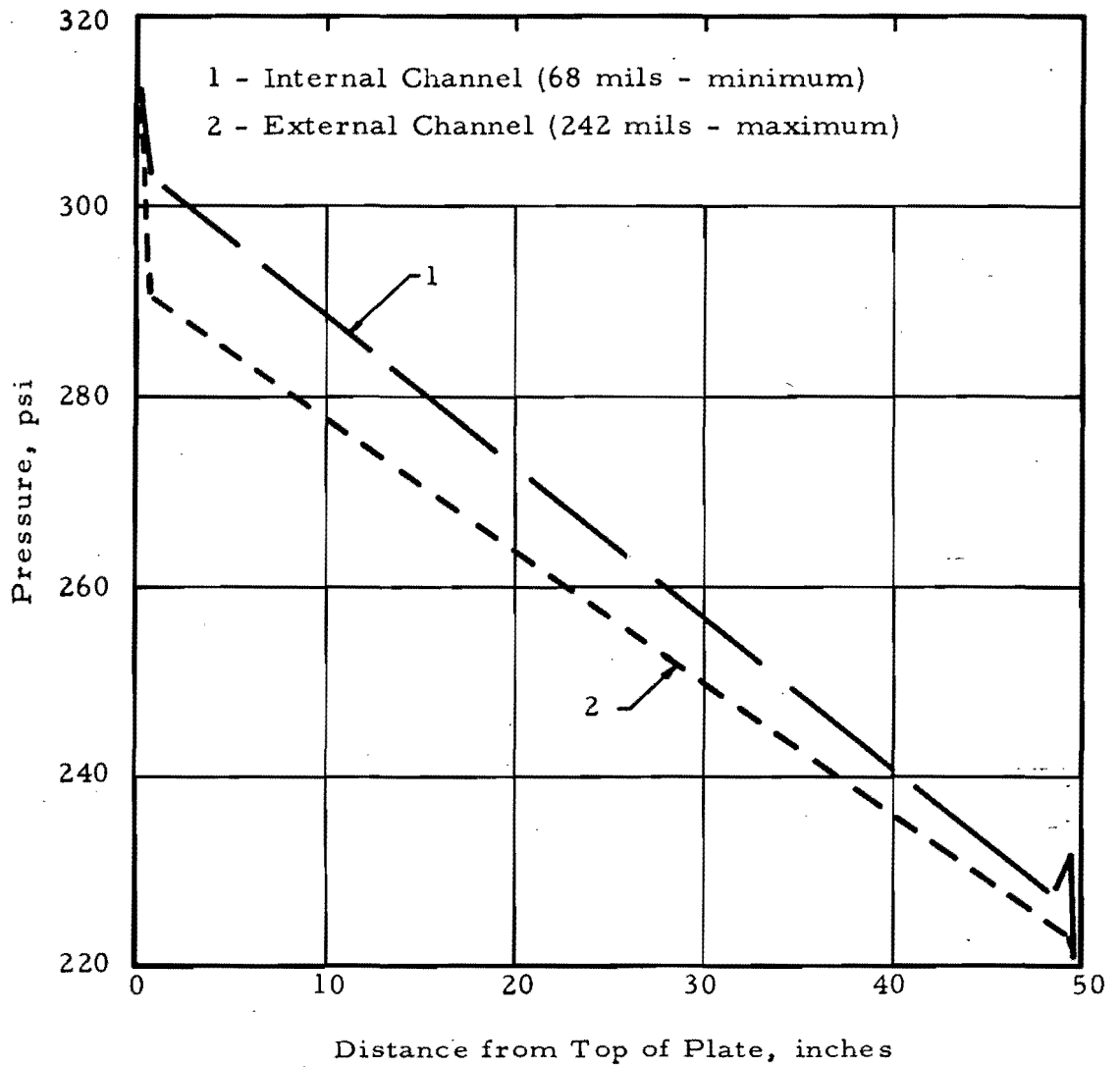


Figure 6. Lateral Pressure Differential Between Internal and External Channels

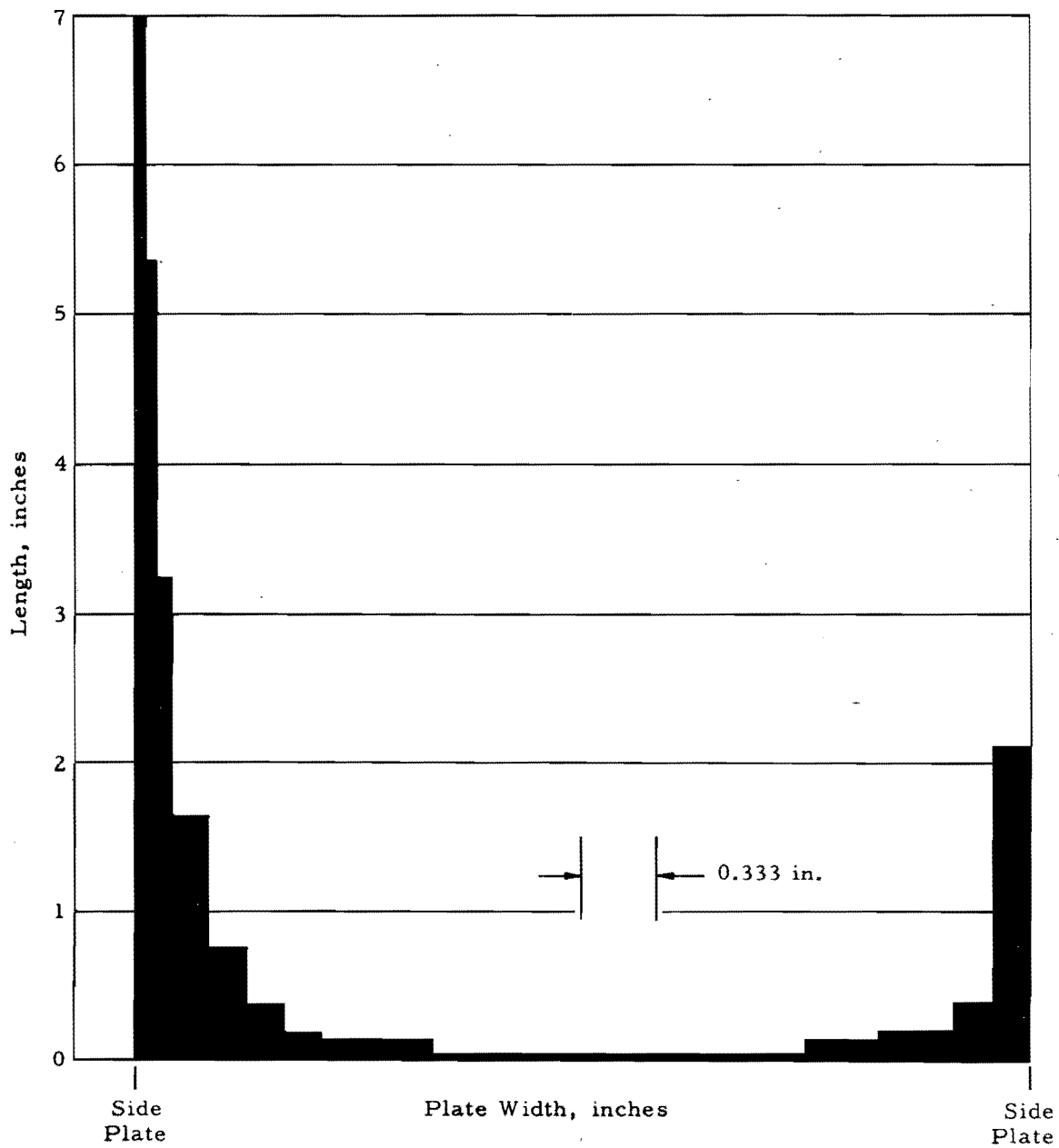


Figure 7. Distribution of Area Above 340 F for Most Critical Fuel Plate

NUCLEAR DESIGN OF THE HFIR

R. D. Cheverton
Oak Ridge National Laboratory
Oak Ridge, Tennessee

Although the present design of the High Flux Isotope Reactor (HFIR) provides considerable versatility in the form of readily accessible beam tubes, engineering irradiation facilities, rabbits, and a variety of reflector through-holes as shown in Fig. 1, the reactor was conceived for a single purpose - to produce, on a yearly basis, milligram quantities of Cf^{252} from a limited supply of Pu^{242} feed material. Preliminary survey analyses of transplutonium production schemes¹ and various reactor types² indicated that the use of a highly enriched, beryllium-reflected, aluminum-water, flux-trap type reactor, similar to that shown schematically in Fig. 2, and having a maximum unperturbed thermal-neutron flux of about 5×10^{15} neutrons/cm².sec in the "flux trap" (referred to as island), would be an economical and feasible way of achieving the desired production rates. The reactor power level required to obtain such a high neutron flux level was ~100 Mw, which, considering the reactor type proposed, appeared to be consistent with the capital funds available. As the concept was developed a nominal power level of 100 Mw became part of the design criteria; however, since the transplutonium production rates were found to be quite sensitive to the neutron flux level, as indicated in Fig. 3, con-

siderable emphasis was placed on achieving the highest island thermal flux that was practical. As a result of these efforts the present design of the HFIR represents a significant step forward in improving the performance (increased power densities and neutron fluxes) of aluminum-water reactors. For example, the maximum thermal-neutron flux in the island region and the total nonthermal-neutron flux in the fuel region are, respectively, 5×10^{15} and 4×10^{15} neutrons/cm².sec, the average steady-state power density is 2 Mw/liter, and the fuel-cycle time is ~15 days; in addition, it appears that a 1% reactivity addition can be made on a 50 msec ramp at any time during the fuel cycle without resulting in core damage. The purpose of this paper is to describe in general how this high performance is being achieved, with particular emphasis being placed on the unique features of the fuel element.

The high thermal flux in the central island region results almost entirely from the moderation of high energy neutrons that leak out of the fuel region into the highly moderating island region. The number of neutrons that leak into the island is essentially independent of the effective island diameter; however, the thermal neutron density and thus flux are strongly dependent upon the average distance required to slow the nonthermal neutrons down and also upon the volume in which they are slowed down. The two conflicting requirements of large volume to produce many thermal neutrons and reduce neutron leakage and of small volume to increase the neutron density and reduce thermal absorption lead to an optimum island diameter for a particular moderating material. By comparison with commonly used moderating materials such as heavy water, graphite, and beryllium, the use of light water in the island results in the greatest value of peak thermal flux per unit of power because of its considerably shorter slowing down distance. Of course the optimum volume of a light water island is smaller than for the other moderators, but it is adequate for the Pu²⁴² targets that will be irradiated in the island region of the HFIR.

Another factor that directly effects the neutron density in the island is the neutron leakage into the island per unit height of the core. For a given power level this leakage depends on two basic factors: the neutron population in the core per unit height of the core and the probability that these neutrons will leak into the island region. For a given core volume, decreasing the core height increases the neutron population per unit height but decreases the probability of leakage into the island. Therefore, there is an optimum height-to-diameter ratio for the core.

The probability of leakage into the island is also increased by decreasing the volume of the core and by increasing the metal-to-water ratio in the core, thus reducing the moderation in the fuel region. A further improvement can be made on a per unit power basis by peaking the power density next to the island; however, as the relative peaking is increased, the power level and thus neutron flux must be lowered so as not to exceed the maximum permissible power density. If the volume of the core is increased to maintain the same power level, the island flux decreases as explained above. Thus, one of the primary objectives in the HFIR design was to increase the average power density and metal-to-water ratio as much as possible while maintaining a 100-Mw power level.

One of the most fruitful ways of increasing the average power density is by reducing the ratio of maximum-to-average power density, $(q_{\max}/q_{\text{ave}})$. For this purpose cylindrical core geometry was selected in lieu of rectangular geometry, reducing $(q_{\max}/q_{\text{ave}})$ by about 35% relative to that obtained with the latter geometry.³ The use of reflector control in the form of two concentric, oppositely driven, cylindrical control plates located in a narrow annulus between the fuel and beryllium reflector and containing an axially graded poison, as shown schematically in Fig. 4, resulted in an estimated 50% decrease in $(q_{\max}/q_{\text{ave}})$ relative to that achieved with rods that are located in the fuel and enter the core from one end only. Also, axial power density peaking caused by excessive neutron moderation at the ends of the core was controlled by extending the non-fuel-bearing portion of the fuel plate a short distance.

Power distribution control during the fuel cycle was supplemented by the use of burnable poisons, which were also used for reactivity control.

The above devices all affect the power distribution through their effects on the flux distributions. Further major benefits in power distribution control were achieved through the use of a radially graded fuel concentration. Since the power density at a point is nearly proportional to the product of the thermal-neutron flux and fuel density, the radial power distribution achieved with a uniform fuel distribution would be similar to the radial thermal neutron flux distribution shown in Fig. 2. In principal, by using a radial fuel distribution that is nearly the mirror image of the thermal flux distribution the radial $(q_{\max}/q_{\text{ave}})$ could be reduced to unity. This scheme, which was achieved by varying the thickness of the fuel-plate cores across the width of the radially oriented involute-shaped fuel plates, as shown in Fig. 5, reduced the radial $(q_{\max}/q_{\text{ave}})$ from about 3 to 1.2. A value of unity could not be achieved because of flux and fuel distribution variations associated with control rod movement and nonuniform fuel burnup during the fuel cycle.

Application of the above methods for reducing $(q_{\max}/q_{\text{ave}})$ in the HFIR design resulted in an overall $(q_{\max}/q_{\text{ave}})$, excluding hot-spot effects, of about 1.5.

Additional benefits are realized in reducing $(q_{\max}/q_{\text{ave}})$ by very carefully controlling the power-density and heat-flux variations that result from fabrication inaccuracies. In order to significantly reduce the associated statistical safety factor, HFIR fuel-plate specifications include 100% inspection to check on fuel inhomogeneity, fuel contour, and lack of bonding of the cladding.

Another general method of increasing the permissible power density is to increase the surface-area-to-volume ratio or to increase the maximum permissible heat flux or both. What could be accomplished in these respects for the HFIR design was defined only after much trial and error analysis that involved many interrelated parameters, such as fuel plate strength and creep behavior, coolant velocity and associated hydraulic lateral pressures, manu-

facturing tolerances, burnout behavior during steady-state and transient conditions, oxide film formation rates and associated thermal resistance, and control and safety system characteristics, to mention a few. A very significant amount of uncertainty associated with several of the individual factors in the analytical analysis was eliminated by extensive experimental investigations and measurements of the nuclear kinetics' constants, fuel-plate stability and creep behavior, aluminum-oxide formation rate, fabrication tolerances, burnout heat flux, and the water-film heat transfer coefficient. The core design that resulted from these studies consisted of two cylindrical fuel annuli each about 3 in. in radial thickness containing 0.050-in.-thick involute-shaped fuel plates and 0.050-in.-thick coolant channels; the active height of the core was 20 in. and the coolant velocity 42 ft/sec. By using an essentially single-fuel-element core design with involute plates, instead of circular-segment plates in numerous pie-shaped elements, about 13% excess side-plate volume was eliminated.

As indicated in Fig. 2, a water annulus about $3/8$ in. thick has been provided between the two fuel annuli. There were primarily three reasons for doing this: (1) to help flatten the thermal flux distribution and thus lessen fuel distribution difficulties, (2) to increase neutron multiplication, and (3) to facilitate assembly and disassembly of the two fuel annuli. The width of the water gap selected was a minimum (consistent with the minimum flux flattening and neutron multiplication requirements) because excess water in the fuel reduces neutron leakage to the island.

The fuel loading required for an average fuel-cycle time of about 15 days is 9.4 kg of U^{235} , 2.3 kg of which is in the inner annulus. The reactivity associated with this loading is $\sim 0.15 \Delta k/k$. A burnable poison, tentatively composed of boron and cadmium and located in the fuel-plate core filler piece in the inner fuel annulus as shown in Fig. 5, reduces the maximum core worth during a fuel cycle to about $0.11 \Delta k/k$; this poison, distributed as indicated, also helps to maintain a uniform power distribution during the fuel cycle.

The large excess neutron multiplication associated with the core is controlled by positioning the two 1/4-in.-thick control cylinders symmetrically in the axial direction, thus minimizing the "roof topping" effect. Axial variations in the power distribution are further reduced by dividing the control cylinders into three axial regions: a highly absorbing region on one end (20 in. long) containing Eu_2O_3 dispersed in and clad with aluminum, a medium absorbing region (about 7 in. long) containing tantalum dispersed in and clad with aluminum, and a low absorbing region of aluminum (20 in. long) on the other end. The outer control cylinder is physically divided into four equal circular segments, each having a shim drive rod and scram mechanism; the inner control cylinder, which is not equipped with a scram mechanism, is used for both shim and regulation. With three of the outer control segments completely inserted, the fourth completely withdrawn, and the inner control cylinder completely withdrawn, the reactor will be subcritical by a minimum of $0.03 \Delta k/k$.

The adequacy of the HFIR design from a heat removal point of view is reflected in the amount of conservatism inherent in the hot-spot analysis,⁴ which considered the occurrence of the most pessimistic combination of hot-spot factors. The HFIR critical experiments verify that a peak thermal-neutron flux of about 5×10^{15} neutrons/cm².sec can be achieved at a power level of 100 Mw; and fuel-element development work thus far indicates that the unusually tight dimensional and fuel distribution tolerances can be attained. Therefore, it appears that the high performance desired in the HFIR will be achieved.

References

1. H. C. Claiborne and M. P. Lietzke, Californium Production in the High Flux Isotope Reactor, ORNL CF-59-8-125 (August 1959).
2. R. D. Cheverton, HFIR Preliminary Physics Report, ORNL-3006 (Oct. 4, 1960).
3. S. M. Feinberg et al., An Intermediate Reactor for Obtaining High Intensity Neutron Fluxes, Geneva Conference Paper 2142 (1958).
4. N. Hilvety and T. G. Chapman, Summary of HFIR Hot-Spot Studies, personal communication (January 1962).

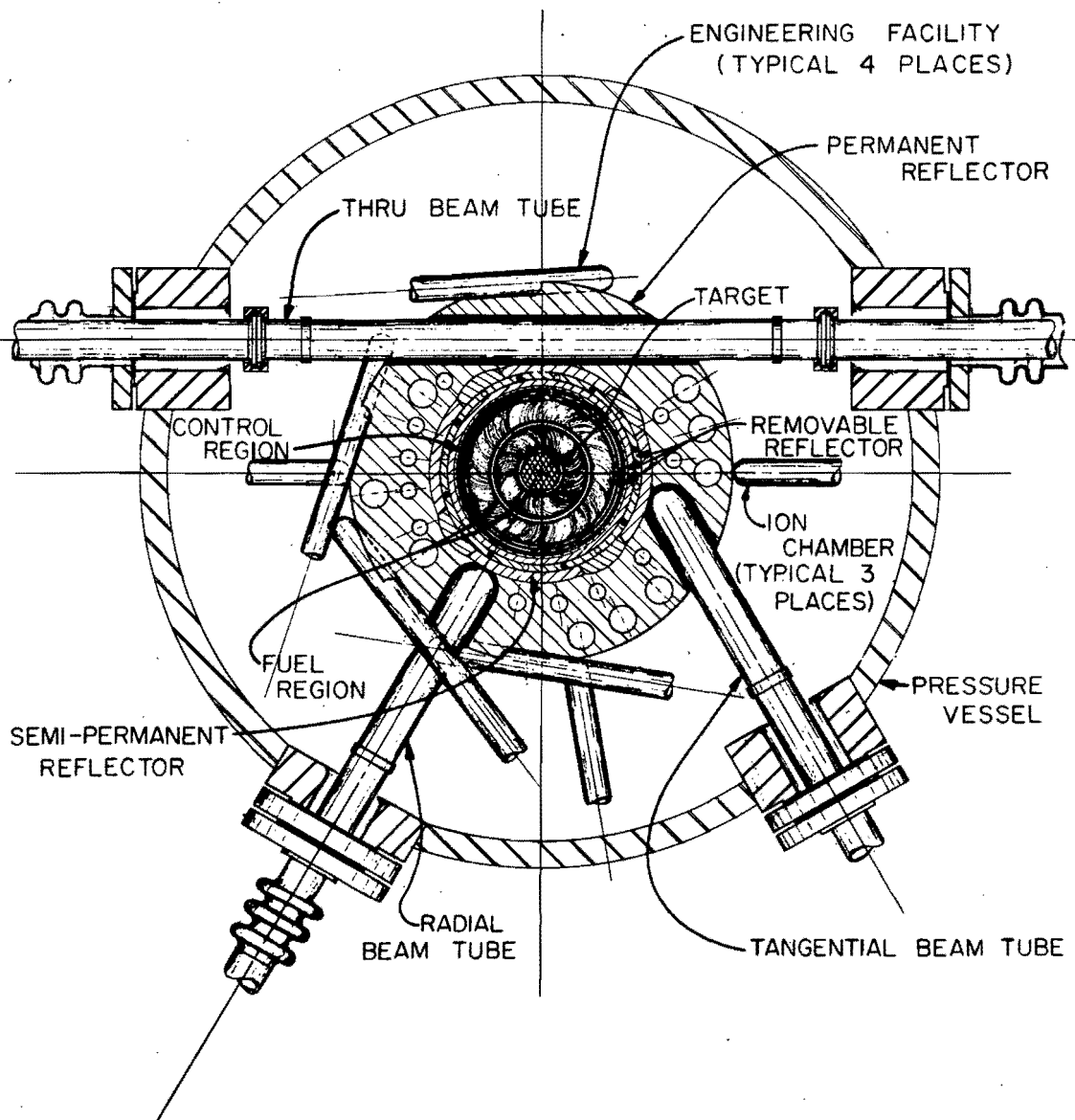


Fig. 1. Horizontal Cross Section Through HFIR Core and Pressure Vessel

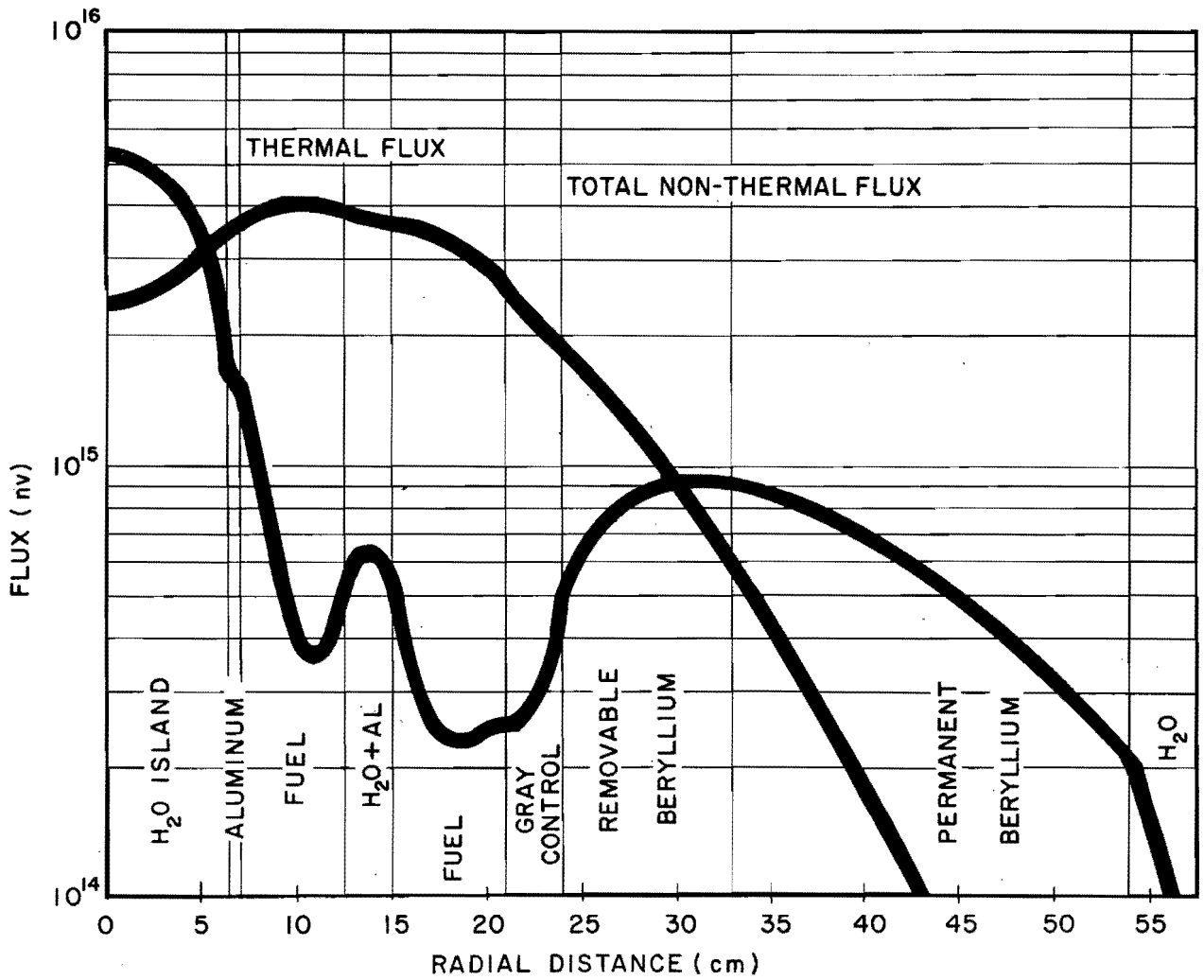


Fig. 2. Neutron Flux at Horizontal Midplane of Clean HFIR Core

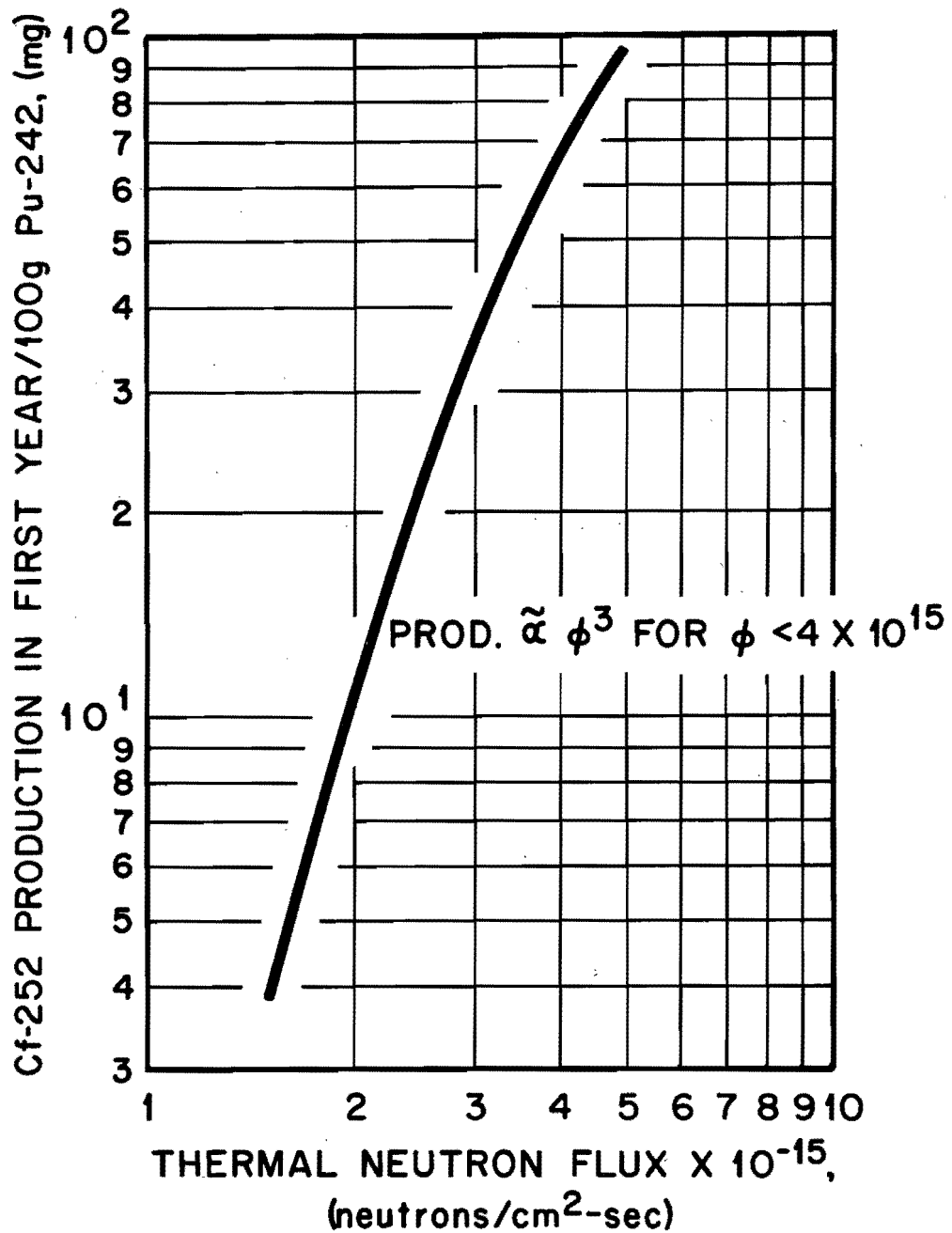


Fig. 3. Total Production of Cf-252 from Pu-242 During the First Year of Irradiation as a Function of Thermal Flux Level

GRAY
 WHITE
 BLACK

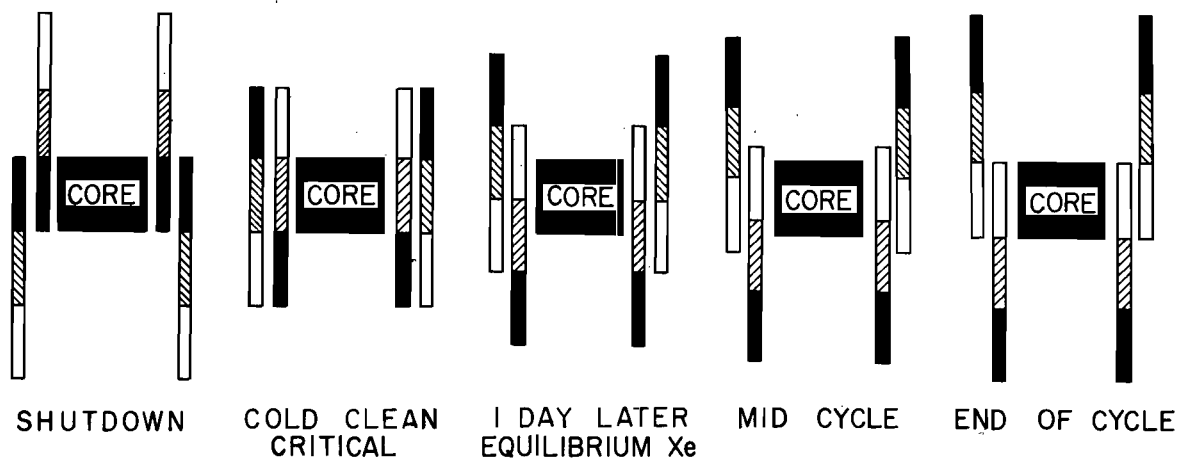


Fig. 4. Schematic Representation of HFIR Cylindrical Control Plates

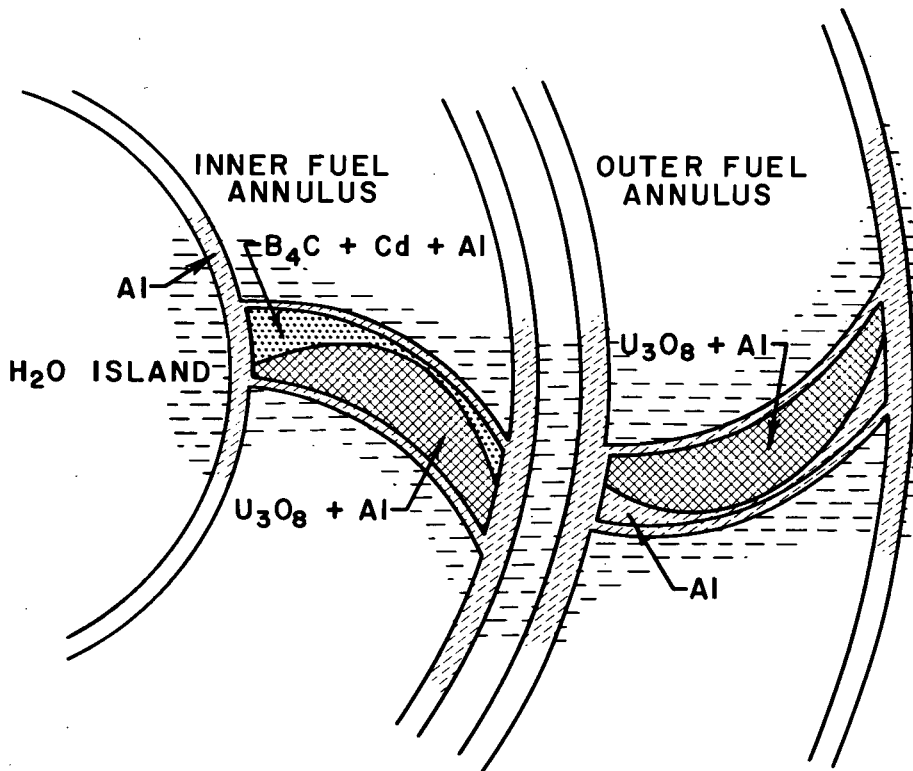


Fig. 5. Schematic Representation of Core Cross Section, Showing Fuel Contours

MECHANICAL AND HYDRAULIC DESIGN OF THE HFIR

By J. R. McWherter and T. G. Chapman

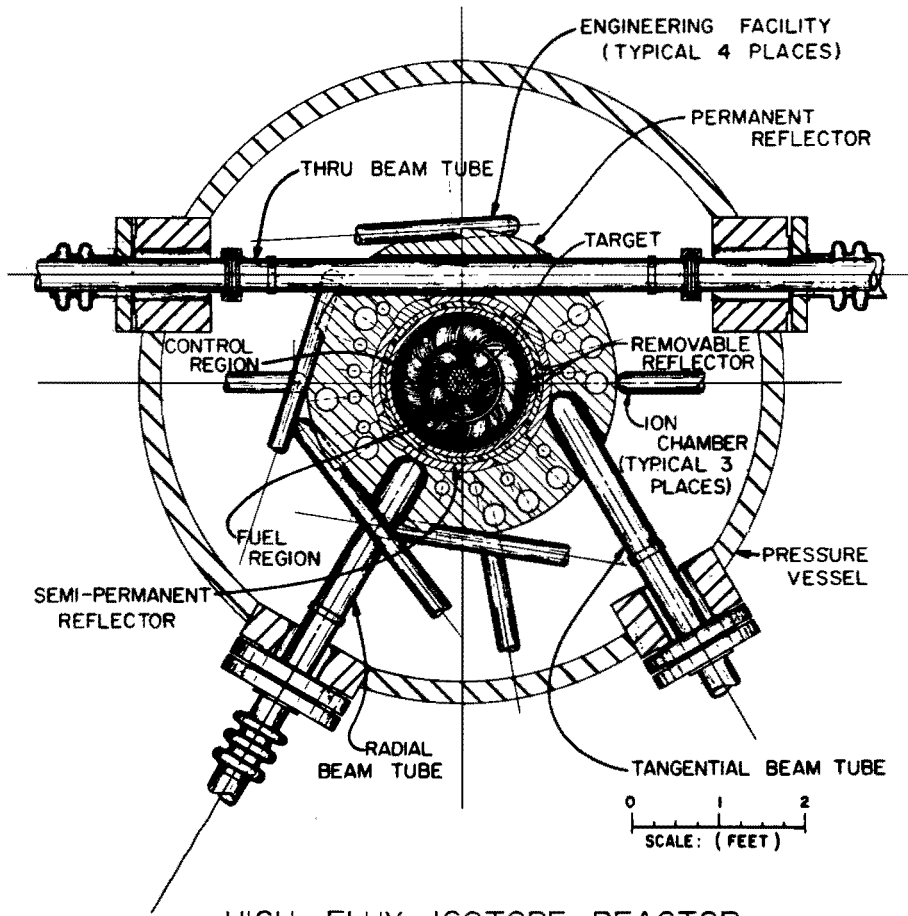
Oak Ridge National Laboratory
Oak Ridge, Tennessee

The High Flux Isotope Reactor is a light-water-cooled and -moderated reactor with an aluminum-clad plate-type fuel element and a beryllium reflector.¹ As shown in Fig. 1, the fuel element is cylindrical with a central target region. The 17-in.-diameter fuel element is separated from the 43-in.-OD, 24-in.-high reflector by a thin control region.

The core assembly is contained in an 8-ft-diameter pressure vessel;² where, as shown in Fig. 2, the core assembly is supported by concentric pedestals. The vessel has a quick-opening hatch in the large upper head through which underwater refueling is accomplished. The vessel is located in a water-filled pool in which the spent fuel is stored. A lower extension of the vessel penetrates the shielding below the reactor to permit operation of the control rods from a subpile room.

The coolant flow required to remove the heat from the reactor assembly is 15,000 gpm. The coolant enters near the top of the pressure vessel and leaves at the bottom. Approximately two-thirds of the water flows through the fuel element with a pressure drop across the element of about 70 psi. The water enters the fuel element at 120°F and leaves at 181°F.

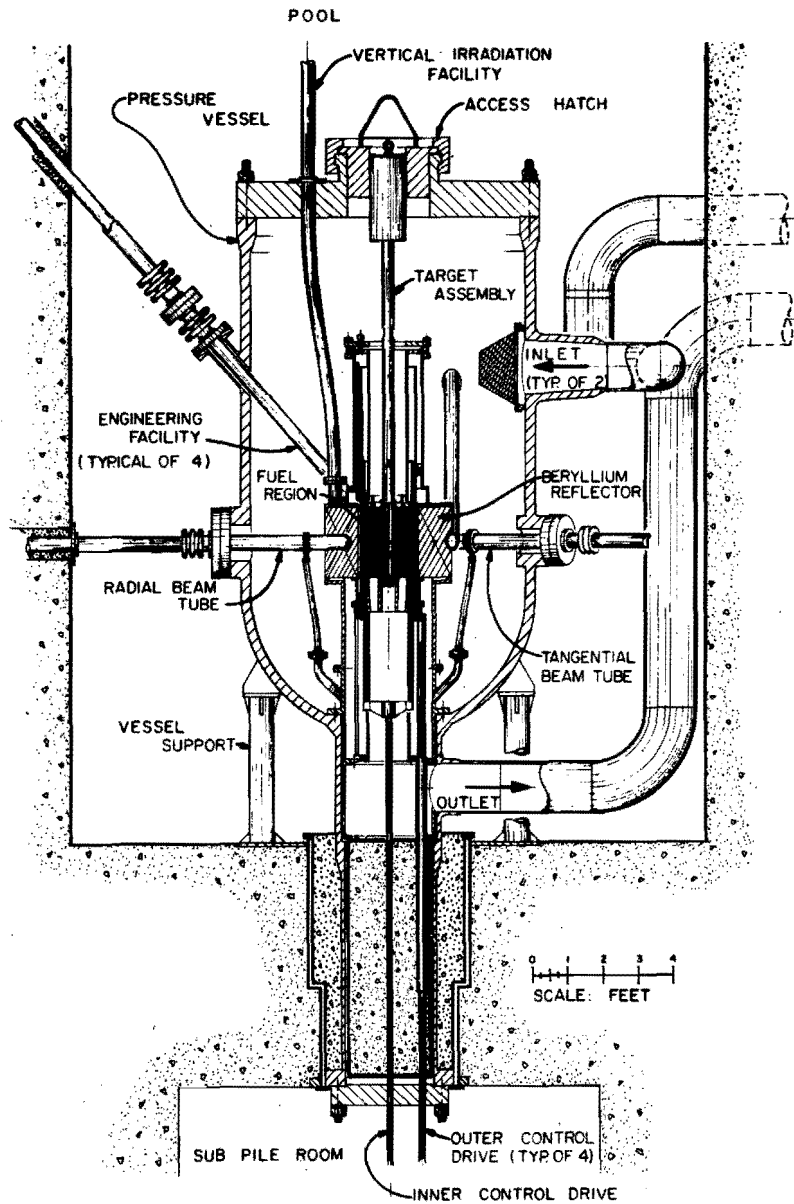
As shown in Fig. 3, the primary water is circulated through the reactor vessel by three centrifugal pumps in parallel. The heat is removed



HIGH FLUX ISOTOPE REACTOR

Figure 1

Horizontal Section Through Pressure Vessel



HIGH FLUX ISOTOPE REACTOR

Figure 2

Vertical Section Through Pressure Vessel

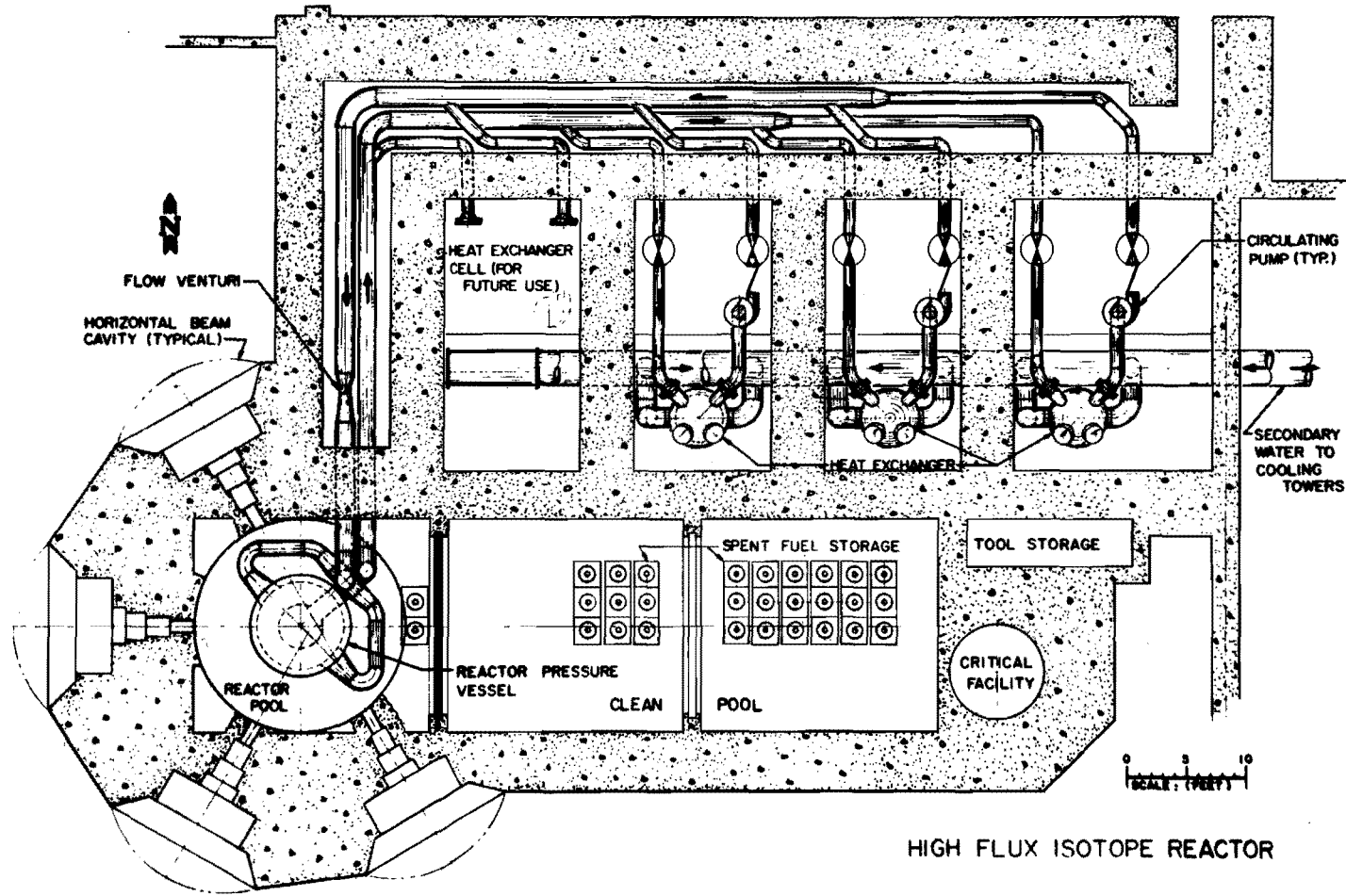


Figure 3
Reactor Shield, Heat Exchanger Cells, and Pool Structures
(Horizontal Section)

from the primary water in three tube-and-shell heat exchangers. The primary water system is designed for 1000-psi internal pressure and is constructed primarily of stainless steel or steel clad with stainless steel.

The mechanical, hydraulic and thermal design parameters of the fuel element were analyzed simultaneously in an effort to satisfy the stringent criteria set forth by the nuclear considerations. As a result of the extensive analysis, an element with an average power density of 2 Mw/liter and a metal-to-water ratio of unity was achieved. As shown in Fig. 4, the cylindrical fuel annulus was divided into two equal-thickness annuli containing 50-mil-thick involute-geometry fuel plates and 50-mil-thick coolant channels. The coolant design velocity is 42 ft/sec. The diameter of the light-water-filled central target region is approximately 5 in., the over-all diameter of the fuel region is about 17 in., and the active fuel length is 20 in., with an over-all fuel plate length of 24 in.

Some of the more important fuel element specifications that resulted from the nuclear design studies¹ are given below:

Power level	100 Mw
Power density (average)	Maximize
Length-to-diameter ratio	Fixed
Central water target region	~ 5 in.
Metal-to-water ratio	Maximize
Fuel cladding	Aluminum
Coolant	H ₂ O
Fuel distribution (radial)	Contoured
U ²³⁵ loading	9.4 kg
Fuel lifetime	15 days

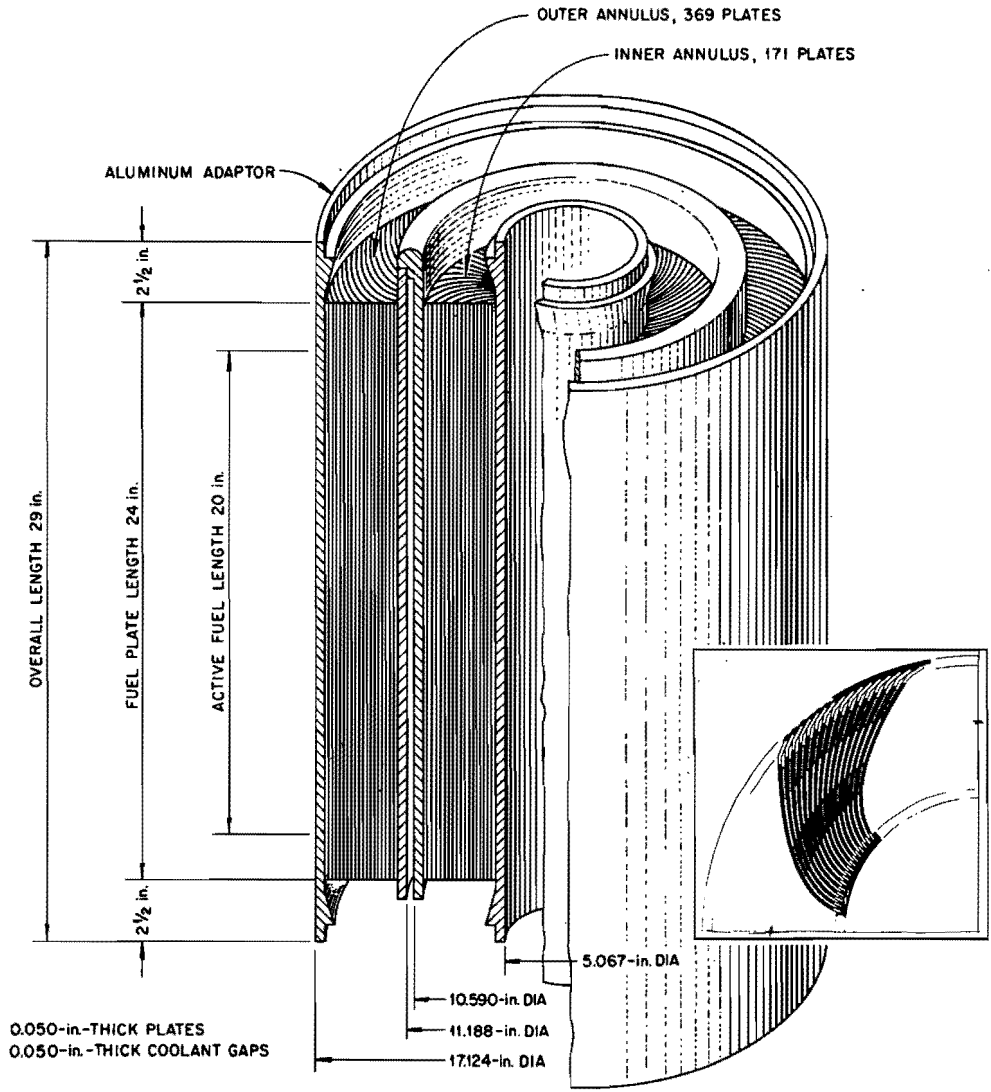


Figure 4

Dimensional Illustration of the Assembled High Flux Isotope
 Reactor Fuel Element

The parameters which could be varied in the mechanical, hydraulic, and thermal studies were:

1. The configuration of the heat transfer area.
2. The surface-to-volume ratio.
3. The coolant velocity.

Preliminary studies led to the choice of a plate-type element containing involute-geometry fuel plates. This configuration was selected primarily because it provided the following features:

1. A high surface-area-to-volume ratio.
2. A constant coolant channel thickness and uniform metal-to-water ratio in a cylindrical annular core.
3. The ability to vary fuel concentration radially.
4. Curved geometry is favorable from the standpoint of hydraulically and thermally induced fuel plate deflections.
5. All the plates within a single fuel annulus are identical.

The more important mechanical and hydraulic considerations included in the analysis of the fuel element were:

1. Hydraulically induced lateral pressure differentials across the fuel plates.
2. Radial and longitudinal thermal expansion of the fuel plates.
3. Tolerance requirements for manufacture of the fuel element.

Analytical expressions were developed to be used in the hot-spot analysis³ for the formation and effect of lateral pressure drops across the plates and for the effect of thermal expansion of the plates. The hot-spot analysis was then used to establish the required manufacturing tolerances.

In order to determine the pressure loading, equations⁴ were developed and used in the analysis of the formation of hydraulically induced lateral pressure differentials across the fuel plates. The equations described the local velocity distribution, velocity pressure drop, and frictional pressure drop in nominally flat channels that are either undistorted or distorted by any nonabrupt deviations from flatness such as those shown in Fig. 5. Two important postulates are: the static pressure is independent of position across the width of the channel at any distance along the channel, and frictional forces are transmitted solely across the thickness of the channel, with none in the direction of the width. (The width of the channel is defined as the length of the involute arc.) These two postulates are justified for very thin channels if it is assumed that there are no abrupt changes in channel shape. This assumption also permits the postulate that changes in velocity do not result in expansion or contraction losses. It is believed that the equations developed permit reasonably accurate analysis of the effect of deviations in plate contour and coolant-gap thickness on the hydrodynamics in the HFIR fuel element coolant channels.

Elastic beam theory was used to obtain analytical solutions⁵ for the stresses and deflections of involute plates as a result of the pressure loadings. Both pinned- and fixed-edge restraint were considered. The analyses performed were limited by the following assumptions:

1. The pressure load variations along the length of the plate were neglected.
2. The pressure load distribution across the width of the plate was uniform.
3. Both membrane and bending stresses were considered; however, deflection due to membrane stresses was not considered.

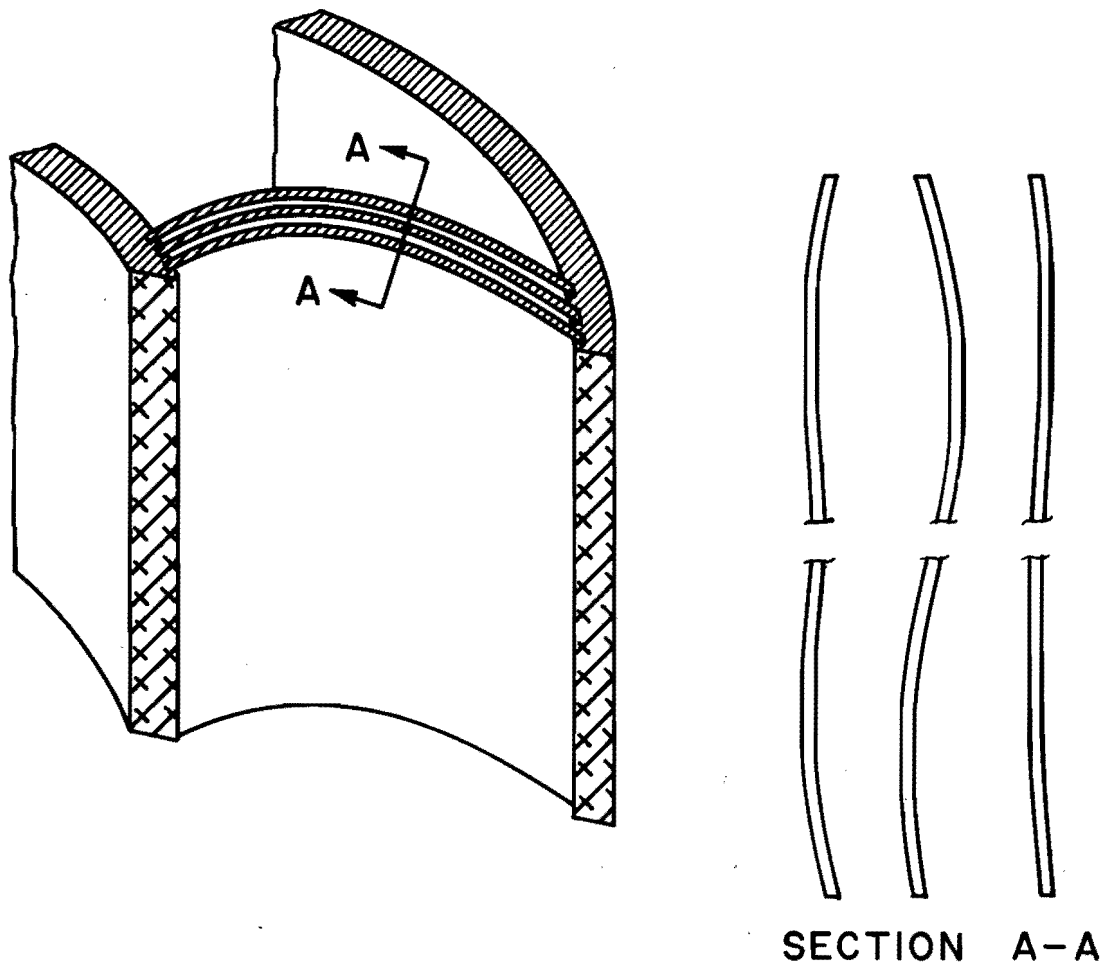


Figure 5

Involute Fuel Plates & Coolant Channel Deviations

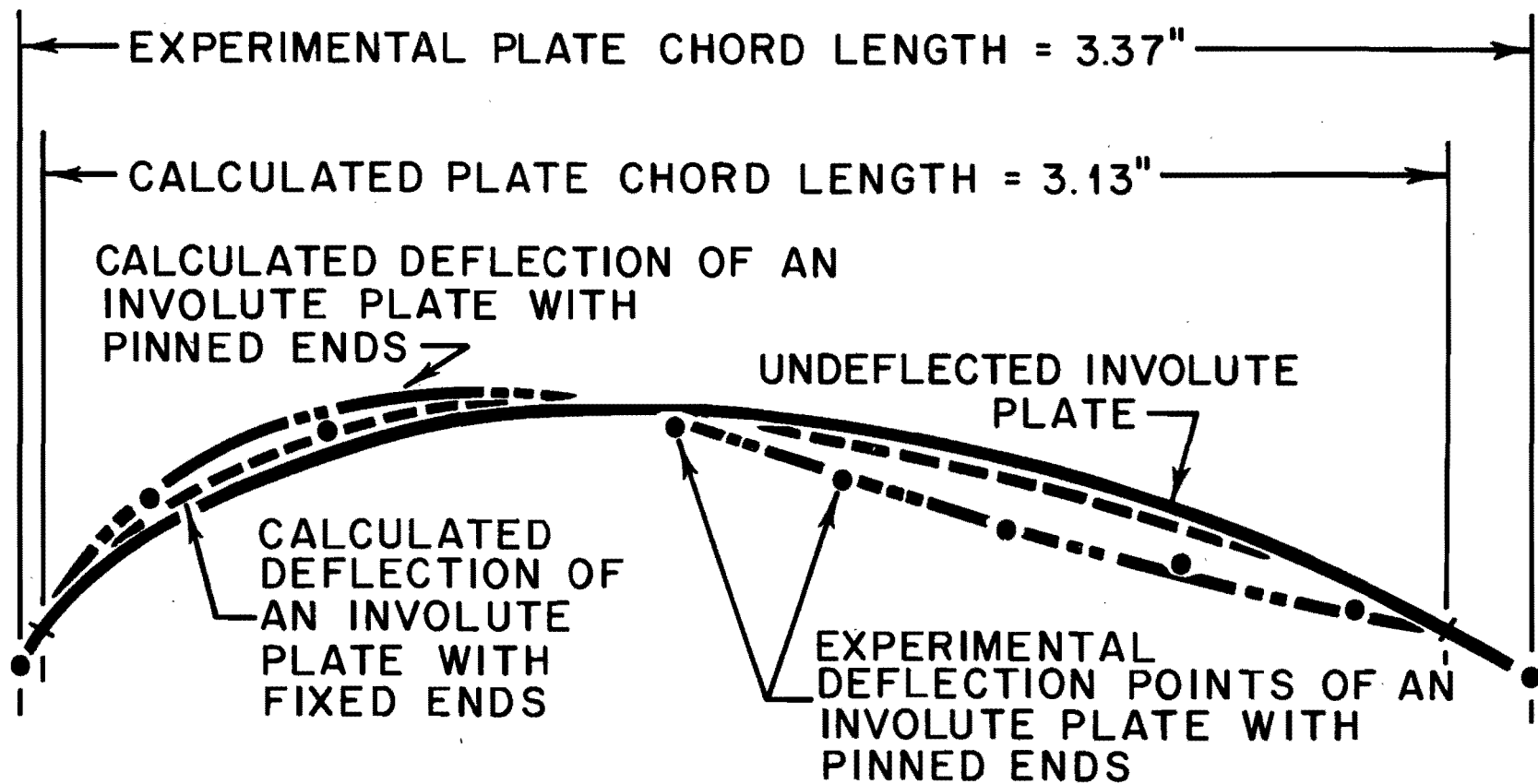


Figure 6

Deflections of an Involute Plate with Uniform Pressure on
the Convex Side

4. The fuel plate was at a uniform temperature.

As a back-up effort to the analytical approach, an experimental program⁶ was initiated. Aluminum involute plates having appropriate edge restraints were subjected to differential pressures. Strain gages and dial indicators were used to measure the associated strains and deflections. Using this equipment, a determination of the deflection as a function of the pressure differential across the plate indicated that the deflected shape was in the form of an S relative to the initial involute contour; that is, both positive and negative deflections existed for a given loading, as shown in Fig. 6. This figure also shows the rather good agreement between the pinned-edge analytical results and the experimental results. The maximum deflection determined experimentally for pinned-edge, 40-mil-thick plates with pressure on the convex side was about 1 mil/psi; the analytical calculations indicated that the corresponding deflection for a 50-mil-thick plate would be about 0.5 mil/psi. Also shown in Fig. 6 is the comparison between calculated pinned- and fixed-edge plate deflections.

During the experiments, the static stability characteristics of the fuel plates were investigated. It was determined within the pressure and deflection ranges of interest that plate buckling resulting from pressure differentials should not occur.

In addition to the static pressure deflections, the creep behavior of the plates was also considered because of the unusually high aluminum fuel-plate temperatures. To obtain this information experimentally, an aluminum involute plate was clamped in a carbon steel frame in such a manner that the difference in thermal expansion between the carbon steel and aluminum simulated the appropriate temperature difference between the

fuel plates and side plates. The assembly was subjected to a suitable operating fuel-plate temperature. The fuel plate was simultaneously subjected to an appropriate differential pressure. In this manner combined static and creep deflections resulting from both pressure and temperature differentials were investigated over periods of time consistent with the proposed fuel element lifetime.

The experimental results⁷ indicated that differences in fuel-plate and side-plate temperatures resulted in sinusoidal longitudinal buckling of the fuel plates as shown in Fig. 5. Plate deflections associated with this buckling were included in the over-all thermal and mechanical design of the fuel element by means of an analytical representation⁷ of the thermally induced buckling behavior.

In order to alleviate problems associated with the differences in radial thermal expansion between the fuel plates and side plates, each fuel annulus is supported by only one side plate. The other side plate is free to rotate.

In addition to the use of the involute-fuel-plate analytical expressions in the hot-spot analysis to help establish the plate dimensions and associated tolerances, the expressions were also used to establish the fuel plate-to-side plate attachment requirements;⁵ that is, the plate-edge loadings. The final fuel plate design permitted a pinned-edge attachment to the side plate with the following provisions: first, that the joint withstand an axial force of 5 pounds per lineal inch of attachment; and second, that the joint withstand a 100 pound per lineal inch force normal to the attached edge of the fuel plate.

References

1. R. D. Cheverton, "HFIR Preliminary Physics Report," ORNL 3006, Oct. 4, 1960.
2. J. R. McWherter et al., "Preliminary Design of the HFIR Core and Pressure Vessel Assembly," ORNL TM-172, August 25, 1961.
3. N. Hilvety and T. G. Chapman, "Thermal Design of the HFIR Fuel Element," paper presented at the Research Reactor Fuel Element Conference, Gatlinburg, Tennessee, Sept. 17-19, 1962.
4. Personal Communication, R. N. Lyon, Oak Ridge National Laboratory, to J. R. McWherter, March, 1960.
5. T. G. Chapman, "Thermal Expansion and Pressure Differential Induced Stresses and Deflections in HFIR Involute Contoured Fuel Plates," (to be issued).
6. J. R. McWherter, T. G. Chapman and C. A. Burchsted, "Deflection of an HFIR Involute Fuel Plate Under a Uniform Load," (to be issued).
7. Personal Communication, R. N. Lyon, Oak Ridge National Laboratory, to J. R. McWherter, Sept. 1962.

BURNOUT HEAT FLUX PREDICTION FOR FLOWING,
SUBCOOLED, WETTING LIQUIDS*

W. R. Gambill
Oak Ridge National Laboratory
Oak Ridge, Tennessee

ABSTRACT

It is generally recognized that a boiling system is characterized by a peak or critical heat flux at which a transition is made from efficient nucleate boiling to high-thermal-resistance film boiling. With essentially constant heat-input systems such as nuclear reactors, particle accelerator targets, and electromagnets, the heat flux is imposed independently of the thermal resistance of the coolant. With such systems, the rapid rise of surface temperature which follows attainment of the critical heat flux usually results in melting or burnout of the heating surface, so that "burnout heat flux" is often used to denote the heat flux at the critical boiling condition.

A new generalized two-term additive prediction method has been developed for burnout flux in which one term represents the boiling contribution in the absence of forced convection and the other the equivalent forced-convection contribution in the absence of boiling. The predictions of this superposition method have been compared with all available experimental data (1326 points)

* A lengthier version was presented at the Fifth National Heat Transfer Conference, Houston, Texas, August 5-8, 1962, and a fully detailed description will be given in an ORNL report to be issued in early 1963.

for burnout with flowing, wetting liquids in the absence of significant net vapor generation. The data compared are for seven fluids in axial, swirl, and cross flow in tubular, annular, rectangular, and rod geometries over broad ranges of flow conditions: velocities of 0.05 to 174 fps, pressures from 4.2 to 3000 psia, subcoolings from 0 to 506°F, centrifugal intensities of 1 to 57,000 gees, and burnout heat fluxes from 0.1×10^6 to 37.4×10^6 Btu/hr.ft².

When the data which can be shown to be unrepresentative of burnout under the experimental conditions are excluded, a selected data field of 878 tests remains. For these data, 96% of the predictions agree with the experimental values within 40%. If deviations which include 90% of the data are compared for all available points for burnout with water coolant only (943 tests), it is found that the additive correlation gives a deviation ~35% less than Bernath's method, which is sometimes considered the best of the previously available generalized burnout correlations.

I. Introduction

The fact that a boiling system is characterized by a peak or critical heat flux at which a transition is made from efficient nucleate boiling to high-thermal-resistance film boiling has prompted the proposal of a great number of equations for predicting critical or "burnout" heat fluxes. There are at least 40 of these; space limitations prevent separate discussion of them here, but most have been described in the reviews of Bonilla,¹ Emmerson,² and Roberts & Bowring.³ Most of these correlations, useful as they have been for specific purposes or for making estimates in the absence of any other information, are characterized by one or more weaknesses which considerably restrict their generality:

(a) The form of the equation may be such as to predict a zero ϕ_{bo} when the subcooling is zero. One example of many is the Gunther equation:⁴

$$\phi_{bo} = 7000 V^{1/2} \Delta t_{sub} \quad (1)$$

This prediction is, of course, at variance with the experimental evidence.

(b) The equation may be applicable only to a single fluid, usually water. Of the correlations thus far proposed for the forced-convection case, only those of Griffith⁵ and of Bernath⁶ include physical properties as variables and have been applied to several fluids.

(c) The equation may have been statistically derived in a fashion far removed from any physical considerations, an arbitrary attempt being made to relate the ϕ_{bo} with the numerous experimentally controlled variables. The ultimate example of this approach to date is the unwieldy 24-term equation of Jacobs & Merrill,⁷ which is applicable only to water in circular geometries. As indicated by the authors and later emphasized by this writer,⁸ extrapolation of the equation, and others of this type, is to be scrupulously avoided. Since a fully adjustable equation can be forced to fit any data set (even if in error) which conforms to the general pattern of the equation, it seems desirable to reduce rather than increase equation adjustability in order to progress toward a more completely defined system.

(d) The equation may be marred by the use of widely variable exponents and "constants", as exemplified, e.g., by the early and now obsolete Jens & Lottes correlation:⁹

$$\phi_{bo} = C (G/10^6)^m \Delta t_{sub}^{0.22}, \quad (2)$$

wherein both the coefficient C and exponent m are pressure dependent.

(e) A given correlation, when compared with data other than those from which it was derived, is very often found simply to give poor agreement with the other data. Of equations which have been proposed for the subcooled forced-convection case, only those of Griffith,⁵ Bernath,⁶ Jacobs & Merrill,⁷ and Zenkevich¹⁰ have been compared with even a reasonable variety of such data (~300 points in each case).

The prediction method to be described will be shown to be relatively free of the shortcomings outlined above.

II. Description of the Correlation

A. Boiling Contribution

The premise on which the correlation is based is that boiling and convective heat-flux terms can be independently formulated and added to yield the total heat flux at burnout. The boiling contribution is obtained from:

$$(\phi_{bo})_{boil} = (\phi_{bo})_{pool} = (\phi_{bo})_{pool,sat} \left[\frac{(\phi_{bo})_{sub}}{(\phi_{bo})_{sat}} \right]_{pool} \quad (3)$$

All available evidence indicates that at least the primary factors influencing saturated pool-boiling burnout are included in the dimensionless equation originally proposed by Kutateladze^{11,12} in 1951:

$$(\phi_{bo})_{pool,sat} = K L_v \rho_v \left[\frac{\sigma g_c a \Delta \rho}{\rho_v^2} \right]^{1/4} \quad (4)$$

Equation (4) has been rederived on several bases by Zuber,¹³ Sterman,¹⁴ and Chang & Snyder.¹⁵ Available experimental saturated pool-burnout data^{12,16} (~125 points) give a maximum K range of 0.08 to 0.23. The observed variation of K values is probably caused by (a) the different experimental techniques utilized by various investigators [whether burnout protection devices are used, e.g.], (b) the use of different criteria for defining the location of the burnout or critical point on the boiling curve, (c) the occasional use of relatively uncertain values of the pertinent physical properties, caused in some cases by purity variations of the test liquids, and (d) the apparently intrinsic random nature of the boiling process, whereby values characterizing the peak-flux condition fluctuate around the most probable value.

Average values which have been proposed for K in Eq. (4) include 0.13 (Kazakova¹⁷), $\pi/24$ (Zuber¹³), 0.145 (Chang & Snyder¹⁵), 0.15 (Deissler¹⁸), 0.16 (Kutateladze¹²), 0.168 (Sterman¹⁴), and 0.18 (Rohsenow¹⁹). Zuber¹³ further proposes that $0.120 < K < 0.157$ is the most probable range, and Chang & Snyder¹⁵ suggest that $\pi/12$ is the absolute maximum attainable. Borishanskii¹⁶ also proposed a correlation in which K is weakly dependent on a dimensionless

group which includes liquid viscosity. With two exceptions (the NH_3 and N_2O_4 data), the K values used in the calculations of the present work were limited to the range 0.12 to 0.17, so that K was regarded as a finitely adjustable rather than completely arbitrary constant.

The factor completing Eq. (3), the ratio of the subcooled to saturated pool-boiling burnout heat fluxes, was calculated in the present work from Kutateladze's semiempirical dimensionless factor¹¹ as described by Bonilla:¹

$$F_{\text{sub}} \equiv \frac{(\phi_{\text{bo}})_{\text{pool,sub}}}{(\phi_{\text{bo}})_{\text{pool,sat}}} = 1 + \left(\frac{\rho_{\ell}}{\rho_v} \right)^{0.923} \left(\frac{c_p \Delta t_{\text{sub}}}{25 L_v} \right), \quad (5)$$

which correlates available small-wire data within $\sim \pm 20\%$.

Kutateladze later proposed¹² the following correlation, which is based on pool data for water, ethanol, and iso-octane over the range $0^\circ < \Delta t_{\text{sub}} < 216^\circ\text{F}$:

$$F_{\text{sub}} = 1 + \left(\frac{\rho_{\ell}}{\rho_v} \right)^{0.80} \left(\frac{c_p \Delta t_{\text{sub}}}{15.38 L_v} \right). \quad (6)$$

More recently, Zuber^{13,20} has derived the dimensionless equation:

$$F_{\text{sub}} = 1 + \frac{2 k \Delta t_{\text{sub}}}{\sqrt{\pi \alpha \tau}} \frac{24}{\pi} \frac{(\rho_v^2 / \sigma g_c a \Delta \rho)^{1/4}}{L_v \rho_v}, \quad (7)$$

where

$$\tau = \frac{\pi}{3} \sqrt{2 \pi} \left(\frac{\sigma g_c}{a \Delta \rho} \right)^{1/2} \left(\frac{\rho_v^2}{\sigma g_c a \Delta \rho} \right)^{1/4}. \quad (8)^*$$

If $a/g = 1$, τ , which is a function only of P and of a/g for a given fluid, is given (for water) by:

$$\tau = (1.169 \times 10^{-5}) \frac{\sigma^{1/4} \rho_v^{1/2}}{\Delta \rho^{3/4}}, \quad (9)$$

*Still more recently, Ivey and Morris²¹ have modified Eq. (5) to read:

$$F_{\text{sub}} = 1 + (\rho_{\ell}/\rho_v)^{0.75} \left(\frac{c_p \Delta t_{\text{sub}}}{9.8 L_v} \right).$$

when the units are chosen as hr, dynes/cm, and pcf. As pointed out by the writer,²² if the subcooling factors of Eqs. (5), (6), and (7) are represented by K_1 , K_2 , and Z , respectively, parametric comparisons for water over the ranges $5 < P < 3000$ psia and $10^\circ < \Delta t_{\text{sub}} < 300^\circ\text{F}$ show that at low pressures (5 to 30 psia), $K_2 < Z < K_1$; at intermediate pressures (30 to 400 psia), $K_2 < K_1 < Z$; and at high pressures (400 to 3000 psia), $K_1 < K_2 < Z$. It may be concluded that the choice of the best over-all equation for F_{sub} has yet to be made; but, except under vacuum conditions, the differences between values predicted by the equations were not large in the comparisons cited above for water. Equation (7) might be expected to possess the greatest generality.

From the preceding, it may be seen that the first term of the prediction method as used in the calculations to be reported is:

$$(\phi_{\text{bo}})_{\text{boil}} = K L_v \rho_v \left[\frac{\sigma g_c a \Delta p}{\rho_v^2} \right]^{1/4} \times \left[1 + \left(\frac{\rho_\ell}{\rho_v} \right)^{0.923} \left(\frac{c_p \Delta t_{\text{sub}}}{25 L_v} \right) \right], \quad (10)$$

in which K is ordinarily taken as 0.12 to 0.17. In all cases, c_p in Eq. (10) was evaluated at $t' = t_{\text{sat}} - (\Delta t_{\text{sub}}/2)$.

B. Convective Contribution and Summation

The nonboiling convective contribution is written in the form of the conventional Newton cooling law:

$$(\phi_{\text{bo}})_{\text{nb}} = h_{\text{nb}} (t_w - t_b)_{\text{bo}}, \quad (11)$$

and $(t_w)_{\text{bo}}$ of Eq. (11) is evaluated with Bernath's generalized plot⁶ of $(\Delta t_{\text{sat}})_{\text{bo}}$ versus T_{sat}/T_c , shown as Fig. 1.

The final correlation, therefore, is:

$$\phi_{\text{bo}} = (\phi_{\text{bo}})_{\text{boil}} + (\phi_{\text{bo}})_{\text{nb}} = \text{Eq. (10)} + \text{Eq. (11)}. \quad (12)$$

Since most nonboiling film-coefficient correlations are in the form of:

$$N_{\text{Nu}} = K' N_{\text{Re}}^m N_{\text{Pr}}^n, \quad (13)$$

Eq. (12) may be written as:

$$\phi_{bo} = K L_V \rho_V \left[\frac{\sigma g_c a \Delta \rho}{\rho_V^2} \right]^{1/4} \left[1 + \left(\frac{\rho_l}{\rho_V} \right)^{0.923} \frac{c_p \Delta t_{sub}}{25 L_V} \right] + K' \left(\frac{k}{D} \right) N_{Re}^m N_{Pr}^n (t_w - t_b)_{bo}, \quad (14)$$

and used in three different ways; which are, in the order of auxiliary-data needed:

(a) For conservative calculations in the absence of any data or related experience, K and K' may be chosen as the minimum values characterizing their normal ranges. Minimum values will be discussed in a following section.

(b) Pool-boiling tests may be made to determine K_{min} and nonboiling convective tests or the literature utilized to determine K'_{min} . Such an approach obviates to a considerable degree the need of conducting forced-convection burnout tests.

(c) K and K' may be regarded as adjustable constants and evaluated with limited relevant forced-convection burnout data.

A further illustration of the flexibility inherent in the additive approach is the generally acceptable use of alternative expressions for Eq. (4). If, e.g., σ is not known or easily predicted, the Rohsenow-Griffith equation,²³ as later modified by Rohsenow & Choi¹⁹ by inclusion of $(a/g)^{1/4}$, may be substituted:

$$(\phi_{bo})_{pool,sat} = 143 L_V \rho_V (a/g)^{1/4} (\Delta \rho / \rho_V)^{0.6}, \quad (15)$$

in which units of Btu/hr·ft², Btu/lb, and pcf are commensurate. Finally, knowledge of only P_c allows one to estimate $(\phi_{bo})_{pool,sat}$ from a generalized curve of ϕ_{bo}/P_c versus P/P_c , as proposed by Cichelli & Bonilla.²⁴

It should be noted that additive types of correlations, though quite different in detail from that described here, have been proposed in the area of boiling heat transfer three times in the past, first by Rohsenow²⁵ for the correlation of forced-convection local-boiling heat-transfer rates below burn-

out. Sonnemann later proposed²⁶ a burnout correlation, applicable only to water at 2000 psia, which consisted of the sum of the ϕ required to initiate nucleate boiling (taken directly from ref. 9), and an incremental ϕ required to cause burnout, the incremental term containing four empirical constants for each of two Reynolds number ranges. Hines²⁷ has semiempirically correlated hydrazine burnout data by expressing the theoretical Eq. (64) of ref. 28 as follows:

$$\phi_{bo} = A + B \Delta t_{sub} + h_{nb} \Delta t_f, \quad (16)$$

in which A and B are treated as pressure-dependent "constants", and the first two terms constitute the boiling contribution. Of the three proposals, that of Rohsenow²⁵ is the most similar to the one described here.

The method as now formulated is not applicable to forced-convection bulk-boiling burnout - i.e., for flow with significant net-vapor generation. In the comparisons to follow, only four of the burnouts listed occurred under low-quality conditions, and these were satisfactorily correlated by use of Guerrieri & Talty's multiplying factor²⁹ for two-phase heat-transfer coefficients in the forced-convection region.

III. Physical Properties

All physical properties in Eq. (10) are evaluated at t_{sat} with the exception of c_p , which is taken at $t' = t_{sat} - (\Delta t_{sub}/2)$. The property reference temperature for Eq. (11) varies with the particular heat-transfer-coefficient correlation used. The fact that many of the several physical properties required had to be calculated or extrapolated would be expected to decrease to some extent the accuracy of the final ϕ_{bo} predictions. Property data are surprisingly sparse for the rocket propellants listed. This situation has apparently arisen from the empirical correlation of ϕ_{bo} (which most frequently limits liquid-fuel rocket heat-transfer design) in terms of V, P, and Δt_{sub} for each propellant; and the fact that the nonboiling heat-transfer regime, for which physical properties are required, is not critical in the design.

Available physical-property data were taken from refs. 30 through 45.

IV. Results of the Comparison of Data with Prediction

A. Background

Numerical calculations were made with slide rule and desk calculator.

For a given fluid, the calculation time can be reduced considerably by plotting $(\phi_{bo})_{pool,sat}$ versus P , and the isolated physical-property groups of both F_{sub} and h_{nb} versus t . Burnout heat fluxes for all tests of each data collection were calculated with Eq. (12), but some were, for the specific reasons to be cited in the detailed report, excluded from further consideration. Some data have been reported in insufficient detail to allow the present comparisons to be made. This is especially true of the Russian literature.

Literature values were generally chosen for both K and K' of Eq. (14). K was, with two exceptions, taken in the range 0.12 to 0.17; and, where the form of Eq. (13) applied, K' was taken in the range 0.018 to 0.027 - i.e., between the minimum and maximum values established as characteristic of the Dittus-Boelter, Sieder-Tate, and Colburn correlation forms. In several instances where the convective contribution was a small fraction of the boiling contribution, properties were evaluated at t_p in equations normally used with t_f as the property reference temperature. The large variety of slightly differing correlations which have been proposed for h_{nb} for various geometries allows considerable latitude in the selection of an appropriate equation. Though no effort was made to select optimum values of K and N_{Nu} (within the permissible ranges) in order to formally minimize the resulting deviations between experiment and prediction, first-order changes were made when the initial calculation resulted in a deviation distribution which could obviously be improved by selection of different values of K and K' (again within the permissible limits).

In comparing the predictions of any burnout correlation with experimental values, two points should be kept in mind:

(a) The boiling transition is a typical crisis phenomenon which is not characterized by exact values; and, at best, only the average or most probable value can be indicated for the specific conditions. Though not yet quantitatively established, Zuber's approach,¹³ e.g., indicates an inherent $\pm 14\%$ uncertainty in the value of the mean ϕ_{bo} under conditions of saturated pool boiling.

(b) As pointed out by Larson with regard to liquid-phase physical properties,⁴⁶ it is true also of experimental burnout fluxes that the variations for similar conditions between the results of competent investigators are normally significantly larger than each investigator's own estimates of uncertainty, so that the possible margin of error is considerably greater than is generally admitted.

B. Data with Water Coolant

These results are outlined in Table 1. As noted, the average and maximum deviations for the 87.0% of the data accepted (766 tests) are 17.8% and 96.6%. If, in addition, the BMI tube data, ANL 1/16-in.-dia rod data, and Columbia Task X and Task IV annulus data are rejected (for reasons to be discussed in the detailed report), the average and maximum deviations for the remaining 573 points are 14.7% and 59.4%. The corresponding deviation-distribution curves for these data are shown in Fig. 2. Detailed comments regarding the heat-transfer-coefficient correlations used will be given in the final report.

It seems worthwhile to mention specifically the Soviet data of ref. 62. In his comparisons, Bernath⁶ omitted these data, stating "unequivocally" that they were "unsuitable" for inclusion with the other data. This does not, however, seem to be the case, and the data actually yield valuable information on the effect of flow gap on ϕ_{bo} . As shown in Table 1, 55 points of the higher-pressure data, all taken with a constant flow gap of ~ 79 mils, are in excellent agreement with prediction. For one test of this series, the burnout was obviously premature since $(\phi_{bo})_{\text{exptl.}}$ was only 77% of the calculated $(\phi_{bo})_{\text{pool,sub}}$ - even though V was 6.1 fps.

In the low-pressure (~ 14 psia) tests, however, the deviation between experiment and prediction increases sharply when the flow gap (varied from 220 to 20 mils) is reduced below ~ 80 mils, as shown in Fig. 3. For tests with flow gaps ≥ 71 mils (63 of the 99 points), the predictions are quite satisfactory, as shown in Table 1. Other studies^{10,65,66} combine with these data to suggest that a diameter effect is encountered in subcooled boiling only when the flow-gap dimension becomes comparable to bubble dimensions.⁸

Kutateladze has suggested⁶⁷ that the "critical" flow-passage diameter below which D affects ϕ_{bo} (adversely) can be approximated by:

$$D_c \approx [\sigma g_c / a \Delta\rho]^{1/2}, \quad (17)^*$$

which is $1/\sqrt{2}$ times the so-called Laplace constant; which has been shown, if bubble contact angle is included as a variable, to give a good correlation of bubble volume at the moment of the bubble's departure from a heated surface. The very limited experimental evidence^{62,66} suggests, however, that the critical diameter at which the effect becomes significant is $\sim 3/4$ of the prediction of Eq. (17), as depicted in Fig. 4, which is proposed for use on a tentative basis. It remains, of course, to quantitatively predict the large effect of gap width on ϕ_{bo} when $D < D_c$.

Values for h_{nb} were calculated from the Mikheev equation for annuli:⁶²

$$N_{Nu,b} = 0.023 N_{Re,b}^{0.8} N_{Pr,b}^{0.4} \left(\frac{D_1}{D_2} \right)^{0.5}. \quad (18)$$

C. Data with Other Coolants

Test results are outlined in Table 2. As noted, the average and maximum deviations for the 96.1% of the data accepted are 19.4% and 79.4%. If, in addition, the newer Aerojet data for diphenyl and the Reaction Motors data for NH_3

* 2π times the right-hand side of this equation is Zuber's critical wave length.¹³

Table 1. Comparison of Burnout Data for Water with the Additive Prediction Method*

Data Source	Type of Flow	Geometry	Experimental Ranges ^a				Number of Points	Number of Points Accepted ^b	% Deviation ^c		% Positive Deviations	K Value Used ^d	Ref.
			P (psia)	Δt_{sub} (°F)	V (fps)	ϕ_{bo} (10 ⁻⁸ Btu/hr-ft ²)			Avg.	Max.			
UCLA	Axial	Tube	500 - 2000	5 - 163	6.3 - 54.7	1.04 - 3.78	42	42	12.5	34.9	57	$\pi/24$	9
Purdue	Axial	Tube	600 - 3000	5 - 148	5.7 - 42.0	1.20 - 4.21	24	24	14.2	44.5	42	$\pi/24$	9, 47
ANL	Axial	Tubes	620 - 2000	0	5.7 - 33.1	0.81 - 2.16	8	7	16.0	48.2	86	$\pi/24$	48
USSR	Axial	Tube	29 - 3000	0	5.9 ^e	0.44 - 1.29	22	22	13.6	35.8	77	$\pi/24$	49
ORNL	Swirl	Tubes ^f	15 - 545	0 - 260	14.7 - 156	2.77 - 37.35	40	32	15.6	42.0	59	$\pi/24$	50
ORNL	Axial	Tubes	15 - 74	78 - 222	23.6 - 174	2.23 - 17.25	29	29	25.2	47.1	10	0.168	50, 51
USSR	Axial	Tubes	495	0 - 362	11.8 - 147.7	1.37 - 16.71	31	27	20.5	46.1	44	$\pi/24$	52
BMI	Axial	Tubes	1500 - 2750	10 - 81	10.1 - 20.0	0.66 - 2.14	180	126	19.5	67.3	54	0.12	53
IIT	Cross	Single Rods	17 - 30	43 - 199	1.0 - 6.8	0.85 - 3.75	31	31	6.3	21.6	74	$\pi/24$	54
IIT	Cross	Rod Matrix	31 - 35	72 - 179	3.9 - 12.9	1.14 - 7.44	27	25	15.3	27.2	44	0.168	55
Stanford	Cross	Single Rods	17	14 - 48	0.3 - 0.5	0.50 - 0.94	2	2	13.6	16.3	100	$\pi/24$	56
ANL ^g	Cross	Single Rods	15	44 - 164	3.0 - 12.3	1.68 - 4.16	43	43	16.9	47.2	30	$\pi/24$	57
ANL ^h	Cross	Single Rods	15	50 - 116	2.6 - 10.0	2.86 - 6.69	42	42	41.3	51.4	0	0.168	57
WAPD	Axial	Rectangular Channel	2000	5 - 97	9.9 - 30.7	1.13 - 2.02	17	17	11.3	25.2	88	0.12	58
SRL	Axial	Rectangular Channel	25 - 86	11 - 133	5.4 - 41.6	1.02 - 3.18	51	51	9.7	29.4	35	$\pi/24$	59
ORNL ^j	Axial	Rectangular Channel	160 - 566	26 - 90	30.4 - 85.4	3.04 - 7.36	7	7	13.5	26.0	29	0.16	60
ORNL ^k	Axial	Rectangular Channel	462 - 521	0 - 64	34.9 - 46.0	3.25 - 3.67	4	4	10.8	18.8	50	0.12	60
JPL	Axial	Rectangular Channel	14 - 164	22 - 282	4.8 - 40.0	0.42 - 11.41	35	34	37.0	59.4	41	$\pi/24$	4
Aerojet	Axial	Annulus	254 - 493	11 - 115	5.8 - 22.7	0.77 - 2.68	4	3	7.1	15.3	100	$\pi/24$	34
MIT	Axial	Annulus	30 - 90	14 - 99	1.0 - 12.0	0.49 - 2.01	9	6	9.1	19.1	83	$\pi/24$	61
SRL	Axial	Annulus	37 - 65	12 - 130	10.0 - 33.5	0.81 - 1.43	14	14	11.6	32.4	43	$\pi/24$	59
USSR	Axial	Annulus	14 - 313	28 - 278	4.5 - 13.4	0.64 - 5.95	56	55	11.4	29.5	33	0.168	62
			14	24 - 153	4.9 - 49.5	0.56 - 5.35	99	63	9.8	28.1	46	0.168	62
Columbia ^m	Axial	Annulus	93 - 248	8 - 239	0.05 - 0.13	0.51 - 1.84	7	7	11.4	36.7	43	0.12	63
Columbia ⁿ	Axial	Annulus	4.2 - 248	30 - 313	0.06 - 0.66	0.34 - 3.21	30	28	12.8	44.9	39	0.15	64
Columbia ^p	Axial	Annulus	500 - 700	24 - 132	0.5 - 26.7	0.95 - 1.95	12	12	32.7	80.5	75	0.12	6
Columbia ^q	Axial	Annulus	23 - 69	41 - 79	5.9 - 27.6	0.36 - 1.56	14	13	49.5	96.6	100	0.12	6
Over-all:			4.2 - 3000	0 - 362	0.1 - 174	0.34 - 37.35	880	766	17.8 ^r	96.6 ^r	-	0.12-0.17	-

*Sixty-three new values of ϕ_{bo} for water in tubes and annuli have recently been reported by the Savannah River Laboratory in Report DP-725. These data, taken at $60 < P < 1220$ psia, $41 < \Delta t_{sub} < 157$ °F, and $8.5 < V < 39.6$ fps, covered a ϕ_{bo} range of 1.55×10^8 to 3.74×10^8 Btu/hr-ft². Using the same K value and h_{nb} equation used for the SRL data tabulated above, the average and maximum deviations are 13.7% and 29.4%, respectively.

^aAt burnout site.

^bBases of selection will be given in the detailed report.

^c(Calc. - Exptl.) 100/Exptl.

^dThe K of Eqs. (4), (10), and (14).

^eMaximum used in test series.

^fWith internal twisted tapes

^gWith 1/8-in.-OD rods.

^hWith 1/16-in.-OD rods.

^jWithout spacers.

^kWith axially oriented, centered spacer strips.

^mTask IX data with tubular heaters.

ⁿTask IX data with solid rod heaters.

^pTask X data; four tests were run with flow inside tubes.

^qTask IV data.

^rSee text Section IV-B for over-all deviations with another selection of data.

Table 2. Comparison of Burnout Data for Fluids Other than Water with the Additive Prediction Method

Data Source	Fluid	Type of Flow	Geometry	Experimental Ranges ^a					Number of Points Accepted ^b	% Deviation ^c		% Positive Deviations	K Value Used ^d	Ref.
				P (psia)	Δt_{sub} (°F)	V (fps)	ϕ_{bo} (10^{-6} Btu/hr·ft ²)	Number of Points		Avg.	Max.			
JPL	Hydrazine	Axial	Tubes	100 - 1200	98 - 506	1.0 - 93.0	0.74 - 14.10	62	61	11.8	41.0	43	0.14	37
Rocketdyne	Hydrazine	Axial	Tube	191 - 1025	102 - 473	13.2 - 120.5	1.41 - 13.72	22	22	14.4	45.5	100	$\pi/24$	27
JPL	Ammonia	Axial	Tubes	170 - 1820	3 - 208	3 - 156	0.90 - 7.42	45	44	15.2	44.1	25	Eq. (15) with K = 232	40
RMI	Ammonia	Axial	Tube	165 - 1275	1 - 201	12.4 - 81.8	0.78 - 5.19	111	111	26.7	79.4	52	"	68
Aerojet	Monoisopropyl-biphenyl	Axial	Annulus ^e	386 - 400	159 - 322	5.1 - 15.0	0.39 - 0.95	6	6	14.6	24.9	33	$\pi/24$	34
Aerojet	Diphenyl	Axial	Annulus ^e	197 - 406 23 - 326	77 - 328 0 - 159	4.8 - 17.3 0.5 - 14.8	0.23 - 0.89 0.07 - 0.28	23 25	23 15	15.2 31.1	26.2 57.8	35 100	0.12 0.12	34 34
JPL	Nitrogen Tetroxide	Axial	Tube	150 - 615	0 - 200	10.2 - 59.8	0.55 - 3.59	73	72	17.2	44.5	50	0.17, 0.27, 0.29	45
ORNL	Ethylene Glycol	Swirl	Tubes ^f	20 - 279	77 - 426	21.4 - 97.5	2.33 - 9.00	11	9	12.5	39.3	67	0.16	33
ORNL	Ethylene Glycol	Axial	Tube	20 - 88	155 - 264	17.3 - 88.4	2.06 - 6.25	5	5	42.8	54.1	0	0.16	33
			Over-all:	20 - 1820	0 - 506	0.5 - 156	0.1 - 14.1	383	368	19.4 ^g	79.4 ^g	-	0.12-0.29	-

^aAt burnout site.^bBases of selection will be given in the detailed report.^c(Calc. - Exptl.) 100/Exptl.^dThe K of Eqs. (4), (10), and (14).^eBetween a heated outer tube and an unheated inner rod.^fWith internal twisted tapes.^gSee text Section IV-C for over-all deviations with another selection of data.

are rejected (for reasons to be discussed in the detailed report), the average and maximum deviations for the remaining 242 tests are 15.0% and 54.0%. The corresponding deviation-distribution curves for these data are shown in Fig. 5.

Some burnout data are available^{1,69} for mixtures such as white and red fuming nitric acids, JP-3 and JP-4 fuels, hydrazine with unsymmetrical dimethyl hydrazine,⁷⁰ and hydrazine with ethylenediamine.³⁷ A lack of adequate physical-property data has delayed comparisons for these mixtures. Data have also been taken but not published for the following pure liquids⁶⁹ - isopropanol, diacetone alcohol, chlorine trifluoride, and diethylenetriamine; though requested from JPL,⁷¹ these data have not been received.

D. Prediction of Minimum ϕ_{bo}

In Tables 1 and 2, an effort was made to roughly adjust the two terms of the burnout equation, within the allowed ranges for K and K', so as to obtain an approximately minimum average deviation from the data. In practice, there is usually more interest, however, in prediction of the minimum burnout heat flux, since burnout is to be avoided, for safety, at all times and places in the heated structure. All available nonaqueous burnout data of Table 2 were accordingly recalculated using K = 0.12 in all cases and K' = 0.019 in Eq. (14). The swirl-flow heat-transfer coefficients were reduced by 20% below the average values used previously. The results are:

<u>Data Source</u>	<u>% Negative Deviations</u>
JPL, N ₂ H ₄	96.8
Rocketdyne, N ₂ H ₄	86.4
JPL, NH ₃	88.9
RMI, NH ₃	56.8
Aerojet, MIB	66.7
Aerojet, (C ₆ H ₅) ₂	35.4
JPL, N ₂ O ₄	98.6
ORNL, C ₂ H ₄ (OH) ₂ - axial	100.0
ORNL, C ₂ H ₄ (OH) ₂ - swirl	66.7

Taken in the context of the discussion of the individual data sets and their respective limitations, it would seem that such a calculation would approximate the true minimum burnout heat flux. Both K and K' could, of course, be decreased arbitrarily still further to obtain all negative deviations.

The deviation distribution for the minimum burnout heat flux predictions for the selected nonaqueous data (242 tests) is tabulated below:

<u>% Deviation</u> *	<u>% of Points with Deviation \leq Indicated %</u>
-10	4.96
-20	15.70
-30	41.74
-40	65.70
-50	84.71
-65	90.91

Twenty-two tests, or 9.09% of the total, deviated positively as follows:

+5	2.48
+10	5.79
+15	7.02
+20	7.85
+25	8.68
+30	9.09

E. Deviation between Prediction and Experiment for the Over-all Data

Population

Deviation distribution curves are shown in Fig. 6 for the total data field. The legend indicates the data used for each curve.

V. Burnout in Liquid-Metal Systems

The value of the additive technique was first recognized in March 1961 when the writer was estimating burnout heat fluxes for liquid-metal nuclear reactor systems utilizing boiling K or Rb as the heat carrier.⁷² Even though Eq. (4) [with $K = 0.16$] gave values of $(\phi_{bo})_{pool,sat}$ at 1 atm less than that for water, burnout fluxes of tens of millions of Btu/hr.ft² are predicted by the Griffith relation,⁵ and of hundreds of millions by Bernath⁶ for a $V - \Delta t_{sub}$

* Of predicted with respect to experimental value.

combination of 10 fps and 60 to 180°F. This result appeared quite unreasonable and the additive technique was investigated as an alternative procedure. The convective contribution was calculated for the liquid metals with the Lubarsky-Kaufman equation:⁷³

$$h_{nb} = 0.625 (k/D) (N_{Re} N_{Pr})^{0.4}, \quad (19)$$

which applies for $N_{Pe} > \sim 10^2$ for fully developed flow in round tubes with a uniform wall heat flux. The results of this comparison are shown in Table 3, extracted in part from the paper describing the above comparisons in detail,⁷² in which it is concluded that at low V and Δt_{sub} , ϕ_{bo} for K and Rb should be comparable to that for water. The difference in predicted values is large indeed. Three sources of experimental data are now available:

(a) Russian studies^{74,75} of the pool boiling of mercury outside a horizontal tube, presumably at atmospheric pressure, with 0.04 wt % magnesium added as a wetting agent, yielded a ϕ_{bo} of only $\sim 130,000$ Btu/hr.ft² at $\Delta t_{sat} \approx 27^\circ\text{F}$. The magnesium addition was varied from 0 to 0.04 wt %, and the curve of ϕ_{bo} versus % magnesium is almost flat by 0.04%, indicating full wetting.

(b) Krakoviak⁷⁶ has found in preliminary forced-convection studies that burnout heat fluxes for K under atmospheric pressure, low inlet velocity, high exit-quality conditions are in the range of tens of thousands of Btu/hr.ft² and may be approximately correlated by the NACA two-phase burnout curve for water.⁷⁷

(c) Noyes⁷⁸ has made measurements of $(\phi_{bo})_{pool,sat}$ for sodium at 0.5 to 1.5 psia; these give a broadly extrapolated ϕ_{bo} at 1 atm abs of $\sim 1.9 \times 10^6$ Btu/hr.ft². He has correlated his results, along with some of the pool data available for H₂O and four organic liquids, with N_{Pr} to obtain the dimensionless equation:

$$(\phi_{bo})_{pool,sat} = \frac{0.144 L_v \rho_v}{N_{Pr}^{0.245}} \left(\frac{\Delta\rho}{\rho_v} \right)^{1/2} \left(\frac{\sigma g_c a}{\rho_l} \right)^{1/4}, \quad (20)$$

which is presumably applicable to wetting liquids at $P \ll P_c$. Unlike Eq. (4),

Table 3. Axial-Flow Forced-Convection Local Boiling
Burnout Heat Fluxes - Liquid-Metal Comparison^a

(P = 1 atm abs, a/g = 1, D_i = 3/8 in., V = 10 fps)

Δt_{sub} (°F)	ϕ_{bo} (10 ⁻⁶ Btu/hr·ft ²)				
	Bernath ⁶	Gunther ⁴	Griffith ^{5,b}	Additive Method ^c	
H ₂ O	60	0.96	1.33	2.34	1.64
	120	1.52	2.65	3.54	2.69
	180	2.07	3.98	4.65	3.51
K	60	488	-	36.2	0.80
	120	834	-	45.6	1.21
	180	1180	-	54.1	1.62
Rb	60	340	-	29.5	0.59
	120	585	-	37.1	0.87
	180	825	-	43.5	1.16

^aThe predictions are point predictions, without consideration of specific values of inlet temperature and tube length which would result in sub-coolings at the burnout site equal to those selected for burnout calculation.

^bMean line through correlation plot used.

^cCombination of Eqs. (4) [with K = 0.16], (5), (11), and (19).

which evolved from the purely hydrodynamic theory of burnout, Eq. (20) contains transport properties of the liquid phase in the form of the Prandtl number. Equation (20) predicts an increased ϕ_{bo} when μ is decreased, whereas Borishanskii's modification¹⁶ of Kutateladze's equation indicates the inverse. Should Eq. (20) prove to be general, it can, of course, be utilized in the first term of Eq. (14) in place of Eq. (4).

These three studies seem to indicate that the predictions of the additive method, as proposed, are at least more qualitatively correct for liquid metals than are those of other generalized methods.

VI. Final Remarks

In summary, this method may be used quite flexibly and satisfactorily to either predict or correlate burnout data over extremely broad ranges of fluid properties, velocity, acceleration, subcooling, and pressure.

The writer wishes to emphasize that the additive approach avoids many of the problems inherent in typical correlations composed of the product of various variables taken to different powers. In the cases of velocity and subcooling, e.g., past equations have been expressed in terms of a wide range of exponents on each variable. The additive method makes it clear that the "effective exponent" on each term in such an equation can vary widely depending on the relative contributions of the boiling and convective terms to the total heat flux at burnout.

Acknowledgment

The author wishes to express his appreciation to J. Lones for his conscientious assistance in making the comparison calculations and to Dolores Eden for her typing of the manuscript.

Notation (Units for dimensional relations are given where they occur)

a	local acceleration	L	heated length of test section
C	constant	L_v	latent heat of vaporization of coolant
c_p	constant-pressure specific heat of liquid	m, n	exponents
D	diameter (equivalent) of flow passage	N_{Nu}	Nusselt number, dimensionless, hD/k
D_1, D_2	outer and inner diameters of annular flow passage	N_{Pe}	Peclet number, dimensionless, $N_{Re} \cdot N_{Pr}$
F_{sub}	subcooling factor [defined in Eq. (5)]	N_{Pr}	Prandtl number of liquid, dimensionless, $c_p \mu / k$
g	local gravitational acceleration	N_{Re}	Reynolds number, dimensionless, DG/μ
g_c	conversion constant, $L \cdot M / F \cdot \theta^2$	P	absolute pressure
G	mass velocity of coolant, ρV	t	temperature ($^{\circ}F$ or $^{\circ}C$)
h	surface heat-transfer coefficient	T	absolute temperature ($^{\circ}R$ or $^{\circ}K$)
k	thermal conductivity of liquid	Δt_{sat}	film superheat, $(t_w - t_{sat})$
K, K'	adjustable constants of boiling and convective terms of Eq. (14)		

Δt_{sub}	degree of subcooling, ($t_{\text{sat}} - t_b$)	ρ	fluid density
V	axial coolant velocity	$\Delta\rho$	phase density difference, ($\rho_l - \rho_v$)
x	vapor quality, weight fraction vapor	σ	surface tension
α	thermal diffusivity of liquid, $k/\rho c_p$	τ	period of unstable inter- facial wave
μ	dynamic viscosity of liquid	ϕ	heat flux into liquid

Subscripts

a	axial	max	maximum
b	bulk	nb	nonboiling
boil	boiling	r	reduced
bo	burnout	s	swirl
c	critical	sat	saturation
f	film	sub	subcooled
i	inside	v	of vapor
l	of liquid	w	at heated wall
m	mean		

Literature Cited

1. C. F. Bonilla, pp. 399-431 of Chapter 9 ("Heat Removal"), Nuclear Engineering, McGraw-Hill, New York, 1957.
2. G. S. Emmerson, "Heat Transmission with Boiling," Nuclear Engineering, 493-500 (Nov., 1960).
3. H. A. Roberts and R. W. Bowring, "Boiling Effects in Liquid-Cooled Reactors," Nuclear Power, 96-101, 118 (March 1959).
4. F. C. Gunther, "Photographic Study of Surface-Boiling Heat Transfer to Water with Forced Convection," Trans. ASME 73, 115-123 (Feb., 1951).
5. P. Griffith, "The Correlation of Nucleate Boiling Burnout Data," ASME Preprint No. 57-HT-21 (not published); MIT Tech. Rep. No. 9 (March 1957); also described in ref. 19.
6. L. Bernath, "A Theory of Local Boiling Burnout and Its Application to Existing Data," Chem. Engrg. Progress Symposium Series 56, No. 30, 95-116 (1960).
7. R. T. Jacobs and J. A. Merrill, "The Application of Statistical Methods of Analysis for Predicting Burnout Heat Flux," Nuclear Sci. and Engrg. 8, 480-496 (1960).
8. W. R. Gambill, brief communication re ref. 7, Nuclear Sci. and Engrg. 10, No. 1, 92 (1961).
9. W. H. Jens and P. A. Lottes, Analysis of Heat Transfer, Burnout, Pressure Drop, and Density Data for High Pressure Water, ANL-4627 (May 1, 1951).

10. B. A. Zenkevich, "Similarity Criteria for Critical Heat Loading in Forced Liquid Flow," J. Nuclear Energy, Part B: Reactor Technology 1, No. 2, 137-140 (1959).
11. S. S. Kutateladze, "A Hydrodynamic Theory of Changes in the Boiling Process under Free Convection Conditions," Izv. Akad. Nauk, SSSR, Otd. Tekh. Nauk, No. 4, 529-536 (1951).
12. S. S. Kutateladze, Heat Transfer in Condensation and Boiling, 2d ed., Moscow-Leningrad, 1952, Chapter 10; AEC Transl. 3770, August 1959.
13. N. Zuber, Hydrodynamic Aspects of Boiling Heat Transfer (Thesis), AECU-4439 (June 1959).
14. L. S. Sterman, "On the Theory of Heat Transfer in Boiling Liquids," Zhur. Tekh. Fiziki 23, 342 (1953).
15. Y. P. Chang and N. W. Snyder, "Heat Transfer in Saturated Boiling," Chem. Engrg. Progress Symposium Series 56, No. 30, 25-38 (1960).
16. V. M. Borishanskii, "An Equation Generalizing Experimental Data on the Cessation of Bubble Boiling in a Large Volume of Liquid," Zhurn. Tekh. Fiziki 25, 252 (1956).
17. E. A. Kazakova, "Influence of Pressure on the Production of the First Crisis in the Boiling of Water on a Horizontal Plate," pp. 86-94 of Problems of Heat Transfer During a Change of State: A Collection of Articles (ed. by S. S. Kutateladze), Moscow-Leningrad, 1953; AEC Transl. 3405.
18. R. G. Deissler, Columbia University Heat Transfer Symposium, New York, 1954; reference by R. Cole, "A Photographic Study of Pool Boiling in the Region of the Critical Heat Flux," AIChE Journal 6, No. 4, 533-538 (1960).
19. W. M. Rohsenow and H. Y. Choi, Heat, Mass, and Momentum Transfer, Chapter 9, pp. 211-236, Prentice-Hall, 1961.
20. N. Zuber, M. Tribus, and J. W. Westwater, "The Hydrodynamic Crisis in Pool Boiling of Saturated and Subcooled Liquids," 1961 International Heat Transfer Conference (Boulder, Colorado), Part II, Paper No. 27, pp. 230-236.
21. H. J. Ivey and D. J. Morris, On the Relevance of the Vapor-Liquid Exchange Mechanism for Subcooled Boiling Heat Transfer at High Pressure, AEEW-R 137 (January 1962).
22. W. R. Gambill, submitted written discussion regarding the paper of ref. 20 (October 1961).
23. W. M. Rohsenow and P. Griffith, "Correlation of Maximum-Heat-Flux Data for Boiling of Saturated Liquids," Chem. Engrg. Progress Symposium Series 52, No. 18, 47-49 (1956).
24. M. T. Cichelli and C. F. Bonilla, "Heat Transfer to Liquids Boiling Under Pressure," Trans. AIChE 41, 755-787 (1945).
25. W. M. Rohsenow, Heat Transfer Symposium, 1952, pp. 101-149, Engrg. Research Institute, University of Michigan, Ann Arbor, Michigan, 1953.

26. G. Sonnemann, "A Method of Correlating Burnout Heat Flux Data," Nuclear Sci. and Engrg. 5, 242-247 (1959).
27. W. S. Hines, Forced Convection and Peak Nucleate Boiling Heat Transfer Characteristics for Hydrazine Flowing Turbulently in a Round Tube at Pressures to 1000 Psia, Rocketdyne (Declass.) Rept. R-2059 (August 1959).
28. N. Zuber and M. Tribus, Further Remarks on the Stability of Boiling Heat Transfer, University of California Department of Engineering Report 58-5 (January 1958).
29. S. A. Guerrieri and R. D. Talty, "A Study of Heat Transfer to Organic Liquids in Single Tube, Natural-Circulation, Vertical-Tube Boilers," Chem. Engrg. Progress Symposium Series 52, No. 18, 69-77 (1956).
30. W. R. Gambill, "Physical Properties of Water," Chem. Engrg., 241 (May 18, 1959).
31. J. H. Keenan and F. G. Keyes, Thermodynamic Properties of Steam, John Wiley and Sons, New York, 1936.
32. G. O. Curme, Jr., and F. Johnston, Glycols, ACS Monograph 114, Reinhold, New York, 1952.
33. W. R. Gambill and R. D. Bundy, "High-Flux Heat-Transfer Characteristics of Pure Ethylene Glycol in Axial and Swirl Flow," Paper No. 2, AIChE National Meeting, Los Angeles, California, February 1962; to be published in the AIChE Journal.
34. T. C. Core and K. Sato, Determination of Burnout Limits of Polyphenyl Coolants, IDO-28007 (February 1958).
35. W. R. Gambill, 32-article series on physical property prediction, Chem. Engrg., February 1957 - January 11, 1960.
36. K. Anderson, Engineering Properties of Diphenyl, ANL-5121 (August 1953).
37. M. B. Noel, Experimental Investigation of Heat-Transfer Characteristics of Hydrazine and a Mixture of 90% Hydrazine and 10% Ethylenediamine, JPL Tech. Report No. 32-109 (June 1961).
38. R. E. Kirk and D. E. Othmer (editors), Encyclopedia of Chemical Technology, vol. 7, p. 570, Interscience, New York, 1951. [Hydrazine properties.]
39. N. B. Vargaftik, "The Thermal Conductivity of Liquids and Compressed Gases," pp. 142-149 of Proceedings of the Conference on Thermodynamic and Transport Properties of Fluids, London, July 1957, published by the Institution of Mechanical Engineers, London, 1958. [Hydrazine and N₂O₄ properties.]
40. M. B. Noel, Experimental Investigation of the Forced-Convection and Nucleate-Boiling Heat-Transfer Characteristics of Liquid Ammonia, JPL Tech. Report No. 32-125 (July 1961).
41. W. E. Forsythe (editor), Smithsonian Physical Tables, 9th Rev. Ed. (second reprint), published by the Smithsonian Institution, 1959. [Ammonia properties.]
42. N. A. Lange (editor), Handbook of Chemistry, 7th Ed., pp. 1463-1464, 1949. [Ammonia properties.]

43. International Critical Tables, vol. IV, pp. 442, 447, McGraw-Hill, New York, 1928. [Ammonia properties.]
44. R. M. Drake, Jr., p. 500 of Heat and Mass Transfer, by E. R. G. Eckert and R. M. Drake, Jr., 2d Ed., McGraw-Hill, New York, 1959. [Ammonia properties.]
45. D. E. Birdseye, Experimental Investigation of Heat-Transfer Characteristics of Liquid Nitrogen Tetroxide, JPL Tech. Report No. 32-37 (October 1960).
46. D. B. Larson, The Liquid State, IX - Review and Appraisal, privately circulated, December 1961.
47. H. L. McGill and W. L. Sibbitt, Heat Transfer and Pressure Drop of Water Flowing in a Small Tube, ANL-4603 (Part I), pp. 1-58 (February 1951).
48. A. S. Jameson and P. A. Lottes, Burnout Newsletter No. 1 (December 1954); data taken from ref. 6.
49. S. M. Lukomskii, "An Investigation of the Maximum Heat Flux during the Boiling of Water in Vertical Tubes," 1951, IG-Transl.-(R)-3, UKAEA (1955).
50. W. R. Gambill, R. D. Bundy, and R. W. Wansbrough, "Heat Transfer, Burnout, and Pressure Drop for Water in Swirl Flow Through Tubes with Internal Twisted Tapes," Chemical Engrg. Progress Symposium Series 57, No. 32, 127-137 (1961).
51. W. R. Gambill and N. D. Greene, "Boiling Burnout with Water in Vortex Flow," Chemical Engrg. Progress 54, No. 10, 68-76 (1958).
52. P. I. Povarnin and S. T. Semenov, "Investigation of the Abrupt Change in Boiling of Subcooled Water at High Flow Rates Through Pipes," Teploenergetika, No. 4, 72-79 (1959).
53. H. M. Epstein, J. W. Chastain, and S. L. Fawcett, Heat Transfer and Burnout to Water at High Subcritical Pressures, BMI-1116 (July 1956).
54. S. P. Kezios and R. K. Lo, Heat Transfer from Rods Normal to Subcooled Water Flow for Non-Boiling and Surface-Boiling Conditions up to and Including Burnout, ANL-5822 (January 1958).
55. S. P. Kezios, Tong-Soo Kim, and F. M. Rafchick, "Burnout in Crossed-Rod Matrices under Forced Convection Flow of Water," Paper No. 31, pp. 262-269 of 1961 International Heat Transfer Conference (Boulder, Colorado), Part II.
56. G. Leppert, C. P. Costello, and B. M. Hoglund, "Boiling Heat Transfer to Water Containing a Volatile Additive," Trans. ASME, 1395-1404 (Oct. 1958).
57. R. T. Weatherhead, "Boiling Burnout Heat Flux for Wires in Water Crossflow at Atmospheric Pressure," Report NDA-9 (Boiling Burnout Progress No. 5) (June 1955).
58. M. Troy, Upflow Burnout Data for Water at 2000 Psia in 0.097 in. x 1 in. x 27 in. Long Rectangular Channels, WAPD-TH-340 (July 1957).
59. S. Mirshak, W. S. Durant, and R. H. Towell, Heat Flux at Burnout, Savannah River Laboratory Report DP-355 (February 1959).
60. W. R. Gambill and R. D. Bundy, HFIR Heat-Transfer Studies of Turbulent Water Flow in Thin Rectangular Channels, ORNL-3079 (June 1961).

61. W. H. McAdams et al., "Heat Transfer at High Rates to Water with Surface Boiling," Ind. and Engrg. Chem. 41, No. 9, 1945-1953 (1949).
62. V. S. Chirkin and V. P. Iukin, "Critical Point in Heat Removal from Boiling Water Flowing Through an Annular Gap," in English, J. Tech. Physics 1, 1503-1515 (1956).
63. D. Lee, "Nucleate Boiling Heat Transfer," pp. 1-38 of NYO-9646, Columbia University Chemical Engineering Department, Engineering Research Labs, Progress Report IX-QPR-2-61.
64. D. Lee, Columbia University Chemical Engineering Department, Engineering Research Labs, "Solid Rod Burnout Data," personal communication, August 1961.
65. S. Mirshak and W. S. Durant, Savannah River Laboratory, personal communication (January 1960).
66. N. L. Kafengauz and I. D. Bauarov, "The Effect of the Height of a Flat Aperture on the Transformation of Heat Flow into Water," Teploenergetika 3, 76-78 (1959).
67. S. S. Kutateladze, "Critical Thermal Flow for the Flow of a Wetting Liquid Containing an Underheated Core," Energetika, No. 2, 229-239 (1959).
68. T. H. Dimmock, Heat Transfer Properties of Anhydrous Ammonia, Reaction Motors Report No. RMI-124-81 (June 1957).
69. D. R. Bartz, "Factors Which Influence the Suitability of Liquid Propellants as Rocket Motor Regenerative Coolants," Jet Propulsion, 46-53 (Jan. 1958).
70. A. B. Witte, Experimental Investigation of Heat Flux at the Upper Limit of Nucleate Boiling for Two Mixtures of Hydrazine and UDMH, JPL Tech. Report No. 32-78 (April 1961).
71. W. R. Gambill, personal communication to D. R. Bartz, September 1961.
72. W. R. Gambill and H. W. Hoffman, "Boiling Liquid-Metal Heat Transfer," ARS Preprint No. 1737-61, presented at ARS-ORNL Space-Nuclear Conference, Gatlinburg, Tennessee, May 3-5, 1961.
73. B. Lubarsky and S. J. Kaufman, Review of Experimental Investigations of Liquid-Metal Heat Transfer, NACA Report 1270 (1956).
74. M. I. Korneev, "Heat Transfer in Mercury and Magnesium Amalgams during Boiling under Conditions of Free Convection," Teploenergetika 2, No. 4, 44 (1955); No. 7, 30 (1955).
75. S. S. Kutateladze et al., "Heat Transfer in Liquid Metals," J. Nuclear Energy, II, 2, 214-229 (1959).
76. A. I. Krakoviak, Oak Ridge National Laboratory, Reactor Division, personal communications, May 1961 and March 1962.
77. W. H. Lowdermilk et al., Investigation of Boiling Burnout and Flow Stability for Water Flowing in Tubes, NACA-TN-4382 (September 1958).
78. R. C. Noyes, from preliminary draft version of "An Experimental Study of Heat Transfer During Pool Boiling of Sodium," August 1961, now indexed as NAA-SR-6769, An Experimental Study of Sodium Pool Boiling Heat Transfer (March 30, 1962).

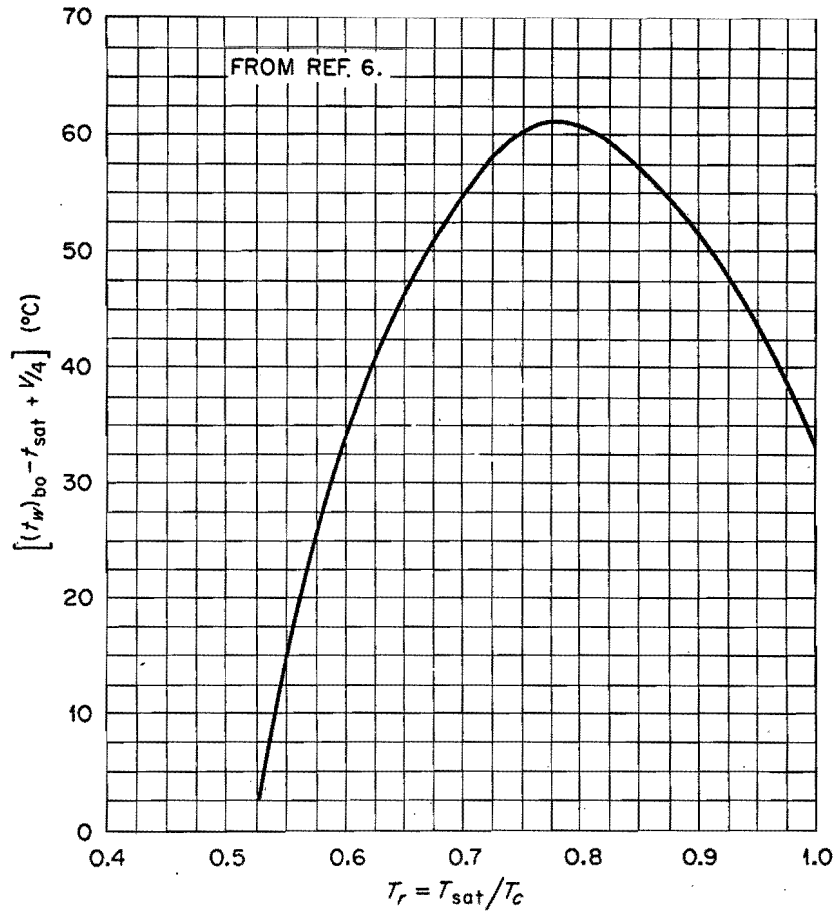


Fig. 1. Generalized Correlation of Wall Superheat at Burnout.

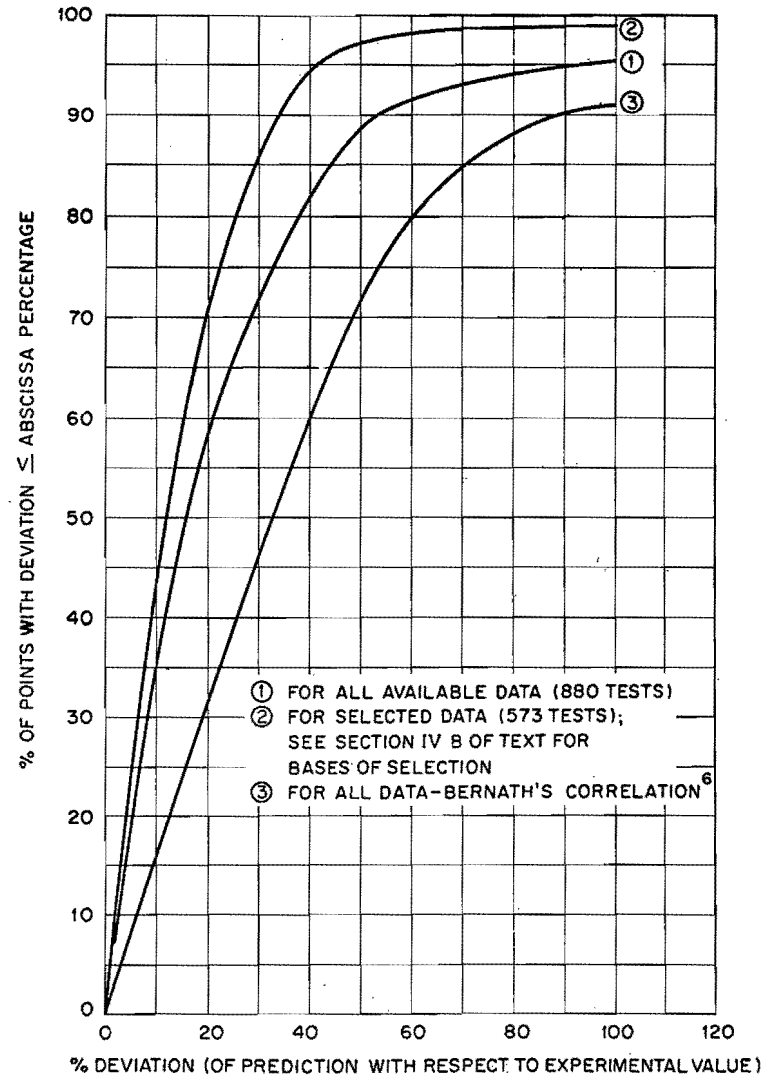


Fig. 2. Deviation Distributions for Water Burnouts.

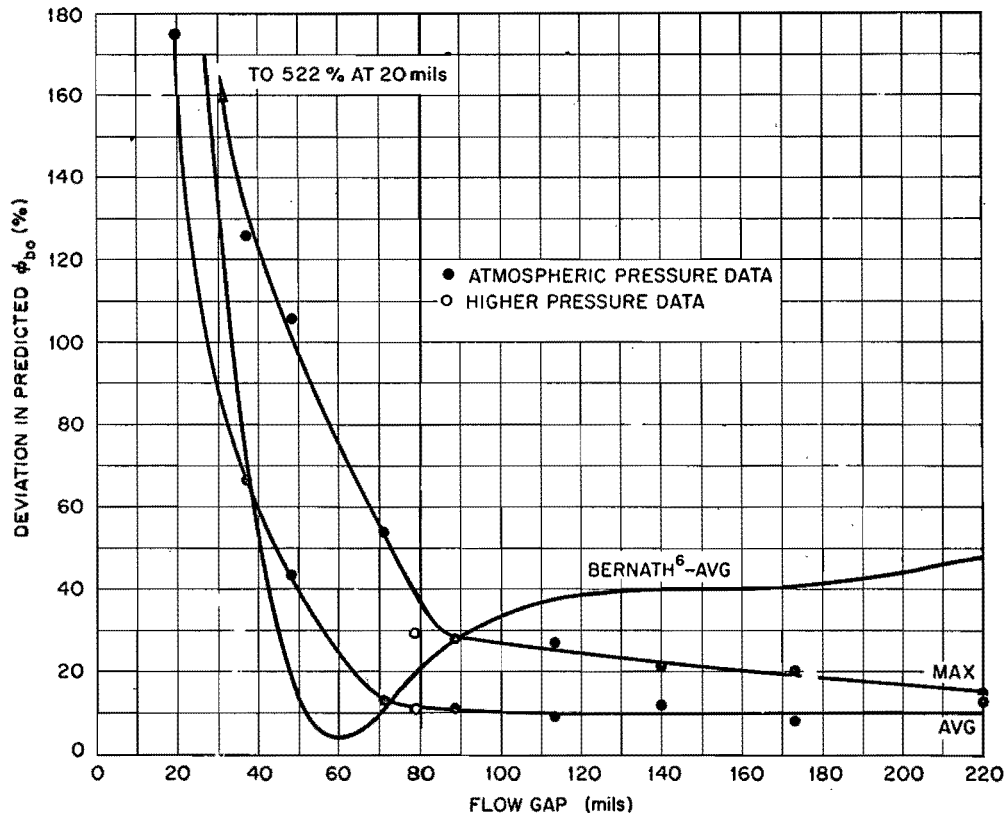


Fig. 3. Variation of Prediction Deviation with Flow Gap for Annulus Burnout Data of Chirkin and Iukin⁶².

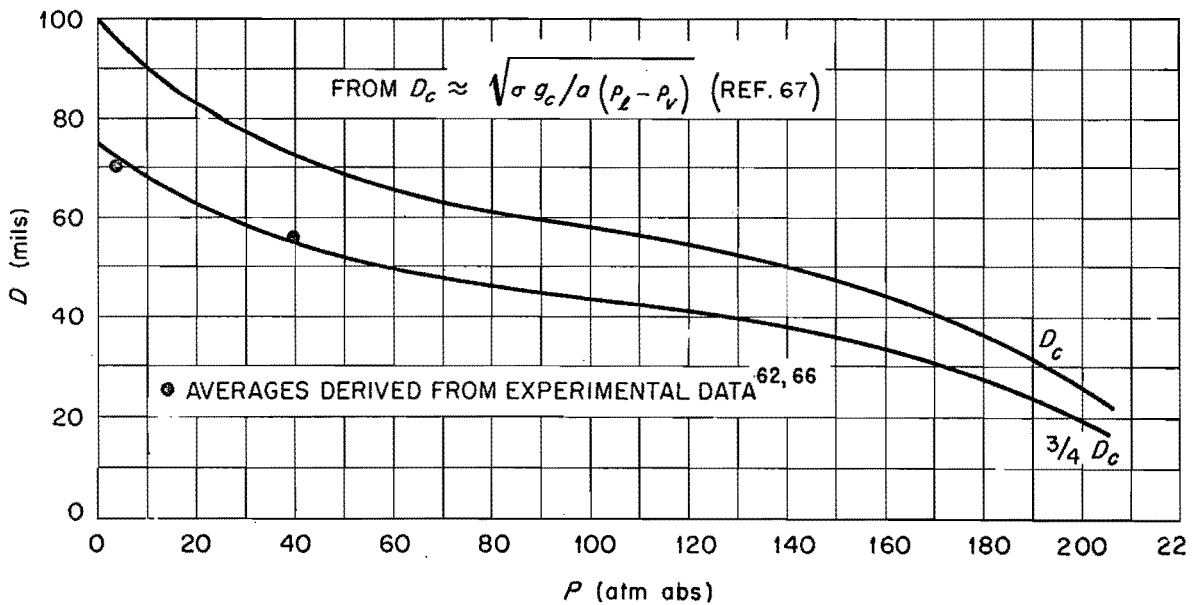


Fig. 4. Variation of "Critical" Flow-Passage Diameter with Pressure for Water.

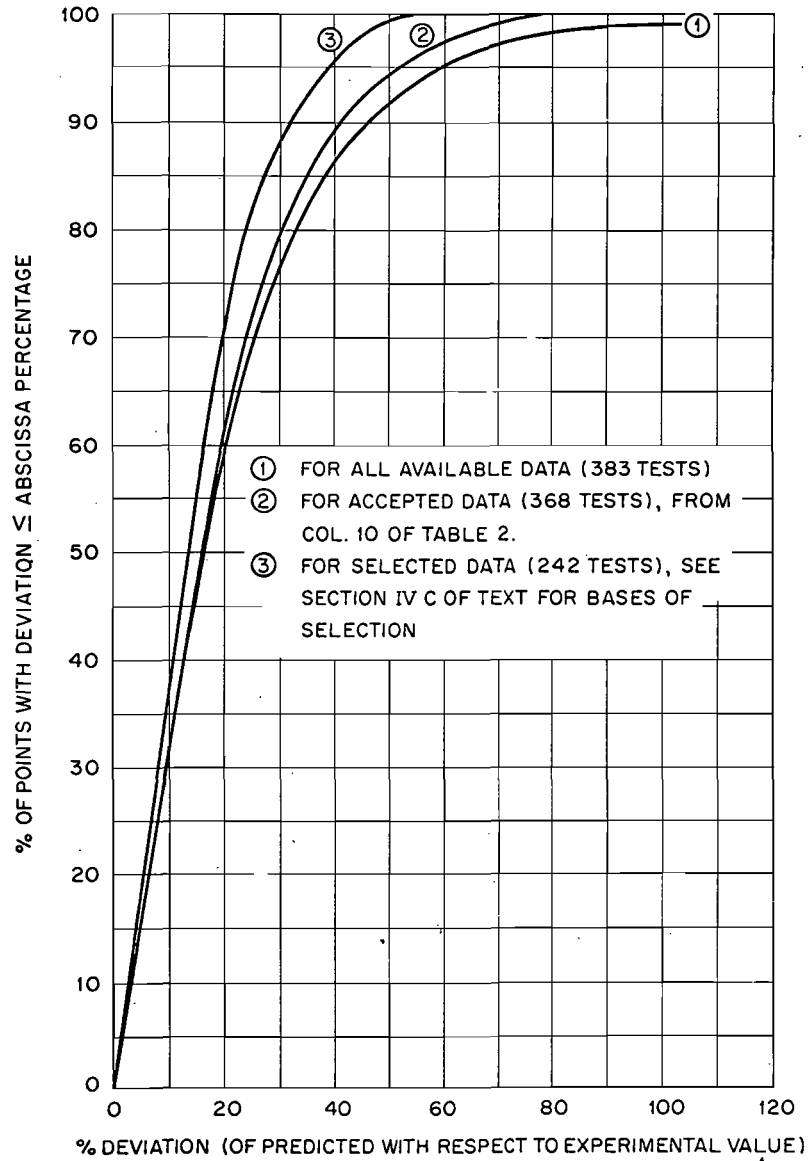


Fig. 5. Deviation Distributions for Non-Aqueous Burnouts.

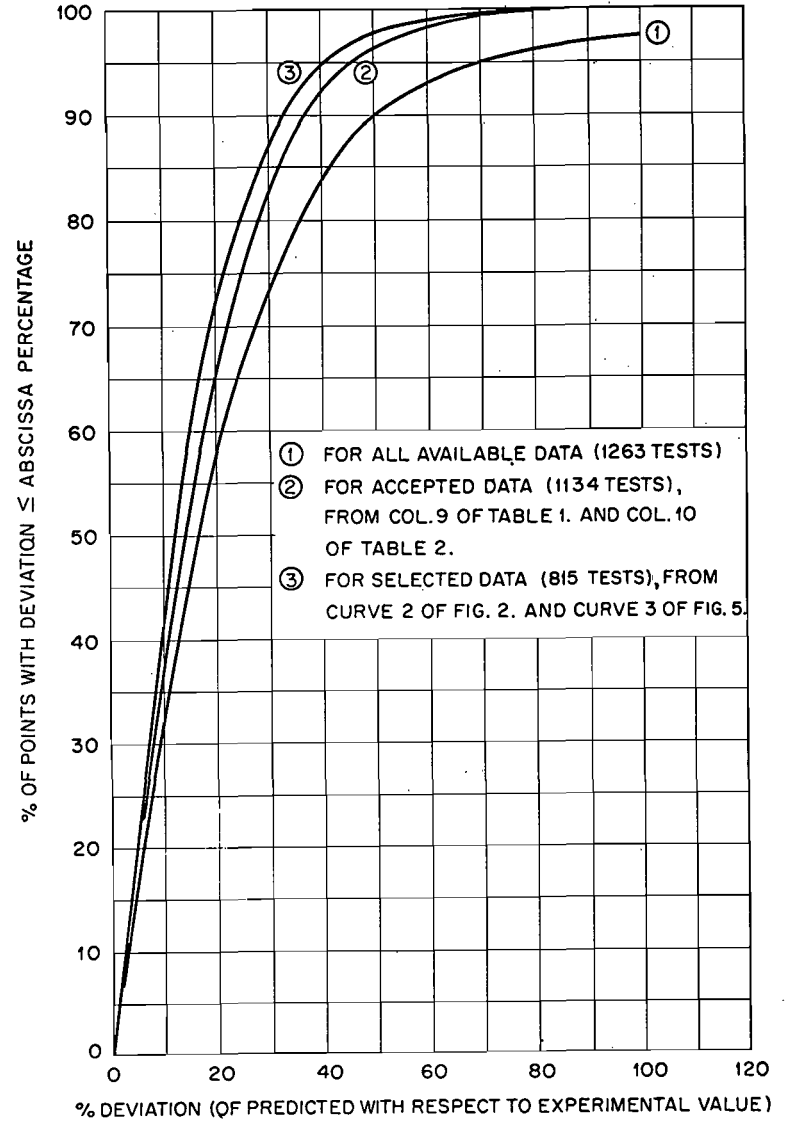


Fig. 6. Deviation Distributions for all Burnouts (Water and Non-Aqueous).

THERMAL DESIGN OF THE HFIR FUEL ELEMENT

By Neil Hilvety and T. G. Chapman

Oak Ridge National Laboratory
Oak Ridge, Tennessee

Three basic criteria were involved in establishing the thermal design of the HFIR. These were:

1. The total reactor power level, which was fixed at 100 Mw by a combination of economic considerations and californium production requirements.
2. The fuel element inside diameter and length-to-diameter ratio, which were fixed by the nuclear optimization studies.
3. The requirement that the reactor operate at the maximum permissible average power density in order to produce the maximum neutron flux in the water island.

In order to ensure that the reactor was capable of meeting these criteria, it was necessary to integrate into the thermal analysis those nuclear¹ and mechanical² parameters which influence the heat transfer characteristics. The thermal design of the HFIR fuel element was based on a series of hot-spot parameter studies which were conducted to establish the reactor design rather than to check out the adequacy of a particular design.

Besides the nuclear flux peaking, there were four basic types of factors considered in this hot spot analysis:

1. Fuel element fabrication tolerances (coolant channel dimensions, plate fuel content, fuel distribution, etc.).

2. Fuel-plate defects (nonbonds and local fuel segregation).
3. Changes in coolant channel dimensions caused by fuel-plate deflections resulting from hydraulic and thermally imposed loads.
4. Uncertainties in plant operating parameters (neutron flux peaking, power level, coolant temperature, pressure level, circulation rates, etc.).

In the final fuel element design, the average power density at design power level is 2 Mw/liter, which corresponds to an average heat flux of 0.8×10^6 Btu/hr-ft². Taking into account neutron flux peaking, fabrication tolerances, fuel-plate-defect factors, and uncertainties in operating parameters, the hot-spot effective power density could be as high as 5 Mw/liter. The hot spot problem is further accentuated by the requirement for high fuel element reliability. In the HFIR, failure of a single fuel plate would mean that the entire fuel assembly would have to be replaced. Because of the symmetry built into the reactor, the worst possible hot spot cannot be limited to just a few fuel plates that could be specially fabricated and inspected.

In order for the hot spot analysis to guarantee an adequate burnout margin and because of the lack of sufficient statistical data on many of the factors involved, the more-or-less conventional approach was adopted of assuming that all hot-spot factors would be simultaneously superimposed in the worst possible way at one given point in the reactor. The principle difficulty with this approach is that it usually results in a high degree

of conservatism. With the high local power densities of the HFIR, an excessively conservative analysis could result in limiting the reactor performance. Also, since it was necessary to conduct parameter studies on the effects of individual factors, the procedure had to account directly for the effects of these factors, rather than to combine effects in overall hot-spot factors. The hot-spot analysis was tailored to minimize the usual thermal contingency factors and to facilitate the necessary parameter studies.

The system was described mathematically so that each of the heat transfer parameters (flow rates, coolant temperature rises, film temperature drops, etc.) was a function of the tolerances and the uncertainty and defect factors by which it could be influenced. In this way the effects of the individual factors could be conveniently determined. This system also eliminated inclusion of conflicting factors in the same calculation and gave proper advantage credit to one parameter caused by a disadvantage to another. For example, one calculation cannot take into account adjacent wide and narrow channels for calculating pressure-induced fuel-plate deflection and at the same time assume adjacent narrow channels for calculating plate temperature and buckling, and factors that cause an increase in bulk water temperature also result in an increase in heat transfer coefficient. It was also decided to base burnout on steady-state operation at the calculated burnout power level rather than on the required increase in local heat flux to cause burnout; that is, in determining the burnout point, all temperature-dependent variables were evaluated at the burnout power level.

Experimental data correlations were examined to ensure that they applied at HFIR operating conditions and that the experimental data spread was reduced to the practical minimum. Special experiments were run that simulated as nearly as feasible the actual HFIR conditions. Included in these investigations were experiments on core pressure drop,³ fuel plate oxide film buildup,⁴ heat transfer coefficient,⁵ burnout heat flux,⁵ and fuel plate deflection due to hydraulic pressure,⁶ creep and buckling.⁷

Many factors not normally considered were included directly in the analysis. In addition to the effects of fuel-plate deflections local heat-flux peaking factors, such as nonbonds and fuel segregation, were considered. In the case of those factors which could be limited to small plate areas by proper inspection techniques, both heat conduction in the plane of the plate and the effects of changes in local heat transfer coefficient on this conduction were taken into account. It was assumed in evaluating these factors that the burnout heat flux correlation was independent of hot spot size and therefore applied to these very local areas. (The hot-spot size effect is currently being investigated and may be included at a later date.) The buildup of oxide film on the fuel plates was also considered.⁴ This factor enters into the fuel plate deflections by effecting both the fuel plate mechanical strength and the temperature differences that cause thermal deflections.

The basic approach to the HFIR hot spot analysis of assuming all factors to be simultaneously superimposed at a given point is conventional.

The application of this approach and the degree of detail involved in this particular study depart, however, from the conventional.

The principle factors and design parameters used in the hot spot analysis are listed below:⁸

Core Dimensions

a	Distance from top of core to hot spot, ft.
w	Fuel plate thickness, mils
e	Coolant channel thickness, mils
L	Active core length, in.
H	Coolant channel length, in.
b	Side plate thickness, in.

Design Operating Conditions and Nuclear Characteristics

ΔP	Core pressure drop, psi
P	Core inlet pressure, psia
T_i	Coolant inlet temperature, °F
Q/A	Average core heat flux, Btu/hr-ft ²
q_m/q_a	Core maximum to average power density ratio
$(q_a)_{hc}/(q_a)_c$	Hot channel average to core average power density ratio
$(q_m/q_a)_{E, hc}$	Hot channel radial maximum to average power density ratio
q_s	Side plate heat generation rate at 100 Mw, Btu/hr-in ³
N	Side plate cold streaking factor, fraction of nominal bulk temperature rise
t_i	Time since start of fuel cycle, hr
$(Q/A)_i$	Core average heat flux during cycle period between t_{i-1} and t_i , Btu/hr-ft ²
$(\Delta P)_i$	Core pressure drop during cycle period between t_{i-1} and t_i , psi

Fuel Element Fabrication Tolerances

$\Delta\epsilon_{\text{avg.}}$	Average coolant channel thickness variation, mils
$\Delta\epsilon_{\text{max.}}$	Maximum coolant channel thickness variation, mils
ΔW_{plate}	Deviation in total plate fuel loading, % of design value
$\Delta W_{\text{profile}}$	Deviation in local plate fuel loading, % of design value

Fuel Plate Defects

ΔQ_1	Local heat-flux peaking caused by nonbonds, fractional increase
ΔQ_2	Local heat-flux peaking caused by fuel segregation, fractional increase

Uncertainties in Performance and Operating Conditions

U_1	Fuel-element-header flow-distribution factor
U_2	Core friction-loss-correlation deviation
U_3	Degree of mixing in hot channel
U_4	Reactor-power-level measurement accuracy
U_5	Inlet temperature measurement and control accuracy
U_6	Pressure control accuracy
U_7	Heat-transfer-coefficient correlation uncertainty
U_8	Burnout-heat-flux correlation uncertainty
U_9	Uncertainty in calculated neutron-flux peaking

All of the basic reactor design parameters were specified, including the location of the hot spot. The analysis program was set up so that any

desired hot-spot location could be examined. The HFIR hot-spot calculations were all based on a hot spot at the core outlet and at the radial point of maximum closing of the channel resulting from pressure-induced fuel-plate deflection. The pronounced flux peaking at the ends of the active fuel region fixes the axial location of the hot spot. Since the radial point of maximum pressure deflection gives a maximum hot-streaking effect, this was the radial location chosen for these studies. The axial location of the hot spot is fixed by the first input number. The radial location enters into the constants in the plate deflection equations.

In addition to the hot-spot location, the individual coolant channel nominal thickness and length, the fuel plate thickness, and the active core length were specified, and the nominal core pressure drop, inlet temperatures, and operating pressure were fixed. The core average heat flux was an input parameter when it was desired to examine operating conditions at some fixed power level and was an output number in calculating the burnout power level. Calculated neutron-flux peaking constants established the nuclear contribution to the hot-spot operating conditions. Heat generation and removal from the side plate were important variables in the fuel-plate-buckling calculations. The time in the cycle and previous reactor operating history were specified for calculating fuel-plate oxide buildup.

In evaluating the factors that give rise to hot spots, it was necessary to consider hot plates and hot streaks in addition to hot spots. Since plate deflections are based on the average plate temperature at the hot-spot elevation, anything that can influence this average temperature must be applied as a hot-plate factor. The tolerance on the average coolant

channel thickness, which determines the channel flow area, is such a factor, since it affects the entire channel width. The tolerance on the local coolant channel thickness, which influences only a small portion of the channel, can, at worst, influence a narrow streak down the plate length, so it was applied as a hot-streak factor. Maximum plate loading tolerances can affect an entire plate, while a tolerance on fuel contour is influential only over a local spot, or at worst, a hot streak. Local heat flux peaking caused by nonbonds and segregation can be limited to small plate areas by proper inspection techniques, and therefore was considered as a hot spot factor.

The uncertainty factors were applied in a similar manner. Header flow distribution is a hot streak factor, core friction loss deviation is a hot-plate factor, mixing is a hot-streak factor, power-level-measurement accuracy is a hot plate factor, etc. Similarly, the plate deflection calculations were separated as to their influence on either the hot streak or the hot spot. A pressure deflection was assumed to be uniform down the plate length. Pressure differentials across an involute result in an S shaped deflection curve.² This does not result in an appreciable change in average coolant channel thickness, but does result in a change in local channel thickness. Pressure deflection is thus a hot-streak factor. Buckling caused by fuel plate-to-side plate temperature differences was shown by experiments to be a local phenomenon and is thus a hot-spot factor affecting local coolant velocity.

Some of the results of the HFIR hot-spot calculations are presented in Table 1. Heat flux and operating temperature values are listed for both

Table 1.

HFIR Fuel ElementThermal Characteristics at Design Conditions

	Start of Cycle			End of 15 Day Cycle		
	Fuel Average	Hot Streak	Hot Spot	Fuel Average	Hot Streak	Hot Spot
Heat flux, Btu/hr-ft ²	0.8×10^6	1.1×10^6	2.1×10^6	0.8×10^6	1.1×10^6	2.1×10^6
Mean fuel plate temp., °F	214	349	428	220	469	627
Metal-oxide interface temp., °F	206	337	407	212	457	606
Oxide-water interface temp., °F	206	337	407	206	344	417
Water inlet temp., °F	120	121	121	120	121	121
Water outlet temp., °F	189	257	257	189	255	255
Calculated minimum burnout power level (nominal vessel inlet pressure = 900 psia.), MW.	165			150		

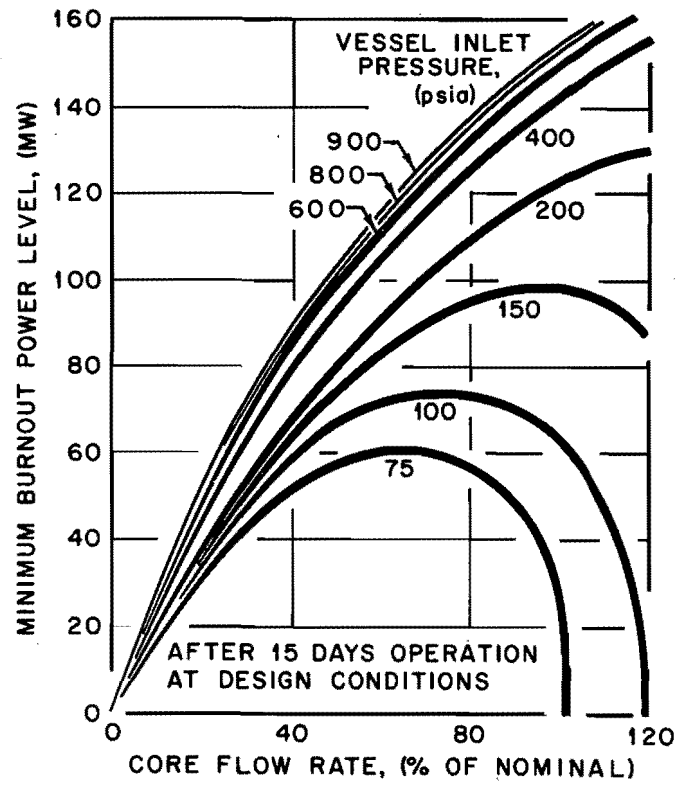
beginning and end of cycle for the average fuel element conditions, the outlet from the maximum hot streak, and the maximum hot spot. As would be expected, buildup of the oxide film on the fuel plates results in a decrease in burnout power level as the fuel cycle progresses (165 to 150 Mw). the oxide buildup also results in an appreciable increase in plate temperatures, as evidenced by the hot spot mean metal temperature, which increases by 200°F during the fuel cycle. Since plate strength is dependent upon the hot-plate temperatures, which are somewhat lower than the hot streak values listed here, it appears from these data that, with the possible exception of very local hot spots, the temperatures are such that plate strengths can be expected to remain at reasonable values throughout the fuel cycle.

Buildup of the oxide film also produces another interesting result, in that the arrangement of wide and narrow coolant channels that produces the lowest burnout power level at the start of the cycle is not the one that is nearest to burnout at the end of the cycle. (The computer program has the capability of examining all potential limiting channel arrangements, such as alternate narrow and wide channels, alternating pairs of narrow and wide channels, all narrow channels, etc.) There is a slight unexplained discrepancy between tabulated temperatures at the beginning and end of cycle. The hot-streak outlet temperature, according to the table, decreases slightly during the cycle. This occurs because, at the start of the cycle, pressure-induced plate deflection resulting from unequal adjacent coolant channels is an important hot-streak factor, while at the end of the cycle, the additional local plate deflections caused by fuel plate-to-side plate temperature differences become controlling, and the case of adjacent narrow channels is the nearest to burnout.

The effects of vessel inlet pressure and coolant flow rate were of special interest in establishing the desired reactor operating conditions, and in examining accidents such as loss of pumping power. The effects of these variables are indicated in Fig. 1. It is evident that there is little to be gained by operating at pressures in excess of about 600 psia, especially when consideration is given to the effect high operating pressures might have on the usefulness of a boiling detector or on void coefficient effects that might otherwise be of benefit during a transient.

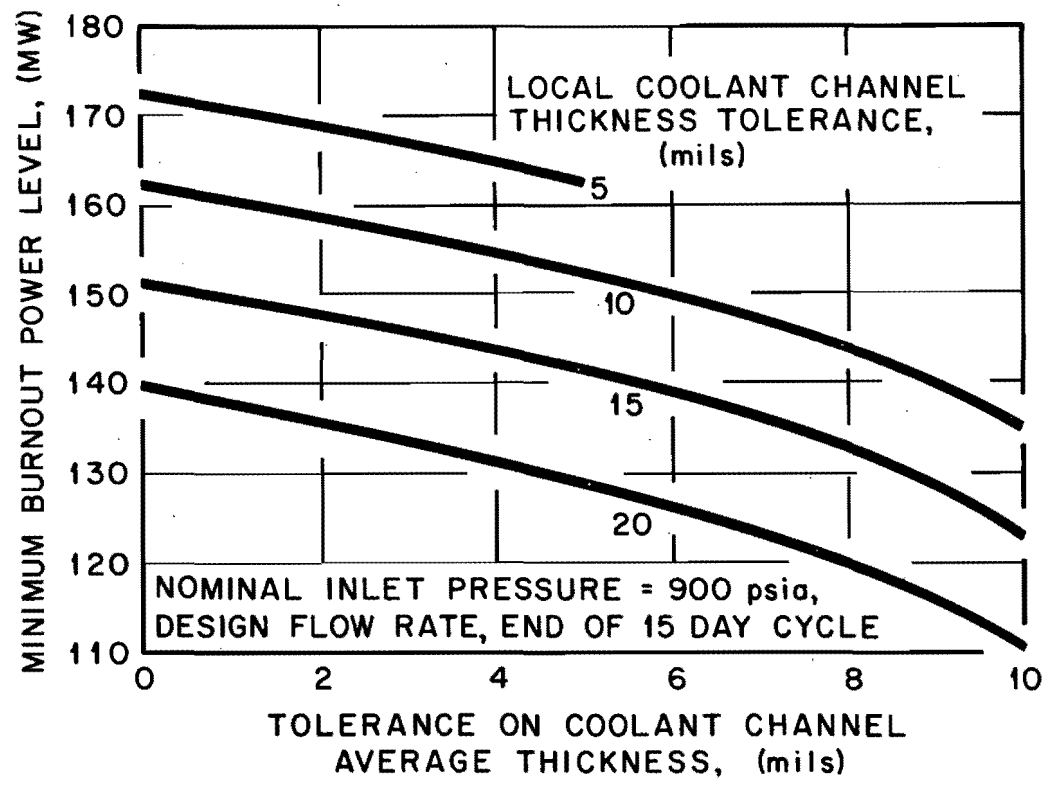
The effect of coolant channel tolerances on minimum calculated burn-out power level is shown in Fig. 2. These curves indicate that for a constant average coolant channel thickness tolerance, a change in local channel thickness tolerance of 5 mils results in about a 7.0-Mw change in burnout power level. A 5 mil change in average channel thickness tolerance, with the local tolerance constant, would result in about a 12.5-Mw change in burnout power level. Studies such as this have been used to establish the required fuel element fabrication tolerances.

In addition to the steady-state hot-spot data, useful information was obtained from this analysis for conducting transient hot-spot studies. The time constant for transfer of heat from the fuel plates to the coolant in the HFIR is so small that relatively slow transients, such as pump coastdown, are essentially equivalent to steady-state operation, so the steady-state procedure can be used directly. For extremely fast transients, the steady-state results give a possible basis for estimating the consequences of the excursion. If it is assumed that, during a transient, film



EFFECT OF FLOW RATE AND OPERATING PRESSURE ON BURNOUT POWER LEVEL

Figure 1



EFFECT OF COOLANT CHANNEL THICKNESS ON BURNOUT POWER LEVEL

Figure 2

blanketing occurs when the hot-spot heat flux reaches the burnout heat flux calculated by the steady-state procedure, the safety system can be required to limit the peak heat flux to this point, which would probably result in no permanent core damage, or it can be assumed that the hot spot becomes insulated at this heat flux and hot-spot melting can be set as the limiting level for the excursion. An excursion of this magnitude would, of course, result in permanent core damage, and would necessitate replacing of the fuel assembly, but it would not be expected to result in excessive contamination of the reactor system.

The results obtained to date indicate that the HFIR can meet the thermal design criteria. Plans are being made to expand the hot-spot computer program to permit the programming of fuel cycles for the HFIR. This might permit the use of below standard fuel elements to their best advantage and programming for above design point operation.

Bibliography

1. R. D. Cheverton, "Nuclear Design of the HFIR," Sept. 17, 1962, Proceedings of the Gatlinburg Research Reactor Fuel Elements Conference.
2. J. R. McWherter and T. G. Chapman, "Mechanical and Hydraulic Design of the HFIR," Sept. 17, 1962, Proceedings of the Gatlinburg Research Reactor Fuel Elements Conference.
3. T. H. Mauney, personal communication, 1960.

4. J. C. Griess, et al., "Effect of Heat Flux on the Corrosion of Aluminum by Water, Part III. Final Report on Tests Relative to the High-Flux Isotope Reactor," Dec. 5, 1961, ORNL-3230.
5. W. R. Gambill and R. D. Bundy, "HFIR Heat Transfer Studies of Turbulent Water Flow in Thin Rectangular Channels," June 5, 1961, ORNL-3079.
6. T. G. Chapman, "Thermal Expansion and Pressure Differential Induced Stress and Deflections of HFIR Involute Contoured Fuel Plates," 1962 (to be issued).
7. R. N. Lyon, personal communication, Sept. 6, 1960.
8. Neil Hilvety, "Preliminary Hot Spot Analysis of the HFIR," March 1, 1960, Supplement, Sept. 18, 1961, CF 60-3-12.

Acknowledgements

The authors wish to express their gratitude to R. D. Cheverton for the many helpful suggestions provided throughout the course of these studies, to C. D. Griffies for his conscientious coding of the hot spot analysis program and for his continuing efforts in expediting the numerous machine calculations involved, and to Louise Ferguson for her very efficient secretarial assistance in preparing this report.

PART I : Design and hydraulic tests of some special fuel elements
FUEL ELEMENTS FOR THE BELGIAN HIGH FLUX TEST REACTOR BR2

Written by : J. HERPIN , Technology Department

C.E.N.-EURATOM Operating group

I. INTRODUCTION AND SUMMARY.

The experimental assemblies to be installed into the reactor BR2 - the Belgian high flux engineering and test reactor - give numerous problems concerning the level of the neutron flux required for the samples or specimens to irradiate.

The standard BR2 fuel element is made of six concentric fuel tubes with an inner central support tube. In order to comply with the nuclear desiderata or requirements of the various experimenters, special types of fuel elements have been studied, designed and tested. For two types of special fuel elements, a description is given in this paper : one type is a five concentric fuel tubes type without an inner central support tube, the other type is a two concentric fuel tubes type with an inner central tube acting as a neutron screen.

One reason for this special design of fuel element is to bring to a minimum the volume of moderator between fuel and experimental assembly in order to have a maximum neutron fast flux. With this type of fuel element, it is possible to achieve, in a high flux research reactor, experimental conditions encountered in power reactors.

2. BRIEF DESCRIPTION OF THE EXPERIMENTAL FACILITIES OF THE BR2 REACTOR.

2.1 The BR2 reactor.

BR2 is a high flux engineering and test reactor, light water cooled and moderated, having a matrix in beryllium and loaded with fully enriched uranium fuel elements. (Fig. 1). One main feature of the reactor is the individual access to each canal or channel at the top cover of the pressure vessel. Each canal is cylindrical and the fuel elements are also cylindrical. The reactor has 64 standard channels (85 mm or $3\frac{1}{2}$ inches nominal diameter) , 5 large channels (200 mm or 8 inches nominal diameter) and 10 small channels (50 mm or 2 inches nominal diameter). The five large channels and thirteen standard channels are through.

The versatility of the experimental facilities is important due to the fact that the 64 standard channels are identical and that it is possible to obtain, with a special beryllium plug, three standard channels out of one large.

The reactor permits the installation of the following experimental facilities :

- through loops (in large and standard channels),
- thimbles with top or bottom external connections,
- capsules with or without temperature control,
- basket with or without instrumentation,
- hydraulic rabbits.

The list of documents giving the description of the reactor is mentioned in Appendix VII.

2.2 The BR2 standard fuel elements.

Each standard fuel element is an assembly of six concentric tubes ranging in size from 3.30 to 7.62 cm (1.3 in to 3 in) in diameter, each tube with 276.2 cm (30 in) fuel length. A tubular experimental space for a very high neutron flux is available in the center of the element and may be enlarged by removing one or more of the innermost tubes. The fuel tube wall cross section is the same as that of the MTR or ETR (U.S.A. research reactor) fuel plate. The tube wall is 1.27 mm (50 mils) thick, consisting

of a 24 w/o uranium-aluminum meat 0.50 mm (20 mils) thick, (uranium 90% enriched), clad on both sides with aluminum 0.38 mm (15 mils) thick. The nominal coolant passage between plate is 2.95 mm (118 mils). For a six tube assembly, the loading is 244 grams of U-235 per fuel element, which are divided between the different plates as follows :

Plate 1 : 7,420 g	Plate 4 : 14,791 g
2 : 9,872 g	5 : 17,245 g
3 : 12,306 g	6 : 19,70 g

A central aluminum support tube acts as structural member of the assembly.

As far as the manufacturing of the fuel element assembly is concerned, three solutions have been examined :

- a) the basic solution : coextruded tube;
- b) an intermediate solution : tube made by three curved plates, each being a section of 120° of angle ; the longitudinal sides of the plates are bent and welded or brazed one to another to form a tube;
- c) an alternative solution : tube made of three curved plates, each being a section of 120° of angle; the longitudinal sides of the plates are set in longitudinal webs attached to a central support tube.

The fuel element type used for the time being in the reactor is the one made of plates set in longitudinal spacers (Fig. 3 and 4).

The principal components of the standard fuel element are :

- the fuel element tubes,
- the inner support tube,
- the end fittings,
- the bayonet locking device.

3. BRIEF DESCRIPTION OF SOME SPECIAL FUEL ELEMENTS.

The differences between standard fuel element and special fuel element concern mainly :

- a) the number of fuel element tubes,
- b) the present or not of the inner support tube.

Different designs with and without inner support tubes are shown on Fig. 5, 6, 7, 9, 10 and 11. On those figures, nominal diameters are given. In the present stage of development, all fuel elements are made of curved plates set in longitudinal webs.

3.1 Design of the fuel element without a central support tube.

For the fuel element without central support tube, the three longitudinal straighteners or spacers are held together at their ends in hollow rings of small thickness giving a minimum of water pressure drop.

To be used in the reactor, these elements must be supported : for this purpose, the ring interlocking the webs has a sloping surface which rests on three supporting points. These points are part of the experimental device installed in the center of the fuel element. To remove it from the reactor channel, the fuel element is loosely attached to one suspension tube. The suspension tube is designed and built such that the fuel element will never be suspended during normal operation of the reactor.

This fuel element has no centering devices ; these are transferred to the thimble itself or to the suspension tube.

3.2 Design of the fuel element with inner support tube.

This fuel element is almost similar to the standard one with the exception that the number of fuel tubes is reduced. For the element with four or five fuel tubes, the last inner tube has been replaced by the support tube and the bayonet device and the inner tube presents a larger diameter ; the centering devices or end fittings are almost identical.

For the element with less than four tubes, the centering device is changed. In addition, it is possible to have a special inner support tube, for instance with an absorber, to obtain in the central volume of the fuel element a given neutron flux spectrum. This inner support tube could be made of cadmium sheeted in aluminum or stainless steel.

3.3 Design of the fuel element with outer support tube

This configuration has not been used yet ; it will be, when the inner tube has to be a fuel tube and when the experimental device cannot support the fuel element.

4. DETAILED DESCRIPTION OF THE ELEMENT WITH FIVE PLATES AND WITHOUT SUPPORT TUBE, TO BE USED WITH THE "I.P.M.T.L."

4.1 The I.P.M.T.L. (x)

The I.P.M.T.L., studied and manufactured under contract in the scope of a research and development program on a high temperature gas reactor, will permit to study the effect of fast neutrons on the mass transfer of graphite up to 1500°C, exposed to a helium flow carrying a known amount of impurities such as oxygen, water and carbon oxide and dioxide.

The pressure tube is a thimble, which penetrates into the reactor vessel through the bottom cover. Its upper section, situated in the reactor core, carries the fuel element (Fig. 13). In order to obtain a spectrum of eipthermal and fast neutrons, the fuel plates should be very close to the pressure tube.

4.2 The fuel element with five plates and without support tube.

This element is shown in Fig. 7 and is of the type described in section 3.1. (xx)

The results of the hydraulic tests are given in Appendix II and III.

(x) I.P.M.T.L. In Pile Mass Transfer Loop

(xx) Mechanical study and prototype fabrication were made by "Metallurgie & Mécanique Nucléaires" (M.M.N.) Europalaan, Dessel.

4.3 Handling tube.

The design of the handling tube has been subject to numerous transformations during the hydraulic tests in order to decrease the pressure drop. Fig. 14 shows the actual design whose dimensions and general characteristics take into account the following facts :

- in operation position, the element rests on the thimble, and is not suspended anymore by the handling tube ,
- during operation, the element cannot become free of the handling tube.

The maximum relative values of displacement have been calculated and are 20 mm, the fuel element rising with respect to the tube. In order to avoid an eventual rotation of the element, a blocking plate hanging from the handling tube remains in contact with the top of the spacers by means of a spring.

4.4 Hydraulic tests with thimble.

These hydraulic tests consist of :

- a) endurance tests and pressure drop measurement,
- b) determination of speed in annulus.

These tests are given in Appendix II and only the results are discussed below.

- a) Endurance or long run tests and pressure drop measurement.

The prototypes of the fuel elements will be submitted to the following tests:

- 24 hours at 100 % of the nominal flow
- 24 hours at 110% " " " "
- 24 hours at 120% " " " "
- 24 hours at 130% " " " "
- 6 hours at 140% " " " "

The nominal flow is the flow obtained in the fuel elements for a pressure drop of 48 p.s.i. or 3.360 kg/cm^2 at the limit of the matrix i.e. from the top of the upper extension piece to the bottom of the

lower extension piece. This value has been chosen arbitrarily for the tests and might slightly change for the reactor.

A dummy element (number SV n.02) of $34.6 \text{ mm} \begin{matrix} + 0 \text{ mm} \\ - 0,2 \text{ mm} \end{matrix}$ inner diameter allowing an easy handling, has been subjected to this test ; no damage was observed which could have resulted from the clearance between the spacers and the thimble.

Besides, the dummy element SV n.01 (of $34 \text{ mm} \begin{matrix} - 0 \text{ mm} \\ + 0,5 \text{ mm} \end{matrix}$ inner diameter) has been subjected to an endurance test of 1840 h at the above mentioned nominal flow.

The endurance test proved that the element resisted well to the vibrations and no damage was observed even after 6 hr. tests at 140 % of the nominal flow.

b) Speed between plate.

Speed has been measured at various flows and at various pressure drops at the matrix. Only two values are mentioned here.

	Element SV n-01 Test with pressure drop at the matrix of 2.8 kg/cm^2 (40 psi)	Element SV n-01 Test with pressure drop at the matrix of 3.36 kg/cm^2 (48 psi)
annulus 1	9.0 m/sec	9.7 m/sec
annulus 2	8.9	9.9
annulus 3	8.9	9.8
annulus 4	9.0	9.8
annulus 5	8.8	9.6
annulus 6	8.8	9.6

More details about these tests and the mode of operation are given in Appendix II.

5. FUEL ELEMENT WITH FIVE PLATES AND WITHOUT SUPPORT TUBE COMBINED WITH AN IRRADIATION CAPSULE.

The fuel element with five plates combined with an irradiation capsule is shown in Fig. 16.

The basic principles of the element are identical to those of the element with a thimble ; however, the mean speed in the element is

about 10.7 m/sec with a pressure drop at the matrix of 40 psi (2.8 kg/cm²).

6. FUEL ELEMENT WITH TWO PLATES AND WITH SUPPORT TUBE TO BE USED WITH THE EXPERIMENT M.F.B.S.*

6.1. The M.F.B.S. loop.

By means of this loop will be studied the behaviour of a fuel pin for a fast reactor cooled with sodium. A fast neutron flux without thermal neutrons is required.

In order to obtain neutrons of the required energy, a boron carbide screen and a cadmium screen have been interposed between the pin and the surrounding fuel element to form a selective neutron filter. The cadmium screen is part of the fuel element and is thus situated in the primary water of the reactor, while the boron carbide is part of the experiment (Fig. 17)/

The primary coolant of the experiment is sodium ; it is wholly contained in a thimble which penetrates through the upper cover of the vessel to the core of the reactor and occupies a large reactor channel. The bottom end of this thimble is reduced in diameter to form the experimental section which is placed in the special fuel element. The experiment and the element are inserted in one of the three 84 mm channels of the large Be-plug. The other two channels are loaded with standard fuel elements ; so is obtained the compact loading necessary for the required neutron flux inside the pin.

6.2 The fuel element with two plates and with support tube.

The fuel element with two plates is shown in Fig. 12. As already mentioned the support tube consists of the 52-57 mm cadmium screen clad by 52-50 mm and 57-59 mm aluminum. The drums

*M.F.B.S. = Manipulation Franco-Belge Sodium

brazed to the extremities support the guide elements, which are extended by the bayonet hooking systems.

The centring devices had to be adapted to the small space available between the drum and the channel. The roller has been mounted at the extremity of a stainless steel arm, attached to the pins by two screws.

The hooking system is identical to that of the standard element but the inner diameter has been increased.

6.3. Hydraulic tests.

This element has not yet been subjected to hydraulic tests. The programmed tests are identical to those of the element SV n.

APPENDIX I.

Water loop for hydraulic tests.

The water loop in which are carried out hydraulic tests with BR2 type fuel elements - dummy and prototype - is actually equipped with three vertical channels working in parallel. Each channel represents the geometry of one standard (85 mm or 3 in nominal diameter) channel of the BR2 reactor.

The experimental section "2 A" is shown on Fig. 19 ; it simulates a BR2 channel surrounded with adjacent matrix pieces and cooling holes. The total water flow passing through the experimental section "2 A" is divided into two parts, one going inside the channel and the other passing outside the channel, in the cooling spaces provided between the hexagonal pieces.

The experimental section "2 B" simulates only a standard channel of the reactor ; it is shown on Fig. 20. This section is mainly used to study water flow distribution in fuel element annuli.

The experimental section "2 C" simulates a standard channel over its total length from the top of the reactor vessel to the bottom

cover. This section is mainly used to study water flow distribution in fuel element with through loop or with thimble having bottom connections.

Other experimental sections are presently in design or in construction ; one simulating a large reactor channel (200 mm or 8 in nominal diameter), one simulating a small reactor channel (50 mm or 2 in nominal diameter).

The water loop is presently equipped with two pumps, capable to work in series or in parallel. One pump unit has a speed variator to adjust water flow. One heat exchanger permits to regulate temperature. The operation of the loop is completely automatic and under servo-control as far as temperature, flow and pressure are concerned.

APPENDIX II.

Hydraulic tests I.

1. Introduction.

These tests are carried out on the fuel element type SV n-01. The dummy element is inserted into the experimental section "2 A", then into the experimental section "2 C", of the water loop, around a dummy of the I.P.M.T.L. experiment. The dummy thimble has an outer diameter of 33 mm instead of 34 mm; these tests are therefore to be considered as trials and afterwards they will be carried out with a thimble of 34 mm. Besides, the bottom tube of the loop has a diameter of 60 mm whereas the real tube is 57 mm.

2. Tests.

2.1. ----- In the experimental section "2 A".

Taking into account the pressure drops at the limits of the reactor matrix and at the end pieces, the static pressures are recorded at various points in order to establish the pressure curve of the whole device.

2.2. In the experimental section "2 B".

Speed measurements are made by means of pitot tubes ; the tests are carried out for various flows at a pressure of 5 kg/cm^2 and a temperature of 40°C .

3. Results.

3.1. Pressure curve recorded in the experimental section "2 A".

The pressure curve recorded in section 2 A for the elements SV n is shown in Fig. 25.

This diagram is established for a pressure drop at the limits corresponding to a total flow in the loop of 2274 liters/min ; this flow consists of : outer flow 545 liters/min

flow in the element 1729 liters/min

The mean speed in the element is 8.9 m/sec .

3.2. Long run test.

The dummy element, which is mounted on a thimble of 33 mm outer diameter, has been subjected to a long run test of 1840 hours for a pressure drop at the matrix of 48 psi or 3.4 kg/cm^2 corresponding to a mean speed between plates of 9.8 m/sec .

3.3. Measurement of speed between plate.

Fig. 22 gives a summary of the speeds measured by pitot tubes positioned at the center of the annuli 1 to 6 of the elements ; these speeds are corrected for the flows corresponding to the pressure drop of 40 psi (2.8 kg/cm^2) and 48 psi (3.4 kg/cm^2). The pitots are calibrated before installation in the fuel element and they differ at most $\pm 0.5\%$ from one to another. The measurements are carried out in each of the sectors of 120° delimited by the spacers and labeled I, II, III.

APPENDIX III.

Hydraulic tests II.

The tests are carried out in the experimental section "2 C" with a real thimble ; its upper part has an outer diameter of 34 mm, its lower part has a diameter of 57 mm. In this case, the circle inscribed in the three webs has a diameter of 34.6 mm.

1. Measurement of pressure drop and total flow.

1.1. Test conditions.

Temperature of the water is 40 °C ; pressure is : 5 atmospheres ; pressure drop at the limits of the matrix is 40 psi or 2.8 kg/cm². Fig. 26 shows the inner and outer pressure curve of the channel. The pressure curve of the test, already mentioned in Appendix II, is also shown.

1.2. Results.

For a pressure drop 2.8 kg/cm², the flow in the element is 1800 l/min ; this corresponds to a speed of 9.4 m/sec.
For a pressure drop 3.4 kg/cm², the flow in the element is 2000 l/min ; this corresponds to a speed of 10.5 m/sec.

2. Long run tests.

The following long run tests have been carried out, on the dummy element SV n-02.

Flow of 2000 liters/min or 10.5 m/sec	-	135 h
" " 2200 " " 11.5 " "	-	93 h
" " 2400 " " 12.6 " "	-	48 h
" " 2600 " " 13.6 " "	-	32 h
" " 2800 " " 14.6 " "	-	12 h

The dummy element SV n-02 has been subject to a total test period of 322 hours under severe conditions and no damage results on the spacers.

3. Measurement of speeds between plate.

These tests are not carried out yet.

APPENDIX IV.

Hydraulic calculations for the element S II s with experiment in place.

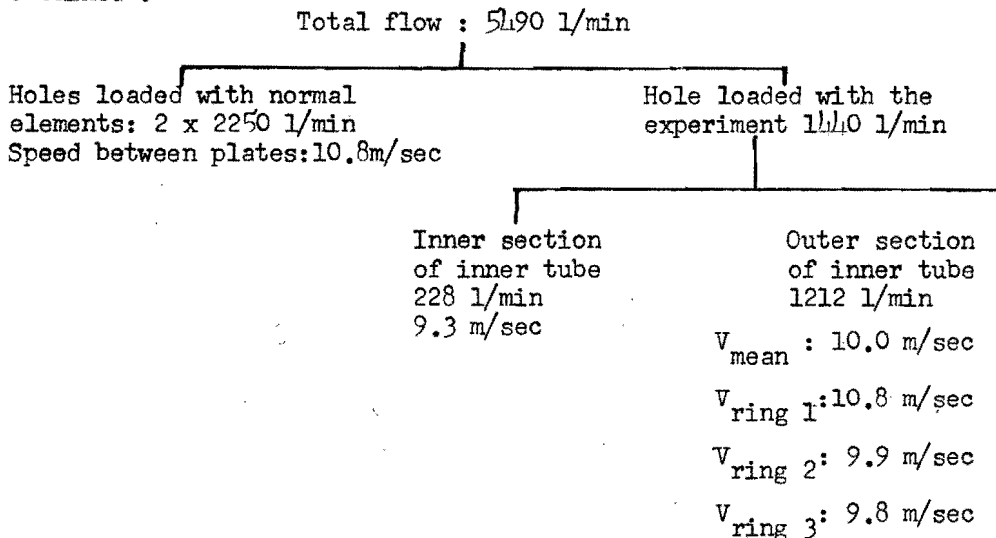
1. Purpose.

The purpose is the determination of the flows between the fuel tubes of the particular element S II s and in the inner tube.

The formulas used are those generally encountered in hydraulic studies.

2. Results.

For 60 mm diameter of the inner tube, the following results are obtained :



APPENDIX V.

Results of nuclear calculations giving the fluxes at the centre of the experiment inside the element SV n.

1. Hypotheses of calculation.

The experiment and its surrounding fuel element with five tubes is put in a channel which is surrounded by six fresh fuel elements and

fifteen poisoned elements in order to take into account the effect of control rods and other experiments.

All data concerning the fuel elements are those at the start of the operation cycle of the reactor.

The calculations are carried out in cylindrical geometry.

2. Results.

The radial flux distribution is shown in Fig. 25 where $\bar{\Phi}_1$ represents the epithermal flux and $\bar{\Phi}_2$ the thermal flux at the mid-plane of the reactor.

At the graphite sample the following values are expected :

$$\bar{\Phi}_1 = 2.1 \cdot 10^{15} \text{ n/cm}^2 \cdot \text{sec}$$

$$\bar{\Phi}_2 = 4.2 \cdot 10^{14} \text{ n/cm}^2 \cdot \text{sec}$$

if the fuel elements operate at a thermal neutron flux of $6 \cdot 10^{14} \text{ n/cm}^2$ per sec or 380 W/cm^2 power density.

APPENDIX VI.

Results of nuclear calculations giving the fluxes in the fuel pin of the experiment inside the element S II s.

1. Hypotheses of calculation.

The experiment with its surrounding special fuel element is put in one of the three holes of the barrel occupying a large channel of BR2. The two remaining holes are loaded with standard fuel elements. The barrel is surrounded by five new fuel elements and fifteen 15 % burned up elements. This second layer is poisoned to take into account the effect of control rods, the burnup, and the presence of other experiments. A reflector consisting of poisoned Be-plugs surrounds them.

2. Geometric model of the reactor.

The calculations are carried out in cylindrical geometry ; the model has ten regions which are somewhat homogenized.

3. Mode of calculation.

The calculations are carried out by means of a multigroup diffusion code MODIC (25 energy groups) on the digital computer Mercury. No correction, however, is applied for the approximation of the diffusion theory. The calculations are carried out for various compositions of the barrel (Be or Al) and of the fuel pin ; the results mentioned in this Appendix refer to an aluminum barrel and a UC-PuC pin. The maximum thermal flux in the fuel is 6.10^{14} n/cm².sec.

4. Results.

Fig. 26 and 27 show the neutron spectra in the centre and at the edges of the fuel pin as a function of the lethargy groups (listed in ANL-5800, page 157) for the 24 epithermal groups ; for the thermal groups the lethargy interval is chosen arbitrarily to be unit.

APPENDIX VII.

List of documents describing the BR2 reactor and its experimental facilities.

1. - CEN-R.1996/Blg 59 : 01.05.61 : Belgian Engineering Test Reactor
BR2
Safety and Design - Final Report
2. - CEN-R.1528/Blg 30 : 09.58 : Le réacteur Belge d'Essais des
Matériaux
H. Dopchie - J. Planquart
Conférence de Genève P/1679
Séance B-5
3. - CEN-R.1374 : 15.08.57 : BR2 Fuel Element Testing Facilities
J. Planquart
4. - CEN-R.1375 : 15.08.57 : Fitting of Loop in BR2
J. Planquart
5. - CEN-R.1830 : Février 1960 : Essais hydrauliques et mécaniques
effectués sur les éléments combustibles postiches du type BR2
J. Herpin
(Internal Report)
6. - CEN-R.1878 : 30.09.59 : Rapport d'avancement du programme
des études sur le modèle mécanique du réacteur BR2 (1958-1959)
L. Valette
(Internal Report).

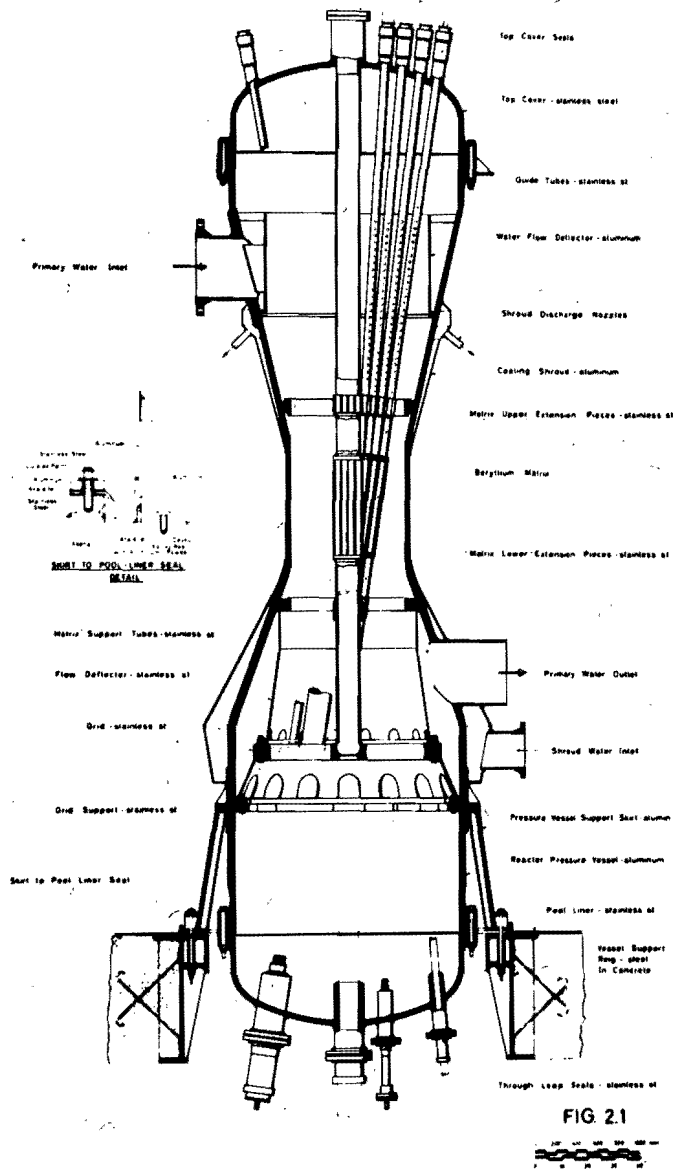


FIG 2.1

Fig. 1 The BR2 reactor

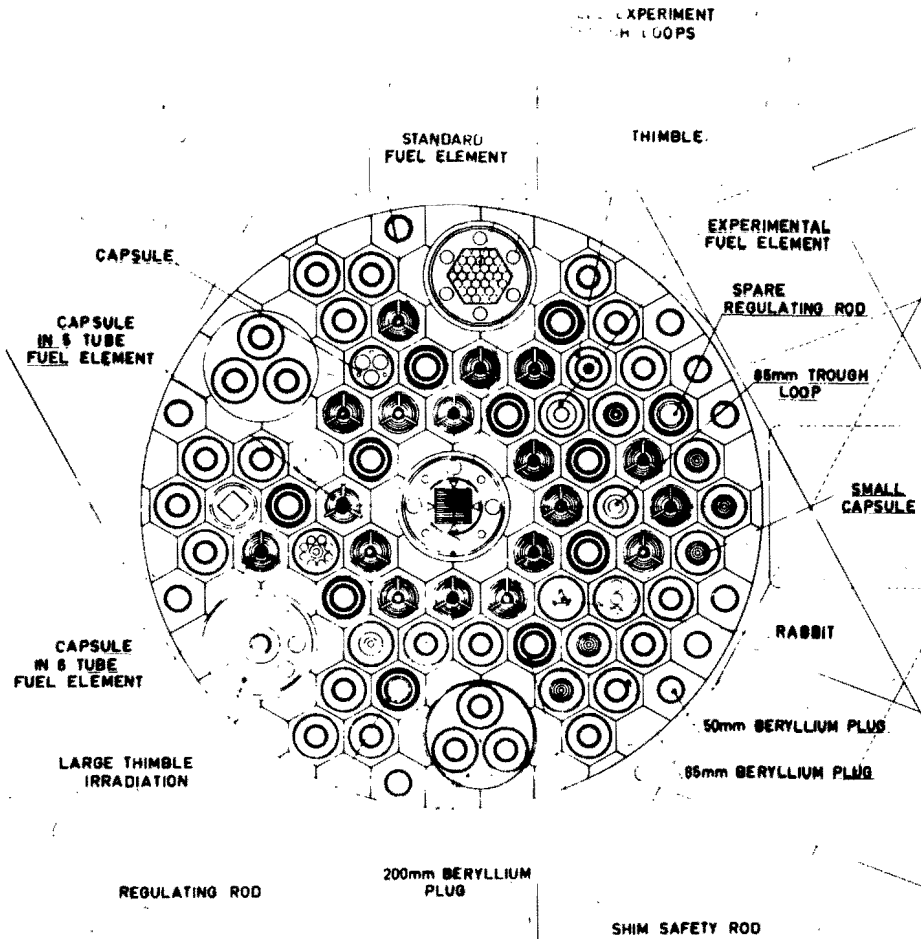
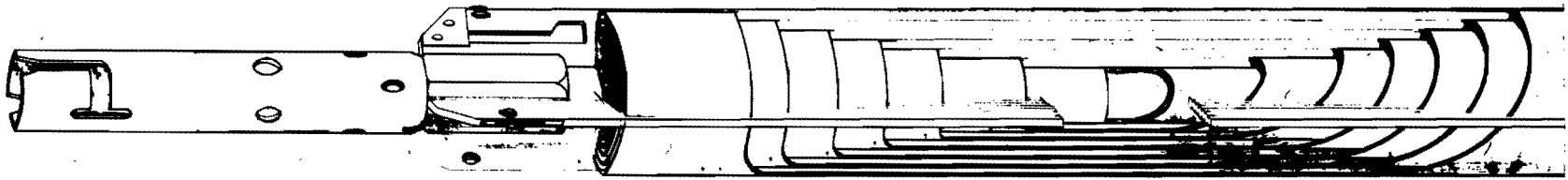


FIG. 1.2

BR-2 TYPICAL CORE LOADING

Fig. 2 The experimental facilities of the BR2 reactor Cross-section at mid-plane and typical loading configuration



DISPOSITIF D'ACCOMPLISSEMENT
 TYPE MANOMÈTRE
 BA JONKHOFFLIJND

COPPE D'EXTREMITÉ AVEC DISPOSITIF
 DE CENTRAGE
 EINDKAP MET CENTERRIJND

TUBE 1
 BUS 1

TUBE 2
 BUS 2

TUBE 3
 BUS 3

TUBE 4
 BUS 4

TUBE 5
 BUS 5

TUBE 6
 BUS 6

TUBE SUPPORT
 STEUNBUS

Fig. 3 Fuel element SVI i - Exploded view

168

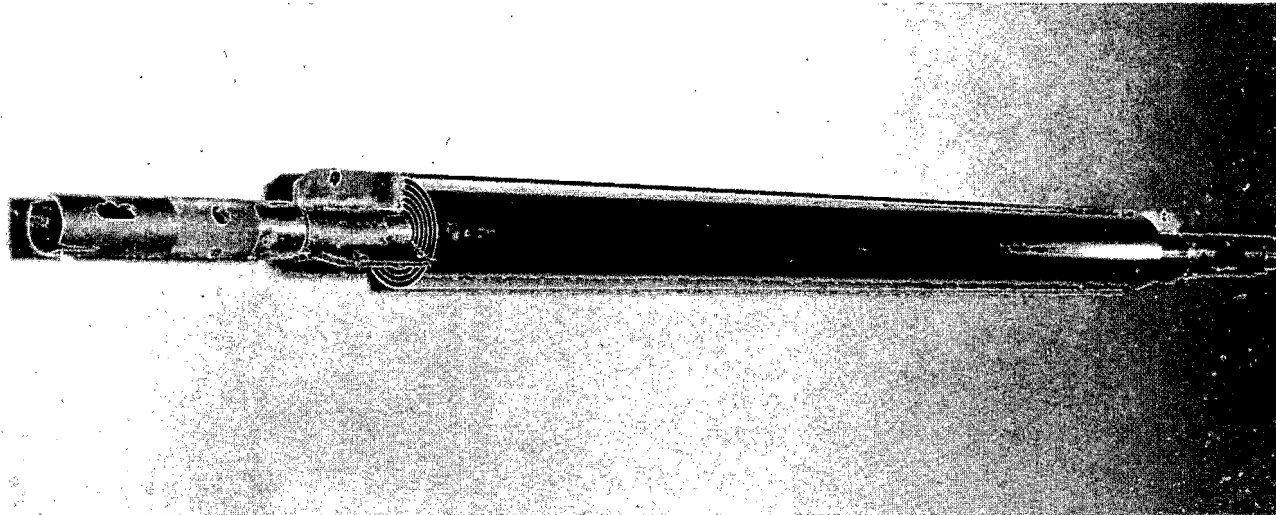


Fig. 4 Fuel element SVI i - Photo

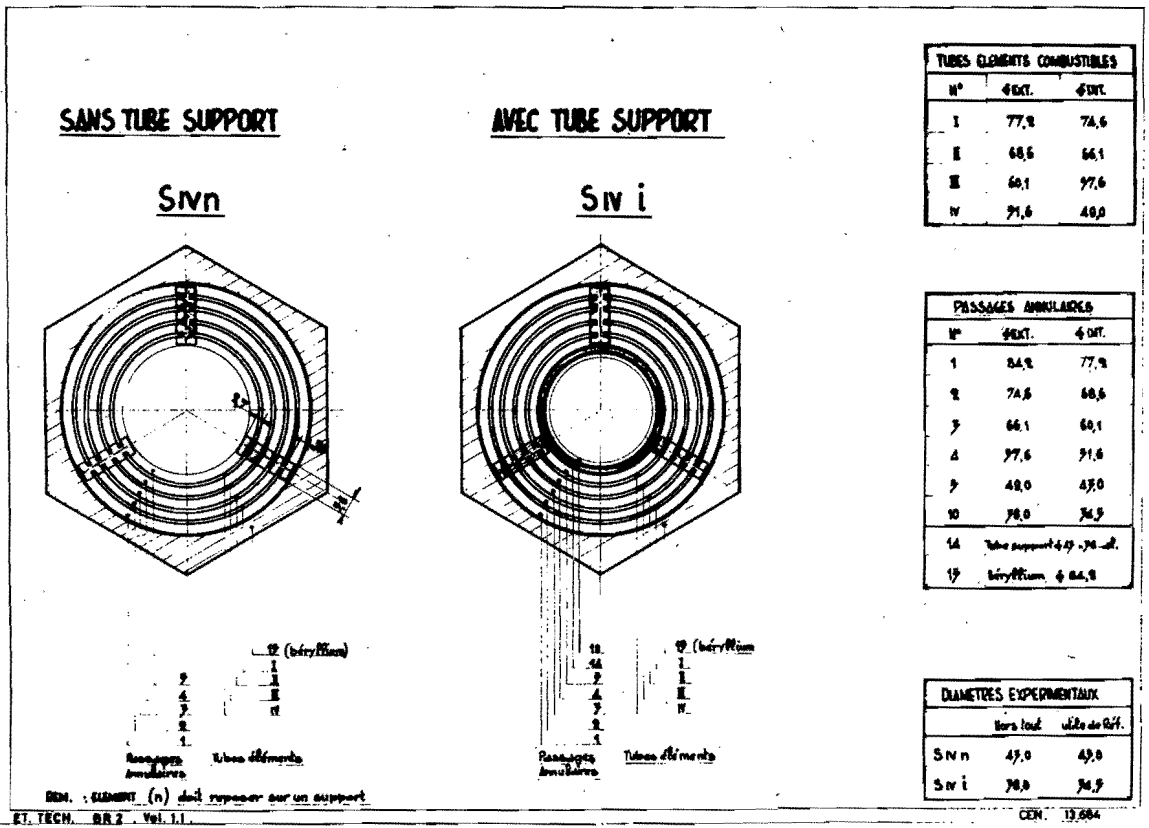


Fig. 5 Fuel element S IV i and S IV n - Cross-section at the mid-plane

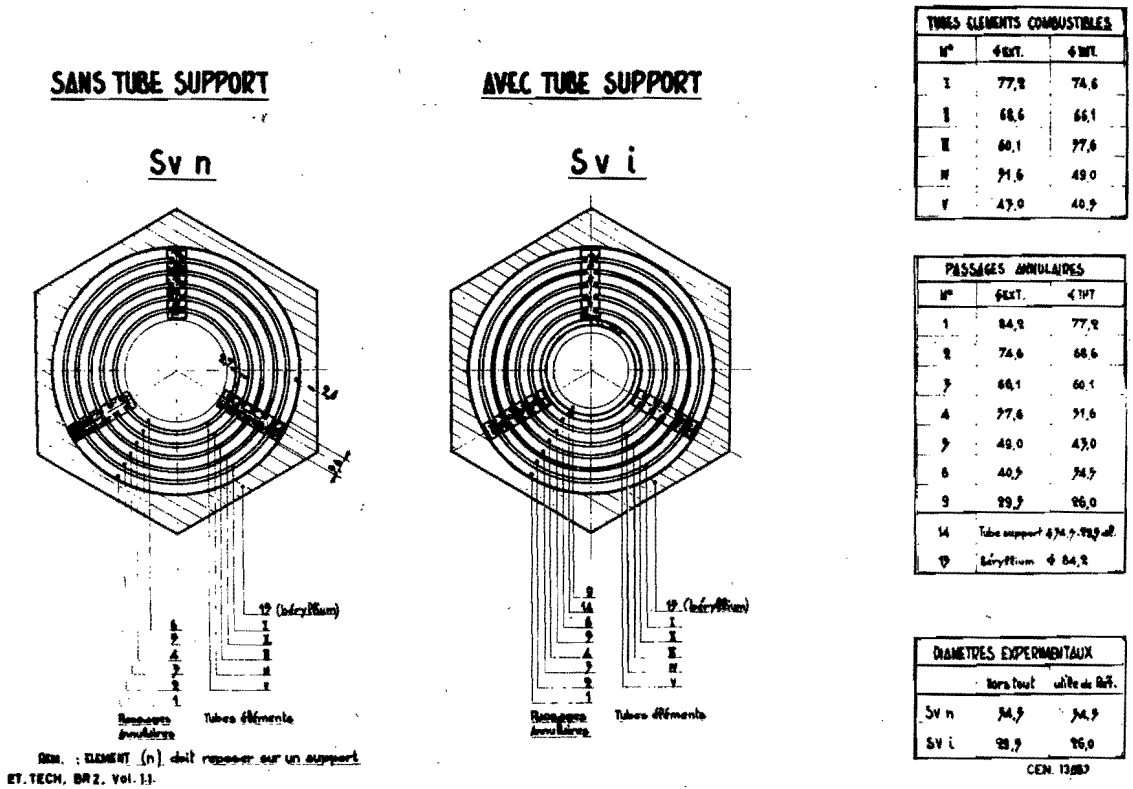


Fig. 6 Fuel element SV i and SV n - Cross-section at the mid-plane

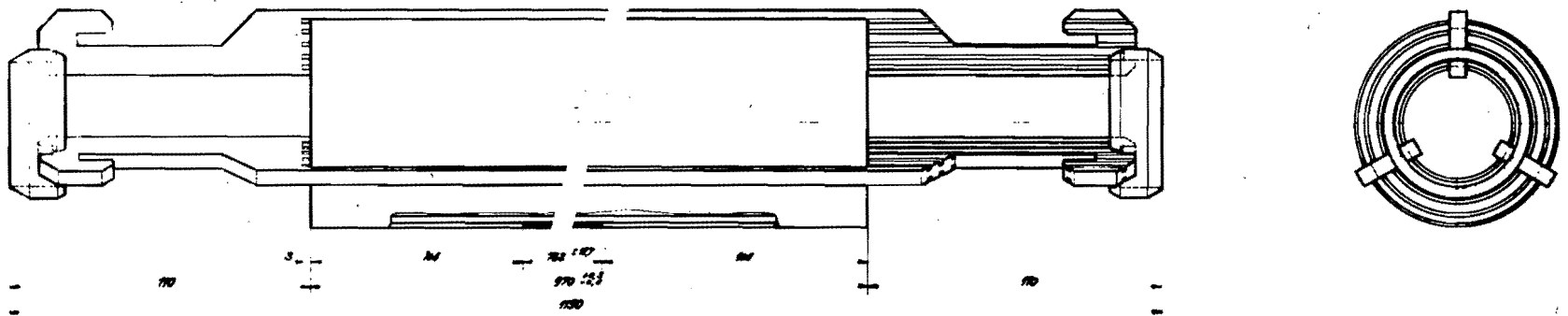


Fig. 7 Fuel element SV.n - Conceptual design

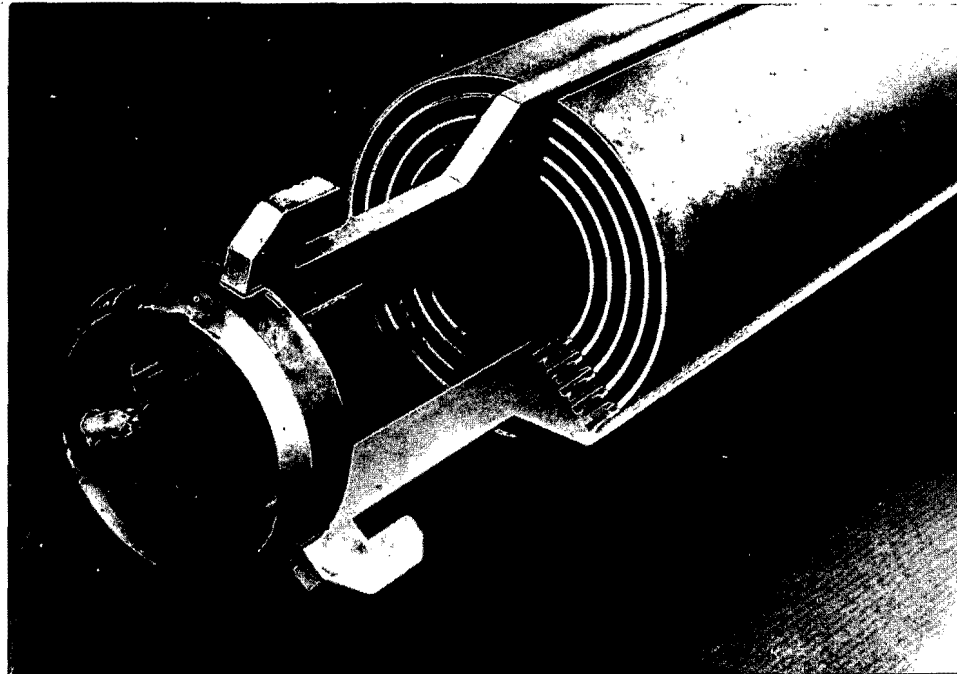


Fig. 8 Fuel element SV n - Photo

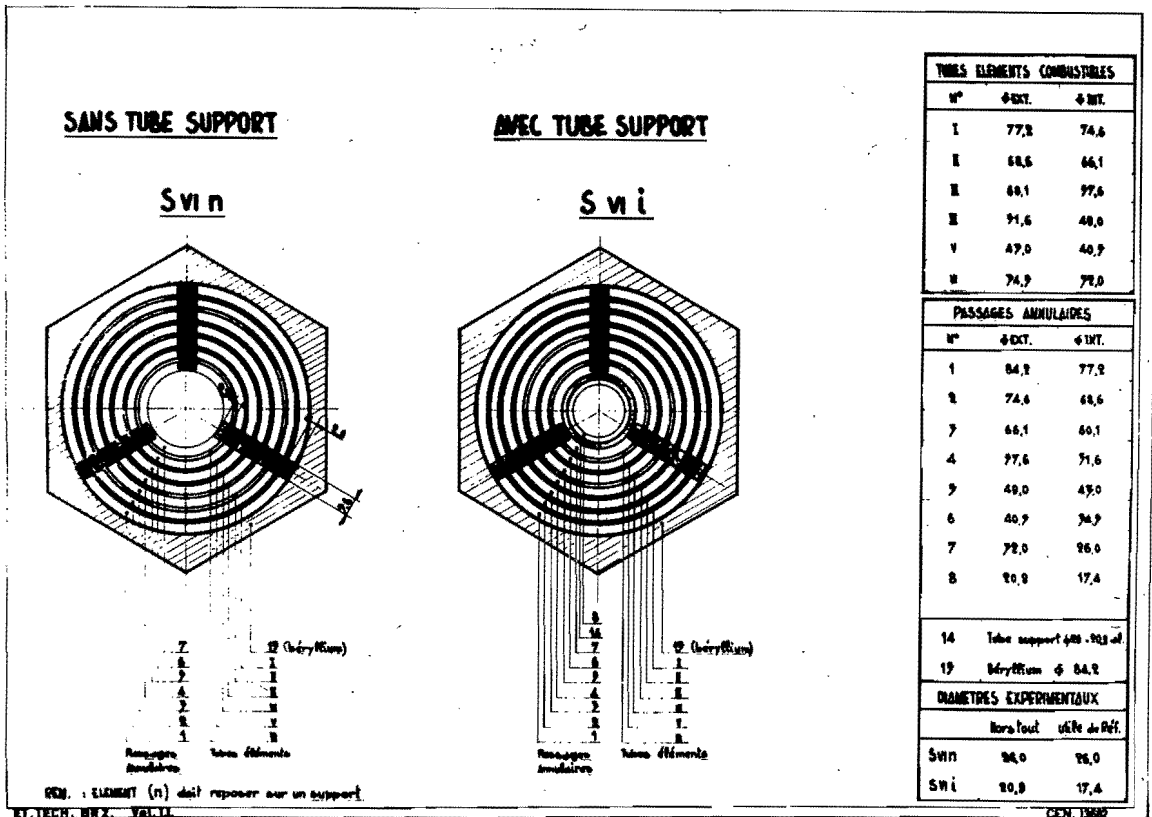


Fig. 9 Fuel element Svi i and Svi n - Cross-section at the mid-plane

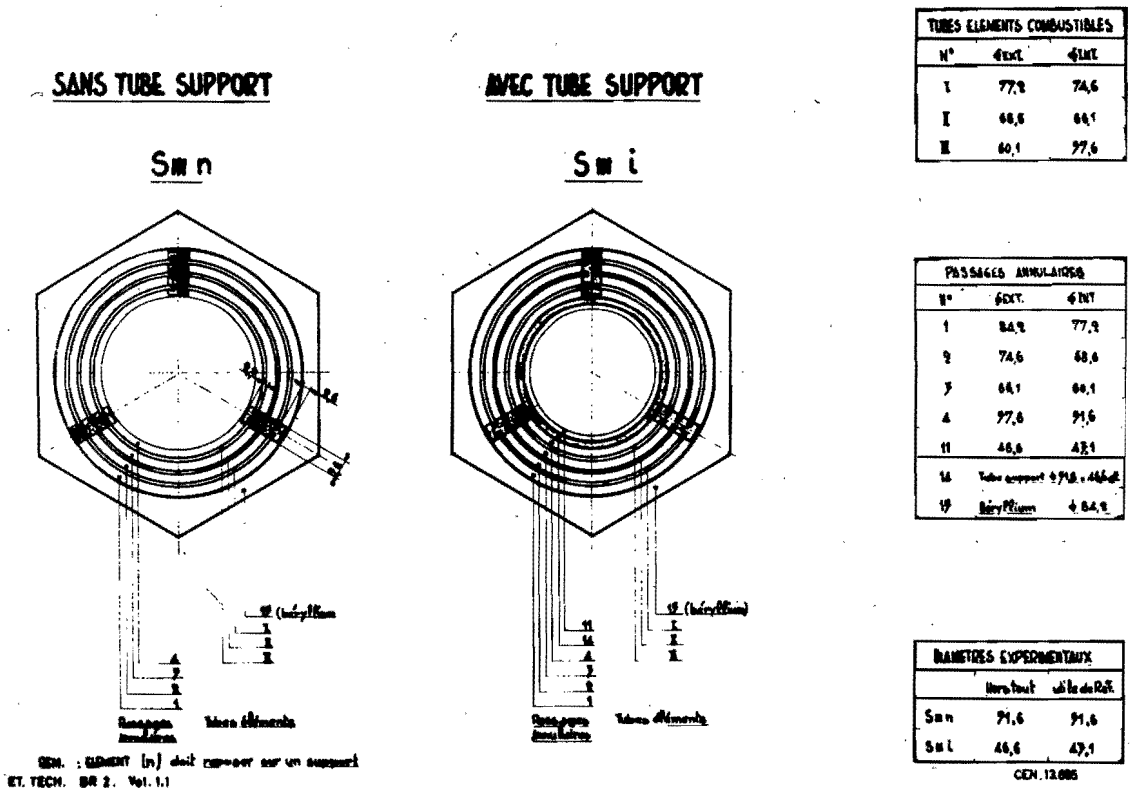
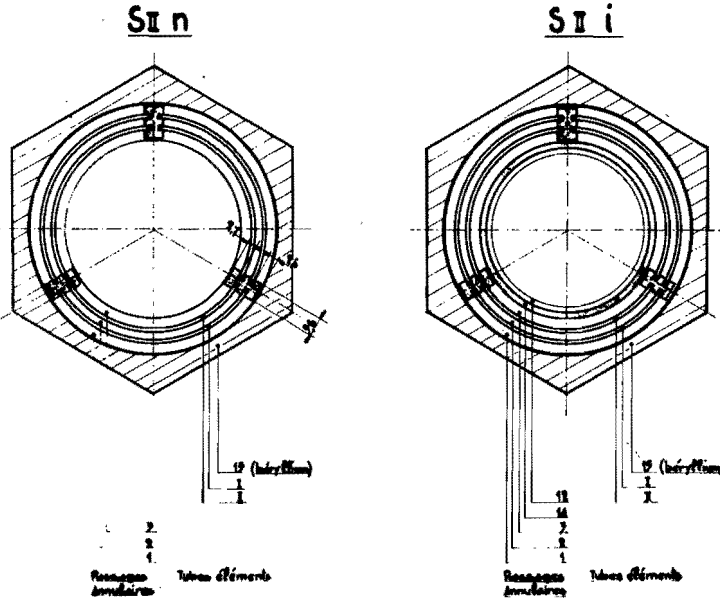


Fig. 10 Fuel element S III i and S III n - Cross-section at the mid-plane

SANS TUBE SUPPORT

AVEC TUBE SUPPORT



REM. : ELEMENT (n) doit reposer sur un support.
ET. TECH. BR 2. Vol.1.1.

TUBES ELEMENTS COMBUSTIBLES		
N°	Ø EXT.	Ø INT.
I	77,2	74,6
II	68,6	66,1

PASSAGES ANNULAIRES		
N°	Ø EXT.	Ø INT.
1	84,9	77,2
2	74,6	68,6
3	66,1	60,1
12	32,1	21,6
14	tube support Ø int. 22,1 ad.	
19	zirconium Ø 88.	

DIAMETRES EXPERIMENTAUX		
	hors tout	à l'intérieur
S II n	66,1	66,1
S II i	77,1	71,6

CEN. 12086

Fig. 11 Fuel element S II i and S II n - Cross-section at the mid-plane

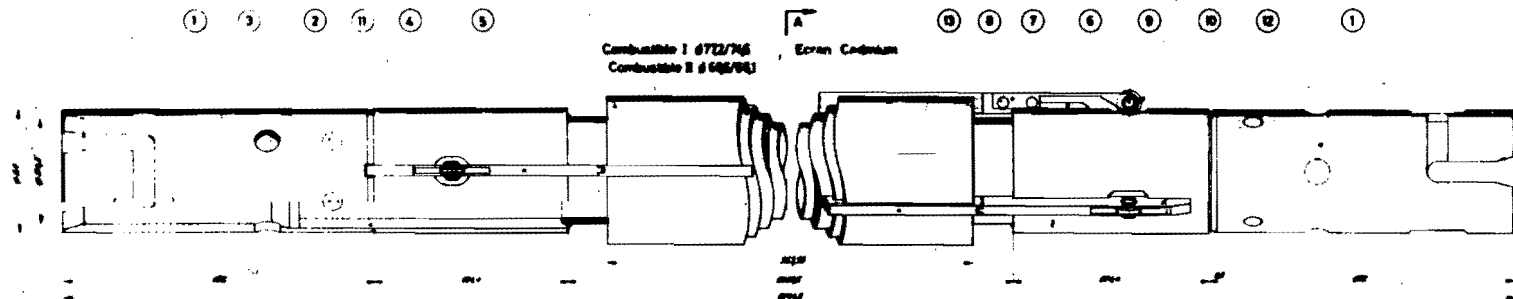


Fig. 12 Fuel element S II s - Conceptual design

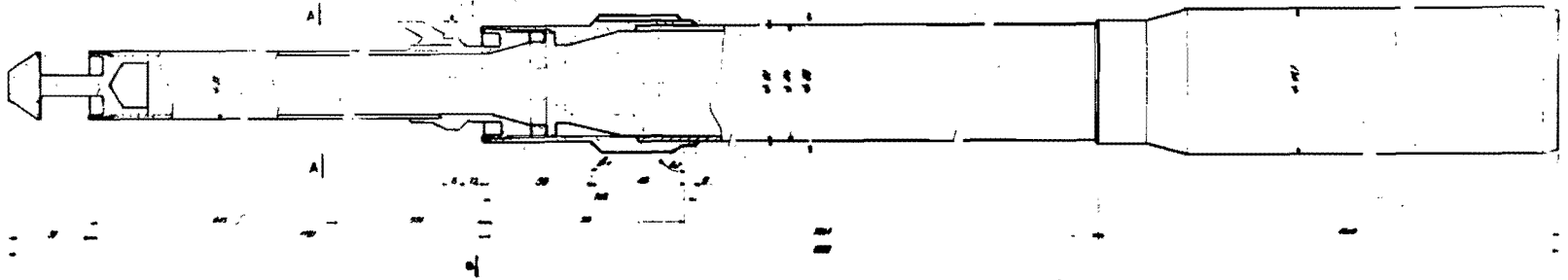


Fig. 13 Upper section of the I.P.M.T.L. - Conceptual design

178

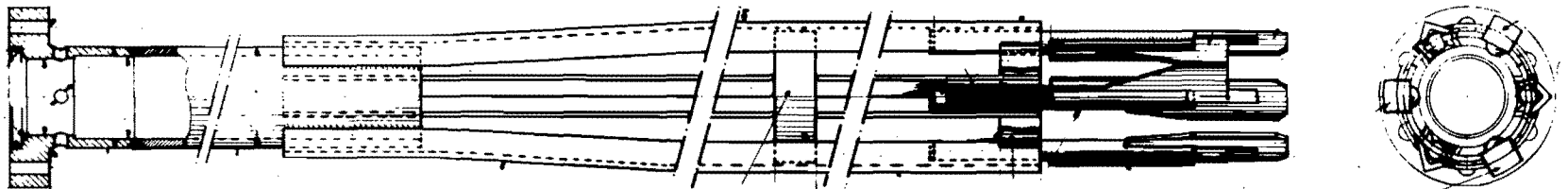


Fig. 14 Handling tube for the element SV n

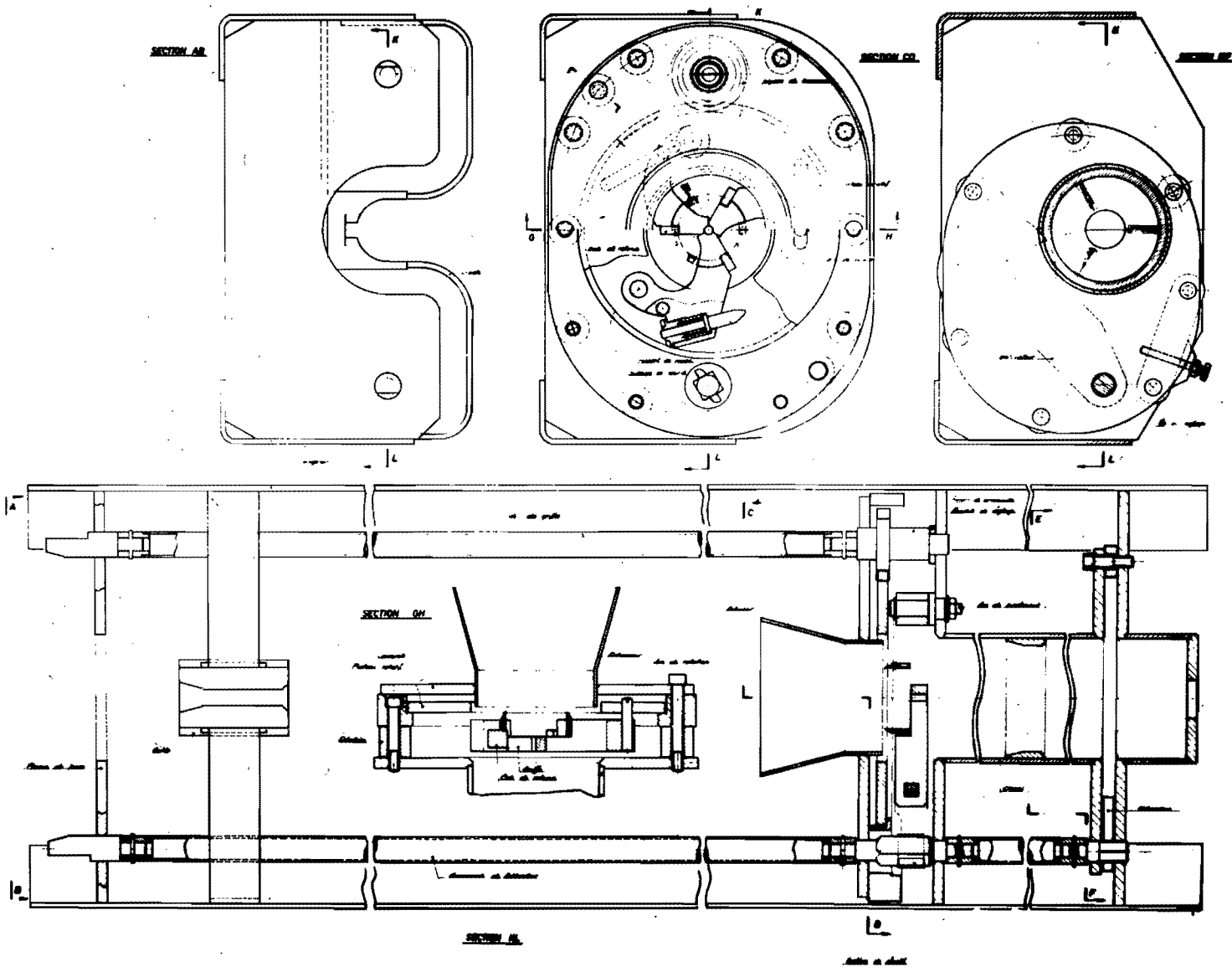
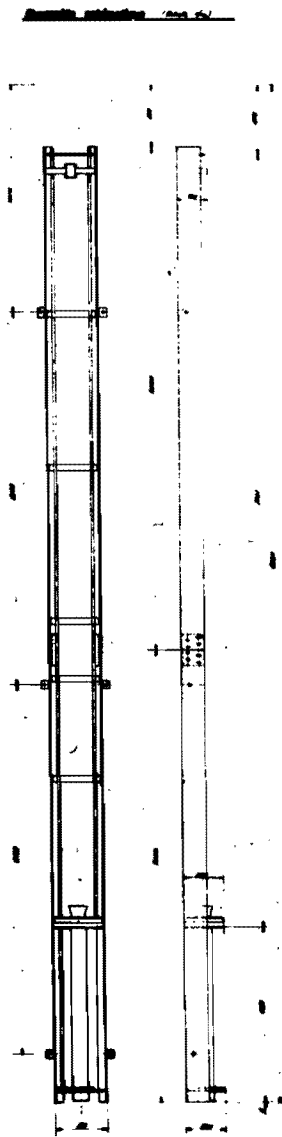
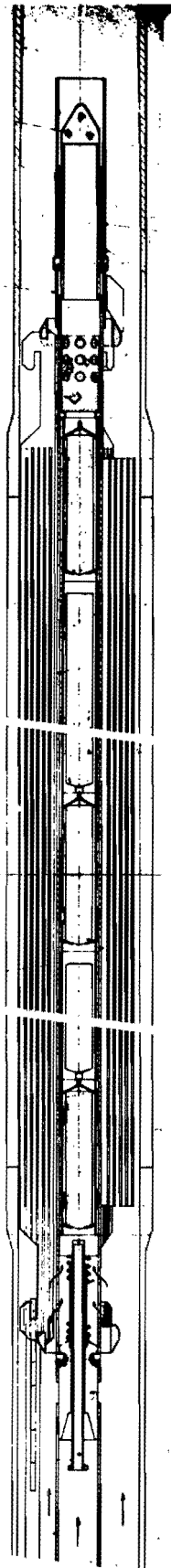
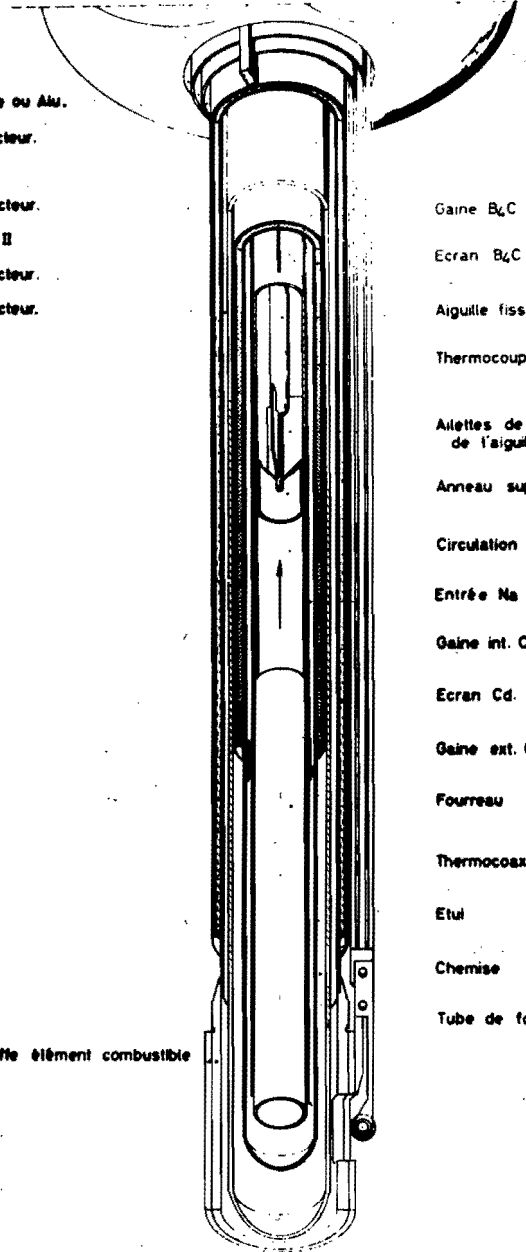


Fig. 15 Unhooking device for the element SV n



Beril ou Be ou Al.
 Eau du réacteur.
 Combustible
 Eau du réacteur.
 Combustible II
 Eau du réacteur.
 Eau du réacteur.

Coiffe élément combustible



Gaine B₄C
 Ecran B₄C
 Aiguille fissile
 Thermocouple
 Ailettes de guidage
 de l'aiguille.
 Anneau support de l'aiguille.
 Circulation Na
 Entrée Na
 Gaine int. Cd.
 Ecran Cd.
 Gaine ext. Cd.
 Fourreau
 Thermocox de chauffage
 Etui
 Chemise
 Tube de force

Fig. 17 The MFBS loop - Exploded view

Fig. 16 Fuel element SV n combined with irradiation capsule

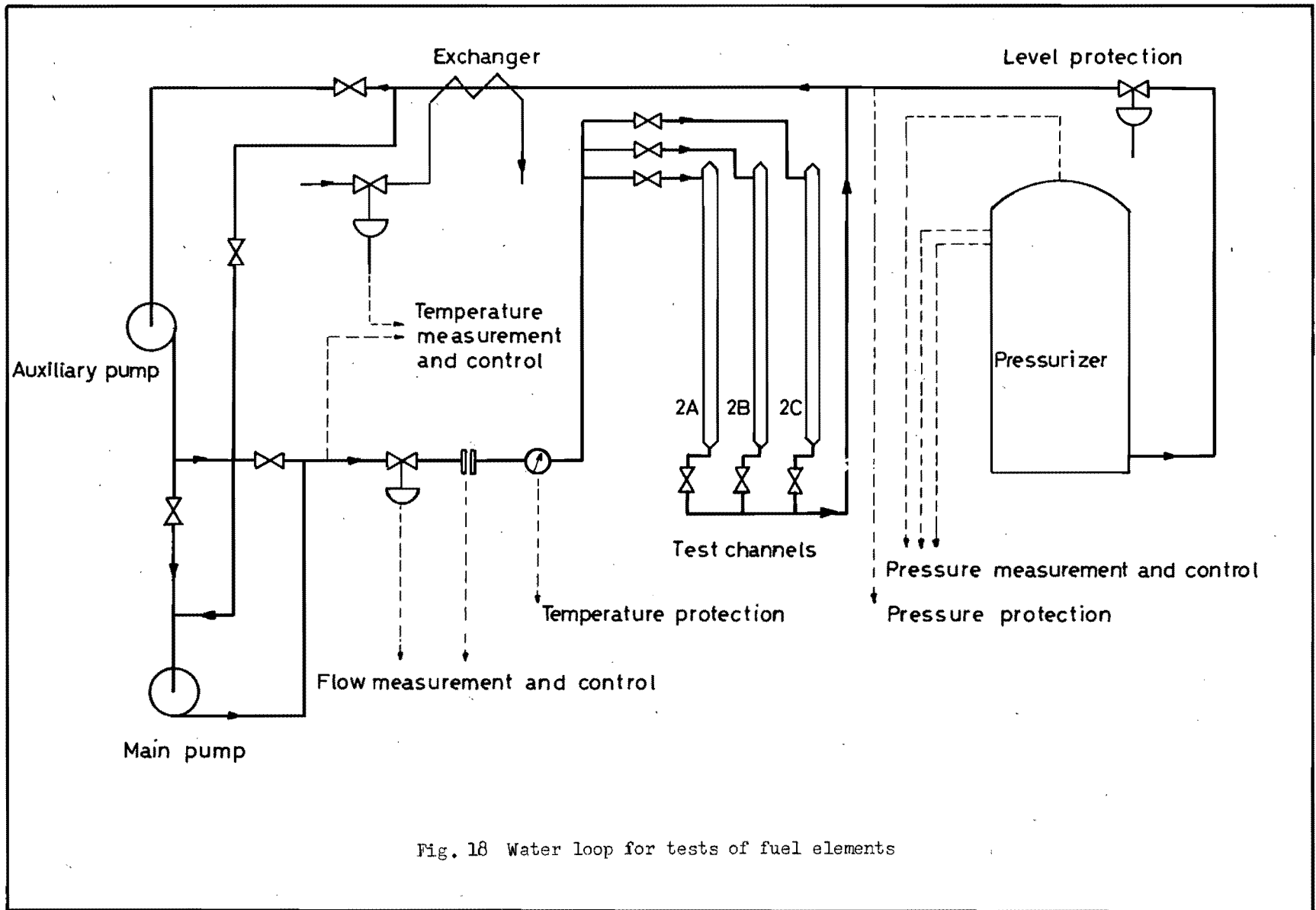


Fig. 18 Water loop for tests of fuel elements

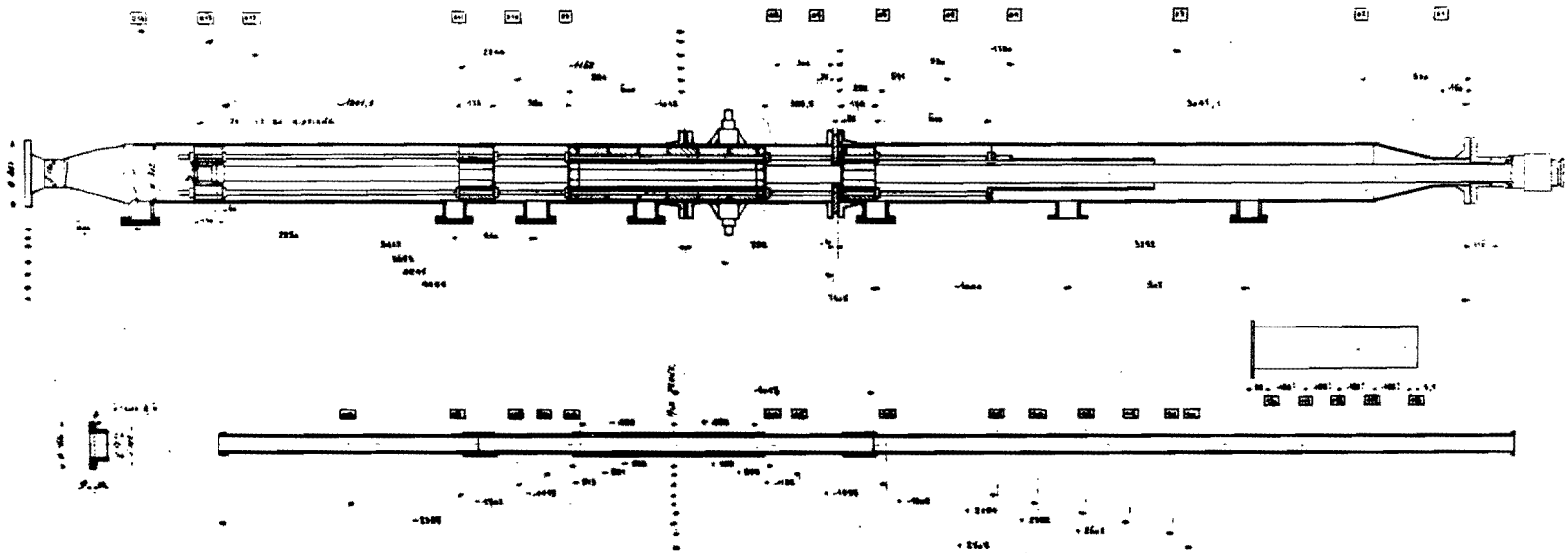


Fig. 19 Experimental section "2A" of the water loop

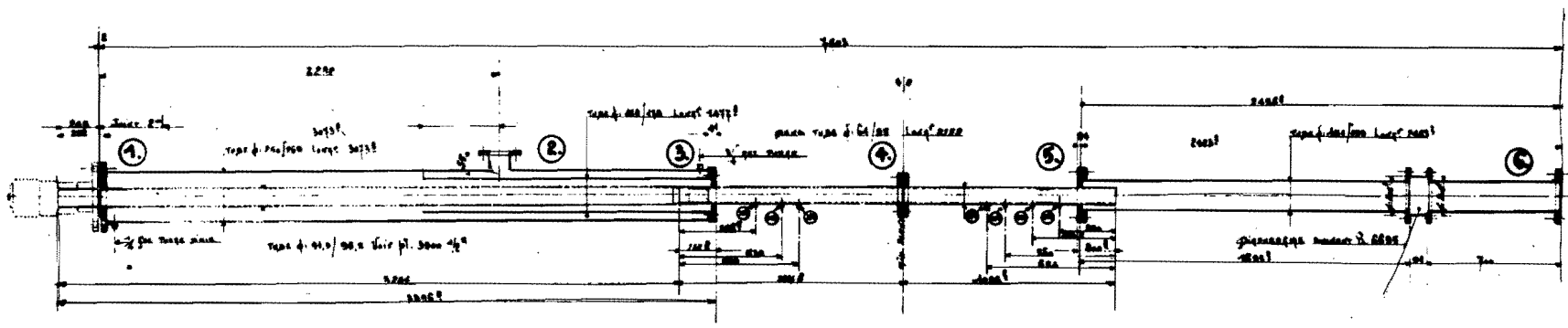


Fig. 20 Experimental section "2B" of the water loop

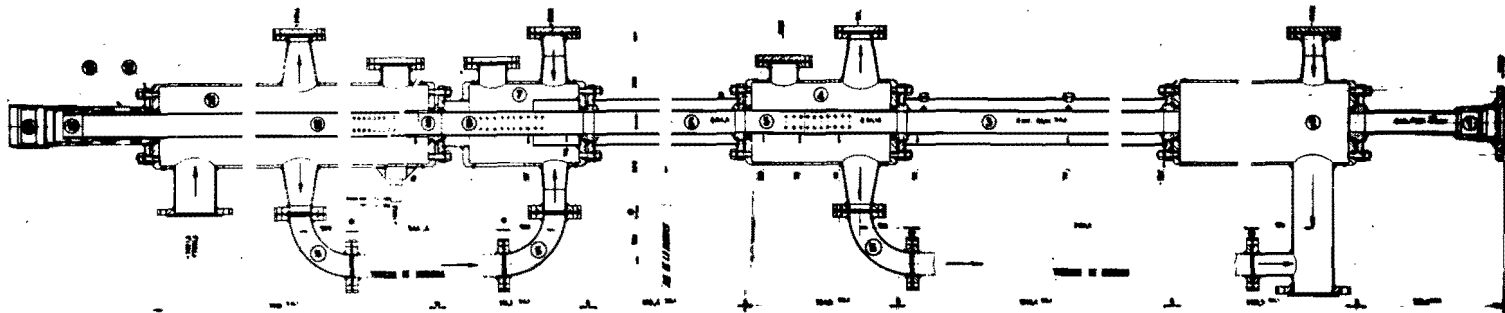


Fig. 21 Experimental section "2C" of the water loop

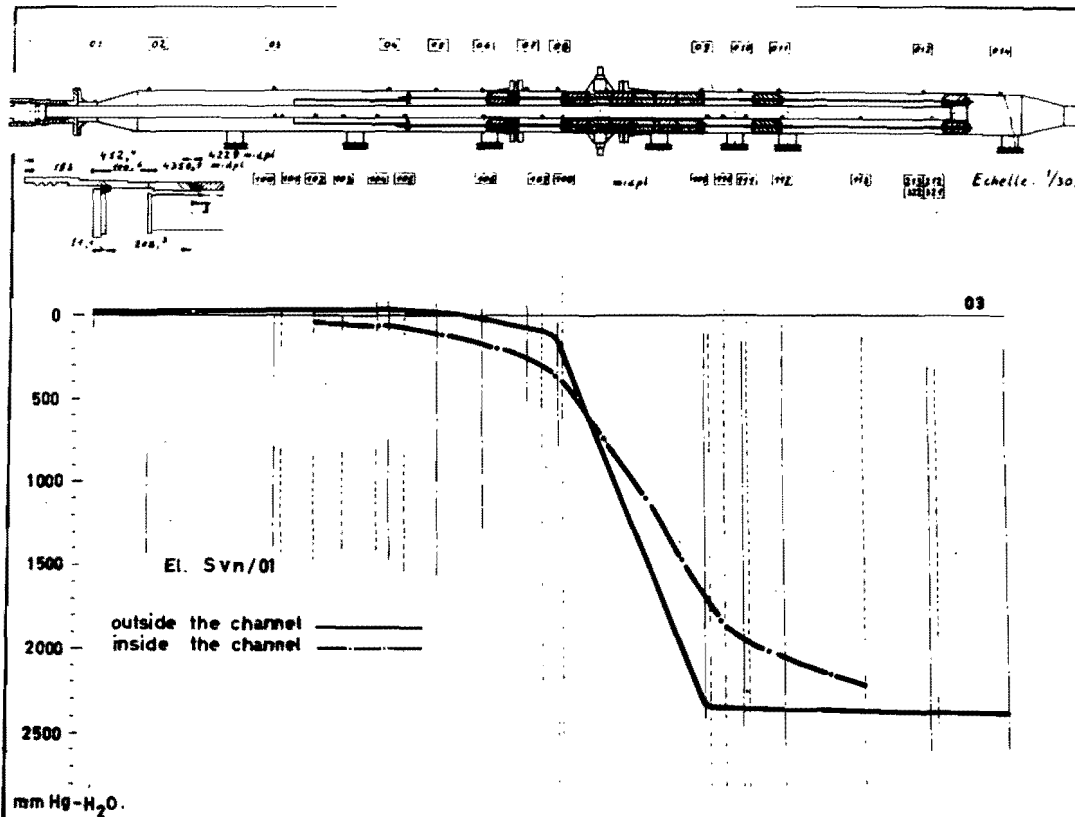


Fig. 22 Static pressure curves inside and outside experimental section "2A" for fuel element SV n/01 with thimble

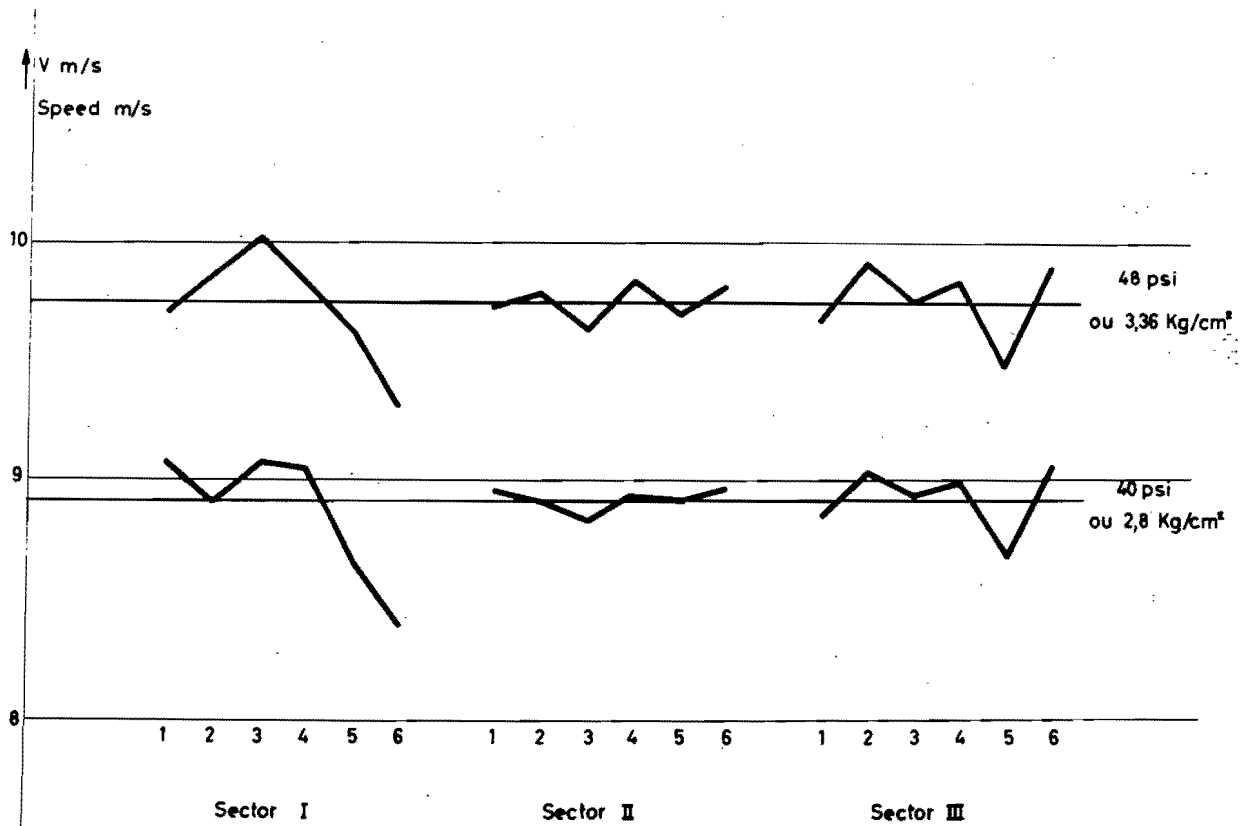


Fig. 23 Speed distribution in annuli of fuel element SV n/01

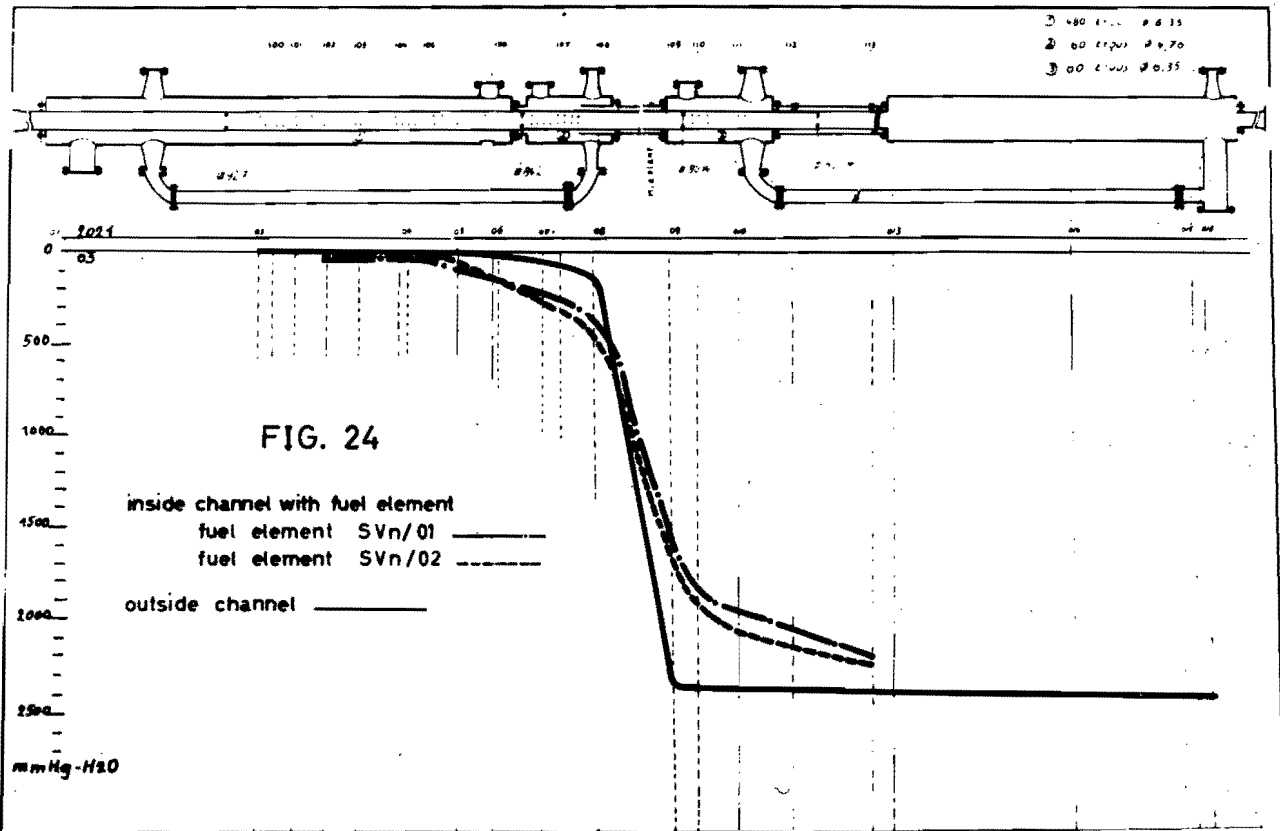


Fig. 24 Static pressure curves inside and outside experimental section "20" for fuel element SV n/02 with thimble

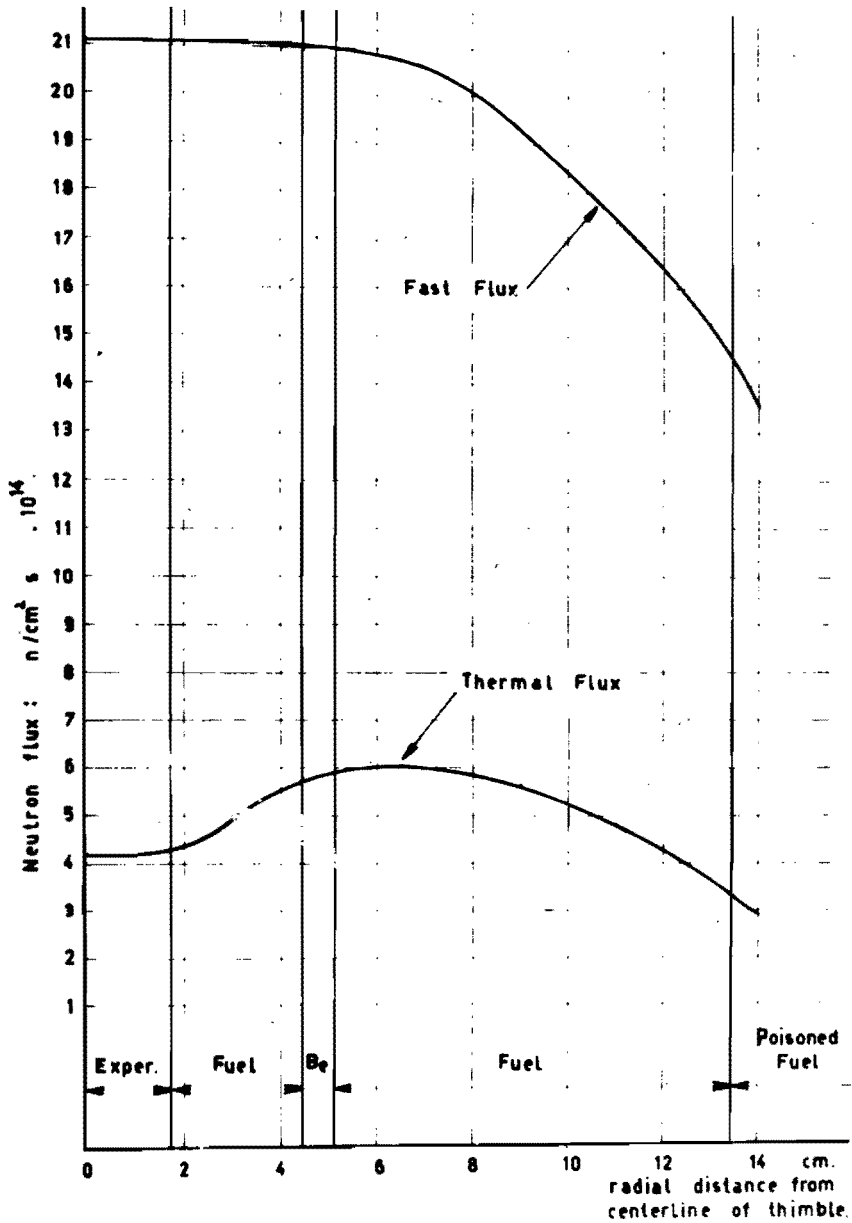


Fig. 25 Fast (Φ_1) and thermal (Φ_2) flux distribution at reactor core mid-plane in thimble inserted in fuel element SV n

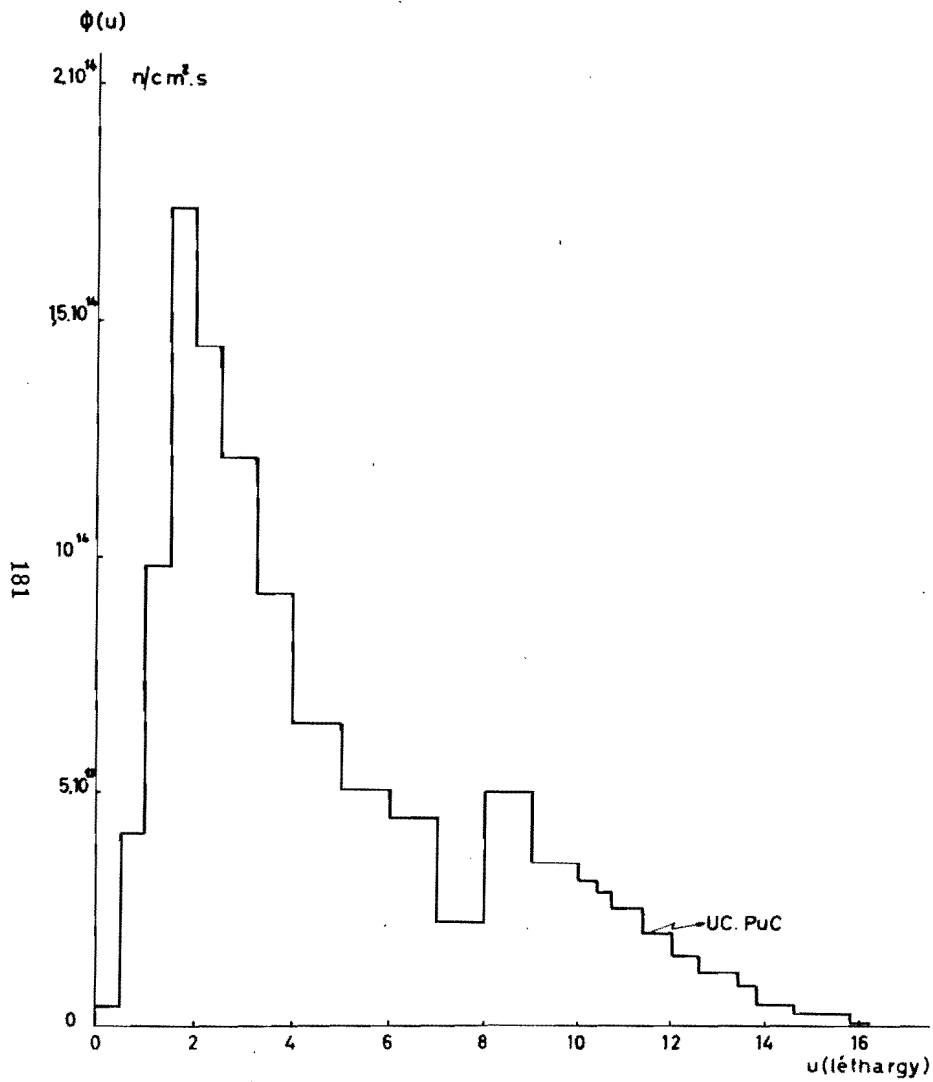


Fig. 26 Neutron spectrum at the center of fuel pin inside fuel element S II s

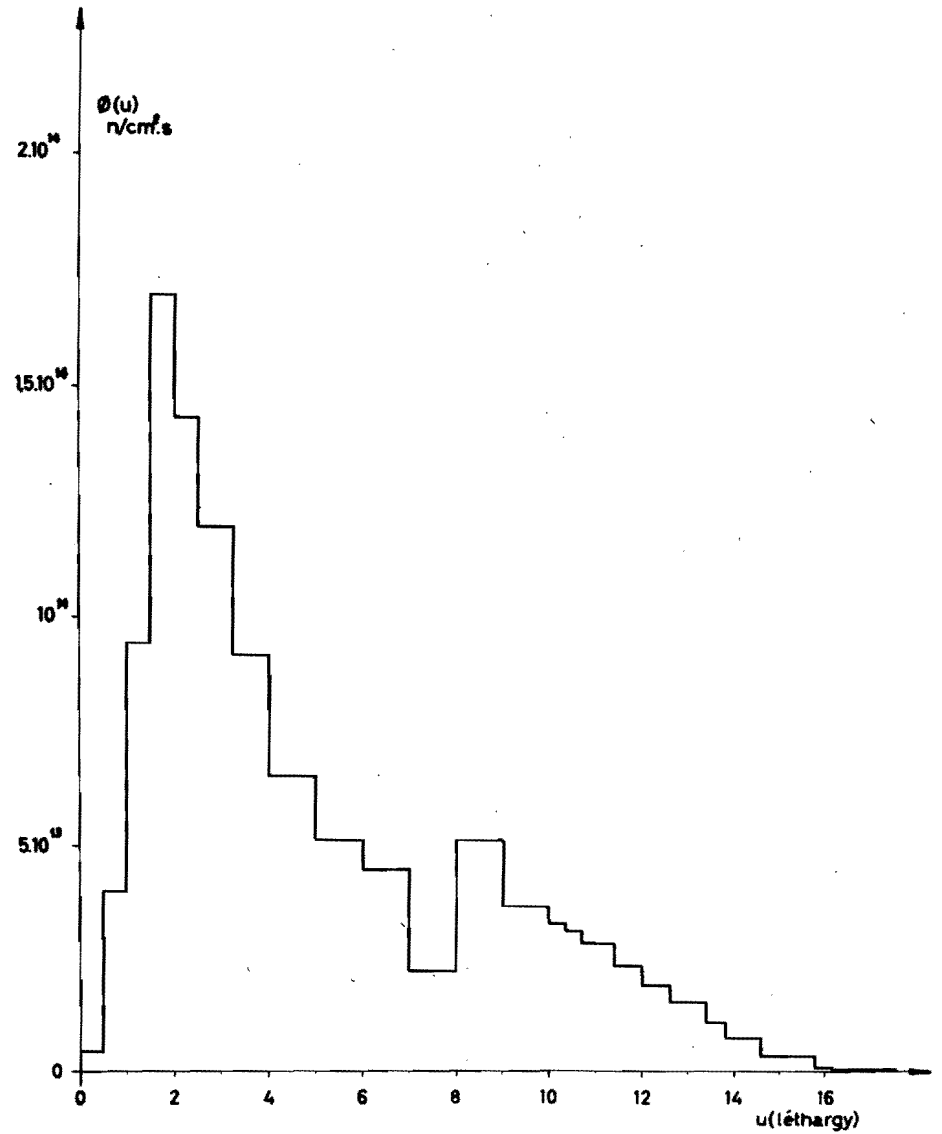


Fig. 27 Neutron spectrum at the periphery of fuel pin inside fuel element S II s

FUEL ELEMENTS FOR THE BELGIAN HIGH FLUX TEST REACTOR BR2

Part II: Non-destructive testing of plates

Including work of C.E.N.: P. De Meester, L. Binard,
M. Brabers, R. De Knock, E. Gourski, and D. Tytgat;
and of Sylcor (U.S.A.): R. Alto

Paper presented by M. D'hont

ABSTRACT

The BR2 fuel elements consist of five to six concentric tubes; each tube is formed by assembling three MTR-type fuel plates, joined mechanically or by welding or by brazing.

Among the various tests performed during and after plate fabrication and assembling, two devices are described:

Ultrasonic tester of the core-cladding bond.

Controller of U^{235} homogeneity throughout the plate by beta-gamma-scanning.

Data obtained on a complete batch are reported.

1. THE BR2 FUEL ELEMENT

The BR2 fuel elements consist of five to six concentric tubes; each tube is formed by assembling three MTR-type fuel plates of one size, joined mechanically or by welding or by brazing.^{1,2} The plate sizes are numbered from 1 to 6, so that the smaller tube is formed out of plates with the lower number; the dimensions of plates and tubes are given on fig. 1. For fuel elements containing only five concentric tubes, size 1 is omitted. The core of the plates consist of a 24 wt % U - 76 wt % Al alloy, the uranium being 90% enriched.

2. DESCRIPTION OF THE ULTRASONIC TESTER

2.1 General considerations

The ultrasonic inspection is done by the transmission technique. The fuel plate is immersed in water (fig. 2-3).

The surface of the fuel plate is scanned horizontally along its length, at the end of each line the scanning equipment undergoes a small vertical displacement. The motors are actuated manually or automatically.

A generator supplies electrical pulses of adjustable amplitude to the emitter transducer. The receiver triggers a discriminator if the amplitude of the transmitted signal exceeds the fixed threshold. The discriminator is not triggered when a defect is present, as in this case the signal transmission is stopped or attenuated. The smallest defect to be detected will depend on the generator pulse amplitude.

The recording is performed on paper which is metallized on one side. The amplified discriminator output signal burns the metallization under the stylus. Unburned recording paper indicates the presence of a defect. As the stylus is attached to the transducer assembly, a recording is obtained which localizes the defects on a one to one scale (fig. 4). However, the size of the defects as shown on the recording, is larger by an amount approximately equal to the radius of the acoustical beam. As the paper is translucent at the burned spots, photographic copies are easily made.

2.2 The transducers

Most of the ultrasonic testers generate a wave train which after transmission through the fuel plate and multiple reflection on its faces produces a signal whose amplitude depends strongly on the transit time. The internal reflections may indeed give rise to different waves that are more or less out of phase at the receiver. Thus a change of thickness or density of the plate will cause an important change of the transmitted acoustical signals. If the section of the acoustical beam is not made too small in order not to decrease the area to be tested at each pulse, it will be large compared with the smallest defect to be detected. Hence this defect will cause a small signal variation and it will be detected accurately only if the various reflections are separated by decreasing the duration of the acoustical signal. One obtains a short signal without using too high a frequency, by decreasing the number of periods.

Transducers have been made in which the piezoelectric disc is backed by a metallic alloy of comparable acoustical impedance, so that the interface cannot cause reflections and the piezoelectric disc will not resonate. In this way an aperiodic acoustical signal is generated.

The piezoelectric disc is made of barium titanate ceramic material and the metallic alloy is a low-temperature melting one (Cerrobend-MP. 70°C).

The acoustical beam has a diameter of 2 mm. It consists of rectangular pulses of 50 ns duration.

2.3 Defect detectibility

With this instrument one can easily and accurately detect a lack of bond having an area equal to or greater than $\frac{1}{2}$ mm² which corresponds to a circle of $\frac{1}{32}$ " diameter.

3. CONTROL BY BETA GAMMA COUNTING

3.1 Principle

The measurement of the gamma counting through a collimator defining a small surface of the fuel element gives an indication of the local uranium content.

When the uranium is 90% enriched, the 184 kev peak of the U^{235} can be used.^{3,4}

The radiation of this energy is not very sensitive to the absorption variations in the element (total absorption is only a few per cent); on the other hand, it is easily collimated (1 cm of lead gives an attenuation factor of 10^4).

The simultaneous measurement of the beta emissions from the same area but on both sides of the plate, gives, in relation with the gamma counting, an indication of the can thickness.

The radiation used is mainly the 2.32 Mev beta of the U^{238} .

On the other hand, the beta counting can help to control the uniformity of elements fabricated for technological purpose with natural uranium. In this case, an additional measurement can be made with 90 kev gamma, but this counting is slow.

3.2 Description of the apparatus (fig. 5, 6, 7)

The gamma radiation counting is done with a scintillator composed of a NaI(Tl) crystal of 1 inch diameter and 1 inch height, mounted with a photomultiplier 6342A and a cathode follower. The photoelectric efficiency for 1 inch of NaI is about 90% at 184 kev. Therefore, it is not interesting to use a larger crystal.

The crystal is placed into a lead cylinder of 10 cm ϕ , performing both shielding and collimating. The scintillator is fixed to the lead cylinder which is vertically fixed to a steel base plate.

The collimator is formed by a hole in the lead cylinder axis of the following sizes 14 mm ϕ and 13 mm height, the entry being reduced by a lead ring of 5 mm thickness perforated with a square hole of 1 cm \times 1 cm.

The shielding is completed by a lead block of 3 cm thickness and 10 cm ϕ which is placed on the base plate and guided by a hinge system.

The fuel element to be controlled is placed between the base plate and the top lead block which keeps it in place by its own weight (fig. 6).

Small teflon pieces avoid any scratching of the fuel plate.

The beta counting is made by two proportional counters, one being the proper gamma collimator and the other being formed by a symmetrical cavity in the upper lead block. Those cavities are penetrated in their center and perpendicularly to their axes by nickel wires of 0.05 mm held by teflon insulators and forming anodes.

Some tubing permits the circulation of the counting gas (90% argon + 10% methane).

The counters are closed by mylar windows of 6 μ (1 mg/cm²) made conductive by a gold deposit.

The signal is transmitted by short cables, without preamplifiers, to the measuring circuit, the sensitivity of which (4 mv on 10 pf) gives a counting plateau between 1800 and 2000 V (slope: 5% per 100 V).

The electronic equipment involves: (fig. 5):

- for the gamma counting: 1 high voltage stabilized source
- 1 amplifier, gain 500
- 1 one-channel pulse height analyzer
- 1 scaler

for the beta counting: 1 high voltage stabilized source
1 double discriminator with high sensitivity
2 scalers

One electronic timer and a low voltage source common to the three scalers complete the installation.

3.3 Measurements

For a 90% enriched uranium element with a U-Al alloy of 0.51 mm thickness (30 mg U per cm²) between two aluminium clads of 0.38 mm thickness and with collimators of 1 cm², following values are obtained:

Beta counting: 32 counts/sec. (BG = 0.15 counts/sec.)

Counting variation of 12% for a cladding thickness change of 20% (0.076 mm).

Gamma counting (from 160 to 210 kev) = 92 counts/sec. (BG = 0.23 counts/sec.)

The counting time is determined by the aimed precision. Measurements up to a few percent precision are obtained by using 100 sec counting time per location.

4. BR2 PLATE SCANNING AT THE C.E.N.

A batch of 150 MTR-type fuel plates made by Sylvania, Sylcor Division U.S.A., has been tested before assembling. The test is going on for another batch of fuel plates. All will be loaded in the Belgian BR2 test reactor.

The ultrasonic testing proved the excellent bonding of all plates tested. A typical recording is given in fig. 8, while a faulty record looks like fig. 9 (this plate was made as a standard in our laboratory).

Complete beta-gamma recordings of the whole area of fuel plates were registered and compared to graphics of routine checked plates. This leads, together with several other experiments, to the following procedure which proved to be satisfactory.

The serial numbered end will be held at the left side.

By cold start of equipment: count for 3000 seconds in order to reach the equilibrium conditions. Afterwards start with a 100 s. standard count.

Count the plate core on centerline for sizes 1, 2 and 3; on centerline and on both sides of the centerline at 2 cm of it, for sizes 4, 5, and 6.

Count the plate core on each line at ten locations from the end of the core to the middle, i.e., at 14 - 15 - 16 - 17 - 22 - 28 - 31 - 40 - 46 - 52 cm of each end of the plate.

Count the standard after every ten counts.

The data for a typical set of 15 plates, to be assembled to one BR2 fuel element, are given in Figs. 10, 11, 12, 13, and 14. Each of these figures represents the counting of three plates of the same size. The location of measurement is given on the abscissas, starting from the numbered plate-end; the length of the active core is 76 cm (30"). In ordinate the number of gamma-counts per second is indicated.

For sizes 4, 5, and 6 only the mean values of measurements along three different length-axes are given. Underneath each diagram, the plate numbers are given and the total U-235 content in g/plate.

5. BR-2 PLATE GAMMA SCANNING IN THE U.S.A.

An agreement was arranged between CEN and Sylcor for Sylcor to gamma scan a number of the fuel plates manufactured by Sylcor for use in the BR2 test reactor in Belgium.

a. Fabrication of the standards

In order to eliminate the potential of error introduction by gross geometry variation from the standard scanning to the sample, it was decided that the standards should be basically fuel plates, however, for ease of handling and evaluation for U-235 content, the standard plates should be considerably smaller than fuel plates.

Two production fuel plates rejected because of blisters over the core were obtained and radiographed. The plates were PBN-21 and PBN-32. Three locations on each plate were chosen for use to develop standards. Selection of the locations was based on:

1. Homogeneity of the uranium content within the area.
2. Apparent level of uranium content from one area to another to provide a reasonably broad span of contents for the standards.

Three sections measuring $2.187'' \times 4.500''$ X plate thickness were blanked from the selected areas of each plate, and identified with the plate serial number followed by a digit (1, 2, or 3) to identify the location of the section on the radiograph. The sections were cut so that the full thickness of the original plate core was maintained to all edges of the platelet.

b. Gamma evaluation of the standards

The gamma scanning was done with a model 413 Fuel Element Analyzer manufactured by Packard Instrument Company, La Grange, Illinois, USA. A NaI crystal with a $\frac{1}{2}''$ diameter collimator nearly in contact with the plate is used; the one-channel analyzer is set up on 184 keV midpoint with a 20 keV window. Counting time is one minute on a 0.196 square inch area.

Each of the six standard sections was gamma scanned using the $\frac{1}{2}$ inch diameter collimator. Scanning of the platelets was done using one minute counts at each of 32 locations on each platelet. The 32 locations were made up of eight steps (non-overlapping) on each of four lengthwise tracks (again non-overlapping). Five of the six pieces were scanned twice in the same manner for assurance of repeatability. All scanning was done in conjunction with an independent standard from another job, to permit relating the scans of the standard platelets to each other.

Scanning 32 locations of one-half inch diameter on each platelet resulted in examining 64% of the area of the platelet, which was considered to be well representative of the pieces.

Evaluation of the difference between the average platelet count relation to the independent standard for the duplicate scans shows differences ranging from .00080 to .00900. Noting that the average count was approximately 12300, based on a 95% confidence level, statistically the count relation can vary up to .01774 and still be valid. Therefore, all counts made were considered valid and used to calibrate the standards.

c. Chemistry evaluation of the standards

Two of the platelets, PBN-21 (2) and PBN-32 (1) were chosen for retention as permanent standards based on the criteria of their relative count rate to the others (roughly mid range), and their apparent homogeneity within themselves. The balance of the platelets were released to the chemistry laboratory, and three replicate analyses made on each after total dissolution of the platelet.

d. Relating gamma counting to U-235 content

Platelet PBN-32 (1) was chosen for the primary permanent standard, and the average of all counts for each of the four analyzed platelets was related to it by the computation,

$$R_p = \frac{\text{Average count of plate}}{\text{Average count of PBN-32 (1)}}$$

The R_p value of each analyzed platelet was then applied with the replicate U-235 values to a least square Regression Analysis to derive the linear equation relating total U-235 gram content of the platelet to R_p gamma count relation value.

The equation derived is, $U-235 = .1297 + 2.4253 R_p$.

Since that equation resulted in total U-235 content of the platelet, and we were interested in the U-235 content under the one-half inch diameter area, the equation was multiplied through by the factor relating the area scanned (A_s) to the area of the platelet (A_p) resulting in the equation,

$$U-235 \times 10^{-2} = .2583 + 4.8299 R_s$$

where $R_s = \frac{\text{Count of particular area being considered}}{\text{Average count of PBN-32 (1)}}$

$$A_p = 9.842 \text{ in}^2$$

$$A_s = .196 \text{ in}^2$$

e. Gamma scanning instructions

Two groups of measurements have been made

Group I

- a. Count the standard.
- b. Count the plate core on centerline for entire core length moving the plate $\frac{1}{4}$ inch after each count.
- c. Re-count the standard after every 15 counts on the plate core. Be careful to return to the proper location on the fuel plate after counting the standard.

Group II

- a. Count the standard.
- b. Count the plate core on centerline (unless otherwise specified) at four locations on each end of the core starting at the core ends and moving the plate $\frac{1}{2}$ inch after each count.
- c. Count two random locations on the plate core centerline (unless otherwise specified) other than the core ends.

- d. Re-count the standard.
- e. The counting for steps b and c may be modified from time to time for particular plates.

f. Results

Group I

A scanning summary of seven plates is presented in table 1. The average count is the average of 120 measurements.

The comparison between U-235 content of plates measured by gamma-counting and Archimedes density method, indicates in a few plates a disagreement, sometimes as great as 10% between the two methods. Sylcor is still investigating the problem, to develop a consistent, inexpensive scanning procedure for all nuclear fuel using gamma-scanning which might give more accurate figures than the density method.

Group II

As an example, results on three plates are given in table 2.

CONCLUSIONS

1. Ultrasonic testing: the C.E.N. has developed an ultrasonic tester which is a reliable device for control of nonbonding.
2. Gamma-counting: a development program has been conducted both at the C.E.N. and at Sylcor, U.S.A.
Gamma-counting shows that the distribution of U-235 in the plate is not homogeneous. Dog-boning up to 25% of normal core thickness was noted. This effect may be eliminated by giving a chamfer on the active core before the rolling of the triplex plate. But it leads to a fading at the end.
Due to the heterogeneity, measurements of the centerline do not seem sufficient for plates of large-size (nrs. 4, 5, and 6). A counting of three parallel lines was included in the counting instructions at the C.E.N.
The results are much clearer than those obtained by radiographic inspection. By using a proper standard the absolute amount of U-235 can be calculated. A certain disagreement was observed between the values obtained by gamma counting and Archimedes density method.

REFERENCES

1. Stanley Davis et al "Special design considerations for high flexibility in BR-2", TID-7584, pp 71-83, Symposium on high flux materials Testing Reactors, held in Brussels, Sept. 21-26, 1959 (Published June 1960).
2. Alfred Strasser "Fabrication of BR2 fuel elements" American Society of Mechanical Engineers Symposium, April 1959.
3. Fred K. White and Ronald B. Perry "A method of determining total U-235 in flat configurations," C00-272, Nov. 1960.
4. Fred H. Tingey "Non-destructive fuel assay at NRTS", Nucleonics, Vol. 20, no. 7, pp 76-81. (July 1962).

Table 1—Scanning Summary. Group I

Plate Nbr	Set	Avg Count	Hi count		Low count not end	Std Avg	U-235 × 10 ⁻²			% of AVG		Area of core in sq. in.†	Total U-235 content according to counting	Total U-235 content according to Archimedes density measurement		
			with dogboning (a)	without dogboning (b)*			Avg	Hi	Low	Hi	Low					
							(a)	(b)*	(a)	(b)*						
PBH-25-4	1	12.611	15.137	12.923	12.105	13 271	4.848	5.767	4.963	4.664	119	102	96	60.04	14.92	14.34
PBA-33-5	12	11.732	13.337	12.331	11.077	13 332	4.508	5.090	4.722	4.271	113	105	95	71.8	16.50	15.83
PBC-35-6	4	12.397	13.753	12.988	11.870	13 332	4.749	5.240	4.968	4.558	110	105	96	81.7	19.80	19.30
PBJ-02-3	5	12.896	15.287	13.432	12.181	13 361	4.920	5.784	5.118	4.661	118	104	95	49.0	12.31	12.14
PBE-46-2	7	12.773	15.940	13.116	11.536	13 465	4.732	5.976	4.964	4.396	126	105	93	40.7	9.83	9.71
PBZ-03-6	11	13.688	14.991	14.991	10.652	13 581	5.197	5.590	4.046	4.046	108	108	78	81.5	21.58	20.30
PBZ-02-6	14	15.125	16.079	16.079	13.029	13 532	5.657	5.997	5.997	4.909	106	106	87	81.5	23.50	20.46

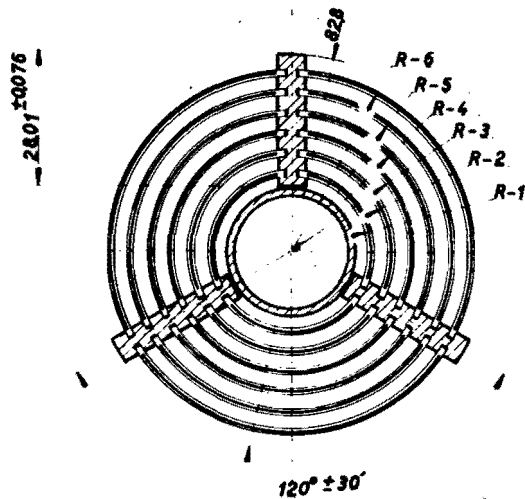
*Disregarding 5 cm at each end where dogboning occurs.

†Measured on the radiograph.

Table 2 — Scanning of 3 plates of Group II

Plate	PBJ-58-2	PBJ-18-3	PBK-20-6
Standard	13.355	13.265	13.120
1	13.378	13.595	12.419
2	12.411	12.233	12.149
3	11.993	12.025	12.042
4	11.938	12.008	12.446
Random	12.003	11.947	12.334
Random	12.056	12.186	13.281
7	11.949	11.821	12.285
8	11.974	12.011	12.499
9	12.040	12.171	12.764
10	13.512	13.465	13.714
Standard	13.131	13.018	13.175

Sylcor fuel element



Length of plate : 969,96
of active core : 762 ± 12,7

Scale: 1/1

Tube No	R	Minimum width of active core
1	15,976	24,5872
2	20,243	33,147
3	24,511	41,5544
4	28,778	50,0788
5	33,045	58,6232
6	37,312	67,2084

All dimensions in mm

Fig. 1 - Cross-section of the six-tube Sylcor fuel element

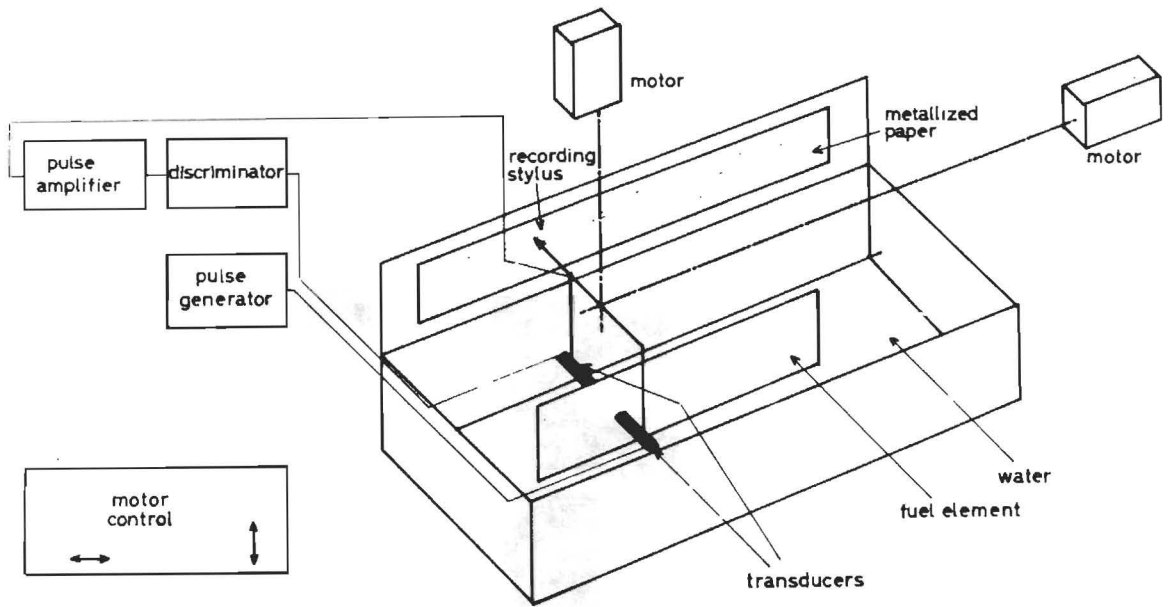


Fig. 2 - Overall view of the ultrasonic tester

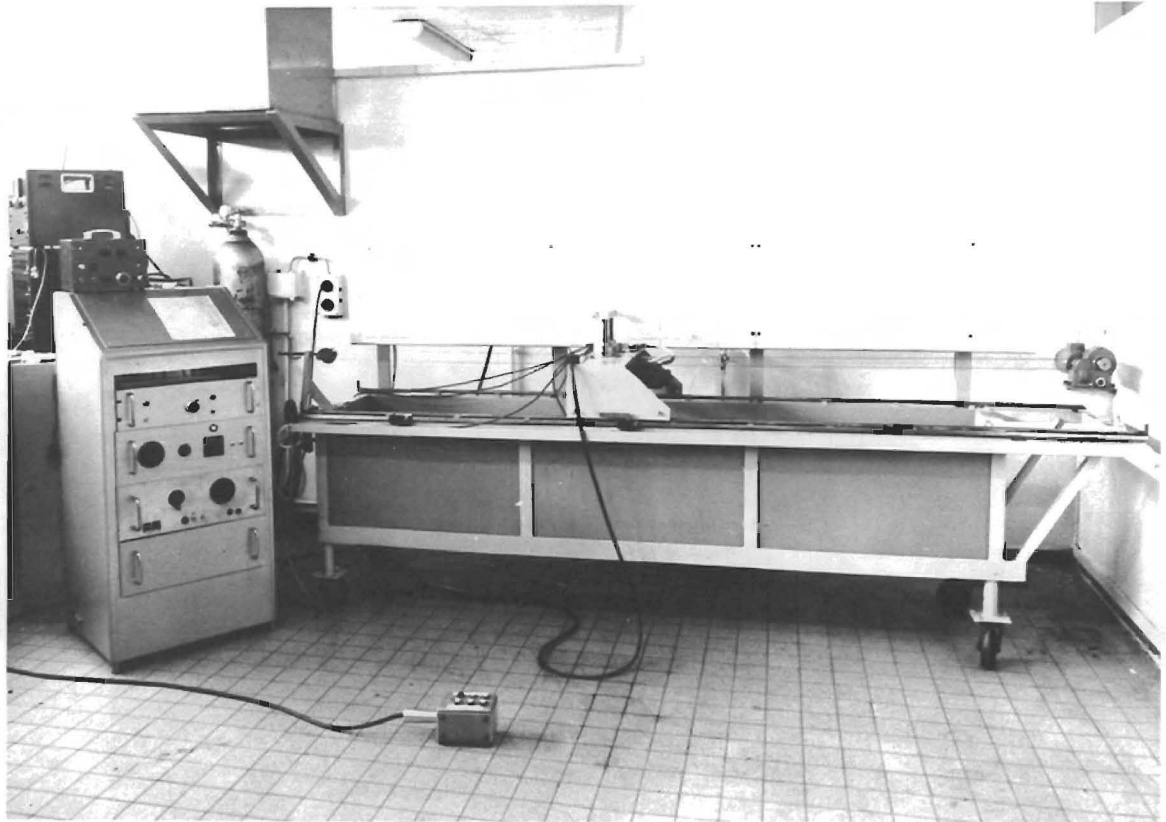


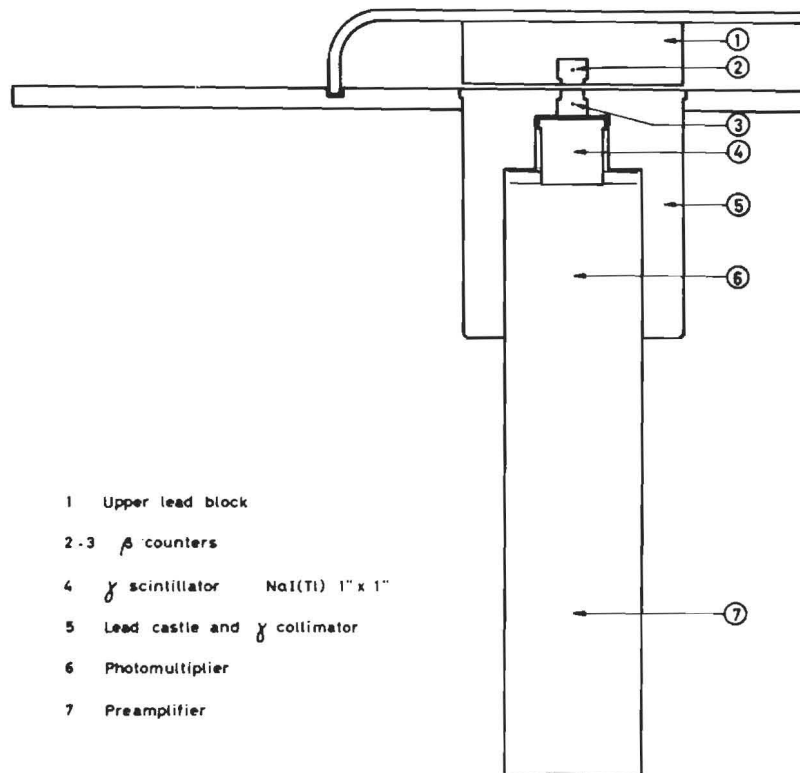
Fig. 3 - Overall view photo of the ultrasonic tester



Fig. 4 - Detail view of the ultrasonic tester



Fig. 5 - Overall view photo of the beta-gamma scanning apparatus



- 1 Upper lead block
- 2-3 β counters
- 4 γ scintillator NaI(Tl) 1" x 1"
- 5 Lead castle and γ collimator
- 6 Photomultiplier
- 7 Preamplifier

Fig. 6 - Sketch of the beta and gamma counters

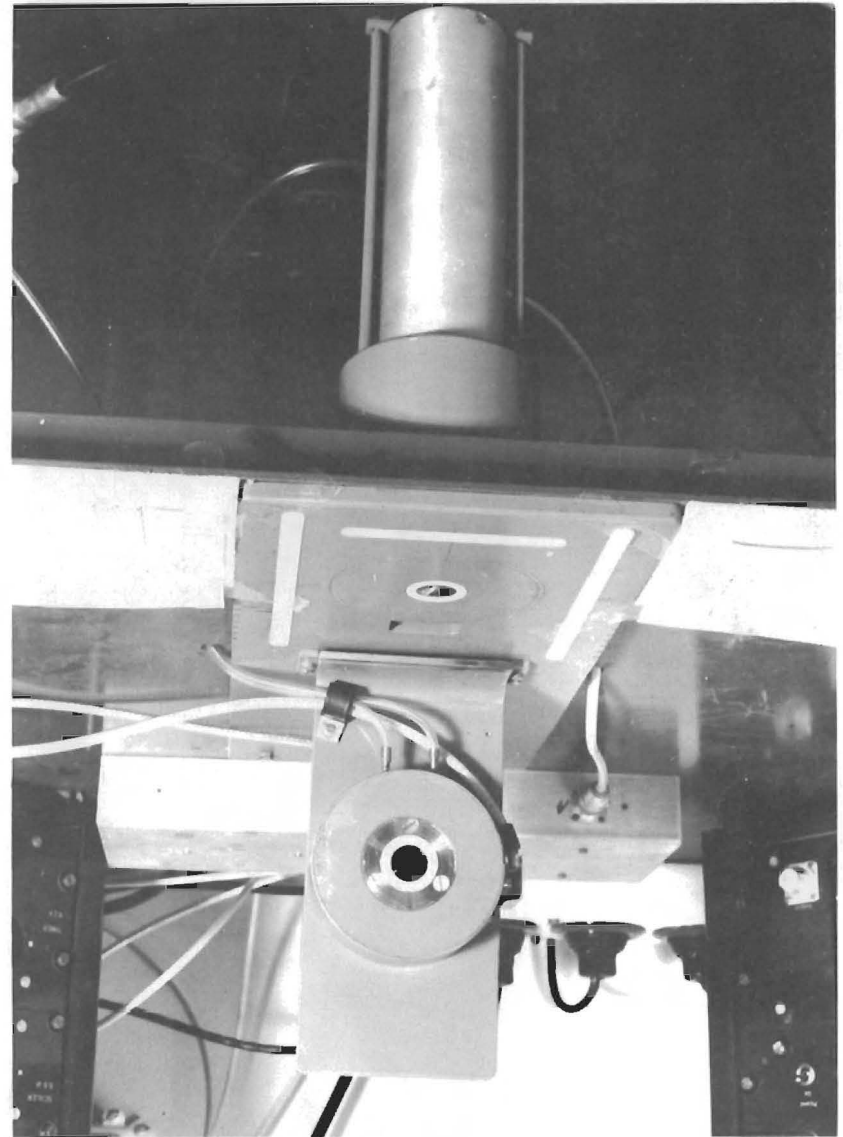


Fig. 7 - Detail view of the beta and gamma counters

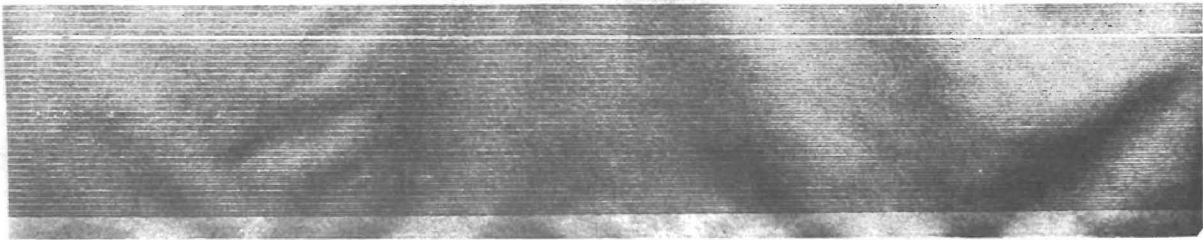


Fig. 8 - Typical ultrasonic recording

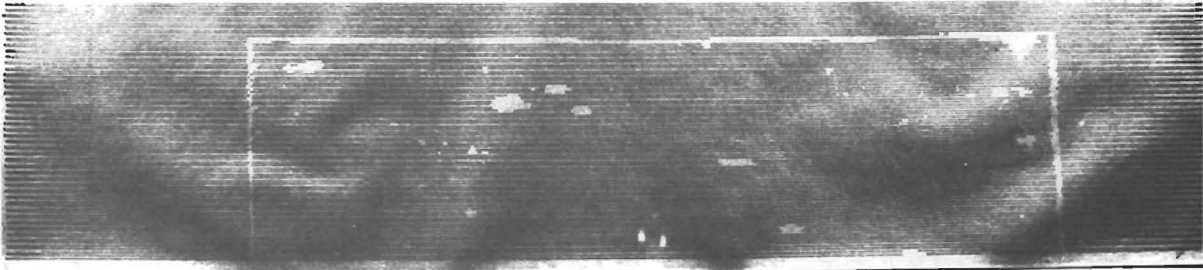


Fig. 9 - Faulty ultrasonic recording

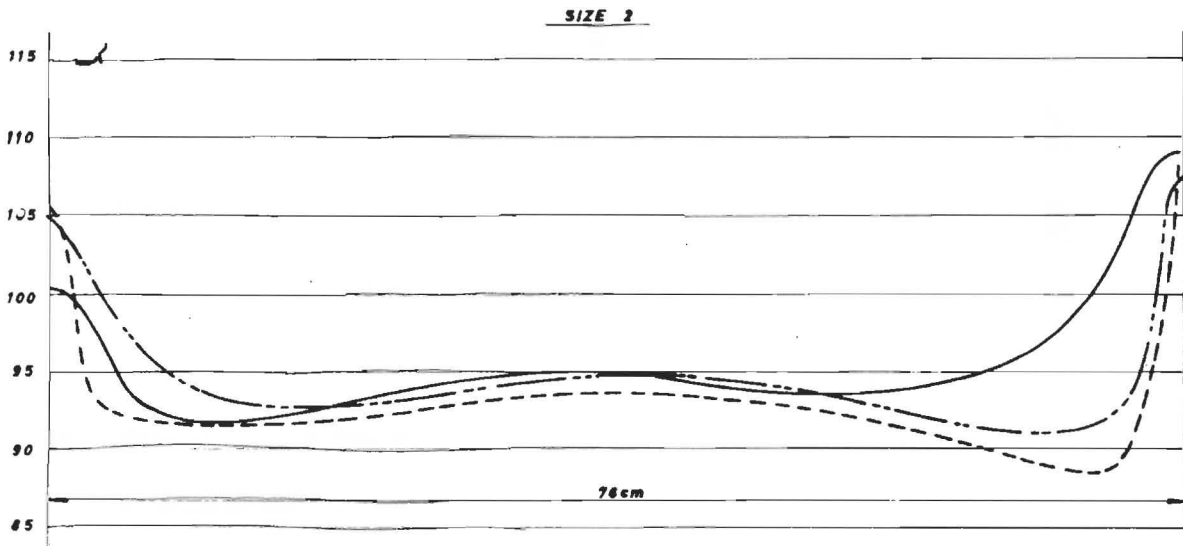
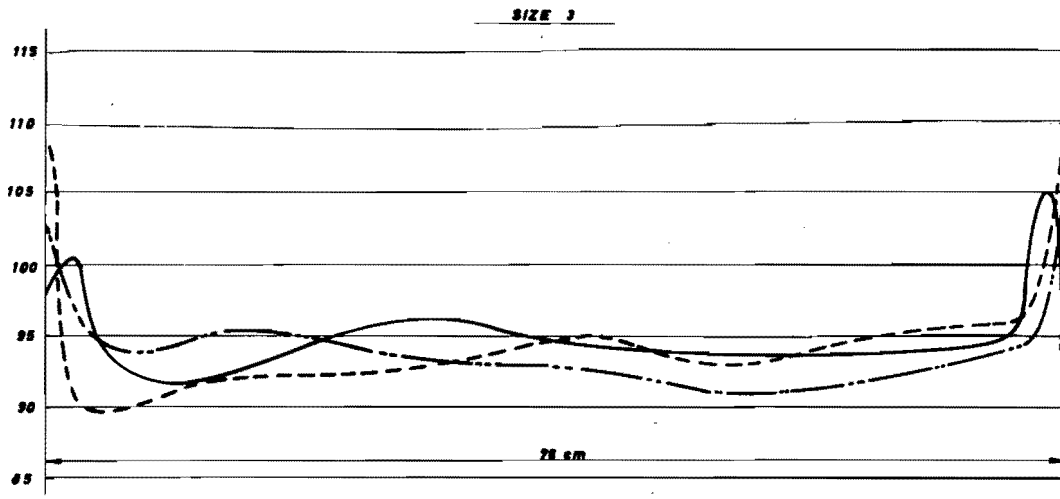


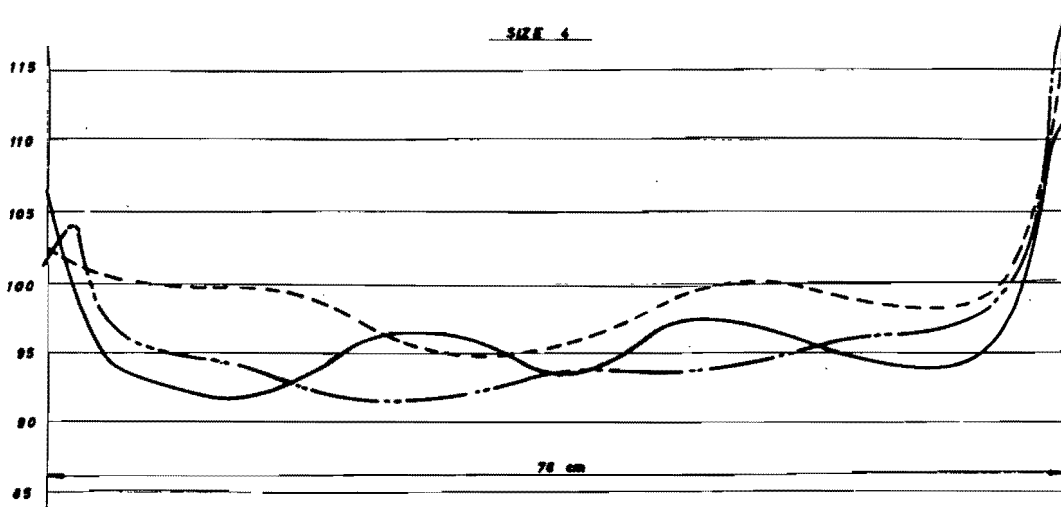
PLATE N°	U^{235} g/PLATE
— PBE - 62 - 2	2.50
- - - PSD - 88 - 2	2.05
- · - PBE - 54 - 2	2.64

Fig. 10 - Gamma-counting diagram - Size 2 plate



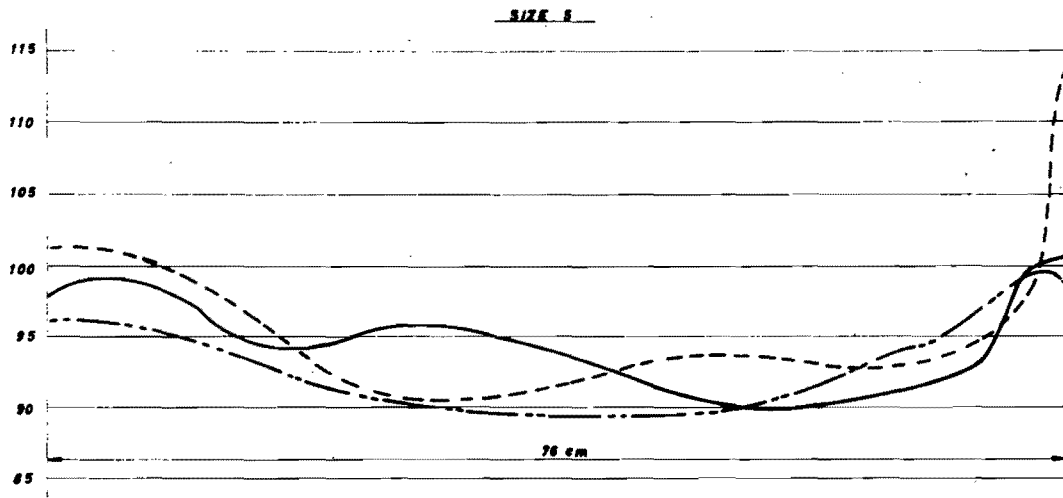
<u>PLATE N°</u>	<u>U²³⁵ g/PLATE</u>
— PBD - 41 - 3	11.60
- - - PBJ - 42 - 3	11.70
- · - PBJ - 44 - 3	11.69

Fig. 11 - Gamma-counting diagram - Size 3 plate



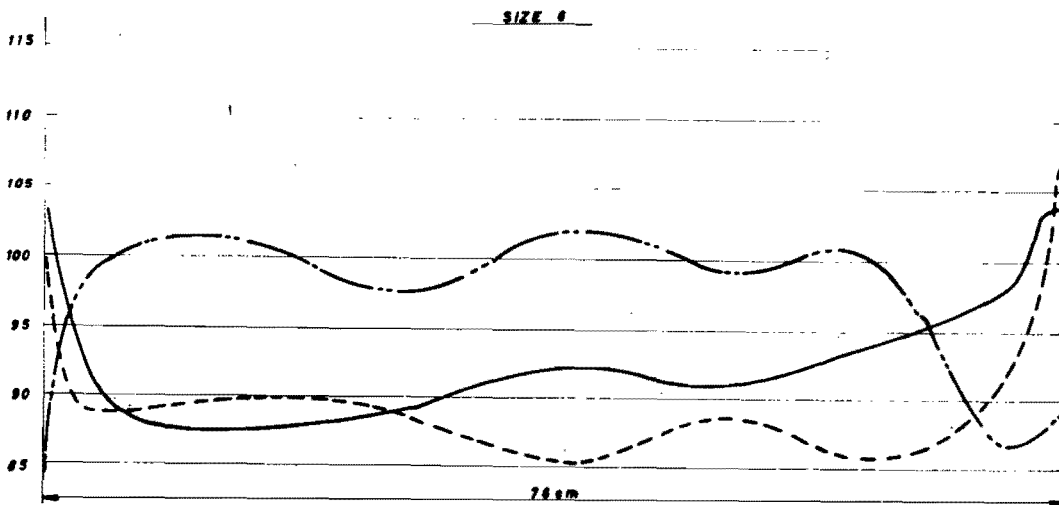
<u>PLATE N°</u>	<u>U²³⁵ g/PLATE</u>
— PDN - 29 - 4	14.46
- - - PBH - 32 - 4	14.43
- · - PBH - 37 - 4	14.43

Fig. 12 - Gamma-counting diagram - Size 4 plate



<u>PLATE N°</u>	<u>U²³⁵ g/PLATE</u>
— PBL - 42 - 5	16.41
- - - PBL - 19 - 5	17.09
- · - PBL - 27 - 5	17.07

Fig. 13 - Gamma-counting diagram - Size 5 plate



<u>PLATE N°</u>	<u>U²³⁵ g/PLATE</u>
— PBC - 33 - 6	16.98
- - - PBC - 40 - 6	16.82
- · - PBY - 17 - 6	20.47

Fig. 14 - Gamma-counting diagram - Size 6 plate

BOTTLE TYPE FUEL ELEMENT FOR POOL TYPE REACTORS

Prepared by: Commissariat à l'Energie Atomique, Compagnie pour l'Etude et la Réalisation des Combustibles Atomiques (CERCA), INDATOM

Presented by: P. Ageron, C.E.A.

by:

Atomiques

1. INTRODUCTION

In a usual pool-type reactor, where the forced convection circuit is open on the pool, it appears that the surface activity of the pool water is the first limitation in raising the power of this type of reactor.

- either in raising the power of an existing pool-type reactor (for instance from a nominal power of 1-2 Mw to a proposed power of 5-10 Mw) ; sizing of the fixed components is too low to allow, at the proposed power, for sufficient dilution, decay time and demineralization rate.

- or in the design of a new pool-type reactor of the maximum possible power (range : 20 to 30 Mw), size of the pool, decay tank and purification system would be prohibitive. The maximum power of an open circuit pool reactor (as the Austrian reactor ASTRA or the French reactor SILOE) seems to range in the 10-15 Mw region.

A well known and proved solution is to put the core in a tank in the pool, with a closed cooling circuit. But the tank cancel the main advantages of the pool reactor.

- simplicity and low cost of the in-pile part of the reactor
- easy access and manipulation of all elements and loops in or against the core
- flexibility of the reactor (size and shape of the core, size and place of the loops)
- higher neutron flux, at same specific power for loops close to the pool reactor core, than for loops close to the tank reactor core (neutron absorption in the tank wall, larger distance between fuel region and loops, impossibility of half penetration of the loops in the fuel region.

In answer to this problem, adding the advantages of the usual pool reactor to the advantages of the closed circuit tank reactor, is to put each fuel element in an individual tank connected to the inlet and the outlet of the cooling circuit. Such a fuel element will be called "bottle" type fuel element.

2. THE BOTTLE TYPE FUEL ELEMENT

2.1. Hair pin fuel element

As it is desired that the fuel element keeps the same easy accessibility from the top as does the usual one, inlet and outlet of coolant have to be placed in the foot of the element and water flow has to be of the double-pass type.

The foot of the bottle type element with inlet and outlet orifices, fit in a guid plate, which incorporates two water boxes, one for incoming, the other for the outgoing flow, as shown on figure n° 2.1 a.

Fuel plates can be parallel (curved or flat) or concentric (circular, hexagonal or square cylinders). In both cases a fuel plate acts as separation between upward and downward flow.

In a concentric plates fuel element, the flow can be :

- upward in the central fuel region of the element and downward in the peripheral region (this flow will be called "outward flow").
- upward in the peripheral region and downward in the central region (this flow will be called "inward flow")

The merits of this different dispositions will be discussed later on, but each one offers, beyond the containment of the active water in a closed circuit, the thermal advantage of the double pass cooling : for the same velocity of the water in identical channels, at the same specific power, the flow in each element will be half of that for a MTR element, and the temperature raise will be twice. That leads to a smaller size and cost of the primary cooling circuit and heat exchangers.

2.2. The open top fuel element concept

The top of a fuel element has to be opened and in communication with the pool in two occasions

- when the reactor and its refrigeration are stopped for rearranging the core and during the transfer of irradiated fuel element, it is necessary to provide a natural convection, upward flow cooling.
- in case of over heating of the water (accidental over rating of the power, or loss of coolant flow) boiling and or degassing may occur and vapor and gasses (also radiolyse gasses) can accumulate in the top of the element and have to be evacuated.

This opening of the top can be achieved :

- occasionally, by means of valves acting some by loss of pressure, the other ones by overpressure.
- permanently by means of a permanent opening, called "tapping orifice".

Only the first solution allows a pressurisation of the whole element and primary circuit above the hydrostatic pressure in the pool, and thus, much better thermal performances than the classical pools reactors. But the second solution exhibits a much greater simplicity and, probably, safety. Moreover as it will be shown later, :

- the thermal performances of such an open top, double passe fuel element can reach an interesting range (a specific power of 200 to 300 Kw/1 that is to say a power of 20 to 30 Mw for usual size of pool reactor core).
- with a proper design of the top opening, one can prevent any loss of active water from the inside of the element to the pool. On the contrary a certain amount of pool water will flow into the fuel element (this flow called "tapping flow" will be about one tenth of the main cooling flow) entraining the active water formed between and above the elements, and will be returned to the pool after sufficient decay of its short life radionuclides, and fixation of its middle and long life radionuclides on ions exchange resines (see figure 2.1 a)

The present paper deals mainly with this last concept.

2.3. Geometry

- The aims of geometrical studies of the element are :
 - To obtain the largest ratio of heat transfer surface (S) to volume of core (V) : S/V
 - To reduce as much as possible the local flux peaking in the element.

- Types of geometries

Different arrangements of the fuel plates are possible :

- parallel plates (flat or curved) as in the MTR Type, fuel element with a longer plate separating the upward and the downward flows.

Their advantages are:

- for all plates the meat dimensions are standard
 - there is no region in the core without fuel plates except the water holes where the control rods are to take place (special elements)
- Thus S/V is good

Their drawbacks are:

- the local flux peaking near the water hole for usual control rod is important

$$\frac{\phi_{m,x}}{\phi_{local}} \approx 1,7$$

- this type of element is not symmetrical around a vertical axis and it will be sometimes difficult to place the best cooled region (upward flow region) in the highest flux peaking region.
- concentric plates: cylindrical with circular, hexagonal or square base

Drawbacks:

- this type of element leaves regions without fuel plates in the center of the element (because it is not possible to have so small plates to fill the central region) and, with circular plates, between elements. Thus, the ratio S/V will be lower than for parallel plates types.
- there will be flux peaking in the center of the element, if the central region without fuel is left filled of water; this peaking can be lowered by putting in this region an

irradiation container, or a dummy aluminium piece.

Advantages:

- it is possible to have in the whole peripheral region of the element, where flux peaking is to be the highest, a better cooling (upward flow region)
- maximum flux peaking near the water hole between elements seems to be lower than for water holes in parallel plates elements:
For circular plate element $\frac{\phi_{max}}{\phi_{local}}$ is about 1,4 and only 1,1 for hexagonal or square plates elements (the water width between element being constant).

- Parameters involved in optimization of a circular bottle element

- Inner diameter of the inner fuel plate:

by reducing this diameter one can reduce the diameter of the water hole thus, lower the flux peaking in the central region (Use of a dummy aluminium piece can also help in this way) with the technology of laminated fuel plate, hold by 3 aluminium holders, it seems that this diameter could not be economically reduced more than about 2 cms. More reduction could be expected from co-extruded fuel tubes. Any way, improvement in the whole S/V ratio of the element is small in this way.

- Outer diameter of the outer fuel plate:

by increasing the outer diameter of the outer fuel plate the ratio of the fuel region section on the total section of the cellule is increased, thus the ratio S/V also, (other things remaining the same). But the size of fuel element is limited, to keep its neutronic weight in reasonable limits Gap between fuel elements and lattice size for a given fuel element influence sharply the flux peaking in this region.

- Plate thickness .

Thinner fuel plates are the best and well known mean to improve S/V ratio. Numerous studies and tests on thin fuel plates will probably make available in a near future plates thinner than the 50 mills plate, which we consider actually as a minimum.

Deflection of the separating plate between upward and downward flow, under differential pressure, will be an other limitation of the thickness of this plate.

3. STUDIES AND TESTS PERFORMED

Studies and tests described in this chapter were performed by "Sté INDATOM" and "La Compagnie pour l'Etude et la Réalisation des Combustibles Atomiques" (C.E.R.C.A.).

3.1. Fuel element choice and description

The principle of double flow element enclosed in individual tank naturally leads to a cylindrical plates element with coaxial outlet and inlet set on hexagonal lattice. This form has been adopted.

For detailed studies and tests, a type of fuel element was to be selected. Several types of elements have been studied, they differ by the quantity of plates, the thickness of uranium and cladding and the width of water channels.

A high power density and a low head loss were the objectives. Besides, the manufacturing possibilities were taken into account.

Finally an element called B3, with 20% enriched uranium has been choiced for neutronic and heat transfer studies and hydraulic tests. An element C3 with 90% enriched uranium has also been selected and design is under way.

In table bellow are shown the main features of these elements and for comparison, features of some known elements.

Fuel element	Fuel Thickness mm	Cladding Thickness mm	Plate Thickness mm	Channel Width mm	Enrichment
Russian Reactor 20 MW)	0,7	0,65	2,0	2 & 2,5	90 %
B R 2	0,508	0,38	1,27	2,97	90 %
E T R	0,508	0,38	1,27	2,74	-
M T R	0,508	0,38	1,27	3,24 ou 2,99	20 ou 90 %
B3	0,9	0,38	1,66	2,34 et 2,84	20 %
C3	0,508	0,38	1,27	2,73 et 3,23	90 %

B3 element is composed of six 1.66 mm plates mounted on 3 holders set at 120° (see fig. 3.1.a and 3.1.b.)

The inert plates, not part of the fuel system, form the basic frame, the outer plate being used as a "bottle".

3.2. Neutronics

Observation bears mainly on flux distribution in cell. Bottle elements being of circular form, the core made of elements arranged in a hexagonal pitch, show more or less important water holes. To these water holes correspond flux peaking and hot spots on the plates. At a first look, these hot areas might have been unacceptable.

Therefore, we had to observe the microscopic flux distribution in each element, to determine the flux coefficient necessary for the hot spot computation and to decide if final result was acceptable.

Most of the work was on type B3 elements (20 %) and C3 (90 %).

Flux peaking computation.

Computation is performed using the total thermal power (P watt) as a base multiplied by a coefficient K specific of flux variation (maximum to average flux).

The coefficient K is composed of two factors :

$$K = K_1 \times K_2$$

- K_1 = macroscopic coefficient specific of macroscopic flux variation from center to edge of core.
- K_2 = microscopic coefficient specific of microscopic flux variation from center to edge of cell.

Average macroscopic flux $\bar{\phi}$ is given by formula :

$$\bar{\phi} = \frac{3 \cdot 10^{10} \cdot P}{V \Sigma_f}$$

P = power (watts)

V = core volume (cm³)

Σ_f = average macroscopic fission in core (cm⁻¹)

True macroscopic flux is similar to the flux observed at every point of an homogeneous core having finished dimensions.

Maximum value ϕ M at center :

$$K_1 = \frac{\phi M}{\bar{\phi}}$$

Microscopic flux ϕ is the true flux at every point of an heterogeneous element disposed in an area where macroscopic flux is constant and whose value is 1.

$$\text{True flux} = \phi \times \phi$$

In the case of cylindrical cells arranged in a hexagonal pitch flux irregularities may be defined by two coefficients Ψ and θ

- Ψ radial microscopic coefficient is the ratio between maximum flux in outer uranium cylinder of element and average flux in uranium of cell taken as a whole, this being in direction of average water thickness.

- θ angular microscopic coefficient is the ratio between both flux in outer uranium cylinder of element in respective direction of maximum and average water thickness.

Therefore :

$$K_2 = \Psi \theta$$

Flux distribution :

To emphasize pitch importance on distribution, 4 average half-widths of water surrounding the element have been observed :

(a)	half width	1 mm	pitch	78 mm
(b)	" "	3 mm	"	82 mm
(c)	" "	7 mm	"	90 mm
(d)	" "	12 mm	"	100 mm

In a hexagonal lattice having mean half width of 3 mm correspond minimum half width of 1 mm and maximum of 7 mm. Alternatives (a), (b) and (c) allow to determine the microscopic coefficients ψ and θ for a lattice pitch of 82 mm.

Computation method used here was double P1. Successive stages in computation were :

- double P1 on type B3 (plane) and C3 (plane)
- diffusion B3 and C3 (plane and cylindrical)
- transfer of B3 and C3 (plane) to B3 and C3 (true) through the previous curves.

It is then admitted that :)

- local flux variations are due to the heterogeneous structure of the elements.
- Curve shape is due to geometry.

Curves on fig. 3-2a and 3-2b show the results of these computations.

Flux maps are shown on fig. 3-2c and 3-2d.

Results of study

Table below shows results as B3 and C3 elements and alternatives (b) and (c) are concerned.

An intermediary alternative B3 is also shown, it was necessary for the continuation of study.

Thermic and neutronic results emphasize 82 mm pitch (better repartition of neutronic and thermic flux, lower ψ θ coefficients)!

84 mm pitch alternative has been retained to leave an acceptable clearance between the elements.

ELEMENTS	B 3 (b)	B 3 described	B 3 (c)	C 3 (b)	C 3 (c)
Lattice pitch (mm)	82	84	90	82	90
Cell dimensions : (mm)					
Minimum Radius	39	40	42,86	39	42,86
Average radius	41	42	45	41	45
Max. Radius	45	46.2	49.49	45	49.49
Clearance between elements (mm)	†	2	4,86	1	4,86
U 235 g/L of core	48,31	45,49	40,10	40,18	33,35
Metal volume/water volume : (without support)	0,5991	0,5417	0,4406	0,4583	0,3451
Microscopic flux peaking : K_2	1,329	1,335	1,357	1,295	1,262
Material buckling $B^2 : m^{-2}$	94 to 100	94.5 to 104.5	94 to 104		
Critical weighty : Kg U - 235	3.15 to 3.50	3 to 3.3	2.6 to 2.9		
Geometrical buckling m^{-2} (25 elements)	91.3	88,7	81,8	91,3	81,8

For chosen B3 element, we have :

$$K_2 = \psi \theta = 1.335$$

Approximately, K1 is given the same value as in the case of a M T R elements core. Readings of the MELUSINE reactor being taken into account we have :

$$K_1 = 1.6$$

from which :

$$K = 1.335 \times 1.6 = 2.14$$

This value will be used for heat transfer computation.

However it should be noted that this value is applicable only if control rods may be housed into ordinary water holes of the lattice and not in place of fuel elements.

3.3. Heat transfer

Heat transfer study covers several types of fuel elements. Below are shown results as for B₃ type element which has been selected for testing.

Features of B3 element

- 6 tubes composed of bent fuel plates and two inert tubes.
- Metal/water ratio = 0.568
- Uranium 235 weight per element = 151 g.
- Fuel density : 47,8 g U 235/l of core
- Enrichment : 20 %
- Fuel alloy : 45 % U , 55 % AL (weight)
- active height : 600 mm
- Core composed of 27 elements type B3
- Thermal power : 10 MW

- Direction of flow : centrifugal (upward water flow through central plates, downward water flow through peripheral plates).

Cooling Features

- Total cooling flow : 600 m³/h
- flow per element (upward flow) : 5.55 L/s
- flow per element (downward flow, after tapping) 6.17 L/s
- Upward flow : through 4 inner channels 2.84 mm thick, except center channel 2.50 mm thick (with fuel plate on one side only).
- Downward flow: through 3 outer channels 2.34 mm thick
- Head losses in upward and downward flow : same value to the nearest 10 %
- Water velocity in element : upward flow : 6.25 m/s
downward flow : 5.07 m/s
- Water temperature : inlet of core : 30 ° C
outlet of core : 44.35 ° C
- Heat transfer coefficient on plates (as per COLBURN)

Upward flow	:	3.26 W/cm ²	°C
Downward flow	:	2.87 W/cm ²	°C
- Maximum surface temperature is computed using ratio $\phi_{max} / \bar{\phi}$ 2.5 thus increasing the computed value of 2.14 as a safety measure.

Maximum surface temperature is 82.4°C. As uncertainty about this temperature is 18.1°C (see below) and boiling point at channels center is 111.2°C, we still have an allowance of 10.7°C which permits the statement that no local boiling is likely to occur.

Uncertainty about maximum plates temperature

The "hot spots factors" method has been used here. The following values have been retained concerning elementary uncertainties in this computation :

- Velocity : measure of average velocity : 5 %
- distribution heterogeneousness between elements 15 %
- distribution heterogeneousness into one element 15 %
- Spacing between plates :
 - Manufacturing tolerance (0.25 mm) : 9 %
 - Distortion in operation 15 %
- Heat generation and transfer :
 - Flux measurement 10 %
 - Heterogeneousness of U 235 content 15 %
 - Water temperature (inlet) 5°C
 - Incertitude about COLBURN formula 20 %

Computation shows an incertitude of 18,1° C.

Therefore, max. sheath temperature will be lower than :
 $82.4 + 18.1 = 100.5^{\circ} \text{ C}$

Fuel element 90 % enriched

At the start a 20 % enriched fuel has been selected as it was more easily available at that time.

However, 90 % enriched uranium enables the user to utilize thinner plates and consequently to lower head losses. This is why, a C3 90 % enriched element has been designed, similar to B3 although plates thickness is 1.27 mm.

Computation showed that for constant maximum plates temperature (82.4° C) head losses were reduced about 14 %.

3.4. Hydraulic tests on mock up

Test purpose was to check the viability of hydraulic design in bottle element, in the same time as clearing up incertitudes on the following main points.

- head losses, flow distribution between channels.
- Possibility to obtain a satisfactory head shape although opposite requirements of forced convection (no leakage of active water at top orifice) and natural convection (low head losses through top orifice)
- Possibility to annihilate loosening force to avoid mechanical locking, by proper flow direction and foot shape.

Hydraulic tests were performed in GRENOBLE at the SOGREAH laboratories member Company of the INDATOM Group.

For these tests a stainless steel mock up of the selected element has been used (see fig. 3 -4A). Experiments were performed on a testing facility including pump, heat exchanger, flow meters on main circuit and draining circuit.

Natural convection experiments were performed on special testing facility shown on fig 3 - 4b.

Head losses in forced convection

Full measurements of head losses in outward flow of element have been taken (water flowing upward in central plates and downward in peripheral plates). Reduced tests of inward flow (water flowing upward in peripheral plates and downward in central plates) showed that the change in distribution direction did not alter the results very much.

Pressure measurements were performed at different points of circuit in order to obtain a check of head losses as tight as possible. Measurements points locations are shown on fig. 3 - 4c.

Measurements show the different output values. Draining flow was 1/10 of total flow. Main results are shown by curves of fig. 3 - 4d giving versus flow, the total and partial head losses.

Total head loss may be written :

$$H = K_a \frac{V_B^2}{2g}$$

Where V_B is the velocity in peripheral plates, K_a is the head loss coefficient of the unit.

Curve in fig. 3 - 4e gives K_a in terms of Reynolds number in peripheral plates.

Results obtained have been compared with the values computed in H. Rouse "Elementary Mechanics of Fluids". head losses are always lower than values thus calculated

When total nominal flow is 6.17 L/sec which corresponds to a thermal power of reactor of 10 MW head losses are :

$$H \text{ total} = 16.3 \text{ m}$$

$$H \text{ downward drain} = 8.5 \text{ m}$$

Downward head loss is important as far as pumps cavitation is concerned Taking into account hydrostatic pressure at draining level. the value obtained shows that no cavitation is likely to occur and that a higher head loss may be understood. This result permits the concept that with selected element it will be possible to have a higher water output e, i, more reactor power. A better design of water flow should result in a more important increase.

Head losses in natural convection

The purpose of natural convection tests in conjunction with draining tests was to define a head shape satisfying the two following conditions; to allow a sufficient natural convection flow of cooling water while forced cooling not in operation and prevent cooling water leaks through tapping orifice while in operation.

Studies of head loss have been made in an element flowed with water in one direction only and mounted with the different heads :

- A : Without head
- B : Mushroom head 70 mm dia. without chimney (see fig 3-4-h)
- C : Mushroom head 56 mm dia. without chimney
- D : Half mushroom head and cylindrical chimney
- E : Ogive head and venturi (see fig. 3-4-i)
- F : Ogive head and cylindrical chimney.

In each case, head loss for natural convection has been measured. Results are shown on fig. 3 - 4f.

Total head loss coefficient K_a may be written :

$$H = K_a \frac{v^2 B}{2g}$$

Fig. 3,4g shows the values of this coefficient in terms of Reynolds number. In general, the operation of the bottle element in natural convection corresponds to transitory areas between turbulent and laminar flow.

In natural convection, tests show that moving flow particles reach approximately a speed of 20 cm/s. This corresponds to an output element of 420 cm³/s. It is possible to obtain a head shape so as the head loss be about 3cm of water. It is certain that density forces will be higher than these viscosity forces and that mentioned flow will be reached. For comparison, the 18 plates MTR element gives 1 cm of water head loss for a speed of 11 cm/s.

Leaks through tapping orifice.

Draining tests were performed to check the possibility of having tapping orifice allowing solely outside to inside flow, without any leak in opposite direction.

For these tests potassium bichromate had been injected into the cooling circuit and traces of this product has been measured outside the head.

Main flow was 6.17 L/s and tapping flow 0.617 L/sec.

Measure was taken with a 2 cells model VI, Lange photo-electric colorimeter allowing to detect traces to the nearest 0.01 ppm. In these conditions, this device could detect a leak of $0.1 \text{ cm}^3/\text{s}$.

Following results was obtained :

- Head shape B, outward flow = No leak
- Head shape E, inward flow = No leak
- Head shape A, inward flow = Very low leak

Therefore, it is no difficult to install a tapping orifice giving no leak to the outside. The right head shape, according to water flow, will be selected comparing the results of natural convection tests, and leak tests

Flow distribution between plates

Water velocity distribution into different channels is important as far as cooling calculations are concerned. Flows and velocities slightly differ from one channel to the other due to :

- difference between channel diameters
- manufacturing tolerances
- lack of symetry in channel distribution

Water velocity in channels has been measured with a progressive travelling rotary tester designed at the "SOGREAH",

Conditions of tests performed :

- Constant total flow at different points of element
- Variable flow at specific point

Tests showed that speed variations were lower than 10 % except in the two smaller channels where variations reach 15 % . On the other side, speed variations diminished when total flow increases. However, it should be noted that machining accuracy of test element was higher than machining tolerance of fuel element.

In general, velocity distribution may be taken as acceptable, but thickness might be increased in both smaller channels.

Loosening tests

While in operation, bottle element may be subject to a vertical upward force imputable to pressure difference and water friction on walls. This force should be counterbalanced either with balance weight or foot locking.

Loosening tests purpose was to determine the value of this force, they were performed with a rather rudimentary device shown in fig. 3 - 4j. A cable on pulley is fixed at the top part of the element. At the other end of cable is a weight p . P being the weight of element, downward force F will be determined when element will be lifted.

$$F = P - p$$

The test covered both flow directions and various flow values.

Obtained results have been corrected taking into account the following facts :

- test performed in open air (not in water)
- test element weight is different from the element weight proper.

On the other hand theoretical calculation give loosening forces values. Computed values differ from experiment values. This difference results partly from lack of precision of tests, and from the impossibility to perform an exact calculation, the bottle element geometry being very complex.

Finally, nominal output being 6,17 L/s. test values are :

- outward flow, loosening force : 8 Kgp
- inward flow, pressing force : 4 Kgp

Actual weight of bottle element being 6 Kgp, this one should be lifted in normal operation condition. (1st case) and a balancing or locking system should be provided.

As a conclusion as far as loosening is concerned, inward flow is preferred to outward flow. With a proper design of foot, the inward flow element would not be loosened and might merely be set into the grid.

3.5. Realisation studies

Theoretical studies have been performed on the manufacturing problems and on the mechanical strength of a bottle type fuel element. Further developments will comprise construction and tests of prototypes.

The fuel region of the element consist in 6 concentric fuel tubes, each consisting in 3 curved plates fit to aluminium holders. The fabrication of aluminium uranium alloy, aluminium clad plates, their curving (diameter from 22 to 68 mm) and their crimping on the holders will use known

Outer diameter of the outer aluminium shell cm	9,2
Diameter of the central aluminium piece cm	1,54
Lattice type	Triangular
Dimension cm.	10
Ratio $\frac{\text{Volume metal}}{\text{Volume water}}$	0,627
Ratio $\frac{S}{V} \text{ cm}^{-1}$	3,39

4.2 - Heat transfer

For the hottest channels (in upward and downward flow) maximum wall temperature have been calculated in fonction of the velocity of water :

- in upward channel :

$$(\theta_{\max})_u = t_i + \frac{1}{2} \frac{k_r \bar{\phi} S_u}{C_p s_u V_u} + \frac{0,9 k_1 (k_2)_u \bar{\phi}}{h_u}$$

- in downward channel :

$$(\theta_{\max})_d = t_i + \frac{k_r \bar{\phi} S_u}{C_p s_u V_u} + \frac{1}{2} \frac{k_r \bar{\phi} S_d}{C_p s_d V_d} + 0,9 \frac{k_1 (k_2)_d \bar{\phi}}{h_d}$$

where :

$\bar{\phi}$ watt/cm² : mean heat flux defined as $= \frac{P}{S}$ where P watt is the total power of the reactor

p watt/cm³ : mean specific power

h watt/cm²/°C : heat transfer coefficient

t_i °C : inlet temperature of water

S cm² : exchange surface

s cm : flow section

V cm/sec : water velocity

k_r : radial macroscopic flux peaking

k_1 : total macroscopic flux peaking

k_2 : total microscopic flux peaking

C watt/cm³ : specific heat of water

indices "u" and "d", refers to upward flow and downward flow

- Inlet temperature is 28°C
- Tapping flow have been included in downward flow as 10% of the upward flow
- Uncertainty $\Delta \theta_{\max}$ on θ_{\max} have been calculated by statistical method used for SILOE and PEGASE and with the same elementary uncertainties as in 3-3; it was found to be 18°C.
- an another margin $\sqrt{\theta_{\max}}$ was taken to allow for accidental power increase of 10 %
- the total maximum wall temperature to be considered at the hot spot was :

$$\theta_{\max} = (\theta_{\max})_{\text{calculated}} + \Delta \theta_{\max} + \sqrt{\theta_{\max}}$$

- According to MELUSINE experience, and SILOE calculations

$$k_r = 1,27 \text{ ; } k_1 = 1,6$$

- Two local flux distribution have been studied :

A relatively flat distribution :

$$(k_2)_u : \left(\begin{array}{l} \text{for the outer fuel plate} \\ \text{of the upward flow region} \end{array} \right) = 1,3$$

$$(k_2)_d : \left(\begin{array}{l} \text{for the outer fuel plate} \\ \text{of the downward flow region} \end{array} \right) = 1,1$$

A distribution with more flux peaking in peripheral region and more depression in central region :

$$(k_2)_u : 1,4$$

$$(k_2)_d : 1,0$$

- The ratio of upward water velocity to downward water velocity $\frac{V_u}{V_d} = 1,24$ was a compromise between geometry requirement and optimum value (about 1,1)
- Setting the condition : $\theta'_{\max} = \theta_{\text{saturation}}$

The maximum mean specific power can be calculated and is plotted versus water velocity in downward flow on the graph figure N° 4.2 a

According to possible water velocity between 600 cm/s and 800 cm/s, and local flux distribution, this specific power lie in the range of 200 - 300 watt/cm³.

That is to say, for a core volume of about 100 liters, a total power of :

20 - 30 MW

4.3. Head losses

Head losses was calculated by methods used in SILOE fuel element calculation which has been verified by hydraulic tests on a dummy fuel element.

The first aim of this calculation was to obtain an order of magnitude of the differential pressure on the separating fuel plate.

The maximum differential pressure at the maximum water velocity considered ($V_d = 800$ cm/sec.) was found to be

3.400 cm of water

The following head losses are plotted versus water velocity on graph figure N° 4.3 a.

ΔH_{AB} between inlet and top of the fuel region (upward flow)

ΔH_{BC} between top and outlet of the fuel region (downward flow)

$\Delta H_{AC} = \Delta P_{PC} + \Delta H_{BC}$ maximum differential pressure at the bottom of the separation fuel plate.

4.4. Deflection of the separating fuel plate

A rough calculation of the deflection of the separating plate can be made by analogy with a vertical, cylindrical tank, of constant wall thickness, submitted to an outside hydrostatic pressure (assuming that differential pressure is linear versus height and zero at the top), with free upper edge and fixed lower edge.

According to TIMOSHENKO, "Theory of Plates and Shells", the deflection is given by the general equation :

$$\frac{d^4 w}{dx^4} + 4 B^4 w = \frac{P}{D}$$
$$B^4 = \frac{3(1-\nu^2)}{a^2 h}$$

w cm : deflection
x cm : height

$$D = \frac{E h^3}{12 (1 - \nu^2)}$$

$$P = \gamma (d - x)$$

d cm : total height

a cm : half diameter

h cm : wall thickness

: Poisson coefficient

E $\frac{\text{kg}}{\text{cm}^2}$: Elasticity modulus

γ $\frac{\text{kg}}{\text{cm}^3}$: Fictive specific weight

The general equation, with the above edges conditions can be solved :

$$w = \frac{a^2 d}{Eh} \left[1 - \frac{x}{d} - \theta (\beta x) - \left(1 - \frac{1}{\beta d}\right) \zeta (\beta x) \right]$$

where : $\theta (\beta x) = e^{-\beta x} \cos \beta x$

$\zeta (\beta x) = e^{-\beta x} \sin \beta x$

For the separating plate :

d : 60 cm

a : 3,419 cm

h : 0,127 cm

E : $7,22 \cdot 10^5$ kg/cm²

ν : 0,3

} for an aluminium plate

For a maximum differential pressure $p_{\max} = 3,42$ kg/cm² the fictive specific weight γ is : 0,057 kg/cm³.

Thus :

$$w = 4,35 \cdot 10^{-4} \left[1 - \frac{x}{d} - \theta (\beta x) - 0,9915 \zeta (\beta x) \right]$$

The maximum deflection is $4,5 \cdot 10^{-4}$ cm at 0,15 cm above the bottom.

5 - CONCLUSION

The possibility of an open top, unlocked bottle fuel element has been proved by hydraulic tests, in particular :

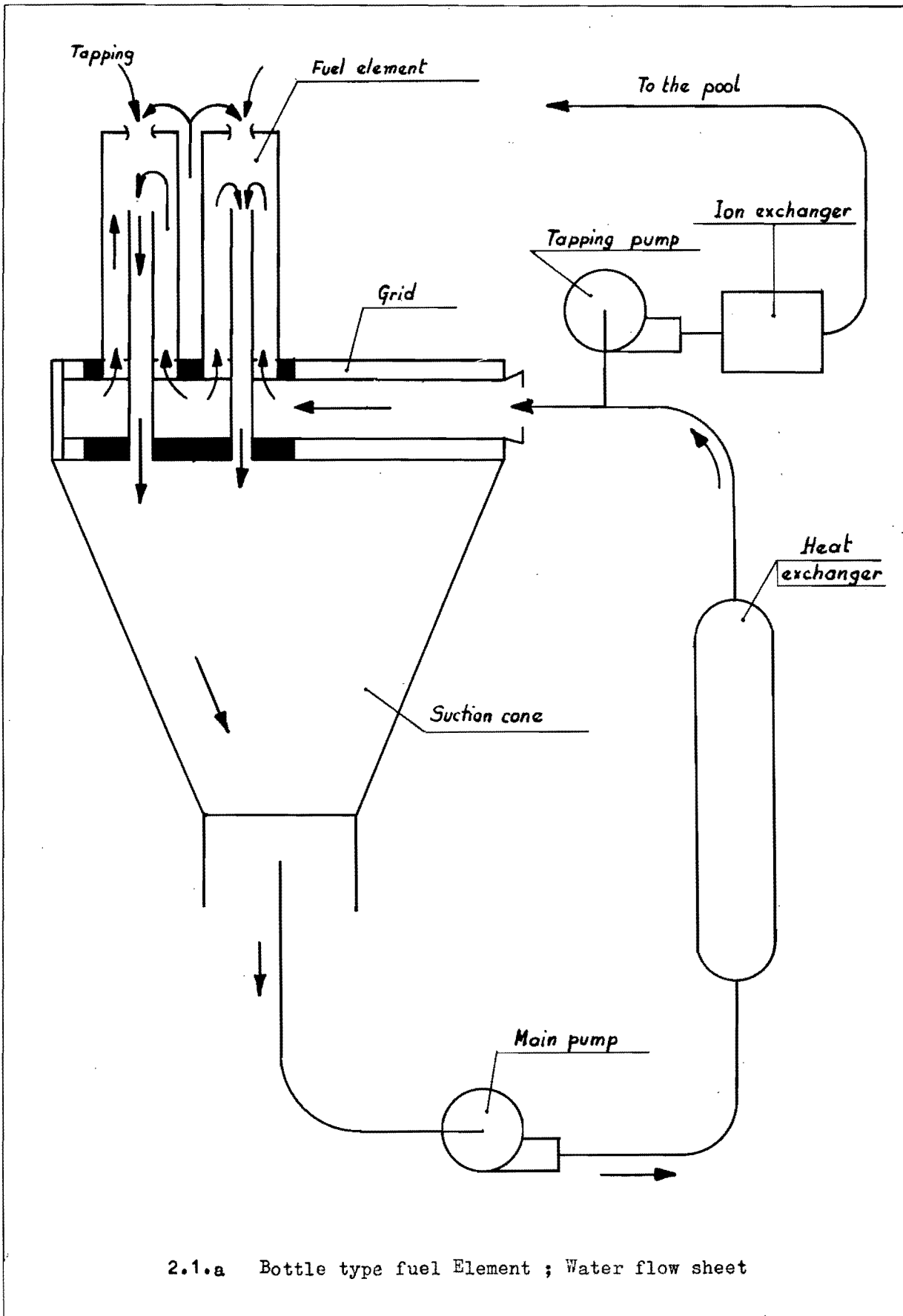
- there was no loss through the opening of radioactive water,
- with inward flow and proper design of the foot, the resulting vertical force on the element was downward, thus pressing the element on the grid-plate and permitting to avoid locking system.

Bottle elements could thus be used in pool reactor with no more difficulties than ordinary M.T.R. elements and permitting important increase on power rating, by minimizing the activity of water in surface.

Uncertainties remain on active water losses and by-passing between grid-plate and elements.

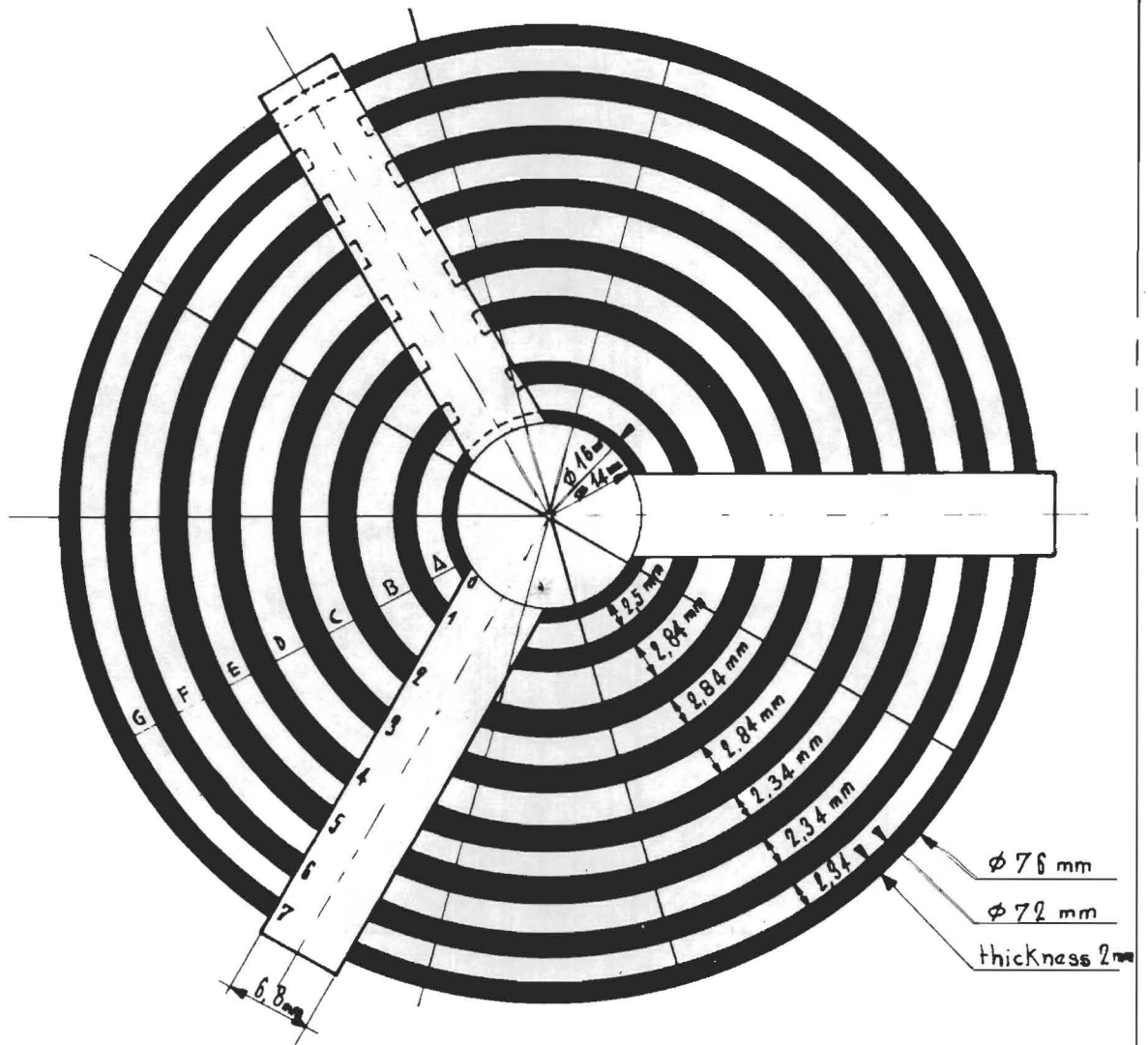
First studies on cooling problems have shown that the maximum mean power density for an optimized bottle element lies in the range of 200 to 300 kw/l; uncertainties remain in the following fields :

- accurate knowledge of the flux peaking (importance and position) in the element,
- minimum thickness of available and proved fuel plates - Until now this minimum thickness is 1,27 mm (50 mills) but improvements in this way are expected,
- resistance and deflection of plates under important differential pressure and at operating conditions,
- vibrations of elements at large water velocity.



2.1.a Bottle type fuel Element ; Water flow sheet

Fig 3-1a
 BOTTLE-TYPE ELEMENT
 HORIZONTAL SECTION



Fuel plates 1, 2, 3, 4, 5 and 6 (thickness 1.66 mm)

Fig 3.1 b
BOTTLE-TYPE ELEMENT
VERTICAL SECTION

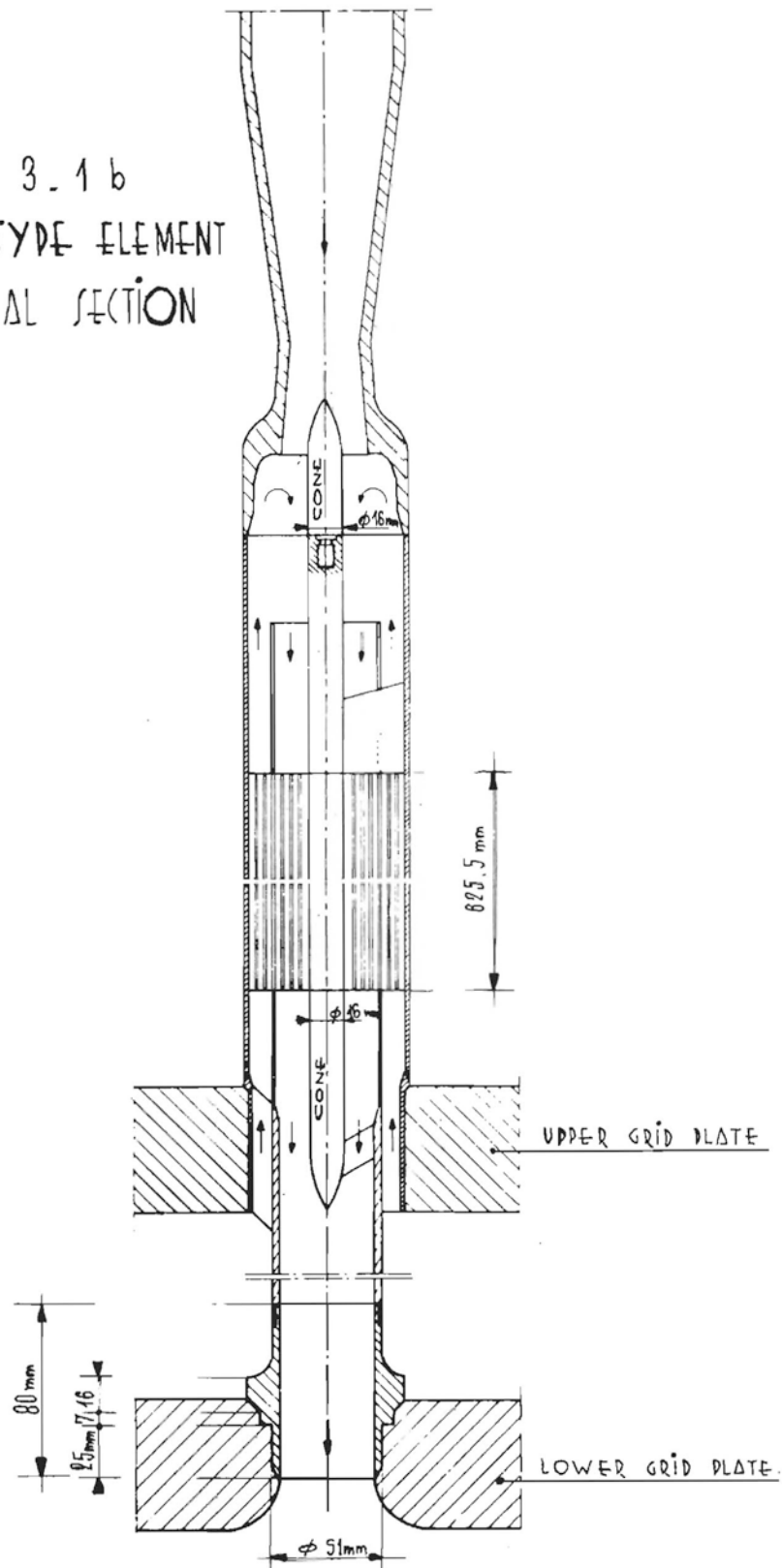


Fig 3.2 c
FLUX MAP
IN B3 TYPE ELEMENT
SCALE : 5

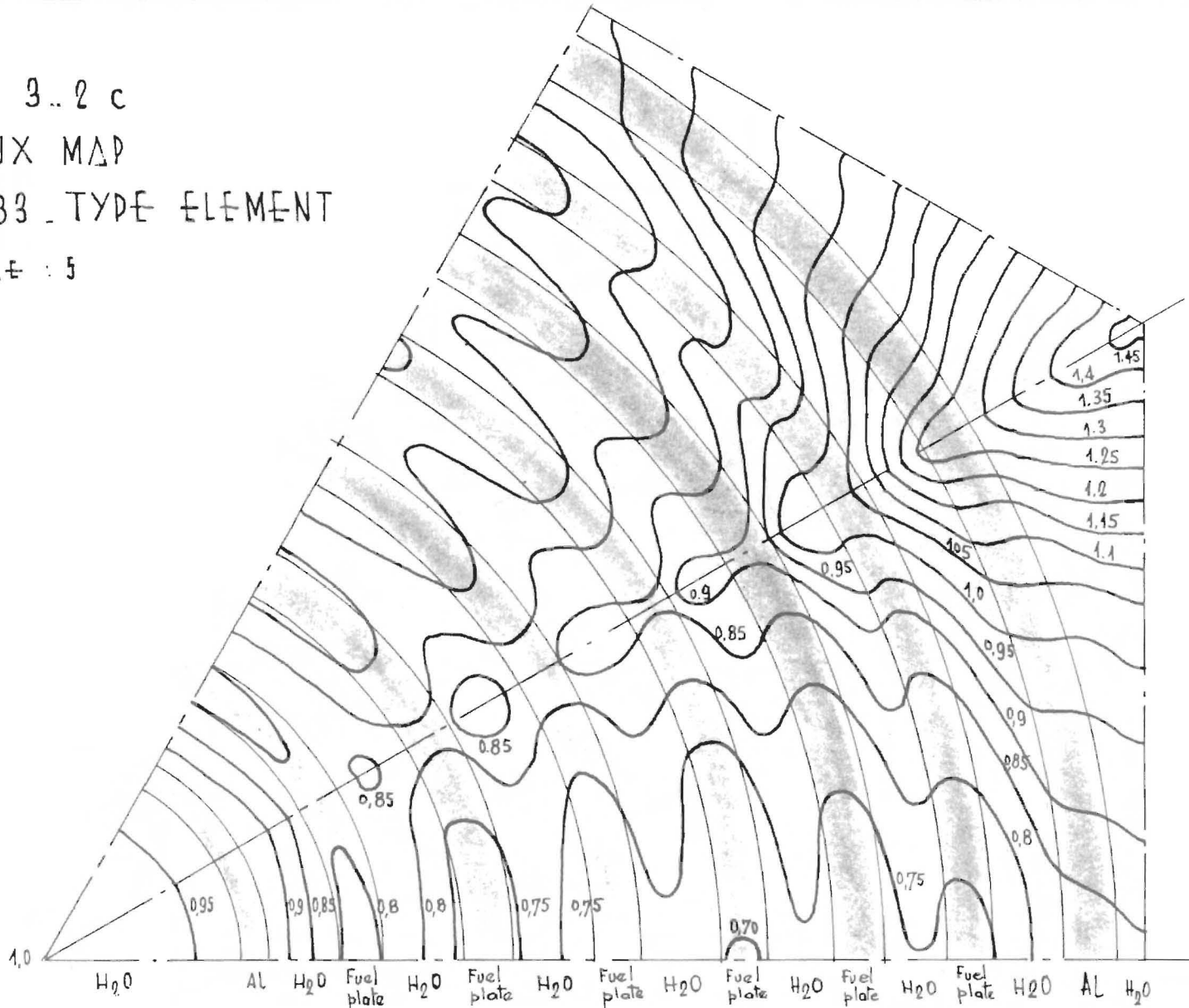
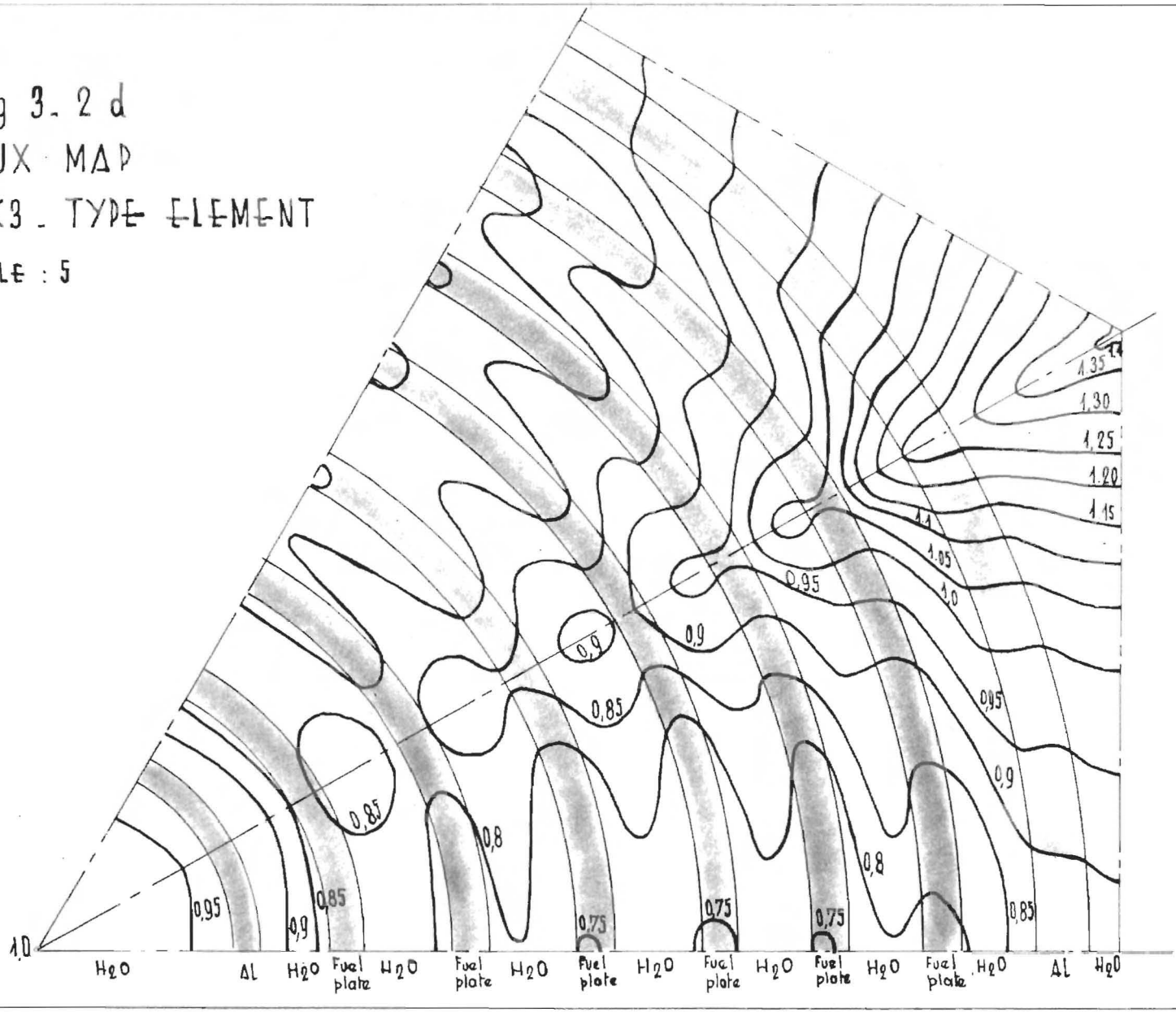
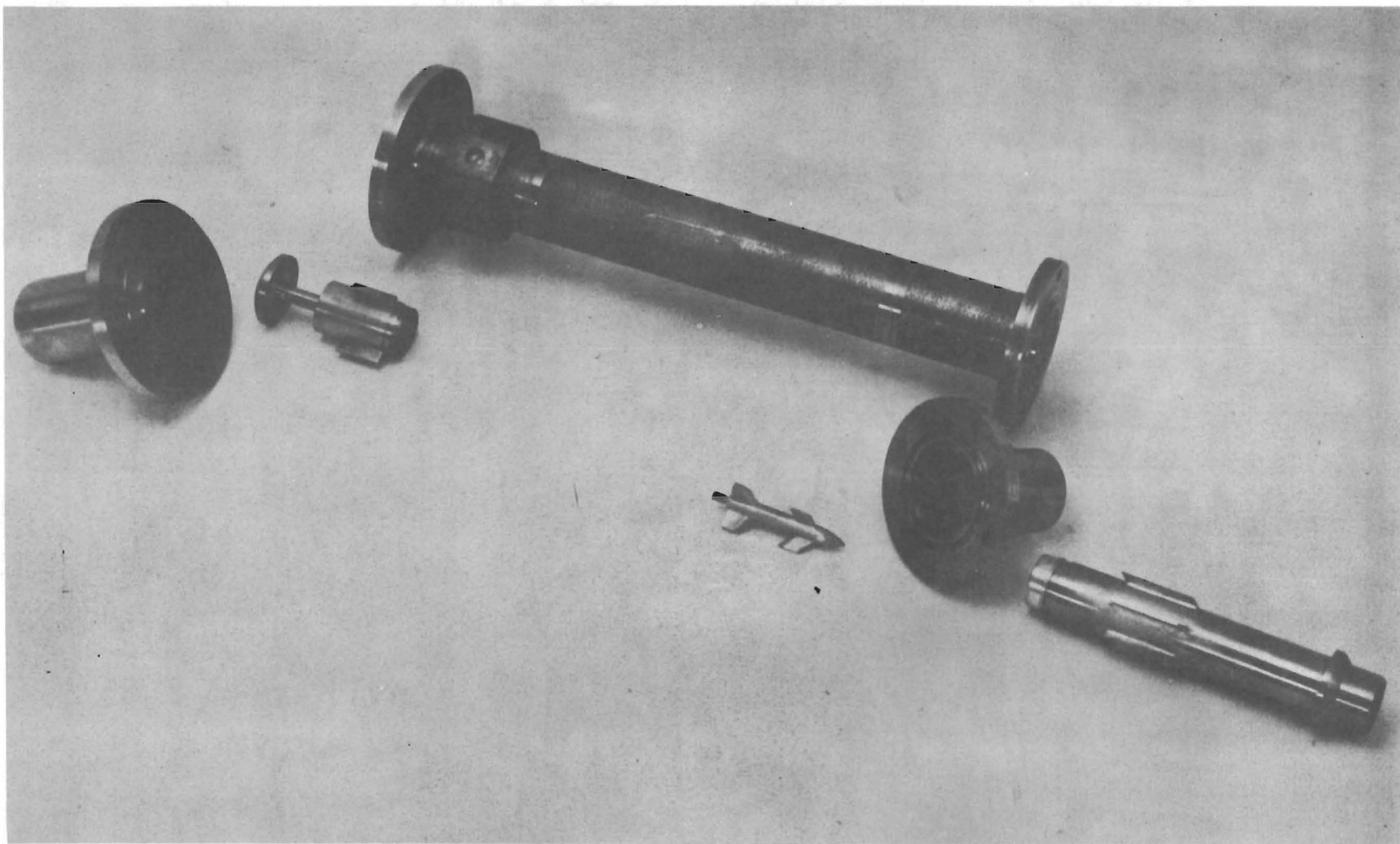
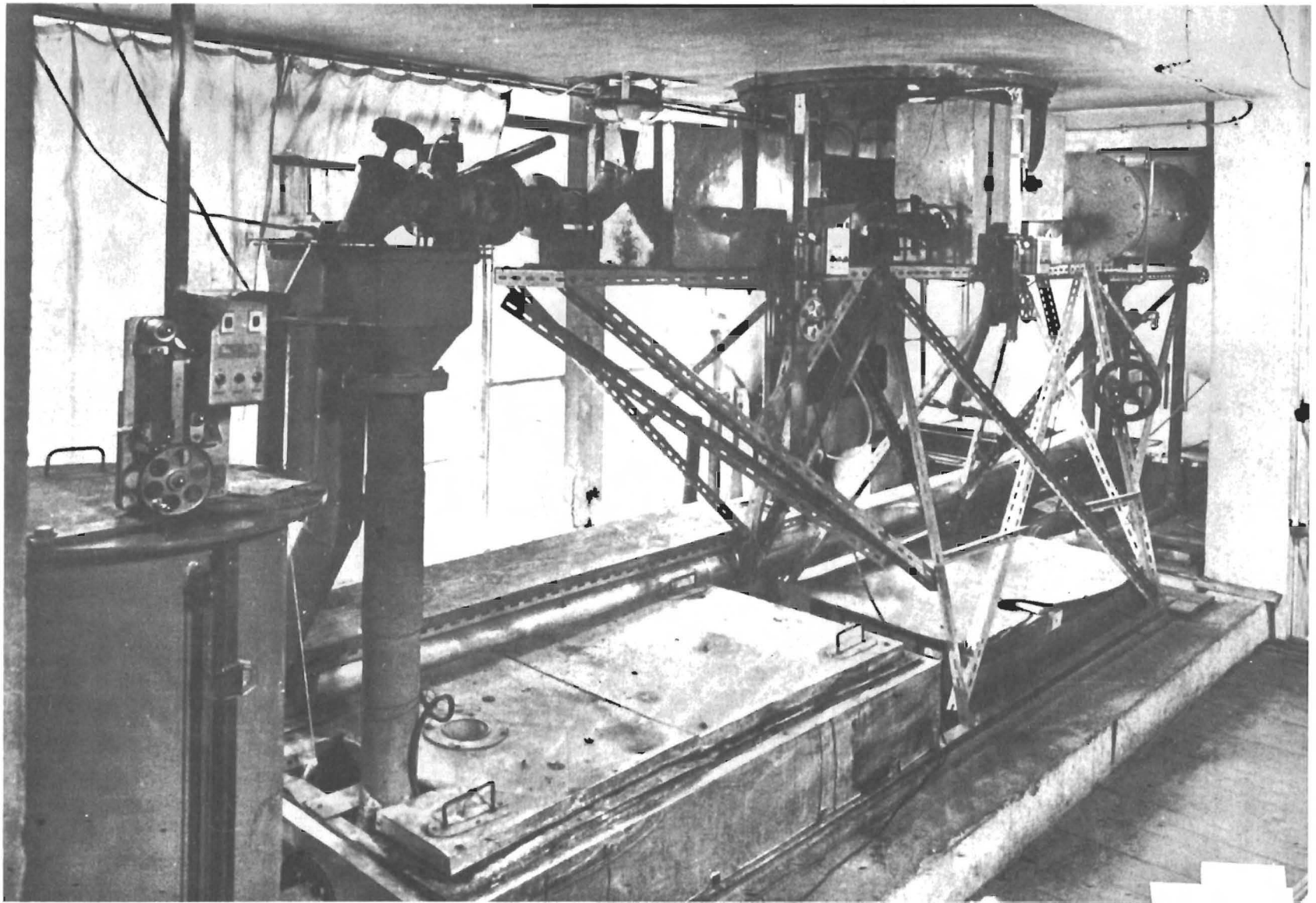


Fig 3.2 d
FLUX MAP
IN C3 - TYPE ELEMENT
SCALE : 5





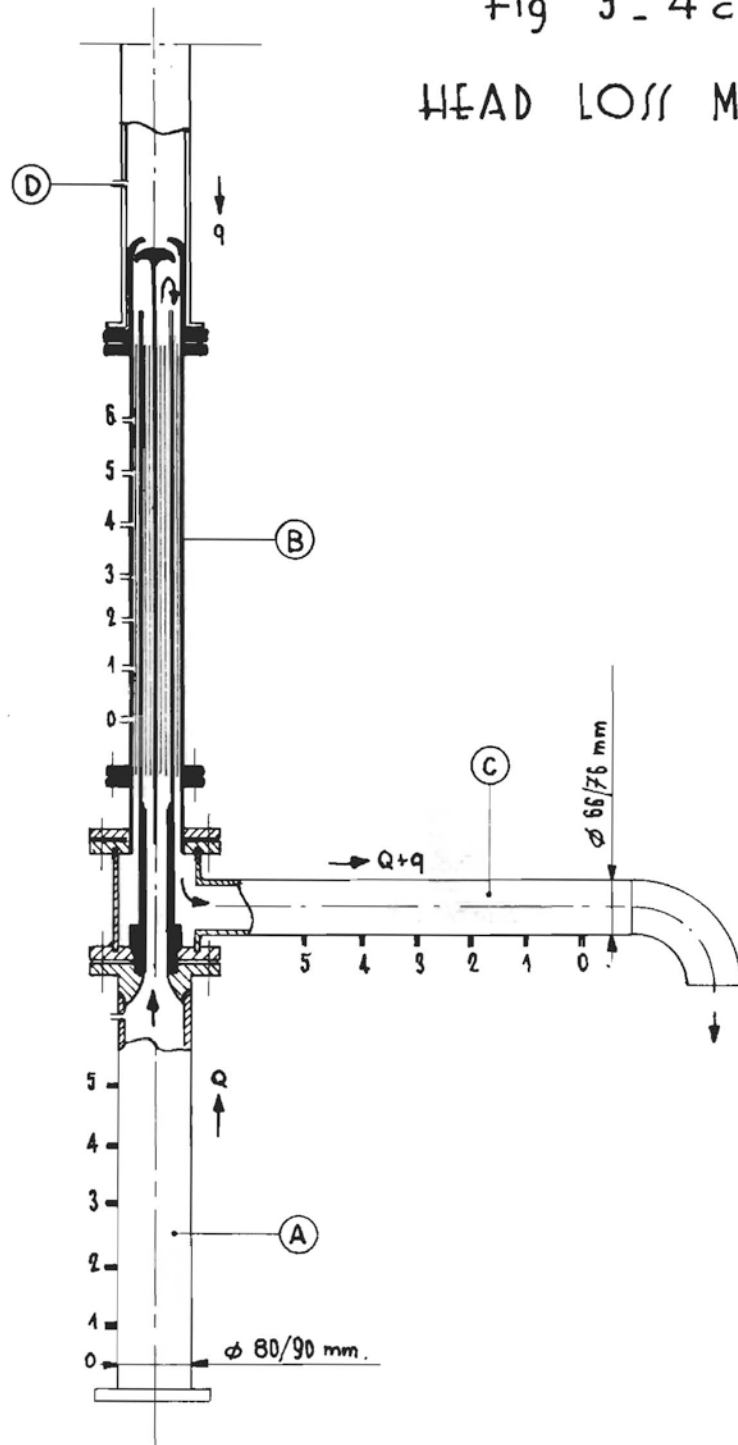
3.4.a Mock up of B3 element for hydraulic tests



3.4.b Hydraulic test facility

Fig 3-4c

HEAD LOSS MEASUREMENTS



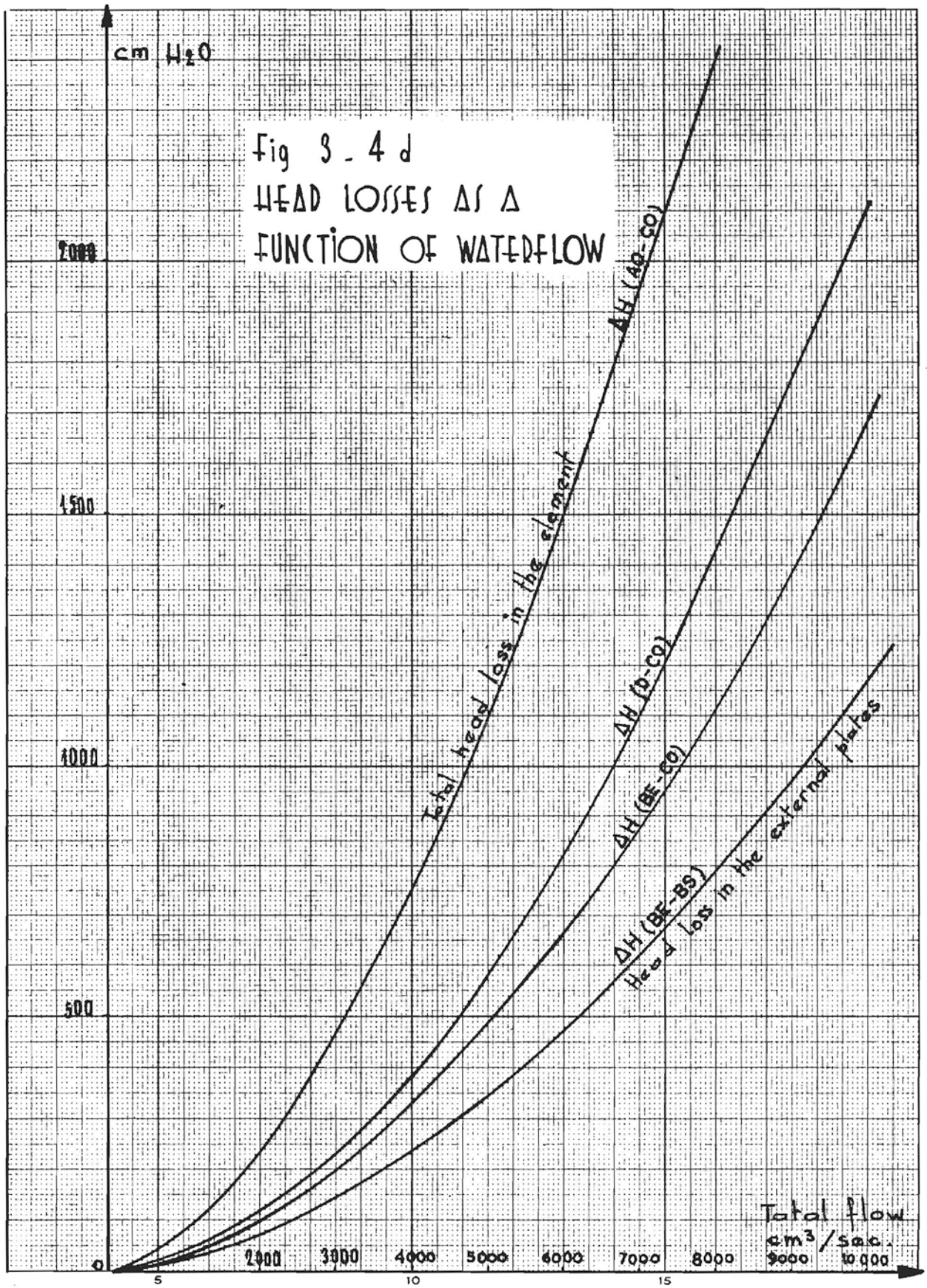
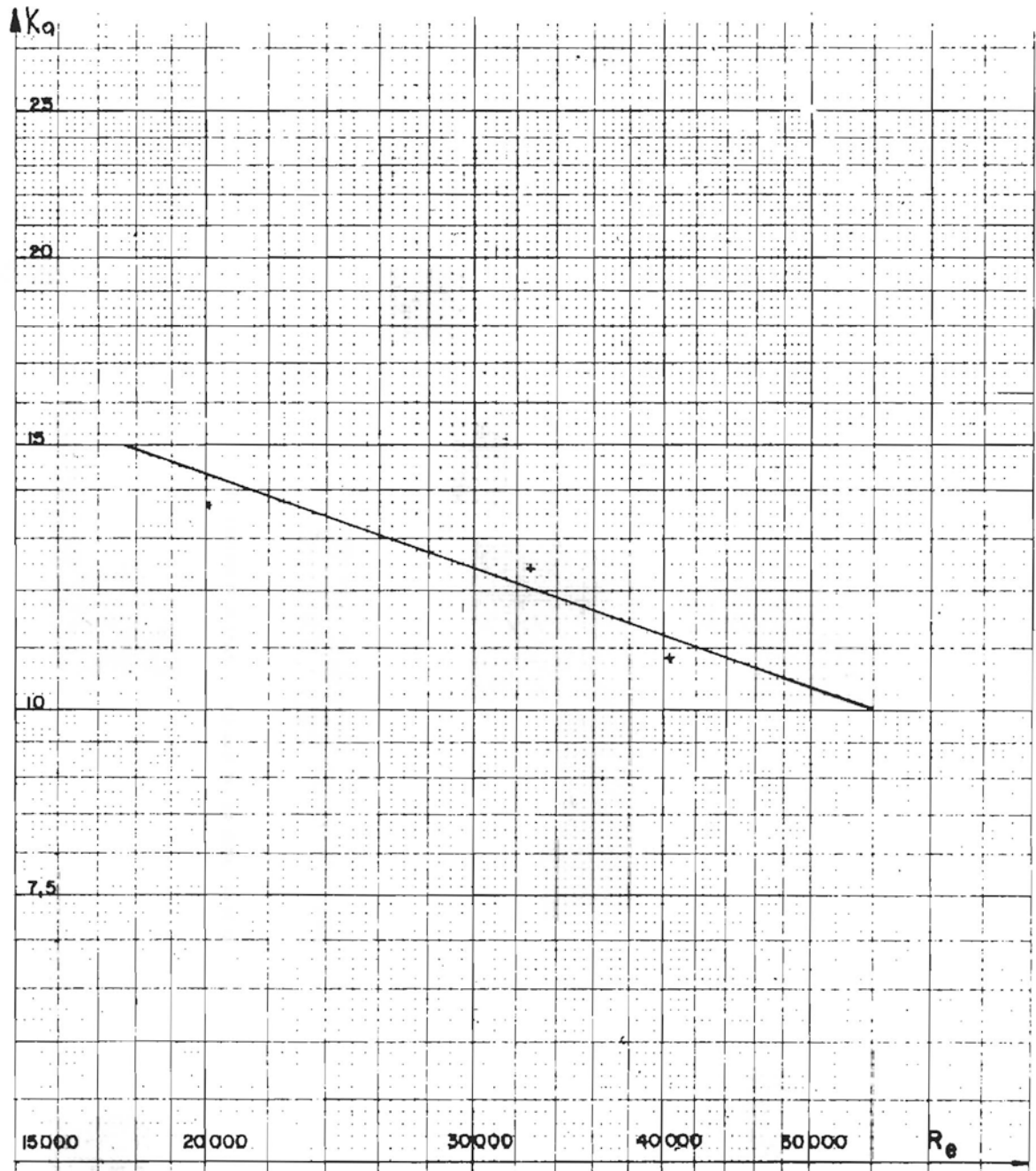


Fig 3.4 e

TOTAL HEAD LOSS FACTOR Δ AS A FUNCTION OF REYNOLDS' NUMBER



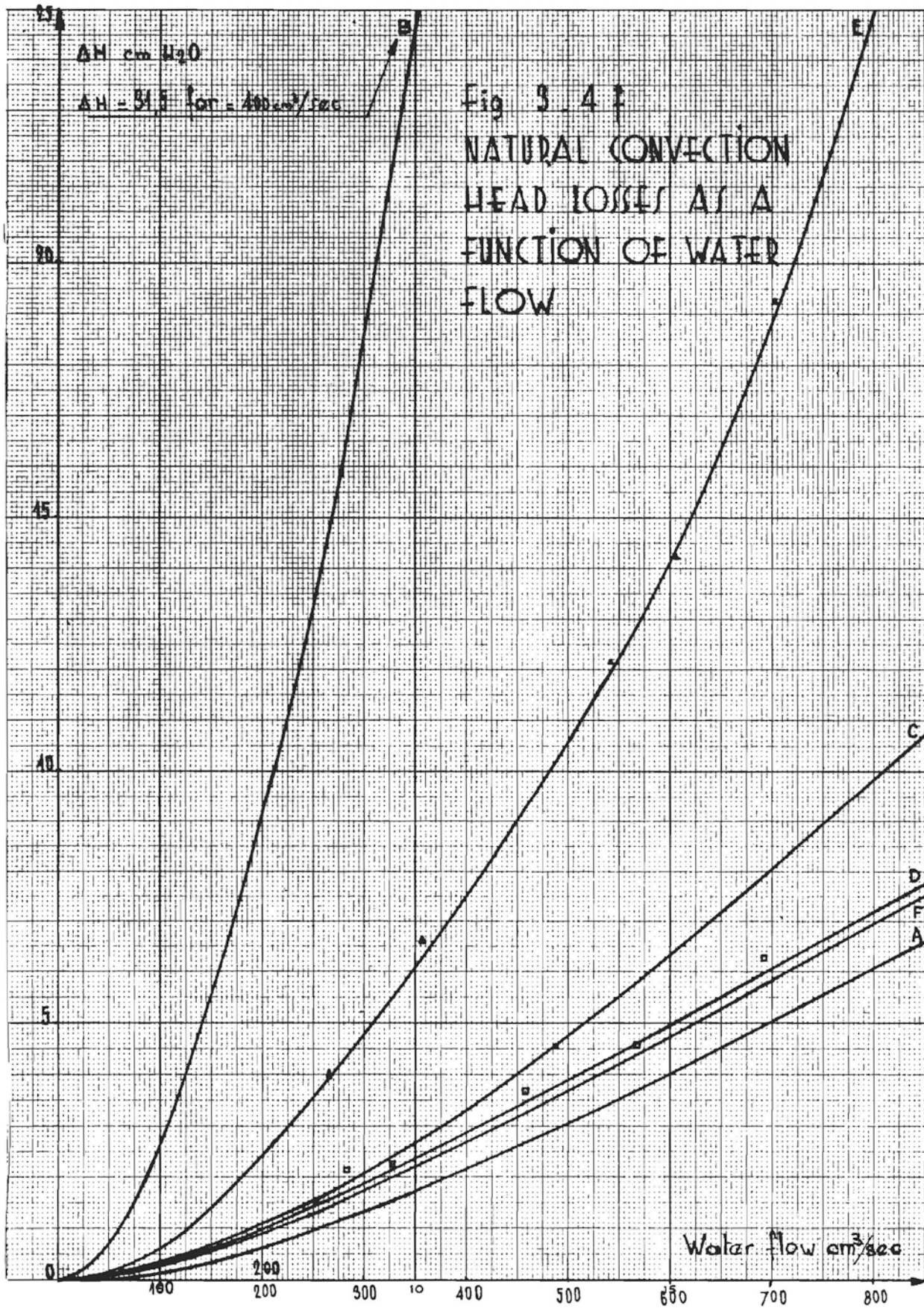
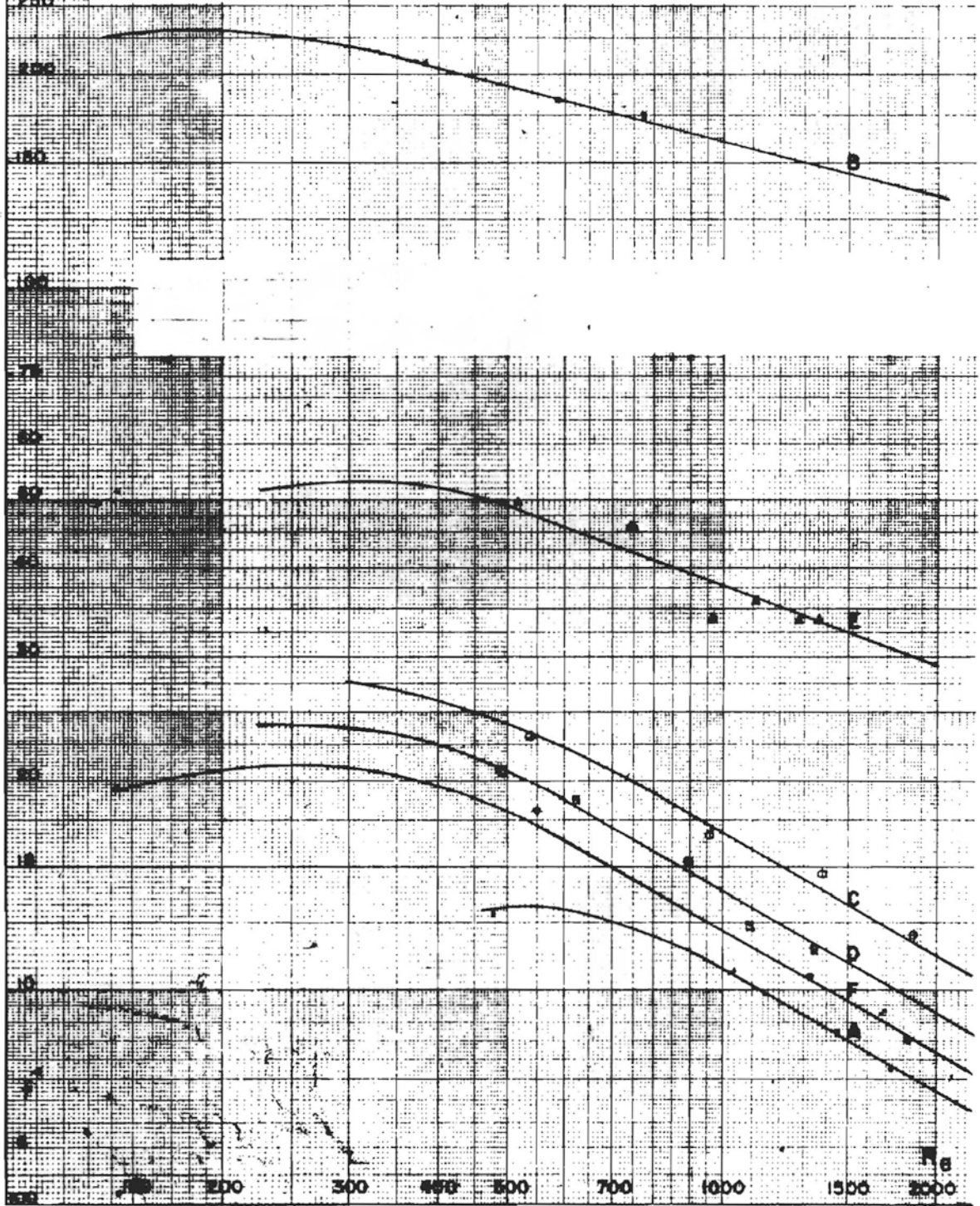


fig 3 4 g

NATURAL CONVECTION
HEAD LOSS FACTOR AS A FUNCTION
OF REYNOLDS NUMBER



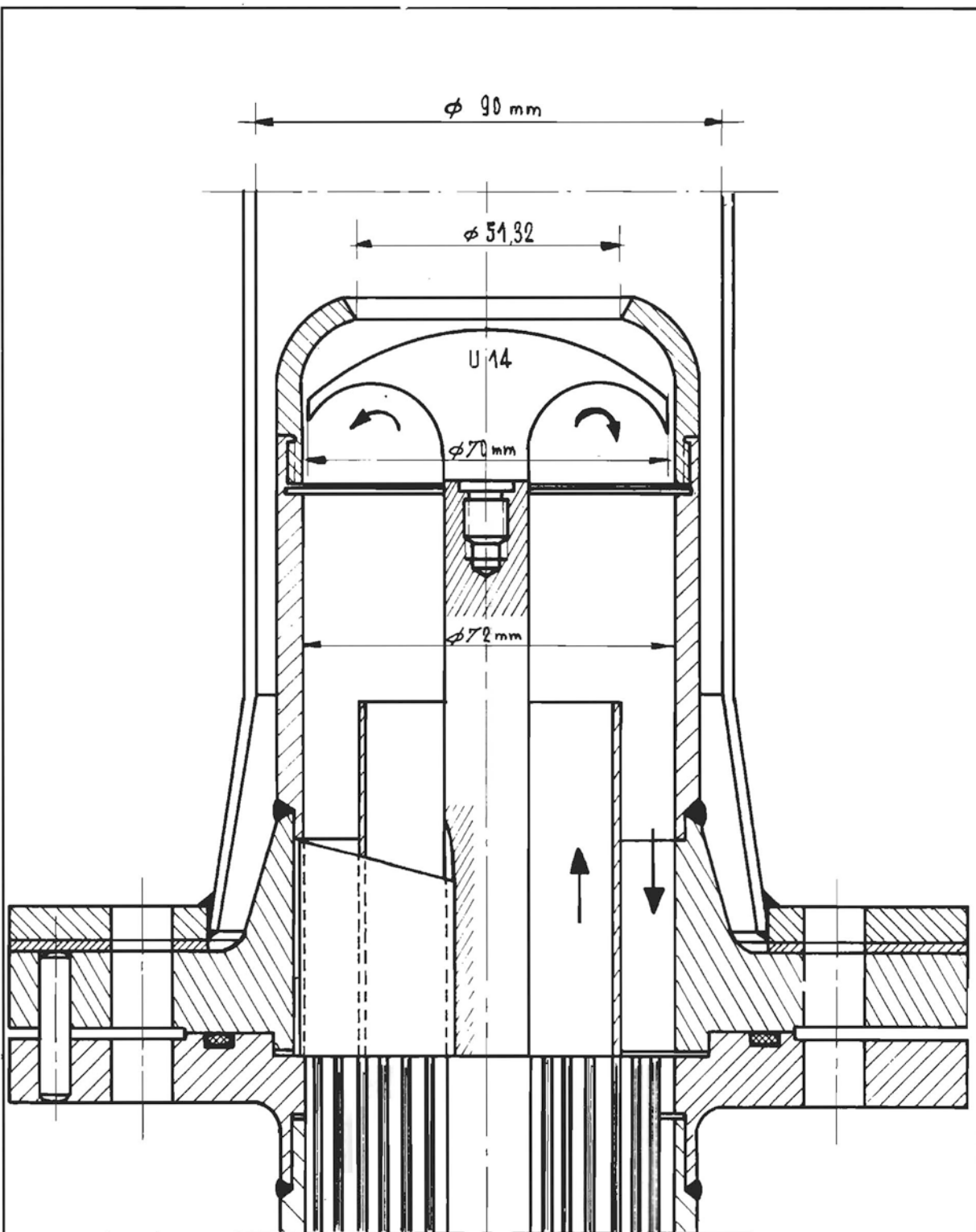


Fig 3 - 4 h

TAPPING TESTS TYPE B MUSHROOM HEAD $\phi 70 \text{ mm}$ AND CHIMNEY

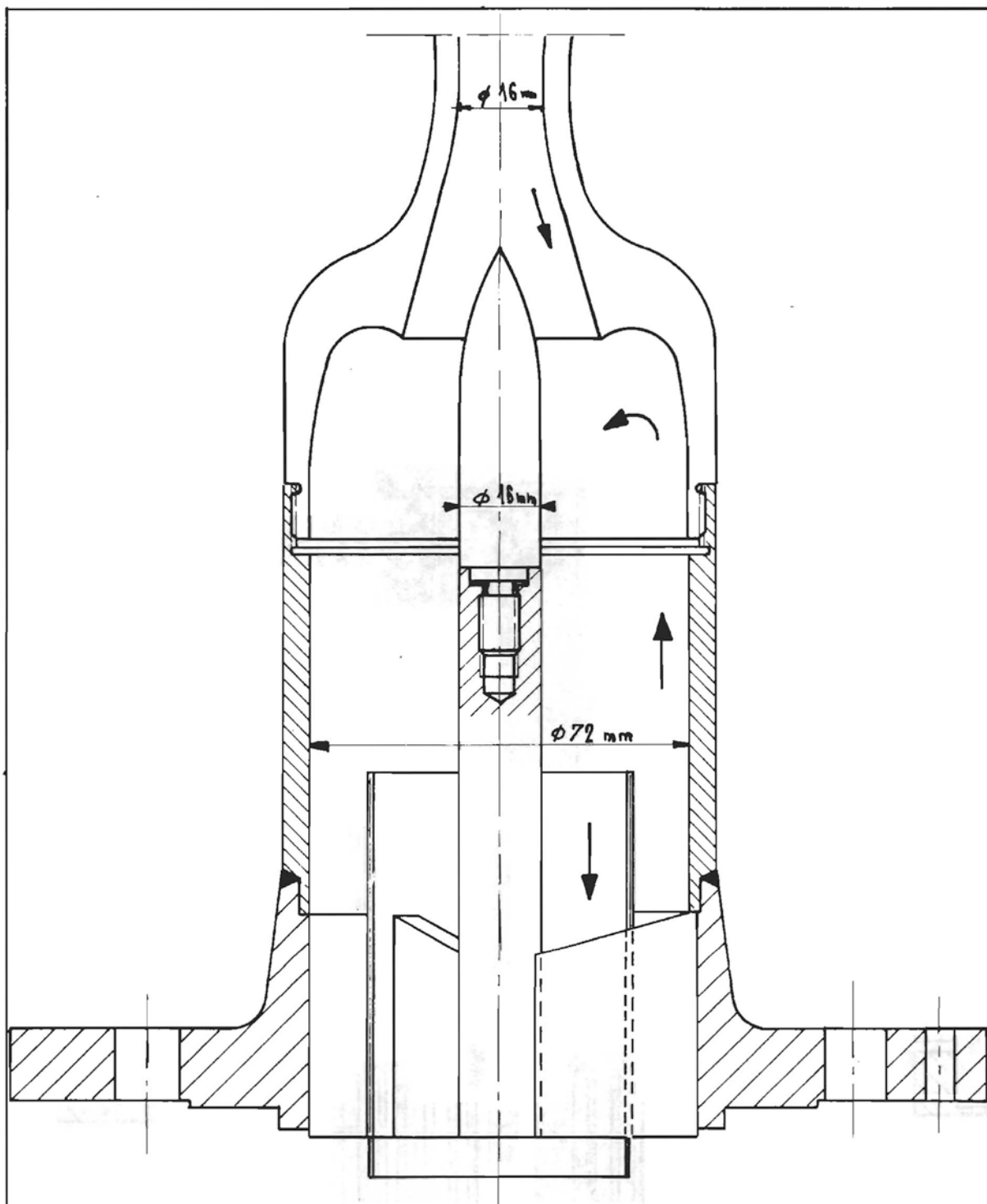
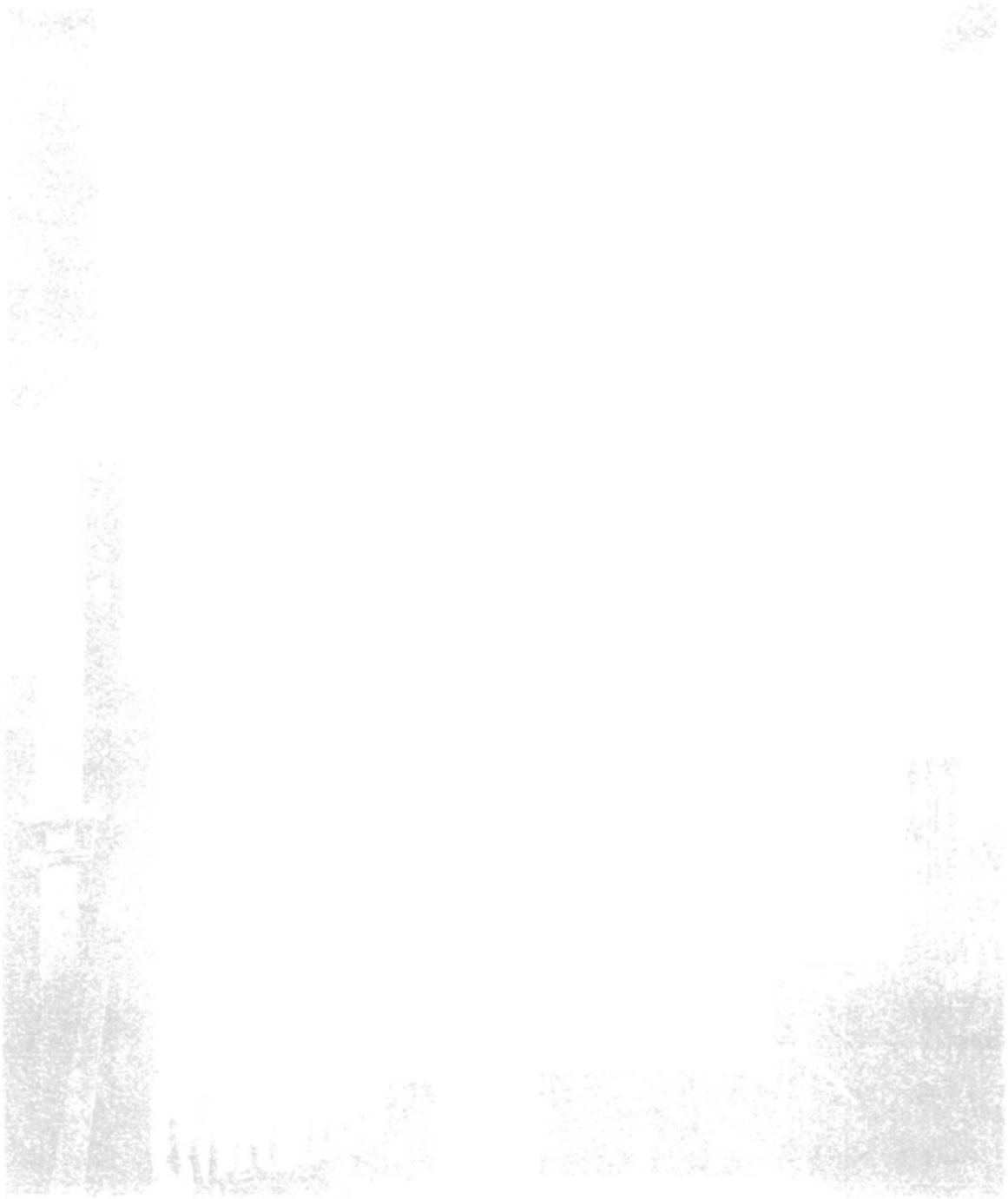
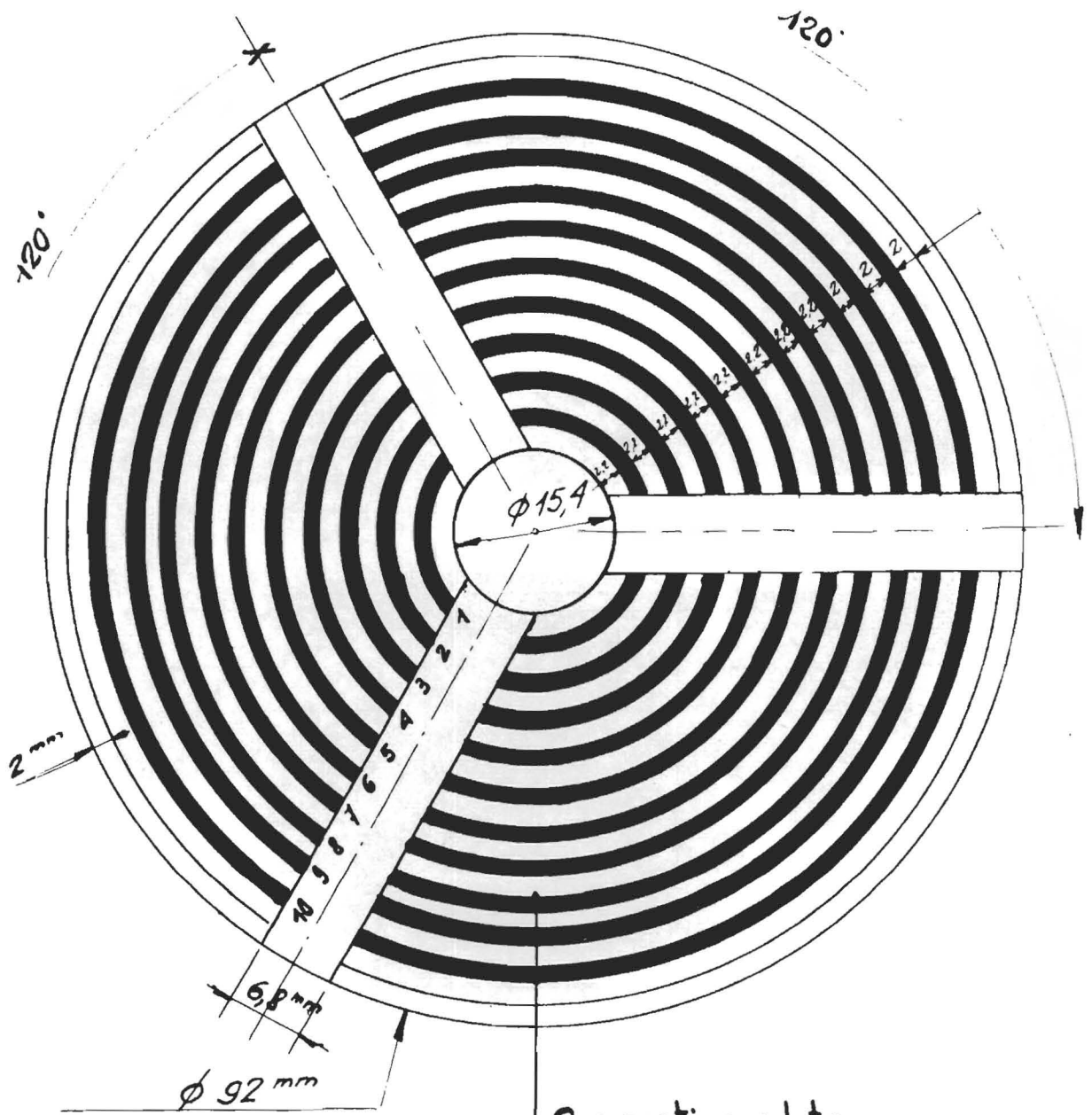


Fig 3.4 i
 TAPPING TESTS TYPE F (CONE HEAD AND VENTURI
 CHIMNEY)

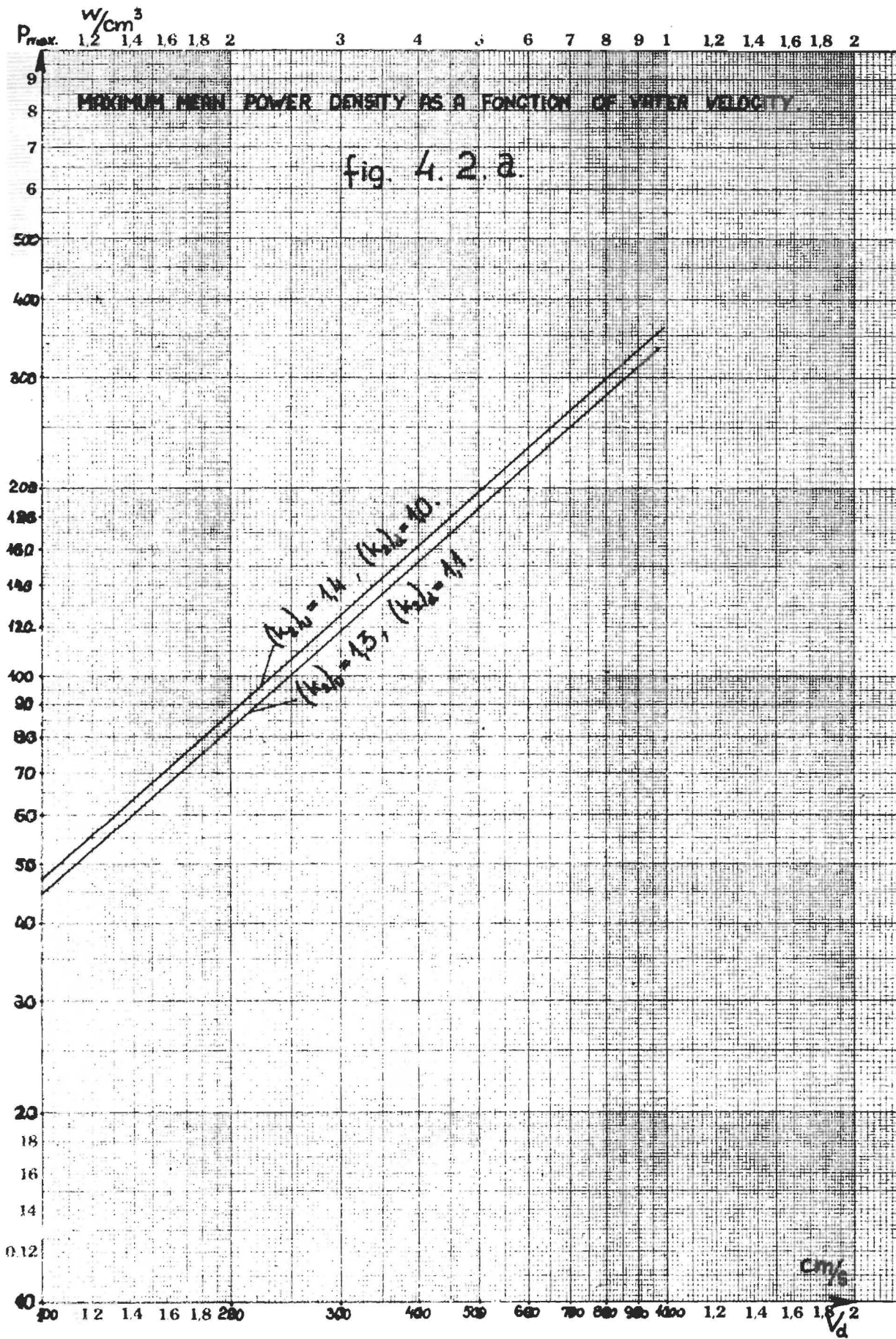


Bottle Type Element <10 Plates>

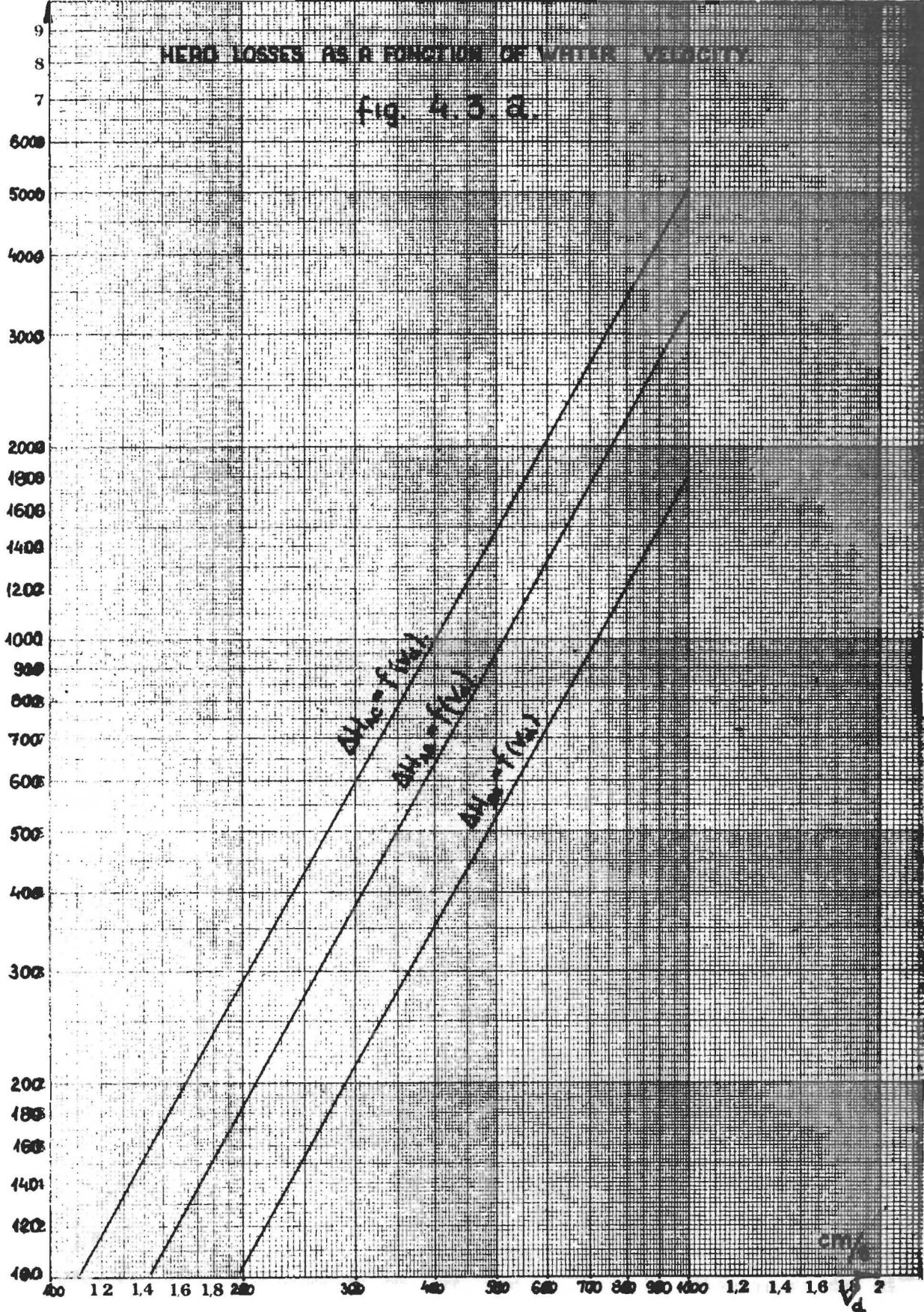


Horizontal Section

Separating plate
fuel plates : 1, 2, 3, 4, 5, 6, 7, 8, 9, 10.
Thickness $1,27 \text{ mm}$



ΔH_1 cm of water . 2 3 4 5 6 7 8 9 1 12 14 16 18 2



PROTOTYPE STUDIES OF MODIFIED FUEL ELEMENT GEOMETRIES*

By

W. C. Francis and M. L. Griebenow

Phillips Petroleum Company
Atomic Energy Division
Idaho Falls, Idaho

Prepared for presentation to the Research Reactor Fuel Element Conference to be held at Gatlinburg, Tennessee, September 17 through 19, 1962.

ABSTRACT

A logical sequence in any fuel element development program involves the testing of fuel materials, usually as samples in the reactor; the design and testing of geometries, usually in ex-reactor facilities; and the final combination of the most promising materials and an optimum geometry in a full scale reactor proof test. This paper is concerned with the geometry and proof test aspects which resolves primarily into a determination of the engineering properties of the fuel element. This requires a thorough study of the hydraulic and heat transfer characteristics of the fuel element so that an optimum design results.

At the MTR/EPR, the initial development work or the solution of some particular problem of design geometry may be determined in a single or double channel hydraulic facility. Such parameters as entrance effects, surface roughening, differences in channel widths and plenums have been studied.

Full scale mock-ups of the proposed design in hydraulic loops then provided pressure drop vs gpm (or velocity) curves, flow distribution, vibration

*Work done under contract to the U. S. Atomic Energy Commission

and life tests. In the pre-start-up for the ETR it was this test which illustrated most vividly the need for stronger fuel elements. It is now routine practice at the MTR/ETR to test a statistical sampling of MTR and ETR production fuel elements before accepting that particular shipment of elements. Tests to date have been based on 140% of normal reactor flow and are performed at temperatures of about 100°F. A high temperature hydraulic facility capable of 500°F operation is being designed to extend the range of these tests.

Static pressure tests of simulated fuel sections have been useful in determining the amount of elastic and plastic deflection to be expected due to lateral pressure differences in the reactor. The degree of restraint afforded by the side plates may also be evaluated in such a facility.

Most of the heat transfer work at the MTR as been preformed in a 200 KW electrically-heated single channel test section inserted in an out-of-pile hydraulic loop. Heat transfer coefficients, the inception of nucleate boiling and burnout have been determined on special geometries.

These procedures have been applied to artificially roughened fuel plates, a tubular MTR fuel element, a concentric rounded square fuel element, and a 32-plate MTR fuel element. This latter prototype combines a geometry capable of operating at higher power levels with a fuel composition readily adaptable to incorporation of burnable poisons and non-uniform fuel and poison distributions and tests the merit of a heat-treated and aged aluminum alloy for increased strength with less material.

I. Introduction

A fuel element development program logically resolves itself into two major endeavors: (1) a materials study which usually involves a broad compatibility study in the literature followed by a testing program, including irradiation, of a selected group of materials and (2) a geometry study involving a thorough paper study of hydraulic, stress, and heat transfer characteristics followed by adequate testing of mockups. Ultimately, of

course, an optimization of the two areas of investigation in the form of prototypic irradiations in an existing reactor but in which the conditions are scaled (usually upwards) towards the desired application.

In this paper we are concerning ourselves generally with the engineering aspects of fuel development and specifically in those areas of investigation being conducted by Phillips Petroleum Company at the National Reactor Testing Station.

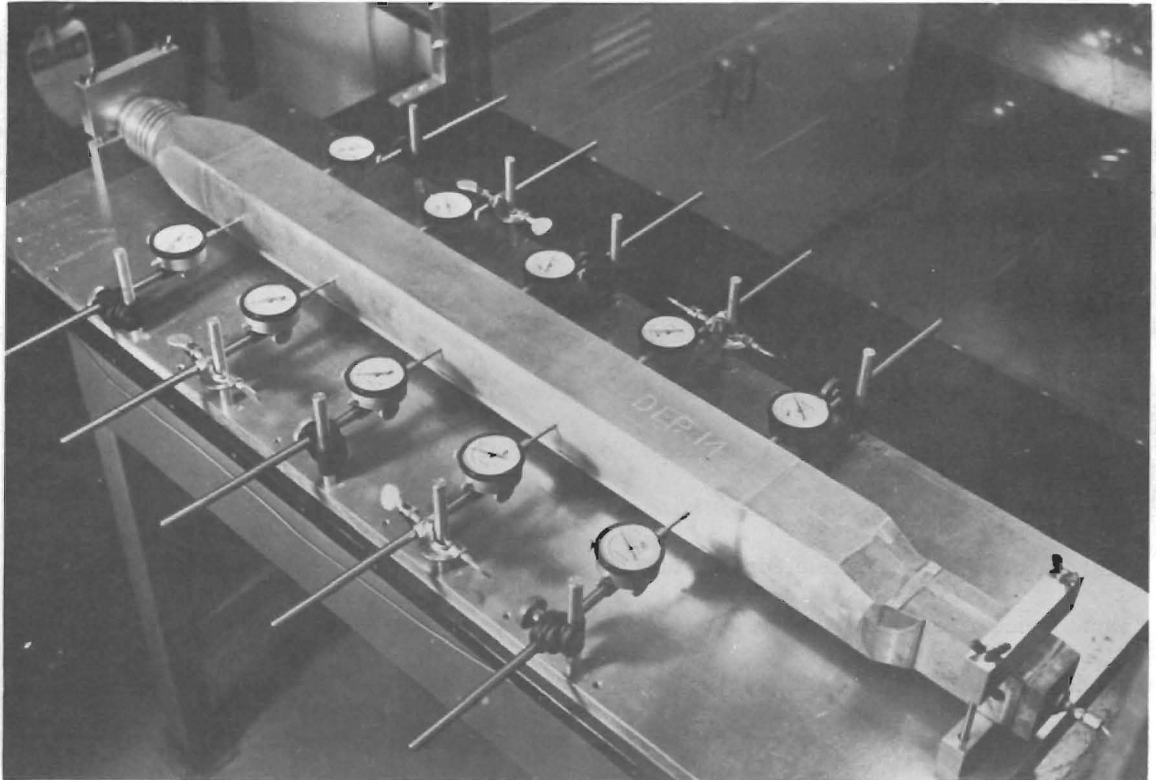
Since reactor power is limited by the maximum allowable fuel temperature it is advantageous to put as much coolant through the core as possible to reduce the fluid boundary layer to a minimum. To increase the heat transfer area without unduly increasing the metal/water ratio requires reducing the fuel plate thickness and thereby its strength. Increasing the coolant velocity to reduce the boundary layer, increases the lateral pressure differentials tending to collapse the fuel element. The trend therefore is toward stronger fuel plate materials, to the use of mechanical methods of strengthening the plates, or to relieving the forces tending to collapse them while promoting turbulence either through increased coolant velocities or by some mechanical method. The materials development and hydraulics-heat transfer relationships must be combined to optimize the heat removal, consistent with the best materials design. The approach we have chosen is to analyze separately the strength, hydraulics and heat transfer in out-of-pile experiments. The most promising concepts are then incorporated into a full scale prototype for out-of-pile testing followed by in-pile evaluation of the promising design.

II. Test Techniques

A. Static Pressure Tests

A simple technique for evaluating materials strengths under conditions simulating in-pile hydraulic forces but, of course, without the radiation damage, involves testing a fuel element, with plates containing either no fuel or with depleted fuel, by pressurizing it internally with a gas and measuring

the corresponding plate deflection. The test apparatus is shown in Figure #1. Although a deflection traverse would produce a more complete picture of the deflection, an accelerated test involves measuring the deflection at a limited number of points as shown in the figure. The test results include the combined effects of fuel and side plate deflection and fuel plate to side plate slippage.



**STATIC PRESSURE DEFLECTION MEASUREMENT RIG
THE APPARATUS FOR MEASURING DEFLECTION
OF FUEL PLATES WITH APPLIED PRESSURE**

Figure 1

There seems to be very little difference in the observed deflections for solid aluminum plates or for fueled plates of the same dimensions. Another interesting effect is that the deflection differs considerably down the length of the element and that the peak deflection tends to shift as the load is increased.

Deflection measurements have been taken for several of the fuel plate cladding materials. These deflection curves are shown in Figure # 2. The

plates were 0.080" x 4" x 24" solid aluminum. The advantage of the stronger plate material is obvious. The 6061-0 curve represents one of our first swaged joints, and the high deflections are probably the result of a poor joint between fuel plate and side plate. The empirical stress-strain equation based on early MTR work, shown in the figure, predicts a slope of 0.0023" deflection/psi. The values read from the curves range from 0.0015 to 0.0035. The increased deflection over the predicted value could be explained by increased side plate deflection, since the side plate thickness has been reduced from 0.187 to 0.150, or by slippage of the swaged joint. This is substantiated by the fact that the curve for the 0.250" side plate and a pinned joint had a 0.0015 slope.

Table I shows the measured yield points for the same plates compared to the value predicted by flat plate theory for all edges fixed. Here again, with the same exception, the yield is below the predicted value. The poorest correlation is for the 6061-0 plate.

While the recommended equations for predicting deflection and yield lack the refinement required to give precise results under complex reactor conditions, they have proven of considerable value in MTR and ETR work and clearly indicate the potential gain from the stronger aluminum alloys.

One of the difficulties encountered when using aluminum clad fuel plates is, of course, the low mechanical strength of aluminum at elevated temperatures. These properties can be improved by alloying additions. Another means of increasing the transverse stiffness of fuel plates is through the use of beads formed across the plate. Some of the variables to be considered in the design of these beads are the amplitude, spacing, and the shape to be used. It was believed to be desirable to have the amplitude no more than one-half the water channel thickness in the fuel elements so as to minimize the possibility of blocking the water channels. The shape chosen had to be such that there would be no danger of rupturing the core

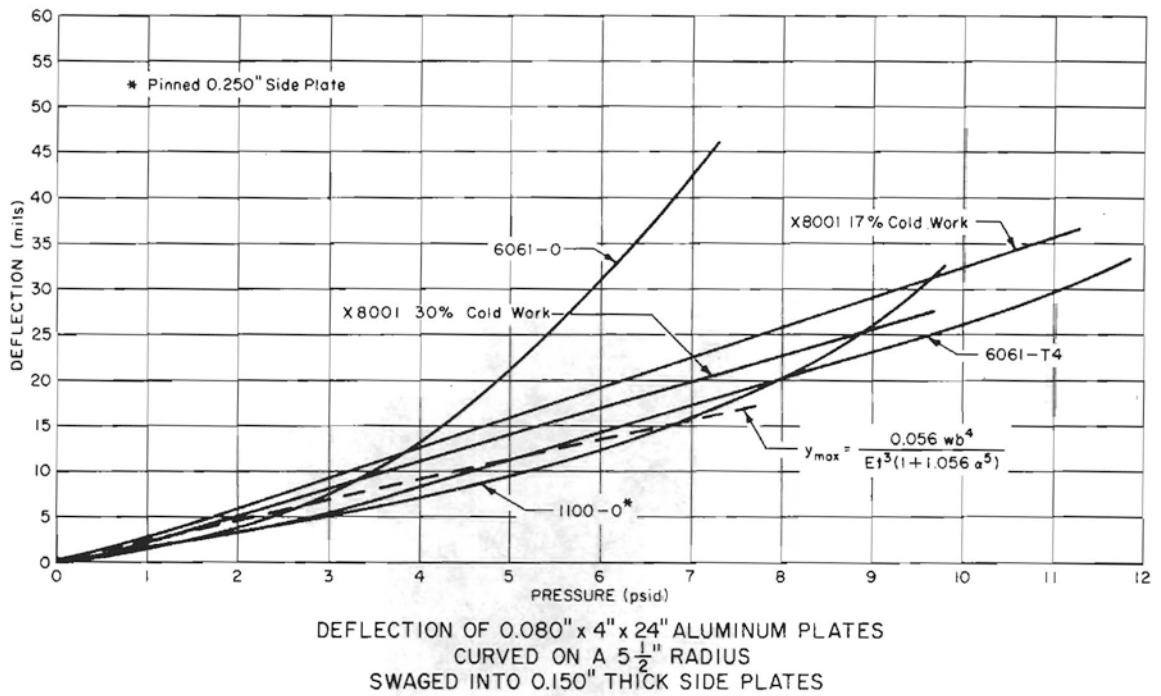


Figure 2

MEASURED vs COMPUTED PRESSURE DIFFERENCES TO CAUSE YIELDING
IN 0.080" x 4" x 24" PLATES CURVED ON 5 1/2" RADIUS

VALUES SHOWN IN THE TABLE ARE THOSE GAUGE PRESSURES APPLIED TO THE CONCAVE SIDE OF THE PLATE WHICH PRODUCE THE FIRST INDICATION OF PLASTIC STRAIN.

	COMPUTED LOAD - psi $w = \left[\frac{St^2 (1 + 0.623 a^6)}{0.5 b^2} \right]$	MEASURED LOAD - psi (AT ROOM TEMPERATURE)
1100-0	4.4	4.5
6061-0	7.1	2
X8001 17% COLD WORK	14.3	12
X8001 30% COLD WORK	17.0	14
6061-T4	18.6	10.5

Table I

or cladding during fabrication. Figure # 3 is a view of a typical bead in the MTR fuel plate showing the height and shape used.

The desired frequency with which the beads were spaced along the plate was determined to be a compromise between strength, resistance to fluid flow and the effects on heat transfer. It was desirable to achieve the maximum

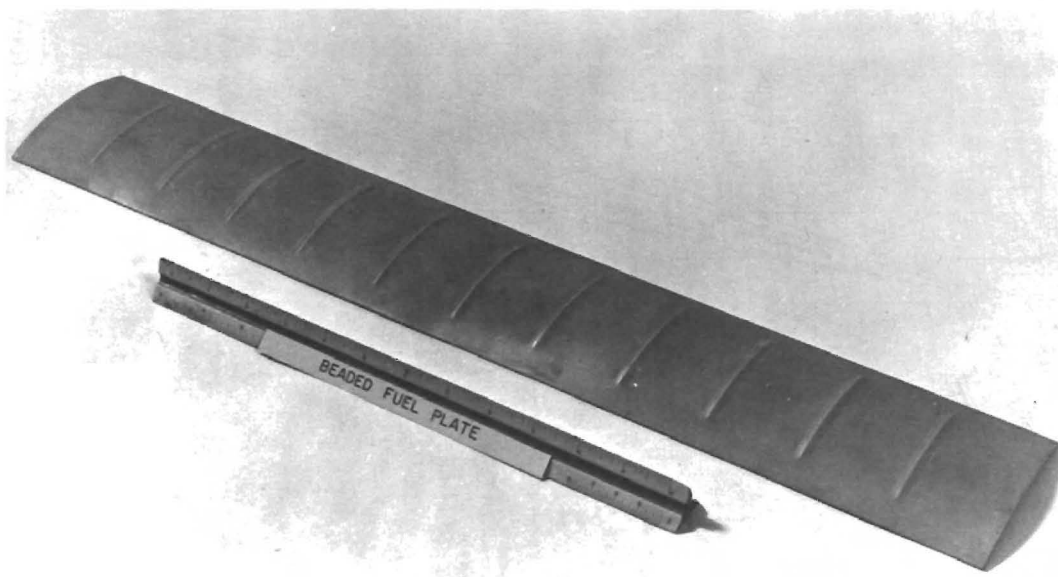


FIG. 3

strength with the minimum effect on the other factors. A spacing of 2" between beads gave good results as illustrated by the deflection data shown in Figure # 4. The plate used for this test was made from fully annealed 1100 aluminum.

B. Hydraulics

1. Single-Double Channel Assembly

The simplest method of measuring the hydraulics effect of the coolant on the fuel assembly is in a single or double channel test piece such as shown in Figure # 5. This test section is 3" wide by 37" long and can be assembled with either one or two channels the dimensions of which are maintained by brass spacers. Rapid measurement of entrance and exit effects,

lateral pressure differentials and the effects of turbulence promoters are obtainable on simulated fuel channels by use of such a test section in a hydraulic loop.

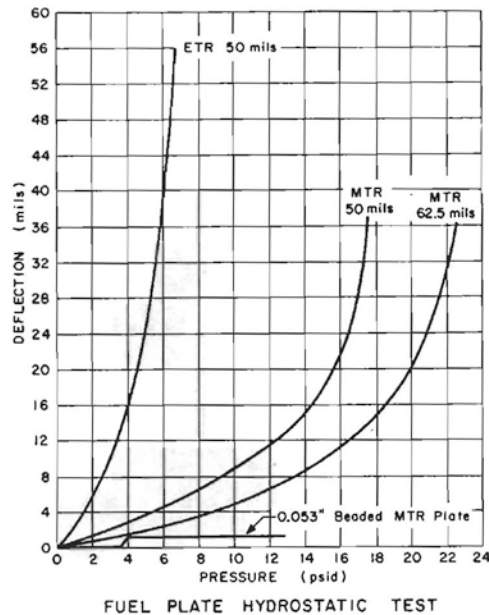
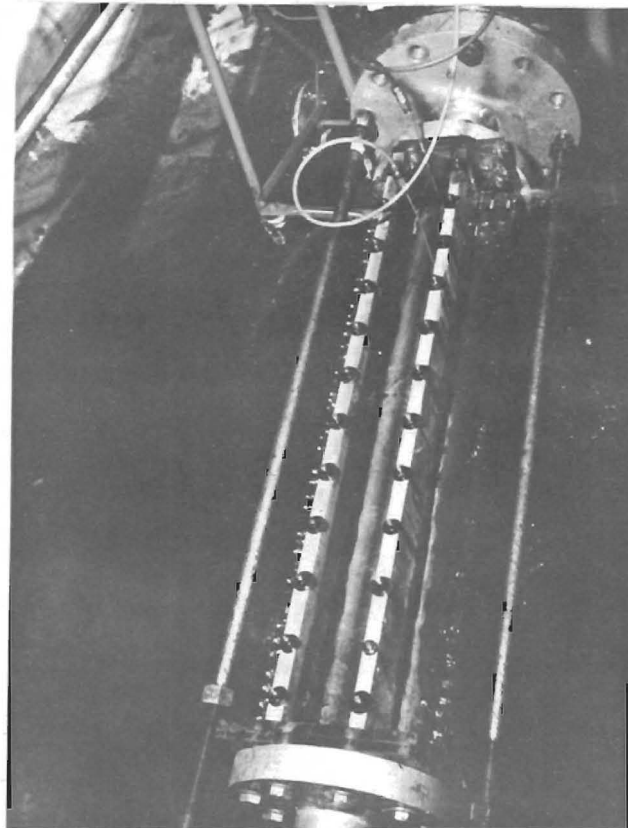
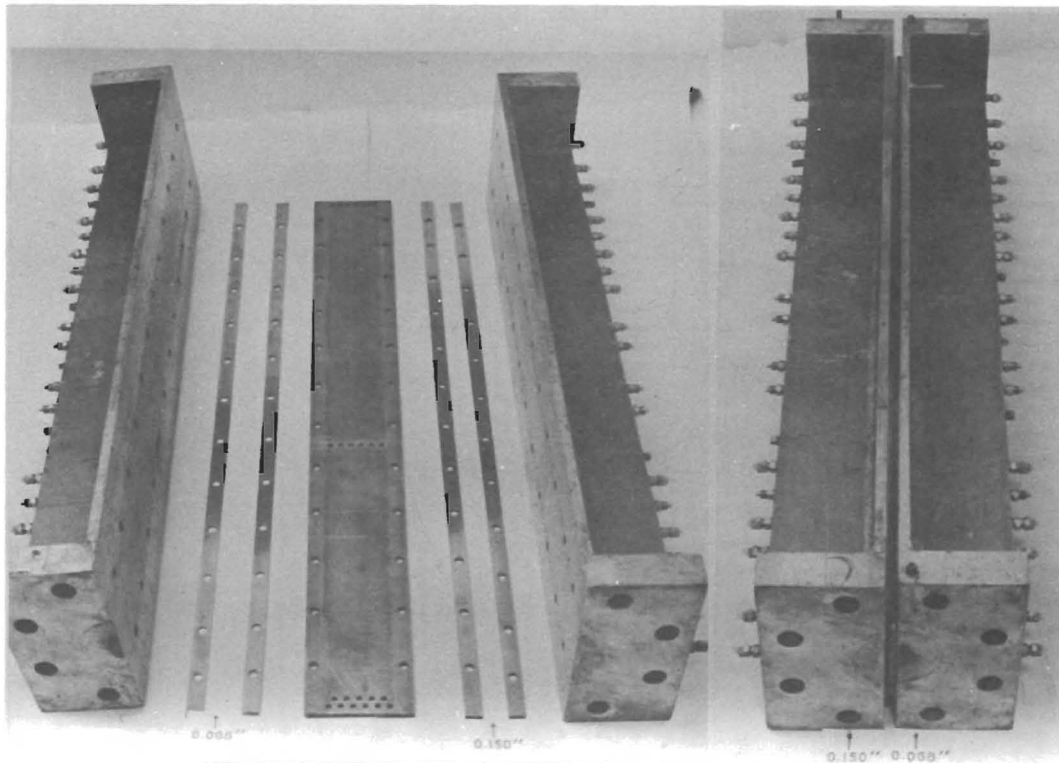


Figure 4

a. Entrance Effects

One of the first requirements in fuel element design is an evaluation of the forces tending to collapse the element. These forces are produced by channels of unequal size and therefore unequal hydraulic resistance. The larger the channel the lower the hydraulic resistance and the higher the subsequent coolant velocity. As the coolant velocity is thus increased, the static pressure in the channel decreases. Figure # 6 shows the measured pressure differential between unequal channels and compares these values with the results computed from standard friction factors and entrance-exit coefficients. In all cases the computed values are within 2.0 psi of the measured values with the maximum values agreeing to within less than 1.0 psi.

One method of reducing the lateral pressure gradients is to permit communication between channels by use of pressure-relieving passages



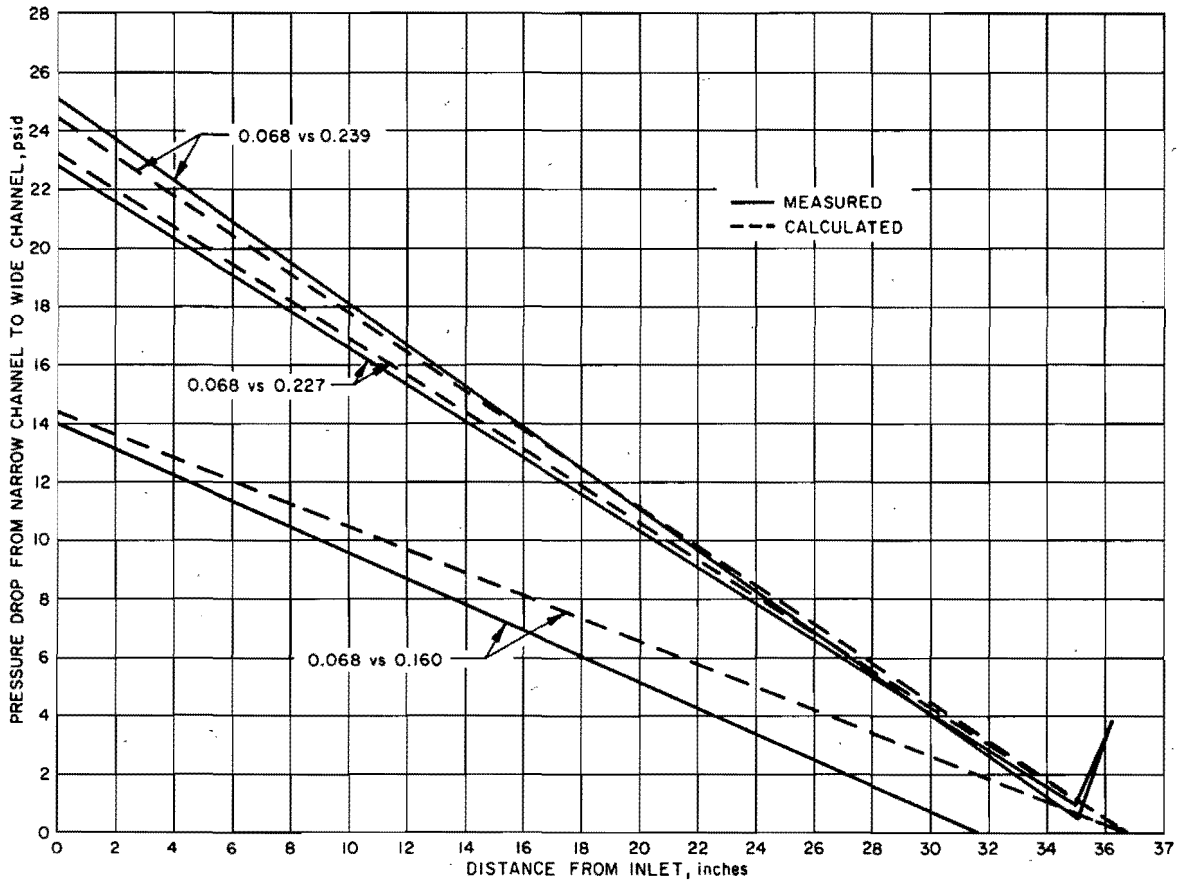
SINGLE CHANNEL TEST ASSEMBLY

Figure 5

either in the fuel plates or through the side plates. Probably the most logical location for these holes is in the fuel plate itself either above or below the fuel zone. Analysis shows no advantage for holes below the fuel zone, but a potential reduction of 20-30% is obtainable through holes above the fuel zone. The exact value is a function of the division of hydraulic resistance between expansion-contraction losses and frictional losses. Figure # 7 shows the results of several combinations of hole numbers and locations. Two to six 1/4" holes 3/8" below the leading edge of the plates reduced the lateral ΔP by 2-3 psi at any location. This amounts to better than 20% at the vertical centerline, where because of temperature effects, the plate is weakest. Additional holes tended to change the slope more toward the theoretical value but failed to reduce the magnitude.

b. Surface Roughening

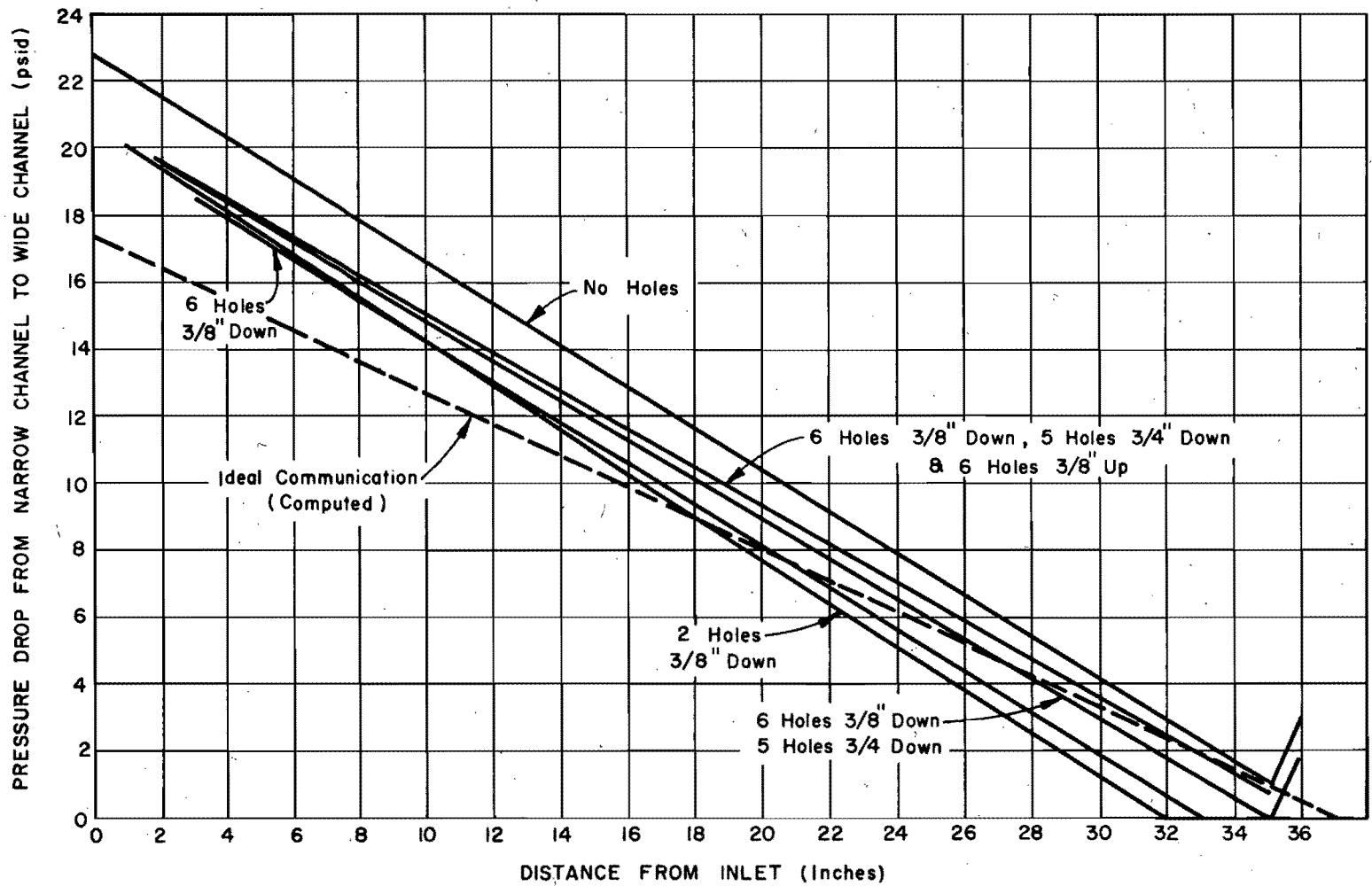
The method of reducing the laminar boundary layer in narrow channels without increasing the pumping rate and thereby the destructive forces is to roughen the cladding surface. Dummy fuel plates were knurled to varying degrees of roughness and tested in the single channel assembly to develop a technique to produce a given increase in turbulence as measured by the friction factor. A series of tests were run to check the measured roughness height against the increase of friction factor. The results as shown in Figure # 8 agree quite well with published tube values with the same roughness height to hydraulic diameter ratio. The effect of knurling the plates was optimized assuming the change in film coefficient to be proportional to the change in friction factor and allowing only the existing core pressure drop. The potential gain is shown in Table II. An additional gain may be obtained by allowing the entire primary ΔP to remain fixed as this would leave a higher loss in the element and result in higher coolant flow rates.



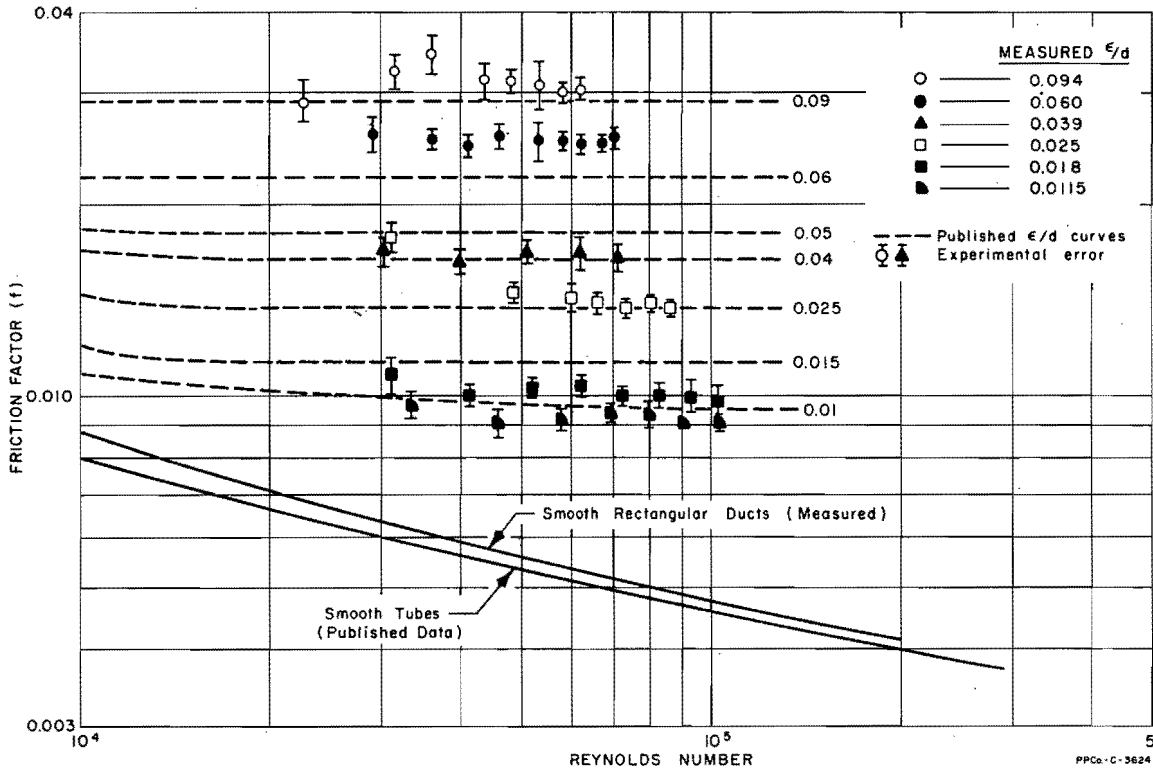
MEASURED vs CALCULATED
 PRESSURE DIFFERENTIAL BETWEEN UNEQUAL CHANNELS
 (3" x 37" x VARIABLE THICKNESS) AT 70 psi DIFFERENTIAL
 OVER LENGTH OF TEST SECTION

Figure 6

Figure 7



MEASURED PRESSURE DIFFERENTIAL FROM 0.068" CHANNEL TO 0.227 CHANNEL
 AS A FUNCTION OF QUANTITY AND LOCATION OF 1/4" HOLES AT
 70 psi. DIFFERENTIAL OVER LENGTH OF TEST SECTION
 (VELOCITY IN 0.068 CHANNEL = 38 ft/sec)



ROUGHENED PLATE FRICTION FACTOR DATA

Figure 8

Table II

ROUGHENED FUEL PLATE OPTIMIZATION

	<u>MTR</u>	<u>ETR</u>
1. HOT ELEMENT POWER Mw/L	0.832	1.087
2. METAL/WATER RATIO	0.6362	0.6655
3. NUMBER OF PLATES	19	19
4. POTENTIAL INCREASE IN POWER AT SAME METAL/WATER RATIO TO,		
(a) YIELD EXISTING HOT ELEMENT NOMINAL WALL TEMPERATURE.	81% ($\epsilon/D=0.060$)	20% ($\epsilon/D=0.015$)
(b) YIELD EXISTING HOT SPOT-HOT CHANNEL WALL TEMPERATURE	86% ($\epsilon/D=0.060$)	33% ($\epsilon/D=0.028$)
5. POTENTIAL REDUCTION IN PUMPING RATE AT SAME METAL/WATER RATIO TO,		
(a) YIELD EXISTING HOT ELEMENT NOMINAL WALL TEMPERATURE.	66% ($\epsilon/D=0.060$)	34% ($\epsilon/D=0.015$)
(b) YIELD EXISTING HOT SPOT-HOT CHANNEL WALL TEMPERATURE.	68% ($\epsilon/D=0.060$)	47% ($\epsilon/D=0.028$)

outer channels. The total coolant flow through the element was also reduced, but it was compensated for by the increased heat transfer area. As the number of fuel plates is increased, while holding the metal/water ratio constant, the calculated wall temperature decreases.

Recent advancements in aluminum research and development have produced techniques for manufacturing high strength fuel plates. These techniques coupled with the more advanced high density fuels technology have made it possible to reduce the required fuel plate thickness thus producing fuel elements with higher thermal efficiencies, i.e., fuel elements that operate cooler and/or require less coolant at reactor power.

The MTR fuel element configuration has been optimized consistent with present technology, and two elements have been purchased for reactor use. These elements have 32-0.030" 6061-T6 clad fuel plates, separated by 0.068" water channels and contain a total of 250 grams U²³⁵.

To permit testing these elements in reactor positions adjacent to standard MTR elements without increasing the lateral ΔP across the standard element external plate, the 32 plate elements have been constructed with a standard external channel (nominal 0.116" between elements).

The elements were hydraulically tested to 140% of reactor flow at 100°F (flow at 40 psi across the elements) and withstood the hydraulic forces produced by the unequal channels (there was actually a 0.0655" internal channel adjacent to the 0.120" external channel). The hydraulic tests showed the average internal channel velocity to be 26.1 ft/sec with a variation of + 6% - 12%.

This element provides a 68% increase in heat transfer area (for the same metal/water ratio) and has the capability of a 46% increase in power or a 44% reduction in pumping rate (gpm) while maintaining the same maximum surface temperature. (See Table III)

Safeguards and AEC approval have been received to test the elements in the MTR.

C. Concentric Rounded Square Fuel Element

A concentric rounded square fuel element has also been designed. This fuel element consists of nine concentric square tubes with the corners rounded off and one cylindrical tube in the center. A "dummy" fuel element of this design, made of mild steel, has been tested in the hydraulic facility. Although a detailed analysis has not been made, a preliminary investigation of the data indicates that with a given ΔP across the fuel element, the total flow for the element is larger than for a standard ETR fuel element. The data indicate that the minimum velocity in any channel is approximately 30 ft/sec and in addition, the flow distribution across the fuel element appears to be relatively uniform.

It is anticipated that a detailed analysis will indicate the desirability of obtaining fully-fueled and operational prototypes to complete the testing.

D. Hydraulic Acceptance Tests on Production Elements

It is current practice to hydraulically test a sample of all production MTR and ETR fuel elements and specifications for the tests and sampling plan are incorporated in MTR and ETR fuel contracts. The test consists of subjecting an element to 140% of normal reactor flow for periods up to 6 hrs at 90-120°F. (normally about 10 minutes is adequate to produce a failure in a sub-standard element) The sampling plan consists of 100% testing of the first 25 units produced. If these pass the test, up to 20% of the remaining assemblies to be delivered are randomly selected from each lot of 10 assemblies and tested. If a single failure occurs, the 100% inspection is resumed and may be extended to previously accepted but untested assemblies. Evidence of failure is taken as a change in thickness of a coolant channel of 0.010 inch or more, plate distortion, or changes in dimension across side plates. In recent periods, no failures have occurred in the 600 ETR elements received (of which 116 were hydraulically tested). 64 of 325 MTR elements failed (of 264 tested) but most of these occurred in one period of consecutive production, caused

Table III

FUEL PLATE OPTIMIZATION

	MTR	ETR
1. HOT ELEMENT POWER – MEGAWATTS/LITER	0.832	1.087
2. METAL – TO – WATER RATIO	0.6362	0.6655
3. NUMBER OF PLATES (STANDARD)	19	19
4. POTENTIAL INCREASE IN POWER AT SAME METAL – TO – WATER RATIO TO		
a. Yield Existing Hot Element Nominal Wall Temperature With Optimum Practical Number Of Smooth Plates	(32 Plates) 46%	(28 Plates) 16%
b. Yield Existing Hot Spot – Hot Channel Wall Temperature With Optimum Practical Number Of Plates	(32 Plates) 47%	(30 Plates) 25%
5. POTENTIAL REDUCTION IN PUMPING RATE AT SAME METAL – TO – WATER RATIO TO		
a. Yield Existing Hot Element Nominal Wall Temperature With Optimum Practical Number Of Plates	(32 Plates) 44%	(28 Plates) 21%
b. Yield Existing Hot Spot – Hot Channel Wall Temperature With Optimum Practical Number Of Plates	(32 Plates) 44%	(30 Plates) 30%

by the same defect. All of the latter elements appeared acceptable by all other inspections.

The 140% flow figure used in these acceptance tests has been somewhat arbitrarily set (but supported by considerable experience) to compensate for the higher temperature and the neutron effects encountered in the reactor. Because the ATR will extend even further the operating temperature of the fuel elements, a hydraulic facility capable of testing at elevated temperature and pressure is required. Such a facility is currently in design stages by the Architect-Engineer and is expected to be operational by next summer. This loop will be capable of circulating 1000 gpm of 500°F water through a test section with a pressure differential of about 200 psi. A comparison of the loop capabilities with the present MTR/ETR loop characteristics is shown in Table IV. Normal MTR, ETR and ATR fuel element operation is also shown in Table IV. An interesting feature of the new facility will be the control of flow by means of the pressure difference across the test section. It is believed that this procedure comes very close to simulating the true reactor condition of essentially constant core ΔP .

E. Heat Transfer

An essential parameter in any reactor fuel design is of course the heat transfer capability. In the test reactor the heat removal from fuel experiments is equally important. For development work a heat transfer test facility is available at the NRTS as shown in Figure 10. This loop consists of a 200 KW electrically heated test section paralleled by an "infinite" bypass. The loop is capable of testing simulated single MTR or ETR fuel channels with up to 45 ft/sec coolant velocity. Because of the limited power supply, only a portion of the test section length can be heated to the high heat fluxes desired. Figure # 11 illustrates a typical ETR test piece. The flow channel is a full 3' long but only the central 6" is heated. The heated section has 0.008" thick walls, and is relieved on the corners to reduce the flux. This and similar test sections have been employed to measure the

Table IV

HYDRAULIC LOOP CHARACTERISTICS

LOOP	TEST HANDLING CAPABILITIES	DIRECTION OF FLOW THROUGH TEST SECTION	MAXIMUM OPERATING TEMPERATURE (°F)	MAXIMUM OPERATING PRESSURE (psi)	MAXIMUM FLOW (gpm)	MAXIMUM PRESSURE DIFFERENTIAL ACROSS TEST SECTION (psi)
MTR/ETR	SINGLE CHANNEL TO ETR FUEL ELEMENT	HORIZONTAL	160	220	1000	90
ATR	SINGLE CHANNEL TO ATR FUEL ELEMENT	VERTICAL	500	1000	1200	200

FUEL ELEMENT OPERATING CONDITIONS

FUEL ELEMENT	FUEL PLATE LENGTH (inches)	FLOW THROUGH ELEMENT (gpm)	FLOW VELOCITY (ft./sec.)	PRESSURE DIFFERENTIAL ACROSS ELEMENT (psi)	MAXIMUM WALL TEMPERATURE (°F)
MTR	25 $\frac{1}{8}$	650	33	40	330
ETR	37 $\frac{1}{4}$	550	32	43	400
ATR	49 $\frac{1}{2}$	650	44	92	420



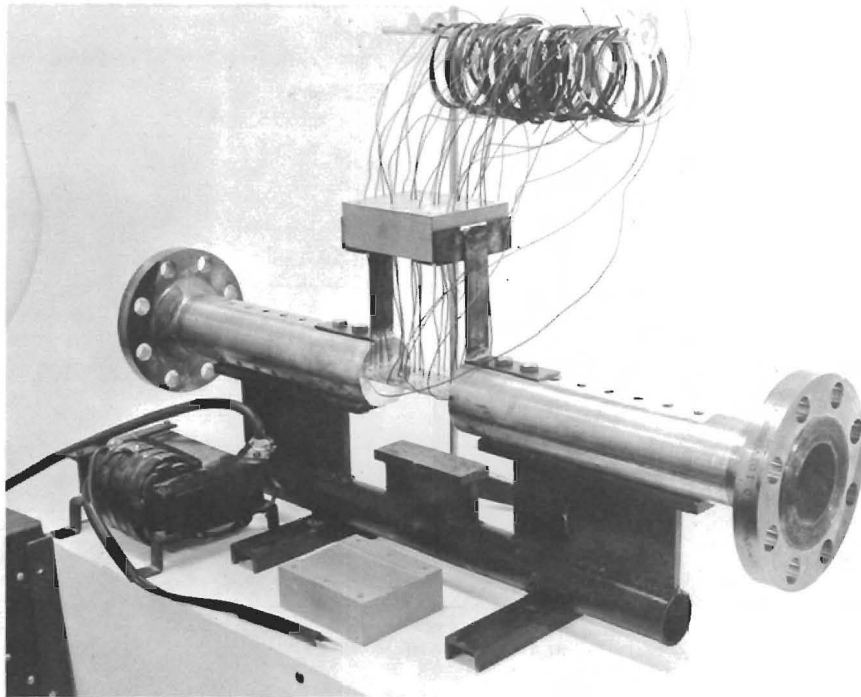
HEAT TRANSFER TEST FACILITY

Figure 10

fuel temperature that could be expected in the reactor as the power is increased. Nucleate boiling and burnout data are also an important part of this test work. The bulk water temperature at the outlet of the heated portion was maintained at the value that would be encountered at the channel hot spot for the particular reactor power. Figure # 12 shows the results of these tests and compares the observed data with the Dittus-Boelter and the Modified Colburn equation. While both equations yield coefficients that are optimistic the resulting temperature error is relatively small and is well within the 20% tolerance usually allowed.

The nucleate boiling data to date has been quite limited but it appears that the temperatures predicted by the Jens and Lottes correlation will be close once this heat transfer mechanism is fully developed.

To test the assumed relationship between friction factor and film coefficient used in optimizing the roughened MTR and ETR elements, a heat



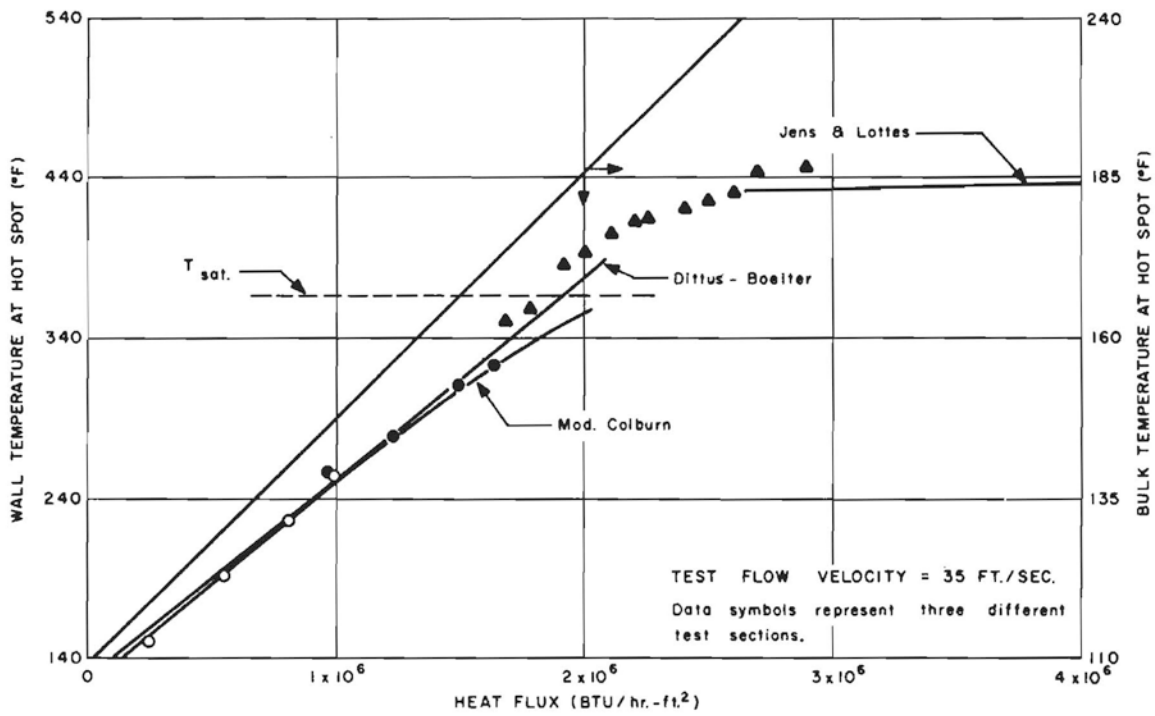
HEAT TRANSFER TEST SECTION

Figure 11

transfer test assembly was fabricated with the degree of roughness recommended for the MTR. The results are shown in Figure 13. The data agree quite well with the values predicted by assuming that the film heat transfer coefficient was directly proportional to the friction factor.

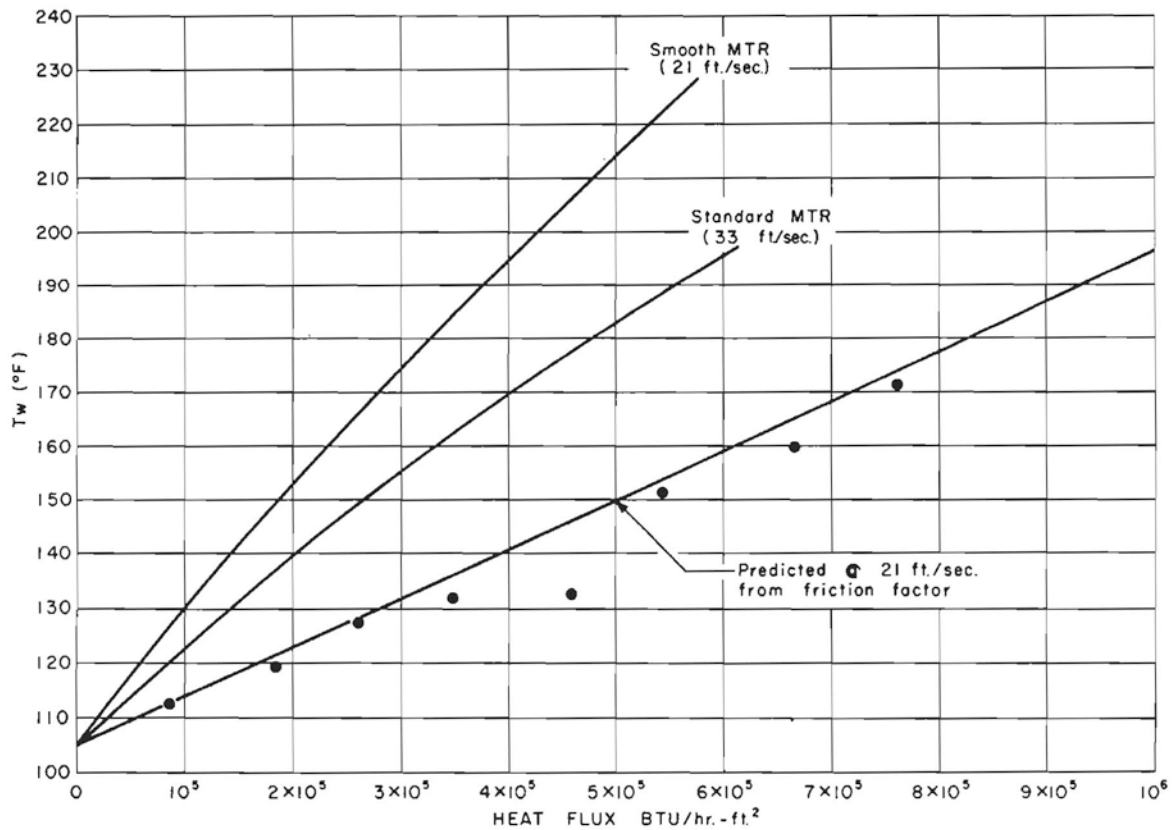
V. Conclusions

In summary, we believe that optimization of fuel plate strength, channel spacing, number of fuel plates and surface roughening offers considerable potential for increasing power density, reduction in pumping requirements or greater safety of operation. Heat transfer calculations and hydraulic tests on a 32-plate MTR element show that increases of 46% in power or 44% reduction in pumping rate are possible with this design. This is, of course, only one example of optimized geometries.



HEAT TRANSFER TEST RESULTS ON SIMULATED ETR FUEL ELEMENT

Figure 12



HEAT TRANSFER DATA ON OPTIMIZED MTR ROUGHENED CHANNEL

Figure 13

VI. Future Work

Future effort in Fuel development at Phillips will place more emphasis on materials development both in fabrication and in radiation testing. However, a limited effort will continue on prototype testing of interesting geometries in the MTR and ETR and in heat transfer and hydraulic studies on roughened fuel surfaces. A whole new correlation for acceptance testing will be developed based on high temperature hydraulic tests.

FABRICATION DEVELOPMENT OF THE INVOLUTE-SHAPED HIGH FLUX ISOTOPE REACTOR FUEL PLATES

M. M. Martin, J. H. Erwin, and C. F. Leitten, Jr.*

Abstract

The 100-Mw High Flux Isotope Reactor (HFIR) being designed and constructed at the Oak Ridge National Laboratory (ORNL) will utilize type 6061 aluminum-clad involute-shaped fuel plates containing a radial fuel gradient. This paper is concerned with the fabrication development of the plates utilized in the first critical-test elements as well as the dimensional and fuel homogeneity problems imposed by radially grading the uranium concentration. Since the inner-annulus plate contained a burnable poison, a dispersion type fuel consisting of 26 wt % U_3O_8 and 0.07 wt % B_4C in aluminum was selected for the fuel-bearing portion of the plate. A 24 wt % U-Al alloy was utilized in the outer-annulus plate. Various methods for forming the involute-plate contour to the tight tolerances dictated by the element design are evaluated and several factors that effect the duplication of the plate curvature are reported.

Introduction

The development of high-strength, corrosion-resistant, aluminum fuel plates has been under way for application in the High Flux Isotope Reactor (HFIR). This reactor, which is presently under construction at the Oak Ridge National Laboratory (ORNL), will operate with elevated central fuel temperatures of 400 to 475°F, at high neutron fluxes (approximately 5×10^{15} neutrons $cm^{-2} sec^{-1}$), and with average heat fluxes of approximately 0.8×10^6 Btu/hr-ft².

The reference design of the HFIR fuel assembly is shown in Fig. 1. The array consists of two cylindrical elements: an inner-annulus element

*Oak Ridge National Laboratory, Oak Ridge, Tennessee.

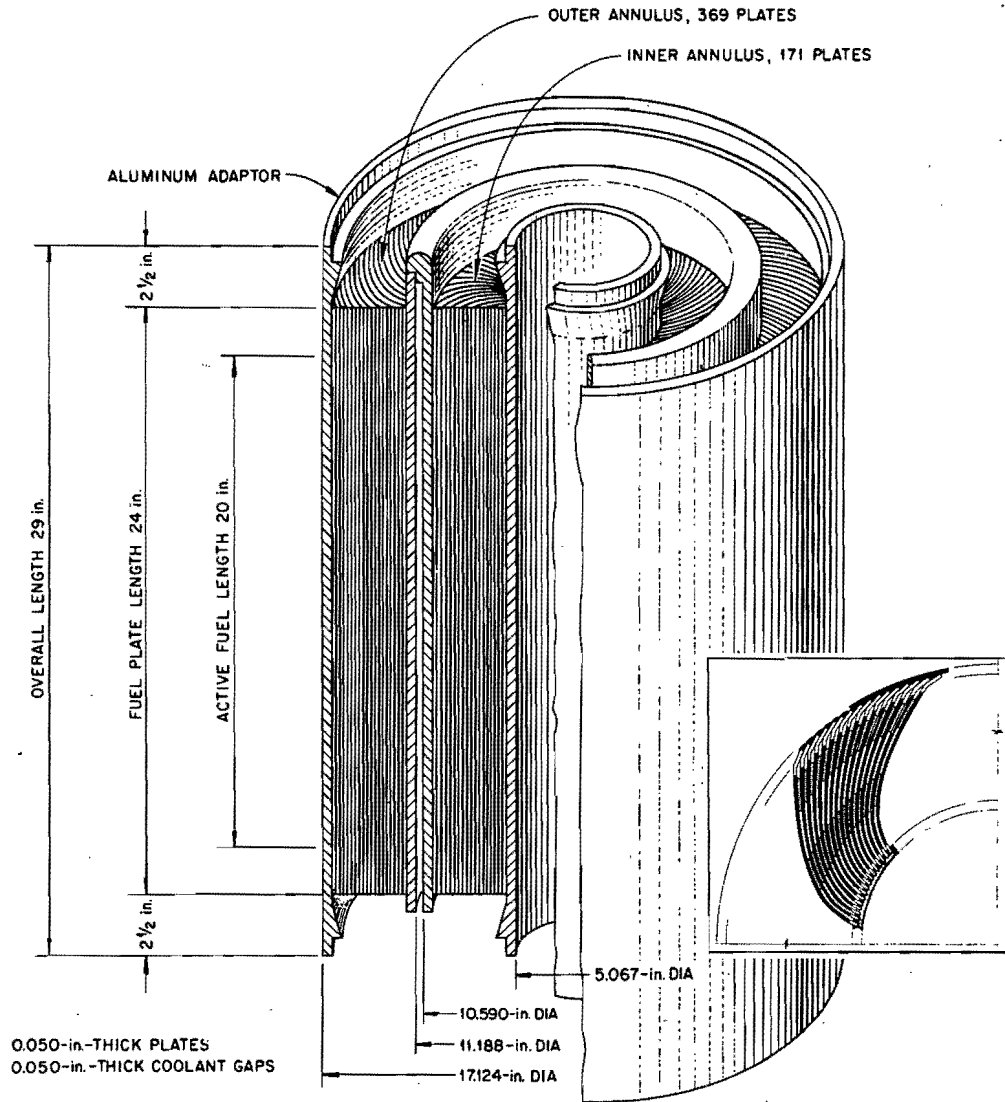


Fig. 1. Dimensional Illustration of the Assembled High Flux Isotope Reactor Fuel Element.

containing 171 involute-shaped plates and an outer-annulus element containing 369 plates. It is the purpose of this paper to describe the fabricational development of these plates and, in particular, the fuel plates utilized in the first critical-test elements. Procedures developed for assembling these elements are described elsewhere in this report.¹

A unique feature of the HFIR fuel plates is the incorporation of radial fuel gradients, as illustrated in Fig. 2, to achieve a uniform radial power distribution in the elements. Incorporating this radial fuel gradient and the subsequent roll cladding of the fuel with type 6061 aluminum imposed several fabrication problems. Of prime concern were the reproducibility of the gradient, the resulting fuel distribution in the plate, and the bonding characteristics of the type 6061-0 aluminum. In addition, the compactness of the fuel array and the rigid water-coolant spacing tolerance of 50 ± 0.006 in. have dictated rigid control of the involute curvature.

Fuel Plate Specifications

The reference design specifications for the inner- and outer-annulus fuel plates utilized in the first critical-test elements are shown in Table 1. The overall plate length of 24 in. and thickness of 0.050 in. are identical for both types of plate. A minimum clad thickness of 0.010 in. is specified in both plates which, therefore, permits a maximum core thickness of 0.030 in. in the plates. As previously shown in Fig. 2, the fuel is radially distributed in the inner plate varying from a thickness of 0.009 in. at the narrow edge to a maximum thickness of 0.028 in. Correspondingly, the fuel in the outer-annulus plate is distributed from a minimum thickness of 0.015 in. to a maximum of 0.028 in.

As previously indicated, the fuel plates are formed into an involute curvature since the design requires uniform water-channel spacings of 0.050 ± 0.006 in. To meet this rigid tolerance, it was tentatively established that the involute curvature must be reproduced within ± 0.004 in.

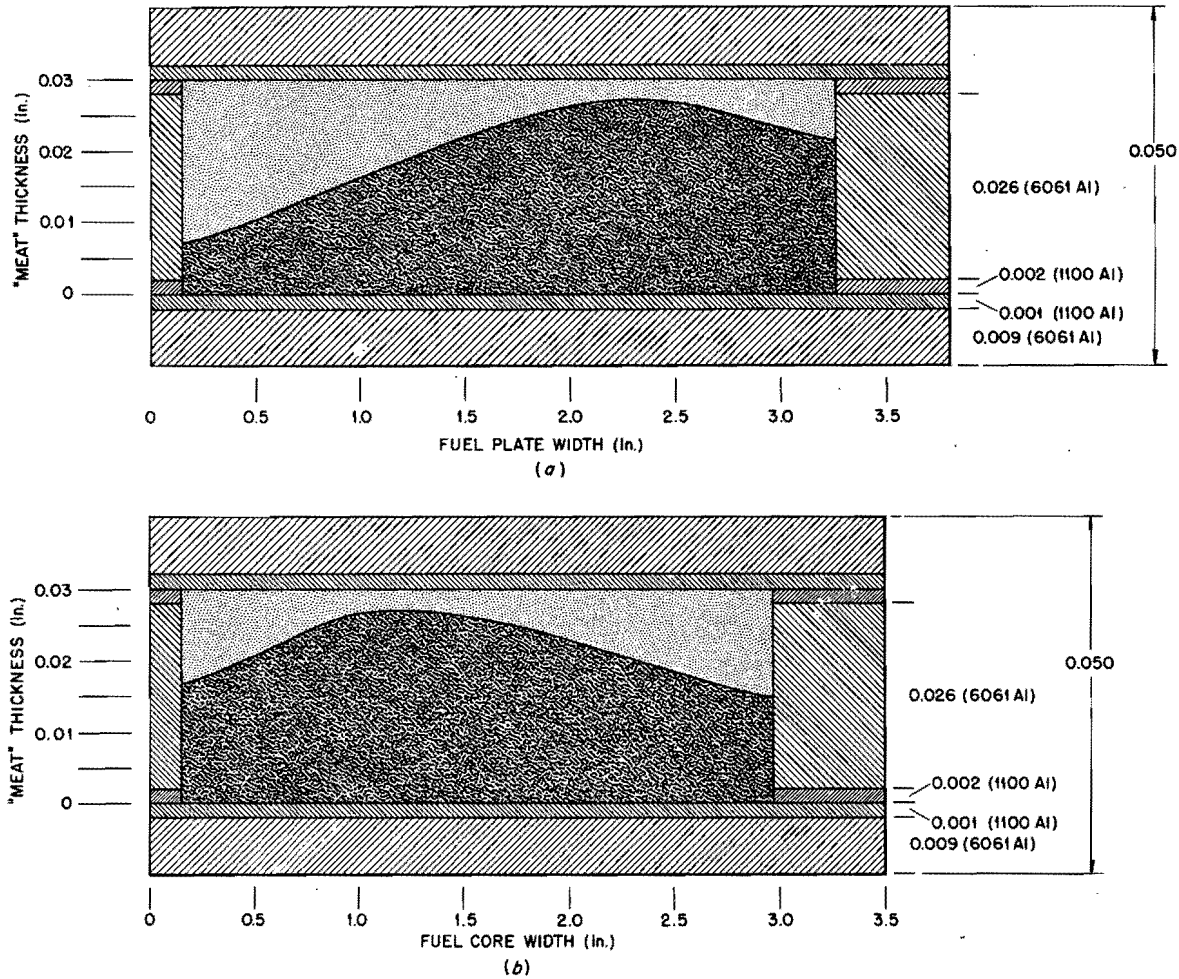


Fig. 2. Idealized Cross Sections for Experimental High Flux Isotope Reactor Fuel Plates.
 (a) Inner annulus; (b) outer annulus.

Table 1. Design Specifications for the Development of Inner Annulus and Outer Annulus Fuel Plates for the High Flux Isotope Reactor

	INNER ANNULUS PLATE	OUTER ANNULUS PLATE
NUMBER OF PLATES	171	369
OVERALL SIZE (in.)		
LENGTH	24.000 ± 0.005	24.000 ± 0.005
WIDTH	3.800 ± 0.001	3.500 ± 0.001
THICKNESS	0.050 ± 0.001	0.050 ± 0.001
NARROW EDGE CLAD	0.140/0.203	0.140/0.203
FUEL-SECTION SIZE (in.)		
LENGTH	20.0 ± 0.5	20.0 ± 0.5
WIDTH	3.067 ± 0.063	2.777 ± 0.063
THICKNESS, MAX.	0.030	0.030
MATERIALS		
CLADDING	ALCLAD TYPE 6061 ALUMINUM	SAME
FRAME	ALCLAD TYPE 6061 ALUMINUM	SAME
FUEL SECTION	26 w/o U_3O_8 - 0.07 w/o B_4C - Al	24 w/o U - Al
FILLER PIECE	0.65 B_4C - Al	TYPE 1100 Al

Material Selection

The core of the inner-annulus fuel plate consists of a fuel section composed of U_3O_8 and B_4C dispersed in type 1100 aluminum and a matching filler piece containing 0.65 wt % B_4C in type 1100 aluminum. Because of large and erratic boron losses when alloying boron with uranium and aluminum, the powder metallurgy dispersion of U_3O_8 and B_4C in aluminum was selected in preference to a uranium-boron-aluminum alloy. The particle size of U_3O_8 utilized in the development program was $-100 +325$ mesh.

In the outer-annulus plate, the core also contains a fuel section and a matching filler piece. The fuel section is composed of a 24 wt % U-Al alloy which is basically a mixture of UAl_4 in aluminum. Since a burnable poison is not specified for this plate, the filler piece is made from wrought type 1100 aluminum.

The operational characteristics of the fuel elements dictate the use of a high-strength, corrosion-resistant cladding material. As is described elsewhere in this report,^{2,3} type 6061-0 aluminum is well suited for this application. This alloy is age-hardenable and contains alloy additions of silicon, copper, magnesium, and chromium. As the cladding for the HFIR fuel element, type 6061 aluminum is used in the fully annealed condition.

Fuel Plate Fabrication

The basic scheme employed in fabricating the fuel plates is shown in Fig. 3. As previously stated, the fuel material in the inner-annulus plate consisted of a dispersion of 26 wt % U_3O_8 and 0.07 wt % B_4C in aluminum. A 24 wt % U-Al alloy was used in the outer-annulus plate. In addition to these fuel-bearing compacts, complementary filler pieces were necessary to achieve a rectangular compact shape suitable for roll cladding. The inner-annulus complementary filler piece also contained B_4C so that a uniform boron distribution could be achieved in the radial direction of the plate.

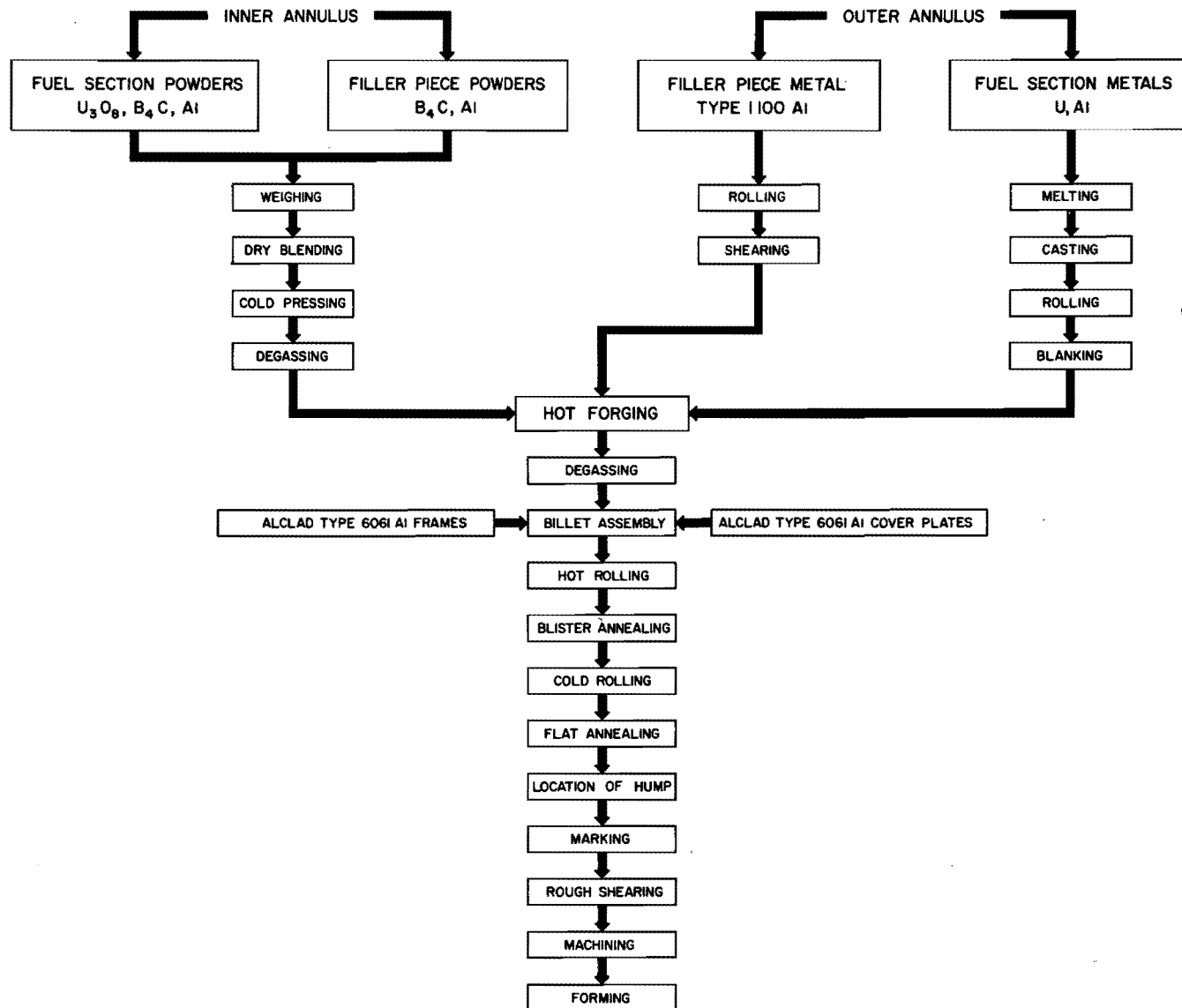


Fig. 3. Flowsheet: Inner and Outer Annulus Fuel Plate Fabrication; High Flux Isotope Reactor.

As can be seen in Fig. 3, conventional powder metallurgy techniques were employed in blending and pressing both the fuel section and the filler piece for the inner-annulus plates. The mixtures were blended dry and a compaction pressure of 50 tsi was utilized to obtain highly dense rectangular shapes. The fuel section for the outer-annulus plate was prepared by induction melting and casting in air a 7-kg ingot of uranium-aluminum alloy, hot rolling the ingot to plate, and blanking rectangular slugs. The filler piece was prepared from commercial type 1100 aluminum plate which was properly sized by cold rolling. Core components for both the inner- and outer-annulus plates were then hot-press forged at 500°C to obtain the contoured shapes previously illustrated in Fig. 2. A heavy-weight oil was applied to the dies during forging to prevent adhesion to the dies.

Cladding of the fuel compacts with type 6061 aluminum was achieved by hot-roll bonding using the picture-frame technique with alclad frame and cover plate materials. As illustrated in Fig. 4, the inner-annulus rolling billet was assembled by inserting the contoured fuel section and complementary filler piece into the frame cavity and attaching the cover plates by tack welding. It should be noted that a double picture frame was utilized which permitted tandem rolling of two plates simultaneously.

The outer-annulus billet also contained a double picture frame. In this case, the frame was prerolled with the fuel section and filler piece in place to ensure that voids were not present at the periphery of the window cavities. The prerolled frame was then sheared in half, and rolling billets were prepared by inserting each cored frame in a preformed wraparound cover plate.

The inner- and outer-annulus billets were hot rolled at 500°C with reductions in thickness of 81 and 91%, respectively. After blister annealing at 500°C, the fuel plates were cold rolled to final dimensions, flat annealed at 500°C, marked, sheared, and machined. It was necessary to conduct all heat treatments prior to final machining in order to prevent bowing. This bowing was attributed to the unsymmetrical positioning of the core within the plate and to the radial gradient in the core.

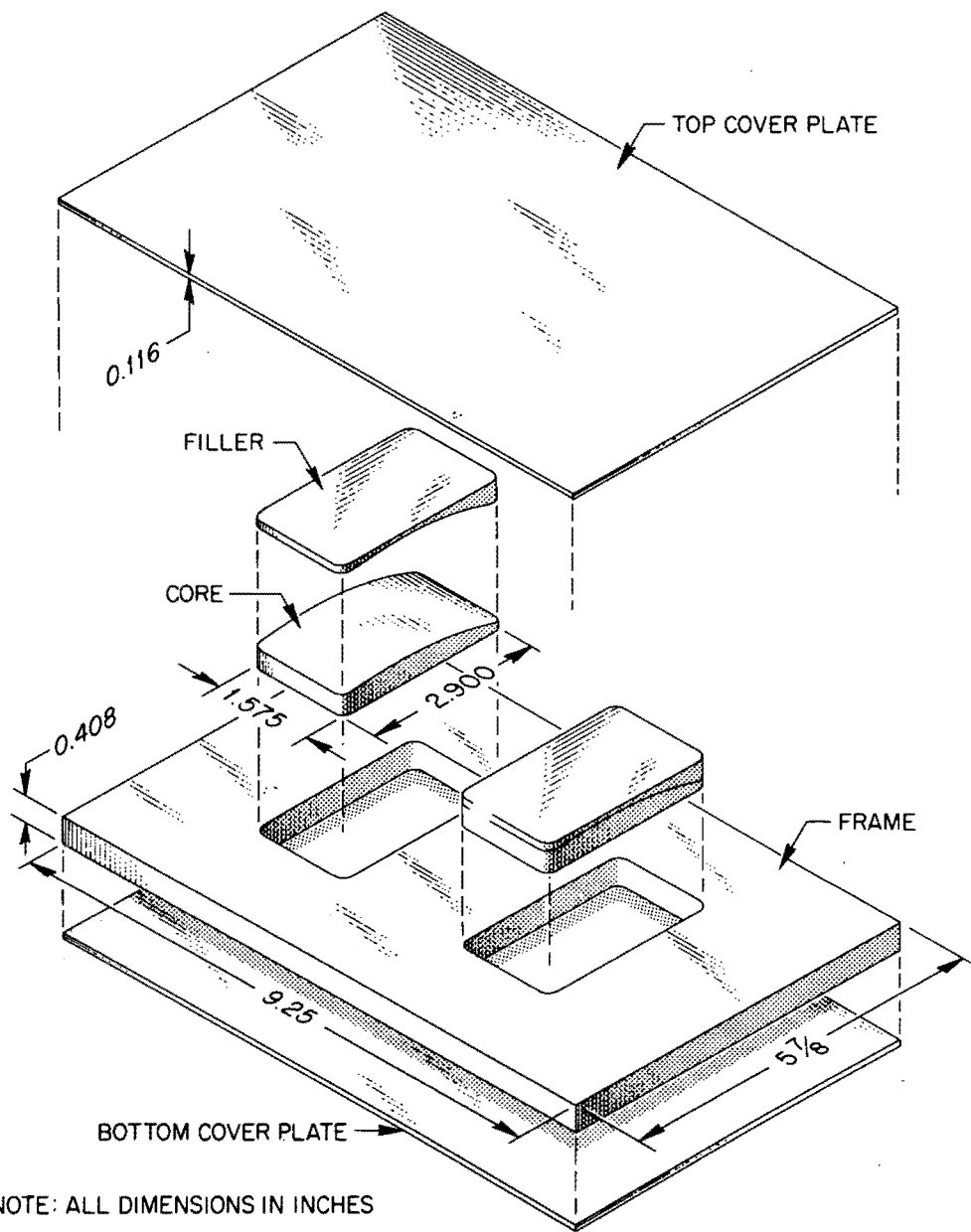


Fig. 4. High Flux Isotope Reactor Inner Annulus Double Plate Billet Assembly.

Discussion of Fabrication Results

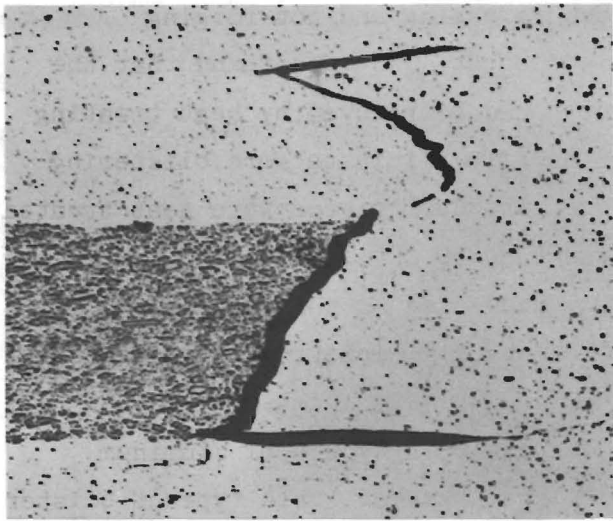
The principal problems in producing satisfactory composite fuel plates were blister formation, reproducibility of the involute shape, and fuel homogeneity. The results of the development work undertaken to eliminate these problems are discussed below.

The prime problem in roll cladding the fuel sections and filler pieces with type 6061 aluminum was blister formation in both the inner- and outer-annulus plates. Gas blisters appeared within the cladding, fuel section, or filler piece and between those pieces in nearly all fabricated and annealed composites. A classification of blister types, illustrated by the photomicrographs in Fig. 5, was utilized in a systematic analysis of the problem. Blisters of the nonbond and core types were predominant.

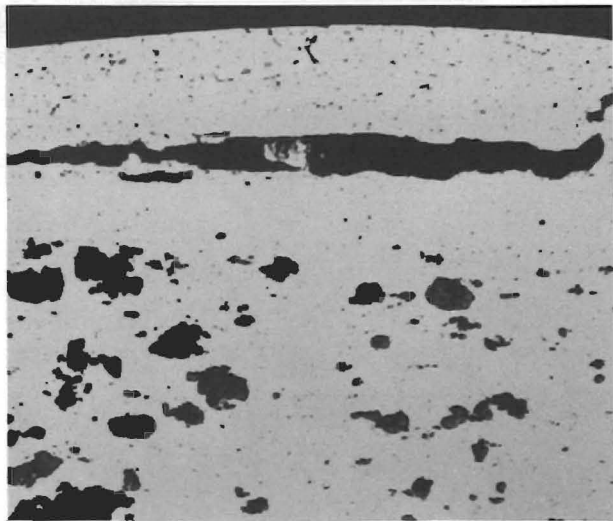
Fit blisters occurred in the volume of material associated with the vertical core-frame edge and resulted primarily from air entrapped in the billet. A slight reduction in the picture-frame cavity dimensions and a differential of 15 mils between the core and frame thicknesses eliminated this type of blister in inner-annulus plates. In the case of the outer-annulus plates, however, it was also necessary to preroll the frame, with the fuel section and filler piece in place, to a reduction in thickness of 40%. These procedures allowed the core to completely fill in the cavity before the billets were sealed in roll cladding.

Nonbond blisters in composite plates occurred at mating surfaces that lacked metallurgical bonding. A typical clad-to-filler piece nonbond is shown in Fig. 5. It is believed that this type of blister nucleates and grows by the desorption of dissolved atomic hydrogen at these free surfaces. Nonbond blisters were eliminated in inner- and outer-annulus plates by inserting a thin layer of type 1100 aluminum between the major mating interfaces. This was accomplished by utilizing alclad type 6061 aluminum for the cladding and frame material.

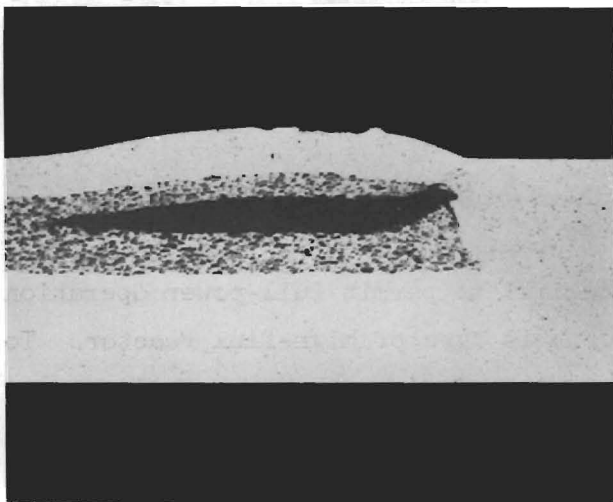
Core blisters were associated with the gas content of the core components. It was observed early in the HFIR program that large amounts of gases were released in hot-rolling inner-annulus billets. Mass spectrometer analysis of the released gases revealed various proportions of H₂, CH₄, N₂, CO₂, and CO. Further experiments indicated that substantial



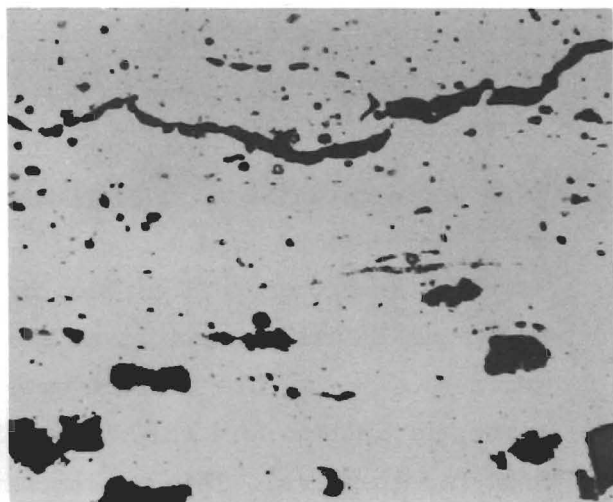
Fit 100X



Nonbond 100X



Core 33X



Skin Blisters 250X

Fig. 5. Illustration of Blister Types Observed in High Flux Isotope Reactor Fuel Plates.

quantities of lubricant from the "green" pressing and hot-forging operations were retained by the core components. It was found that the volatile constituents of the lubricant could be removed by heat treating the compacts in vacuum at 600°C for 3 hr. To eliminate core blistering in inner-annulus fuel plates, therefore, the fuel pieces were heat treated for 3 hr at 590°C at a pressure of less than 50 μ . The forging blanks as well as the forged core components were subjected to this degassing operation. This procedure was also successfully employed to reduce core blistering in outer-annulus fuel plates.

Profuse skin blisters sometimes occur within type 6061 aluminum cladding and literally cover the fuel plate surface. This type of blister was eliminated by restricting the fabrication temperature to 500°C. Further studies are required, however, to firmly establish the role of temperature on this type of blister. As illustrated in Fig. 6, a marked change in the surface oxide film occurred on type 6061 aluminum heat treated above 500°C. At temperatures above 500°C, the oxide appears porous, thereby permitting direct exposure of the aluminum to the atmosphere and the subsequent absorption of hydrogen. This degree of oxide film porosity increases with temperature. Similar studies on the stability of the oxide film on type X8001 aluminum have failed to show porosity formation at temperatures as high as 600°C.

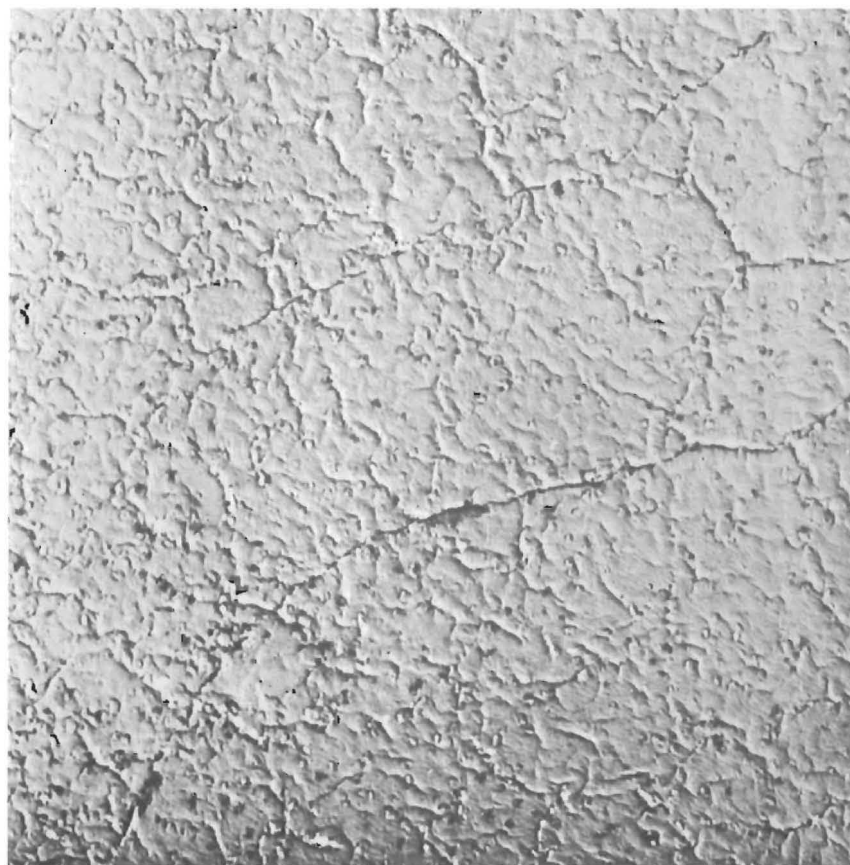
Homogeneity

The homogeneity specification required to permit full-power operation of the HFIR fuel element is unique for this type of high-flux reactor. To avoid "hot spots," the present specification requires that the fuel concentration shall not be greater than 30% of the nominal concentration in any 5/64-in.-diam area. Since a lateral gradient of fuel exists within these plates, it is obvious that the overall distribution of fuel depends on the contour height at the point of measurement as well as the homogeneity of the fuel at that point.

To ascertain the variations on contour that were expected along the length of a fuel section, ten transverse profiles were measured in an



(a)



(b)

Fig. 6. Appearance of Surface Oxide on Type 6061 Aluminum After Annealing in Air for 1 hr at (a) 500°C and (b) 515°C.

inner-annulus plate and statistically analyzed. The results are presented in graphic form in Fig. 7a. The actual thickness of the fuel section is plotted against the distance from the narrow edge of the plate. The dotted curve is the desired nominal contour; the solid lines and I bars represent the average fuel section profile and statistical variation found in the plate.

This variation in the thickness of the fuel section leads to local variations in the uranium content per unit area of the fuel plate which are shown in Fig. 7b. It can be seen from Fig. 7b that because of dimensional variations alone inhomogeneities of uranium as high as 20% can be expected, particularly in the thin section of the fuel core.

To assess the distribution of fuel, a destructive statistical analysis was performed by punching 5/64-in.-diam samples from a representative fuel plate and chemically analyzing these punchings for total uranium content. The results are shown in Table 2. In general, the average uranium content for each row does not differ significantly from the calculated theoretical value. The largest and smallest values found within each of the nine rows are compared to the theoretical in the last two columns of the table. The maximum uranium content in specimens from the edges of the fuel section, rows 1 and 9, did not exceed the nominal. The rows which exhibited large positive deviations, 2 and 4, are located on the long tapered side of the fuel section profile.

Similar experiments were conducted to determine the variations in uranium content that were expected along particular rows within a batch of plates. The results, when expressed in the form of statistical tolerance limits, indicated variations in uranium of $\pm 40\%$, $\pm 20\%$, and $\pm 19\%$ for rows 2, 5, and 8, respectively. As expected, considerable variations in uranium distribution are indicated for position 2 by the large statistical tolerance. Arbitrarily, the limits were calculated at the 95% confidence level to include 99% of the batch of fuel plates.

A nondestructive technique for determining the uranium distribution in every fuel plate will be described elsewhere in this report.⁴

To fully evaluate the uranium homogeneity in the fuel section of rolled HFIR plates, it is necessary to compare 5/64-in.-diam samples on

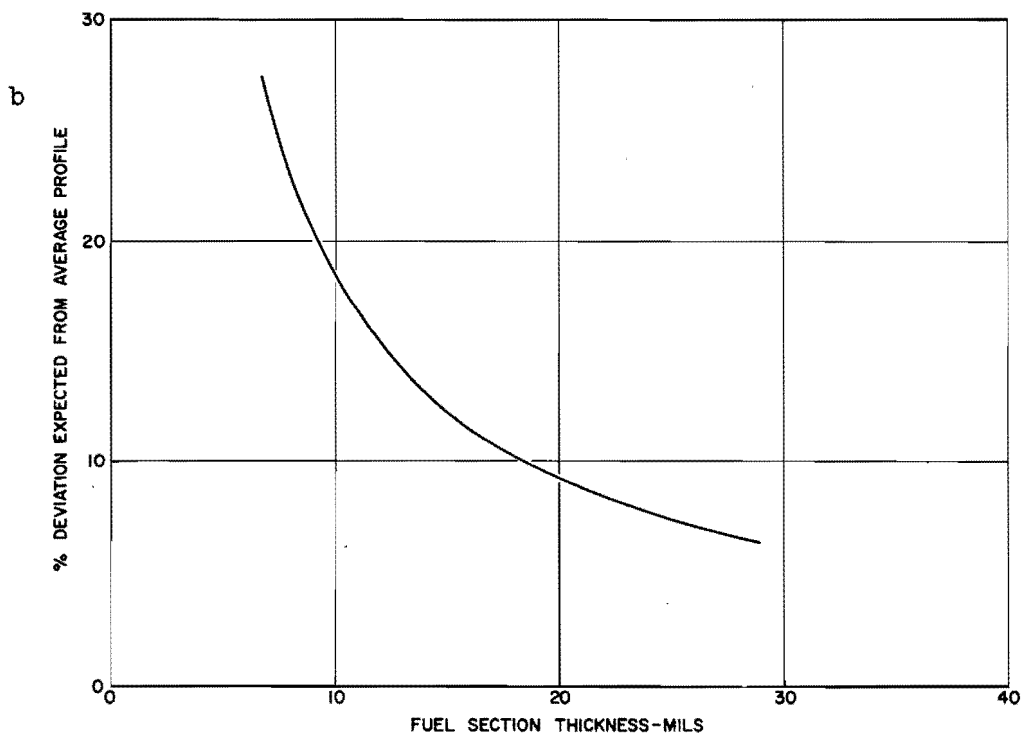
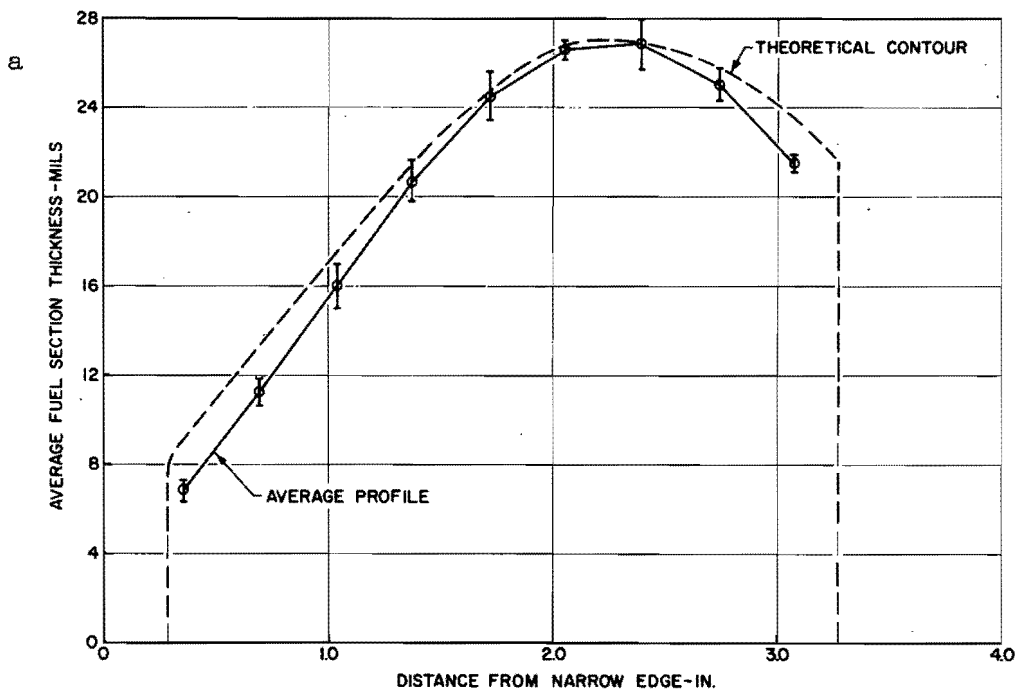


Fig. 7. Variation in Fuel Section Profile for Inner-Annulus Plate H-990: (a) Average Fuel Section Thickness vs Distance from Narrow Edge and (b) Percent Deviation Expected from Average Profile vs Fuel Section Thickness.

Table 2. Distribution of Uranium in Experimental Inner-Annulus Plate H-969^a

ROW NUMBER	DISTANCE FROM NARROW EDGE OF PLATE (in.)	URANIUM CONTENT ^b		MAXIMUM DEVIATION FROM THEORETICAL	
		THEORETICAL (mg/in. ²)	AVERAGE (mg/in. ²)	POSITIVE (%)	NEGATIVE (%)
1	0.328	114	84	0	39
2	0.656	158	164	42	24
3	0.984	208	189	8	28
4	1.312	257	254	31	16
5	1.640	300	282	2	9
6	1.968	327	328	1	0
7	2.296	335	312	2	26
8	2.624	327	308	8	15
9	2.952	302	262	0	21

^aSAMPLE SIZE - 5/64 in. DIAMETER PUNCHING

^bTOTAL NUMBER OF RANDOM SAMPLES - 60

a uranium density basis, thereby eliminating contour thickness as a variable. The result of dividing the uranium distribution values by the actual "meat" thickness is presented in Table 3. The average overall uranium density in this particular fuel section is 0.78 g/cm^3 , which compares very closely with the calculated theoretical value of 0.76 g/cm^3 . In general, the uranium density appears to pass through a maximum at position 2. In the last two columns, the largest and smallest values found within each of the nine rows are compared to the theoretical uranium density. The positions which show large positive deviations, rows 1, 2, 3, and 4, again occur on the long tapered side of the fuel section profile. Based on the statistical variation of the data, a tolerance limit of $0.78 \text{ g/cm}^3 (\pm 5\%)$ results for the fuel section density.

Several factors could conceivably cause this increase in uranium content in the thin portion of the fuel section. The contour height variation in this region accounts for a large percentage of the increased uranium content. The initial size of the U_3O_8 particles and the subsequent forging of the contour also conceivably contribute to this effect. The effect of particle size on uranium distribution is presently under study. Powder metallurgy procedures are being developed to prepare the fuel contour and mating filler in one piece by direct cold pressing. This scheme is particularly attractive since it does not require the lateral flow of the powders to obtain the desired gradient as does forging.

FORMING OF FUEL PLATES

The assembly of the roll-clad fuel plates into the required fuel element geometry, as previously shown in Fig. 1, dictates reproducible fuel plate curvatures in order to meet the rigid water-channel tolerances. To meet the tolerance restriction of 50 ± 6 mils for the water-channel gap, it appears that the involute radii must be reproduced to within ± 4 mils on all fuel plates. As a result, studies have been aimed at developing economical techniques to reproducibly form the fuel plates to close tolerances. Because of the simplicity of the die design and the ease in which a plate can be formed, a modified marforming technique was adopted as the reference forming method.

Table 3. Uranium Homogeneity in Fuel-Bearing Portion of Inner-Annulus Plate H-969

ROW NUMBER	DISTANCE FROM NARROW EDGE OF PLATE (in.)	AVERAGE URANIUM DENSITY ^a (g/cm ³)	MAXIMUM DEVIATION FROM THEORETICAL ^{b, c}	
			POSITIVE (%)	NEGATIVE (%)
1	0.328	0.87	33	5
2	0.656	0.97	54	4
3	0.984	0.79	31	23
4	1.312	0.78	50	12
5	1.640	0.73	6	9
6	1.968	0.73	0	4
7	2.296	0.71	2	24
8	2.624	0.74	6	9
9	2.952	0.68	0	20

^aAVERAGE OVERALL CORE DENSITY 0.78 g/cm³

^bTHEORETICAL DENSITY 0.76 g/cm³

^cCALCULATED HOMOGENEITY TOLERANCE 0.78 g/cm³ ± 55%

The die assembly, illustrated in Fig. 8, consists of a die punch which is mounted to a movable ram and two "Maple Heights Hi Temp" rubber packs placed in the female die. Forming is accomplished by inserting a flat plate in the positioner frame and lowering the male punch into the rubber pack. A force of 65 tons (approximately 1600 psi total pressure) is employed to form the involute shape.

To establish the parameters essential to reproducible forming of the fuel plates, experiments were conducted using type 6061-0 aluminum plate stock. As shown in Table 4, forming this material at 1600 psi resulted in reproducible plate contours with yields greater than 95%. This was achieved by close control of rubber quality, plate positioning, unit pressure, and use of talcum powder lubrication between the plate and the top rubber pack.

A comparison of the reproducibility of forming solid type 6061 aluminum plates with the composite fuel plates for the critical-test element and recently developed outer-annulus plates is also shown in Table 4. Although the critical-test plates were formed under the same controlled conditions, the yield of acceptable involutes (about 20%) was discouraging.

Two approaches are being followed to increase the yield of curved plates. One is refinement of the fabrication procedures to produce fuel plates with uniform characteristics. By increasing the amount of cold work from 5 to 15% and reducing the hot-rolled thickness variations to ± 0.5 mils, the yield of recently processed outer-annulus plates increased to 51%. This gross improvement over the plates marformed for the critical-test element, however, was still considerably below that for type 6061-0 aluminum sheet stock. As a result, alternate forming methods coupled with low-pressure marforming are being explored. These include (a) marforming at unit pressures of 4, 12, and 16 tsi, (b) restrike marforming, (c) stress relief or creep forming, and (d) high-energy electrical discharge forming. Recent data on forming a limited number of plates by the first three alternates indicated sufficient reproducibility of the involute curvature by the restrike and creep-forming

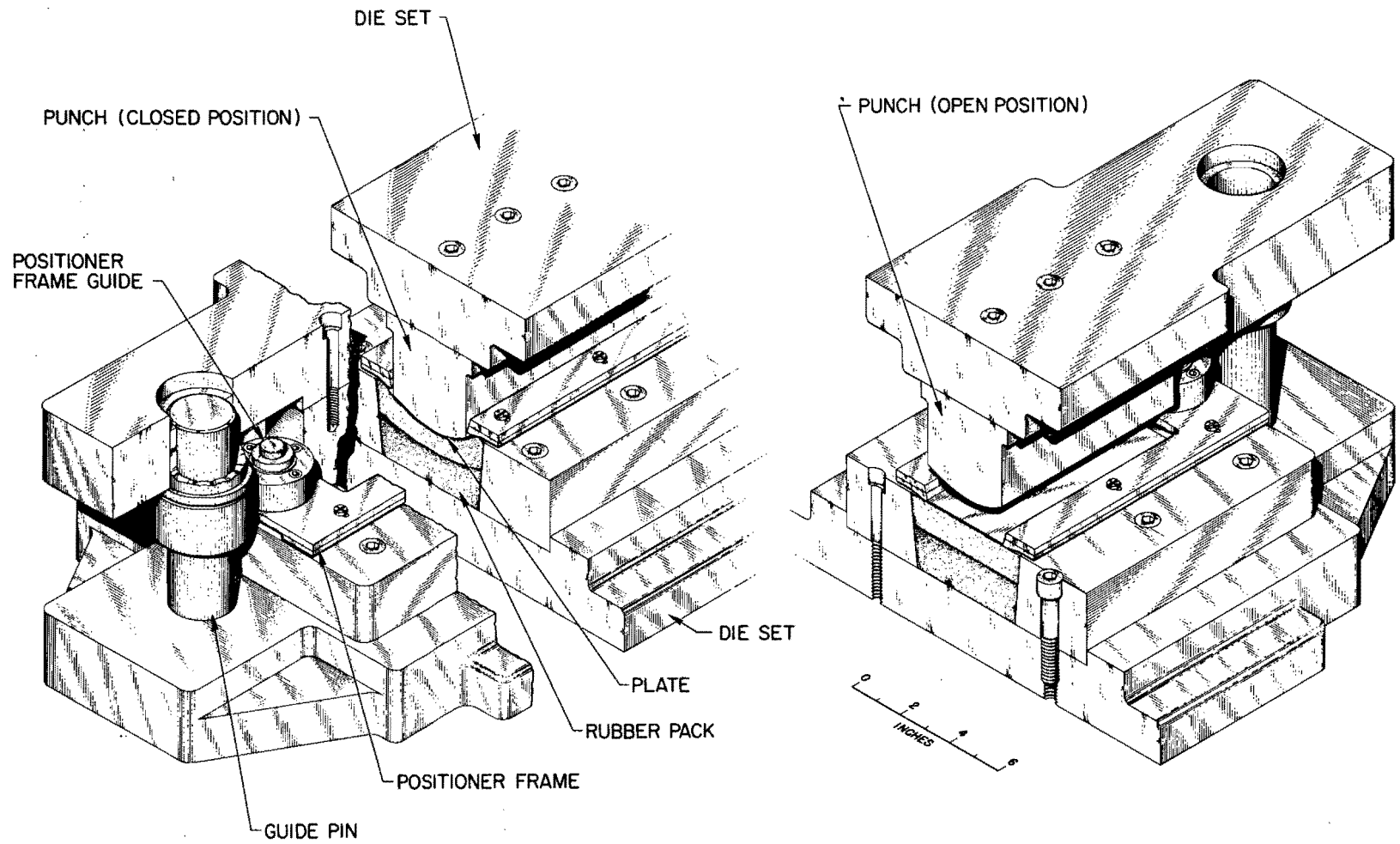


Fig. 8. Marforming Die Assembly.

Table 4. Summary of Data from Low-Pressure-Marformed HFIR Fuel Plates Showing Degree of Duplication of the Involute Radii

	INNER ANNULUS		OUTER ANNULUS		
	Type 6061-0 Aluminum	Fuel Plates Utilized in Critical Core	Type 6061-0 Aluminum	Fuel Plates Utilized in Critical Core	Recently Developed Fuel Plates
Number of plates measured	37	18	68	72	101
Maximum spread in plate radius measurements ^a (mils)	9	36	9	18	20
Statistical variance of measurements in the plate group (28 measurements/plate)	1.65	5.03	1.17	3.26	2.75
Percent of acceptable plates (within ± 0.004 in. duplication)	97.3	27.8	98.5	12.5	51.5

^aMeasurements taken at 7 equidistances along the length of each plate at four radii positions (28 measurements/plate).

methods to warrant further investigation. Experiments are now being conducted to determine the feasibility of high-energy electrical discharge forming. Similar encouraging results were also obtained in forming fuel plates at 1600 psi and subsequent electro-hydraulic reforming with an energy of 2500 j.

Conclusions

Procedures were established for fabricating fuel plates clad with the high-strength type 6061 aluminum for applications in the HFIR. Good reproducibility of the radial gradient contour was achieved in rolling plates containing either powder metallurgy dispersions or conventional alloy fuel compacts. Techniques were developed for preventing the blistering associated in roll cladding the radial gradient fuels with type 6061 aluminum. Blister-free reduction yields comparable to the more conventional alloy plates were thus achieved in fabrication of these high-strength fuel plates.

Methods for reproducibly forming these plates to the required involute contours were investigated and considerable progress was made toward obtaining a satisfactory yield of properly shaped plates.

Acknowledgments

The authors are indebted to R. J. Beaver, G. M. Adamson, Jr., T. D. Watts, and J. P. Hammond of the Metals and Ceramics Division for their immeasurable contributions to this fuel development program.

References

1. J. W. Tackett et al., "Assembly and Welding Development for the HFIR Elements," published elsewhere in this report.
2. J. C. Griess et al., "The Corrosion of Aluminum Alloys Under Simulated HFIR and ATR Conditions," published elsewhere in this report.
3. W. R. Martin and J. R. Weir, "Mechanical Properties of X8001 Aluminum Cladding and X8001 Aluminum-Base Fuel Dispersion at Elevated Temperatures," published elsewhere in this report.
4. R. W. McClung, "Nondestructive Testing on HFIR and ATR Fuel Elements," published elsewhere in this report.

ASSEMBLY AND WELDING DEVELOPMENT FOR THE HIGH-FLUX ISOTOPE REACTOR FUEL ELEMENT

J. W. Tackett, J. H. Erwin,
C. F. Leitten, Jr., and G. M. Slaughter*

Introduction

In order to produce research quantities of transplutonium elements, the High-Flux Isotope Reactor (HFIR) will operate with an extremely high neutron flux. The high neutron flux necessitates rapid fuel burnup and high heat generation in the reactor core. The reactor core will be replaced at 10-15 day intervals in order to maintain the required neutron flux level. Light water flowing at a rate of 11,000 gpm through the core will remove the generated heat.

The problems attendant to (1) the high heat generation in the fuel plates and (2) the rapid flow of coolant water between the plates dictate rigid structural requirements for the manufactured fuel elements. Also the frequency of core replacement limits the manufacturing process to a reasonably economic one.

The reactor fuel element, shown in Fig. 1, consists of two annular rings of aluminum-clad fully enriched uranium-cored fuel plates. After the fuel plates are manufactured and formed to an involute curvature,¹ they are placed between two concentric support tubes such that a 0.050 in. uniform spacing exists between adjacent plates. This spacing must be maintained to within very close tolerances so that each plate is cooled uniformly. The fuel plates must also be rigidly anchored to the support tubes in view of the high flow rate of the coolant water through the channels.

It should be noted that the two fuel annuli are manufactured as separate items; namely: (1) an inner annulus containing 171 fuel plates with an inside diameter of approximately 5 in. and an outside diameter

*Oak Ridge National Laboratory, Oak Ridge, Tennessee.

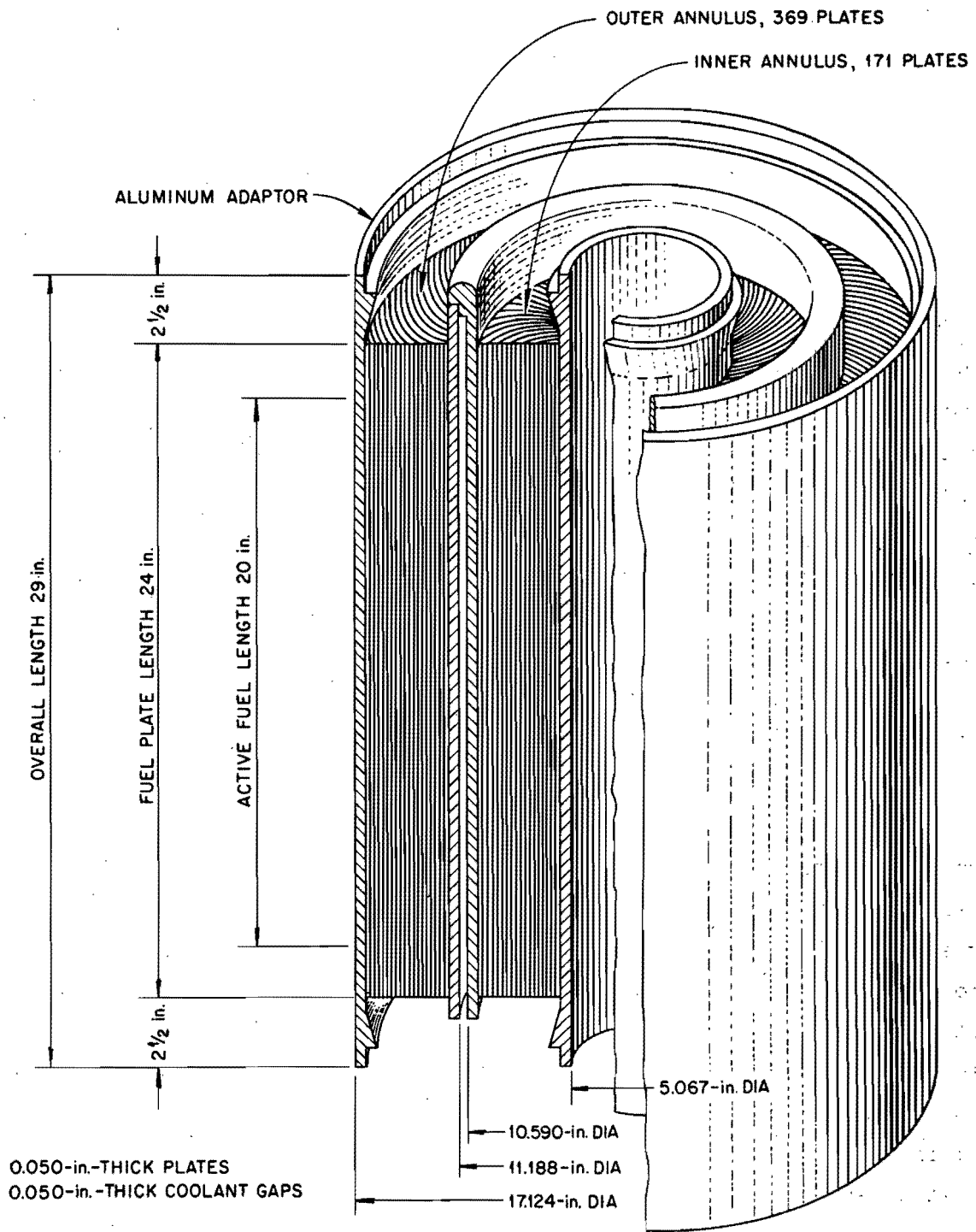


Fig. 1. Sketch of HFIR Fuel Element Showing the Two Annular Rings of Fuel Plates. These plates are formed to an involute curvature and placed between two concentric support tubes.

of approximately $10\frac{1}{2}$ in. and (2) an outer annulus containing 369 fuel plates with an inside diameter of approximately 11 in. and an outside diameter of $17\frac{1}{8}$ in.

The support tubes of the annuli must be perfectly concentric with the center line of the core. Out-of-roundness in the 17-in.-diam tube would introduce installation problems* and encroach on the water gap required between the fuel element and the surrounding control plates. Out-of-roundness of the 5-in.-ID tube of the inner annulus would introduce similar complications with the target assembly. It should be obvious that distortion of any kind, whether occurring during fabrication or during reactor operation, would be undesirable.

Therefore, in developing a suitable manufacturing procedure for the reactor fuel element, one must consider the major fabrication criteria listed in Table 1.

Discussion of Fuel Element Concepts and Fabrication Techniques Investigated

A program was set up in the Metals and Ceramics Division of the Oak Ridge National Laboratory (ORNL) to develop procedures for fabricating fuel elements to the exacting requirements imposed. The program has been broad in scope and a variety of design concepts and joining techniques have been investigated. The three concepts illustrated in Fig. 2 appeared to be the most suitable for fuel element production.

The first concept (shown at the left of Fig. 2) utilizes a "bent lip" fuel plate. The bent lips are located at the outer edges of the fuel plate and, when the plates are assembled in the annular configuration, the lips both generate an outer support tube and establish the approximate channel thickness. The fuel plates are mechanically attached to the inner grooved support tube by peening (plug welds are used to attach the last five plates), and they are joined to the outer edges of adjacent fuel plates by welding.

*The fuel element is installed into the reactor core through a hatch opening in the top of the reactor pressure vessel which will be located under 17 ft of water.

Table 1. Criteria for Manufacture of HFIR Fuel Elements

Dimensional Control

Coolant channel thickness: 0.050 in. nominal

Tolerance: ± 0.010 in. at any location

± 0.006 in. average*

Diametral tolerance: ± 0.005 in.

Joint Requirements for the Fuel Plate Support Tube Attachment

Minimum spacing of joints (if intermittent): 1 in.

Minimum pull-out strength: 100 lb/linear in.**

Economy and Safety

Manufacturing method must be reasonably economical

Procedures must not damage the fuel plates

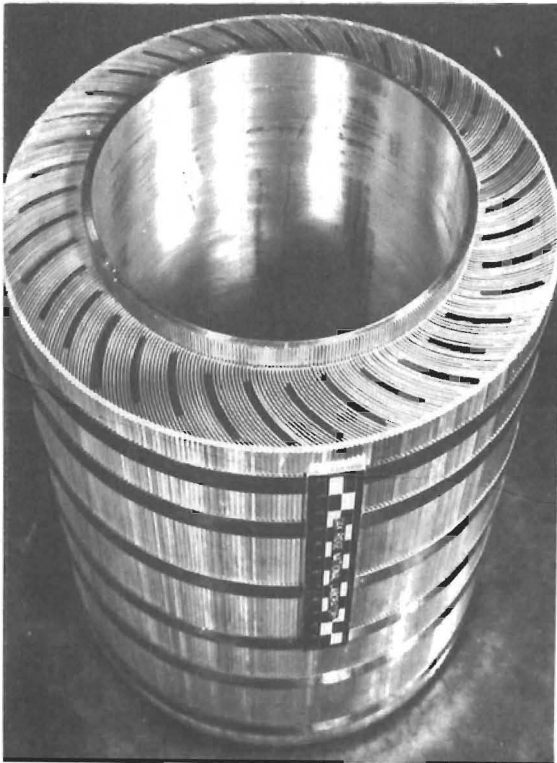
Joining operations must be reasonably immune to process malfunction

*The average channel thickness at any axial location along the channel is obtained by the following formula:

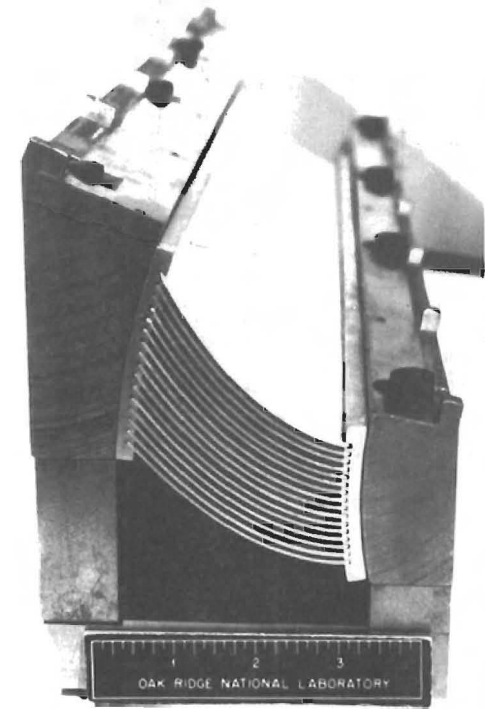
$$\text{Average value} = \frac{50 + A + B + C}{4}$$

where A, B, and C are channel thickness readings (in mils) taken at $\frac{1}{4}$, $\frac{1}{2}$, and $\frac{3}{4}$ of the distance across the channel width at the particular axial location.

**The pull-out strength of a fuel plate-to-support tube joint refers to the force necessary to separate the plate from the tube when applied tangent to the plate curvature at the point of attachment.



BENT LIP DESIGN

CONCENTRIC SIDE PLATE
"ALL WELDED" DESIGN

SEGMENTED DESIGN

Fig. 2. Three HFIR Fuel Element Design Concepts Considered to be the Most Suitable for Production. (a) Bent lip - the lips on the outer edge of the fuel plates generate an outer support tube and establish the approximate channel thickness, (b) sliding plate - fuel plates are slid between concentric tubes which are grooved circumferentially and slotted longitudinally. These plates are attached to both tubes by circumferential welds, (c) segmented - subassemblies are made by roll-swaging fuel plates to support tubes. Annular segments are then installed between two concentric tubes to generate complete annuli.

The second concept (shown in the center of Fig. 2) utilizes two concentric support tubes which are grooved circumferentially and slotted longitudinally. Fuel plates are slid into involute positions between the concentric tubes and are attached to both support tubes by circumferential welds.

In the third concept, annular segments (shown at the right of Fig. 2) are manufactured as subassemblies. A mechanical roll-swaging process is used to attach the fuel plates to the grooved support tube segments. The annular segments are then pinned together and assembled between two concentric tubes in order to generate complete annuli.

Each of these three design concepts will be described in more detail in the following sections of this paper. It should be pointed out, however, that the present developmental status of the three concepts varies considerably. The bent-lip concept was introduced early in the program and became the primary development effort as well as the reference design. The all-welded concept was introduced later and evolved from an exploratory welding study which paralleled the primary effort. The potentially attractive segmented concept is relatively new to the development program and its problem areas are currently under investigation.

In conjunction with the development program, necessary fuel element hardware for flow studies, demonstration purposes, and criticality tests has been manufactured. In fact, the fuel element for the criticality test contained fully enriched uranium-cored fuel plates.

Fabrication Procedures Developed for the Bent-Lip Design

The fabrication techniques developed for the "bent-lip" concept are shown schematically in Fig. 3. A peening process was developed to mechanically attach the inner fuel plate edge to the grooved inner support tube. This peening process was selected over roll-swaging because of the space limitations encountered when the fuel plates close in upon themselves during assembly of a complete annulus. A pneumatically operated peening wire using a hammering motion displaces metal from the edge of the groove into the surface of the adjacent fuel plate. The displaced metal not only rigidly attaches the full length of the fuel plate to the grooved

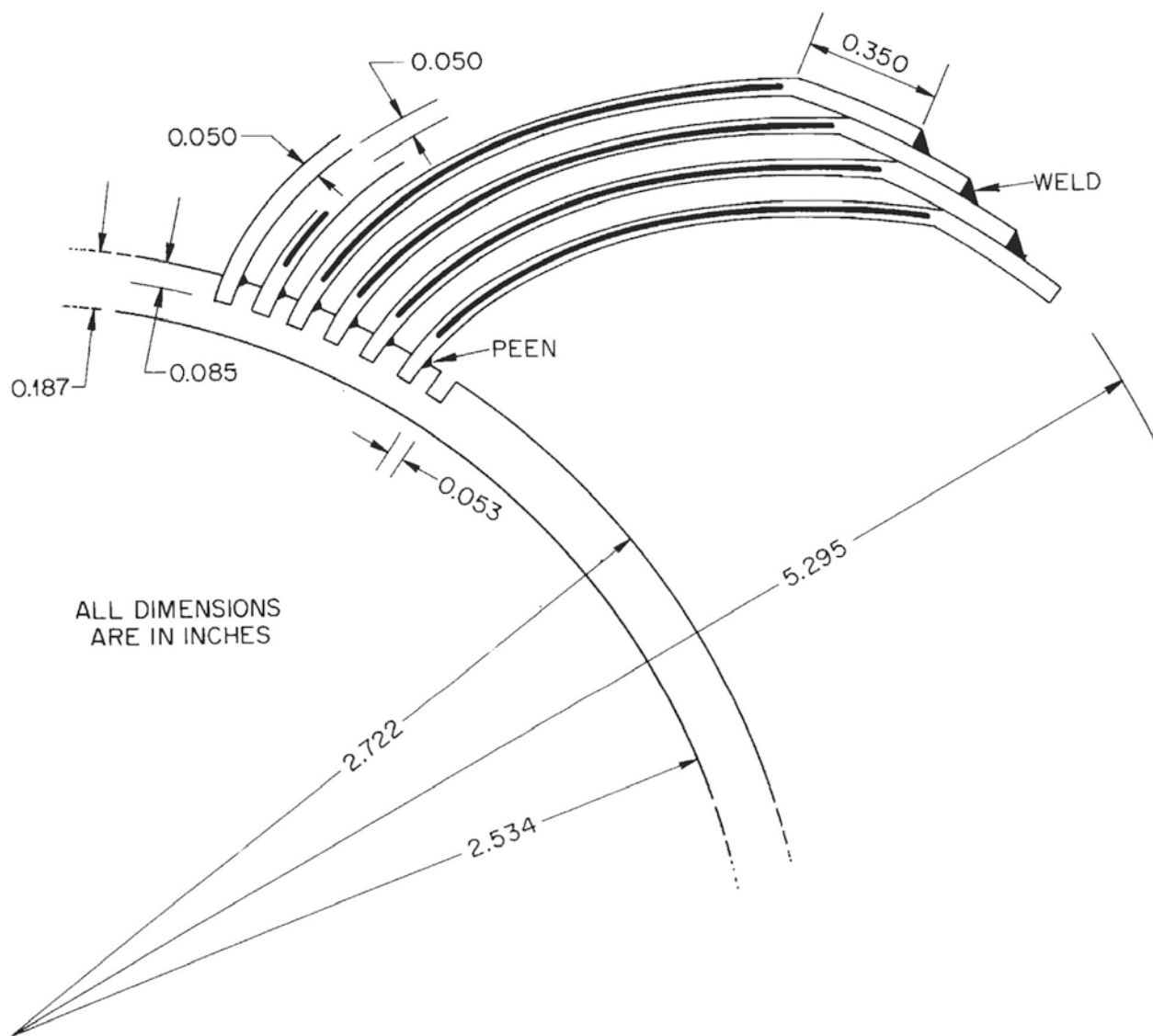


Fig. 3. Schematic Drawing of Fabrication Techniques for Bent-Lip Concept of HFIR Fuel Element.

support tube but also forces the fuel plate against a reference side of the groove. To obtain optimum joint conditions, care and precision were required in correctly positioning the peening tool relative to the groove edge. After all fuel plates have been installed, the outer bent edges are joined by welding. It can be seen that the weld is located well away from the outer edge of the fuel body.

Figure 4 shows an outer annulus fuel element which is almost completely assembled. The peening tool driven by the lathe drive traverses the length of the fuel plate. The large index wheel positions the assembly for locating every plate. Since lack of access prevents the peening tool from being used to attach the last five fuel plates, a supplementary plug-welding operation was developed for this purpose. Prior to assembly, weld grooves were machined into the inside surface of the inner support tube as shown at the top of Fig. 5. After insertion the inner fuel plate edges protrude through the bottom of the weld groove. The short plug welds, made at 1-in. intervals along the length of the plate, can be made either manually or automatically. Special equipment, described later under All-Welded Design, was developed to make the inside welds automatically.

Two welding methods were developed to rigidly secure the outer fuel plate edges. One method, as shown in Fig. 6, used aluminum bands installed around the outer circumference of the fuel element. The bands both secure the plate edges and, when joined together, form the outer tube. To accommodate these bands, circumferential grooves were machined into the outer bent-lip portion of the fuel plates (left of Fig. 6). The steel bands shown in this photograph were used to hold the assembly rigid during machining and subsequent attachment of the aluminum bands. The aluminum bands, precut to length, were installed in the grooves and attached to the raised shoulders formed by the fuel plate edges by welds joining adjacent bands. A network of short tack welds (center of Fig. 6) were made first in order to minimize lateral movement of the bands during deposition of the complete circumferential welds. A completely welded outer annulus is shown at the right of Fig. 6. The second method, shown in Fig. 7, is a simplification of the first method in which "V"-type weld grooves were machined into the outer bent lips of the fuel plates.

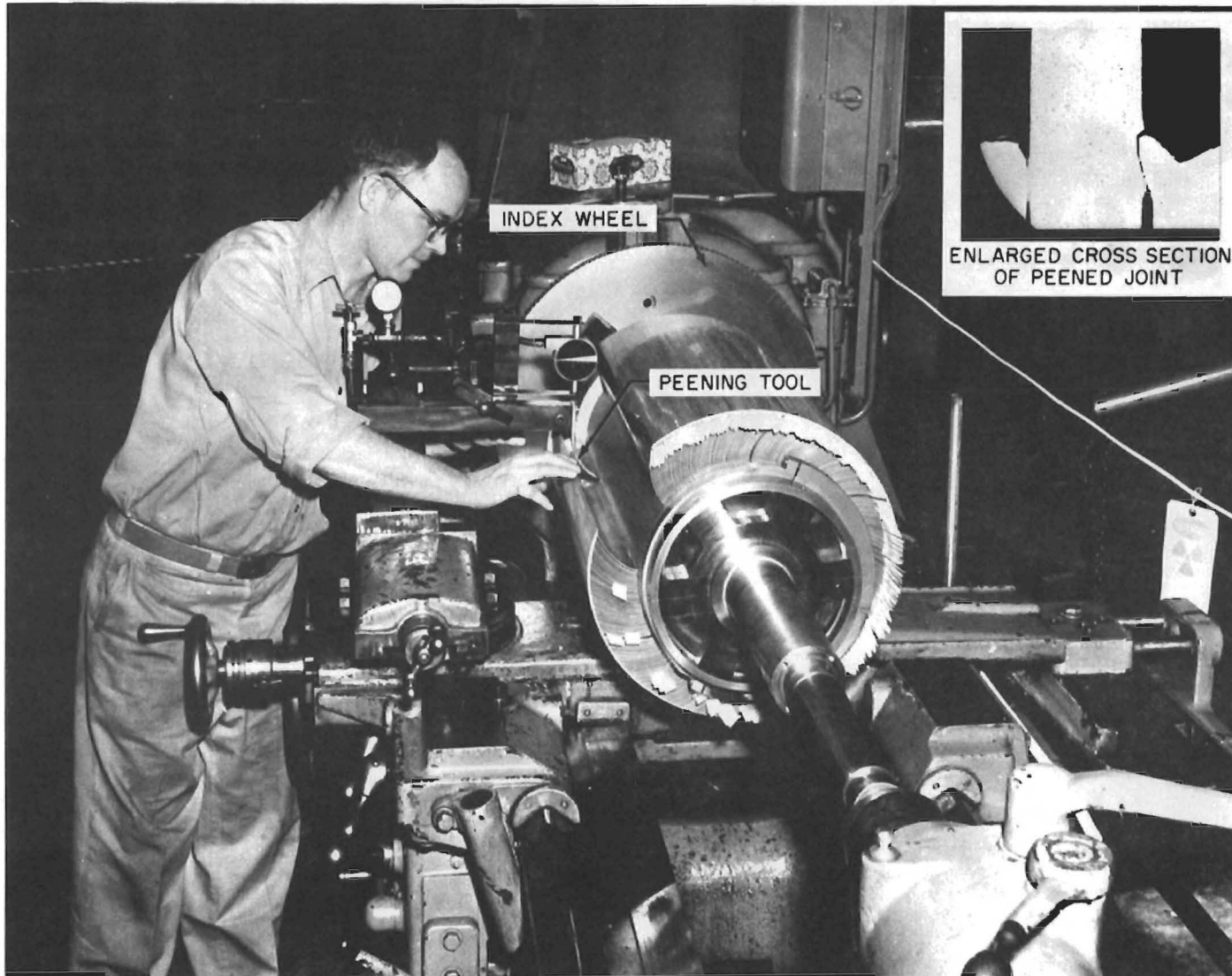


Fig. 4. Photograph Illustrating the Use of Peening to Mechanically Attach Fuel Plates into Longitudinal Slots of Inner Support Tubes. The pneumatically operated tool traverses along the length of the fuel plate.

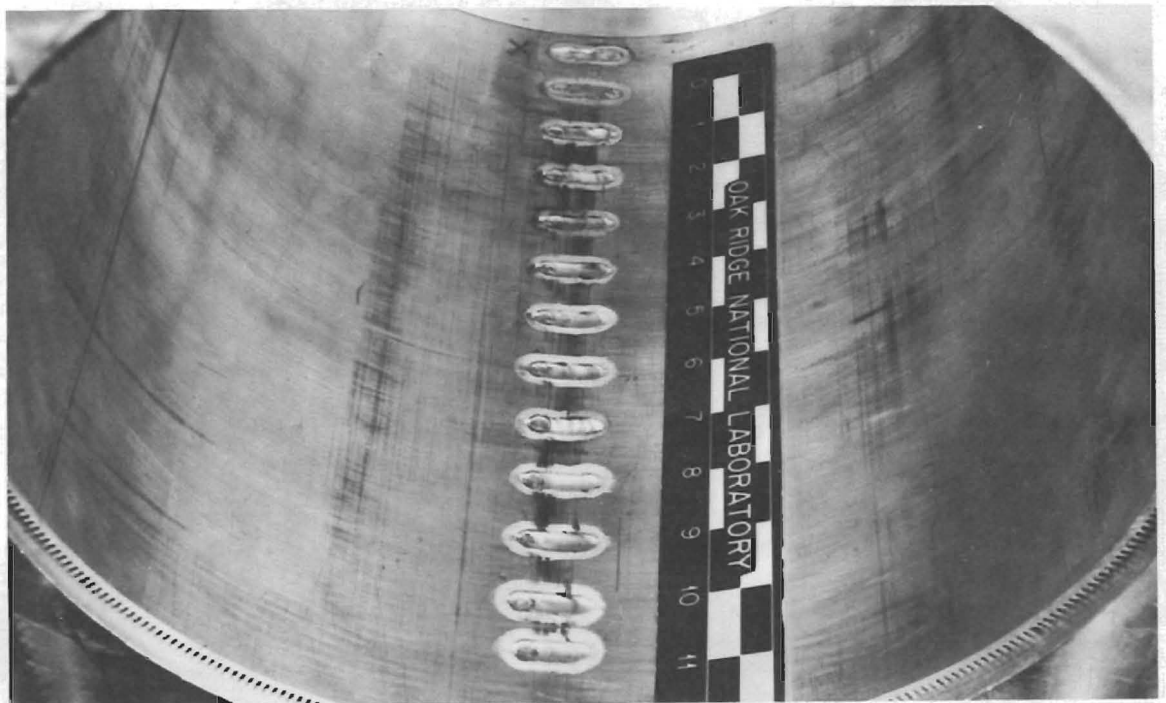
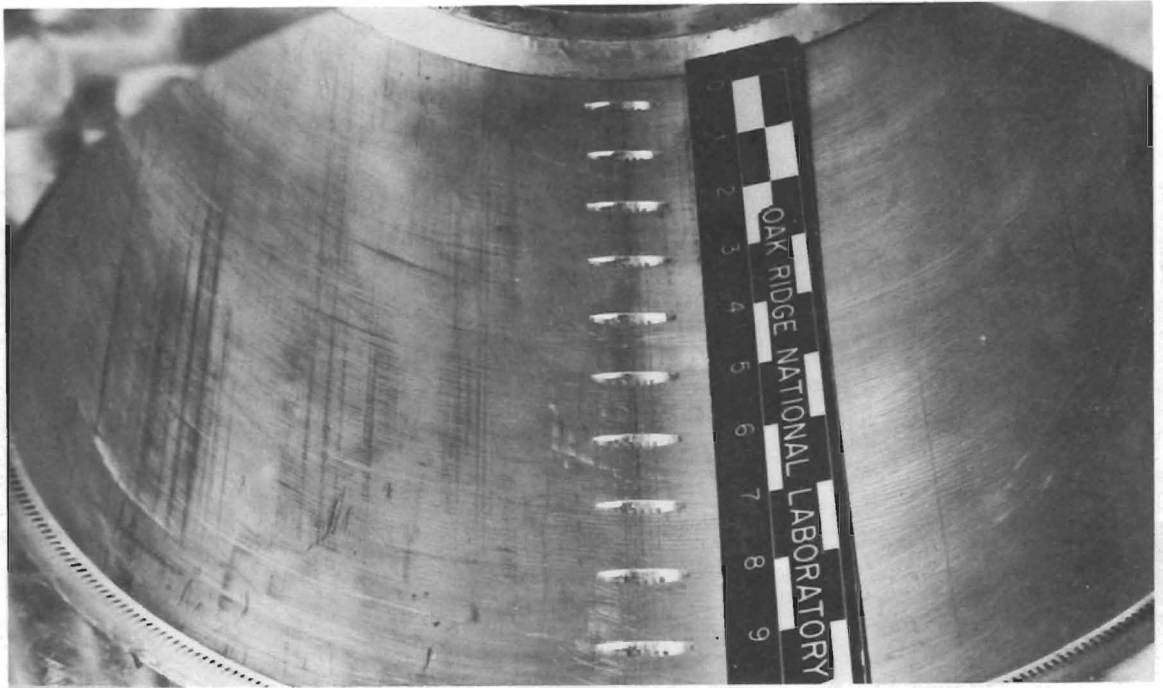
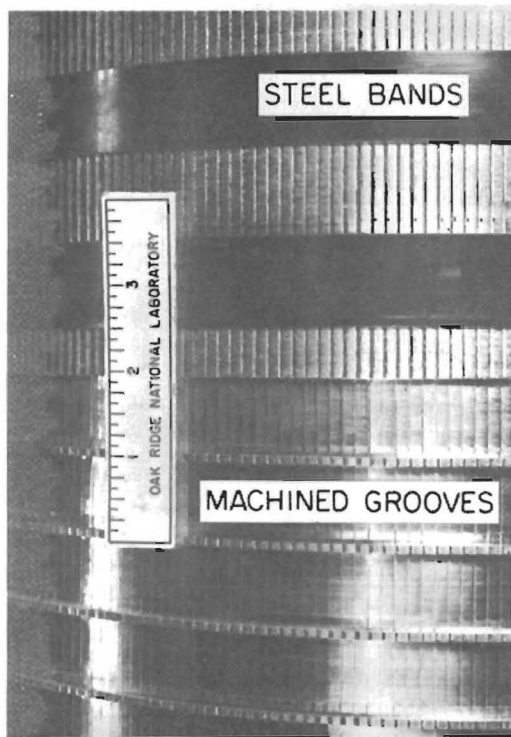
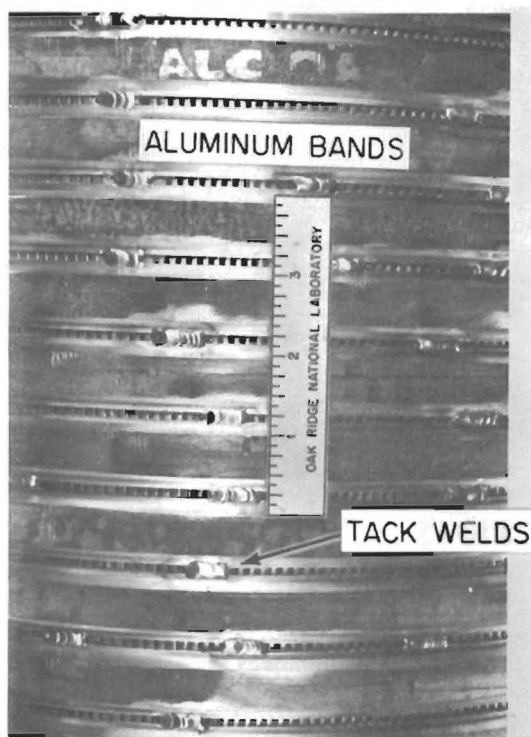


Fig. 5. View of Joint Preparation and Welds Used to Attach the Last Five Plates to the Inner Tubular Side Plate of the HFIR Fuel Element.



CLOSE-UP OF GROOVE PREPARATION PRIOR TO WELDING



CLOSE-UP OF PARTIALLY WELDED ELEMENT



VIEW OF COMPLETELY WELDED ELEMENT

Fig. 6. Steps Involved in Welding the Outer Edges of the Bent-Lip Fuel Plates into a Rigid Fuel Element.

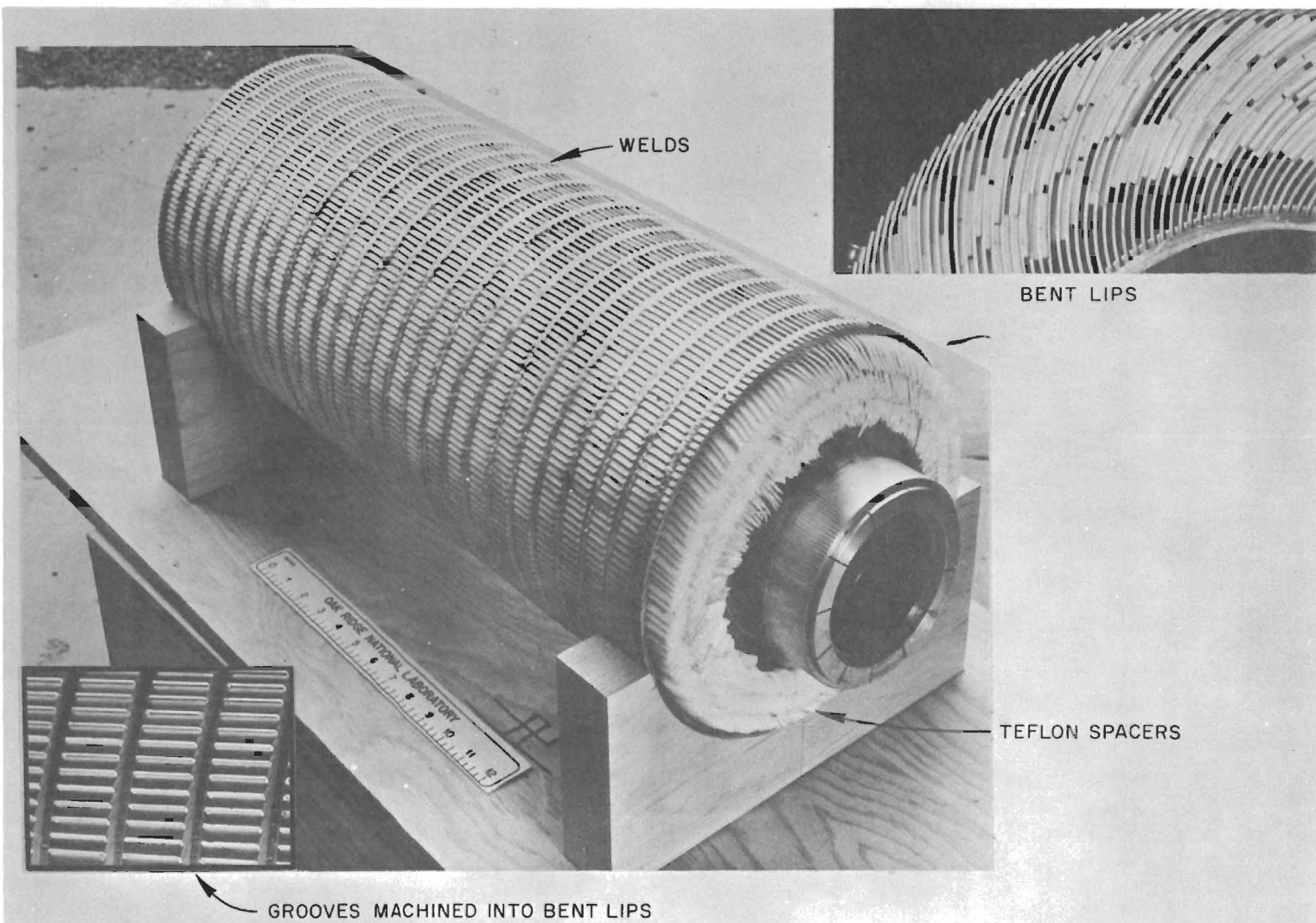


Fig. 7. View of a Bent-Lip Fuel Element Made by a Simplified Assembly Procedure. Machined grooves (shown in close-up) are made prior to welding. No aluminum bands are needed in this fabrication method.

Aluminum bands were not required in the second method. Both manual and automatic welding procedures have been used to make the welds. Following the welding step, the outer surface of the annulus was machined to a true cylinder and an outer tube and associated end fittings were installed to complete the assembly.

Some difficulty was experienced in placing the bent-lip fuel plates into exact involute positions and holding them in the involute position during the outside welding operation. This difficulty was overcome by a unique jiggling technique, illustrated in Fig. 8, involving 0.050-in.-thick "Teflon"* spacer strips placed the full length of the coolant channels between adjacent fuel plates. The spacers tend to be self-lubricating and can therefore be readily slid into and removed from the channels of the assembled element. After the Teflon was installed, stainless steel compression bands were placed around the outer circumference to reduce the diameter, thereby forcing the fuel plates against the Teflon and establishing uniform channel spacing.

In the as-assembled condition (Fig. 8a) many channels were obviously out of tolerance; Fig. 8b shows the Teflon installed; and Fig. 8c shows the greatly improved element after welding. While single narrow strips of Teflon installed adjacent to the outer bent edges of the fuel plates were generally found to be sufficient to locate the plates in the involute positions, two or three wide strips were required to make the assembly sufficiently rigid to withstand the tangential welding shrinkage. For example, tangential shrinkage of only 0.001 in. in the weld between each adjacent fuel plate edge in an outer annulus assembly would result in a total diametral shrinkage greater than 0.1 in. Rotation of the outer side plate from shrinkage would result in a change in the incident angle between the fuel plates and the side plate. Such shrinkage and rotation would encroach upon the diametral tolerance requirement and would seriously affect the nominal channel width adjacent to the outer fuel plate edges.

*A polytetrafluoroethylene plastic marketed by E. I. du Pont de Nemours and Company, Inc.

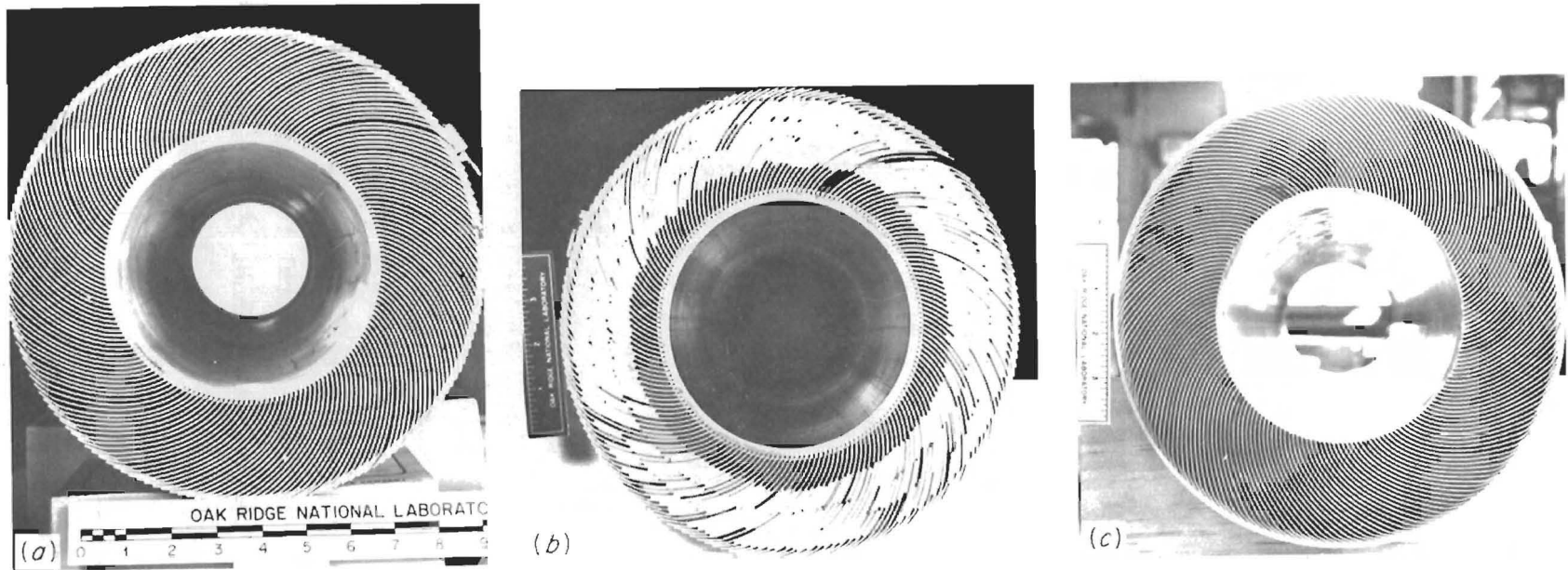


Fig. 8. End Views of an Inner Annulus Showing the Channel Spacing Control Obtained with Teflon Strips (a) As-Assembled, (b) With Teflon Installed, and (c) After Welding With Teflon Removed. The irregular channel spacings present in the as-assembled condition were corrected by this technique.

Since experience in fabricating early test assemblies had indicated that the bent-lip portions of the fuel plates could not be depended upon for overcoming this shrinkage, Teflon strips have been used in subsequent units. Excellent control of both channel spacing and diametral shrinkage was obtained. For example, the diametral weld shrinkage experienced was less than 0.010 in. on the 10-in. OD of the inner annulus assembly and approximately 0.025 in. on the 17-in. OD of a similar outer annulus assembly. The channel width control obtained is discussed in a later section.

Fabrication Procedures Developed for the All-Welded Design

After preliminary design studies and exploratory welding experiments, an all-welded fuel element design of the type shown in Fig. 9 was proposed. A typical annulus would consist of two grooved concentric (outside and inside) support tubes. Fuel plates would be installed between the concentric tubes and attached to them by circumferential welds at intervals along their length.

The preliminary study and welding experiments indicated the following:

1. Little or no diametral contraction would occur as a result of weld shrinkage. The transverse cross-sectional area of the weld or area causing shrinkage (illustrated in Fig. 9) was small in comparison with the cross-sectional area of the supporting tube wall. If desirable, additional support may be achieved by making the wall oversize in thickness. After welding, the outside and inside of the annulus would both be machined to the final dimensions.

2. The overall length of the support tubes shrinks a reproducible amount (approximately $\frac{1}{4}$ in. total). Shrinkage of this order of magnitude would be expected since the amount of tube wall available for support in the weld area is small in comparison with the size of the weld deposit.

3. The fuel plate length would not be changed, measurably distorted, or rippled by the longitudinal contraction of the support tubes if the correct welding procedure were used.

4. By using a proper weld groove geometry, adequate pull-out strength of the weld joint could readily be obtained. Further improvements in

FUEL PLATES BETWEEN
CONCENTRIC GROOVED TUBES

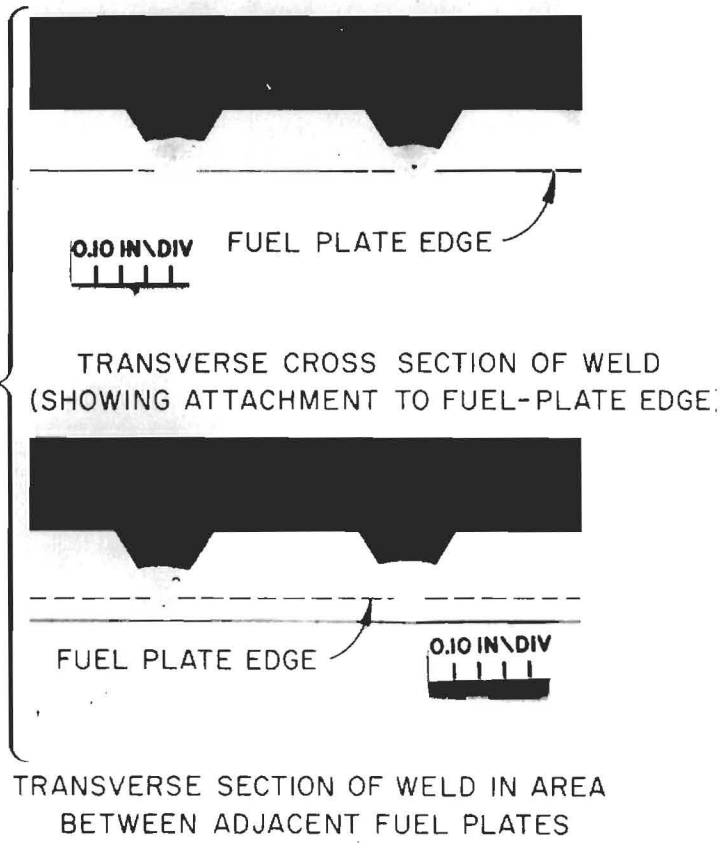
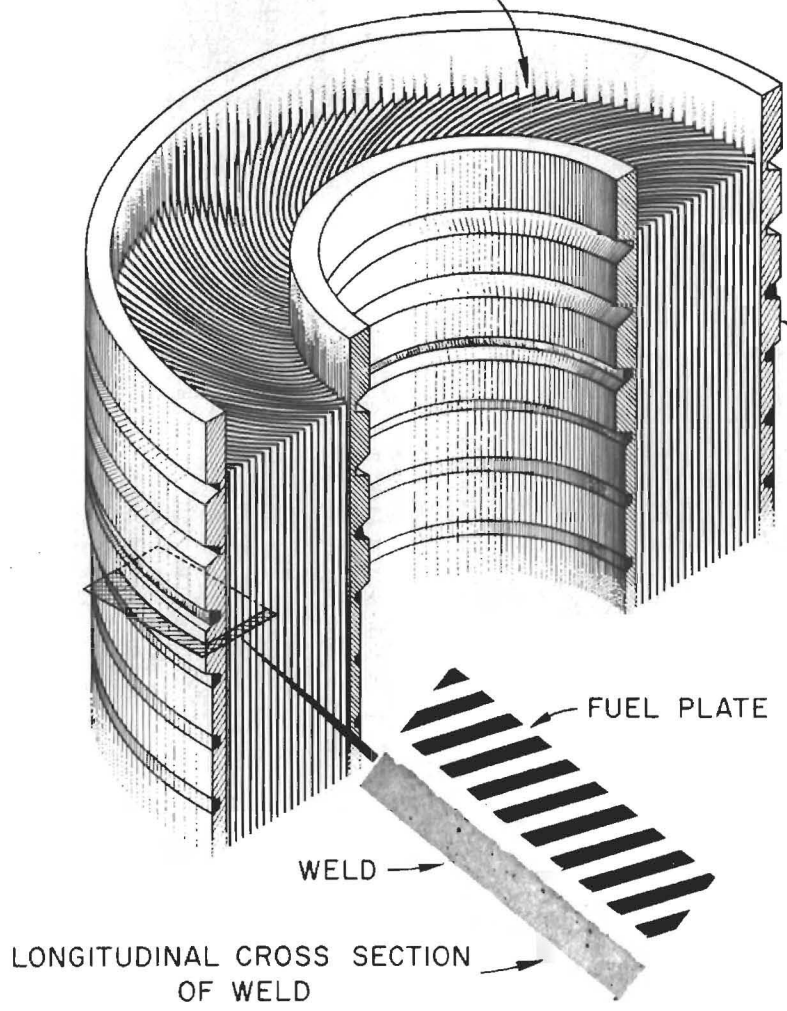


Fig. 9. The "All-Welded" Concentric Support Tube Fuel Element Concept. The fuel plates are slid between the support tubes and are rigidly attached to these tubes by circumferential welds.

joint strength could be made by increasing the overlap of the plate slot and weld groove, thereby causing the fuel plate edge to protrude deeper into the weld. Also the bottom width of the weld groove could be increased in order to increase the total length of the fuel plate edge which would be joined.

5. The residual hoop stress in the welds at any position around the circumference of the annulus would be uniform and, therefore, would not affect the roundness of the support tubes.

Areas of unknown problems, however, were also indicated by the preliminary investigation. Some difficulty was experienced with the concentric positioning of the grooved support tubes and with the fuel plate assembly steps. The subsequent welding operation precluded the use of nonvolatile lubricants to overcome galling between the fuel plate and the groove. Also, automatic gas-metal arc-welding equipment small enough for making the inside welds was not readily available. An assembly fixture, a rotating fixture for welding, and a special welding torch capable of welding inside the 5-in. ID of the inner annulus were therefore designed and procured.

In order to fully evaluate and demonstrate the feasibility of the design, an unfueled outer annulus was manufactured as shown in step sequence in Fig. 10. After the outside and inside support tubes were scrupulously cleaned of all oils and loose chips, they were installed concentrically in a Lucite assembly jig (left side of Fig. 10). The assembly jig was designed and constructed to rigidly align the support tubes to within 0.005 in. of concentricity. Involute curved fuel plates were then slid into place using a volatile camphor-alcohol mixture as a lubricant. All 369 fuel plates were installed without difficulty in approximately 2 hr. The assembled fuel element was heated in a ventilated oven to remove any residual lubricant. Teflon spacer strips were then installed for channel spacing control (center of Fig. 10). The fuel element was then positioned in the welding fixture and both inner and outer circumferential welds made using a new low-energy automatic gas-metal arc-welding process. The photograph on the right of Fig. 10 shows the fuel element after welding.

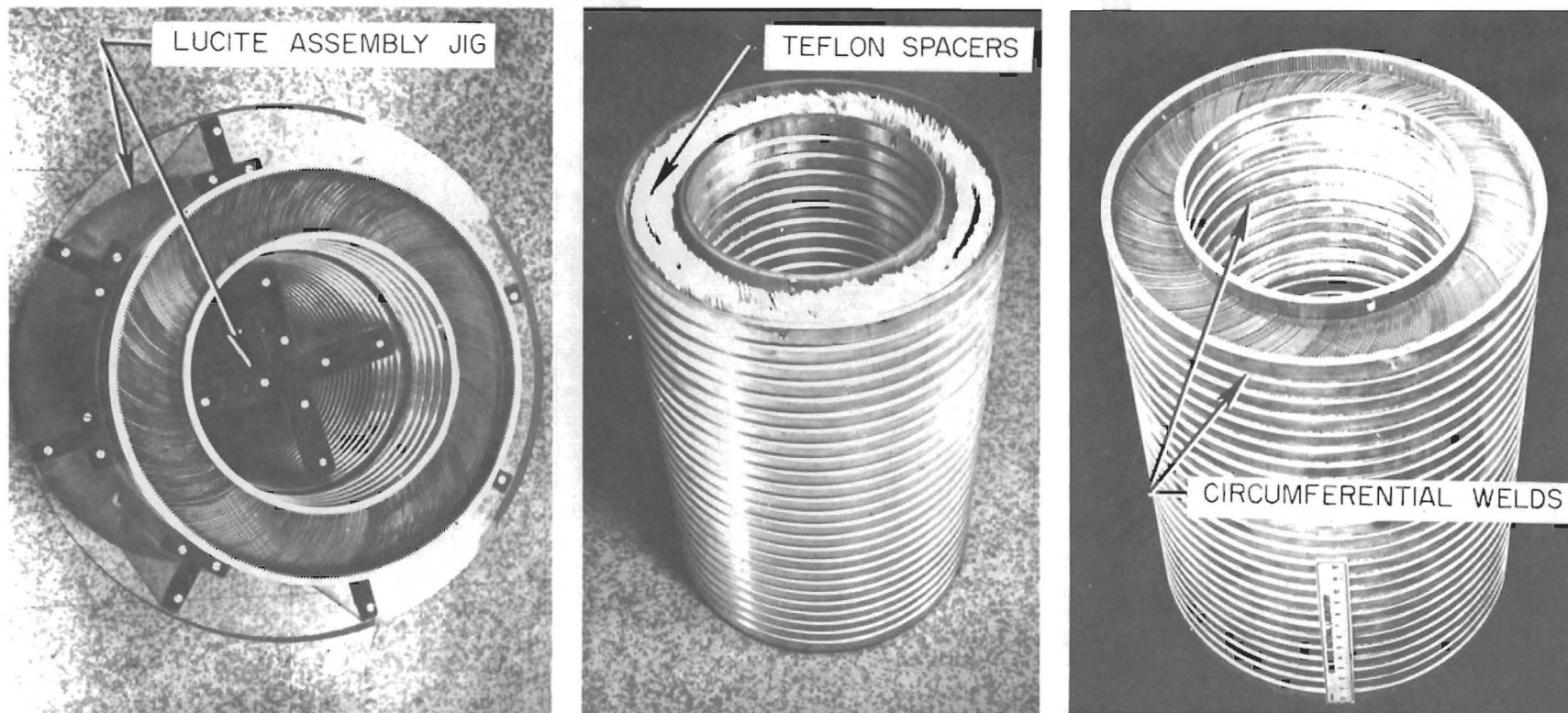


Fig. 10. The Manufacture of an "All-Welded" Fuel Element in Step Sequence. (1) The fuel plates were installed between grooved concentric support tubes, (2) Teflon channel spacers were inserted for dimensional control during welding, and (3) the fuel plates were attached to the support tubes by circumferential welds.

The automatic welding setup is shown in Fig. 11 and consists of a variable-speed motor-driven rotating fixture, a conventional gun for outside welding, and a special torch for inside welding. The gun used for making the outer circumferential welds is commercially available and was operated from the welding control panel shown in the photograph. A close-up view of the special inside welding torch is shown in Fig. 12. The consumable-electrode wire is pulled from a spool container (attached to the rear of the torch beam) around a 90-deg bend by drive rolls (located in the torch) and is pushed through the contact tip immediately above the weld groove. The special torch was designed specifically for welding inside the 5-in. ID of the inner annulus, but was also used successfully for welding inside the 10-in.-ID tube.

As previously mentioned, this equipment was also used in fabricating assemblies involving the bent-lip fuel plate design. The commercially available welding torch was used in making the outside circumferential welds, while the special torch was used in making the short inner plug welds.

No unforeseen difficulty was encountered during welding; however, some diametral shrinkage did occur. The outside diameter of the annulus was 0.015-0.020 in. smaller after welding while the inside diameter changed less than 0.010 in. It is worth noting that the inner support tube was 0.060 in. out-of-round on one end in the as-received condition. The tube was forced into roundness when installed in the Lucite assembly fixture and was held round by end fixtures during the subsequent welding steps. When the end fixtures were removed after welding, the tube was found to be within the ± 0.005 -in. tolerance requirement. A special welding sequence was required for the circumferential welds to minimize plate distortion and to prevent shrinkage of the fuel plate length. In the case of both the inside and outside welds, the circumferential joints located at the center line of the annulus were made first. The adjacent welds were made next, and the sequence was followed until all welds were completed. This sequence permitted the support tube to contract in length during each weld without materially affecting the length of the fuel plate.

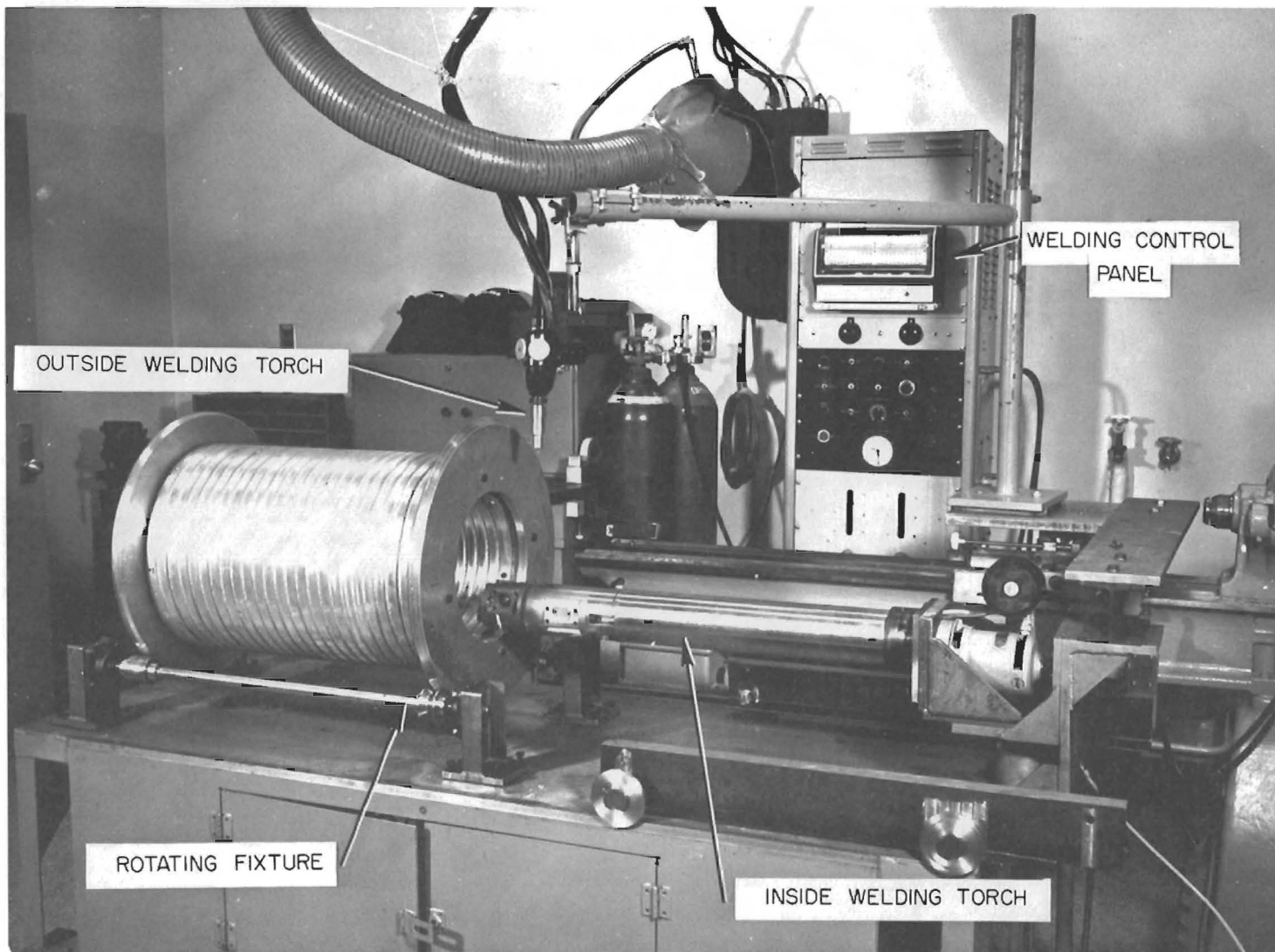


Fig. 11. The Automatic Welding Setup Consisted of a Variable-Speed Rotating Fixture, a Conventional Gas-Metal Arc Gun for Outside Welding, and a Special Torch for Inside Welding.



Fig. 12. A Close-Up View of the Special Gas-Metal Arc-Welding Torch Required for Inside Welding.

Each of the outside welds required approximately $1\frac{3}{4}$ min to complete, and the inside welds required about 1 min, each using a 30 in./min tangential travel speed.

The Segmented Element Design

The roll-swaging method, shown in Fig. 13, also utilizes grooved inner and outer support tubes. Fuel plates are installed individually between correctly positioned tube segments and are attached by roll swaging to both grooved outside and inside support tubes. The roll-swaging wheel moves along the length of the fuel plate so as to displace metal from the groove edge and press it into the fuel plate as shown in the enlarged cross-sectional view of Fig. 13. It is interesting to note that the enlarged view of the joint cross section is very similar in appearance to the peened joint. However, a guide groove for the swaging wheel helps to eliminate much of the alignment problem experienced with the peening method.

Joint Evaluation and Dimensional Inspection

Each of the fuel element designs was evaluated on the basis of joint strength and dimensional control. In the case of each joining method investigated, the pull-out strength of the joint was determined and all methods easily exceeded the 100 lb/linear in. requirement. The geometry of the joint was made as realistic as possible so the force required to remove the fuel plate was indicative of the pull-out joint strength.

The method used to establish the as-built plate spacing tolerances is discussed elsewhere.² In the case of each annulus evaluated, 21 spacing measurements were obtained at three radial and seven axial locations from each water channel. With an inner annulus containing 171 channels and an outer annulus containing 369 channels, a complete element involves 11,340 individual spacing measurements. The tolerance on the spacing measurements required that (1) all spacing measurements be 0.050 ± 0.010 in. and (2) the average channel width at any axial location be 0.050 ± 0.006 in.

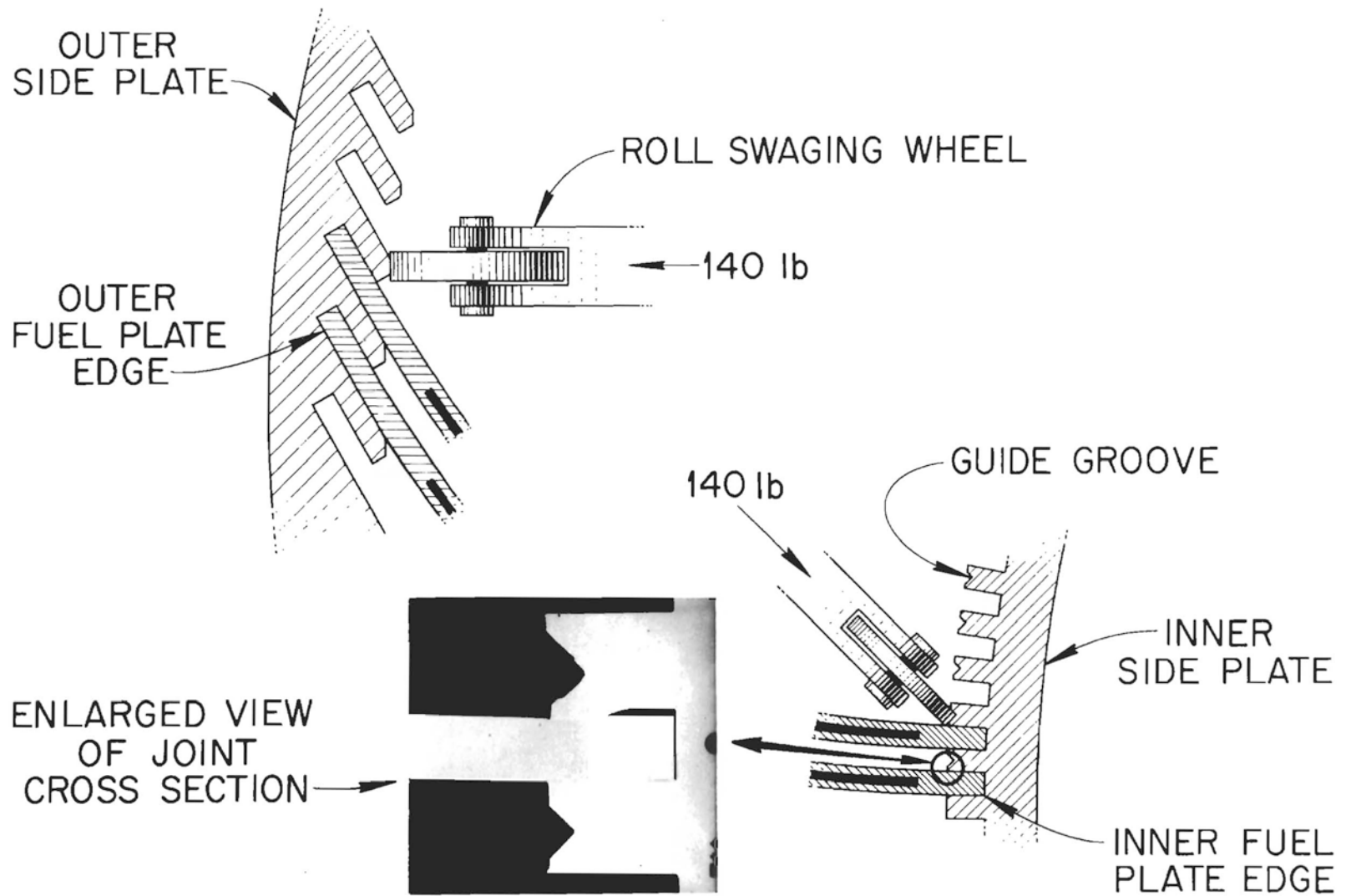


Fig. 13. Roll-Swaged Attachment Process Used in Segmented HFIR Fuel Element Concept.

To give some idea of the tolerances that can be obtained, the inner annulus* of the fuel element for the reactor mockup facility which is shown in Fig. 14 had the following as-built plate spacing tolerances:

- (1) all individual measurements were within 0.050 ± 0.006 in., and
- (2) all average channel widths were 0.051 ± 0.002 in.

In summary, it can be said that suitable fabrication procedures for each of the three potential fuel element designs have been developed. In the process of constructing the various fuel element components, it has been demonstrated that the rigid tolerance requirements imposed by the design criteria can be met. Future work will include an additional evaluation of all three concepts in order to determine the design most suitable for production.

Acknowledgments

The authors would like to acknowledge G. M. Adamson, R. J. Beaver, G. Goldstein, R. Knight,** and R. Shooster of the Metals and Ceramics Division who made immeasurable contributions to the overall HFIR fuel element development program. The craft assistance of the Engineering and Mechanical Division Shops in the preparation of fuel element components was very instrumental in the success of this program.

References

1. M. M. Martin et al., "Fabrication Development of the Involute-Shaped HFIR Fuel Plates," given elsewhere in this report.
2. R. W. McClung, "Nondestructive Testing on HFIR and ATR Fuel Elements," presented elsewhere in the report.

*The fabrication procedure used in manufacturing this inner annulus assembly has been previously described in Figs. 7 and 8.

**On loan from Engineering and Mechanical Division.



Fig. 14. Photograph of the Completed Fuel Element Constructed for the HFIR Mockup.

FABRICATION DEVELOPMENT OF THE ADVANCED TEST REACTOR
FUEL ELEMENT

R. L. Heestand and C. F. Leitten, Jr.*

R. W. Knight**

Abstract

At the Oak Ridge National Laboratory (ORNL), a program is under way to develop techniques for manufacturing fuel elements for the Advanced Test Reactor (ATR). The operational characteristics of the reactor impose rigid requirements on the integrity and radiation stability of the elements. To meet these requirements, aluminum-base dispersions containing U_3O_8 were selected as the fuel system. Mechanical strength and corrosion resistance are achieved by hermetically sealing the dispersion in either type X8001 or 6061 aluminum.

Due to the wide range of dimensional requirements which necessitated the development of the 19 fuel plates, the ATR has provided a unique opportunity for investigating fabrication variables. The 49 1/2 in. fuel plate length is greater than that normally encountered, and plate widths vary from 2.221 to 4.055 in. Dimensional requirements were met by varying the initial compact thickness, using compacts in tandem, and cross rolling to obtain the desired widths. The effect of these fabrication parameters on plate quality is discussed. Plates were formed to the required radii by a modified marforming technique and mechanically assembled into the element array by roll swaging. Dimensional inspection of the experimental fuel plates and elements indicate that fuel elements of high quality can be produced by the above techniques.

*Oak Ridge National Laboratory, Oak Ridge, Tennessee.

**On loan from the Engineering and Mechanical Division.

Introduction

The Advanced Test Reactor (ATR) under construction at the National Reactor Test Station was designed primarily to provide additional experimental loop irradiation space for the various Atomic Energy Commission (AEC) testing programs.¹ The Oak Ridge National Laboratory (ORNL) is supporting the design effort at Babcock and Wilcox and has the responsibility of developing the fuel element technology.

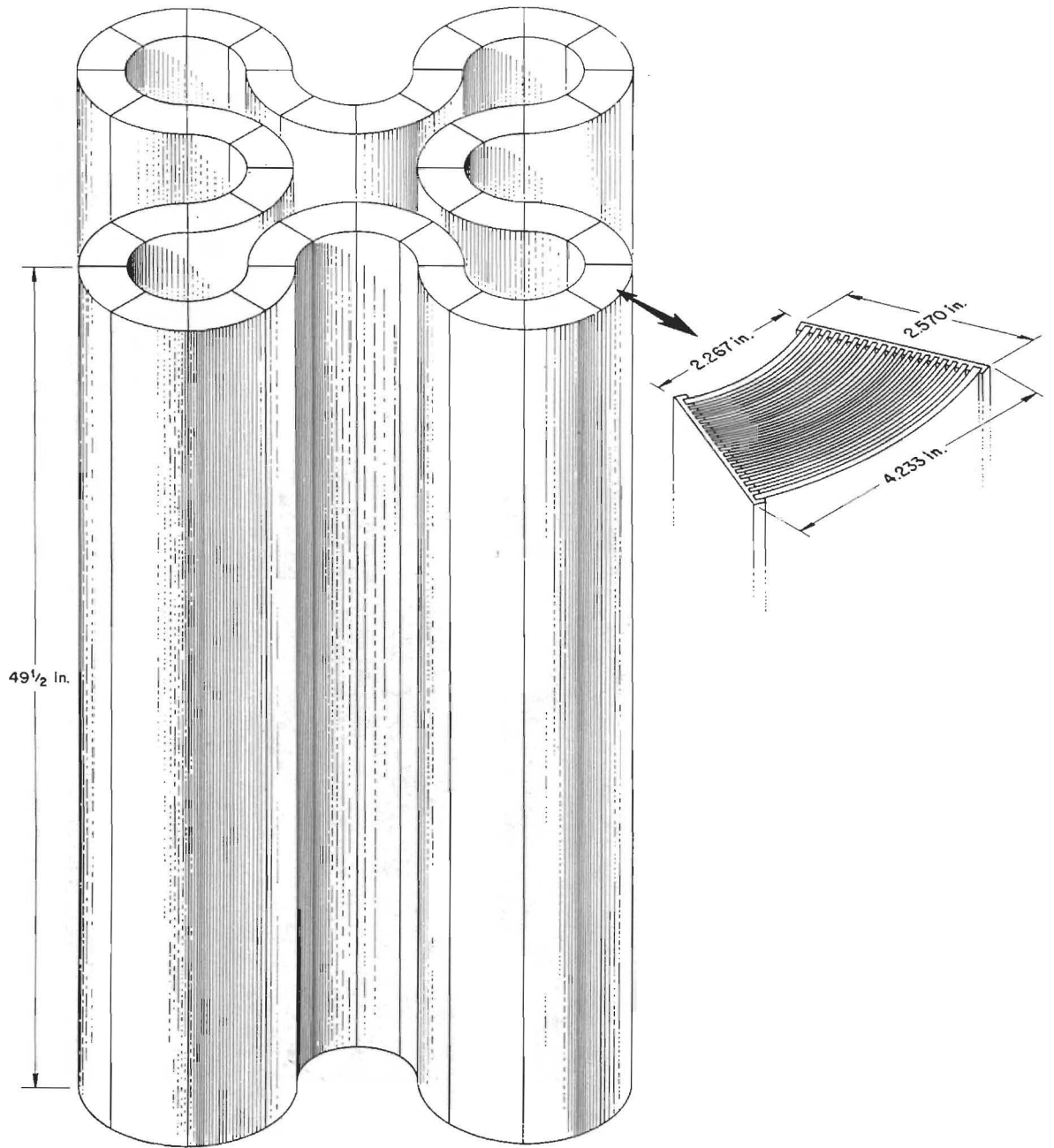
The core configuration of the ATR, as schematically shown in Fig. 1, provides for nine flux traps for experimental loops. The fuel array consists of 40 individual 45-deg wedge-shaped elements, over four feet in length, which are interchangeable in regard to location within the core assembly.

Although the feasibility of fabricating fuel elements similar in design has been demonstrated previously, a number of unique fabrication problems are encountered in manufacturing the ATR fuel elements.

The unusual length of the fuel plates require stringent process control to meet the core straightness specifications. The geometry of the ATR element requires the development of 19 plates which differ in both width and radius of curvature, in contrast to the usual need for one repetitive plate. Forming of the plates to the specified radii was of particular concern because each plate must be formed independently. Thus variations in the forming behavior of the plates will directly affect the water-channel spacings in the assembled elements. Such effects are compensating in fuel elements assembled from identical plates.

Fuel Element Specifications

The conceptual design of the ATR fuel element is illustrated in Fig. 2. The fuel element contains 19 plates, 49 1/2 in. long and varying in width from 2.221 to 4.055 in. In order to achieve a uniform water-channel spacing of 0.078 in., each plate must be formed to a different specified radius to close tolerance. Pertinent design specifications as well as tolerances for the element and fuel plates as set forth in the conceptual design are listed in Table 1.



ATR Core Assembly.

Fig. 1. Advanced Test Reactor Core Assembly.

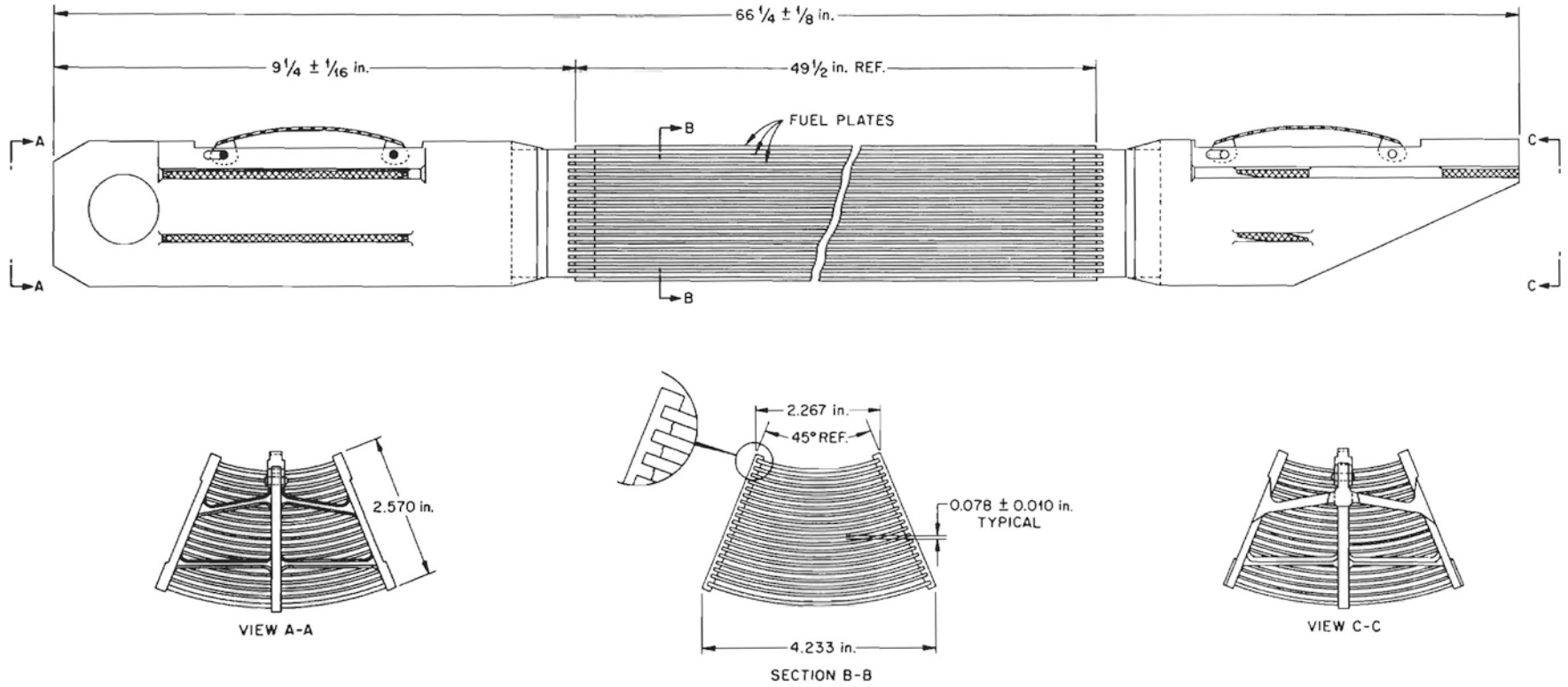


Fig. 2. Conceptual Design of the Advanced Test Reactor Fuel Element.

Table 1. Tentative Design Specifications and Tolerances
for the Advanced Test Reactor Fuel Components

	<u>Specification</u>	<u>Tolerance</u>
Overall fuel plate size, in.		
Length	49 1/2	±1/32
Width	2.221 to 4.055	±0.002
Thickness		
Inner plate	0.050	±0.001
Outer plate	0.080	±0.001
Number of elements	40	
Number of plates per element	19	
Fuel section size, in.		
Length	48	±0.375
Width (average)	1.770 to 3.60	±0.080
Thickness	0.020	±0.001
Minimum fuel plate edge cladding	0.185	+0.080 -0.000
Fuel element loading		
Uranium, g U ²³⁵	750	±1/2%
Enrichment, % U ²³⁵	>93	
Burnable poison - boron, g	3.2	±2%
Boron enrichment	natural	
Core composition	34 wt % U ₃ O ₈ -0.15 wt % B ₄ C-bal type X8001 Al	
Fuel plate radius, in.		
Minimum width plate	3.043	±1/16
Maximum width plate	5.337	±1/16
Material		
Cladding	Type X8001 or 6061-0 Al	
Frame	Type X8001 or 6061-0 Al	
Side plate	Type 6060-T6 Al	

Material Selection

The design specifications of the ATR dictate rigid control on the quantity of fuel and burnable poison contained in the fuel element. To achieve this requirement, a dispersion-base fuel was selected as the core material for the individual plates. In contrast to conventional alloy fuels, dispersion fuels provide excellent reproducibility of the uranium and boron contents in the fuel plates as well as close control of the homogeneity within an individual plate. Incorporation of the fuel by the dispersion route also potentially affords improved radiation performance. The core material selected for the fuel plates consists of a

dispersion of 34 wt % U_3O_8 and 0.15 wt % B_4C in a matrix of aluminum powder. Type X8001 aluminum powder was selected as the matrix material on the basis of ease of fabrication and good corrosion resistance.

Two aluminum alloys, each with a specific advantage, were selected as possible cladding materials. Type X8001 aluminum was given prime consideration due to its excellent corrosion resistance at the fuel element operating temperature. Type 6061-0 aluminum was selected as an alternate material based on the strength of this alloy at the fuel element operating temperature; ultimate selection of the cladding material will depend upon establishing which criterion is more important for satisfactory operation.

Fuel Plate Fabrication

The basic scheme developed for fabricating the ATR fuel plates is illustrated in Fig. 3. The fuel dispersions were prepared by a standard powder metallurgy technique of weighing, dry blending, and cold pressing. After blending for 3 hr in an oblique-type blender, the powders were compacted in a double-acting die at 33 tsi pressure. The powder metallurgy compacts were assembled into billets using the "picture-frame" technique as illustrated in Fig. 4. Cover plates were tack welded in place and the billet was hermetically sealed by hot rolling at 500°C to the desired thickness. After blister annealing at 500°C, the fuel plates were dimensionally sized by cold rolling, annealed at 500°C, radiographed, marked and sheared, edge machined, and inspected.

Fabrication of reactor fuel plates by conventional procedures would dictate independent tooling for the production of each type of plate required. Because of the number of differently shaped fuel plates required for the ATR, the time required and cost of such tooling would be prohibitive for the development program. To circumvent this problem, techniques were developed for fabricating the various plates using a minimum of tooling. By utilizing the parameters shown in Table 2, the 19 different fuel plate geometries were satisfactorily fabricated using only three powder metallurgy dies. The individual frames were prepared by broaching, which significantly reduced the machining cost.

FABRICATION SEQUENCE

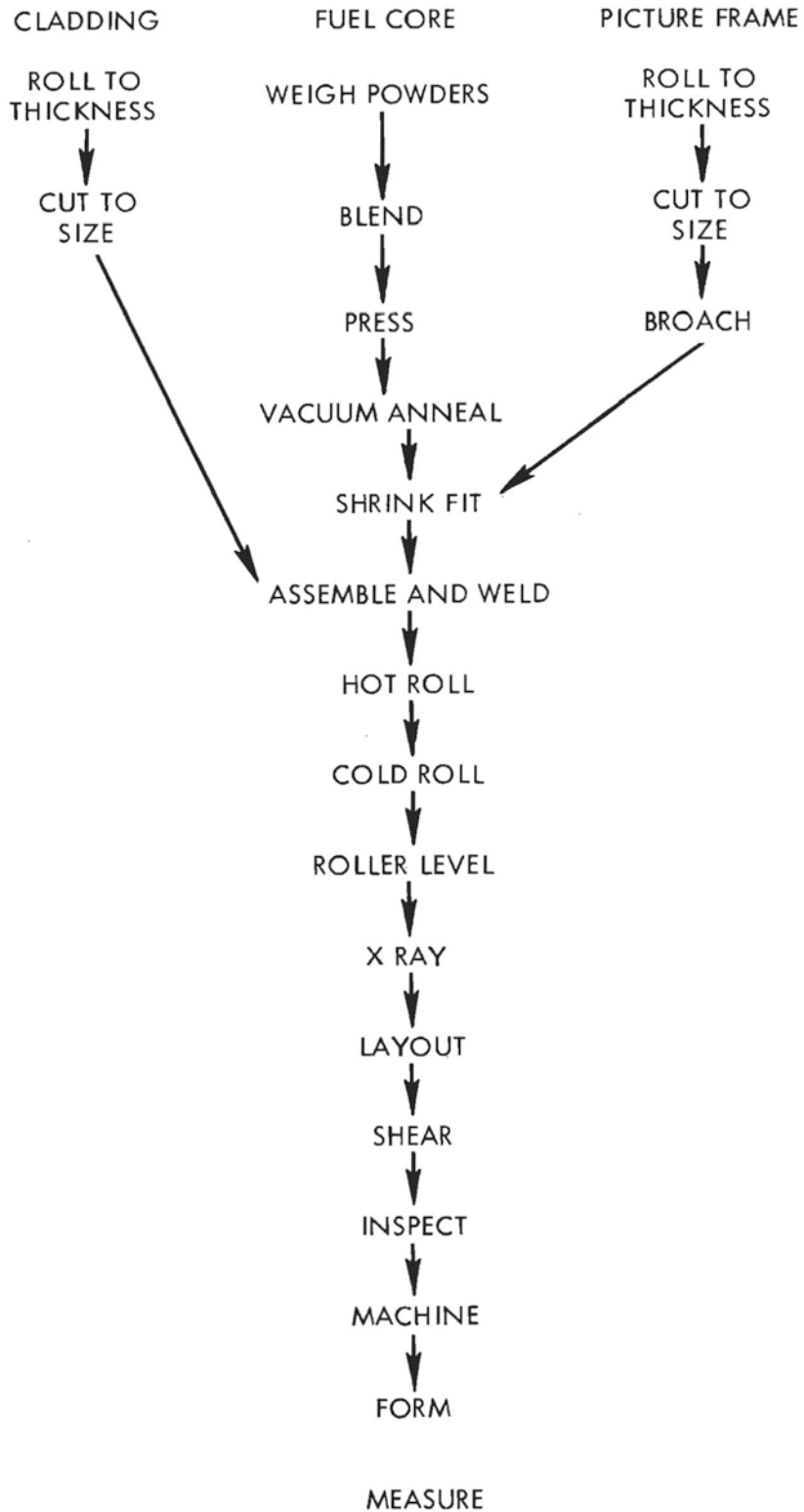


Fig. 3. Fuel Plate Fabrication Sequence.

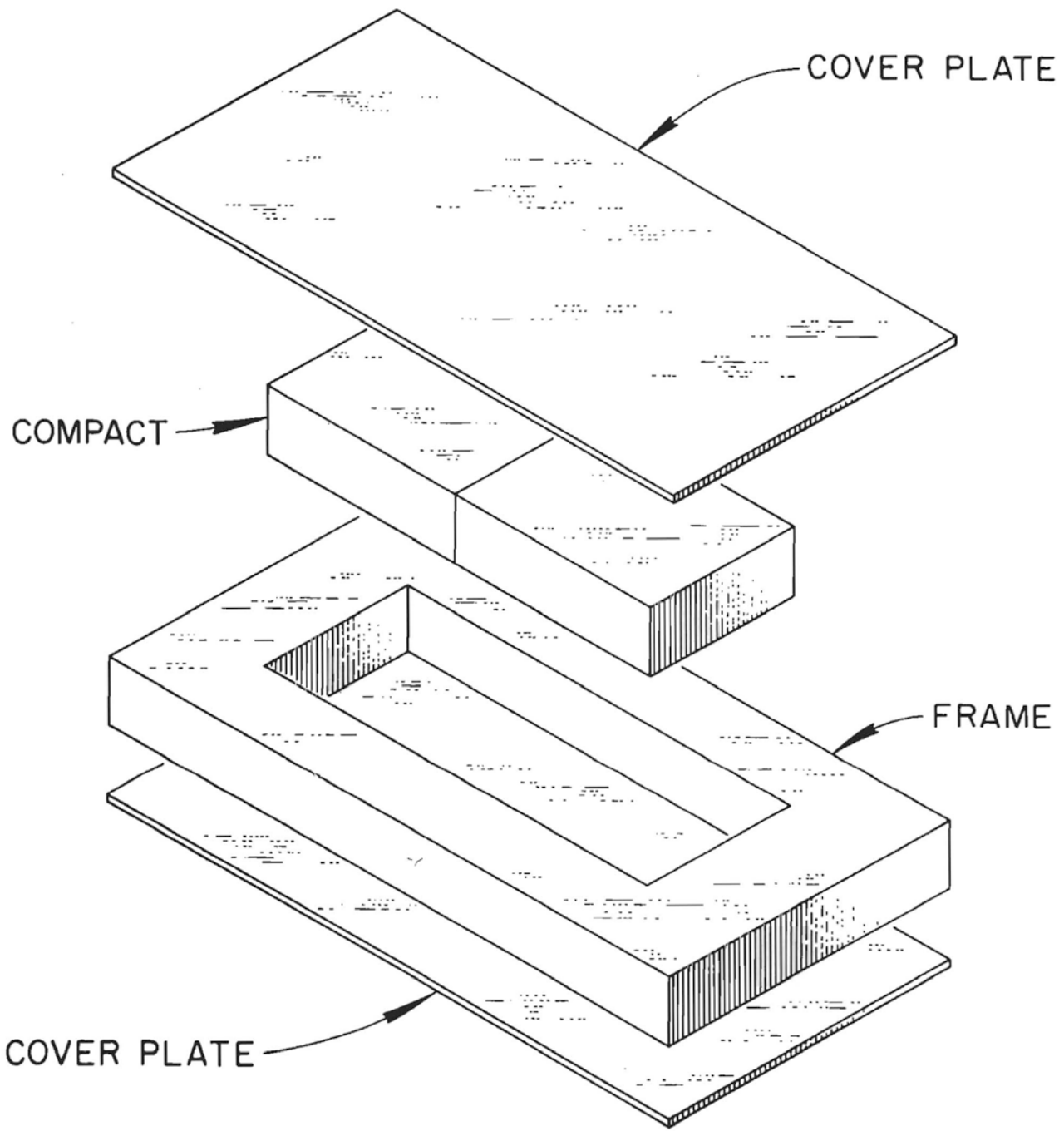


Fig. 4. Fuel Plate Billet Assembly.

Table 2. Advanced Test Reactor Fabrication Parameters

Reduction ratios	9/1 to 18/1
Cross rolling	0 to 25%
Core thickness	0.188 to 0.360 in.
Core widths	1.660 to 3.475 in.
Fuel widths	1.823 to 3.636 in.
Cores per frame	Single and tandem
Cladding materials	Types X8001 and 6061 Al

The cross rolling was performed after the billet received an initial hot reduction in the normal rolling direction. Deviating from conventional fabrication practices by incorporating cross rolling proved to be a satisfactory technique to reproducibly fabricate plates with different fuel section widths. Dimensional examination of numerous fuel plate radiographs indicated that the fuel core width was controlled within the required tolerance of ± 0.080 in.

Metallographic evaluations were conducted to determine the effect of cross rolling on the transverse edge characteristics of the fuel core in plates roll clad at various reduction ratios with types X8001 and 6061-0 aluminum. The core edge in plates roll clad with type X8001 aluminum was concave. The degree of concavity was found to increase primarily with the reduction ratio. Although cross rolling did effect the core edge characteristics, the overall contribution was insignificant. Figure 5 illustrates the typical concave appearance of the fuel core edge in type X8001 aluminum-clad plates rolled at 9 to 1 and 18 to 1 reduction ratios. It should be noted that the plate rolled at the high reduction ratio also was cross rolled 15%. Edge effects of the magnitude shown in this figure are acceptable.

A difference, as shown in Fig. 6, was noted between the fuel core edge characteristics in plates roll clad with types X8001 and 6061-0 aluminum. The core edge in the type 6061-clad plate appears relatively straight in contrast to the concave edge noted in the type X8001-clad plate. Both plates were roll clad at a 12.5 to 1 reduction ratio

Y-46384



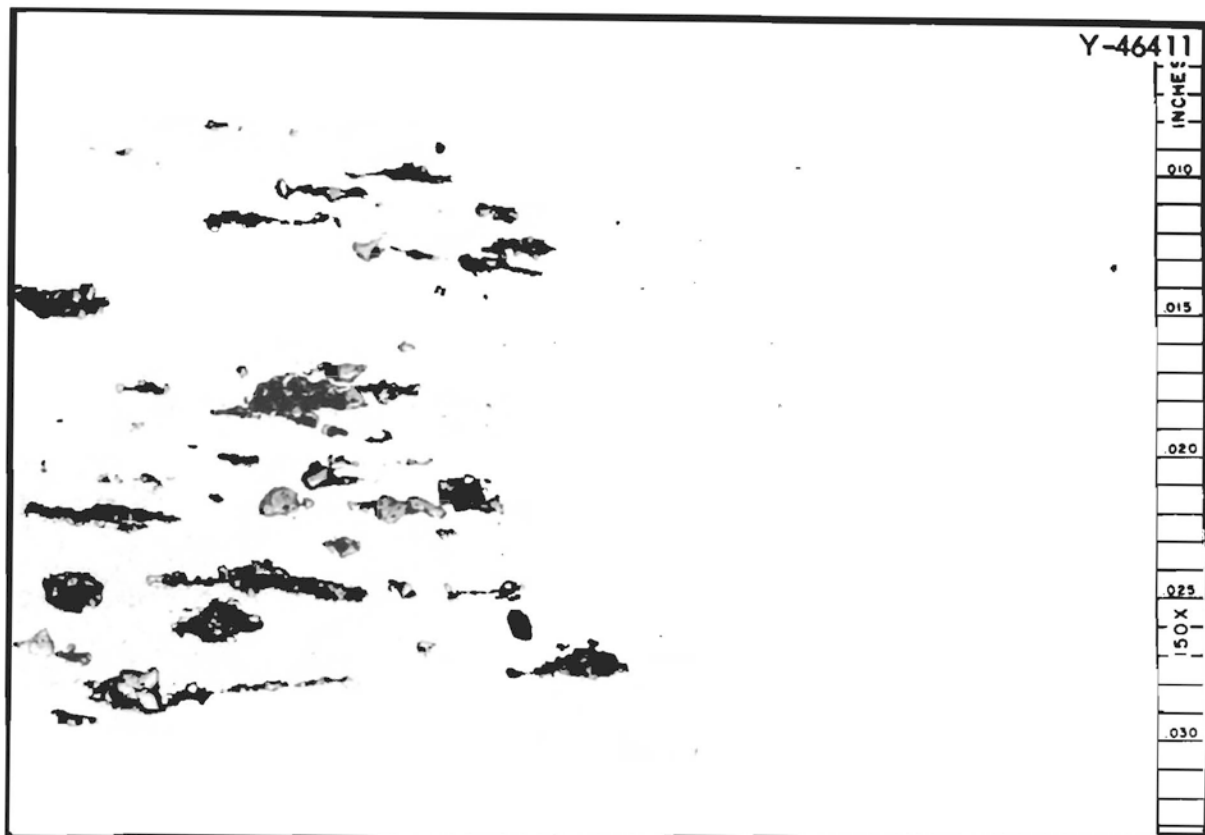
Plate 5 - 9/1 Reduction Ratio. No Cross Roll. Type X8001 Core and Clad.

Y-46366



Plate 4 - 18/1 Reduction Ratio. 15% Cross Roll. Type X8001 Core and Clad.

Fig. 5. Effect of Reduction Ratio and Cross Roll on Fuel Edge Characteristics. As-polished. 150X.



Type X8001 Aluminum Core and Clad



Type X8001 Core - Type 6061 Clad

Fig. 6. Effect of Cladding Material on Fuel Edge Characteristics.

and received 25% cross rolling. It should be noted that the cross rolling did not significantly affect the shape of the core edge in the type 6061-0-clad plate. Similar differences were not noted in the fuel core end characteristics. As shown in Fig. 7 the amount of fuel core tapering (approximately 0.30 in.) is essentially the same with both of the cladding materials. It is interesting to note that the degree of tapering did not increase with the reduction ratio as would normally be expected. Since the fuel plates fabricated at the higher reduction ratios (>9 to 1) also receive 25% cross rolling, cross rolling may have reduced the overall fuel core end effect.

In examining the fuel plate radiographs for dimensional control of the fuel section, it was noted that the straightness of the core within the plate varied with thickness in the initial powder metallurgy compacts. This effect was further substantiated by grading a series of compacts according to thickness variations and dimensionally examining radiographs of the resultant plates. It was found that transverse variations in compact thickness in excess of 0.003 in. resulted in excessive core bowing. To achieve this pressed-compact thickness tolerance, extreme care was essential in leveling and cold pressing the powder metallurgy dispersions.

Typical examples of the metallurgical bonding achieved in roll cladding the dispersion fuels with both types X8001 and 6061 aluminum can be seen in Fig. 8. To assure reproducible metallurgical bonding in the type 6061 aluminum-clad fuel plates, the mating surfaces of the frames and cover plates were preclad with approximately 0.003 in. of type 1100 aluminum. No difficulties were encountered in achieving reproducible metallurgical bonds in the type X8001 aluminum-clad fuel plates. Vacuum degassing the fuel compacts at 600°C prior to billet assembly essentially eliminated core-gas blistering from both type plates.

Evaluations were made of the fuel homogeneity within various fabricated fuel plates. Chemical analyses of randomly selected samples ranging from 0.090 to 0.250 in. in diameter showed the uranium concentration in the fuel to be uniform within $\pm 15\%$. The uranium concentration did not depend on sample size in the range investigated.

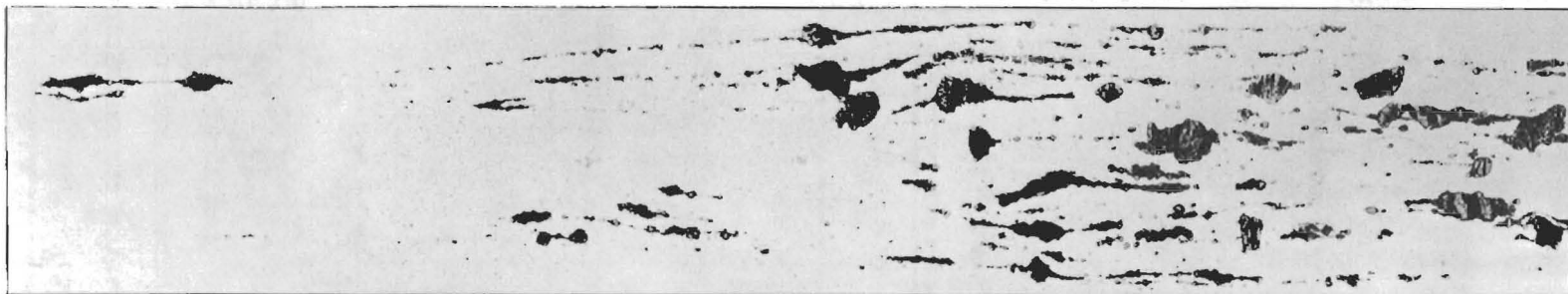


PLATE 5-9,1 REDUCTION RATIO TYPE X-8001 ALUMINUM CORE AND CLAD

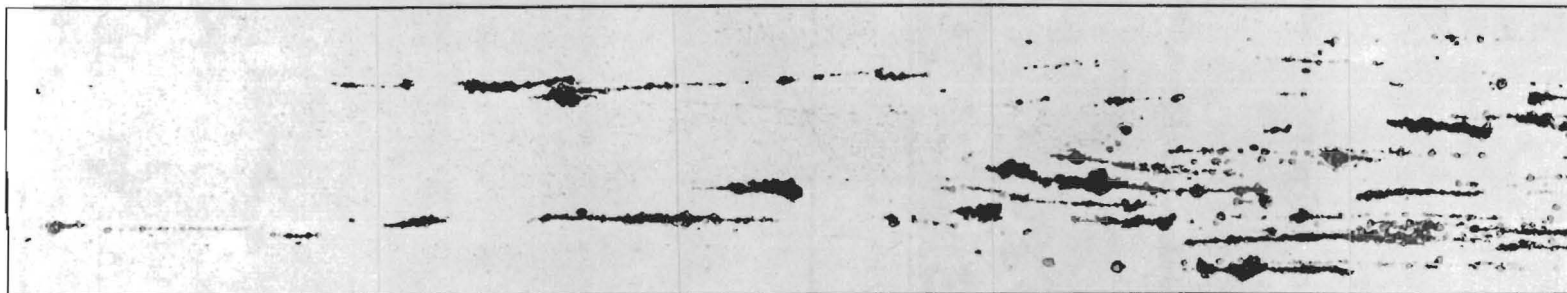


PLATE 12-12.5,1 REDUCTION RATIO TYPE X-8001 ALUMINUM CORE AND CLAD



PLATE 12-C-12.5,1 REDUCTION RATIO TYPE X-8001 ALUMINUM CORE-TYPE 6061 ALUMINUM CLAD

Fig. 7. Fuel Plate End Characteristics.

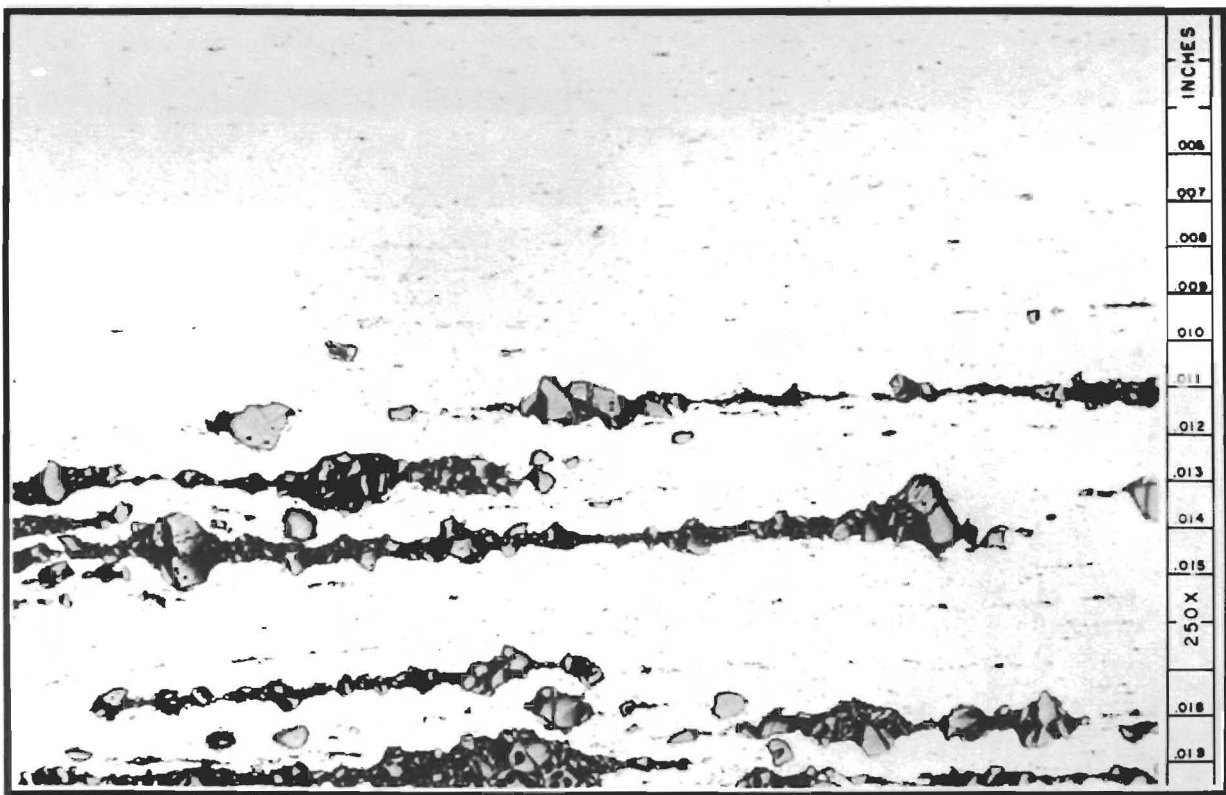


Plate 12 - 12.5/1 Reduction Ratio. 25% Cross Roll. Type X8001 Core - Type 6061 Clad



Plate 12 - 12.5/1 Reduction Ratio. 25% Cross Roll. X8001 Core and Clad

Fig. 8. Comparison of Core-Clad Interface Bonding in Fuel Plates Roll Clad with Types X8001 and 6061 Aluminum.

Fuel Plate Forming

The assembly of the roll-clad fuel plates into the required fuel element array as shown in Fig. 2 dictates reproducible fuel plate curvatures in order to meet the rigid water-channel tolerances. Because of the simplicity of the die design and the ease in which a plate can be formed, a modified marforming technique was adopted as the reference method for forming the ATR fuel plates. As illustrated in Fig. 9, the die basically consists of a conventional die set, in which is positioned a double rubber part and a variable male punch shaped to the desired curvature. Forming is accomplished by positioning a flat plate on the rubber packs and lowering the male punch into the part. To establish the parameters essential for reproducibly forming the various fuel plates, experiments were conducted using commercial types X8001 and 6061 aluminum sheet stock. Forming these materials at approximately 1600 psi pressure has yielded good reproducible plate curvatures. The type 6061 aluminum exhibited greater springback than type X8001.

Since only a limited number of each of the 19 fuel plates have been fabricated to date, insufficient data exist to evaluate the feasibility of forming the fuel plates by this technique. A sufficient number of fuel plates were formed to assemble elements for the thermal and mechanical testing programs. Proper fuel plate radii were achieved by additional hand forming.

To assure success in forming the fuel plates to the required radii, alternate techniques are being explored, such as hydroelectric forming and an improved rubber contained marforming process.

Fuel Element Assembly

The conceptual design of the ATR fuel element required rigid attachment of the fuel plates to assure dimensional stability. Because of inherent advantages, mechanical joining by either peening or roll swaging was selected in preference to mechanical pinning or the conventional brazing process. Exploratory demonstrations of mechanically attaching

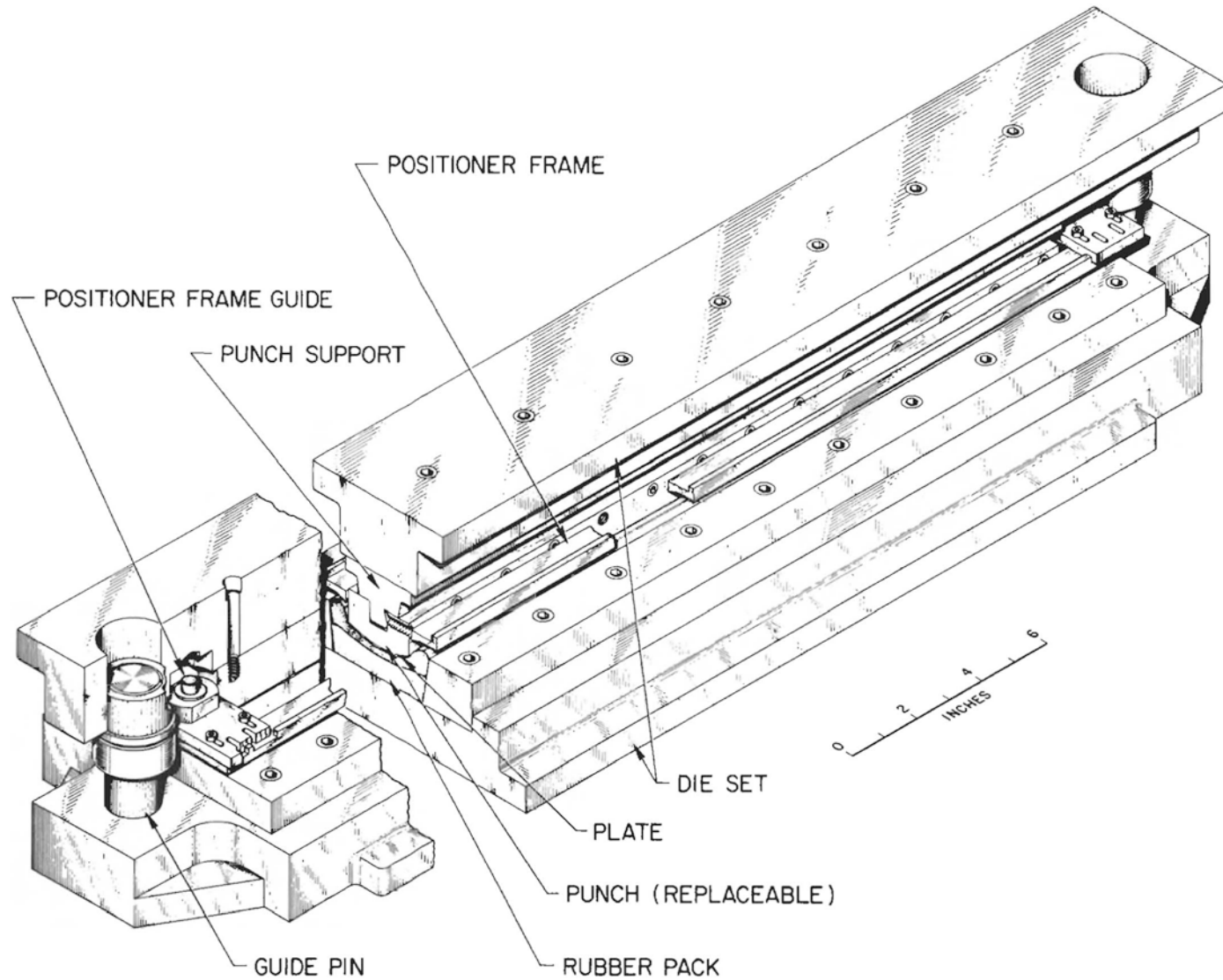


Fig. 9. Advanced Test Reactor Fuel Plate Forming Die.

the fuel plates to the side plates by both peening and roll swaging achieved joint strengths greater than 200 lb/in. Since in all cases more reproducible joints resulted from roll swaging, this method was selected for assembling the ATR elements.

The fuel element was assembled in a fixture adapted to a lathe bed as shown in Fig. 10. In assembly, the side plates were first inserted into the fixture, aligned, and clamped into place. The fuel plates were then inserted into machined slots in the side plates, as illustrated in Fig. 11; and individual plates are attached by rolling a small-diameter wheel under pressure along the length of the side plate immediately above the inserted fuel plate. To maintain alignment in traversing the length of the side plate with the wheel, guide lands were machined to position the swaging wheel. A contact pressure of approximately 140 lb resulted in the most reproducible joints. To achieve maximum thickness and strength in the element side plates, the minimum depth of groove required to securely attach the fuel plates was determined. A depth of 0.070 in. was established as the optimum, based on the strength of the joint and metallographic examination.

Five prototype fuel elements were fabricated to supply fuel elements for the ATR test program. Although the dimensional specifications were not completely met in any of the assemblies, as shown in Table 3, a marked improvement was made as the manufacturing progressed. The improvement in element quality, as manifested by the water-channel spacing measurements, is attributed mainly to the corrections made in the fuel plate radii.

An overall view of one of these test elements equipped with end boxes is shown in Fig. 12. The success in processing these elements clearly demonstrated the feasibility of manufacturing the ATR fuel elements by mechanical joining techniques.

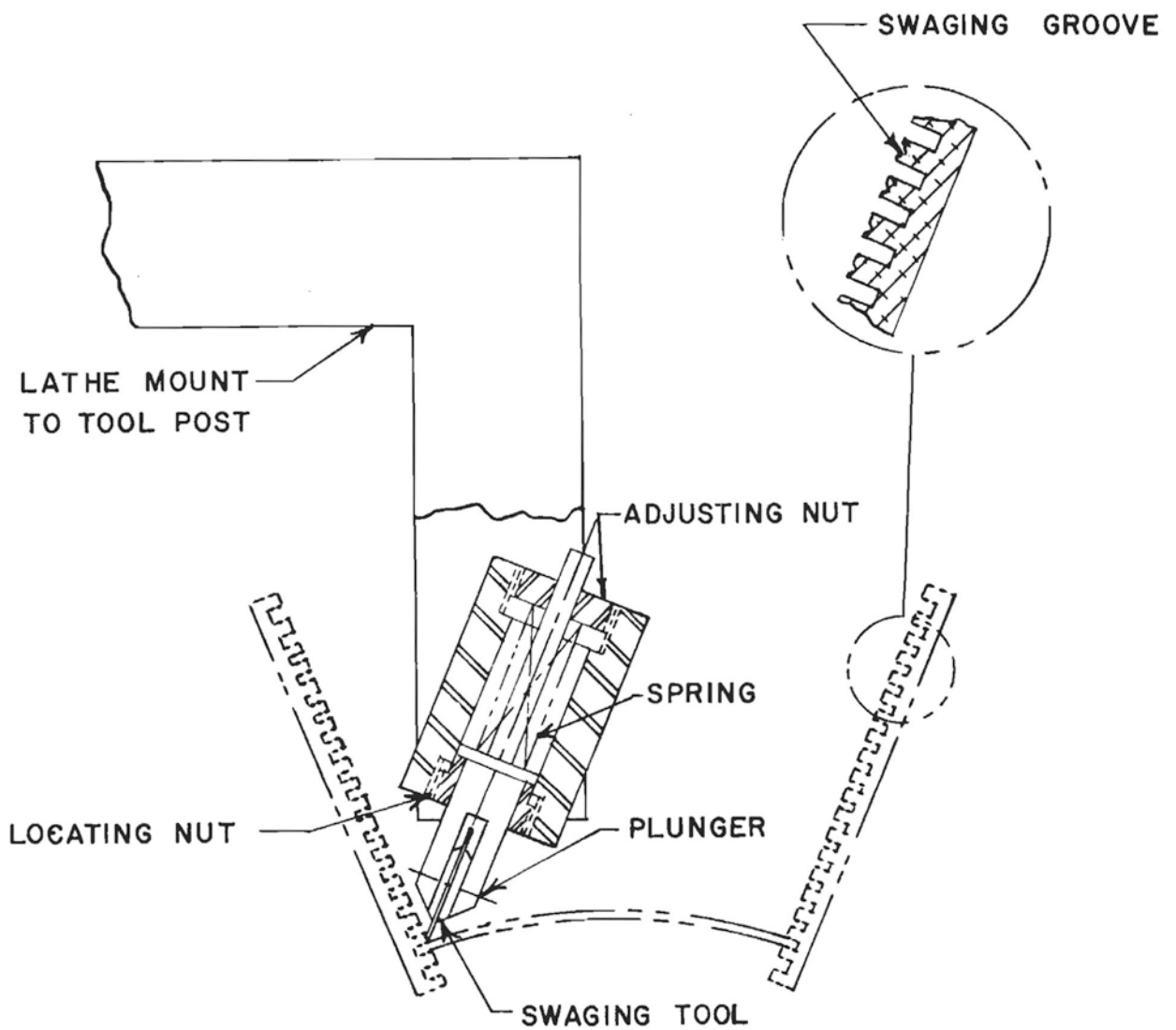


Fig. 11. Swaging Mechanism.

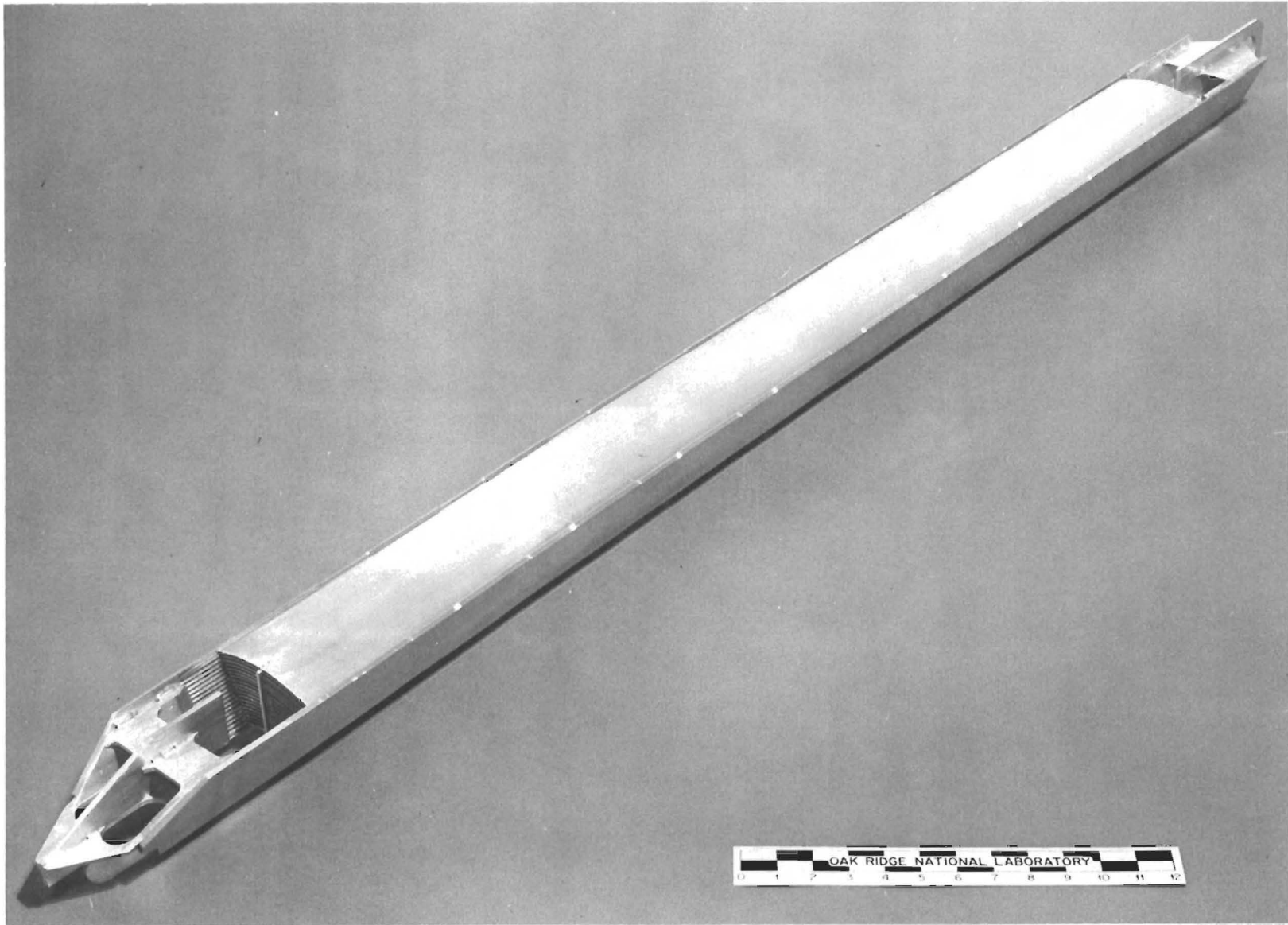


Fig. 12. Advanced Test Reactor Fuel Element.

Table 3. Advanced Test Reactor 1-5 Inspection Summary
Total Measurements Taken Per Element 1296

	Fuel Element No.				
	1	2	3	4	5
Plate channel (volume) in specification	5	4	7	8	14
Plate channel (volume) out of specification	13	14	11	10	4
Plate spacing (area) in specification	274	342	323	364	415
Plate spacing (area) out of specification	158	90	109	68	17
Total measurements within ± 0.010	1098	1249	1234	1253	1292

Conclusions

Although the ATR fuel element development program is not completed, the feasibility of manufacturing fuel elements within the design specifications has been demonstrated. Procedures were established to fabricate the 19 different fuel geometries within the required tolerances. Cross rolling was established as a suitable technique for reproducibly obtaining fuel plates of different fuel widths. Metallurgical bonding was achieved in roll cladding the dispersion fuels with either type X8001 or 6061 aluminum.

Experience to date in assembling the fuel elements indicates that reproducible forming of the fuel plate radii is essential to achievement of dimensional requirements. Techniques to reproducibly form the fuel plates and parameters which affect the forming reproducibility are being vigorously explored.

Acknowledgment

The authors wish to acknowledge G. M. Adamson, Jr., R. J. Beaver, J. H. Erwin, and T. D. Watts of the Metals and Ceramics Division for their contribution to this fuel element development program. The authors are also indebted to J. L. Gregg, consultant from Cornell University, for his contribution to the fuel plate fabrication studies.

References

1. D. R. deBoisblanc et al., The Advanced Test Reactor (ATR) Fuel Conceptual Design, IDO-16667 (November 1, 1960).

NONDESTRUCTIVE TESTING OF HIGH-FLUX ISOTOPE REACTOR
AND ADVANCED TEST REACTOR FUEL ELEMENTS

Robert W. McClung*

Introduction

The satisfactory performance of high-flux reactor fuel elements demands assurance that design tolerances have been met. One step toward the necessary high confidence for the High-Flux Isotope Reactor (HFIR) and the Advanced Test Reactor (ATR) has been the establishment of a nondestructive testing development program to provide techniques that will allow evaluation of various fuel element properties. Most of the work has been directed toward the detection or measurement of those conditions that could cause uneven heat distribution leading to premature fuel element failure. Ultrasonic techniques have been studied for the detection and evaluation of non-bonded areas between the core and cladding material in the fuel plates. The x-ray attenuation method has been investigated as a tool for measuring fuel concentration variations within each fuel plate. Electrical impedance techniques have been developed for the measurement of coolant-channel spacing. The above systems have been or are

*Oak Ridge National Laboratory, Oak Ridge, Tennessee.

being developed for both the ATR and the HFIR. In addition, an eddy-current technique has been devised for the identification of core orientation in the HFIR fuel plates. Previous description at this Conference of both HFIR and ATR fuel plates and assembled elements makes further elaboration and design details unnecessary. Because of the basic similarities between the two fuel plates, discussion of the inspection development will be common to both except as noted:

Nonbond Detection

Nonbonded areas between the fuel-bearing core material and the aluminum cladding would act as barriers for heat flow causing localized hot spots and probable fuel plate failure. The through-transmission ultrasonic technique has been utilized successfully for nonbond detection in alloy-core reactor fuel plates;¹ however, the principal unknown for application to the HFIR and ATR plates was the effect of the cermet-dispersion core on the ultrasonic transmission. In particular, there was no information relative to the minimum size nonbond which could be detected in the presence of acceptable or designed variations in fuel concentrations.

Theory

The basic through-transmission ultrasonic technique is illustrated in Fig. 1. A high-frequency ultrasonic beam is generated by a piezoelectric transducer and transmitted through a coupling medium such as water. As the beam encounters an interface, a portion of the beam will be reflected and a portion will be transmitted through the interface. The amount of reflection is dependent, in part, on the acoustic mismatch. Thus, a beam being transmitted from one transducer to a similar receiving transducer will be attenuated by the presence of intermediate interfaces and such other factors as scattering, absorption, divergence, etc. As long as the intermediate material is uniform, a constant signal amplitude will be detected by the receiving transducer.

A localized condition of nonbond with its drastically different acoustical impedance, however, will cause a reduction in transmission. The amount of reduction will be primarily a function of the nonbond area as compared to the cross-sectional area of the ultrasonic beam.

Equipment

Commercially available pulsed-ultrasonic instrumentation has been used during this study. The principal component is the instrument that produces the electrical signal to feed the piezoelectric transducer. This signal is a continuous series of one-microsecond pulses at a repetition rate of approximately 600 pulses/sec. For rapid scanning over the plate surface, it is necessary to have the fast repetition rate to assure that every section of the plate which has been scanned has also been investigated by the ultrasound. Other features of the basic unit are detection, amplification, and display circuitry to process the data relative to the amount of sound transmitted through the fuel plates.

An item of auxiliary equipment provides an electronic gate to select and process the transmitted signal. This pulse subsequently operates visual and audible alarms and generates an output signal suitable for actuating the stylus of a plan-view recorder. Thus a map of the plate and its nonbond areas is provided as a permanent record.

Mechanical scanning equipment is required to provide precise control of the scanning parameters. Figure 2 is a photograph of the temporary scanning system which is being used. The fuel plate is held with the transverse direction (width) vertical. It is moved in a longitudinal direction to accomplish the linear scan by means of a continuous roller-chain drive. Transverse indexing of the transducers before reverse parallel scans is accomplished with the cross-feed mechanism of a small lathe. Longitudinal scanning speeds in excess of 200 in./min were readily attainable.

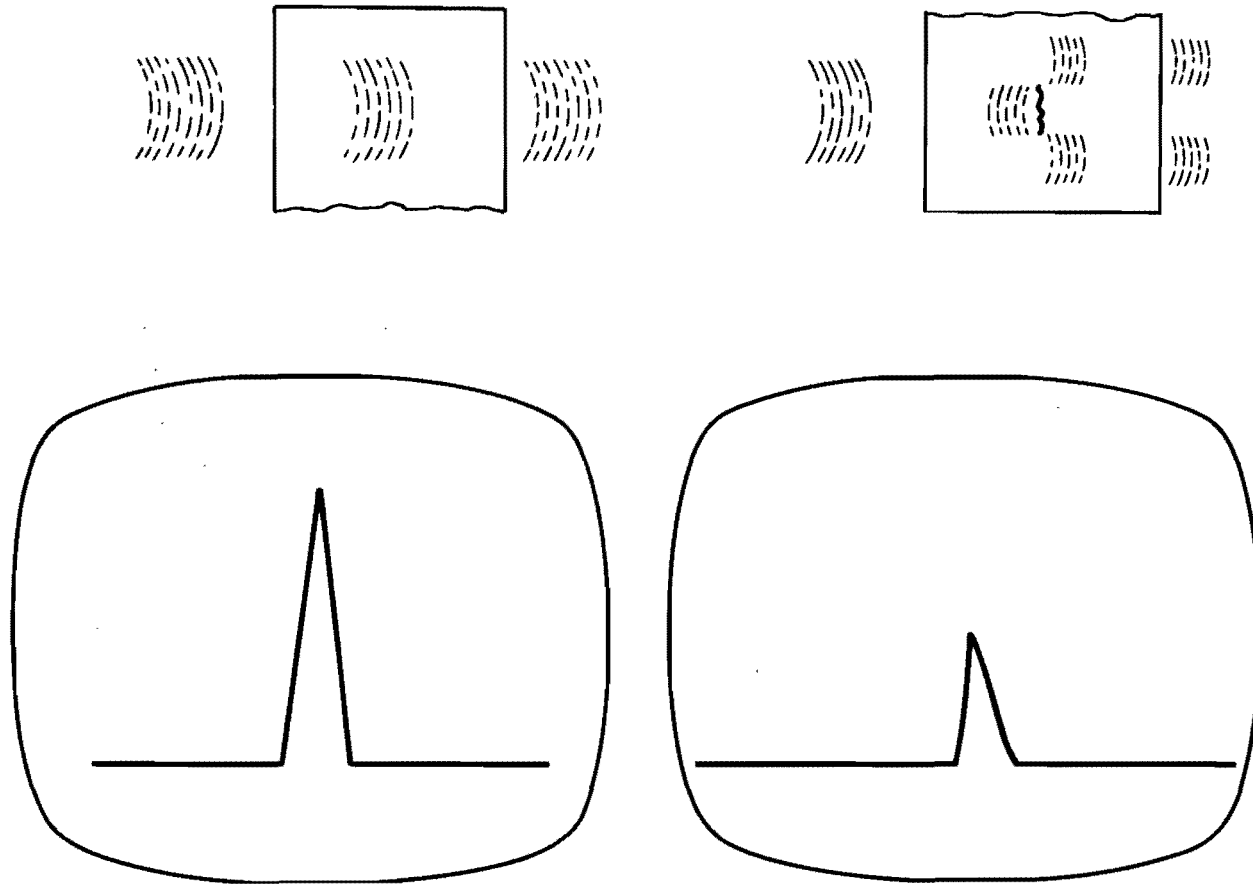


Fig. 1. Through-Transmission Ultrasonic Test Method.

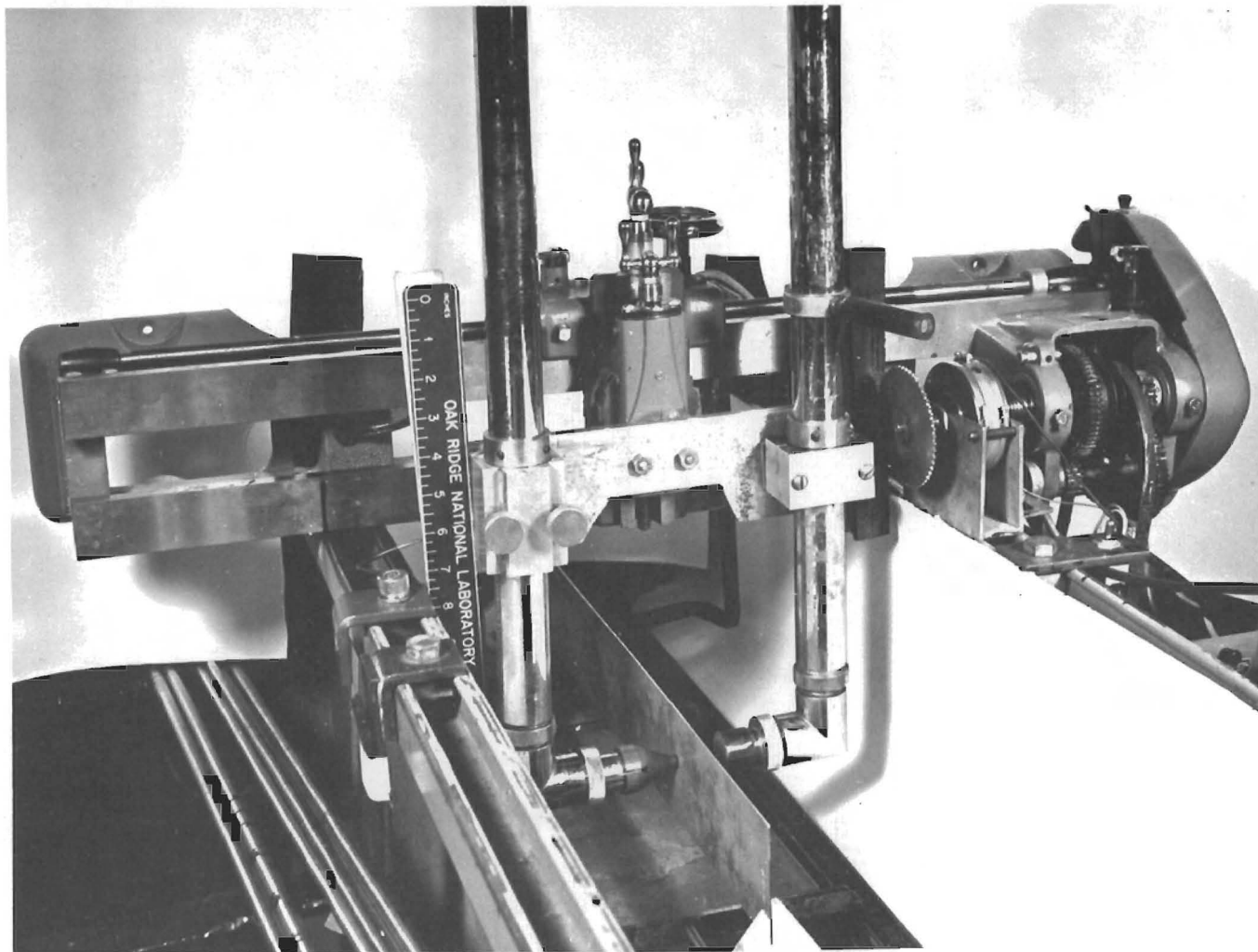


Fig. 2. Temporary Scanning Mechanism for Ultrasonic Nonbond Detection on Fuel Plates.

Reference Standards

Nonbond areas of known size in standard fuel plates are needed for instrument calibration, inspection standardization, and, more particularly in the early stage, for the determination of attainable sensitivities. The best and most reproducible fabrication technique for simulated nonbonds has been the use of end mills to produce shallow, flat-bottom holes of known diameter in finished fuel plates. These holes are then plugged in such a fashion that the acoustic mismatch at the bottom of the hole corresponds as closely as possible to that expected from a naturally occurring nonbond.

Tests and Results

Simulated nonbonds of $1/16$, $3/32$, and $1/8$ in. diam have been placed in frame and core areas of both the ATR and HFIR plates. As mentioned previously, the response to a nonbond is noted as a decrease in transmitted sound and the degree of response is a function of the nonbond areas as compared to the cross-sectional area of the sound beam. Therefore, reinforced-plastic collimators are used to restrict the sound beam and thus improve both sensitivity and resolution since the most readily available transducers are $3/4$ in. in diameter.

A number of HFIR and ATR developmental plates have been examined using the reference plates containing the drilled holes. Background variations in ultrasonic transmission due to the core quality have been slightly less than that due to $1/16$ in. nonbonds. Only a few nonbond indications equivalent to $1/16$ in. diam and none larger have been found in recently fabricated plates. An insufficient number of plates have been investigated, however, to decide conclusively that background variations will be of sufficiently low level to permit inspection for $1/16$ in. nonbond with no spurious rejections. Despite this slight uncertainty on the final allowable sensitivity, the ultrasonic method has been demonstrated to be a fast, reliable inspection for nonbond detection.

Fuel Homogeneity

Variations in fuel concentration beyond design tolerances could have an adverse effect on fuel element performance. For this reason, nondestructive techniques are necessary to detect and evaluate changes in fuel loading. Preliminary specifications for both fuel elements require that there be no spots in which the amount of uranium exceeds a prescribed tolerance. The spot size for each is less than 0.007 in.² and the tolerances which are being studied relative to homogeneity for any spot are $\pm 10\%$ for ATR and $\pm 30\%$ for HFIR. The small area-homogeneity combination far exceeds that of any other known specification. The need for 100% inspection of a large number of plates demands a fairly rapid inspection. This, in turn, precludes the use of gamma-counting techniques on as-fabricated plates since the low order of emitted irradiation would require too long a dwell time on a given area to obtain adequate statistical accuracy. An x-ray attenuation method, however, has been demonstrated to be feasible for this difficult inspection problem.

Theory

As x rays are transmitted through a specimen, they are attenuated in accordance with the relation:

$$I = I_0 e^{-\mu\rho x}$$

where

- I = transmitted intensity,
- I_0 = initial intensity,
- μ = mass attenuation coefficient,
- ρ = density, and
- x = thickness of specimen.

The mass attenuation coefficient increases with increasing atomic number and, in general, decreases with higher x-ray energies. Under constant operating conditions, therefore, as the amount of high atomic

number material (uranium) changes, there will be a change in the transmitted irradiation. Appropriate calibration techniques will thus allow correlation of intensity change to fuel concentration change.

Equipment

Industrial x-ray equipment is being utilized as the irradiation source during this development program. Careful control of the input voltage and operating conditions has resulted in very stable and reproducible operation. Two detection systems are being studied to monitor the intensity changes; namely, x-ray film with associated densitometry,² and scintillation crystals with associated circuitry and recorders.

Figure 3 is a block diagram of the gamma scintillation detection system which is being used for both reactor plates. The array of collimators restricts the primary beam to the spot size of interest on the plate and, at the same time, eliminates scattered irradiation from reaching the detector. Thus, as fuel concentration varies, the change in x-ray intensity will be detected, amplified, and recorded. As with the ultrasonic system for nonbond detection, mechanical X-Y scanning of the plate is necessary to evaluate the entire surface area. Figure 4 shows a temporary system which has been assembled to allow the plate to be driven longitudinally with successive vertical indices at the end of each longitudinal scan. A sturdier, more permanent system for mechanical scanning is being fabricated.

Scanning speeds will be limited by the recorder-response time and the beam intensity which can be faithfully accepted by the detector. The latter will, of course, be a major consideration in the determination of the statistical accuracy. Plates have been scanned at a linear speed of 16 in./min, but the maximum scanning speed is not yet known.

The other detection system requires the making of a high-contrast radiograph of the fuel plate and then measuring the gradients of film density which can be related to fuel concentration. Although this

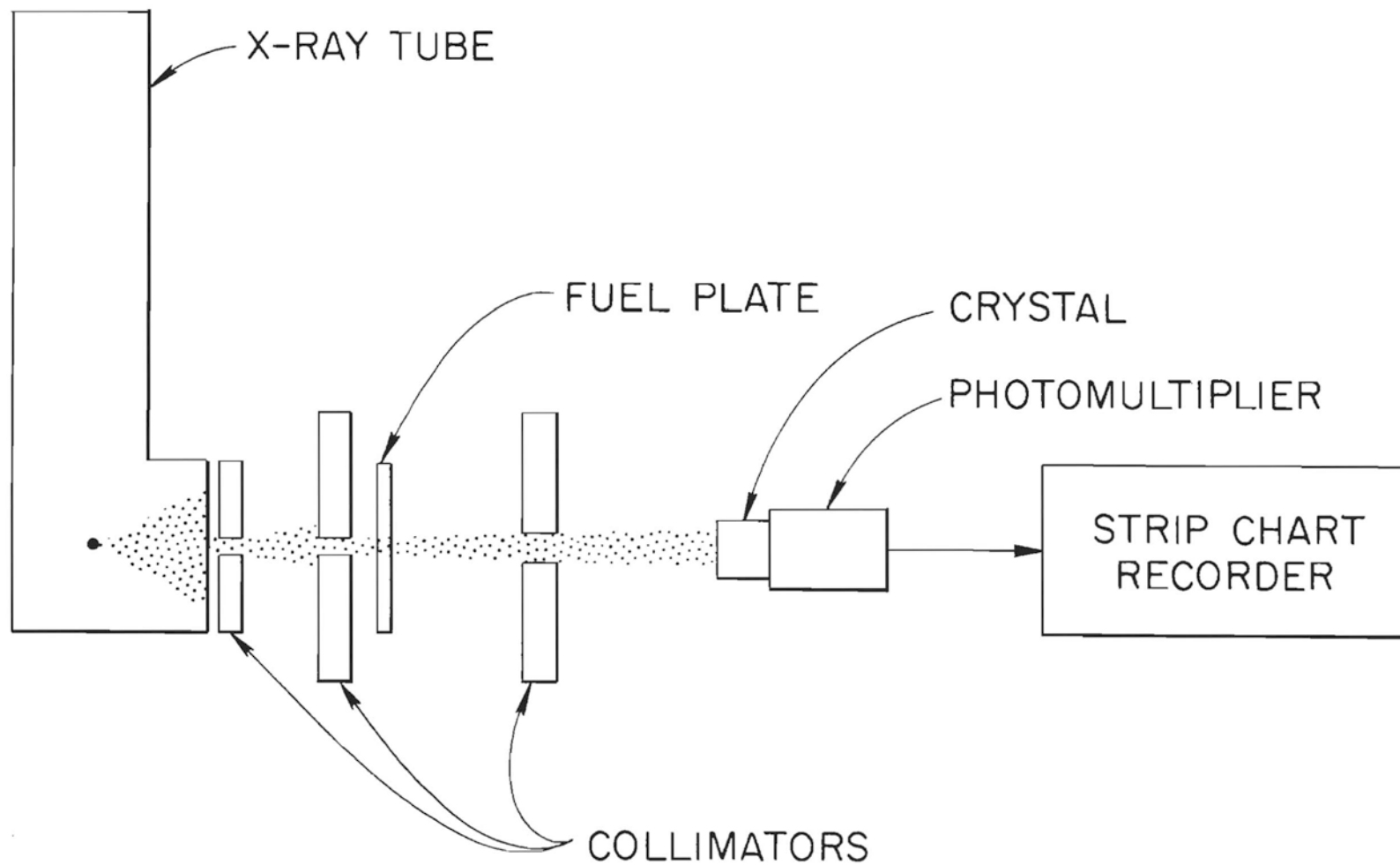


Fig. 3. Block Diagram of Gamma Scintillation System for Evaluation of Fuel Inhomogeneity.

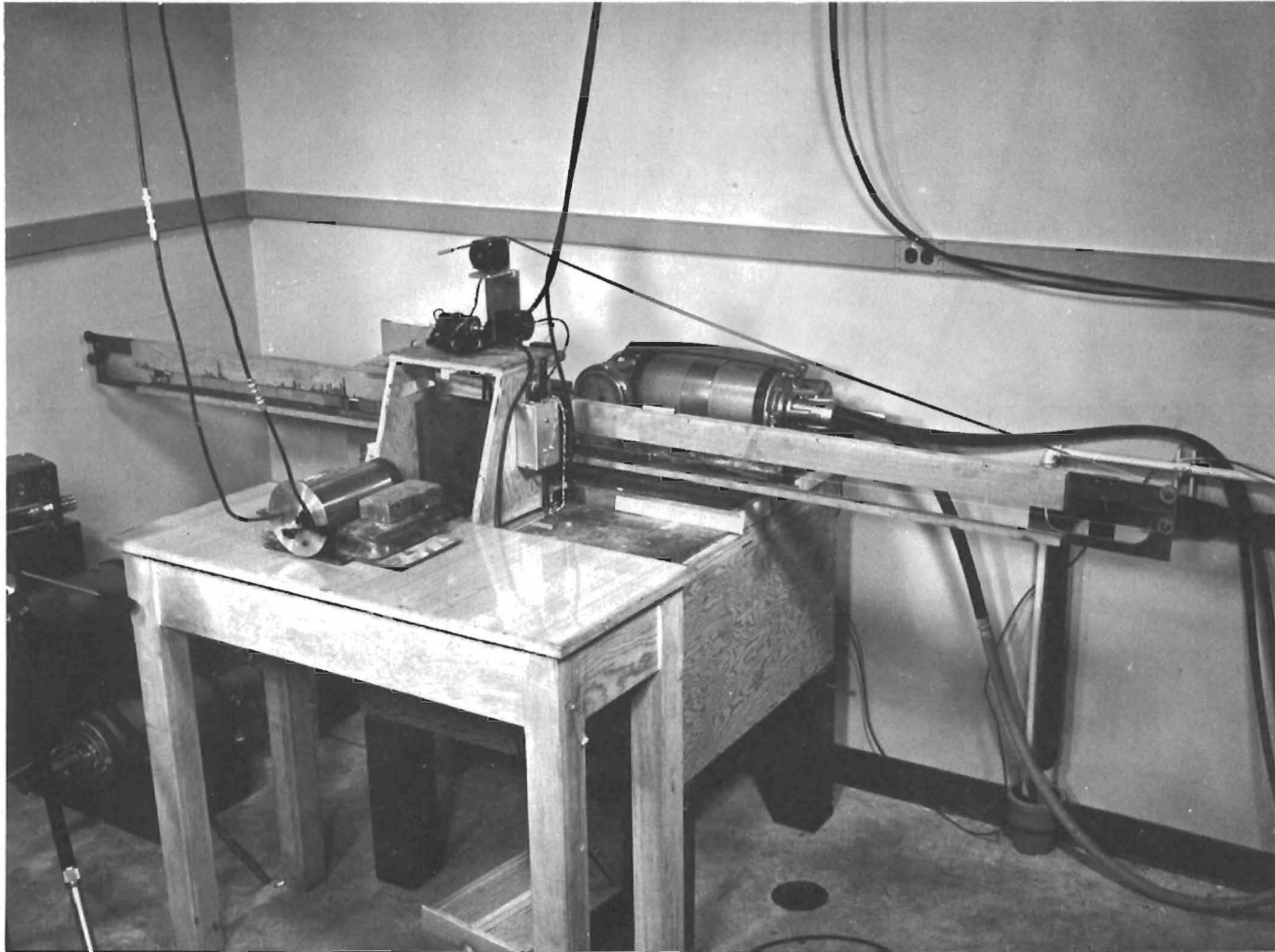


Fig. 4. Temporary Scanning Mechanism for Evaluation of Fuel Inhomogeneity.

seems like a much simpler method, the calibration and measurement of small localized variations require the x-ray film to be scanned in the same fashion as the plate in the gamma scintillation system.

Reference Standards and Calibration

In common with most other nondestructive tests, the measurement of inhomogeneity requires special standards to calibrate and establish the technique. A quantitative relationship must be established between changes in fuel concentration and x-ray attenuation. The most direct method was to produce U_3O_8 -Al compacts which were rolled into thin foils having varying amounts of U_3O_8 per unit area. These were then combined with an appropriate thickness of aluminum to simulate the thickness of a fuel plate. Although there were inhomogeneities in the standards, extensive scanning and integration of attenuation values coupled with analytical chemistry determinations allowed good attenuation relationships to be established. The fuel concentration gradient of the HFIR plate (see Fig. 5) and the need for single-point standardization for go-no-go inspections led to the investigation of thicknesses of homogeneous materials which will have an equivalent attenuation at the energy levels being used. Both tool steel and aluminum have been shown to be applicable for this. Figure 6 illustrates the type curves which were obtained for instrument chart values (x-ray attenuation) vs tool steel thickness and U_3O_8 concentration. Similarly for film radiography Fig. 7 relates the material values to film density. Of course it must be recognized that the chart and density values are relative and not absolute. Exact values must be obtained at the time of inspection.

Tests and Results

A number of HFIR inner annulus plates have been radiographed and scanned with the scintillation system. Although this has been concurrent with the development of calibration standards and no absolute

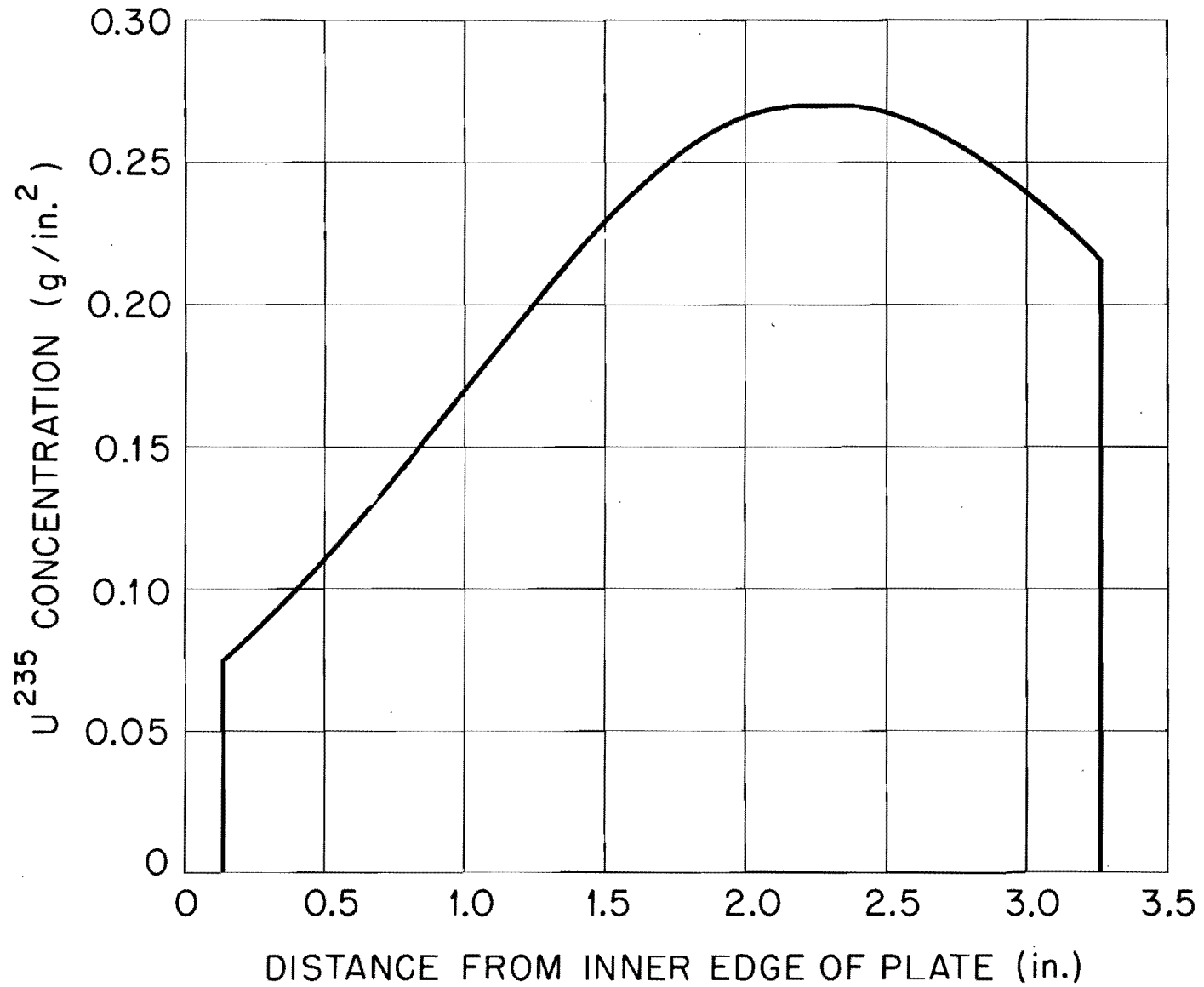


Fig. 5. Fuel Concentration Gradient of the HFIR Inner Annulus Fuel Plate.

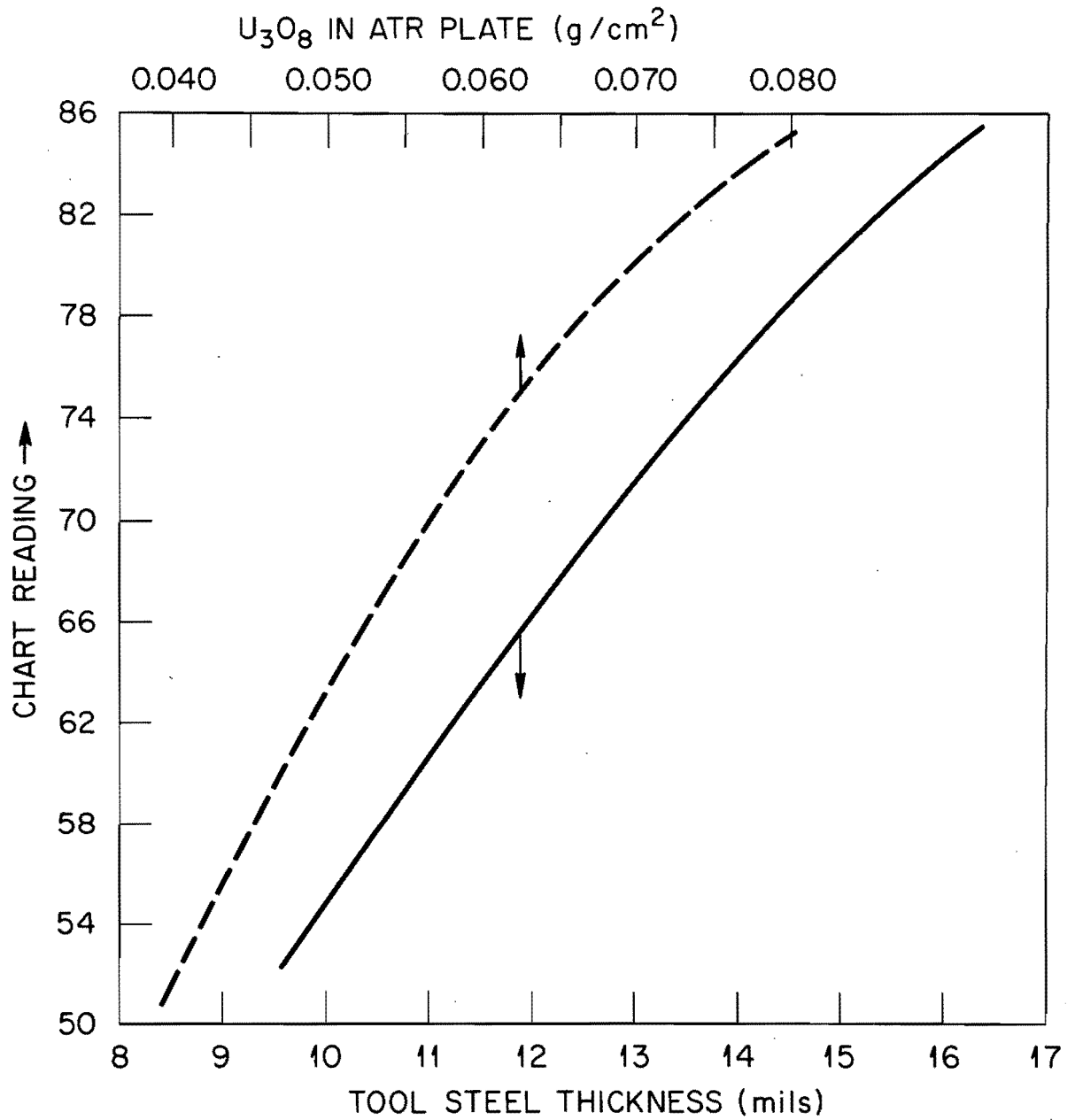


Fig. 6. Typical Chart Values for X-Ray Attenuation Scintillation System for Tool Steel and U_3O_8 Concentration.

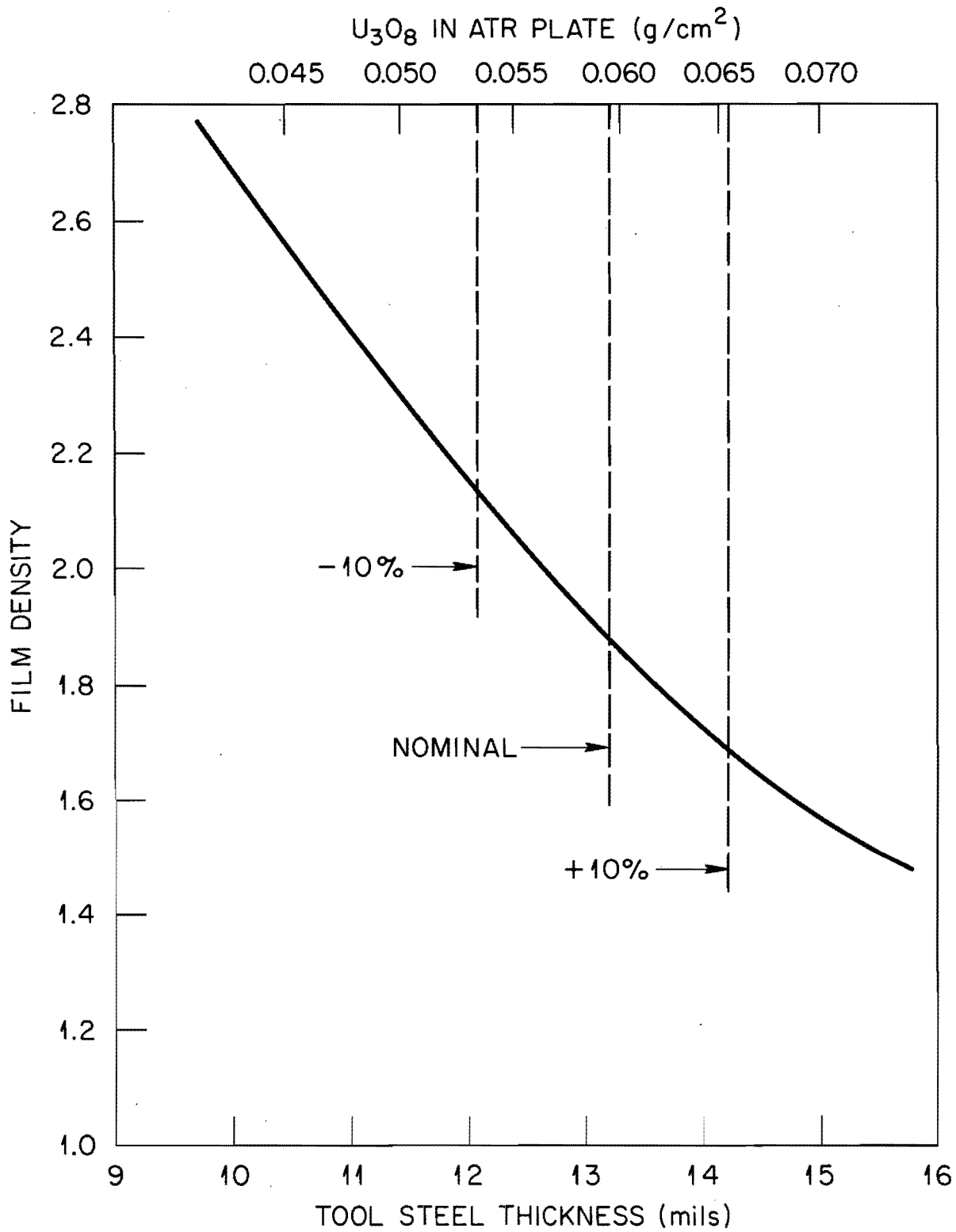


Fig. 7. Typical Film Densities for Varying Tool Steel Thickness and U_3O_8 Concentration.

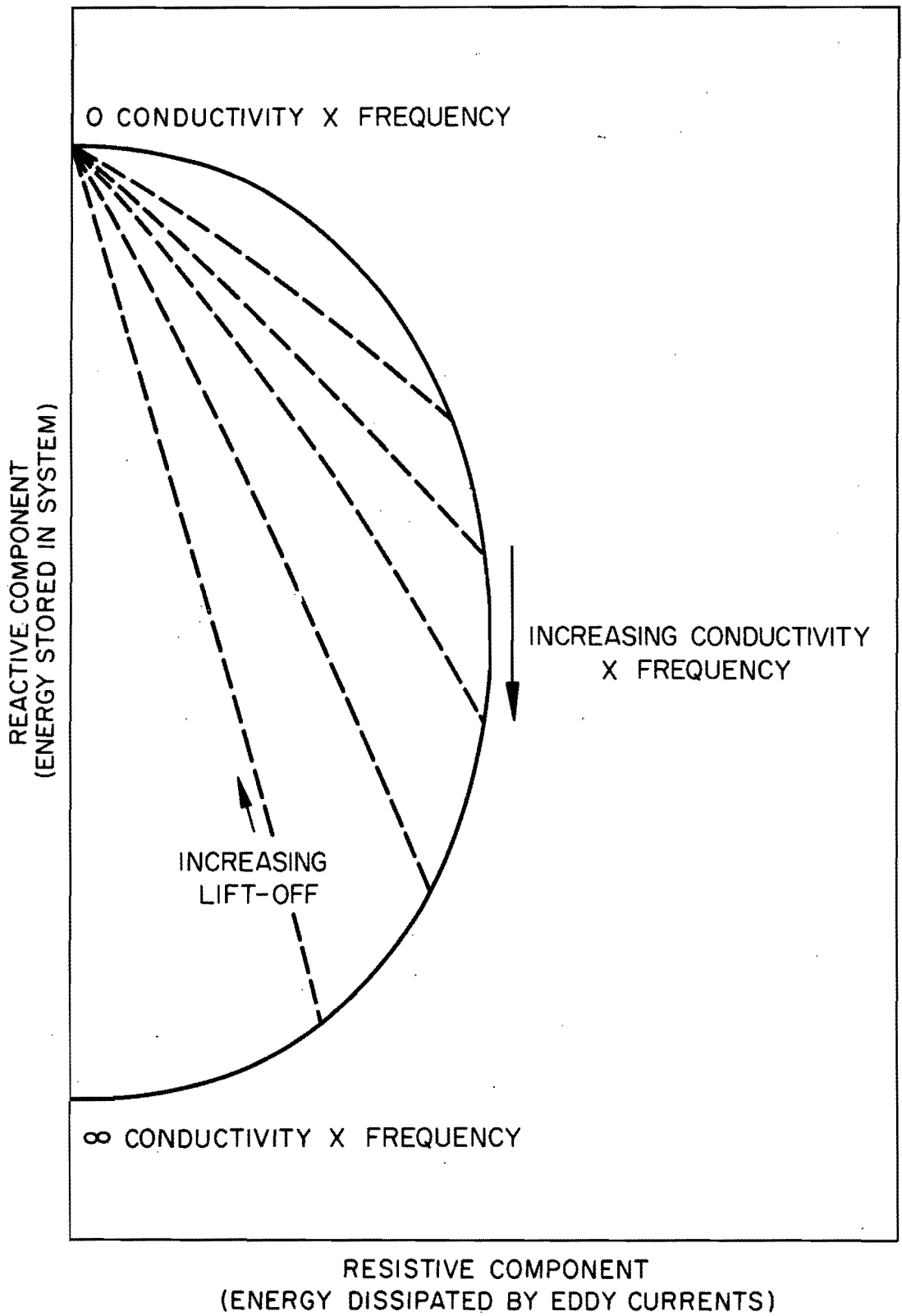


Fig. 8. Idealized Electrical Impedance Curve for Coil Near a Metal Specimen.

values can be assigned, it appeared that there were plates which contained localized fuel variations greater than 30% from nominal.

Because of the rather large planned fuel gradient in the HFIR plates (as much as 4:1), the film densitometric technique does not seem to be practical. The large dynamic range or latitude of the scintillation system is quite amenable, however, to this large inherent variation. It is felt that the ATR plate with a constant core thickness can probably be evaluated by either method.

Coolant-Channel Spacing

Achievement of well-bonded plates with homogeneous fuel dispersions would be of questionable value if the heat which is produced were not removed uniformly. There is a valid requirement, therefore, for consistent coolant-channel spacing. As an example, for the HFIR fuel element the nominal channel dimension has been established as 0.050 in. with a single-point tolerance of ± 0.010 in. and a tolerance on the average at any cross section of ± 0.006 in. (the latter relating directly to cross-sectional area). Because of the very narrow space and the need for accurate measurements throughout the fuel element length, special techniques and equipment have been developed.³

Theory

The electrical impedance of a coil near a metal specimen will change as a function of coil-to-specimen spacing, specimen conductivity, and the electrical frequency (see Fig. 8). At a given frequency, therefore, if the conductivity remains constant, changes in the coil impedance can be calibrated in terms of coil-to-specimen spacing (or "lift-off") variations. Relatively high frequencies (in the megacycle range) are preferred for the best accuracy since this produces the greatest response for a small movement near the coil.

Equipment

Commercial instrumentation has been used to generate the appropriate frequencies and to indicate the impedance changes associated with "lift-off" or spacing variations. Special test probes for indirect measurements were designed and developed for this unique application. Figure 9 is a drawing showing the probe head used to make the desired measurement. The coil is affixed to a long, slender tape which is used as the extension mandrel to insert the coil into the desired position. The ferromagnetic leaf spring, which is mounted over the coil, presses against the opposite fuel plate. Thus, as the fuel-plate spacing varies, the leaf spring will move closer to or farther from the coil. The resultant impedance changes due to coil-to-spring variations can be calibrated in terms of space dimensions. The frequency of the signal and the thickness of the leaf spring prevent unwanted signals due to variations in the fuel plate itself.

Tests and Results

The calibration standards, consisting of clamped assemblies of small flat parallel plates separated by gage blocks, provided known accurate spaces for probe insertion and instrument calibration through the desired span. Direct-reading meter scales have been made to avoid conversion problems. This system has been used throughout the fabrication development program for both HFIR and ATR fuel elements. Measurement accuracy and precision have been demonstrated to be within about 0.001 in. This is somewhat dependent upon the measured span. Use of strip-chart recorders for continuous measurement and recording of coolant-channel profiles has been demonstrated to be feasible.

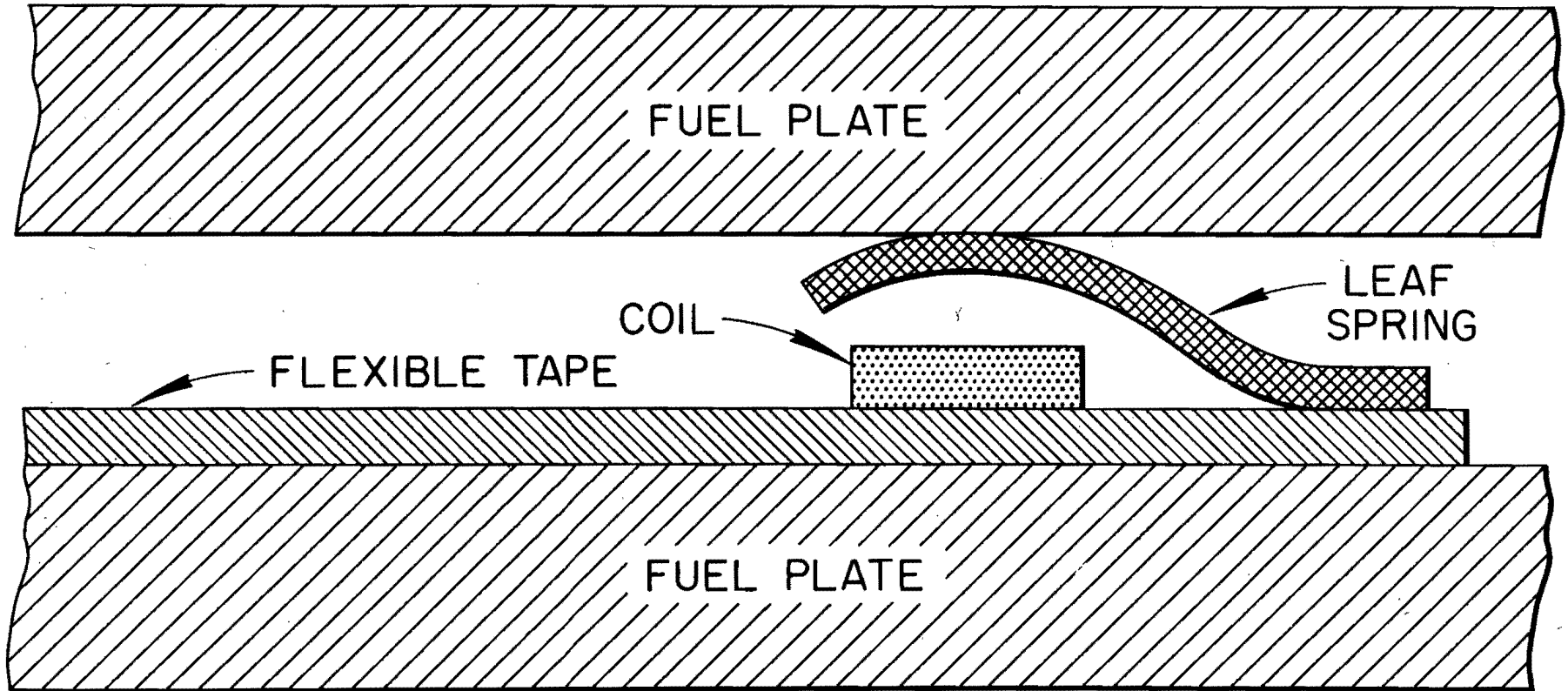


Fig. 9. Probe Head for Impedance Measurements of Coolant-Channel Spacing.

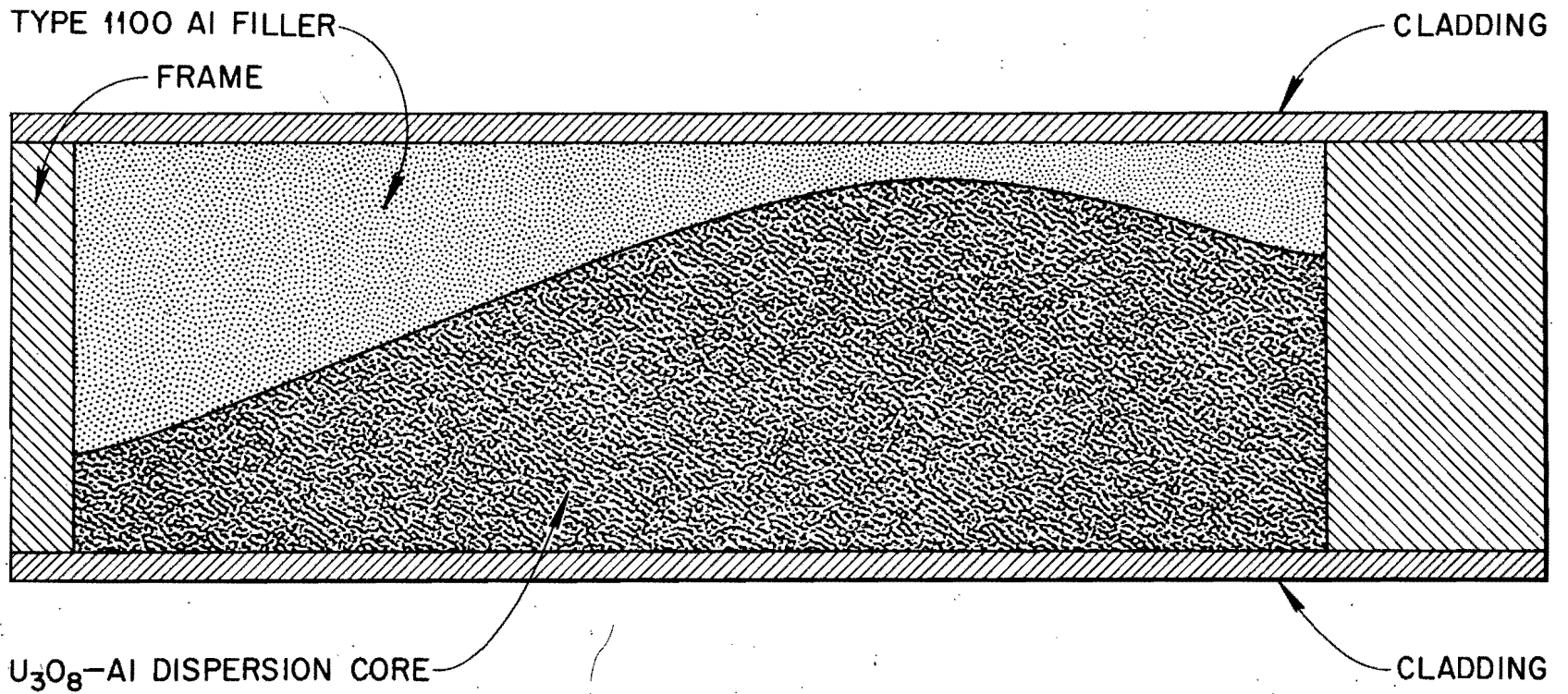


Fig. 10. Cross Section of HFIR Inner Annulus Plate.

HFIR Core Orientation

A problem which is peculiar to the HFIR fuel plate is that of identification of orientation of the fuel gradient. As noted in the discussion on fuel homogeneity, the fuel concentration varies across the plate width, beginning with a minimum value, increasing to a maximum value beyond the plate center, and then decreasing to an intermediate value. For ease of fabrication, the fuel gradient has been achieved through the use of variable thickness core having a nominally constant fuel concentration. To preserve the rectangular symmetry between the cladding, a type 1100 aluminum filler piece has been inserted to match the contour of the uranium-bearing core (see Fig. 10). For thermal flux consideration, there must be assurance that plates are assembled with consistent orientation of the "hump" in the core. This requires a test to identify core orientation.

Technique

As was noted in the discussion on coolant-channel spacing, the normalized impedance of a coil near a metal specimen will vary as a function of specimen conductivity, "lift-off," and electrical frequency. In addition, for thin specimens the impedance change is also related to specimen thickness.⁴

The materials in the HFIR fuel plate vary considerably in electrical conductivity with the type 1100 aluminum filler piece being the best conductor and the aluminum alloy cladding and the U_3O_8 -Al dispersion having lower conductivities somewhat similar to each other. Because of the conductivity similarities between core and clad, there will be little impedance change associated with relative core thickness changes. Thickness changes in the 1100 aluminum (directly associated with core thickness changes), however, can be detected. Thus, by making (through the cladding) a qualitative thickness evaluation of the filler piece, the position of the core hump can be

identified. Through the selection of appropriate frequency, ready identification can be made of the plate surface nearest the filler. Figure 11 shows typical response curves which have been observed on each plate surface.

Two eddy-current instruments have been demonstrated to be suitable for core orientation determination. One, a commercial instrument originally designed for conductivity measurements, provides a well-defined indication, but is very sensitive to variations in coil-to-specimen spacing. The other, an Oak Ridge National Laboratory-designed phase-sensitive instrument, is relatively insensitive to the lift-off variation and is more sensitive, but is more complex and difficult to calibrate. With each instrument a large number of plates have been evaluated rapidly and with a high degree of confidence.

Summary

A number of nondestructive testing techniques have been evaluated or developed for the measurement of certain desired properties for HFIR and ATR fuel plates. These have included through-transmission ultrasonics for nonbond evaluation with an indication that 1/16 in. nonbonds can probably be detected. Calibrated x-ray attenuation measurements are being used for the evaluation of fuel concentration variations. Detection systems include radiographic films as well as scintillation detection and recording systems. Gaging of coolant-channel spacing is being accomplished with an impedance technique using minute probe heads which were custom developed and fabricated. Orientation of the HFIR core can be determined rapidly through the proper use of eddy-current instrumentation. Each of the cited techniques should increase the assurance that the HFIR and ATR fuel elements will perform within the stringent design levels which have been established.

UNCLASSIFIED
ORNL-LR-DWG 71242

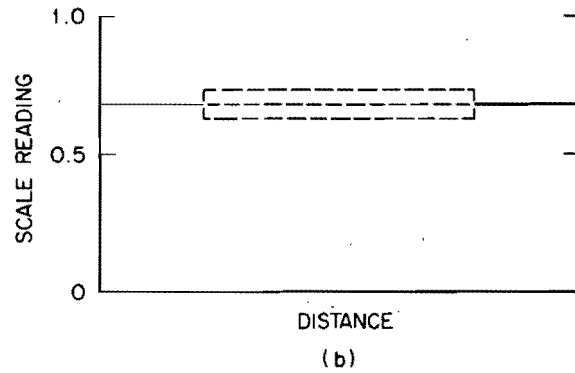
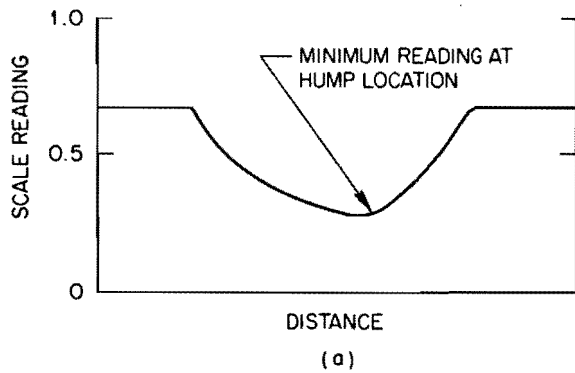


Fig. 11. Typical Response Curves for Identification of Core Orientation by Eddy-Current Technique.

Acknowledgments

Recognition is deserved and must be given to K. V. Cook for his work on ultrasonic nonbond detection; to B. E. Foster and S. D. Snyder for their contributions to the evaluation of fuel inhomogeneities; and to C. V. Dodd for his efforts on the impedance and eddy-current techniques.

References

1. W. N. Beck and W. J. McGonnagle, Development of Ultrasonic Techniques for Inspecting Experimental Boiling Water Reactor Cast Uranium Alloy Cores and Fuel Plates, ANL-5653 (Dec. 1957).
2. R. W. McClung, Feasibility Studies - Nondestructive Testing of the Enrico Fermi Reactor Core B Fuel Element, ORNL-3221 (Dec. 21, 1961).
3. C. V. Dodd and R. W. McClung, Fuel Element Coolant Channel and Other Spacing Measurements by Eddy-Current Techniques, ORNL-TM-129 (March 20, 1962).
4. R. A. Nance and J. W. Allen, Eddy-Current Measurement of Metal Thickness and Cladding Thickness, ORNL-2672 (March 31, 1959).

FUEL ELEMENTS FOR THE BELGIAN HIGH FLUX
TEST REACTOR BR 2

FABRICATION AND TESTING OF A STANDARD TYPE FUEL ELEMENT MADE BY SPOT-WELDING.

M.M.N.- C.E.N. Staff

written by : M. Huberlant (M.M.N.) and D. Tytgat (C.E.N.)

ABSTRACT

Starting from the NDA concept for the Belgian high flux reactor BR2 fuel element, the Metallurgie et Mecanique Nucleaires (M.M.N.) has developed a fuel element with six concentric tubes, each tube being formed of three plates assembled by spot welding.

This method presents incontestable advantages and will lead to an economic realization of this type of fuel element.

Hydraulic testing, under the normal performance conditions, as well as tests under conditions above the standard ones, has shown that the fabrication technique is quite well adapted to the test reactor requirements.

INTRODUCTION

The fuel element for the Belgian high flux test reactor BR2 has been designed by NDA. The element includes six concentric tubes, with a Al-U fuel alloy (24 w/o U, 90% U-235). Each tube is composed of 3 curved plates, assembled at 120°. The six tubes are connected to an aluminum central tube by means of end-fittings which keep at the same time the tube spacing. The fuel plates are each 1.27 mm thick (0.51 mm Al-U alloy, 0.38 mm Al cladding). The nominal water gap value

between the tubes is 2.97 mm. The fueled section of the tube is 762 mm ; the maximum thermal flux is 380 watts per sq. cm. (1).

Different methods have been proposed for the fabrication of the element (2). For example: co-extrusion and drawing of the tubes, brazing of 3 curved plates, deformation locking of 3 curved plates in 3 plate webs.

Co-extrusion produces tubes without interruption of the active fuel, giving a better neutron flux distribution. But this method involves technological difficulties and its efficiency has not yet been proved by an extensive development.

The other methods are based upon assembling three bent plates to form a tube. The active fuel is interrupted, which brings neutron flux perturbation. Assembling can be done by brazing, which introduces the risk of deformation of the plates during the brazing operation and retention of flux and brazing alloy which may affect the corrosion resistance of the fuel element.

The assembling can also be made by deformation locking of the plates in grooved plate webs, which improves the rigidity. But the element cannot be dismounted, the amount of aluminium is increased, the assembly requires machined parts with rather strict tolerances, the quality of the assembly cannot be tested during fabrication.

Starting also from 3 curved plates, the M.M.N. has developed an assembly method by spot welding (3). In this technique the fuel plates are bent with a radially outwards curved rib. The flat parts of the radial rib of three identical plates are assembled by spot welds, spaced along the parallel to the generatrices of the cylindrical surfaces and at a certain distance from the tubes thus formed. After the welding, the ribs are machined to final dimension (fig. 1). Due to this machining, part of the welded surface is eliminated. This allows to control the welded spot quality and to avoid the notch effect which would arise if an unwelded surface was left at the outside part of the rib. The spot welding has the following advantages :

- Due to the development of new machines, the spot welding has become a perfectly reproducible operation.
- The resistance welding does not include any foreign substance and is a quite clean operation.
- Only a local heat-affected zone is produced which does not decrease the mechanical resistance of the parts.

- The welding can be controlled on test specimens welded after a certain number of operations, the immediate examination of which might indicate any misbehaviour of the machine.
- The active fuel part might be brought very near to the edge of the plate; this reduces to a minimum the interruption of the fissile material.
- This fabrication facilitates the mounting and dismounting of the elements. Mounting of the tubes on the spot, depending on the irradiation programs and starting from a limited stock number, will be possible without delay.
- This method does not involve expensive operation or equipment and will result in a reduced assembling cost.

The validity of this technique has been confirmed by hydraulic testing under more severe conditions than the standard operation in the reactor.

2. FUEL ELEMENT FABRICATION

2.1 Fabrication and control of the fuel plates

a. The fabrication of fuel plates for research reactors with an Al-U alloy meat is now classic. M.M.N. has adopted the "picture frame" too but developed a special technique which leaves an exit for the gasses during the first rolling passes of the sandwich and produces directional bonding. (4) (5).

Fig. 2 shows the 200 CV Robertson rolling mill used. Rolling is performed at 600°C.

b. The control of the plates includes radiography, ultrasonic testing, gamma-counting and alpha-counting for external contamination.

2.2 Forming and welding of the plates

a. The forming of the plates is done in two steps: the first is bending the plates, the second forming the ribs. This operation is performed on a 75 ton press shown in fig. 3.

b. Welding : Three plates are assembled on a mandrel to form a tube. A few weld spots are made, the diameter is checked and the mandrel withdrawn. Welding is continued using a judicious welding point sequence to avoid tube deformation. The welding spots are 15 to 25 mm apart and have an approximate diameter of 5 mm. (fig. 4 and 5).

2.3 Dimensioning and control of the tubes

The welded edges are machined to the final dimension. Part of the welded zone is cut; this permits easy control of the weld. Three notches are machined on both ends of each tube in view of the final assembling. Each end of the rib is argon-arc welded to increase the hydraulic stability (see section 3 of the paper), (fig. 6 & 7).

2.4 Assembling of the tubes

The tubes are maintained on both ends by end fittings, those being connected to a central tube.

3. HYDRAULIC TESTS

Some prototype fuel elements have been hydraulically tested at the C.E.N. using the loop described by J. Herpin (5).

3.1 Fuel elements with a longitudinal gap (6)

The concept of the fuel element includes a gap between the tubes and the end fittings to accomodate thermal expansion of the plates during reactor operation.

During hydraulic testing, no expansion occurs. The existing gap permits an hydraulic vibration which induces a wearing of the tubes.

This was confirmed by a test of 188 hrs at a 2385 l/min water flow.

3.2 Fuel elements without longitudinal gap

Two prototypes were mounted without longitudinal gap :

a. Prototype n°37

a.1 endurance test

Time : 1063 hrs

Flow rate : 2688 l/min

Pressure drop on the element : 48 psi

Average speed of water in the element : 40 ft/sec (111% above 35 ft/sec speed).

The thickness of two tubes was measured after the test, the original value being 1.16 mm.

Tube	Water inlet side			Water outlet side		
Dia 78 mm	1.15	1.15	1.16	1.06	1.16	1.11
Dia 68 mm	1.16	1.16	1.16	0.975	1.11	1.07

a.2 Overspeed test

Time : 49 hrs

Flow rate : 3.140 l/min

Pressure drop : 68 psi

Average speed of water : 45.5 ft/sec (130% of the 35 ft/sec speed).

Few welded spots had failed on the external tube, at the water inlet side only.

b. Prototype n°36

At the nominal flow rate of 2700 l/min, this prototype showed defected tubes, even after 2 hrs testing. The rupture start being always at the tube end, it was thought that the unwelded section between the first resistance spot weld and the tube end induced weld fracture.

This was confirmed by a series of 2 hr tests. Progressive rupture of the welds was observed.

3.3 Fuel elements with argon-arc welded ends

The ends of the fuel elements were reinforced, by argon-arc welding few centimeters on each end.

A prototype hydraulically tested has proved the perfect stability obtained.

Time	Pressure drop	Flow rate	Speed
106 hours	48 psi or 3,37 kg/cm ²	2.640 l/min	39 ft/sec
63 "	52 3,66	2.765	41
3	56 3,94	2.895	43
13	60 4,22	2.985	44
907	48 3,37	2.640	39

4. FUTURE PROGRAM

A program will be conducted to determine how to compensate the differential expansion of the tubes and of the central tube, to avoid any wearing of the tube ends.

REFERENCES

- (1) H. Dopchie and J. Planquart "BR2, the Belgian Material and Engineering Test Reactor". Conf. Genève 1958 P/1679
- (2) A. Strasser "Fabrication of BR2 fuel elements". American Society of Mechanical Engineers Symposium". April 1959.
- (3) M.M.N. Patent pending in Holland (n°280.894, July 12, 1962)
- (4) M.M.N. Belgian Patent n°620.577 (July 24, 1962)
- (5) M.M.N. Belgian Patent n°620.596 (July 24, 1962)
- (6) J. Herpin "Fuel Elements for the Belgian High Flux Test Reactor BR2 -Part I- Design and hydraulic tests of some special fuel elements". To be issued at this conference.
- (7) J. Herpin. Internal Report C.E.N. R.1830. February 1960.

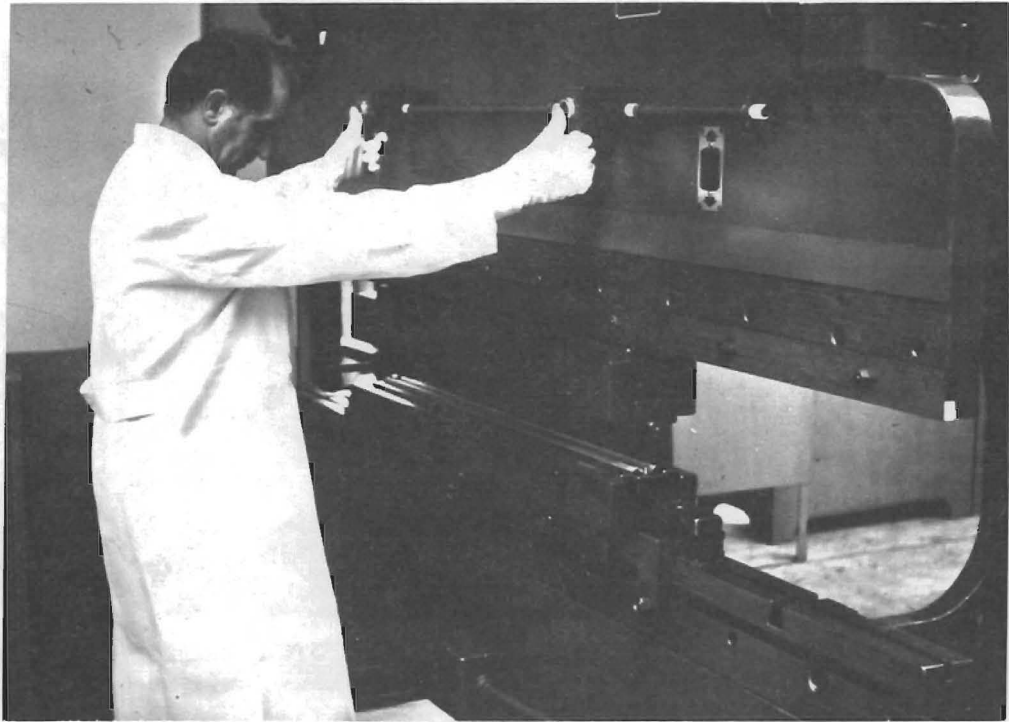


Fig. 3 75 T. Cincinnati Press Brake

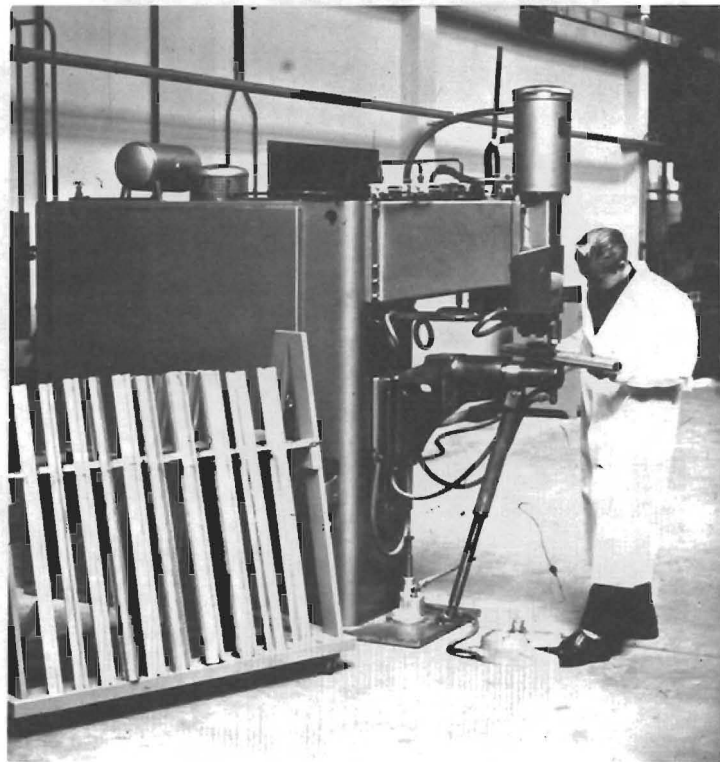


Fig. 4 260 kVA triphase spot welding machine

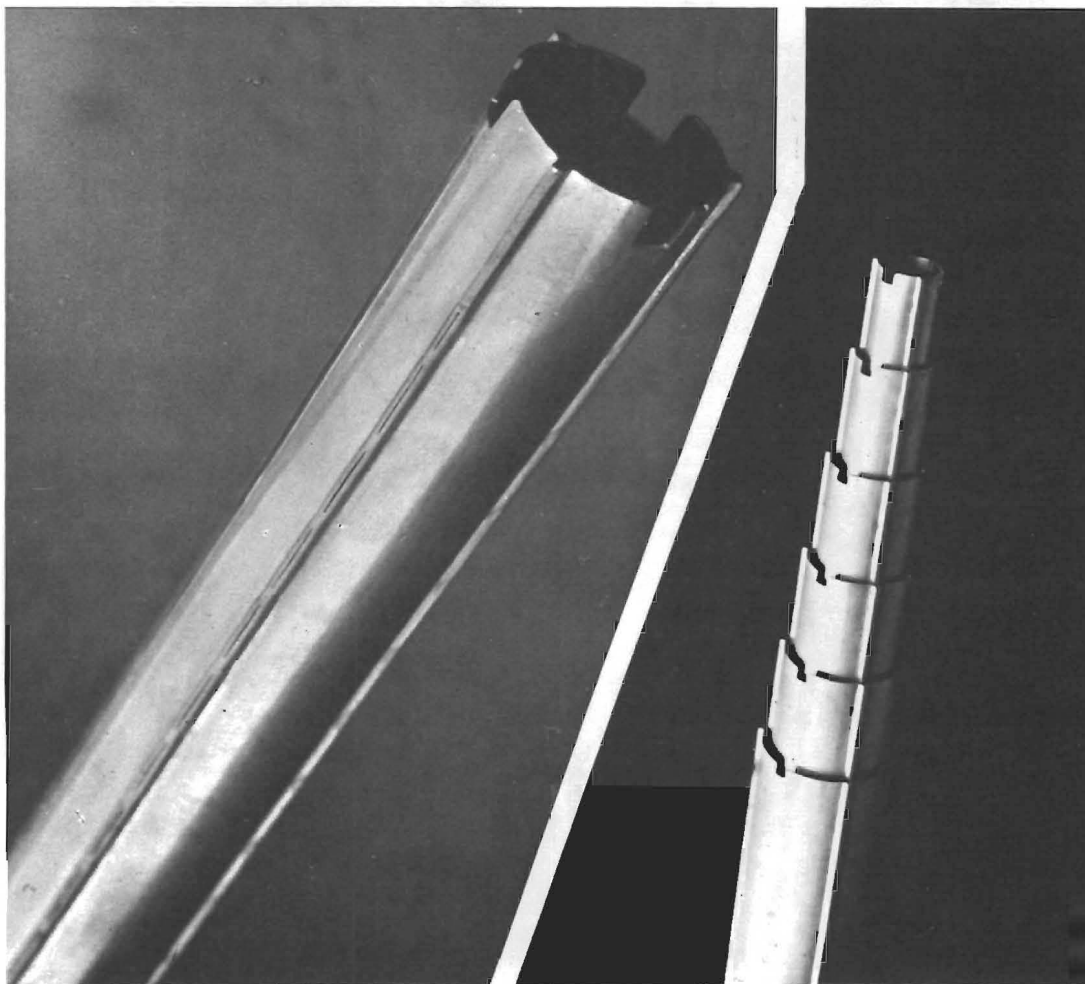
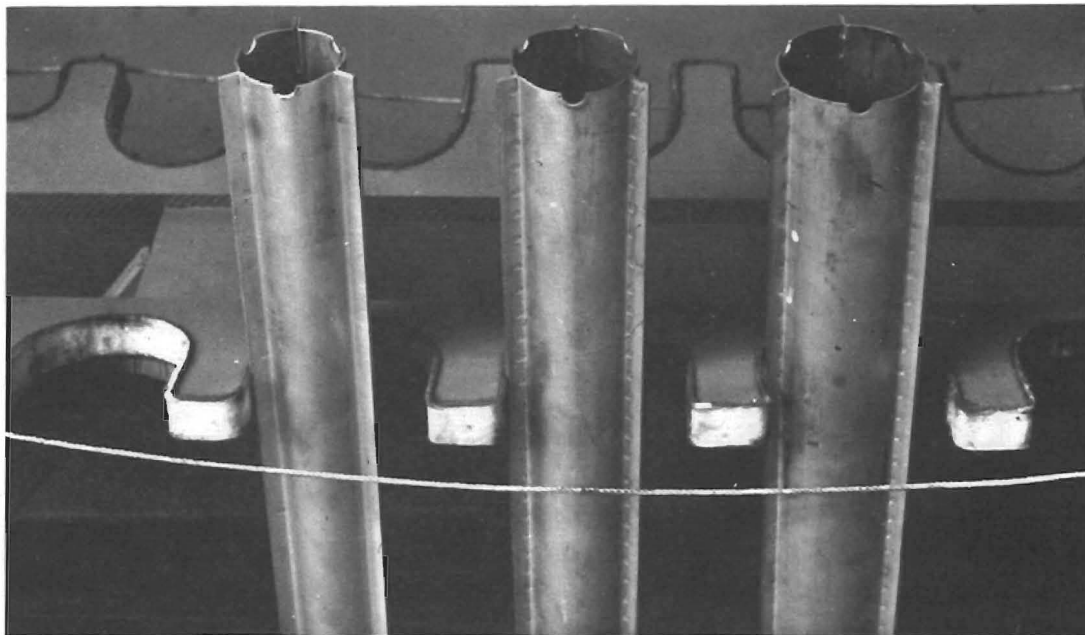


Fig. 5 Unmachined welded tubes

Fig. 6 Finished tube showing argon-arc welded end

Fig. 7 Tubes before assembling